



The author(s) shown below used Federal funding provided by the U.S. Department of Justice to prepare the following resource:

**Document Title: Microspectrophotometry of Fibers:
Advances in Analysis and Interpretation**

**Author(s): Christopher S. Palenik, Jason C. Beckert,
Skip Palenik**

Document Number: 250437

Date Received: December 2016

Award Number: 2012-DN-BX-K040

This resource has not been published by the U.S. Department of Justice. This resource is being made publically available through the Office of Justice Programs' National Criminal Justice Reference Service.

Opinions or points of view expressed are those of the author(s) and do not necessarily reflect the official position or policies of the U.S. Department of Justice.

Microspectrophotometry of Fibers: Advances in Analysis and Interpretation

27 May 2015

2012-DN-BX-K040

**Prepared by:
Christopher S. Palenik, Jason C. Beckert, and Skip Palenik**

Microtrace—

790 Fletcher Drive, Suite 106
Elgin, IL 60123-4755

847.742.9909 (p)

847.742.2160 (f)

www.microtracescientific.com

This project was supported by Award No. 2012-DN-BX-K040 awarded by the National Institute of Justice, Office of Justice Programs, U.S. Department of Justice. The opinions, findings, and conclusions or recommendations expressed in this publication/program/exhibition are those of the author(s) and do not necessarily reflect those of the Department of Justice.

Table of Contents

I – Introduction and Motivation	5
II – Samples	6
III – Investigation of Spectral Variables	6
Choice of Emission Source	7
System Stability	8
Dark Scan Drift	8
Iris Diaphragm	9
Lamp Housing Adjustments	10
Light Leak	10
Latent System Polarization.....	11
Coverslip Tilt.....	13
Light Intensity Reduction with a Polarizer.....	15
Polarizer Rotation.....	16
Polarizer Stability.....	16
Latent Pleochroism.....	19
Resolution Factor	21
Transmission vs. Absorbance	22
IV – Sample Preparation Effects.....	23
Quartz vs. Glass Slides.....	23
Slide Stability	24
Edge Contrast.....	25
Relative Refractive Index of the Medium Compared to the Specimen.....	26
Refractive Index Oils.....	27
Coverslip Thickness	29
V – Sampling Effects.....	29
Analysis Across Fiber Width	30

Cross Sectional Shape	30
Photobleaching	31
VI – Fluorescence Microscopy.....	32
Excitation Conditions	33
MSF Compared to Fluorescence Microscopy.....	33
Volume and MSF	34
Fluorescence of Mounting Media	34
VII – Data Collection Recommendations.....	34
Instrument Setup	35
Collection Conditions	36
Spectral Acquisition.....	36
Post Processing	37
VIII – Fiber Components.....	38
Pure Polymer Classification.....	38
Differentially Dyed Fiber Sections.....	39
Delustrants.....	40
Optical Brighteners	42
IX – Spectral Interpretation and Discrimination.....	43
Spectral Variability in Natural Fibers.....	43
Same Dye at Different Concentrations.....	44
100 Fiber Study	44
Comparison of the Data from the 100 Fiber study to the Original data	46
Preliminary PCA Analysis.....	46
Microscopic Discrimination of Macroscopically Similar Fabrics.....	48
Comparison Microscopy.....	48
MSP	48
Combinations of Four Dyed Fibers	49

Fibers with Individual Dyes	51
Chemically Similar Dyes.....	52
Comparison Microscopy.....	54
MSP	55
Thin Layer Chromatography.....	56
Conclusion	56
Macroscopically Similar Yarns	56
Comparison Microscopy.....	57
MSP	58
TLC.....	59
Conclusions	60
XI - References and Bibliography	61
XI - Figures.....	63

I – INTRODUCTION AND MOTIVATION

Microspectrophotometry was first utilized for performing forensic color comparisons in the 1950s when the Scientific Service of the City Police of Zurich had a purpose-built instrument designed for comparing colored fibers. Still earlier, a microspectroscopic ocular was utilized by Georg Popp in the Margarethe Filbert murder in 1908 to compare the colors of transferred fibers.

This technique is now used in nearly every forensic laboratory throughout the world that performs fiber comparisons. Trace evidence sections of laboratories utilize these instruments primarily for the purpose of color comparisons in fibers; although several additional uses of MSP in forensic science have been implemented (*e.g.*, identification of blood (Peterson, 2010), minerals (Palenik, 2007) and paint examination to name only a few). While MSP can be used to obtain information from a broad range of materials, color comparisons of fiber evidence continues to be the major focus of both casework and recent forensic MSP literature.

An evaluation of the abundant literature from the past two decades on the subject reveals a great number of guidelines, studies, and applications of MSP. Despite the immense amount of information available, much of this literature is designed to address either basic questions of significance and discriminating power. In our own casework experience, we have built a list of a number of interesting questions that arose during various projects. For example, is a microscope lamp capable of altering the visible spectrum of a fiber (and when)? What causes the high and low wavelength spectral variations that cause most laboratories to truncate spectra to the range of 400 to 700 nm (when they are collected on an instrument that collects and stores data from ~250 to 900 nm)? What impact does cross sectional shape or choice of mounting medium have on the spectrum? To the extent that such questions have been previously addressed, they are generally presented in application papers published by instrument manufacturers or in a scattering of talks and papers at forensic conferences. To this point, there has been no comprehensive and reliable source to which the bench analyst can turn for guidance in such matters. In response, this research has attempted to illustrate and explore several of these topics. While we admit that the impact of many of these topics may, in the end, be subtle, they remain important for two reasons a) they represent topics that we believe many examiners are not aware of or are unable to address, and b) as statistical interpretation becomes more significant, subtle artifacts and uncontrolled variations hold the potential to alter the reliability of a spectral comparison (as such, it is critical that the influence of topics such as instrument parameters, sample preparation, and spectral interpretation be better understood).

Similarly, there is no practical source of information to assist examiners in the interpretation of spectra. While statistical approaches are being developed, spectral interpretation remains a largely manual exercise (and will continue this way for at least the near future). While the forensic discipline has been shying away from such methods of interpretation, there is nothing inherently wrong with this approach; however, it is helpful to have an understanding of the sensitivity of the method. To this end, we have evaluated a variety of carefully selected sample sets in order to explore the extent to which manual interpretation can be relied upon. For example, Figure 1 shows quite similar spectra collected from two different purple colored fibers. While the spectra are quite similar, we ultimately concluded that they were not associated with the same source due to subtle differences (which could be noted as a very slight difference in color under the comparison microscope). Ultimately, other independent facts from the case proved definitively that these fibers were from different sources, which confirmed the spectral interpretation. Nonetheless, such a determination was made on the basis of experience built upon looking at many hundreds, if not thousands, of spectral comparisons. The research here presents a number of discrete examples that aim to provide the reader with sets of similar spectra that a) provide them with the context necessary to better understand when true spectral differences exist, b) provide the reader with a context for relating spectral differences to colorant concentrations, and c) illustrate cases in which similar, but different fiber populations (again, with known colorant

concentrations) cannot be discriminated. In some cases, the goal of the data presented is simply to make the reader aware of a particular phenomenon.

II – SAMPLES

Microtrace has accumulated and actively curates a number of reference collections (*e.g.*, paint, colorants, fibers, hairs, glass, *etc.*) to aid in the analysis and identification of a variety of materials. In our experience, reference samples with known origin and documented provenance are essential to facilitate the analysis of unknown materials. Among these databases is a fiber collection containing thousands of man-made fibers that are traceable back to their manufacturer and tens of thousands of fibers from dye manufacturers' shade cards.¹ We believe these collections to be among the largest forensic fiber collections in the world. The large number of authentic specimens allows for groups of fibers that share numerous characteristics (*e.g.*, fiber type and dyes) to be selected while varying a single parameter.

III – INVESTIGATION OF SPECTRAL VARIABLES

Quality data collection relies upon, among other factors, proper instrumental setup. While much of the basic setup should be performed and fixed upon instrument installation (*e.g.*, lamp alignment and spectrometer calibration), there remain parameters of each system which are not explicitly written or prescribed at the time of installation. While MSP manufacturers make a good faith effort to ensure that the instruments produce reliable data, the laboratory using the instrument must remember that they are ultimately responsible for understanding the impact of all of the variables that may affect the collected spectra. In our own casework, we have found numerous subtle details that often go overlooked or ignored during routine casework. The following series of experiments were, therefore, designed to isolate and examine particular variables encountered in MSP analysis. Each experiment explores the range of impact a specific variable can have on the spectrum obtained and how, when applicable, the influence of this variable can be identified, understood or, when necessary, avoided. Topics include:

- Differences in Emission Source
- System Stability over Time
- Iris Diaphragm
- Lamp Housing Adjustments
- Light Leak
- Latent System Polarization
- Light Intensity Reduction with a Polarizer
- Resolution Factor
- Rotation with a Polarizer
- Polarizer Stability
- Transmission vs. Absorbance
- Tilted Coverslips

More details about each of these topics are discussed in their respective sections.

¹ Manufacturer produce fibers or fabrics that demonstrate the appearance of specific colorants.

CHOICE OF EMISSION SOURCE

Two emission sources are most commonly used for visible MSP data collection: tungsten halogen and xenon. The goal of this study was to explicitly explore the emission properties of these two sources. While this is not novel research, this information is intended to serve as a useful reference and educational tool to forensic practitioners, as the differences between these sources are significant in certain spectral regions. The emission characteristics² for a 75 W xenon and a 100 W tungsten halogen illuminator were determined from both a quartz³ and a glass slide (*i.e.*, without a sample or coverslip present). Figure 2 shows the spectra across the full range of the spectrometer (200 – 925 nm). As expected, the xenon bulb has a significantly higher intensity across the majority of this range.

Figure 3 shows the spectra between 380 and 760 nm, which is generally regarded as the “visible” spectrum within the MSP forensic community (SWGMAF, 2011). The tungsten halogen bulb has limited emission at both ends of this range, with a significant drop-off above ~ 670 nm (with essentially no emission above ~ 730 nm) and a gradual decline in intensity at the low-end (nearing, but not quite reaching zero counts).

Both sources exhibit a gradual reduction in intensity at the low-end of the full range (Figure 2). The tungsten halogen source has effectively no emission below ~ 330 nm, regardless of the slide composition (*i.e.*, glass or quartz) (Figure 4). The composition of the slide does not significantly affect the emission spectrum of the xenon source except below ~ 340 nm (Figures 4 and 5). Although there are low counts, the quartz slide does extend the emission of spectra collected with it deeper into ultra-violet (UV) region of the spectrum (with essentially no emission below ~ 220 nm) than one obtains with glass. However, in these boundary regions of the spectrum, the signal will only be further reduced when a sample is placed into the optic path as the sample itself, mounting medium, and coverslip will further reduce the signal.

Another way of comparing the spectral output of the two sources is to plot the percent increase of the difference of the intensity of the xenon bulb and the tungsten halogen bulb, relative to the tungsten halogen source (*e.g.*, if the xenon source emitted 500 counts, while the tungsten halogen source emitted 100 counts at a given wavelength, it would be plotted as 400% at that particular wavelength). Figure 6 plots this intensity increase when a quartz slide is examined (using the data from Figure 2). Because the xenon source has high output across regions of the spectrum where the tungsten halogen has essentially no emission, a log scale has been used to facilitate viewing. The shape of this curve can be understood when it is simultaneously plotted with the raw data used to create it on a secondary axis (*i.e.*, the emission spectra shown in Figure 2) (Figure 7). The initial percentage increase (beginning at ~220 nm) is due to the increasing emission of the xenon source itself. The sharp decrease (at ~ 330 nm) is caused by the increasing emission of the tungsten halogen source. Finally, the second sharp increase (at ~670 nm) is the result of the drastic drop-off in intensity of the tungsten halogen bulb at ~ 670 nm.

Figure 8 shows the percentage difference along with the absolute difference in counts between the xenon and the tungsten halogen sources on a secondary axis. This same data is shown in Figure 9 with the secondary axis plotted on a logarithmic scale. These plots demonstrate that there is not always a correlation between percentage gains and absolute counts. More specifically, there are areas with seemingly high percentage increases, but minimal gains with regard to actual counts (Figure 10). For example, xenon emits ~ 10,800% more light at 264 nm compared to tungsten halogen, but this translates into only ~ 195 additional counts. To put this into context, the dark scan has ~ 2,500 counts at this wavelength.

To summarize, over the spectral range of 380 to 760 nm, the xenon source emits significantly more light compared to tungsten halogen with regards to both percentage increase (228% minimum (at 641 nm)) and absolute counts (~ 4230 minimum additional counts (at 380 nm)) (Figure 11). While this is advantageous in many applications, particularly in the

² Collected as absolute counts.

³ GE 124 quartz. Note that there are other grades of quartz slides which have better transmission in the UV region.

near-UV or near-IR regions of the spectrum, there are certain disadvantages such to such strong intensities such as photobleaching (discussed in a later section of this report). The purpose of this section is not to suggest that one form of illumination is “better” than the other, but rather to educate users so they are aware of the differences and can select the source most applicable to their casework.

SYSTEM STABILITY

An attempt was made to explore one aspect of the system stability: the variation in a white light transmission spectrum over time. The goal of this investigation is to provide users with one way to evaluate and understand the timescale and magnitude of drift in their system.

The stability of the system was investigated by repeatedly collecting spectra of air (*i.e.*, no slide or sample present) using the same reference spectrum. Figure 12 shows six spectra, collected in one minute intervals (*i.e.*, over the course of five minutes) using a xenon illuminator. Ideally, the six spectra would each be represented by a straight line at 100% transmission. The actual spectra appear to be relatively stable over time, especially above ~ 460 nm. There is some minor drift below ~ 460 nm, but this represents less than a 1% change in intensity over the course of the five minutes. The individual spectra are more easily observed when they presented in a stacked format (Figure 13). In general, the fine spectral fluctuations (*i.e.*, noise) increase in amplitude as time increases. However, it is interesting to note that this “noise” does not appear to be entirely random. A noise “peak” will often exist at the same position over the course of minutes, which is unexpected if its position was entirely random, as one might expect with true noise. However, while there may be a tendency for these noise “peaks” to stay at the same general location (increasing in amplitude over time), they often gradually shift slightly in position (*i.e.*, along the abscissa). Similar results were observed in subsequent experiments.

The above data represents one of many possible ways to evaluate system stability over time. The exercise above represents one approach and it shows that the overall spectrum of the system studied is extremely stable when considered in light of the data being collected. As noted above, there appears to be some non-random contribution to the system variability that is as of yet unexplained. Ultimately, the cause of this “noise” is not significant enough to impact typical casework data.

DARK SCAN DRIFT

In most laboratories, dark scans are collected less often than their counterpart bright/reference scans. Dark scans are expected to show some change over time based on temperature fluctuations and possibly other variables. Variations in dark scans over time were explored in relation to temperature to examine the potential impact of this change on the dark scan contribution to a spectrum. The results show that small amounts of dark scan drift can be measured and that the effects of this drift are essentially constant across the entire spectrum. The drift is correlated to ambient temperature (*i.e.*, the dark scan counts increase with temperature) (Figure 14). This is not unexpected, but it is interesting to note that the absolute magnitude of the drift observed in our laboratory can be measured on a scale of single counts (under typical office environment temperature variations). The only time during which this could potentially impact a spectrum is during collection of fluorescence spectra (microspectrofluorimetry – MSF) from samples with exceedingly small amounts of fluorescence. Figure 15 illustrates the increasing signal in the MSF spectrum. The results of this experiment show that the increase is not due to a change in the fluorescence, but rather an increase in the dark scan counts. The collection of periodic dark scans will eliminate the effects of this drift completely.

IRIS DIAPHRAGM

The sub stage iris diaphragm is essential to image formation in microscopy; and light microscopists are used to commonly adjusting this diaphragm to provide the most useful image of the particular feature being studied. Adjustment of the iris opening alters the amount of light available to pass through the preparation and changes the contrast/depth of field. Its placement, therefore, greatly impacts image quality. In MSP, the size of the substage iris opening also affects the quality of the spectrum being collected.

The diaphragm accompanying the CRAIC QDI2010 MSP is labeled from one to eight with markings every half interval. Reference spectra were collected at discrete positions as the substage iris was opened. The maximum counts from those reference spectra are listed in Table 1 below.

Table 1. Diaphragm position and corresponding maximum reference scan value

Iris Diaphragm Position	Maximum Reference Counts
1	15,000
1.5	22,000
2	32,000
2.5	48,000
3	57,500
3.5	57,500
4	57,500

It is self-evident that more light reaches the spectrometer as the substage iris is opened. It is interesting to note as well, therefore, that no additional light reaches the spectrometer as the aperture is opened past position 3. This hypothesis was confirmed by removing the ocular and directly observing the substage diaphragm as it was opened and closed (*i.e.*, the rear focal plane of the objective was fully illuminated when the substage aperture was opened to position 3).⁴

To see the effect of varying substage iris positions, spectra were collected along a single fiber at several discrete diaphragm positions. The collection parameters for this study are as follows:

- Scan Range: 300-800 nm
- Averaged Scans: 500
- Integration Time: 8 ms
- Resolution Factor: 2
- Objective: 40 x
- Collection Aperture: #3
- Source: Xenon

The counts recorded by the spectrophotometer increased quickly with increasing substage iris size until reaching a plateau at, or somewhere slightly before, an aperture position of three. Each set of spectra from an iris position was averaged and the resulting seven spectra were compared. Figure 16 is an overlay of the resulting seven spectra. The spectra have been

⁴ It is very important to wear UV protecting goggles before removing an ocular and looking directly into the microscope tube when using a xenon illuminator as it is emitting UV radiation. The oculars supplied with the microscope have appropriate filters in them to allow for safe viewing.

stacked (with 10% offset) for easier viewing. It is readily apparent that the amount of noise present in the spectrum decreases as the aperture size is increased. In other words, at a small aperture size, the signal (*i.e.*, light) is insufficient to collect an appropriate spectrum when the diaphragm is stopped-down.

However, when setting the position of the substage diaphragm, a disparity arises between forming an optically pleasing image and the production of a high quality (*i.e.*, high signal to noise) spectrum. More specifically, the image formed under the optimal photometric acquisition parameters is washed out and of poor quality for visual observations. When asked to adjust the image for comfortable or desirable observation, several scientists at Microtrace closed the substage diaphragm to a position between one and a half and two. The resulting spectra that were obtained under these conditions are of poor quality (*i.e.*, they contain relatively high noise). The position of the substage diaphragm helps to determine the quality of any image formed using a microscope. However to minimize the effects of noise introduced from the instrument, the diaphragm must generally be opened past the point necessary to produce a pleasing and useful image in order to increase the signal reaching the detector. For this reason, the video camera, with a higher dynamic range, is extremely helpful for setting up measurement positions in the relatively “bright” optical conditions. Regardless of how the iris is positioned, it should remain in a fixed location throughout the course of any given experiment.

LAMP HOUSING ADJUSTMENTS

As with all forms of microscopy, lamp setup is a critical component of high quality image formation. The lamp should be centered and a diffusion filter may be used to assist with providing an even illumination across the field of view. It is important to understand that the position of the lamp (*e.g.*, the xenon arc) can affect the relative intensities of various wavelengths. Figure 17 shows that by moving the position of the arc, higher intensities of light can be obtained in specific regions of the spectrum. Therefore, it is possible and may be desirable to maximize or minimize ultra-violet (UV) emission based on the sample and the data being collected from it. For example, UV emission should be maximized when analyzing the clear coat of an automobile paint sample for the presence of UV absorbers. However, UV light can be minimized when analyzing samples which are known to photo-degrade rapidly. Regardless of how the lamp is positioned, it should remain in a fixed location throughout the course of any given experiment. Additionally, we recommend allowing the lamp to equilibrate for at least 30 minutes once it is turned on before spectra are collected.

LIGHT LEAK

Since spectra are, in most laboratories, collected in a room with fluorescent lights that are left on during data collection, the effect of ambient light (*e.g.*, general room lights, computer monitors, lamps, *etc.*) from the room was investigated.⁵ To start, all possible sources of ambient light were turned off for the collection of the dark reference scan. These sources were turned on during the course of the following experiments. A spectrum, in absolute counts, was collected with the beam splitter directing all of the transmitted light from the system to the oculars. The resulting flat (dark) spectrum (Figure 18) was essentially constant between ± 0.1 counts. This confirmed that no stray light is reaching the detector in this configuration.

The beam splitter was then positioned to direct all of the light to the spectrometer. A glass slide was focused on using the 40X objective and a spectrum was collected using the largest aperture (Figure 19). An extremely small “peak” at ~ 543 nm was detected, having an amplitude of approximately 0.2 counts. The peak approximately doubled in size to ~ 0.4 counts

⁵ Our main MSP system is currently located in a room that also houses our Raman microspectrometer and two fluorescence microscopes and therefore, various lights may be turned on and off while a scientist is collecting MSP data.

when the 10x objective was used (Figure 20). Two additional “peaks,” at ~ 435 nm and 611 nm, were also detected (~ 0.2 counts each) with this configuration. Similar results were obtained when the instrument was focused on a polished aluminum slide using the 10X objective (data not shown).⁶ These results indicate that stray ambient light is not expected to provide a significant contribution to the MSP sample signal.

Finally, an angled mirror was placed on the microscope stage and positioned to reflect light from the room’s fluorescent lights into the lens of the 10X objective. This configuration is intended to provide the greatest ambient light signal to the spectrometer. The resulting spectrum (Figure 21) indicates that emission from these lamps is the source of the small amounts of stray light observed. In this figure, it is important to note that the vertical scale has a maximum value of about 25 counts, which is inconsequential when taken in consideration with the thousands to tens of thousands of counts collected for a typical brightfield measurement.

LATENT SYSTEM POLARIZATION

MSP instruments encountered in forensic laboratories generally do not have a polarizing filter located between the source and the sample (*i.e.*, they do not generally use plane polarized light). However, many of the components of the microscope (*e.g.*, coatings on mirrors, beam splitters) can induce some polarization into the system (Eyring, 2002). This becomes relevant because some materials (*e.g.*, uniaxial and biaxial crystalline substances) exhibit pleochroism when viewed using plane polarized light, and their orientation relative to the preferred direction of vibration impacts their appearance and spectrum.⁷

In forensic science, fibers are the most commonly encountered dichroic⁸ materials which are routinely analyzed using MSP.⁹ The high orientation of the fiber matrix (be it natural or man-made) provides the framework for pleochroic colorants (both dyes and pigments) to become oriented as well. In those instances where pleochroic colorants are oriented along the lengths of fibers, they may appear lighter/darker or even different colors when viewed at various orientations relative to the privileged vibration direction of the polarizer.

The cause for concern is that the small amount of latent polarization present in the MSP system can have small, yet significant effects on spectra collected from fibers in different orientations. In essence, if sample orientation is not carefully controlled, inclusionary or exclusionary errors can be made (Purcell, 2013).¹⁰ Because of this, Eyring (2002) recommends that all fibers to be analyzed in a given MSP comparison should be oriented the same way (*e.g.*, all fibers positioned east-west) in order to negate, or at least minimize, any effect of the latent polarization within the system. This recommendation can be implemented relatively easily when using an MSP system equipped with a rotating stage. However, many commercial MSP systems are equipped with mechanical stages which allow for easy navigation, but make slide rotation essentially impossible.

⁶ No “peaks” were observed above the baseline when the instrument was focused on the polished aluminum slide using the 40X objective.

⁷ This property should be assessed during the initial polarized light microscopy examination of the material in question.

⁸ Fibers are referred to as being dichroic because they generally behave as uniaxial crystals with two principle refractive indices. Some dye molecules with dichroic structures, align themselves along the axis of the fiber and change color when the fiber axis is parallel to the polarizer as opposed to perpendicular to it.

⁹ Other pleochroic materials typically encountered in forensic science such as mineral grains are rarely analyzed using MSP.

¹⁰ Purcell (2013) goes further, suggesting the collection of MSP spectra using plane polarized light. His recent dissertation discusses the potential of increased discrimination if spectra are collected in two different orientations relative to the polarizer (*i.e.*, parallel and perpendicular).

Even with the use of a rotating stage,¹¹ the consistently precise orientation of a highly twisted and convoluted fiber is not a trivial accomplishment.

With this in mind, several experiments were conducted in order to:

1. Determine the extent of unintentional (*i.e.*, latent) polarization in our systems.
2. Determine the significance of this polarization with regards to spectral comparisons of samples known to exhibit dichroism.

In order to conduct these experiments, the mechanical stage that came with our instrument was removed and replaced with a rotating stage. This stage was then carefully centered about the optical axis of the microscope. Once adjusted, the area of the sample in the center of the field of view (*i.e.*, where the aperture is located) remains fixed as the stage is rotated about it. It should be noted that even if the stage centration was perfect,¹² because our instrument uses square apertures, the exact same area can only be sampled at the cardinal positions (*e.g.*, 90°, 180°, and 270° relative to the starting position). Simple geometry proves that at all other rotation positions there has to be some amount of discrepancy between the sampled areas. For example, approximately 17% of the original area is not analyzed when the sample is rotated 45° (Figure 22). It follows, that ~17% of the area analyzed after the rotation of the sample is “new,” in that it was not originally analyzed. This issue can be eliminated through the use of a circular aperture (or by only rotating the sample in 90° increments if using a square aperture).

During the initial experiments, samples that were expected to exhibit pleochroism were identified. Preliminary data was collected from numerous fibers and mineral grains in order to view how their spectra differed as their orientation relative to a polarizer (oriented east-west and placed on top of the field diaphragm) changed. Figures 23 - 26 show examples of pleochroic fibers and mineral grains oriented parallel and perpendicular to the vibration direction of the polarizer. In each case, the positions and/or intensities of the absorbance peaks differ dramatically depending on their orientation relative to the polarizer (as one would expect for known pleochroic samples).

Epidote grains were selected for further analysis because they exhibited reproducible fine spectral shifts between ~370 – 490 nm (Figure 27).¹³ Most notable are the two distinct doublet peak inversions at ~ 380 & 400 nm¹⁴ and 455 & 471 nm. In other words, the lower wavelength absorptions (*i.e.*, ~ 380 and 455 nm) are dominant in the parallel orientation and the longer wavelength absorption (*i.e.*, ~ 400 and 471 nm) are dominant in the perpendicular orientation of the epidote grains.¹⁵

In order to determine the latent polarization in the system, an MSP spectrum was collected from an epidote grain every ten degrees as it was rotated through one full rotation (*i.e.*, 360°) without a polarizer present. Aside from this controlled rotation, the epidote grain would maintain a fixed position in order to analyze the same position on the grain.¹⁶

¹¹ It is also possible to have a mechanical mount on a rotating stage.

¹² In reality, there is always going to be some amount of error with any adjustment, and stage centration is no exception.

¹³ Fittingly, this region was where xenon illumination was shown to produce relatively large amounts of potential latent pleochroism (see Latent Pleochroism section).

¹⁴ These values (*i.e.*, 380 and 455 nm) are only listed as nominal peak values as it is recognized that the true absorbance maxima shift depending on the orientation of the mineral grain.

¹⁵ The perpendicular orientation of epidote also produces a broad absorption peak at ~ 605 nm which is completely absent when it is oriented parallel to polarizer (see Figure 26).

¹⁶ As discussed above, it is impossible to analyze the exact same area of a rotating sample when using a square aperture (except every ninety degrees).

The expectation was that any latent polarization in the system would cause some of the effects that were observed when a polarizer was present (*i.e.*, relative peak intensity inversions) to manifest themselves. These effects should occur in two cycles as the grain is brought through one full rotation (*i.e.*, one 180° rotation should constitute one full cycle with regards to any polarization effects).

Figure 28 shows some of the spectral and photographic data from this experiment. The photomicrographs, taken every 90°, demonstrate that the stage was properly centered, and that the same area of the grain was being analyzed throughout the full rotation.

This experiment produced a number of significant observations:

- There were no obvious effects of any latent polarization in the system. For example the relative peak ratios at ~ 455 and 471 nm did not switch (*i.e.*, the peak at 455 nm was always more intense than the 471 nm peak) (Figure 29). In fact, the difference between the intensities of the peaks (calculated using absorbance data) generally increases over the course of the experiment (Figure 30). Interestingly, the two positions which do exhibit localized maxima (*i.e.*, 120° and 300°) are separated by 180° suggesting that there may be some effects of latent polarization. However, there are likely other phenomena which are dominating any effects of the latent polarization. There are two main possibilities for this:
- Because this experiment was conducted using glass slides, the still unexplained low wavelength absorbance (see Quartz vs. Glass Slides section) could be preferentially contributing to the continually increasing absorbance of the lower wavelength 455 nm peak relative to the higher wavelength 471 nm absorbance.
- This epidote grain was mounted in 1.662 Meltmount. Although not known at the time, and not readily observable using the 40X objective, with which this rotation experiment was conducted, the mounting medium was drastically discolored by the xenon illumination over the course of the experiment. This is immediately obvious when the sample is viewed using a lower powered objective (*e.g.*, 10X) (Figure 31). It is impossible to determine the exact contribution of the discolored medium but it is reasonable to assume that it is affecting the spectra in some way (*e.g.*, increased absorbance across some unknown span of wavelengths).
- The noise in the ~ 640 – 800 nm range is relatively constant until it becomes noticeably greater at ~ 210°, remaining relatively high until ~ 330° (see Figure 28). However, the noise in this region reverts to its near original level at ~ 360°. The cause for this observation has not been determined.
- Perhaps most obviously, the spectra (across the full range) oscillate down, then up, and then down again over the course of the full rotation (see Figure 28). This particular phenomenon was observed in all of the early rotation experiments and additional studies were undertaken in an effort to understand the cause.

COVERSLIP TILT

Tilted coverslips were proposed as one of the possible causes for this cyclical effect of oscillating spectra. Several experiments were performed to investigate this possibility.

A quartz grain was placed on a microscope slide and a coverslip was placed on top of it, off-centered, so that it was tilted (Figure 32). The sample was mounted in 1.54 index of refraction oil¹⁷ and spectra were collected from a blank area of the slide as it was rotated. A spectrum was collected every ten degrees (Figure 33). While there is some oscillation, the dominant change in the spectra is the growing absorption below ~ 480 nm. The cause for this absorption was immediately obvious when the slide was removed from the stage of the microscope. A distinct yellow discoloration had formed in the area being analyzed (Figure 34). Examination using a compound microscope indicated that there is some amount of phase separation occurring in this area based on the small liquid droplets on the underside of the coverslip over the stain (see Figure 34).

As a follow-up experiment, another slide was prepared in the same manner (*i.e.*, with a tilted coverslip using 1.54 index of refraction oil as a medium and xenon illumination) and placed on the microscope stage. Spectra were collected every minute for 15 minutes¹⁸ while the slide was not moved (*i.e.*, neither lateral nor rotational movements). By removing the oscillation effects caused by the rotation of the stage, the spectra from this experiment focused on the absorption at the low wavelengths (Figure 35). The spectra exhibit increasing absorbance with a peak at ~ 340 nm, although it shifts to slightly higher wavelengths over time.

The similar timed exposure experiment was conducted using a flat coverslip (*i.e.*, 1.54 index of refraction oil is still present but there is no quartz grain to tilt the coverslip). In this situation there is a more modest increase in absorption (~ 0.125 versus 0.8 absorbance units) with the peak located at a lower wavelength (~ 320 nm) (Figure 36).¹⁹ Similarly, the obvious yellow discoloration was not visible at the conclusion of the experiment, although there was the faintest hint of color (too light to convincingly photograph). While not understood at the time, this absorption at ~ 320 nm was due to the interaction of the glass slide and the xenon illumination (see Quartz vs. Glass Slides section). Evidently, this xenon-glass phenomenon dominates any yellowing of the 1.54 index of refraction oil when the path length through the liquid is relatively small. However, when a tilted coverslip was used, and hence there was a relatively large path length, the absorbance of the medium dominated the resulting spectra. As a final note, the 1.54 index of refraction oil does not exhibit observable yellowing when it is illuminated for fifteen minutes using tungsten light (data not shown).

Glycerol was selected as another mounting medium for the rotation experiments using a tilted coverslip with the expectation that it would not yellow over the time needed to complete the experiment. Figure 37 shows the results of this study. Ignoring the low wavelengths for a moment, there is a definite and relatively predictable oscillation which has a sinusoidal pattern (*i.e.*, one complete sine wave in the full 360° rotation). The midpoint of this pattern occurs at $\sim 30^\circ$ and 210° (separated by 180° as expected). From these midpoints, the spectra quickly rise (or fall), and then slow as they reach their maximum amplitude before reverting back, accelerating as the sample is continually rotated, to the midpoint. While not understood at the time of the experiment, the low wavelength absorption is due to the interaction of xenon light with the glass slide.

At the conclusion of the above experiment, the slide was immediately rotated another full revolution (*i.e.*, from 360° to 720°) with the corresponding spectra collected (the slide was not moved). Because the effect of the xenon-glass absorption lessens over time, the spectrum collected at 720° exhibits only slightly more absorption compared to the spectrum collected at 360° (Figure 38). This is especially obvious when compared to the difference between 0° and 360° (see Figure 37). Again, the approximate midpoints of the sine wave are located at $\sim 390^\circ$ and 570° (180° relative to the midpoints from the first rotation).

¹⁷ Mineral grains are commonly mounted in 1.54 index of refraction oil for examination using polarized light microscopy.

¹⁸ It took approximately 15 minutes to conduct the previous rotation study.

¹⁹ Replicate experiments confirmed these results.

In summary, these experiments show that a tilted coverslip can cause the spectral oscillations initially observed during the rotation experiments.

LIGHT INTENSITY REDUCTION WITH A POLARIZER

It is worthwhile to take a step back, and observe the effect of a polarizer on the system directly by measuring the amount of light reaching the detector, in absolute counts. A polarizing film was placed on top of the field diaphragm oriented east-west and then north-south sequentially as spectra were collected using both xenon and tungsten halogen illumination (the instrument was focused on the surface of a clean quartz slide). Figures 39 and 40 show the effect of the polarizer when using xenon illumination and Figure 41 shows the effect when using tungsten halogen illumination.

The most obvious, and expected, effect of the addition of a polarizer is the drastic reduction in light intensity across the entire spectrum. Figures 42 and 43 show the percentages of light reaching the detector when a polarizer is present relative to the amount of the light when the polarizer is absent. In general, less than 40% of the light reaches the detector with xenon illumination, and these percentages only drop further with tungsten halogen illumination. These experiments were replicated using glass slides and without any slide on the stage (data not shown).

The second, and more germane, observation is that there are distinct differences in the amounts of light reaching the detector when the polarizer is oriented east-west compared to north-south (Figures 39-43). These figures prove that there is some amount of latent system polarization inherent in the system. Interestingly, the differences are not constant across the width of the spectrum. Furthermore, the illumination source (*e.g.*, xenon and tungsten halogen) has an effect on the general pattern of these differences across the breadth of the spectrum. Figures 44 and 45 show the percentage of light gained or lost across the spectrum when the polarizer is oriented north-south and east-west using both xenon and tungsten halogen illumination. In general terms, when the polarizer is oriented north-south with xenon illumination, more light reaches the detector at the lower wavelengths and less light reaches the detector at the higher wavelengths, compared to when the polarizer is oriented east-west. In contrast, when the polarizer is oriented east-west with tungsten halogen illumination, a continually increasing amount of light reaches the detector as wavelength increases compared to when the polarizer is oriented north-south. It should be noted that both illumination housings were simultaneously mounted on the instrument through the use of a beam splitting accessory. It is possible that the optical element in the beam splitter is accentuating the latent polarization of the MSP system.

This experiment was repeated approximately one month later using two separate polarizers (*i.e.*, the same polarizer used in the experiment described above and a different polarizer). A number of observations came out of these experiments. First, regarding the xenon experiments using the same polarizer, while the overall pattern was similar, there was a noticeable shift to higher wavelengths (*e.g.*, the efficiency cross over shifts from ~ 660 nm to ~ 720 nm) as well as sharper drop off beginning at ~ 340 nm (Figure 46). The plot of the newer data hovers near zero percent below ~ 290 nm indicating that there was minimal latent polarization in this region. Minor adjustments in the microscope setup (including the position of the optical element in the beam splitter) as well as slight differences in the orientation of the polarizer likely caused these differences.

Furthermore, while the overall patterns are similar, the plots produced using two different polarizing filters on the same day are different from each other, most notably at either end of the spectral range analyzed (Figure 47). Differences in the polarizing efficiency of the filters across the wavelengths analyzed as well as variations in filter orientation are likely causes for these differences.

Although there are slight differences, the plots resulting from the experiments using tungsten halogen illumination are relatively consistent with each other. Namely, they all demonstrate that the east-west orientation of the polarizing filter

becomes increasingly efficient at progressively higher wavelengths compared to the north-south orientation (Figure 48). Interestingly, this percentage increase in efficiency is roughly linear relative to wavelength. The one exception to this pattern is below ~ 425 nm using the new filter which exhibits wild fluctuations. This boundary correlates with the relatively steep drop-off observed with xenon illumination (see Figure 47).

These experiments highlight the importance of maintaining the position of the polarizer throughout any experiment in which samples are to be compared with each other.

It is important to note that these two polarization positions (north-south and east-west) were selected solely on the basis of convention. There is no absolute reason to believe that these particular orientations would correspond with any latent polarization existing within the system. In other words, the polarization could be maximal at any possible orientation amongst the 360° of potential light vibration directions perpendicular to the propagation of the light.²⁰

POLARIZER ROTATION

A clean slide (no sample or coverslip) was placed on a stage and rotated 360° while being continuously illuminated using light from a tungsten bulb. Spectra were collected every 20° and overall, the spectra are relatively consistent, hovering near 100% transmission across the spectral range, throughout the experiment (Figure 49). There is some minor variation (ranging from $\sim 100.2\%$ to 99.8%) and some evidence of periodic oscillation although they are not particularly regular. Replicate experiments confirmed these results.

This same experiment was conducted when a polarizer was placed on top the field diaphragm in a fixed east-west orientation. Several spectral changes were observed over the course of this experiment. As in the previous experiment, there is some evidence of periodic oscillation but it is not entirely regular (Figure 50). However, individual spectra exhibit variation across the spectral range (in contrast to the spectra from the previous experiment which remained roughly flat throughout the experiment). Figure 51 shows data from the beginning of the experiment. The spectra are relatively stable between ~ 400 ²¹ and 500 nm but they exhibit increasing amounts of negative absorbance (*i.e.*, increased transmission) above this wavelength. The slight oscillations of the spectra tend to shift this entire pattern up and down, sometime bringing the “baseline” between 400 and 500 nm below 100% transmission (*e.g.*, at 160°) (Figure 52). However, this “baseline” is essentially back at $\sim 100\%$ at 360° (*i.e.*, back at the starting point). It would seem that the rotation of the stage is responsible for the slight up and down spectral translations ($\sim \pm 0.2\%$) but that the variation across an individual spectrum is related to the continuous illumination of the polarizer itself.

POLARIZER STABILITY

Additional experiments were conducted to investigate the effects of continuous illumination of a polarizer. A glass slide was placed on the stage and continuously illuminated using tungsten illumination. Spectra were collected every thirty seconds for

²⁰ This is why the experiments involving the analysis of the epidote grain were conducted every 10° throughout a full 360° rotation.

²¹ The spectra become increasingly erratic below ~ 400 nm, likely because of low light levels, especially with the presence of a polarizer (see Figure 41).

five minutes. As expected, the spectra are relatively stable and flat across the entire spectrum throughout the course of the experiment (Figure 53).²²

This same experiment was repeated when a polarizer was placed on top of the field diaphragm in a fixed east-west orientation. The spectra are relatively stable between ~ 400 and 500 nm but they exhibit increasing amounts of negative absorbance (*i.e.*, increased transmission) above this wavelength (Figure 54). There is no spectral oscillation when the slide is not rotated. Again, the spectra below ~ 400 nm are quite erratic, which is almost certainly a function of the low levels of light caused by the use of tungsten illumination and the presence of a polarizer.

Additional experiments were performed using both tungsten and xenon illumination. No slide was used with these experiments, in an attempt to remove one more variable from the experiment. Figures 55 and 56 shows that without a polarizing filter present, the spectra remain relatively stable and flat across the entire spectrum throughout the course of the experiments using either tungsten or xenon illumination. In both cases there is a slight amount of continual drift towards negative absorption. Additionally, a slight negative absorbance peak begins to form between ~ 330 nm and 390 nm with xenon illumination.²³

Similar timed experiments were conducted with two different polarizing filters (oriented east-west and north-south) using both tungsten and xenon illumination. The polarizers will be referred to as "A" and "B" for convenience. Figures 57 - 60 show the results of the experiments conducted using polarizer A. In all cases a broad negative absorbance "peak" forms at ~ 630 nm. A smaller absorbance forms at ~ 410 nm using tungsten and ~ 405 nm using xenon illumination. Two lower wavelength "peaks" (at ~ 320 nm and ~ 360 nm) also form when using xenon illumination. In all of these experiments, the spectral deviations, while continually increasing, decrease with time.

Figures 61 - 64 show the results of the experiments conducted using polarizer B. In all cases there is a broad negative absorbance band, centered between ~ 620 nm and 640 nm, and a sharp absorbance peak just below 400 nm. Interestingly, the spectral changes occur most dramatically in the first minute before slowing considerably (especially in the peak below 400 nm).

The spectral changes depicted in these experiments are always more pronounced when the polarizer was oriented east-west compared to north-south (Figures 65 - 68). As all of the spectra with the polarizer oriented east-west were collected before the spectra with the polarizer oriented north-south, it was thought that this might be a cause for this difference. As such, one additional experiment was conducted using polarizer B with xenon illumination in which the "north-south" spectra were collected before the "east-west" spectra. Figure 69 shows that the east-west spectra still exhibit more intense deviations (across the majority of the spectrum) during the course of the experiment compared to the north-south spectra. It therefore does not seem that order of collection can account for the spectral differences observed with the two different orientations of the polarizers.

Immediately after the end of the previous experiment, the instrument's shutter was closed, blocking the light from reaching the polarizer. After one minute had elapsed (the sixth minute since the reference spectra were collected and the experiment began), the shutter was opened, a spectrum was collected and the shutter was immediately closed. This process was repeated every minute for the next four minutes (*i.e.*, for a total of ten minutes after the start of the experiment). Curiously, these last spectra are very similar to each other and have nearly horizontal shapes near 100% transmission (Figure 70). This is especially obvious when compared to some of the spectra collected earlier (*i.e.*, the initial time study in which the polarizer (oriented east-west) was continually illuminated) (Figure 71).

²² Data from a similar experiment is displayed in Figure 120.

²³ The appearance of this spectral feature was confirmed through additional experiments (data not shown).

As all of these experiments have demonstrated that the changes in the spectra of a polarizer continually illuminated decrease with time, an experiment was conducted to determine if a preemptive conditioning would eliminate this artifact. Polarizer B was continuously illuminated using xenon illumination for more than two hours before the reference scan was collected²⁴ and then spectra were collected every 30 seconds for five minutes. While the spectral deviations are not as pronounced as before (see Figure 63), they are still readily apparent (Figure 72).

Immediately after the last spectrum was collected, the instrument's shutter was closed and the sample was allowed to sit for five minutes. The shutter was opened and a spectrum was immediately collected (10 minutes) and additional spectra were collected every thirty seconds for the next three minutes (the shutter remained open for these three minutes) (Figure 73). Interesting, the first spectrum (10 minutes) actually has a slight broad absorbance, before becoming approximately horizontal (at 10.5 minutes), and finally exhibiting the negative absorbance peak thereafter. The 10 minute spectrum likely has an absorbance peak because it was immediately collected after the shutter was turned on, whereas normally some amount of time elapses, while the reference spectrum is being collected, before the 0 second spectrum can be collected.²⁵ In other words, when there is a time delay between when the shutter is opened and when the reference scan is collected, the reference scan takes into account some amount of the polarizer's negative absorption artifact. When the shutter is closed and the polarizer "resets" itself, a spectrum collected immediately after the shutter is opened will display an inversion of the polarizer's negative absorption, which was taken into account by the reference scan.

Because the shutter was closed, blocking the light to the polarizer for a few seconds (in order to collect the dark scan), before the previous experiment was conducted, a final experiment was undertaken. Again Polarizer B was continuously illuminated using xenon illumination for more than three hours before the reference scan was collected and then spectra were collected every 30 seconds for five minutes. The dark scan was collected immediately before the reference scan by blocking the light to the spectrometer using a beam splitter between the polarizer and the detector (*i.e.*, the polarizer was truly continuously illuminated). The resulting spectra are relatively flat, are located at 100%, and are essentially free of the spectral deviations previously discussed (Figure 74). Immediately following this, the instrument's shutter was used to block the light from reaching the polarizer for one minute, and then two subsequent thirty second intervals (Figure 75). These spectra are very consistent with each other and exhibit the same artifacts discussed above in the previous "conditioning" experiment. While these spectra are consistent with each other, spectra collected after the shutter was used to block the light for five seconds and five minutes exhibit lesser and greater intensity spectral artifacts respectively (Figure 76). This preliminary data set indicates that the "resetting" of the polarizer is time dependent. It would appear that the majority of the resetting happens almost immediately but that there is continued reversion as unilluminated time increases.

In summary, there appears to be some instability with the two polarizing films examined depending upon whether they are illuminated using tungsten halogen or xenon illumination. This instability increases with time when measured against a fixed (in time) reference scan. These artifacts also appear to be negated when the polarizer is not illuminated for a period of time. It is almost as if the polarizer "resets" itself when it is not being illuminated with the light from the instrument.

²⁴ The shutter was briefly closed immediately before this reference scan was collected for the few seconds (<5) required to collect a dark scan.

²⁵ In this experiment, the polarizer had actually been continuously illuminated for more than two hours before the reference scan was collected. This is in contrast to the previous experiment (where the east-west spectra were collected after the north-south spectra) in which the reference spectrum was collected immediately after the shutter was opened. This lack of delay between when the shutter was opened and when the reference scan was collected is the most likely reason why the spectra collected in that experiment, after the shutter was closed, are nearly horizontal (as opposed to exhibiting a broad absorbance).

LATENT PLEOCHROISM

In light of the several factors, it was determined that petrographic thin section samples should be studied using tungsten illumination in order to minimize some of these artifactual effects, namely:

- Tilted coverslips can cause oscillating spectral translations and a thin section should have a cover slip which is closer to being completely parallel with the slide (compared to other preparations)
- Xenon illumination cannot be used because all of our prepared cross sections are mounted on glass which exhibits unexplained absorption (especially at the low wavelengths) (see Quartz vs. Glass Slides section)
- While continual exposure to both light sources affect the polarizer, the light from a tungsten source has less of an effect compared to xenon

A thin section of an epidote grain, oriented along the gamma (γ) refractive index (*i.e.*, the Z vibration direction) was selected for these experiments. First, a polarizing filter was placed on top of the field diaphragm and spectra were collected every 10° as the sample was rotated through a full 360° (Figure 77). There is an obvious color change as the specimen is rotated. Several features were observed in this experiment.

The spectra oscillate up and down in a perfectly regular pattern (two full cycles in the 360° rotation) as expected. This regular oscillation causes the spectra to cluster into groups of four except the “top” group which only has two spectra (*i.e.*, the “crest” of the oscillating spectra) and the bottom group which has six spectra (*i.e.*, the two “trough” spectra are not sufficiently different from the lowest group of four spectra to warrant separation). These groups are color coded in Figure 77 for ease of viewing. It should be noted that the “top” and “bottom” spectra are actually located at 10°, 100°, 190°, and 280° (as opposed to 0°, 90°, 180°, and 270°).

There are several obvious spectral regions, which exhibit distinct dichroic effects. The two most obvious are the peak/shoulder inversion at ~ 360 nm and 400 nm and the change in the relative peak intensity of the doublet at ~ 455 nm and 471 nm (Figure 78). The difference between the absorbances of these two peaks changes in a regular pattern (Figure 79). The horizontal boxes in Figure 79 demonstrate the correlation of the clustering of groups of four spectra seen in Figure 78 (for select groups).

Superimposed on the individual spectra is a sinusoidal absorbance wave which is most apparent in the regions of the spectrum with minimal absorbance due to the mineral grain (*i.e.*, ~490 nm to 750 nm) (Figure 80). Although artifactual, these sinusoidal features are somewhat regular. For example, the positions of the artifact peaks and troughs are somewhat aligned through quarter rotations of 90° (*i.e.*, up or down one oscillation) (Figures 81 and 82). While the “peaks” are aligned in this region through quarter rotations, they are shifted as the rotation continues through the next quarter, only to return to the original positions in the third quarter of the rotation. Figure 83 shows this region of the spectrum at positions 50°, 150°, 230°, and 330° (the royal blue cluster shown in Figures 77-79). These spectra represent the same rotational position in each of the four quarters of the full rotation (*i.e.*, 40° on either side of the “bottom” spectra at 10° and 190°). Each pair separated by 180° (*e.g.*, 50° & 230° and 150° & 330°) are quite consistent with each other although they are quite different from the other pair. The cause for these sinusoidal artifacts is not understood. However, if nothing else, they are a testament to the controlled centration and rotation of the epidote grain for this experiment.

Only the spectra at the “tops” and “bottoms” of the oscillations (*i.e.*, 10°, 100°, 190°, and 280°) are free from the sinusoidal artifact between ~ 490 nm and 750 nm (Figures 84 and 85). The effect of the polarizer in this region is obvious when examining these four spectra (*i.e.*, the broad absorption at ~ 605 nm in the spectra collected at 10° and 190°). The sinusoidal artifacts partially obscure the transitions of this absorbance peak between the extreme positions. Even so, there is a distinct oscillating pattern between the difference in the absorbances between 605nm and 543 nm (*i.e.*, the approximate position of the absorption minimum in the spectra exhibiting a peak at ~ 605 nm) (Figure 86). However, this oscillating pattern does not

correlate with the raw spectra, nor is it as regular in its fluctuations as the pattern between the absorption difference of 455 nm and 471nm (discussed above). For example, its end points are 0°, 110°, 180°, and 290° (these points are shifted from the “top” and “bottom” raw spectra). This means that there are two extended oscillations (*e.g.*, between 0° and 110°) and two compressed oscillations (*e.g.*, between 110° and 180°). Similarly, while data points from the clusters of four grouped nicely in horizontal rows with the 455 nm – 471 nm plot (Figure 79), the data points fluctuate with regards to position in this plot (Figure 86).

In summary, while there is evidence of dichroic changes in this region of the spectra, the patterns are shifted and alternately stretched and compressed. These deviations from the theoretical expectations are almost certainly due to the unexplained sinusoidal artifacts in this region. The instability of the polarizer in this region (see Figure 51) may also be contributing to the irregularities.

The same experiment was conducted, using the exact same area of the thin section of the epidote grain, without the polarizer (Figure 87). There are few, if any, observable color changes in the specimen. Similarly, there does not seem to be much fluctuation in the peak ratios of the absorbances at ~ 455 nm and 471 nm (Figure 88). A plot of the difference between the absorbances at these two positions demonstrates that there are small, but relatively regular oscillations (*i.e.*, there are two up and down cycles within 360°) at these positions (Figure 89). This variation is rather small compared to the variation observed when intentionally polarized light is used (Figure 90). The average value of this difference (without a polarizer) is ~ 0.02 absorbance units which is quite near the absorbance difference half-way between the “top” and “bottom” spectra (rotationally speaking) when a polarizer is present (Figure 90). The following table presents a summary of this fluctuation:

Table 2. Difference in absorbance units (455 nm – 471 nm)

Polarizer Present	Difference in Absorbance Units			
	Min	Max	Range	Average
No	0.018	0.022	0.004	0.020
Yes	-0.045	0.042	0.088	0.012

It should be noted that previous experiments have shown that this region may not exhibit large amounts of latent pleochroism when using tungsten illumination (See Figure 45). These same experiments indicate that more latent pleochroism would be expected at higher wavelengths. Figure 91 shows a close-up view of the spectral region where epidote grains have a broad absorbance (at ~ 605 nm) when they are aligned perpendicular to a polarizing filter.²⁶ A plot of the difference in absorbance values of 605 nm and 543 nm is shown in Figure 92). There are two general down and up oscillations but they are not particularly regular. Part of this variability may be due to the relatively low levels of absorbance in this region but the instability of the polarizing filter in this region may also be a factor. Also, the variation is relatively small compared to the absorbance differences observed when a polarizing filter was present (Figure 93). The following table summarizes this variation:

Table 3. Difference in absorbance units (605 nm – 543 nm)

Polarizer Present	Difference in Absorbance Units			
	Min	Max	Range	Average
No pol	-0.005	0.003	0.008	-0.001
Pol	-0.027	0.033	0.061	0.000

²⁶ It should be noted that this region does not have the sinusoidal artifact superimposed on the spectra when the polarizing filter is not present.

It is worth noting that the average absorbance difference for both experiments is ~ 0.00 . Also, the maximum absorbance difference in this region (~ 0.008 absorbance units) is approximately twice as much as the variation between 455 nm and 471 nm (~ 0.004).

Based on the plot of the difference between 455 nm and 471 nm (the more regular of the two plots), the spectra at 90° and 180° should represent the positions with the most dissimilar spectral features (see Figure 89). Figures 94 - 96 show little to no differences between these spectra.

Based on the plot of the difference between 605 nm and 543 nm (the more irregular of the two plots), the spectra at 10° and 130° should represent the positions with the most dissimilar spectral features (see Figure 92). Figures 97 and 98 show little to no differences between these spectra. The spectral region between 490 nm and 750 nm exhibits some minor differences (Figure 99). Having accounted for, and removing several variables, latent polarization in the system is the most likely cause for these differences.

In summary, while the potential effects of latent polarization within this MSP system have been demonstrated, the variations between the spectra, even in a case which was intended to maximize these differences, are quite minor. Although the latent polarization effects are minor in the system studied here, it is important that each laboratory conduct an independent investigation of their own system as seemingly minor variations in optical components have the potential to impart significant changes on the resulting spectrum. Ultimately, however, the analysis of a large number of randomly oriented fibers would also serve to negate the effects of any latent polarization.

RESOLUTION FACTOR

In the CRAIC MSP software, “resolution factor” is one of the user defined parameters for every spectrum collected. It is a whole number ranging from 0 to 15. Simply put, this number defines the size of the moving average used to determine the ordinate value at each plotted abscissa point. For example, with the resolution factor set to 5, a total of eleven points (five on each side of the point in question) are averaged. It functions as a built-in smoothing function at the moment the data is collected, with “0” representing no smoothing, and “15” representing the maximum amount of smoothing.²⁷ Figure 100 shows spectra of holmium oxide collected using resolution factors of 0, 5, 10, and 15.²⁸ Loss of spectral resolution is immediately obvious as the resolution factor increases (*e.g.*, the three sharp, high-intensity peaks centered at ~ 450 nm gradually morph into a single broad peak). Noise reduction is also immediately apparent, most noticeably on the broad absorbance peak below ~ 320 nm. Interestingly, the area of instability at the extreme low wavelengths actually increases with higher resolution factors (Figure 101). This artifact is likely due to the fact that moving average itself is increasing in size (*i.e.*, the artifact instability begins approximately five data points from the end when a resolution factor of “5” is selected, approximately ten data points from the end when a resolution factor of “10” is selected, *etc.*).

There are also peak shifts, as minor peaks and shoulders drag larger peaks towards themselves. It should be noted that the resolution factor does not affect the number of data points plotted (*i.e.*, 981 data points are always exported between 200 nm and 950 nm regardless of the user defined resolution factor on our CRAIC MSP system). It follows that these data points always have the same abscissa positions.

²⁷ The post-collection smoothing function in the software operates under a completely different principle.

²⁸ Reference and dark scan spectra were collected using appropriate resolution factors (*i.e.*, a resolution factor of “5” was used when collecting reference and dark scans prior to the collection of the “resolution factor 5” spectrum).

TRANSMISSION VS. ABSORBANCE

MSP data, in forensic analyses, is most commonly collected using transmitted light.²⁹ As in infrared spectroscopic analyses conducted in the transmission mode, there are two conventional ways of plotting the data: absorbance and transmittance. Because there is direct conversion between these two scales, the data can be repeatedly converted from one form to the other and back again without affecting any of the data. The mathematical difference between these scales is that absorbance values vary linearly with respect to concentration³⁰ while transmittance values change logarithmically (Figure 102). Because of this, spectra plotted using one scale may appear different when they are plotted in the other. It is worth reiterating that the plotted data is equivalent and that it is only the appearance of the data that changes.

Since the data are equivalent, the natural question is how should the data be plotted, visualized, and compared to other spectra? In some sense, this is a subjective question with room for differing opinions. Some scientists are more familiar with, and feel more comfortable looking at spectroscopic data plotted in a certain manner. In either case it is important to understand the implications of plotting the data using each scale.

As stated earlier, absorbance varies linearly with respect to concentration. Because of this, previous researchers, including Eyring (2002) recommend comparing spectra in absorbance units as opposed to percent transmittance. Both he and the SWGMAT fiber group (2011) specifically cite the benefit of using absorbance units when examining the spectra collected from deeply colored fibers. This is because the logarithmic nature of percent transmittance will compress spectra exhibiting strong absorbances, potentially obscuring subtle spectral detail. Simply put, the absorbance bands of deeply colored materials will look larger (*i.e.*, more expansive in the ordinate dimension) and will be better defined compared to when the exact same data is plotted in percent transmission.

For example, Figure 103 shows spectral data from a black fiber that has been plotted in both absorbance and transmission on independent axes. The figure shows the exact same data but its appearance changes depending on whether it is plotted in absorbance or transmission. The three absorbance peaks are much more obvious, and consequently easier to view, when compared to the more compressed transmission plot. Quantitatively, the peak-to-trough distance of the central absorption represents ~ 36% of the total absorbance plot while it only represents ~ 9% of the total transmission plot.³¹

Because of the sharper peaks, viewing spectra in absorbance can make it easier to determine peak maxima and minima, especially with broad peaks, compared to viewing spectra in transmittance. For example, a fairly rounded peak when viewed in absorbance can appear as more of an inverted plateau in transmittance (Figure 104).

Figures 105 and 106 show additional examples of how deeply absorbing black fibers appear in both absorbance and transmittance. Again, they demonstrate how subtle spectral features appear compressed when viewed in transmittance.

While the above discussion has focused on effects of ordinate intra-spectral compression, it is also important to recognize the effects of inter-spectral compression when viewing data in transmittance. Figure 107 shows spectra collected from two dark blue fibers (from the same source) in both absorbance and transmission. The three absorbance peaks of the two spectra (between ~550 – 650 nm) appear much closer to each other when they are viewed in transmission compared to absorbance.³²

²⁹ This statement is based on informal conversations with other forensic practitioners as opposed to a formal survey.

³⁰ As defined in the Beer-Lambert equation $A = \epsilon bc$

³¹ The two plots were scaled so that they both take up approximately the same physical distance in the ordinate dimension.

³² This effect is much less noticeable at the lower wavelength absorbance.

This effect is potentially important when conducting visual comparisons of Q and K spectra, as deeply absorbing spectral regions will appear closer together when viewed in transmission (compared to absorbance). It could cause bias towards eliminations (using absorbance) or inclusions (using transmittance). Regardless of how the data is viewed, bracketing the Q spectrum with K spectra (*i.e.*, having one with slightly more and one with slightly less absorbance) will ensure that the Q spectrum falls within the range of variation observed in the known source.

Obviously, the compression consequences of viewing spectra in transmission are most obvious when examining darkly colored fibers. Conversely, they are minimized when viewing lightly colored fibers. Figure 108 shows how the spectrum of a lightly colored green fiber has nearly the exact spectral shape (*i.e.*, in its relative proportions) when viewed in both absorbance and transmission. In this case, there is no practical advantage or disadvantage to viewing the data using either scale.

One of the potential benefits of examining data using transmission is the relative increase in the size of minor peaks when they occur in spectra with one or more strongly absorbing peaks. This can be especially valuable in other spectrographic techniques, such as infrared spectroscopy, but minor effects can also be observed in MSP. Figure 109 shows an example in which a minor peak in a red fiber exhibits a modest increase in relative size when viewed using transmission (compared to absorbance). A similar effect is demonstrated in Figure 110 which simultaneously shows the compression of the deeply absorbing peak when viewed in transmission.

Finally, there are different results when mathematical functions (*e.g.*, averaging, standard deviation, first derivative, *etc.*) are applied to the same absorbance and transmission data. The effects of these differences are discussed more fully in another section of this report (“100 Fiber Study”).

IV – SAMPLE PREPARATION EFFECTS

QUARTZ VS. GLASS SLIDES

As noted in a previous section, the emission spectra differ slightly at low wavelengths when quartz slides are used compared to glass (see Figures 4 and 5).³³ However, there is almost no effect when using tungsten halogen illumination because it does not emit light at these low wavelengths. Figure 111 plots the percent increase in the difference of the intensity through a quartz slide compared to a glass slide, relative to the glass slide, when using a tungsten halogen source. Where there is actual emission (~ 340 – 730 nm), the percent difference hovers steadily between ~ 1 and 2% (the data outside this range is essentially meaningless as there is no true emission in these regions).

This small percentage gain is also observed when using xenon illumination across the majority of the range (Figure 112). However, there is a larger percentage gain at the low end of the spectrum (~ 230 to 350 nm) as expected from the earlier discussion (see Figures 4 and 5). It is worth noting that this relatively large percentage increase is caused by relatively few photons (Figure 113). Figure 114 shows that this dramatic percent increase (*i.e.*, between ~230 and 350 nm), which at its maximum point is ~175%, is the result of less than 25 counts at any particular wavelength. In another trial, the resulting plots are similar in shape but reversed in amplitude (*i.e.*, a relatively larger increase in absolute counts (~ 385 counts) results in a small percentage increase (~ 6.5%) (Figures 115 and 116).

³³ It should be noted that different grades of quartz slides are produced which have different transmission properties in the UV.

SLIDE STABILITY

Timed experiments similar to those described above in the “System Stability” section were conducted using combinations of illuminators (xenon and tungsten halogen) and slides (quartz and glass). In all cases, the slide was wiped with a clean Kim-wipe and the upper surface of the slide was focused on (there was no “sample” or coverslip present). The slide was moved to a new area, a reference spectrum was collected and the first “sample” spectrum was collected immediately after the reference spectrum. Additional spectra were collected every thirty seconds (the figures in this section show data from each whole minute for ease of viewing).

The signal reaching the detector appears to be quite stable using tungsten halogen illumination³⁴ with both quartz (Figures 117 and 118) and glass slides (Figures 119 and 120), and using xenon illumination with quartz slides (Figure 121). In all cases the signal stays well within 1% of the original spectrum (*i.e.*, 100%). It is also interesting to note that the “noise peaks,” which have some consistency with regards to abscissa position within an experiment, occur at different locations in sequential experiments (Figure 122).

An unexpected result was observed when this experiment was conducted using xenon illumination and a glass slide. There was an immediate absorption at the lower wavelengths which increased over time, although the rate slowed as the elapsed time increased (Figure 123). This absorption is most dramatic below $\sim 400\text{nm}$ but it occurs to a lesser extent at higher wavelengths. Moving the slide to a new location begins the process anew (*i.e.*, a nearly flat initial baseline with increasing absorption occurring at the lower wavelengths at time progresses).

The fundamental cause for this phenomenon is not clear at this point but one potential factor, slide heating, has been eliminated. In subsequent experiments, the above phenomenon was observed over the course of five minutes, at which point the mechanical shutter was engaged, blocking the light to the slide. After another five minutes had elapsed, the shutter was briefly opened again and a spectrum was collected. The shutter was closed again and a final spectrum was collected five minutes later (*i.e.*, essentially ten minutes of closed shutter time after the initial five minutes of continual exposure). The last two collected spectra appear similar to the spectrum collected after the initial five minutes of continual exposure (Figure 124). If this phenomenon was due to a reversible heating process, the last two spectra would be expected to revert to spectral shapes similar to those observed at the beginning of the experiment (*i.e.*, nearly flat at approximately 100% transmission across the wavelengths measured).

Seven glass slides, from five different manufacturers (representing slides purchased both recently and others likely decades old), were examined to see if they exhibited increasing absorbance at the lower wavelengths when continuously illuminated with xenon light. In all cases, the slides displayed the previously described phenomenon (Figures 125 - 131). There were however, some minor variations in both the amplitude and the position of the absorbance.

After five minutes of continual exposure, transmission dropped to at least $\sim 93.5\%$ (for at least one wavelength) for all slides. Transmission dropped to a minimum of $\sim 84.5\%$ for two of the slides studied with the rest falling somewhere between these two extremes. It should be noted that all of the slides, with one exception, had the same nominal thickness of 1 mm. The outlying slide, at least with respect to thickness, was approximately 1.5 mm thick. Given the increased path length, it is interesting that this slide exhibited moderate absorbance compared to most of the other slides (Figure 126). The positions of absorption maxima (*i.e.*, transmission minima) ranged from $\sim 320\text{ nm}$ to $< 300\text{ nm}$ (the lower spectral limit during these

³⁴ The tungsten halogen illumination is stable in the region of the spectrum where there are moderate amounts of emission ($\sim 350\text{ nm}$ to 720 nm). Large amplitude noise dominates the spectra outside of this region and is not considered in the above discussion.

experiments). It is unknown at this time how reproducible these inter-brand observations are as no replicate studies were performed.

Surficial detergent residues, either from production or cleaning,³⁵ were hypothesized as a possible cause for these absorptions. As such, six (of the seven) slide types were immersed in an equal parts mixture of concentrated sulfuric acid and hydrogen peroxide (~6%) for approximately 60 hours before being thoroughly rinsed using distilled water. This harsh treatment should have removed the vast majority of any organic residues present on the slides.³⁶ The slides were then exposed to xenon illumination and spectra were collected every thirty seconds for a period of five minutes. Absorbance values similar to those observed in the “unwashed” slides were observed in all cases although there was a slight decrease in the total absorption in each case (approximately 1 - 2% difference in percent transmission at the end of the five minutes) (Figures 132 and 133).

A low temperature oxygen plasma asher was also used in an attempt to remove organic residues from a slide. An Esco³⁷ brand slide was placed in the chamber of the asher and positioned so that both surfaces on the slide would be directly exposed to the plasma environment. The slide remained in the chamber for approximately two and a half hours before it was removed, wiped with a Kimwipe, and finally exposed to xenon illumination in the above described manner. Again, a similar pattern of increased absorbance over time was documented, although there was a slight decrease in the total absorption (approximately 2% difference in percent transmission at the end of the five minutes) (Figures 134 and 135).

This unexplained absorbance observed in glass slides may help to explain some of the low-wavelength variability we have observed, especially in lightly colored samples. We have anecdotally observed increased variability in lightly colored fibers (especially below ~ 400 nm). It was previously assumed that this was largely an effect of the decreased light flux in this region. While low levels of light may still be involved, this glass absorbance is another good candidate for the cause of this variability. For example, in the case of a glass slide positioned in a blank area whilst being illuminated using a xenon bulb, it is typical for a few minutes to pass while the collection parameters are being setup in the software. A reference scan is collected and then the slide is repositioned and a scan is quickly collected from the fiber. This spectrum may differ, especially below ~ 400 nm, if the next reference scan is immediately collected from a “fresh” blank area of the slide.

EDGE CONTRAST

It is well understood among microscopists that sample preparation is one of the most critical steps for insuring a high quality microscopical examination. Despite this, specifications or guidelines for MSP sample preparation have been limited in nature. This raises the question: to what degree should sample preparation be defined for MSP analysis? Poor sample preparation may lead to poor image formation or it could impact the quality of the MSP spectra. It follows that guidelines for sample preparation explored and sample preparation methods should be recorded and available, not only to ensure the best quality data is being collected, but to allow different analysts or laboratories to reexamine samples, as necessary, under the same conditions.

We addressed this consideration using fibers, which are arguably the most common class of evidence studied by MSP. Different cross sectional shapes present not only a range of image contrast, but often localized variations in contrast as well. In addition, the presence of delustrants can create large amounts of localized contrast as the refractive indices of some delustrants can be much greater than that of the polymer matrix. For example, the refractive indices of titanium dioxide fall

³⁵ The slides are described as being “precleaned” by the manufacturers.

³⁶ Fine bubbles immediately formed and continued to be generated at the surfaces of the submerged glass slides.

³⁷ There is no reason why this brand of slide was chosen over any of the other brands.

in the range of 2.5 - 2.9 where as a typical fiber forming polymer falls in the range of 1.45 - 1.7.³⁸ In general, the difference between the refractive index of the specimen and the refractive index of the mounting medium is the greatest determining factor of overall contrast in a given sample.³⁹ Large values of this so-called “index of visibility”⁴⁰ result in an image with high contrast.

RELATIVE REFRACTIVE INDEX OF THE MEDIUM COMPARED TO THE SPECIMEN

Edge contrast due to refractive index differences between the specimen and the mounting medium has been studied to determine if either subtle or gross spectral degradation may result from high or low contrast and to provide information to guide analysts in acquiring better and more reproducible MSP data through more careful selection of mounting media.

A series of six colored (light and dark red, green, and blue) acrylic (PAN) fibers was used to demonstrate the effects of various common fiber mounting media (*i.e.*, xylene, glycerin, and water) on spectral quality. The refractive index of xylene (~ 1.50) is relatively close to the refractive indices of acrylic fibers (~ 1.51 - 1.525) while the refractive index of water (~ 1.33) is quite far removed (Palenik, 1999). Glycerin has a refractive index (~ 1.47) between that of xylene and water. Figures 136 - 138 show how these fibers appear in these mounting media when viewed using transmitted light. MSP spectra were collected from each of the six colors of fibers (Figures 139 - 144).⁴¹ The following general observations were noted after examining these spectra:⁴²

- Spectra collected from the fibers mounted in water show the most noise while spectra from the fibers mounted in xylene have the least. Spectra obtained from the fibers mounted in glycerin show an intermediate amount of noise. This effect is much more apparent in the lightly colored fibers as they have less “signal” to begin with compared to the darker fibers (which absorb more strongly).
- The spectra collected from the fibers mounted in water are generally more compressed in the ordinate dimension compared to the spectra collected from the fibers mounted in xylene and glycerin. This compression is caused not only by the relative “shortness” of the absorption peaks, but also by the increased baseline absorbance in the areas of the spectrum where there is little to no absorbance (*i.e.*, the baseline is shifted up). Again, this effect is more prevalent in the spectra collected from the lightly colored fibers.
- Most importantly, subtle spectral features are the most distinct in spectra collected from fibers mounted in xylene, although the spectra from the fibers mounted in glycerin are significantly better defined than the spectra from fibers mounted in water. For example, the relative intensity of small peaks or other spectral features observed when the fibers are mounted in xylene can be decreased or even eliminated when the fibers are mounted in glycerin or water.

³⁸ Moderate to high concentrations of delustrant effectively results in increased contrast over the entire surface of a fiber.

³⁹ Obviously, the optics of the microscope and the way in which the microscope is setup will also affect the overall contrast of any given sample.

⁴⁰ The difference between the refractive index of a specimen and the mounting medium in which it is immersed.

⁴¹ Although data were collected from additional fibers, spectra from only two fibers for each medium are displayed in these figures for clarity.

⁴² In these spectra, and other spectra shown throughout this report, transmission values are sometimes registered > 100% and absorbance values are sometimes displayed as < 0 for particular wavelengths. This is due to the fiber acting as a lens and causing additional photons of light to reach the detector as they refracted from areas beyond the two dimensional projection of the collection aperture. In other words, light rays which would normally pass outside the boundaries of the detector are bent by the fiber and subsequently counted by the detector.

Again, the more drastic differences are generally observed in the lighter colored fibers as they often have only subtle absorbance peaks to begin with (*i.e.*, even under the best conditions, lightly colored fibers often only have small, subtle absorbance peaks). Specific examples are illustrated in the figures.

Given the above, it is necessary to recognize that the choice of mounting medium can produce artifacts that manifest themselves as differences in spectra obtained from even the same fiber, if analyzed in one medium versus another.

REFRACTIVE INDEX OILS

Commercial index of refraction oils are available in wide range of values. These oils can be used to mount fibers in liquids closely matching their nominal refractive index, thereby minimizing the edge contrast between the fiber and the mounting medium. In theory, this should minimize noise and produce high quality spectra. A few preliminary experiments were conducted using a variety of these media. In one such experiment, a fiber sample⁴³ was mounted in liquids with varying indices of refraction (n)⁴⁴ to induce different amounts of contrast (Table 4).

Table 4. Mounting media used in sample preparation

Preparation	Media
1	Distilled water ($n= 1.33$)
2	Cargille Series A $n=1.460 \pm 0.002$
3	Cargille Series A $n=1.560 \pm 0.002$
4	Cargille Series A $n=1.600 \pm 0.0002$
5	Cargille Series B $n=1.6600 \pm 0.0002$

Water and 1.660 index of refraction oil were selected as a common media with relatively low and high refractive indices. A third medium (1.560) was selected to be close to the nominal refractive index of the nylon fiber. The remaining two preparations were selected to bridge the gap from the “match” to the extremes. Figure 145 shows the fibers mounted in the various media and Figure 146 shows the spectra collected from these. Spectra were acquired on a CRAIC QDI 2010 MSP with the following collection parameters:

- Scan Range: 300-800 nm
- Averaged Scans: 500
- Integration Time: 8 ms
- Resolution Factor: 2
- Objective: 40 x
- Collection Aperture: #1
- Source: Xenon

All fibers were oriented in an east-west configuration with the substage iris aperture adjusted to a position of approximately 2.75. No polarizing filters (*e.g.*, polarizer or analyzer) were present in the optical path of the microscope.

Five spectra were collected along the lengths of three different fibers. A new reference spectrum was collected between each point and a new dark scan was collected between each fiber. Due to the large size of the selected aperture, which spanned the width of the fiber, a neutral density filter (N.D. 1.0) was placed on top of the field diaphragm to prevent

⁴³ MT-Fiber – N-0081: A lightly colored nylon fiber ($n_{\parallel} = 1.582$ at 25°C) which is relatively free of delustrant and has a round cross-sectional shape.

⁴⁴ Nominal value as defined on the bottle.

saturating the detector. The spectra collected from each fiber were averaged, and the subsequent averages per mounting medium were averaged to obtain one representative spectrum per preparation.

Although subtle, the amount of noise observed in each spectrum can be directly related to the total contrast of the preparation. The preparations with the largest Δn between the sample and surrounding media result in the highest amounts of noise. As a consequence of the overall darkening effect of the high contrast, they also exhibit the greatest overall absorption. Because the sampling aperture spanned the breadth of the fiber, it seems most likely that the relatively large fiber diameter ($\sim 28 \mu\text{m}$) limits the introduction of edge contrast into the area being analyzed (*i.e.*, only a small percentage of the total area being analyzed has edge contrast). This in turn minimizes the observed effect of edge contrast.

During the course of the above experiment it was observed that this nylon fiber darkens when it is mounted in Cargille series B ($n = 1.6600$) oil and illuminated using xenon light. In a subsequent experiment, MSP spectra were collected periodically over the course of three minutes from the same area of the nylon fiber (Figure 147).⁴⁵ Photomicrographs of the fiber were also taken during this experiment, which illustrate the progressive darkening of the fiber (Figure 148). The localization of the darkening can be easily observed when the fiber is viewed using a lower powered objective (and the field diaphragm is correspondingly opened) (Figure 149). When viewed in plane polarized light, it is interesting to note that the discoloration behaves pleochroically. Elemental analysis, using energy dispersive x-ray spectroscopy (EDS) in a scanning electron microscope (SEM), detected localized concentrations of iodine and bromine in the darkened area of the fiber. Neither of these elements was detected in control areas of the fiber (Figure 150).

It appears that this particular refractive index oil, which contains 1-iodonaphthalene and 1-bromonaphthalene, undergoes a chemical reaction when illuminated with xenon light. Subsequent experiments demonstrated that the oil itself (*i.e.*, without any sample being present) will darken over time when exposed to xenon illumination but this particular fiber was the only sample studied which darkened when it was exposed to these conditions.

It is also worth noting that certain refractive index oils exhibit spectral artifacts at low wavelengths ($\sim < 360 \text{ nm}$). Figure 151 shows some spectral features that are related to the refractive index liquid. Further study suggests that these may be attributed to photochemical breakdown of the mounting medium from the intensity of the xenon illumination. Most refractive index liquids utilize different binary chemical combinations to achieve the desired n , including several conjugated species which absorb UV light. It is thought that the variation in the molecular makeup of the various liquids may account for the variation in the observed absorbance.

Jeremiah Morris of the Johnson County Sheriff's Office Criminalistics Laboratory has also documented how the interaction of fibers and refractive index oils can affect MSP spectra (Morris, 2013). In the case he describes, questioned fibers were first mounted in 1.520 index of refraction oil and identified as cotton. These fibers were then mounted in glycerin and compared to known black cotton fibers (which had not been previously mounted in 1.520 index of refraction oil). Spectra from some of the Q fibers were very similar to the known standard but there were slight differences between 200 - 325 nm. In subsequent experiments he determined that fibers mounted in 1.520 index of refraction oil for thirty⁴⁶ minutes prior to being transferred

⁴⁵ As discussed above, a portion of the increasing absorbance, especially at the lower wavelengths, is apparently due to the fact that this experiment was conducted using xenon illumination in conjunction with a glass microscope slide. The obvious discoloration of the fiber indicates that this phenomenon is clearly not the only factor at work. In fact, it is likely a minor causal agent in this particular case.

⁴⁶ It is not known if these spectral changes would occur in samples mounted in 1.520 index of refraction oil for less than 30 minutes as this was his shortest timed interval.

to glycerin⁴⁷ for MSP analysis exhibit spectral changes. Various solvents including methanol, hexanes, and a xylene substitute were used in an attempt to wash the fibers after they were mounted in 1.520 index of refraction oil. Although the xylene substitute showed the most promising results, there were still subtle spectral differences when compared to fibers that had never been mounted in 1.520 index of refraction oil.

COVERSLIP THICKNESS

When transmitted light is being used to collect MSP spectra,⁴⁸ the sample being analyzed is invariably mounted between a slide and cover slip. Any absorbances originating from the slide and cover slip should be accounted for by the acquisition of a reference spectrum collected from a blank area of the same preparation. Because of this, it is not immediately obvious that parameters such as cover slip thickness would affect spectral data collection.

However, our work in one particular case indicated the importance of accounting for cover slip thickness. In this case, we received fibers already mounted between slides and cover slips, in addition to loose fibers which we mounted for analysis at our laboratory. The spectra from the fibers received pre-mounted and those which were mounted at our laboratory produced similar over much of spectral range but were distinctly different below ~ 320 nm. Note that this is a region of the spectrum that is often truncated in many crime laboratory reports (which often present data only over the range of 400-700 nm). Further investigation using a caliper revealed that the samples received pre-mounted were under thinner cover slips (No. 1) compared to the cover slips used by our laboratory (No. 1 $\frac{1}{2}$).⁴⁹

Subsequently, experiments were performed in an attempt to replicate this phenomenon. Figure 152 shows MSP spectra of fibers from the same source collected using both No. 1 and No. 1 $\frac{1}{2}$ cover slips. While there is some intra-sample variation at certain locations, the most obvious inter-sample difference occurs below ~ 320 nm. The spectra collected from the fibers mounted under the thicker cover slips exhibit a sharp decrease in absorbance below ~ 320 nm, compared to the spectra collected from the fibers mounted under the thinner cover slips. This difference is especially clear when only two spectra, one with each cover slip are displayed (Figure 153). Since it is often on the basis of apparently minor points of comparison that colored fibers (and other microscopic trace evidence) are often ultimately associated or differentiated by MSP, the importance of minute differences or similarities in spectral detail, due to apparently insignificant differences in sample preparation as noted here (*e.g.*, coverslip thickness and/or tilt, refractive index of the fiber or mountant, fiber orientation, *etc.*), must not be overlooked or disregarded.

V – SAMPLING EFFECTS

In addition to instrumental based factors, there are a variety of factors related to the sample being measured. The topics explored here include a) the specific aperture placement relative to the fiber width, b) the impact of cross-sectional shape on aperture placement, and c) the impact of intense illumination on the sample (*i.e.*, photobleaching).

⁴⁷ In these initial studies, there was apparently no attempt to wash the 1.520 index of refraction oil off of the fibers. The fibers were dragged along a slide in an effort to physically remove the adhering mounting media before they were mounted in glycerin.

⁴⁸ The vast majority of all forensic samples are analyzed in this fashion.

⁴⁹ No. 1 cover slips are nominally 0.13 – 0.16 mm thick while No. 1 $\frac{1}{2}$ cover slips (for which most microscope objectives with magnifications $> 10X$ magnification are normally corrected) are nominally 0.16 – 0.19 mm thick. The “0.17” marking on the sides of most modern, “high-dry”, objectives indicate that they are designed for use with No. 1 $\frac{1}{2}$ cover slips.

ANALYSIS ACROSS FIBER WIDTH

Some time ago, while conducting microspectrophotometry using a hyperspectral imaging process based on a liquid crystal tunable filter, in which a spectrum could be produced from any pixel (or group of pixels) in an image, we found that spectra produced from different regions of a fiber could be significantly different. Some of these differences were due to artifacts in the mechanism of measuring the spectrum; however, it raised the question of whether spectra collected from different regions of a fiber using a traditional spectrometer showed variations based on the relative position of the aperture. To explore this, spectra were collected from a nylon fiber⁵⁰ with a round cross section using a small aperture at varying positions across the width of the fiber. The fiber was mounted in a refractive index oil ($n=1.460$) that resulted in a high edge contrast to emphasize (and thus study the extreme case) of spectral differences due to fiber shape.

Five different areas of the fiber were selected for analysis. Two positions were located at the edge of the fiber, where the contrast is the greatest, one on each side. Two additional locations were selected just inside of the dark areas on each side of the fiber, with the final position relatively centered on the fiber. These positions are illustrated in Figure 154.

Five spectra for each location were analyzed across this fiber. The spectra were averaged per location and are plotted in Figure 154. Qualitatively, the spectra collected near the edges of the fiber have the most noise and also exhibit the greatest overall absorbance. This makes intuitive sense as these are the visually darkest areas, and therefore, they would be expected to transmit less signal relative to the other areas. The spectrum collected from the center of the fiber appears to have slightly less noise compared those collected immediately adjacent to it. It certainly has the greatest range of absorption (*i.e.*, the most pronounced peak relative to its baseline absorbance) due to this area having the longest path length (relative to the other areas examined). Conversely, the spectra collected from the edges of the fiber, which have the shortest relative path lengths, have the smallest ranges of absorption.

CROSS SECTIONAL SHAPE

A colored nylon fiber with a trilobal cross-sectional shape (sample 117 from Microtrace's Forensic Fiber Reference Collection) was mounted in glycerin and spectra were collected from four different areas of the fiber (Figures 155 and 156).

The first area is located along the edge of the fiber and is restricted to a relatively thin aspect of a single lobe. This represents the shortest path length of the four areas examined. The second location is the middle of the fiber and it encompasses the full length of a lobe as well as the central portion of the fiber. Consequently, it represents the longest path length. Area 3 is an intermediate position straddling the boundary between the two previously described lobes. The same sized collection aperture was used for these three areas. A lower magnification objective was needed in order to examine the last location which spans the entire breadth of the fiber. Coincidentally, the same collection aperture was appropriately sized for this last area when the lower powered objective was selected (see Figure 155). This evaluation was conducted in order to determine whether or not there is a preferential location for the analysis of samples with a non-round cross section.

Spectra were collected utilizing identical collection parameters as listed above, with two exceptions. The 40x objective, and neutral density filter of 0.5 was used for analysis of positions 1-3. Five areas across three fibers for each position were acquired and the spectra then averaged within the analysis position, fiber and medium.

⁵⁰ From the same source as the nylon fiber used in the refractive index oils experiment.

A comparison of the resulting spectra is shown in Figure 157. As expected, the smallest path length (area 1) yields the least absorption, the largest path length (area 2) results the greatest absorption, and the other two areas are located somewhere in the middle. There is also a correspondence between range of absorption and path length. (*i.e.*, area 2, which has the longest path length, also has the largest range of absorption, and area 1, which has the shortest path length, has the smallest range of absorption).

Ignoring amplitude differences, the spectra are similar to each other and there do not appear to be any major differences with regard to the spectral peak positions. There are, however, significant differences in the positions of many absorbance positions. This suggests that there may not necessarily be an optimal sampling area regarding fibers with complex cross-sectional shapes. Furthermore, this experiment also suggests the fibers with complex cross-sectional shapes allow for an additional degree of freedom with regards to sampling. For example, it may be desirable to collect spectra through a vertical lobe (*i.e.*, area 2) with lightly colored fibers in order to maximize path length, hence signal, in order to reduce the effects of noise. Conversely, it may be preferable to collect spectra through the side lobe (*i.e.*, area 1) of a deeply colored fiber in order to reduce the path length, thereby avoiding spectral bottoming-out. In any case, it is critical that the spectra used to compare fibers should be collected in the same manner in order to minimize errors (be they false exclusions or inclusions).

The one obvious difference amongst the four spectra in Figure 139 is the “dip” at the lower end of the spectrum from aperture area 4. Areas 1, 2, and 3 were reexamined with the 10X objective using a correspondingly smaller collection aperture. All three of these spectra exhibit a similar “dip” below ~ 400 nm compared to their respective spectra collected using the higher powered 40X objective (Figure 158). While the fundamental cause of this artifact is not understood at this time, it is reproducibly associated with the lower powered 10X objective.

PHOTOBLEACHING

MSP is generally considered to be a non-destructive micro-analytical technique, which is one of the reasons it is well suited for forensic work. Katie Steele at the United States Army Criminal Investigation Laboratory was the first person to alert us to the fact that certain colored fibers may be “bleached” when continuously exposed to xenon illumination. Since that time, we have also noted this phenomenon in our own experiments. This potential for sample degradation needs to be considered whenever forensic evidence is being analyzed for obvious reasons.

We selected several fibers colored with single dyes known to have poor lightfastness (*i.e.*, worst case scenarios) from our reference collection and experimented with them using both tungsten halogen and xenon illumination. Individual fibers were mounted in xylene between quartz slides and coverslips and continuously exposed to either tungsten or xenon illumination for five minutes. Spectra were collected every thirty seconds. Photomicrographs were also taken at the beginning and end of each experiment. Figures 159 - 168 show the results of these experiments. In all cases, some amount of photobleaching was detected spectrophotometrically. As anticipated, exposure to the xenon source also always resulted in greater amounts of photobleaching compared to the effect of tungsten illumination for the fibers colored with the same dye.⁵¹ The more extreme instances of photobleaching (*e.g.*, Acid Green 9 with xenon) are obvious in the photomicrographs. In contrast, there are no discernable changes in the appearance of the fibers where minimal amounts of photo-bleaching was detected spectrophotometrically (*e.g.*, Acid Green 7 with tungsten).

As a control, a fiber that had been dyed with a known lightfast dye was analyzed in the same manner using tungsten and xenon illumination (Figures 169 and 170). There is minimal photo-bleaching with the tungsten source and only minor

⁵¹ It should be noted that replicate experiments demonstrated the relatively high amounts of variability with regards to the degree of photobleaching for individual fibers.

amounts with the xenon. However, the detection of any amount of photo-bleaching is significant since this results in what amounts to irreversible sample degradation. While not an entirely satisfactory solution to this problem, the easiest way to minimize the amount of photo-bleaching is to minimize the amount of time a sample is exposed to the xenon illumination. Not surprisingly, tungsten illumination appears to cause less photo-bleaching than xenon.

In addition to photo-bleaching, we have also observed an example of photo-darkening with C.I. Pigment Blue 30 (PB30).⁵² This phenomenon was unexpectedly detected when we were searching for pleochroic materials suitable for detecting the inherent polarization in the system. Individual pigment grains of PB30, mounted in 1.662 Meltmount, gradually darkened over time when continually illuminated by light from a xenon source (Figure 171). Once recognized, MSP spectra were collected from the same area of a “fresh” pigment grain every thirty seconds, subjected to continual xenon illumination, for a total elapsed time of five minutes (Figure 172). There is a general increase in absorption across entire spectrum as well as a progressive spectral shift of the two main absorption peaks. Additionally, there is the formation of a new distinct absorption peak at ~410 nm. This new peak gradually increases in intensity over time. These spectral effects, as well as the visible darkening, are not entirely caused by the darkening of the pigment, as the mounting medium itself has darkened over the course of the experiment. This darkening is not easily observed until the slide is examined using a lower powered objective, at which time it becomes immediately obvious (Figure 173). Illumination of the PB30 grains mounted in 1.662 Meltmount with the xenon source must have initiated/catalyzed a slow chemical reaction because the pigment grain appeared quite different when it was reexamined several months after the initial experiment (Figure 174). The once translucent blue pigment grain is now essentially opaque with fine acicular crystals radiating from its surface. Additionally, a new phase, magenta in color, has separated from the surrounding mounting medium.

These phenomena appear to be the result of a combination of the illumination (xenon), the mounting medium (1.662 Meltmount), and the sample (PB30). More specifically, the darkening is not observed when PB30 grains, mounted in 1.662 Meltmount, are illuminated with tungsten halogen illumination (Figures 175 and 176) nor when they are mounted in water and illuminated using xenon illumination (Figures 177 and 178).

With these concerns in mind, it is suggested that whenever possible, experiments should be conducted first on known materials in order to assess any sample degradation before the more precious questioned material is subjected to potentially damaging conditions. Due its higher intensity, particular care should be given to samples analyzed or examined using a xenon source. In the event that a lack of lightfastness is observed, it can certainly be utilized as an additional point of comparison.

VI – FLUORESCENCE MICROSCOPY

Fluorescence microscopy has been utilized for several decades as an additional means by which to compare and characterize fibers. Although not often utilized, spectroscopic measurement of fluorescence can provide additional information. This section explores and attempts to educate the user as to the considerations one must make when measuring fluorescence spectra (a technique known as microspectrofluorimetry or MSF).

⁵² Copper hydroxide carbonate.

EXCITATION CONDITIONS

Multiple excitation conditions, often through the use of different filter cubes, are commonly used during the examination of forensic evidence for fluorescence. The use of these different excitation conditions has merit because some samples may not exhibit detectable auto-fluorescence under certain conditions and the use of any single filter cube could cause fluorescence to go undetected. Conversely, it is also common for samples to fluoresce under multiple excitation conditions, often exhibiting drastically different fluorescence colors (Figure 179). It is important to recognize that while three different observations are being made, they are not necessarily independent of each other. In fact, although the sample may be fluorescing a different color at each of the excitation wavelengths, the different colors observed are determined primarily by the cutoff wavelengths of the particular filters sets being used and the relative intensity of the fluorescence. For example, Figure 180 shows how the MSF spectra of a green fiber, illuminated using three different excitation conditions, are clearly related to each other, despite appearing dramatically different visually. The green fiber appear bluish-white when using UV excitation because these conditions are relatively inefficient at causing the dye(s) in the fiber to fluoresce and because the emission filter is allowing relatively low ($> \sim 420$ nm) wavelengths of light to reach the detector. The same fiber appears orange when illuminated with blue light because this condition excites increased fluorescence (albeit at the same wavelengths as the UV excitation) and it blocks light below ~ 520 nm (*i.e.*, bluish light) from reaching the detector. Finally, this fiber appears bright red when illuminated with green light because it is stimulating relatively large levels of fluorescence (again at the same wavelengths as the other two conditions) and because it blocks light below ~ 620 nm from reaching the detector. Additional examples confirming these results are shown in Figures 181 - 184. It is important to realize that these three different observations are simply due to the fluorescent emissions from the dye(s) within the fiber and not a manifestation of three variables

MSF COMPARED TO FLUORESCENCE MICROSCOPY

One particular advantage MSF has over fluorescence microscopy alone is the ability to differentiate subtle differences in fluorescence emissions (or observed fluorescence that is too weak to be detected by the naked eye) that may not be detectable by eye. Figure 185 shows how three lightly colored acrylic fibers (all from the same manufacturer) appear bluish-white using UV excitation. While these colors appear to be visually similar (especially in the absence of a fluorescence comparison microscope), Figure 186 demonstrates how they can be easily distinguished using MSF. The fibers appear to have similar fluorescence colors using UV excitation because the majority of the observed fluorescence is due to the polymer matrix of the fiber (which, expectedly, is quite similar between the three fibers), as opposed to the dye(s) coloring the fibers. MSF allows for the small contributions from the fluorescing dyes to be observed. It is worthy of note that while all of these fibers appear essentially colorless⁵³ when examined using PLM, they can also be differentiated using MSP and/or comparison microscopy.

⁵³ The fact that seemingly colorless fibers can be differentiated by MSP is an important point in and of itself. Individual fibers from lightly, but yet distinctly colored fabrics often appear colorless, or nearly colorless, when examined by PLM with transmitted light.

VOLUME AND MSF

While fluorescence is sometimes thought of as a surface phenomenon, sample thickness is an important variable influencing fluorescence intensity. Figure 187 shows photomicrographs of two differently sized mauve colored fibers from the same source (UV excitation). It is obvious that they exhibit significantly different fluorescence intensities, which is demonstrated graphically using MSF (Figure 188).⁵⁴ Therefore, it is important to compare similarly sized fibers when there are significant differences within a given source.

FLUORESCENCE OF MOUNTING MEDIA

In MSF it is important to confirm that the mounting medium is not contributing to the fluorescence of a sample, especially when low levels of fluorescence are detected. As such, the fluorescence of several common mounting media (*i.e.*, xylene, glycerol, air, water, Permout™, and 1.520 index of refraction oil) were examined using UV excitation. Only Permout™ and Cargille 1.520 index of refraction oil exhibited significant fluorescence, which is consistent with visual observations made using a dedicated fluorescence microscope (*i.e.*, a fluorescence microscope that does not have filters in its oculars) (Figure 189). It follows that these two materials should be avoided, if possible, as mounting media when MSF spectra are to be collected, especially if the samples exhibit weak fluorescence. Of the media tested, water exhibits the least, essentially zero, fluorescence (Figure 190).

A brief comparison was conducted in which MSF spectra were collected from three colors of fluorescent fibers mounted in water and xylene (*i.e.*, the two mounting media commonly used when collecting MSF spectra in our laboratory) (Figures 191 - 193). No reproducible differences in fluorescence intensity were identified between these two media, although there is some evidence of very slight spectral differences (*e.g.*, shifted peak positions). It follows that either medium is suitable for MSF but that all samples for a given experiment should be mounted in the same medium.

VII – DATA COLLECTION RECOMMENDATIONS

In the course of our own casework and this research, we have put together a list of information that describes various factors that should be checked, recorded, or considered when conducting an analysis using MSP. Although ISO principals tend to reduce such details to a series of checklists, we have presented this section in the form of a narrative discussion. Due to the variety of systems, samples and preparations studied, we have found that before reducing the relevant parameters to a checklist, it is important that thoughtful attention be given to the instrumental setup, sample preparation, and quality control. For without a basic understanding of these parameters, one is liable to collect misleading data. For example, it is possible to collect data that conforms to a protocol but does not provide any useful information. One example stems from a case in which dark blue fibers were analyzed. The resulting spectra showed a flat 10-20% transmission across the spectrum. It was stated that the spectra from the Q and K were similar to each other. While this is technically true (the spectra were similar), the spectra contained no colorimetric data suggestive of the blue color of the fibers and were thus not a valid point of comparison. A thoughtful analysis would have, at least, provided a valid interpretation of the data and, at best, would have found a way to collect useful spectra from fibers that were observed to be blue by transmitted light microscopy.

⁵⁴ All of the displayed MSF spectra were collected using the same operating conditions and the collection aperture was selected to fit within the boundaries of the smaller fibers.

INSTRUMENT SETUP

Ultimately, a microspectrophotometer is simply a spectrometer attached to a microscope. Similarly, in microspectrofluorimetry, a spectrometer is optically attached to a fluorescence microscope. In general, there is little the user of the instrument can adjust on the spectrometer and modern spectrometers are extremely stable (with regards to wavelength accuracy). Therefore, the quality of the data collected for any given MSP system is most dependent on the user's ability to prepare the specimen and properly setup and fine tune their microscope.

As with all microscopes, everything is dependent on adequate and proper illumination. A diffuser may be used to obtain even illumination across the field of view⁵⁵ and the bulb should be adjusted in the lamp housing in order to provide maximum light flux. Slight adjustments to the position of the bulb may serve to increase or decrease specific portions of the spectrum. For example, it is possible to maximize UV illumination, often at the expense of some light in the visible wavelengths. Generally, this slight loss of intensity in the visible region is not problematic because there is so much light to begin with.

Once the bulb is in the desired location, the optical elements of the microscope can be adjusted for Köhler illumination, which minimizes stray light (*i.e.*, noise) reaching the detector. With the specimen in focus, the leaves of the field diaphragm should next be brought into sharp focus by adjusting the height of the substage condenser. The field diaphragm is then opened far enough so that its edges are not near the vicinity of the collection aperture of the spectrometer.

The substage aperture should be opened until the desired image is produced. However, it may be desirable to further increase the opening of the substage aperture in order to allow more signal (*i.e.*, light) to reach the detector. In our experience, we have found it desirable to leave the substage aperture in a fixed position during the course of an experiment. In other words, spectra that are to be compared to each other should be collected under the exact same conditions as possible, and this includes the opening of the substage aperture.

If the MSP system is equipped with multiple collection apertures, a single aperture should be selected and used throughout the course of an experiment. In general we recommend using the largest aperture that will remain within the boundaries, avoiding edge effects, of the sample being analyzed when collecting MSP data. An oversized aperture (*i.e.*, one that extends beyond the boundary of the sample), is undesirable as the relative intensity of the signal (*i.e.*, the light passing through the sample) decreases relative to the reference scan. This only serves to decrease the absolute absorbance of the spectrum and increase the relative intensity of the noise.

However, larger apertures may be used when collecting MSF spectra, as long as a non-fluorescing mounting medium is being used. In these cases, the resultant spectrum is not produced from a ratio of a reference scan and the strength of the signal is determined by absolute counts. The oversized aperture will increase the signal reaching the detector, and because the background is black, there is no significant increase in noise to detract from the quality of the collected data.

If one's system is equipped with a filter cube turret, it is always a good idea to check to be certain that the appropriate cube is in position (*i.e.*, the transmission cube for MSP and the desired fluorescence cube for MSF).

⁵⁵ One drawback of a diffuser is the inherent loss of light intensity.

COLLECTION CONDITIONS

As discussed above, there are several selections to be made regarding collection conditions, including the type of illuminator, slides, mounting medium, and the use of polarizers. This report has discussed the use of two illuminators for MSP: xenon and tungsten halogen lamps. In summary, xenon offers more light over a broader range of wavelengths compared to tungsten halogen. One potential drawback of this source, however, is accelerated photodegradation compared to tungsten halogen. While most samples will not photodegrade within the timespans typically required for the collection of spectra, the potential for sample degradation should be recognized and guarded against, especially when examining unique samples (*i.e.*, questioned samples). To guard against this, expendable fibers from the reference sample should always be analyzed first when the xenon source is selected and its effect on the fiber and its spectrum should be evaluated before subjecting a questioned fiber to its possible effects.

This report has also discussed the, as of now, unexplained interaction between xenon light and glass slides at low wavelengths (especially $< \sim 400$ nm). This instability was not observed with quartz slides nor was it observed with tungsten halogen illumination (glass or tungsten slides). It should also be noted that quartz slides transmit additional UV light compared to glass slides.

In general, we recommend using a mounting medium which approximates the nominal refractive index of the sample being analyzed for MSP. In our experience and based on our experiments, xylene works well for most fibers. Our limited research with refractive index oils has provided indications that they are not the most suitable media for MSP (especially when using xenon illumination). Xylene and water have been used for the collection of MSF data in our laboratory (water generally being preferred in order to avoid unnecessary exposure to xylene vapor). It is critical to avoid mounting media known to fluoresce (*e.g.*, Permout™ and 1.520 index of refraction oil) in order to ensure that any fluorescence detected actually originates from the sample.

We do not typically use a polarizing filter when collecting MSP spectra (although we recognize the *potential* for increased discrimination when analyzing pleochroic samples). The experiments conducted in this report indicate that there can be instability in the polarizing filters typically placed on the base of compound microscopes. As such, we recommend confirming the stability of any polarizer before it is used for the collection of MSP spectra from evidence.

SPECTRAL ACQUISITION

Most MSP systems allow the user to define the sampling time and the number of scans to average. There are no rules dictating the values of these parameters. Their values will be determined by the sample being analyzed and they should be adjusted until high quality spectra are produced. With a given instrumental setup, it should be noted that long sampling times may saturate the detector, resulting in unusable spectra. Some software packages have a built in functionality which automatically adjust the sampling time. Again, it is highly recommended that all of the data within an experiment be collected using the same conditions. This is especially critical when collecting MSF data because the amplitude of the resulting spectrum is directly correlated with the collection conditions (*i.e.*, there is no reference scan to ratio against).

Our MSP system has a user defined parameter regarding spectrum smoothing (*i.e.*, resolution factor). Again, there is no rule regarding the optimum value of this variable. Therefore, the user should be aware of its effect on the data being collected and select an appropriate value for the experiment being conducted.

Dark (*i.e.*, when the light from the microscope is blocked from the detector) and reference (*i.e.*, when light from the microscope passes through a blank area of the slide preparation and is directed to the detector) scans should be collected throughout the course of data acquisition. In general, we recommend collecting reference scans before every sample scan is collected. This high frequency of reference scan collection compensates for the effects of adjusting the fine focus on the microscope as various portions of the sample are brought into sharp focus. Dark scans can be collected less frequently as long as there are no drastic temperature changes in the room housing the MSP system. In general, we recommend collecting dark scans after changing slides or every few minutes. Because of the speed with which MSP data can be collected on a modern microspectrophotometer, these additional scans do not result in an unreasonable burden with respect to the time expended in carrying them out.

There is no rule dictating the number of spectra which must be collected from any given sample. SWGMAT (2011) recommends collecting data from at least five fibers when analyzing known samples (ten if dealing with natural fibers) but does not mention how many areas along a single fiber should be analyzed. The European Fibres Group specifically states that it is “not recommended to set a definitive rule on the numbers of fibres that should be analyzed.” However, they do suggest that “a minimum of 5 spectra from individual fibres be collected from each known colour and/ or fibre type.”

In general, we base our replicate analyses on the apparent homogeneity of the item being analyzed. Typically, a minimum of three spectra from three different fibers (*i.e.*, nine total spectra) are collected from synthetic or man-made fibers which appear homogeneous. Additional spectra, generally no more than ten, may be collected from natural (*e.g.*, cotton or wool) fibers or other materials which exhibit color variation along their lengths. A particular item may have multiple fiber types (*e.g.*, different colors and/or chemical compositions). Each of these fiber types is treated independently and is sampled and analyzed accordingly. If a sample exhibits observable heterogeneity, additional sampling should be conducted in an effort to capture the range of variation present within the sample (*e.g.*, hue variations, lighter and darker fibers/areas, thinner and thicker fibers/areas, *etc.*).

The location of the collection aperture relative to the sample should remain constant throughout any given experiment. This is especially important for fibers with complex or irregular cross-sections. For example, spectra collected through the relatively broad, flat portions of cotton fibers should not be compared to spectra collected through the twisted areas. Similarly, spectra collected through the projecting side lobe of a trilobal fiber should not be compared to spectra collected through the vertical central lobe. In general, we recommend positioning the aperture in the specific area. It should also be self-evident that areas with obvious foreign debris or other artifacts should be avoided, if possible (unless these areas are relevant to the potential common history of the samples being compared).

POST PROCESSING

In general, multiple spectra are collected from all items (*e.g.*, a fiber) analyzed using MSP or MSF. These spectra are typically averaged and then compared to the averaged spectra of another item. As discussed above, it is important to realize that there is a difference in the resulting spectrum if absorbance or transmission data is averaged. We recommend averaging absorbance data, because it is directly proportional to concentration, but there is not necessarily a significant difference between averaged absorbance/transmission data on a practical level. Nonetheless, the same format of data (*i.e.*, absorbance or transmission) should be averaged for any given comparison.

It is also possible to compare individual spectra, although it must be recognized that this method does not take potential intra-sample variation into account (unless multiple examples of individual spectra are compared between two, or more, items).

We have found that the examination of first derivative spectra can be a useful exercise when trying to distinguish between samples. It has been found to be most useful when demonstrating that two samples are different when examinations of the absorbance/transmission spectra are found to be close, but with potential differences. In other words, some spectra which appear fairly similar by absorbance/transmission may appear distinctly different when first derivative spectra are examined.

While the periodic collection of dark scans throughout the course of MSF data collection makes this unnecessary, it is possible to rescale MSF spectra in instances where the background has drifted (up or down) (Figure 194).⁵⁶ The effects of the drift are generally only noticeable when examining samples with minimal amounts of fluorescence.

VIII – FIBER COMPONENTS

Fibers are composed of polymers and often contain dyes, delustrants and optical brighteners. In this section of the report, these components of the fibers (polymers, dyes, delustrants, and brighteners) have been studied for their contribution to the MSP (or MSF) spectra.

PURE POLYMER CLASSIFICATION

Analyzing colorless fibers is beneficial in understanding the absorbance/transmission and/or emission characteristics of the raw material itself (*e.g.*, for a fiber, the polymer) without any dyes present. Understanding matrix effects can greatly improve spectral interpretation capabilities.

The fluorescence of fibers is typically thought of as arising from optical brighteners, colorants (*i.e.*, dyes and pigments), and/or additives such as finishing agents. A brief experiment was conducted to determine if the polymers used to make man-made/synthetic fibers could be contributing to the observed fluorescence. The following known polymer samples⁵⁷ were examined using MSF (UV excitation) in order to determine if any of them possess native fluorescence:

- Cellulose acetate
- Cellulose triacetate (CTA)
- Nylon 6
- Nylon 6/6
- Low density polyethylene (LDPE)
- High density polyethylene (HDPE)
- Poly (ethylene terephthalate)(PET)
- Poly (methyl methacrylate) (PMMA)
- Polypropylene (PP)

The polyester (PET) sample was the only polymer which exhibited detectable fluorescence (Figure 195). The spectra from all of the other polymer samples resided within \pm two absolute counts (*i.e.*, negligible fluorescence which was not visibly observable) (Figure 196).

⁵⁶ The original spectrum should always be retained and it should be made clear that post-processing was conducted on the displayed spectrum.

⁵⁷ These were not spun fibers but polymer pellets and powders from the Scientific Polymer Products, Inc. polymer reference collection.

Interestingly, this PET sample has a strong, sharp absorbance peak (at ~ 305 nm) when it is examined using transmitted light (*i.e.*, MSP) (Figure 197).

With these results in mind, known colorless PET fibers were examined using both MSP and MSF. All samples examined exhibited a strong absorbance peak between $\sim 305 - 309$ nm (Figure 198). There also appeared to be a correlation between the presence of delustrant particles and general broad absorbance. In other words, the sample with minimal delustrant particles has a relatively flat baseline while the samples with distinct delustrant particles exhibit wide absorbance. In such cases, it is likely that the delustrant is simply doing what it is designed to do: scatter light. Similarly, all of the fibers exhibit bluish-white fluorescence although it is quite weak in the thinner fibers (Figures 199 and 200).⁵⁸

As a follow-up, MSP spectra were collected from colorless fibers composed of other commonly encountered man-made/synthetic polymers (*i.e.*, acrylic, modacrylic, nylon, polypropylene, and rayon) (Figures 201 - 205). All of these fibers exhibit a modest absorbance (generally less than 0.1 absorbance units) between $\sim 300 - 310$ nm. Additionally, many of these fibers display subtle minor absorbances at higher wavelengths. One of the nylon fiber types is exceptional in that it has a distinct absorbance at ~ 360 nm. It is not clear what is causing this particular absorbance band but it highlights the potential value of conducting MSP on colorless fibers to search for unexpected differences and similarities when performing comparative examinations.

MSF spectra were also collected from these ten fiber types using ultraviolet excitation (206 - 210).⁵⁹ With the exception of one type of rayon, all of these fibers exhibit some fluorescence. This fluorescence was confirmed using a dedicated fluorescence microscope. The rayon fibers exhibiting weak fluorescence (< 8 counts at any particular wavelength under the collection conditions of the experiment)⁶⁰ were just barely visible using this fluorescence microscope. Therefore, these conditions approximately correlate with the visual limit of detection regarding sample fluorescence.⁶¹ It is clear that fluorescence could be detected from samples exhibiting less fluorescence if either the collection time or number of scans is increased, since fluorescence is measured in direct counts (*i.e.*, it is not a ratio relative to a reference scan).

In all of the samples exhibiting fluorescence, the greatest fluorescence is always located at the lower wavelengths ($< \sim 525$ nm). It should be noted that the nylon fibers that had the distinct MSP absorbance at ~ 360 nm (Figure 203), exhibit the most intense fluorescence (Figure 208). Additionally, one of the modacrylic fiber types also exhibit intense fluorescence relative to the other fibers examined (Figure 207).

DIFFERENTIALLY DYED FIBER SECTIONS

Color variability is sometimes observed along the length of individual fibers. For this reason, multiple spectra are typically collected along the lengths of such fibers. This color variation is more commonly encountered with natural fibers (*e.g.*, cotton and wool) compared to man-made/synthetic fibers. Because of this, more MSP spectra are typically collected from

⁵⁸ The same, relatively large, aperture was used to collect the MSF data from these four different PET fiber types. While this maximizes the total fluorescence measured, it also accentuates the differences of fluorescence intensity between the thicker and thinner fibers (because larger relative areas of the aperture are filled with the thicker fibers compared to the thinner fibers).

⁵⁹ Water was used as the mounting medium. The colors of the spectra in these MSF figures correspond to the colors of the spectra in the immediately preceding MSP figures (*i.e.*, the black spectra on the nylon MSF figure originate from the same fibers displayed in black on the nylon MSP figure).

⁶⁰ 100 scans using a 100 millisecond sampling time.

⁶¹ Obviously, the aperture used and the dimensions of the sample being analyzed will also affect the counts detected by the spectrometer.

individual cotton and wool fibers, compared to man-made/synthetic fibers, in an effort to capture the range of variation. Similarly, when known objects are composed of natural fibers, larger numbers of fibers are commonly isolated and analyzed in an effort to represent the range of variation, which is typically greater than that found in a population of man-made fibers from a single source.

The type of color variation discussed above is often inadvertent. In other words, the fiber manufacturers do not necessarily intend on producing fibers with small amounts of color variations along their lengths. These variations are typically caused by uneven dye uptake occurring at a microscopic level and manufacturers are not concerned unless the macroscopic appearance of the final product is affected. Figures 211 and 212 illustrate this inadvertent sample heterogeneity on a cotton fiber. This fiber, known to be dyed with a single dye, appears black macroscopically but has distinct deep blue and brown regions when viewed microscopically using transmitted light.

In some cases manufactures differentially dye fibers intentionally in order to produce a desired macroscopic appearance. This heterogeneous coloring of fibers can be produced in a variety of ways and while detected in various textiles, it is often encountered in carpet fibers.

Figure 213 shows a tuft of carpet fibers that have been *mélange* dyed. They are brownish/orange at one end and green at the other with a gradual transition between these two colors in the middle (Figure 214). Distinctly different MSP spectra can be collected along the lengths of heterogeneously dyed fibers. Figure 215 shows spectra collected from the brown/orange, green, and transition areas of the fibers. Note that the orange and green areas exhibit different absorbances which are simultaneously observed in the transition areas.

Individual fibers with areas having distinctly different colors are especially valuable for forensic purposes because each of the areas can be analyzed and compared separately. This heterogeneity adds potential discrimination power when comparing known and questioned fibers.

DELUSTRANTS

Delustrants, often in the form of fine ($\leq 1 \mu\text{m}$) particles of titanium dioxide, are added to man-made fibers in order change the macroscopic appearance of the fabric/material they are to be used in. Generally, it is desired to reduce the reflectivity of man-made fibers so they don't look like plastic fishing line. Titanium dioxide particles embedded in fibers accomplish this task by scattering incident light.

The presence of titanium dioxide delustrant particles in fibers is readily apparent when they are examined using transmitted light with a compound microscope. Although small, individual delustrant particles exhibit good contrast relative to the surrounding polymer matrix due to the large differences in refractive indices between polymer and particles. Although titanium dioxide powder is white macroscopically, and it is used as a pigment in white polymers, fibers with titanium dioxide appear to have dark inclusions when viewed using transmitted light (Figure 216). Again, this is a function of the high contrast and light scattering caused by the differences in the refractive indices between the inorganic delustrant and the organic polymer matrix.

Because delustrant particles alter the visual appearance of fibers, it is not unexpected that their presence can affect the MSP spectra obtained from fibers containing them. A series of bicomponent acrylic fibers, in which delustrant particles are only located in one side of the fiber (*i.e.*, in only one of the two components) was used to demonstrate the effects delustrant particles can have on MSP spectra (Figure 217). MSP spectra were collected from relatively light and dark examples of red,

green, and blue fibers from areas with and without delustrant particles (Figures 218 - 228).⁶² Several general observations were noted after the examination of these spectra:

- The spectra collected through the delustered areas exhibit greater overall absorbance compared to spectra collected through non-delustered areas. This is not unexpected considering the fact that the delustrant particles appear as dark inclusions when viewed using transmitted light. It should be noted that some of the greater “absorbance” in the delustered areas is actually caused by light scattering.
- The spectra collected through the delustered areas have more noise compared to spectra collected through non-delustered areas. This is a result of less light reaching the detector due to the absorbance/light scattering properties of the delustrants (*i.e.*, less signal = more noise). For this reason, the increased noise is especially apparent in the lightly colored fibers because they do not exhibit much absorbance (*i.e.*, signal) to begin with.
- The spectra collected through the delustered areas cut-off at a higher wavelength compared to spectra collected through non-delustered areas. Again this is a result of less light reaching the detector due to the absorbance/light scattering properties of the delustrants.
- Most importantly, subtle spectral features are more distinct in spectra collected through non-delustered areas compared to spectra collected through delustered areas. For example, a small peak in a spectrum collected from a non-delustered area can be reduced to a shoulder or even eliminated altogether in the spectrum collected from a delustered area. In other words, the delustrant particles have a tendency to “smooth” out these subtle spectral features. Again, the more drastic differences are generally observed in the lighter colored fibers as they often have only subtle absorbance peaks to begin with (*i.e.*, even under the best conditions, lightly colored fibers often only have small, weak absorbance peaks). Specific examples are illustrated in the figures.

In summary, these experiments demonstrate that, all other factors being equal, better quality spectra were collected through the non-delustered areas compared to the delustered areas. It is, therefore, obvious that given the choice, as in the case with these bicomponent fibers, spectra should be collected through areas without delustrant particles.

More important, however, are the implications for fibers which have delustrant particles dispersed throughout the entire fiber (which is by far the more common situation). In general, the presence of delustrant particles results in a combination of increased noise and the loss, or reduction, of subtle spectral features. These reductions in spectral quality are likely to be more pronounced in lightly colored fibers and/or fibers containing large concentrations of delustrant particles. Because of this, there is likely less discriminating power regarding MSP when delustrant particles are present. For example, the subtle spectral features required to differentiate two fiber samples with similar colors may be reduced/lost due to the presence of such particles. As a consequence, there may be an increased risk of false associations of very similar, but still different, fibers. It is important to remember that in a practical sense, these concerns are most likely limited to lightly colored fibers containing relatively large amounts of delustrant particles.

As a follow-up, MSF spectra were collected from each half of the darker bicomponent fibers discussed above (*i.e.*, red, green and blue).⁶³ These preliminary results indicate that the presence of delustrant particles does not significantly affect the resulting MSF spectra (Figures 229 - 231).

⁶² Spectra were collected from areas immediately adjacent to each other (*i.e.*, from the delustered and non-delustered halves) at several positions along the analyzed fibers in an attempt to make these comparisons directly analogous. Although data was collected from additional fibers, spectra from only two fibers are displayed in these figures for clarity.

OPTICAL BRIGHTENERS

The majority of commercially available laundry detergents contain an optical brightener. In essence these optical brighteners are colorless dyes which fluoresce bluish-white when illuminated with ultraviolet (UV) excitation (Bart, 2005). This makes the fabric appear “whiter-than-white” and helps to counteract any yellowing which may have accumulated over repeated use. Some detergents specifically formulated for dark or delicate clothes, as well those marketed as environmentally friendly or natural, may not contain these products.

A small survey of commonly encountered commercial laundry detergents was conducted with regards to their fluorescent emissions. A total of twenty-two unique detergents, representing twelve brands were collected and analyzed.⁶⁴ These detergents were applied to an undyed fabric sample labeled “100% unbleached cotton” purchased directly from a fabric store. Each swatch was swirled in a beaker containing 500 mL of warm water (~ 40° C) with 1 mL of detergent for ten minutes.⁶⁵ Each sample was then thoroughly rinsed using tap water, blotted between two pieces of paper towel, and allowed to air dry.

Fabric swatches were also treated⁶⁶ with four different pure optical brightener samples, designed for laundry detergents, and obtained directly from their manufacturer. These known optical brighteners are chemically different from each other, although they are all intended to fluoresce blue under UV excitation.

A control (*i.e.*, unwashed) sample of the fabric did not exhibit any noticeable fluorescence when examined macroscopically using a hand-held UV light (long wave). All of the washed fabric samples, except for the four washed with detergents suspected of not containing optical brighteners, exhibited distinct bluish-white fluorescence using the same hand-held UV light source.

Portions of the fabric swatches were mounted in water between glass slides and coverslips and microspectrofluorimetry (MSF), using UV excitation, was performed on each of them. All of the swatches, including the control, exhibited some measurable fluorescence. Unfortunately for purposes of differentiation, the fluorescence peaks were constrained to an extremely narrow range of wavelengths. All of the spectra have a “main” peak at ~ 440 nm⁶⁷ with a secondary spectral feature (*i.e.*, shoulder or minor peak) at ~ 465 nm (Figure 232). The principal peak does not necessarily represent the true fluorescence maximum of the optical brightener in question, but is rather a consequence of the low-wavelength cut-off of the emission filter.⁶⁸

Although the spectral curves all had similar shapes, there were large variations in intensity (~ 30,000 to 380 counts for the main peak) (Figure 233). The spectra were classified into one of four groups (very low, low, medium, and high) on the basis of the intensity of their fluorescence. The distinctions between the low, medium, and high groups are entirely qualitative and were only made because there appeared to be some natural groupings (it is not known if this grouping would stand-up to replicate analyses). The very low intensity spectra were separated not only by their low intensity but also due to the

⁶³ A relatively small aperture was used in order to sample only one half of the fiber (*i.e.*, either the delustered or the non-delustered portion).

⁶⁴ Four of these were either directly advertised, or suspected of not containing an optical brightener, based on the product description.

⁶⁵ This temperature corresponds to Federal Trade Commission (FTC) guidelines for a “warm” machine wash.

⁶⁶ The swatches were treated in the same manner except a small (approximately the amount adhering to the very tip of a flattened toothpick) amount of the powder (instead of liquid detergent) was dissolved into 500 mL of warm water.

⁶⁷ Range 439.3 nm to 442.4 nm.

⁶⁸ A different filter cube would be required to collect fluorescence spectral data below ~ 440 nm.

appearance on a true minor peak at ~ 468 nm (Figure 234). This peak is located where the other spectra exhibit a shoulder and in actuality, its appearance is almost certainly directly related to the lower intensity of the main “peak” at ~ 440 nm.

The small amount of fluorescence observed in the “very low” fluorescence fabrics is approximately the level of fluorescence observed with the control (*i.e.*, unwashed) fabric swatch (Figure 235). This indicates that these detergents do not contain optical brighteners themselves and that the purchased fabric itself apparently contains low levels of some fluorescing compound(s). It is not clear if this compound is intentionally added or if it is merely a by-product of the manufacturing/finishing process. In contrast and as a true negative control, a mass of fibers from an ordinary cotton ball exhibit negligible, but still instrumentally detectable, fluorescence (Figures 236 and 237).

Regardless, the fabrics exhibiting “very low” fluorescence do not appear optically brightened when they are macroscopically observed using a hand-held UV light or even when individual fibers are examined using fluorescence microscopy.

It should also be noted that these washed fabric samples cannot be differentiated using transmission MSP (*i.e.*, they do not exhibit consistent absorbance differences in the UV region) (data not shown).

IX – SPECTRAL INTERPRETATION AND DISCRIMINATION

Assuming that one is able to successfully collect valid spectra, one must then be able to interpret the data. This portion of the report switches gears to discuss spectral interpretation. A great deal of research is going into the development of various statistical methods for interpreting spectra. In spite of this research, almost all casework data (in the US, at least) is still evaluated through manual spectral comparisons in the form of overlaid spectra. There is nothing inherently wrong about this manual process, and as these results will show, it is an extraordinarily powerful and accurate method for discrimination. Nonetheless, there is little guidance (other than experience) to aid the trace evidence examiner in calibrating their eyes (and judgment) to this end. The various subtopics in this section each represent an experiment (or series of experiments) designed to help the examiner to develop context for deciding how to sample a known (*i.e.*, how many spectra must be collected?), to interpret the significance of subtle spectral features, and to provide some examples of spectra of different samples that are indistinguishable (among other cases).

SPECTRAL VARIABILITY IN NATURAL FIBERS

In these experiments, a series of cotton fibers dyed by the manufacturer to different, known concentrations were studied. The experiment started with the goal of determining whether fibers dyed with the same dye at different concentrations could be distinguished. Given that differences in the color intensity could be observed in the bulk fibers, we were curious to explore:

- Could individual fibers from any of these groups be definitively assigned to a specific group by MSP?
- Given that this is a natural fiber, how much variation might be expected in a given group?
- How many fibers would need to be characterized in order to capture all of the variation within a given sample?
- Could a basic PCA analysis correctly associate a number of questioned fibers to the proper concentration group?

Just as important as the results from these experiments are the experiences gained in understanding the ability of both manual interpretation and statistical interpretation to classify these groups.

SAME DYE AT DIFFERENT CONCENTRATIONS

In this experiment, the spectra collected from five fiber populations dyed at different concentrations with the same single dye were compared. This study was intentionally conducted on natural (cotton) fibers due to the expected intra-sample variation, which would not be as notable in a synthetic fiber population.

Experimental setup:

- Substrate: cotton fibers
- Dye: Reactive Red 43 at five different concentrations (0.25, 1.5, 6, 16, and 40 g/L) (Figure 238)
- Data: collected four spectra from three fibers at each concentration
- Comparison Microscopy: Fiber samples were also examined by comparison microscopy.

While there is general correlation between nominal dye concentration and absorbance intensity, there is significant overlap between adjacent groups (Figure 239). This is somewhat expected given the fact that these are cotton fibers, which like other natural fibers, tend to exhibit more variation in dye concentration both between fibers, as well as along the length of an individual fiber, compared to man-made fibers.⁶⁹ Averaging the four spectra for each individual fiber significantly reduces the amount of overlap between adjacent groups (Figure 240). While the overlap is reduced, there is a general gradient within and between the groups (*i.e.*, they do not form five distinct, separate groups).

This MSP data is in general agreement with observations made using comparison microscopy. At first glance, fibers from the three darker swatches (*i.e.*, 6, 16 and 40 g/L) appear different from each other. However, careful examination reveals that there is overlap between fibers in adjacent groups (*e.g.*, the lightest areas of fibers from the 16 g/L swatch are very similar in appearance to the darkest areas of fibers from the 6 g/L swatch) (Figure 241). This is directly analogous to the figures showing individual spectra and averages from fibers. There is definite overlap when examining individual spectra but the averaged spectra tend to lie further apart.

The fact that these are dyed cotton fibers easily explains the overlap. Cotton, and other natural fibers tend to pick-up dye unevenly, and the dye concentrations on the shade cards from which they were taken are nominal values (as commercial dyers are typically less interested in the absolute concentration than in achieving a specific color). We observed, both directly (through comparison microscopy) and instrumentally (via MSP), localized areas with dye levels that, in reality, amount to some unknown intermediate concentration (perhaps 11 g/L in the above example). This is an important consideration since many, if not most, fibers examined for their evidential value, are fiber fragments.

The majority of the more weakly dyed fibers (0.25 and 1.5 g/L) appear to be nearly colorless under the microscope and are difficult to distinguish from each other via comparison microscopy (Figure 242). Similarly, there is overlap between MSP spectra. As a consequence of the fibers' light colors, their spectra are relatively "noisy," making comparison and interpretation more difficult (*e.g.*, it is more difficult to determine the exact position of the absorbance maxima).

100 FIBER STUDY

As a follow-up, one-hundred cotton fibers dyed with Reactive Red (16 g/L) were analyzed by MSP (three spectra per fiber). Figures 243 and 244 show how the average changes as additional spectra are collected. Spectra were averaged in increments of ten fibers (*i.e.*, the thirty spectra from the first ten fibers, then the sixty spectra from the first twenty fibers, *etc.*). As

⁶⁹ The cotton fibers were analyzed in relatively wide, pristine areas (*i.e.*, areas presenting the maximum width with minimal twisting).

expected, the average fluctuates but appears to settle in as more fibers are averaged. If an infinite number of fibers from this sample were analyzed, we would expect the cumulative average to be located near the one-hundred fiber average as the general trend appears to be “zeroing-in” near this absorption.

The spectra of these fibers absorb minimal light at either end of the examined range (*i.e.*, $< \sim 280$ nm & $> \sim 620$ nm). By definition, the lack of signal causes noise to be more visible in these relatively flat regions. Also as expected, the noise at the low end of the spectrum decreases as additional spectra are collected (Figure 245). However, the “noise” at the high end of the spectrum does not significantly decrease as additional spectra are collected (Figure 246).⁷⁰ The presence of these nearly regular fluctuations, even after the averaging of three-hundred spectra collected over the course of five days, indicates that they are not the result of random noise, but are, rather, systemic.

The standard deviation at each abscissa point was also calculated in ten fiber increments (Figures 247 and 248). Unexpectedly, the standard deviation initially increases before settling in at a relatively consistent level for any particular wavelength.⁷¹ This is unexpected since standard deviation should decrease as sample size increases (assuming the random sampling of a population with a normal distribution). While the fibers were randomly sampled, the selections of collection areas on the fibers themselves were chosen to capture spectra from relatively light, moderate, and dark areas. Perhaps, this selection bias is preventing the standard deviation from decreasing with increasing sample size.

It is also interesting to note that there is a correlation between the absorbance and standard deviation across the majority of the spectrum (*i.e.*, the absolute value of the standard deviation essentially mirrors the absorbance spectrum) (Figure 249). This was initially unexpected but it makes intuitive sense when all three-hundred individual spectra are viewed together (Figure 250). Where there is no/little absorption (*i.e.*, at either end), the spectra cluster near zero absorbance, whether the fibers are relatively lightly or darkly colored (granted the darker fibers tend to exhibit some moderate absorbances in these regions). In this example, the three-hundred spectra have a range of absorbances of approximately 0.1 in these areas. In contrast, there is a much larger range in the regions of strong absorbance. For example, the range of absorbances is nearly 0.4 at ~ 507 nm (*i.e.*, the strongest absorbance peak observed with these fibers).⁷² The intervening wavelengths have intermediate absorbance ranges, and as a consequence, the absolute value of standard deviation mimics the general shape of the original absorbance spectra.

Interestingly, this correlation becomes inverted at the high end of the spectrum (*i.e.*, in this region an absorbance maximum results in a localized minimum in the standard deviation) (Figure 251). This inverse relationship affects the appearance of the plus and minus standard deviation plots (Figure 252). When the standard deviation is repeatedly subtracted from the average, the fluctuations increase in amplitude. In contrast, when the standard deviation is repeatedly added to the average, the fluctuations first essentially disappear, before increasing in amplitude, becoming easily discernable by plus three standard deviations. These consequences are obvious considering the shape of the absolute value of the standard deviation in this region (see Figure 251). It is unclear, however, as to why the standard deviation fluctuates like this in the first place.

Calculation of the standard deviation is affected by the format and choice of spectra used in the calculations. For example, all of the previously described plots in this section have dealt with standard deviations calculated from individual spectra. However, it is possible to calculate the standard deviation after sub-average spectra were generated for each of the fibers examined (*i.e.*, averages of the three spectra collected from each fiber). While the average spectra will be exactly the same,⁷³

⁷⁰ A similar effect is described in the “System Stability” section of this report.

⁷¹ However, there is considerable variation across the wavelength selected.

⁷² This large variation itself is rather interesting because all of the spectra were collected from cotton fibers dyed with the same nominal concentration (16 g/L). The amplitude at the major absorption peak ranges from ~ 0.032 to 0.42 (~ 38 - 93% transmission), when considering the individual spectra.

⁷³ Assuming the same number of spectra was collected from each fiber.

the standard deviation calculated from the sub-averaged spectra will be smaller compared to the standard deviation calculated using the original data (Figure 253). This is intuitive as the sub-averaging has significantly decreased the variation prior to the calculation of the standard deviation calculations in the latter case.

The standard deviation is also affected by whether it is calculated using absorbance or transmittance data (because absorbance scales linearly while transmission data is plotted on a logarithmic scale). There is a loss-less conversion between absorbance and transmission raw data but this does not hold true as soon a mathematical function is applied to the data (*e.g.*, calculations of averages, standard deviations, *etc.*). Figure 254 shows the average, and ± 1 and 2σ for the 300 cotton fibers dyed with reactive red, calculated using the same data in absorbance and transmission units.⁷⁴ Viewed another way, Figure 255 shows the absolute value of the standard deviation calculated using the absorbance data compared to the absolute values of ± 1 and 2σ ⁷⁵ calculated using the transmission data.⁷⁶ Careful examination of these two figures should confirm that calculating standard deviations using transmission data causes the positive standard deviations to be exaggerated, and the negative standard deviations to be depreciated. In contrast, ± 1 and 2σ spectra are all equally spaced from each other and the average when they are calculated and plotted using absorbance data (they become unequally spaced if they are plotted in transmission).

COMPARISON OF THE DATA FROM THE 100 FIBER STUDY TO THE ORIGINAL DATA

The original purpose of collecting spectra from 100 fibers in one group was to see how this large data set compared to the original data. Figure 256 shows the original data from the 16 g/L fibers with the ± 1 and 2 standard deviations generated from the 100 fiber experiment (also dyed at a concentration of 16 g/L). As expected, most spectra fall within one standard deviation and only one spectrum falls outside the range of two standard deviations. Most of the spectra from the more deeply dyed fibers (40 g/L) exhibit absorbances greater than $+2\sigma$, although several spectra fall within 1σ (Figure 257). The absorbances of essentially all of the lighter fibers (dyed at 6 g/L) fall within two standard deviations of the one-hundred fibers dyed at a concentration of 16 g/L (Figure 258). Again, this is a demonstration of the overlap between the fibers nominally dyed at different concentrations.

PRELIMINARY PCA ANALYSIS

As part of a collaboration with Dr. Michael Sigman of the University of Central Florida, principle component analysis (PCA) was used to answer a hypothetical question relating to this data set. In this experiment, the “known” sample consisted of the spectra from the 100 fibers dyed with Reactive Red at 16 g/L (300 total spectra). Spectra from fifteen “Q” fibers (four spectra per fiber) were also submitted (the original data of the three fibers from each of the five dye concentrations). The question posed was, “which, if any, Q fibers were dyed at the same concentration as the known fibers?”

⁷⁴ After the average and standard deviation were calculated using transmission data, the resulting spectra were converted back to absorbance in order to directly compare them to the average and standard deviation spectra calculated using the original absorbance data.

⁷⁵ The absolute value of $\pm 2\sigma$ was calculated by taking the difference between the $\pm 2\sigma$ spectra and the average spectrum, and then dividing this value by 2.

⁷⁶ While slightly confusing, the sign of the standard deviation becomes inverted when σ is calculated using absorbance or transmission data (*e.g.*, calculating $+1\sigma$ using absorbance data actually corresponds to calculating -1σ using transmission data). While technically incorrect, this report will call standard deviation spectra lying above the average as positive and those lying below the average as negative, regardless of whether they were calculated using absorbance or transmission data.

The answer⁷⁷ provided by Dr. Sigman's analysis included six fibers (#'s 5, 7, 8, 10, 11, and 15), while the correct answer has only three fibers (#'s 5, 7, and 15). In other words, the three Q fibers that belonged to the K's were identified but three additional fibers were also included. The Mahalanobis distances and known concentrations for each fiber are shown in Table 5.

Table 5. Mahalanobis distances and known concentrations

Fiber	Score*	Concentration (g/L)
15	1.201447	16
7	1.293276	16
5	1.61179	16
8	1.888898	6
10	2.120114	6
11	2.990152	1.5
4	3.242748	6
12	3.263865	1.5
2	3.677432	1.5
3	3.707898	0.25
6	3.724494	40
14	3.837	0.25
1	3.880018	0.25
9	6.904801	40
13	12.05669	40

* The double red horizontal line represents the defined cutoff between inclusion and exclusion.

It is interesting to note that the three correctly classified fibers (*i.e.*, those dyed to a nominal concentration of 16 g/L) have the lowest Mahalanobis scores. In other words, the classification is correct but the threshold was not properly adjusted.

This highlights one of the main themes regarding MSP and forensic science in general. The techniques and methods are scientifically sound but interpretation is sometimes difficult because it is not always clear where the "line" needs to be drawn regarding the inclusion or exclusion of samples as having potentially originated from a common source. Whether comparisons are made qualitatively by the visual examination of overlaid spectra or quantitatively using PCA, there is a somewhat subjective requirement of deciding where to draw this line.

⁷⁷ The spectra were converted to absorbance and adjusted so that the minimum absorption was zero for each spectrum. Known spectra from each fiber were averaged and the set of averaged spectra were subjected to PCA. Three principle components were retained and a cutoff was calculated at the 97.5% quantile for the Mahalanobis distances calculated for the knowns. The averages of the questioned spectra from each fiber were projected into the PCA space for the knowns and the Mahalanobis distances were calculated from the center of the known distribution to each of the questioned fibers. Questioned fibers having a Mahalanobis distance greater than the 97.5% quantile cutoff (3.057516) were considered outliers.

MICROSCOPIC DISCRIMINATION OF MACROSCOPICALLY SIMILAR FABRICS

Six fabric swatches with similar macroscopic colors known to have been colored with one of three different dyes were selected for examination using both comparison microscopy and MSP (each of the dyes was used to color a fabric swatch a relatively light or dark shade) (Figure 259). For this experiment, the three lighter fabrics were compared to each other and the three darker fabrics were compared to each other.

Table 6. Intralan Red dyes

Dye	Abbreviation	“Light” Concentration %	“Dark” Concentration %
Intralan Red 2G 200%	2G	0.25	1.00
Intralan Fast Red RB	RB	0.50	2.00
Intralan Red SG	SG	0.50	2.00

COMPARISON MICROSCOPY

Fibers from each of the dark and light swatches were compared to each other under a comparison microscope. The dark 2G and RB fibers were indistinguishable from each other (Figure 260), while comparison of the other dark fiber sets showed they were obviously different from each other (Figures 261 and 262). The colors exhibited by individual, lightly colored fibers are subtle, making comparisons difficult. However, it was determined that all three fibers could be differentiated from each other, with 2G and SG representing the closest pair (Figures 263 - 265).

MSP

All six pairs (three dark and three light) could be distinguished using MSP (Figures 266 - 271). It is noteworthy that the darkly dyed 2G and RB fibers exhibit obvious spectral differences, despite being indistinguishable using comparison microscopy alone (Figures 260 and 267). Light 2G and SG produce similar, although still different spectra, which agrees with the comparison microscopy (Figure 263 and 271). This difference is highlighted when the first derivative spectra are examined (Figure 272).

Finally, relative differences were observed when the spectra from the light and dark fibers from each of the three dyes were examined. Every spectrum collected from these fibers exhibits two principal absorbance bands located at ~ 350 – 380 nm and 485 – 515 nm. In the spectra from the dark fibers, the higher wavelength absorbance is always clearly dominant compared to the lower wavelength absorbance (Figures 273 - 275). In contrast, the two peaks have approximately the same intensity in the spectra collected from the light fibers, but the lower wavelength absorbance is actually stronger than the higher wavelength absorbance in spectra collected from the fibers lightly dyed with Intralan Fast Red RB. This result was not expected, as it was thought that relative peak heights would remain qualitatively constant as the concentration of a single dye was increased.

COMBINATIONS OF FOUR DYED FIBERS

Our reference collections contain a group of fourteen black swatches on a shade card that had been dyed with known concentrations of four potential nylanthrene dyes (Figure 276):

- Nylanthrene Black GLWC
- Nylanthrene Rubine 5BLF
- Nylanthrene Navy LFWG
- Nylanthrene Orange SLF

The fabric swatches appear macroscopically similar to each other and each fabric swatch was dyed with one, two, or three of the four potential dyes (total dye concentration of 4% in each swatch) Table 7.

Table 7. Dye concentrations in the fourteen black swatches

Swatch	Dye Concentration (%)			
	Black	Orange	Rubine	Navy
1	3	0.5	0.5	-
2	2.75	0.5	0.75	-
3	3.5	0.25	0.25	-
4	3.25	0.25	0.5	-
5	3	0.25	0.75	-
6	4	-	-	-
7	3.75	-	0.25	-
8	3.5	-	0.5	-
9	3.25	-	0.75	-
10	3.5	-	0.25	0.25
11	3.25	-	0.5	0.25
12	3	-	0.75	0.25
13	3	-	0.5	0.5
14	2.75	-	0.75	0.5

Several fibers were isolated from each swatch and then each of the 91 possible pairs was compared using both comparison microscopy and MSP (spectra were collected from a minimum of three fibers).⁷⁸ Figure 277 shows the results of these comparisons using a color coded scheme. Select examples from this chart will be used to describe the results of these analyses.

The majority (72) of the pairs can be differentiated using both comparison microscopy and MSP (examples of fiber pairs are shown in Figures 278 and 279). This demonstrates the sensitivity and discriminating power of each of these techniques. However, eight pairs cannot be differentiated using either comparison microscopy or MSP (see Figures 280 - 282 for examples). The majority (six) of these pairs have different relative navy and black dye concentrations. This makes intuitive sense as the dark navy is similar in color to black. In fact, with one exception (pair 8 & 11), these pairs represent all of the pairs that differ only in their relative concentrations of black and navy dyes. The other two indistinguishable pairs (2 & 5 and

⁷⁸ Supplementary MSP data was collected from additional fibers when it was difficult to determine whether a particular pair could be distinguished using this technique.

3 & 7) have small relative changes in their orange and black dye concentrations. Interestingly, all of the fibers representing these two pairs are also colored with red dye, which may make it more difficult to detect the minor amounts of added orange dye. The relative dye differences are summarized in Table 8.

Table 8. Differences in dye concentrations of fibers indistinguishable by both comparison microscopy and MSP

Swatch Pair		Relative Differences in Dye Concentration (%)			
		Black	Orange	Navy	Rubine
2	5	0.25	0.25	-	-
3	7	0.25	0.25	-	-
7	10	0.25	-	0.25	-
8	13	0.5	-	0.5	-
9	12	0.25	-	0.25	-
9	14	0.5	-	0.5	-
11	13	0.25	-	0.25	-
12	14	0.25	-	0.25	-

Additionally, there are some pairs where fibers could only be distinguished by one of the two methods. One pair (8 & 11) could be differentiated using comparison microscopy, but not MSP (Figure 283). This is the only pair with a relative black and navy dye concentration difference (0.25%) which could be differentiated.

The remaining ten pairs could be differentiated by MSP, but not by comparison microscopy (examples are shown in Figures 284 - 288). All of these pairs, with the exception of pair 4 & 12, have differences between their relative black/navy and rubine/orange dye concentrations. Again, this makes intuitive sense as the black and navy are similar to each other just as the red and orange are similar to each other. Interestingly, pair 4 & 12 exhibits relative differences in each of the four dye concentrations. The relative dye differences are summarized in Table 9.

Table 9. Differences in dye concentrations of fibers distinguishable by MSP and indistinguishable by comparison microscopy

Swatch Pair		Relative Differences in Dye Concentration (%)			
		Black	Orange	Navy	Rubine
2	9	0.5	0.5	-	-
2	14	-	0.5	0.5	-
3	10	-	0.25	0.25	-
4	12	0.25	0.25	0.25	0.25
5	9	0.25	0.25	-	-
5	12	-	0.25	0.25	-
6	7	0.25	-	-	0.25
10	11	0.25	-	-	0.25
10	13	0.5	-	0.25	0.25
11	12	0.25	-	-	0.25

In summary, 91% of these pairs, which were dyed using the same restricted group of dyes, and differed only by subtle differences in their concentrations, could be differentiated by comparison microscopy or MSP (*i.e.*, 9% could not be distinguished using either method).⁷⁹ Both techniques were able to distinguish 79% of the pairs. In this data set, MSP has slightly more discriminating power (90% versus 80% for comparison microscopy), but it is important to note that comparison microscopy was also able to differentiate one pair which was indistinguishable by MSP.

With regard to absolute dye intensity differences, all pairs could be distinguished when there was a concentration difference greater than 0.5% for any individual dye. Pairs which had a difference of 0.5%, for any individual dye, could be differentiated 95% of the time while pairs which had a difference of 0.25% could be differentiated 81% of the time.

FIBERS WITH INDIVIDUAL DYES

In a follow-up experiment, fibers dyed with the individual rubine, orange, and navy nylanthrene dyes⁸⁰ discussed above were located in our reference collection.⁸¹ MSP spectra were collected from these fibers and compared to the spectra of fibers isolated from swatch 6 (which only had the black dye⁸²) (Figure 289). The main absorbance of the navy dye (~ 620 nm) corresponds exactly with one of the main absorptions of the black dye. This explains why it was difficult to differentiate pairs which had different relative concentrations of these two dyes (discussed above). It is also interesting to note that the main absorbance of the orange dye (~ 450 nm) corresponds exactly with the other main absorption of the black dye. In contrast, the main absorption of the rubine dye (~ 540 nm) does not correspond to a major absorption of any of the other dyes. This explains why the relative differences in rubine concentration, compared to the any of the other dyes concentrations, were always distinguishable. Figure 290 shows the effect of increasing rubine dye concentration at the expense of black dye concentration. As expected, the absorption minimum at ~ 545 nm when only black dye is present becomes less pronounced as the concentration of rubine dye, which has an absorption peak at ~ 540 nm, increases. Table 10 shows a summary table of all of the pairs which involve differences in the relative dye concentrations of only two dyes (*e.g.*, a pair which differs only in their black vs. rubine concentrations).

Table 10. Summary of pairwise comparisons involving head-to-head relative dye differences

Dye comparison	Number of Pairs Differentiated Using:			
	Both MSP and Comparison Microscopy	Only MSP	Only Comparison Microscopy	Neither MSP nor Comparison Microscopy
Black vs. Rubine	11	3	-	-
Black vs. Navy	-	-	1	6
Black vs. Orange	3	2	-	2
Rubine vs. Navy	1	-	-	-
Rubine vs. Orange	1	-	-	-

The exact correlation between the two absorbance peaks of the black dye with the main absorbance peaks of the navy and orange dyes seemed suspicious (*i.e.*, perhaps the “black” dye was actually composed of a mixture of the navy and orange dyes). This suspicion was supported when the averaged spectra collected from the navy and orange fibers were added

⁷⁹ These fibers are not fluorescent and could not, therefore, be differentiated using fluorescence microscopy or MSF.

⁸⁰ Each of these fibers was dyed by the manufacturer at a concentration of 2%.

⁸¹ Although also nylon, these fibers were unrelated to the shade card with the fourteen black swatches utilized in the previous experiments.

⁸² These fibers were dyed at a concentration of 4%.

together (Figure 291).⁸³ While not exactly the same, there is a striking similarity between this synthetic spectrum and the actual averaged spectra collected from the fibers that had been dyed with only the black dye (*i.e.*, from swatch 6).

The dyes were extracted from the subsamples of black, navy, orange, and rubine nylon fibers and developed on a high performance thin layer chromatography (HPTLC) plate in an effort to confirm or refute this hypothesis (Figure 292). Tellingly, the black lane has two distinct bands, one dark blue and the other orange. These two bands have similar retention factors (R_f) as the bands from the navy and orange fibers (although there is some variability in these R_f values when replicate TLC plates are eluted). In conclusion, the purported “black” dye from the shade card is apparently a mixture of the navy and orange dyes (although other dyes may also be present at lower concentrations). Raman spectra collected from the yellow band was similar in the black and orange lanes; however, the dark band has a different spectrum in the black and navy lanes.

CHEMICALLY SIMILAR DYES

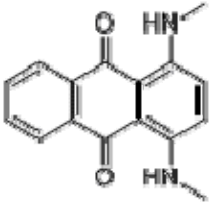
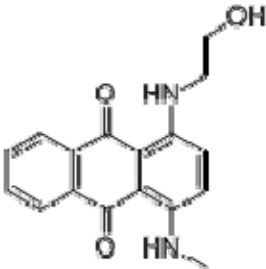
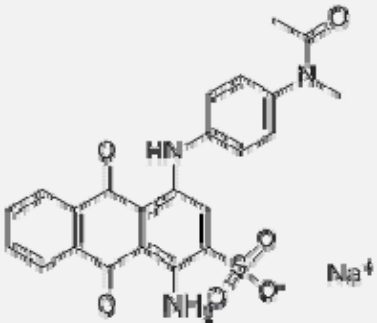
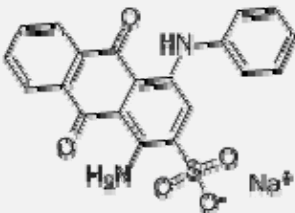
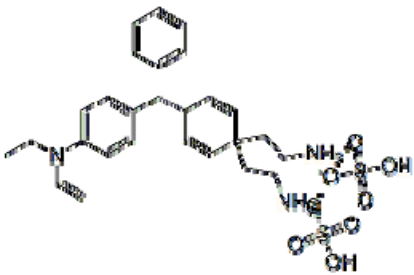
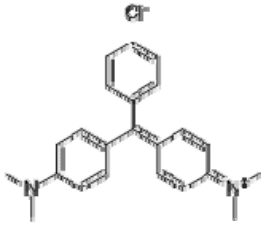
The following work was conducted as part of a collaboration between our laboratory and Dr. Michael Sigman of the University of Central Florida. Six fabrics dyed with six different, but closely related blue dyes were submitted for examination (Figure 293) by traditional microscopical methods (*i.e.*, comparison microscopy and manual overlay interpretation). The samples are listed below:

- Pair 1 (acetate fibers)
 - Disperse Blue 14 (MT Colorants Sample C-65211)
 - Disperse Blue 3 (MT Colorants Sample C-65212)
- Pair 2 (nylon fibers)
 - Acid Blue 41 (Sample C-65213)
 - Acid Blue 25 (Sample C-65214)
- Pair 3 (acrylic fibers)
 - Basic Green 1 (Sample C-65215)
 - Basic Green 4 (Sample C-65216)

Each pair consisted of two fabric samples which had been colored with one of two structurally similar dyes, as shown in Table 11. These pairs were examined using comparison microscopy, MSP, and TLC in order to determine if they were distinguishable from one another.

⁸³ Fortuitously, the fibers colored with the navy and orange dyes were both dyed at a concentration of 2% while the fibers colored with the black dye were dyed at a concentration of 4%. This coincidence, which makes a simple spectral addition reasonable, is offset by the fact that the fibers dyed with the navy and orange dye are different than the fibers dyed with the black dye. Similarly, even if the hypothesis that the “black” dye is actually composed of a combination of navy and orange dyes is correct, there is no reason to believe that the two dyes are present in the same concentration (*i.e.*, 2% of each).

Table 11. Dye structures

Pair 1	
Disperse Blue 14	Disperse Blue 3
	
Pair 2	
Acid Blue 41	Acid Blue 25
	
Pair 3	
Basic Green 1	Basic Green 4
	
Above structures from http://www.chemicalbook.com/ProductIndex_EN.aspx	

COMPARISON MICROSCOPY

Comparison microscopy was performed on fibers from each of the three pairs. A pair was said to be indistinguishable if a single fiber from one source could not be differentiated from a single fiber from the other source (regardless of how different the other fibers from the samples appeared).

Pair 1: Disperse Blue 14 (1) vs. Disperse Blue 3 (2) on acetate.

Observations:

The fibers dyed with Disperse Blue 14 are much lighter compared to those dyed with Disperse Blue 3 (Figure 294). The fibers were dyed thoroughly with very little variation in the dye shade along the length. It was also noted that the fibers dyed with Disperse Blue 3 contained more delustrant particles compared to the other sample, although this was not considered as a distinguishing characteristic for the purposes of this study.

Conclusion:

The fibers from these two samples can be distinguished using comparison microscopy.

Pair 2: Acid Blue 41 (3) vs. Acid Blue 25 (4) on nylon.

Observations:

The fibers dyed with Acid Blue 25 are darker than those dyed with Acid Blue 14 (Figure 295). The amounts of delustrant particles are very similar between the two samples.

Conclusion:

The fibers from these two samples can be distinguished using comparison microscopy.

Pair 3: Basic Green 1 (5) vs. Basic Green 4 (6) on acrylic.

Observations:

The fibers dyed with Basic Green 4 are slightly darker than those dyed with Basic Green 1 (Figure 296). The obvious size difference, while reproducible, was not considered as a distinguishing characteristic for the purposes of this study.

Conclusion:

Although they are quite similar in color, the fibers from these three samples can be distinguished using comparison microscopy.

MSP

- Five fibers from each fabric were studied.⁸⁴
 - Three scans were collected from each fiber (the following figures display the average of each individual fiber)
 - The #4 aperture was used on the MSP
 - Xylene was used as the mounting medium
 - Spectra were collected from 200-800 nm
- The spectra were examined in transmission, absorbance, and as first derivatives

Acid Blue 25 vs. Acid Blue 41

Observations:

While the fibers from the fabrics produce spectra with similar shapes, there are many differences between them (Figure 297). At ~ 390 nm, Acid Blue 25 has a minor, but distinct, absorption peak while Acid Blue 41 has only a shoulder. At ~ 600 nm, there is a large difference in the overall absorbance between the two dyes.

Conclusion:

The fibers from these two samples can be distinguished using MSP.

Disperse Blue 3 vs. Disperse Blue 14

Observations:

The spectra from Disperse Blue 3 and Disperse Blue 14 both exhibit absorption peaks at ~ 580 and 660 nm (Figure 298). However, in Disperse Blue 3, the lower wavelength peak exhibits distinctly greater relative absorbance whereas the higher wavelength peak is more intense in Disperse Blue 14. Inspection of the spectra will show other differences between the spectra from the two dyes as well.

Conclusion:

The fibers from these two samples can be distinguished using MSP.

Basic Green 1 vs. Basic Green 4

Observations:

The spectra from these two samples appear quite similar to each other (Figure 299). This is not unexpected as they were also difficult to distinguish using comparison microscopy. While subtle, the most obvious spectral difference, when viewing the absorbance data, occurs near the strongest absorption peak (~ 630 nm). Basic Green 1 has a sharper absorption peak in this region while Basic Green 4 has a broader peak, which is also slightly shifted towards lower wavelengths. Additional spectral differences are highlighted when first derivative spectra are compared (*e.g.*, ~ 570 and 600 nm) (Figure 300). These leave no doubt about the differences between the dyes in the two fibers.

⁸⁴ This sample size is similar to what we would typically use when performing casework, especially with man-made fibers displaying limited amounts of intra-sample variability. Additional samples can always be studied when deemed necessary but definitive conclusions can generally be reached using samples of this size. This is especially important when dealing with complex cases involving large numbers of samples.

THIN LAYER CHROMATOGRAPHY

The first two pairs of these dyed fibers were extracted in pyridine:water for dye comparison by TLC.⁸⁵ The extracts were dried, spotted and separated on HPTLC plates. These results are consistent with the microscopical results and showed that the dyes could be readily distinguished by TLC (Table 12).

Table 12. Comparison of TLC results

Pair	Dye	Extracted	TLC Result	MSP/Comparison Result
Pair 1 (Acetate)	Disperse Blue 14	Yes	Different by Rf	Distinguished by comparison microscopy and MSP
	Disperse Blue 3	Yes		
Pair 2 (Nylon)	Acid Blue 41	Yes	Different by Rf, Shape and Fluor.	Distinguished by comparison microscopy and MSP
	Acid Blue 25	Yes		
Pair 3 (Acrylic)	Basic Green 1	No	Not run	Distinguished by comparison microscopy and MSP
	Basic Green 4	No		

CONCLUSION

All of the fibers from the dyed fabric pairs can be distinguished from one another through both comparison microscopy and MSP with overlay comparison.

MACROSCOPICALLY SIMILAR YARNS

This subproject was also conducted in association with Michael Sigman's research group. Five red and five blue yarn samples, judged to be macroscopically similar, were supplied by Prof. Sigman (Figure 301). The dye or dyes used to color each of these yarns were not known. Fibers from these two sets were examined using comparison microscopy, MSP, and TLC in order to determine if they could be distinguished from one another. Each yarn was given a letter code (A – J) as illustrated in Figure 301 and summarized (Tables 13 and 14).

⁸⁵ The dyes present in pair 3 did not extract.

Table 23. Summary of red yarns

Code	Fiber Type	Name	Nominal Color
A	100% Acrylic	Caron Simply Soft	Red 9729
B	100% Acrylic	Lion Brand Micro Spun	113 Cherry Red
C	100% Acrylic	Caron Wintuk	Christmas Red 3005
D	100% Acrylic	Red Heart Sport	0912 Cherry Red
E	100% Acrylic	Lion Brand Jiffy	114 True Red

Table 34. Summary of blue yarns

Code	Fiber Type	Name	Nominal Color
F	100% Acrylic	Bernat Satin	04110 (Admiral)
G	100% Acrylic	Caron Simply Soft Quick	Navy 0005
H	100% Acrylic	Red Heart Super Saver	0387 Soft Navy
I	100% Acrylic	Caron Simply Soft	DK Country Blue 9711
J	100% Acrylic	Berant Satin Sport	03110 (Marina)

COMPARISON MICROSCOPY

Fibers from each yarn were mounted in xylene on microscope slides and compared to each other. The focus of this comparison was color alone and other fiber attributes (*e.g.*, diameter, cross-sectional shape, *etc.*) were not considered as cause for discrimination.

Each of the ten possible pairs of red fibers and each of the ten possible pairs of blue fibers were examined using a comparison microscope. A pair was said to be indistinguishable if a single fiber from one source could not be differentiated from a single fiber from the other source (regardless of how different the other fibers from the samples appeared). Figures 302 - 311 show representative photomicrographs of the red fiber comparisons and figures 312 - 321 are photomicrographs representing the blue pairs. All of the pairs could be distinguished by comparison microscopy (looking at color, rather than diameter) except for:

- Red fiber pairs
 - A & D (Figure 304)
 - B & C (Figure 306)
- Blue fiber pairs
 - F & J (Figure 315)
 - G & I (Figure 317)

MSP

Although most of the pairs were distinguishable using comparison microscopy, MSP spectra were collected from fibers from each yarn and the spectra representing all possible combinations were examined and compared.

- Five fibers from each yarn were studied.
 - Three scans were collected from each fiber (the following figures display the average of each individual fiber)
 - The #4 aperture was used on the MSP
 - Xylene was used as the mounting medium
 - Spectra were collected from 200-800 nm
- The spectra were examined in transmission, absorbance, and as first derivatives

Spectrally Similar Red Yarn Pairs

A & D

Surprisingly, the spectra from yarns A & D, which were indistinguishable using comparison microscopy, are quite different from each other (Figure 322). The spectrum from sample D exhibits a distinct shoulder between $\sim 440 - 480$ nm, which is not present in sample A. Also, the main absorbance peak in sample D is shifted to the right (*i.e.*, higher wavelength) of the main absorbance peak in sample A.

B & C

The other pair of red fibers that was indistinguishable by comparison microscopy (*i.e.*, B & C), exhibit similar MSP spectra, although there are some intensity differences (Figure 323). The most notable differences are the slopes between ~ 370 and 440 nm, with sample C exhibiting greater absorbance in this region. This difference can be more easily visualized in a plot of the first derivative spectra (Figure 324). Additional spectra were collected from each sample, which narrowed the gap between these two samples (Figure 325).

It is possible that some of these differences are due to the fact that the fibers from sample C are slightly thicker, and therefore present a greater path length for absorption to occur (Figure 306). Consequently, it becomes difficult to ignore certain fiber characteristics (*e.g.*, diameter) and focus solely on color because MSP data is providing intensity information as well.

Figures 326 and 327 show absorbance and first derivative spectra from two individual fibers (one from each yarn). While not exact duplicates, they are quite similar and may represent the same or very similar hues, but because of variation in fiber diameter between the samples, they appear slightly different.

C & D

The spectra from fibers C and D (Figure 328) appear more similar than might be expected given how dissimilar they appear by comparison microscopy (Figure 310). However, there are distinct and reproducible differences between these two samples, perhaps more easily visualized when looking at their first derivative spectra (Figure 329).

Other Red Yarn Pairs

As expected, all of the other red yarn pairs exhibit distinctly different spectra (Figures 330 - 336).

Spectrally Similar Blue Yarn Pairs

G & I

In general, the spectra from yarns G and I exhibit very similar spectral shapes and have similar ranges of absorption (Figure 337). This is not unexpected based on their similar appearance using comparison microscopy. Examination of their first derivative spectra does not unveil any reproducible differences (Figure 338). Figures 339 - 342 show absorbance and first derivative spectra from fiber pairs which have particularly similar spectra.

F & J

Interestingly, the spectrum from fiber sample J appears to be bimodal with respect to absorbance intensity (*i.e.*, there is a distinct gap between fibers which have relatively high absorbance values and those with relatively low absorbance values) (Figure 343).⁸⁶ Additional spectra, obtained from new fibers, were collected from this sample while maintaining consistent fiber positioning in order to rule out potential orientation effects (*i.e.*, possible dichroic fibers producing varied spectra as a result of uncontrolled orientation in an MSP system with latent polarization). These additional spectra proved that orientation is not the cause of this bimodal absorbance distribution (Figure 344).

Only the more deeply colored fibers from sample J have spectra similar to the spectra collected from sample F (Figures 345 and 346). Figures 347 - 350 show absorbance and first derivative spectra from fiber pairs, which have particularly similar spectra, although there are some minor differences in the fine spectral details between ~ 550 – 590 nm. At this level of analysis, we would, in practice, hesitate to conclude that these two samples were different.

Other Blue Yarn Pairs

As expected, all of the other blue yarn pairs exhibit distinctly different spectra (Figures 351 - 358).

TLC

Fibers were extracted in pyridine:water and separated on HPTLC plates. The extracts were dried, spotted and chromatographed. The TLC results are consistent with the microscopy results, which showed that pairs that could not be distinguished by comparison microscopy or MSP could not be distinguished by TLC (the converse also holds). These results suggest strongly that these yarns used the same combination of dyes to achieve the same colors. Of particular interest is the pair G/I, which are qualitatively similar by all methods of comparison; however, TLC suggests a possible quantitative difference in the amount of the blue component by TLC (further experimentation would be required to confirm this suggestion).

⁸⁶ All of the spectra from the fibers exhibiting the low absorbance have similar intensities (*i.e.*, the relatively low absorbance is consistent along the lengths of these particular fibers and therefore the averaged spectra displayed in Figure 268 are not the result of one anomalous spectrum).

Table 45. Comparison of TLC results

Sample	Color	Extracted	TLC	TLC Result	Raman Result	MSP/Comparison Result [§]
A	Red	Yes	DNR*			Differentiated by MSP
D	Red	Yes	Yes	Similar by TLC	Similar by Raman	Similar by Comparison
B	Red	Yes	Yes			Similar by MSP/Comparison
C	Red	Yes	Yes			
E	Red	Yes	DNR*			
F	Blue	Yes	Yes	Similar by TLC	Similar by Raman	Similar by MSP/Comparison
J	Blue	Yes	Yes			
G	Blue	Yes	Yes	Similar by TLC [#]	Similar by Raman	Similar by MSP/Comparison
I	Blue	Yes	Yes			
H	Blue	Yes	DNR*			

[§]This table only presents selected MSP and Comparison results. Please see earlier data and text for a full discussion of these results.

*DNR: Did not run. This sample is not part of a group of samples identified by MSP and comparison microscopy as indistinguishable.

[#]TLC spectra are qualitatively similar based on number of bands, Rf values, and band fluorescence; however, the blue bands have different intensities, suggesting a possible quantitative difference in dye concentration between these two samples.

CONCLUSIONS

All of the red and blue yarn pairs can be distinguished by employing comparison microscopy or MSP except for the following:

- Red yarns:
 - A & D – these yarns are indistinguishable by comparison microscopy but are readily differentiated by MSP
 - B & C – these yarns are indistinguishable by comparison microscopy alone and have very similar MSP spectra. The slight spectral differences between these two yarns are mostly due to absorbance intensity variations, which may be caused by the differing diameters of the fibers (which we were trying to ignore in this particular study).
- Blue yarns:
 - G & I – these fibers are indistinguishable from each other by both comparison microscopy and MSP
 - F & J – these fibers are indistinguishable by comparison microscopy and have very similar MSP spectra. While there are some very slight variations with regards to fine spectral detail, these differences are not convincing enough at this level of analysis to conclude that they are distinctly different.

XI - REFERENCES AND BIBLIOGRAPHY

- Adolf, F., and Dunlop, J. (1999). *Microspectrophotometry / colour measurement*. In J. Robertson and M. Grieve (Eds.), *Forensic examination of fibres* (2nd ed.). Boca Raton, Florida: CRC Press.
- Barrett, J. A., Siegel, J. A., and Goodpaster, J. V. (2010). Forensic Discrimination of Dyed Hair Color: I. UV-Visible Microspectrophotometry. *Journal of Forensic Sciences*, 55 (2), 323 - 333.
- Bart, J. C. J. (2005). Additives in polymers: industrial analysis and applications (pp. 322 – 323). Chichester: John Wiley & Sons.
- Beck, K. R., Hinks, D., Crawford, A. and Weisner, N. (2012). Liquid Chromatographic and Mass Spectrometric Analysis of Dyes for Forensic Purposes . *AATCC Review*, 12 (1), 60 – 65.
- Buzzini, P. and Massonnet, G. (2007). The analysis of colored acrylic, cotton, and wool fibers using Raman spectroscopy. *Proceedings of the FBI Trace Evidence Symposium, Clearwater, FL*.
- De Wael, K. and Vanden Driessche, T. (2011a). Dichroism measurements in forensic fibre examination. Part 1 – dyed polyester fibres. *Science and Justice*, 51, 57 – 67.
- De Wael, K. and Vanden Driessche, T. (2011b). Dichroism measurements in forensic fibre examination. Part 2 – dyed polyamide, wool and silk fibres. *Science and Justice*, 51, 163 – 172.
- De Wael, K. and Lepot, L. (2011). Dichroism measurements in forensic fibre examination. Part 3 – dyed cotton and viscose fibres. *Science and Justice*, 51, 173 - 186.
- De Wael, K. (2012). Dichroism measurements in forensic fibre examination. Part 4 – dyed acrylic and acetate fibres. *Science and Justice*, 52, 81 – 89.
- De Wael, K. and Lepot, L. (2012). Dichroism measurements in forensic fibre examination. Part 5 – pigmented fibres. *Science and Justice*, 52, 161 - 167.
- De Wael, K., Lepot, L. and Lunstroot, K. (2012). Dichroism measurements in forensic fibre examination. Part 6 – validation and practical aspects of MSP-PPL. *Science and Justice*, 52, 249 - 258.
- European Fibres Group Best Practise Guidelines (n.d.). *Microspectrophotometry of textile fibres*.
- Eyring, M.B. (2002). Visible Microscopical Spectrophotometry in the Forensic Sciences. In R. Saferstein (Ed.), *Forensic Science Handbook, Vol 1* (2nd ed.). Upper Saddle River, NJ: Prentice Hall.
- Goodpaster, J. V., and Liszewski, E. A. (2009). Forensic analysis of dyed textile fibers. *Analytical and Bioanalytical Chemistry*, 394, 2009-2018.
- Hartshorne, A.W. and Laing, D.K., (1991). Microspectrofluorimetry of fluorescent dyes and brighteners on single textile fibres: Part 1 — Fluorescence emission spectra. *Forensic Science International*, 51 (2) 203-220.
- Kubic, T. A., King, J. E., and DuBey, I. S. (1983). Forensic analysis of colorless textile fibers by fluorescence microscopy. *The Microscope*, 31, 213-222.
- Liszewski, E.A., Lewis, S.W., Siegel, J.A., and Goodpaster, J.V. (2010). Characterization of Automotive Paint Clear Coats by Ultraviolet Absorption Microspectrophotometry with Subsequent Chemometric Analysis. *Applied Spectroscopy*, 64 (10), 1122 - 1125.

- Morgan, S.L., Nieuwland, A.A., Mubarak, C.A, Hendrix, J. E., Enlow, E. M., Vasser, E. M., and Bartick, E.G. (2004). Forensic Discrimination of Dyed Textile Fibers using UV-VIS and Fluorescence Microspectrophotometry, Proceedings of the European Fibres Group (Annual Meeting, Prague, Czechoslovakia).
- Morgan, S.L., Hall, S.H., Hendrix, J.E., and Bartick, E.G. (2007a). Pattern recognition methods for the classification of trace evidence textile fibers from UV/visible and fluorescence spectra. Proceedings of the FBI Trace Evidence Symposium, Clearwater, FL.
- Morgan, S.L., Vann, B. C., Baguley, B. M., and Stefan, A. R. (2007b). Advances in discrimination of dyed textile fibers using capillary electrophoresis/mass spectrometry. Proceedings of the FBI Trace Evidence Symposium, Clearwater, FL.
- Morris, J. (2013). How Sample Handling Can Contaminate the Analytical Results of Trace Evidence Examinations. MAFS 2013 Annual meeting.
- Palenik, S. J. (1999). Microscopical Examination of Fibres. In J. Robertson and M. Grieve (Eds.), Forensic examination of fibres (2nd ed.). Boca Raton, Florida: CRC Press.
- Palenik, S.J. (2007). Heavy Minerals in Forensic Science. In M. A. Mange and D. T. Wright (Eds.), Heavy Minerals in Use. Amsterdam, The Netherlands: Elsevier.
- Palenik, S. J. and Fitzsimons, C. (1990a). Fiber Cross-Sections: Part I. The Microscope, 38, 187-195.
- Palenik, S. J. and Fitzsimons, C. (1990b). Fiber Cross-Sections: Part 2 - A simple method for sectioning dingle fibers. The Microscope, 38, 313-320.
- Palenik, S.J. and Palenik, C.S. (2005). Microscopy and microchemistry of physical evidence. In R. Saferstein (Ed.), Forensic Science Handbook, Vol 2 (2nd ed.). Upper Saddle River, NJ: Prentice Hall.
- Peterson, L.K. (2010). Microspectrophotometry (MSP) of Blood – An Update. The Microscope, 58 (2) 81-84.
- Purcell, D. K. (2013). UV-visible microscope spectrophotometric polarization and dichroism with increased discrimination power in forensic analysis, Ph.D. dissertation, CUNY.
- Steele, K. (2009). Photobleaching of Fibers by UV-Visible-NIR Microspectrophotometry. Proceedings of the FBI Trace Evidence Symposium, Clearwater, FL.
- Suzuki, S., Suzuki, Y., Ohta, H., Sugita, R., and Marumo, Y. (2001). Microspectrophotometric Discrimination of Single Fibres Dyed by Indigo and its derivatives using Ultraviolet-visible Transmittance Spectra. Science and Justice, 41 (2), 107 - 111.
- SWGMAAT (2007). Standard Guide for Microspectrophotometry and Color Measurement in Forensic Paint Analysis. www.swgmat.org.
- SWGMAAT (2011). Ultraviolet-Visible Spectroscopy of Textile Fibers. www.swgmat.org.
- SWGMAAT (n.d.). Forensic Fiber Examination Guidelines. www.swgmat.org.
- White, K.M. (2011). Statistical analysis of visible absorption spectra and mass spectra obtained from dyed textile fibers. M.S. Thesis, University of Central Florida.

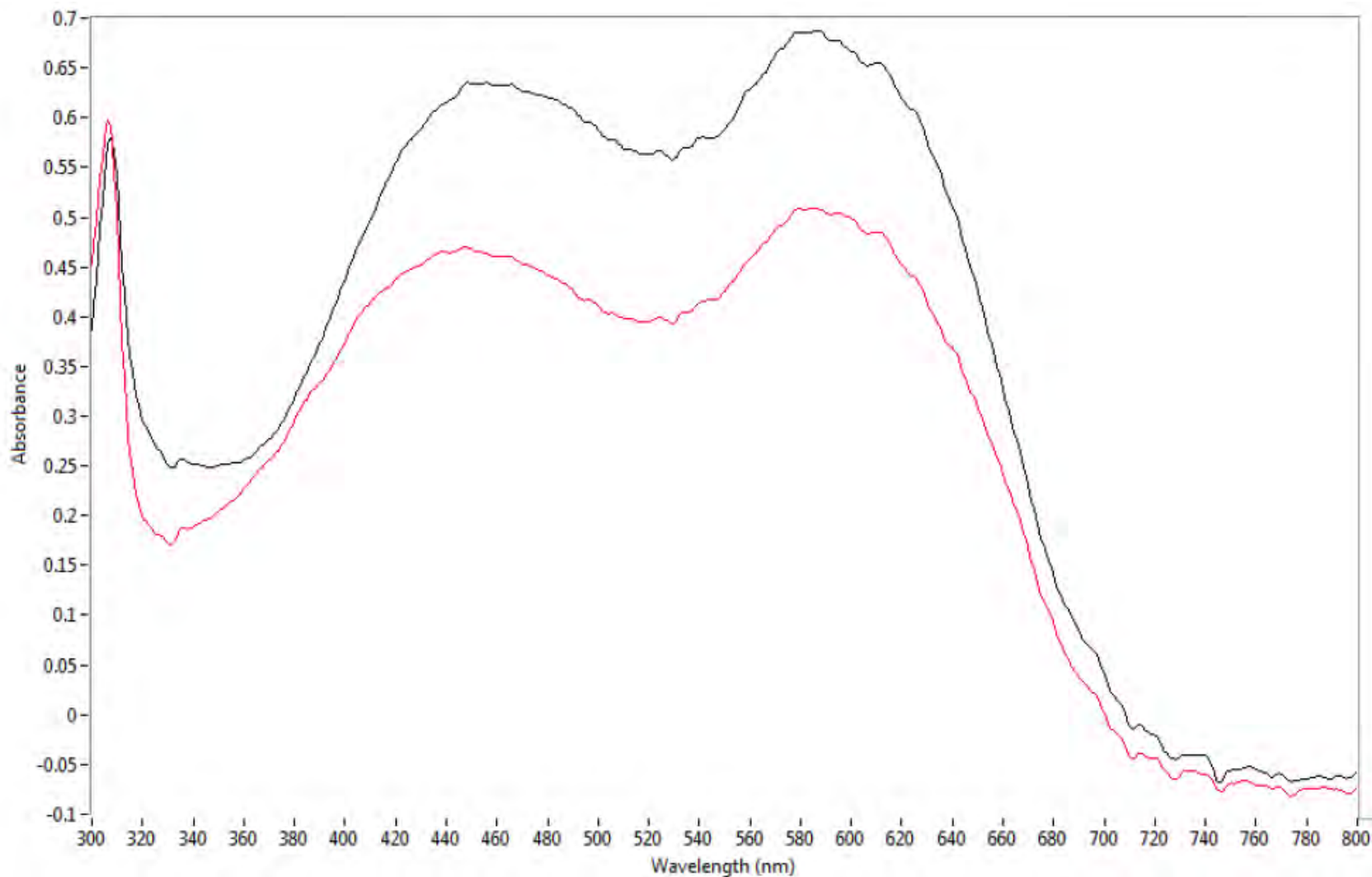


Figure 1. MSP spectra collected from questioned (black) and known fibers (red). It was concluded that the fibers could not be associated with a common source (although they shared many spectral, physical, and chemical consistencies). This conclusion was subsequently confirmed when new information (independent of this data collection) was uncovered.

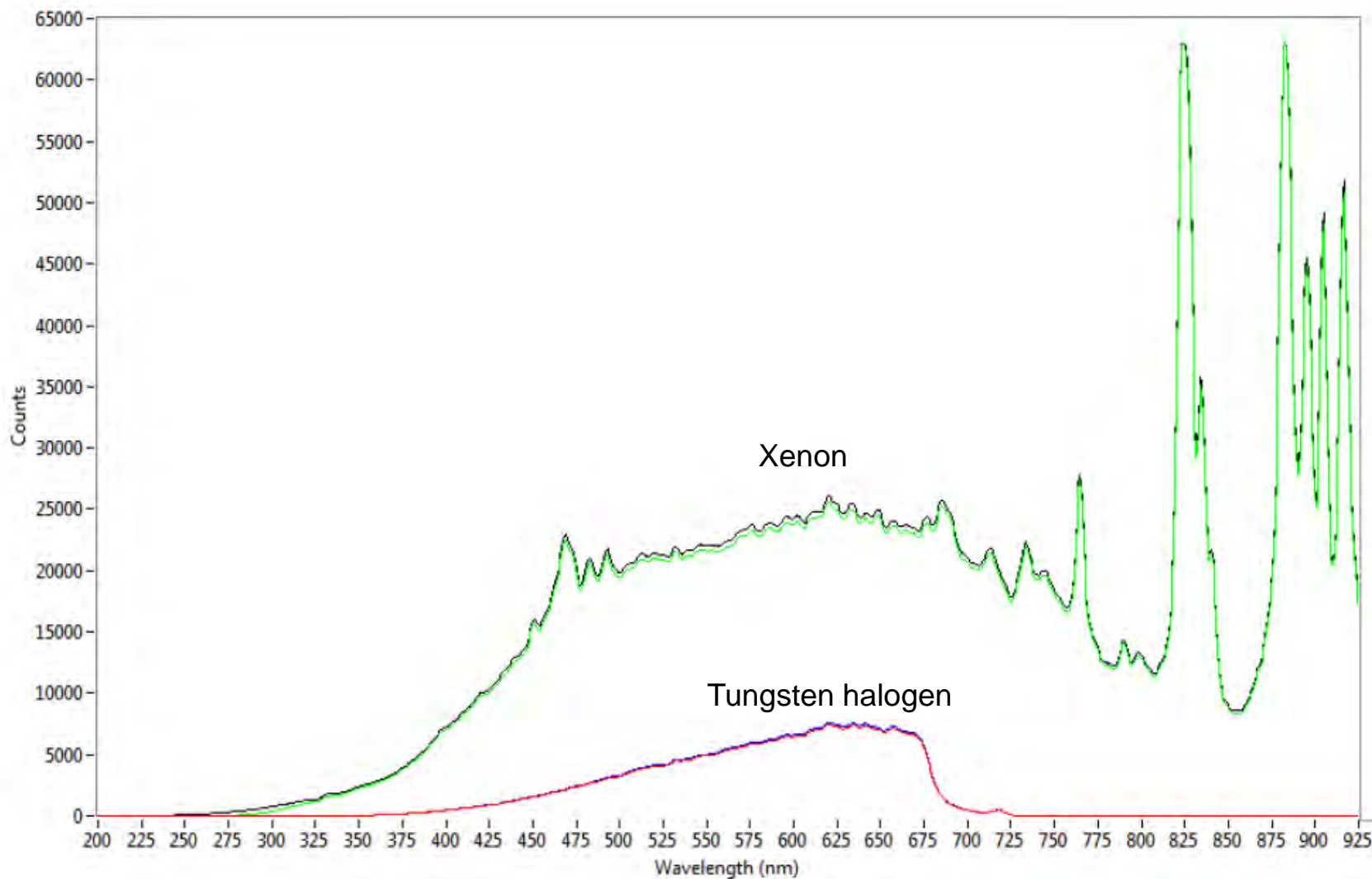


Figure 2. Emission spectra collected using both xenon (upper) and tungsten halogen (lower) bulbs through quartz (black & blue) and glass (green & red) slides.

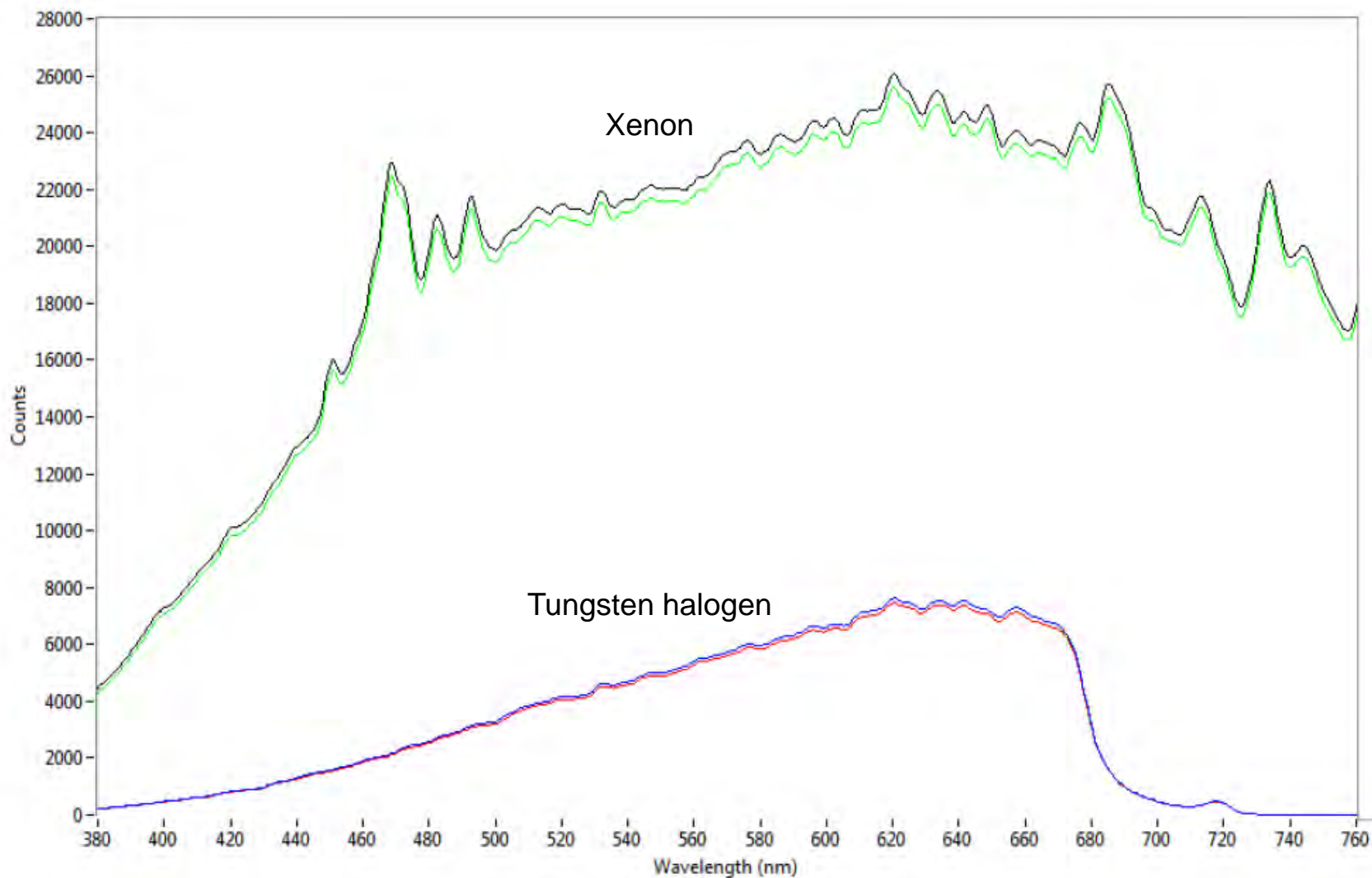


Figure 3. Emission spectra collected using both xenon (upper) and tungsten halogen (lower) bulbs through quartz (black & blue) and glass (green & red) slides (380 – 760 nm).

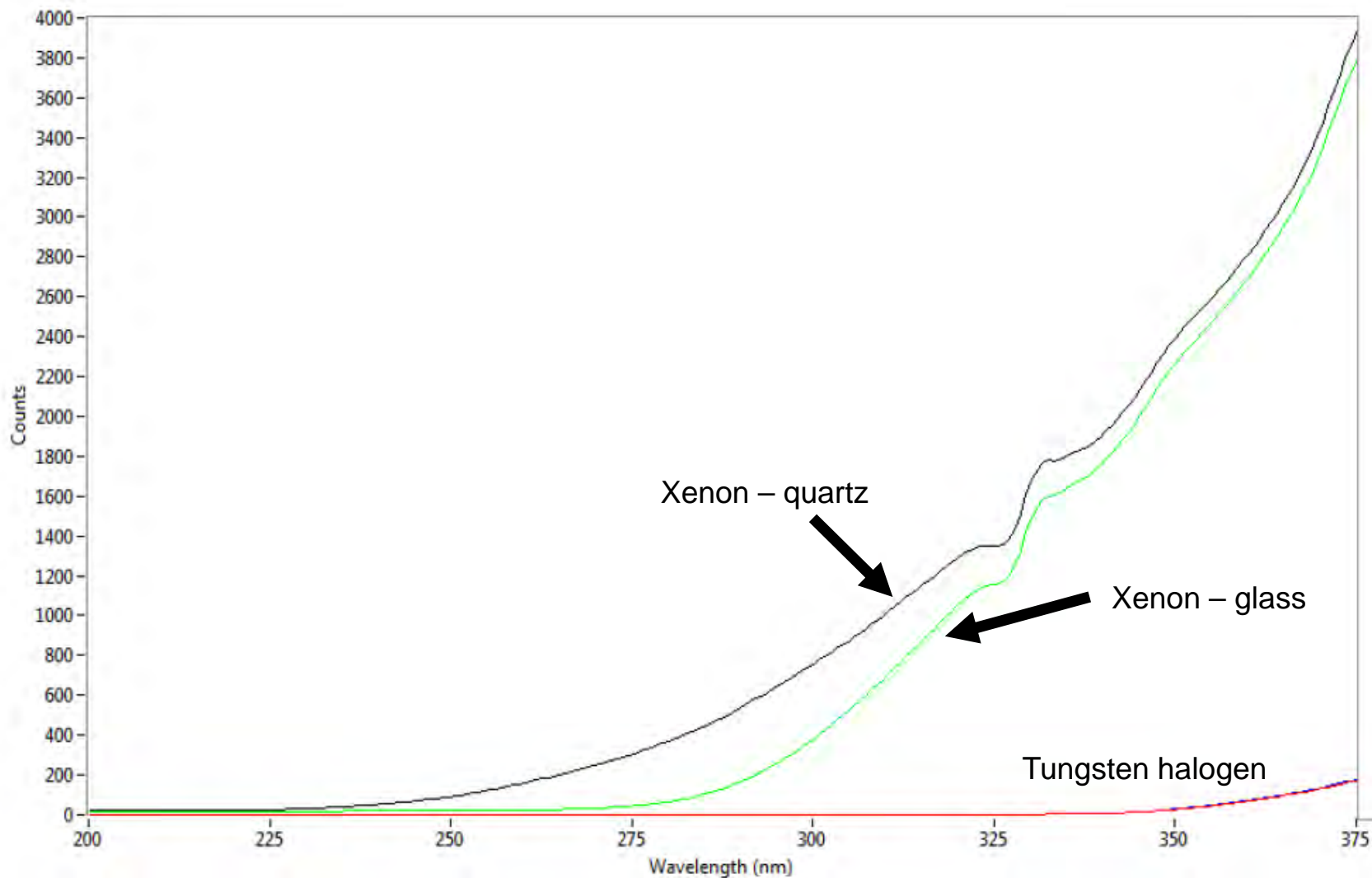


Figure 4. Emission spectra collected using both xenon (upper) and tungsten halogen (lower) bulbs through quartz (black & blue) and glass (green & red) slides (200 – 375 nm).

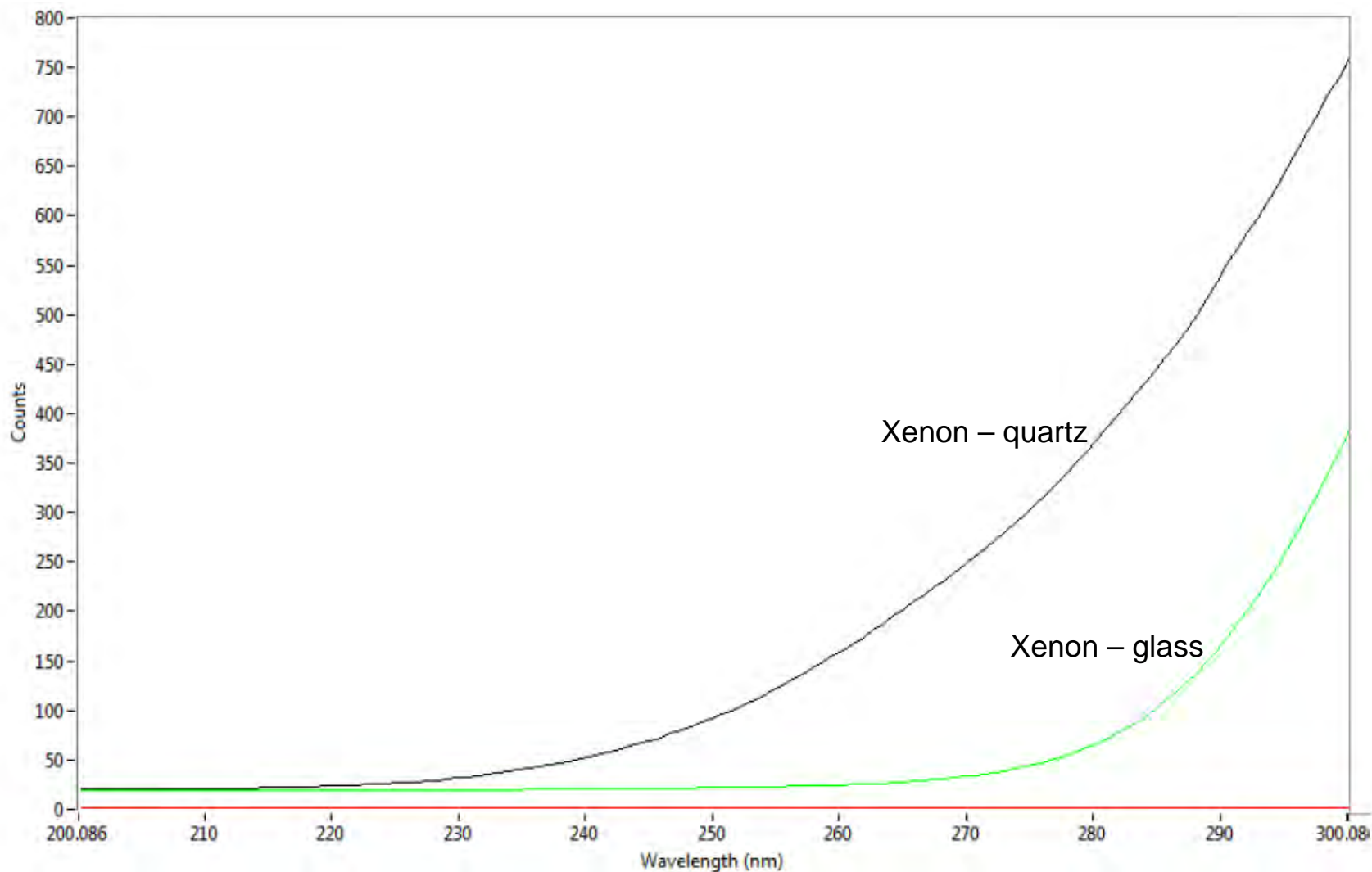


Figure 5. Emission spectra collected using xenon through quartz (black) and glass (green) slides (200 – 300 nm).

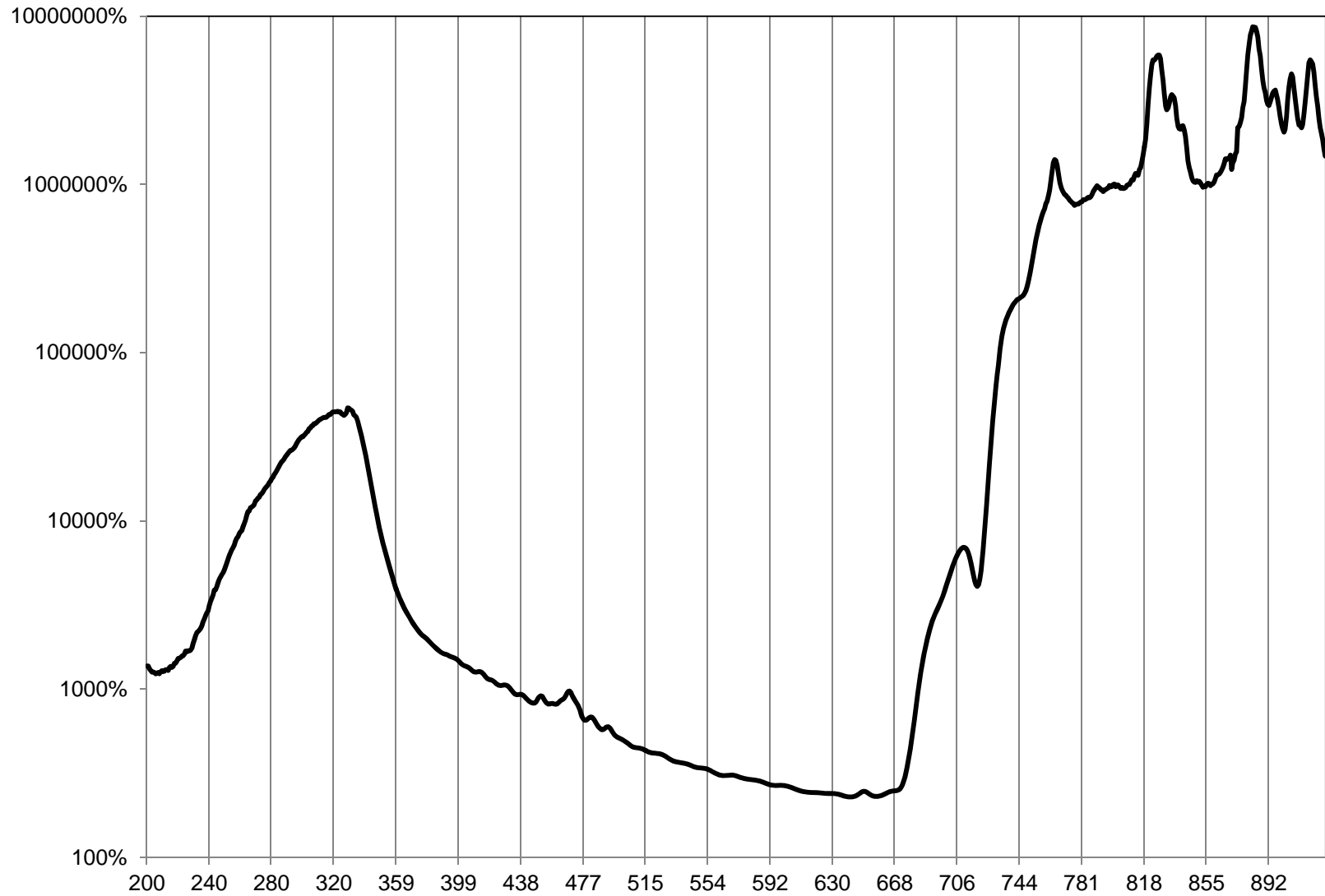


Figure 6. Percent increase in intensity of the emission from the xenon bulb relative to the emission of the tungsten halogen bulb (plotted on a logarithmic scale).

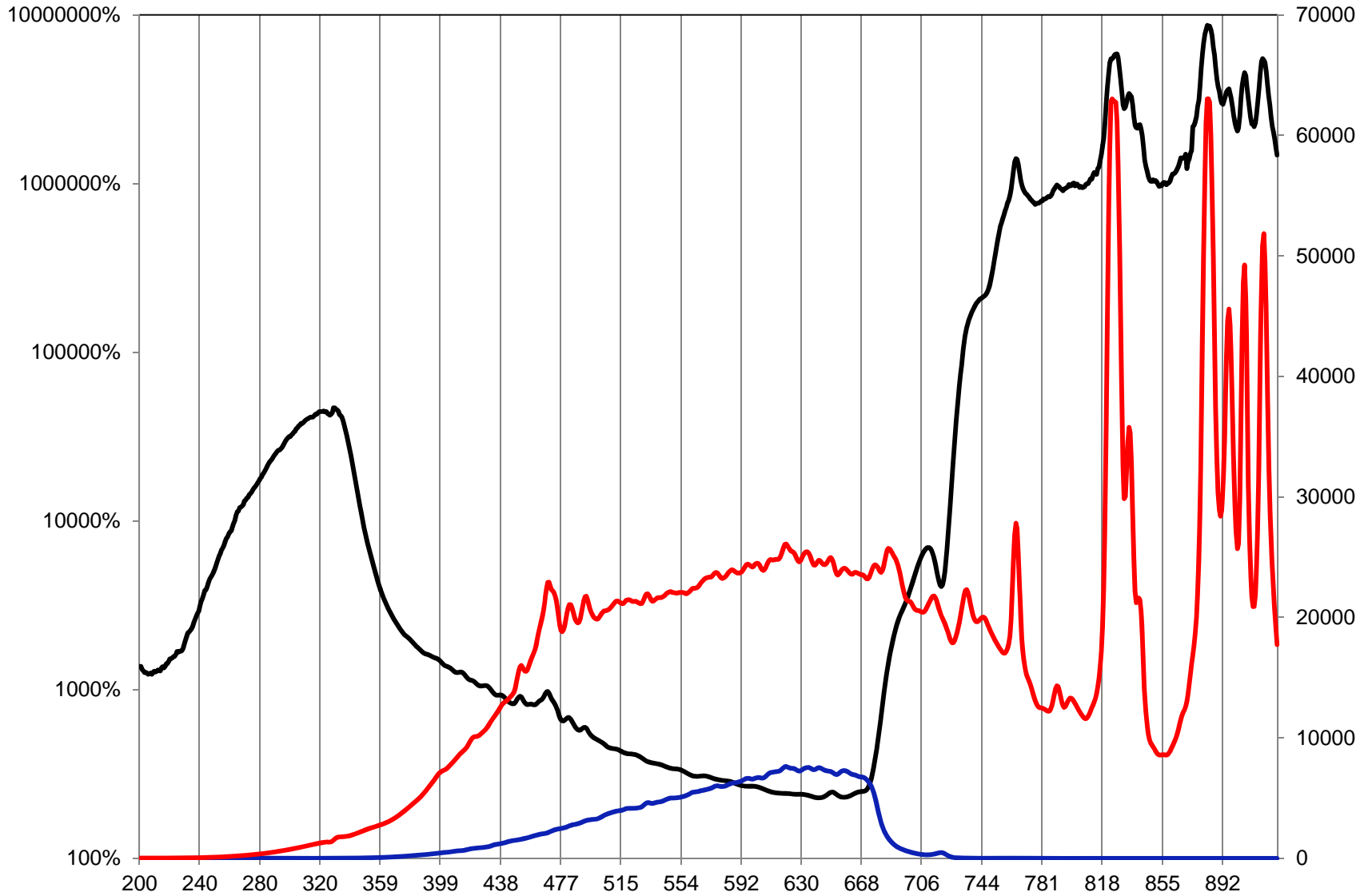


Figure 7. Percent increase in intensity of the emission from the xenon bulb relative to the emission of the tungsten halogen bulb (black - plotted on a logarithmic scale [left axis] compared to the emission spectra of the xenon (red) and tungsten halogen (blue) bulbs (plotted on the secondary [right] axis).

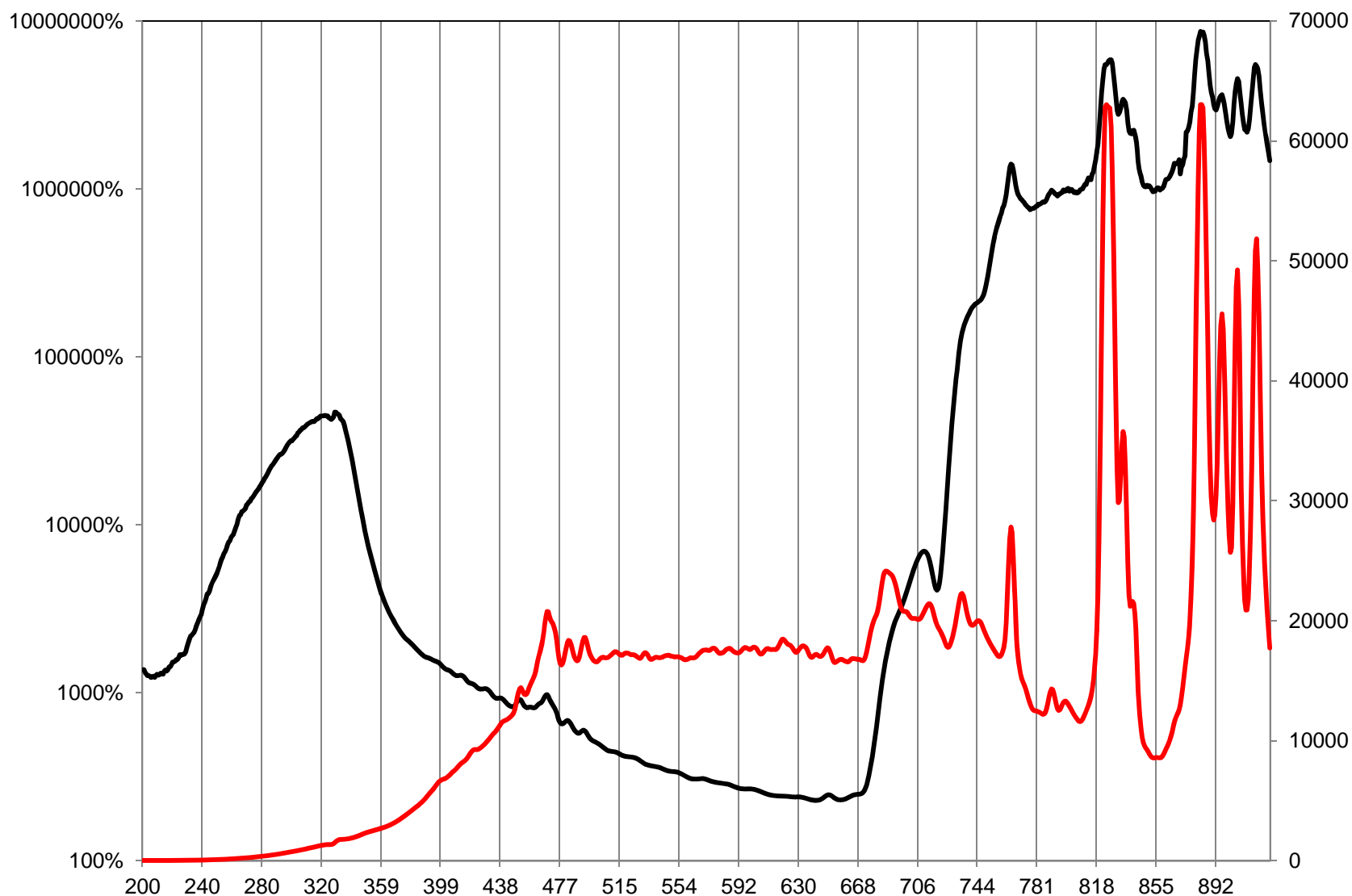


Figure 8. Percent increase in intensity of the emission from the xenon bulb relative to the emission of the tungsten halogen bulb (black - plotted on a logarithmic scale [left axis]) compared to the difference, in absolute counts, of the emission spectra of the xenon and tungsten halogen bulbs (red - plotted on the secondary [right] axis).

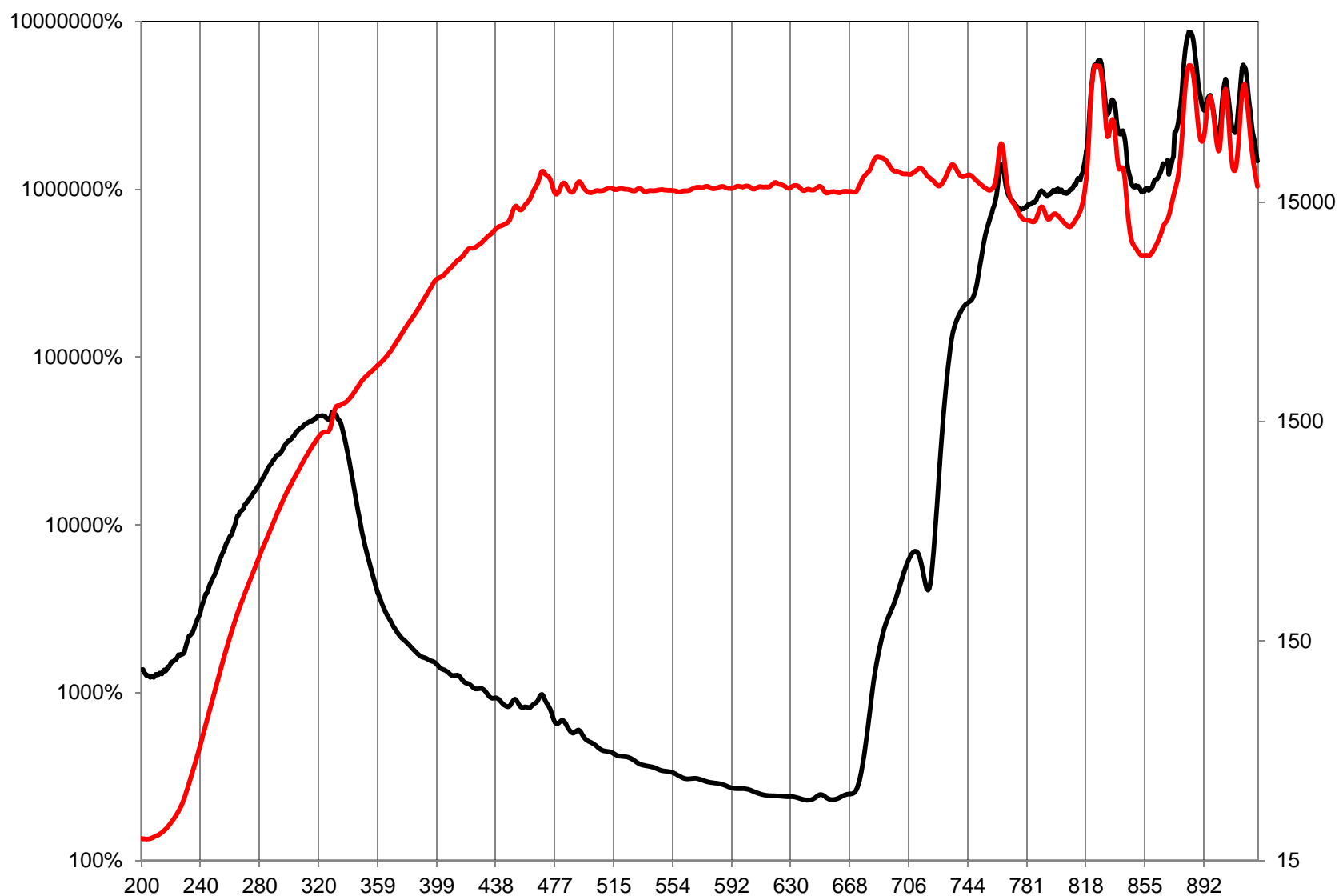


Figure 9. Percent increase in intensity of the emission from the xenon bulb relative to the emission of the tungsten halogen bulb (black - plotted on a logarithmic scale [left axis]) compared to the difference, in absolute counts, of the emission spectra of the xenon and tungsten halogen bulbs (red - plotted on the logarithmic secondary [right] axis).

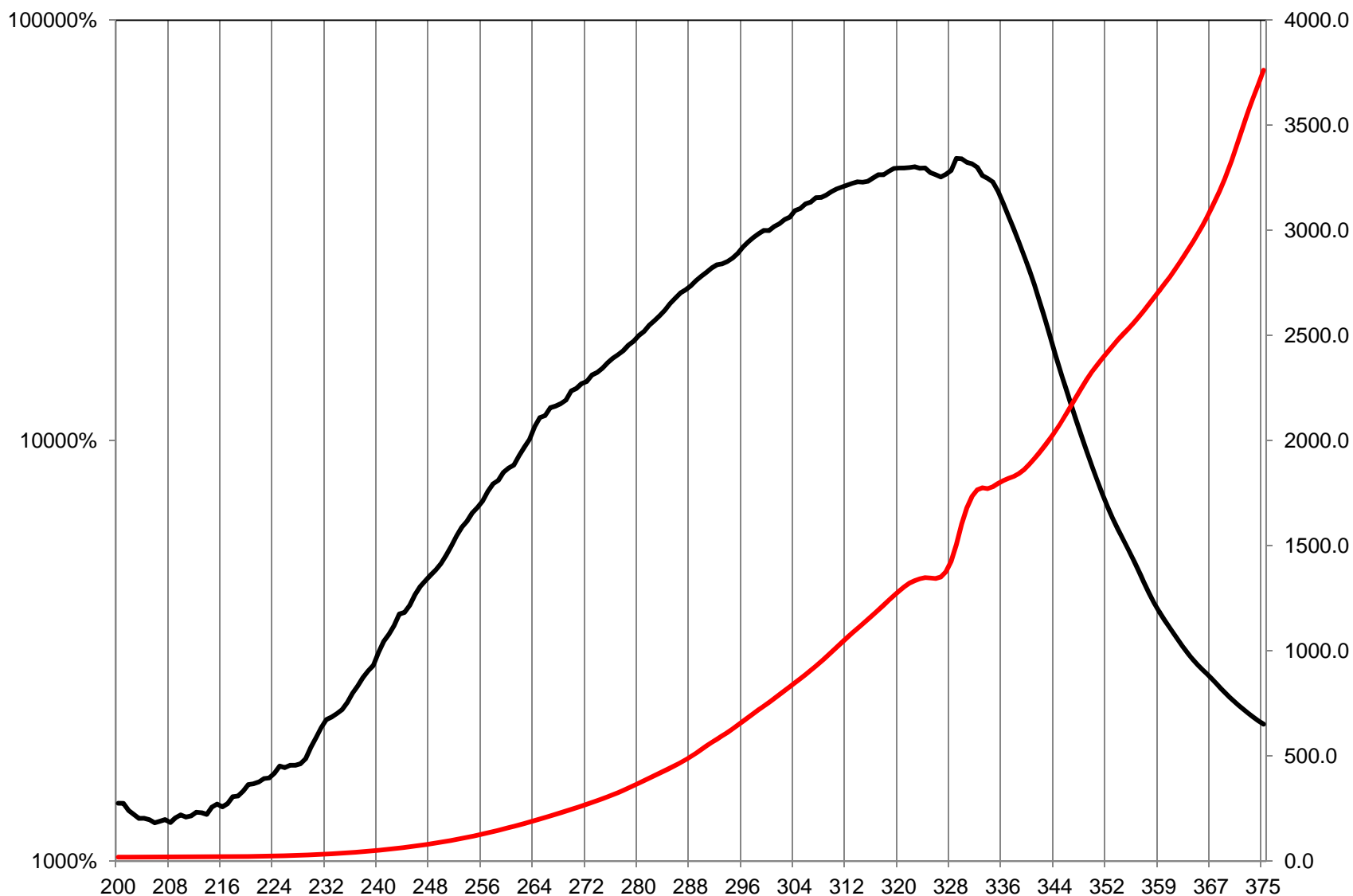


Figure 10. Percent increase in intensity of the emission from the xenon bulb relative to the emission of the tungsten halogen bulb (black - plotted on a logarithmic scale [left axis]) compared to the difference, in absolute counts, of the emission spectra of the xenon and tungsten halogen bulbs (red - plotted on the secondary [right] axis).

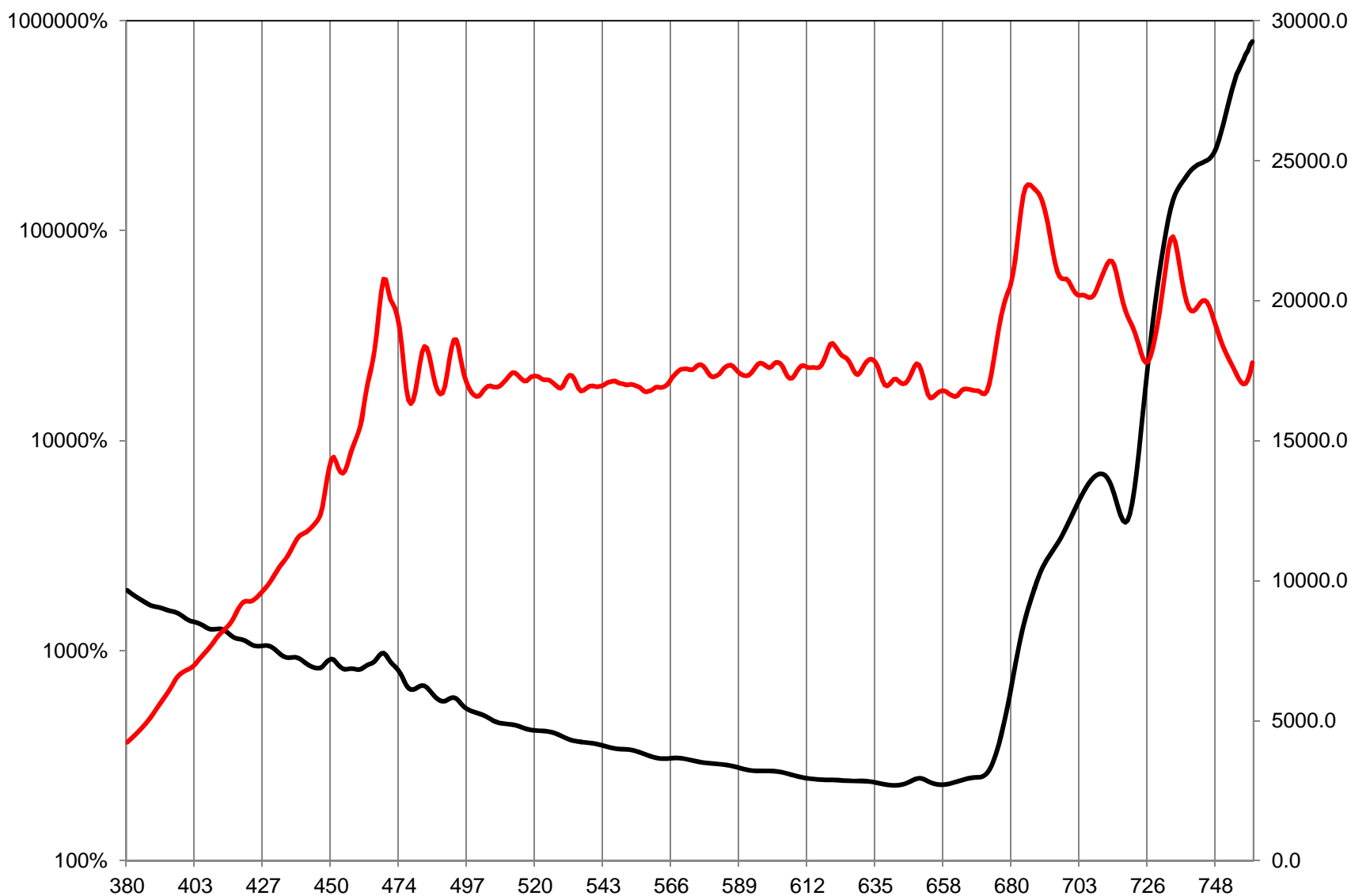


Figure 11. Percent increase in intensity of the emission from the xenon bulb relative to the emission of the tungsten halogen bulb (black - plotted on a logarithmic scale [left axis]) compared to the difference, in absolute counts, of the emission spectra of the xenon and tungsten halogen bulbs (red - plotted on the secondary [right] axis).

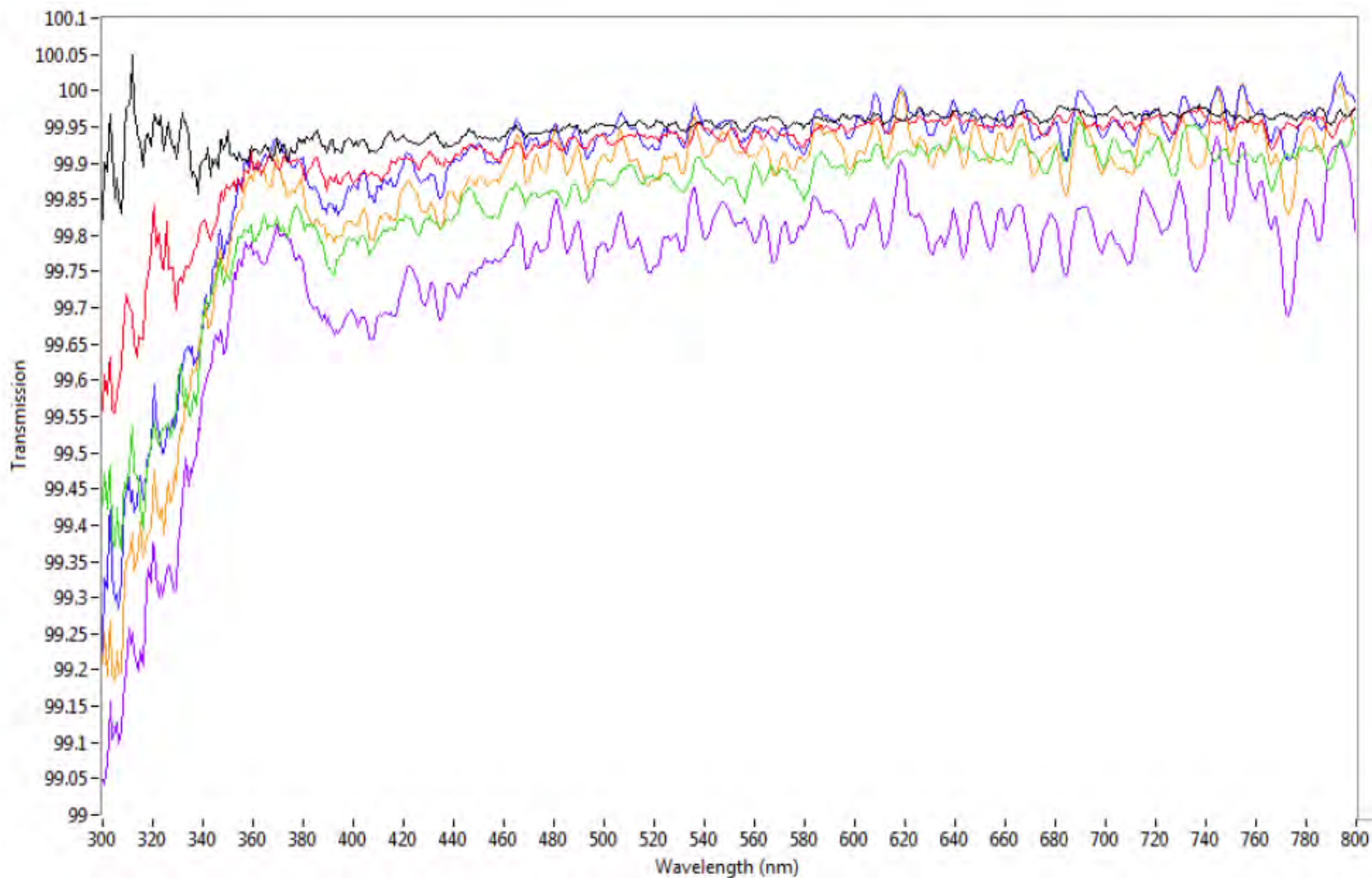


Figure 12. Spectra of air collected in one minute intervals using the same reference spectrum (0 min = black, 1 min = red, 2 min = green, 3 min = blue, 4 min = orange, 5 min = purple).

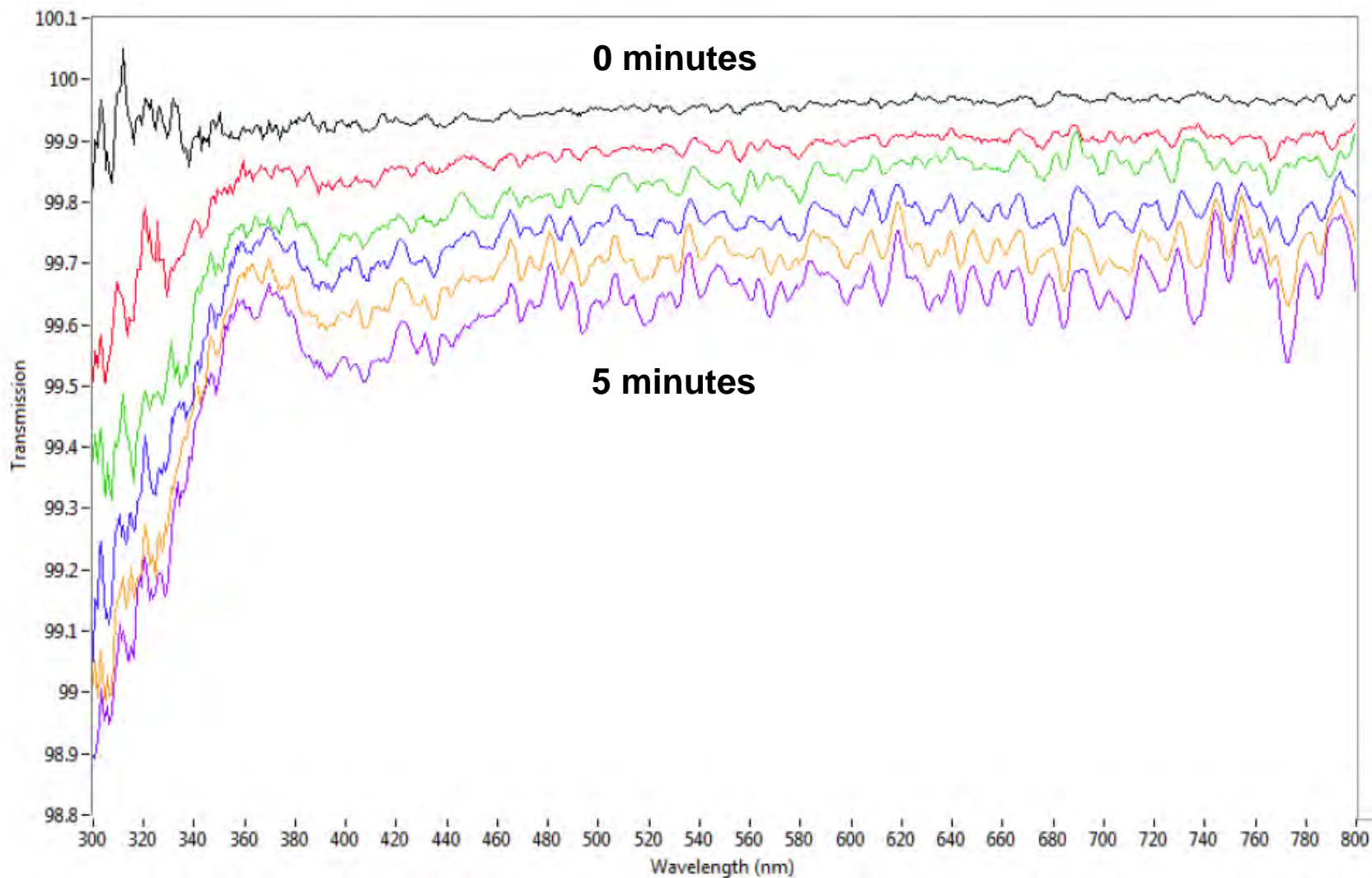


Figure 13. Spectra of air collected in one minute intervals using the same reference spectrum (spectra are artificially stacked (spaced) for easier viewing).

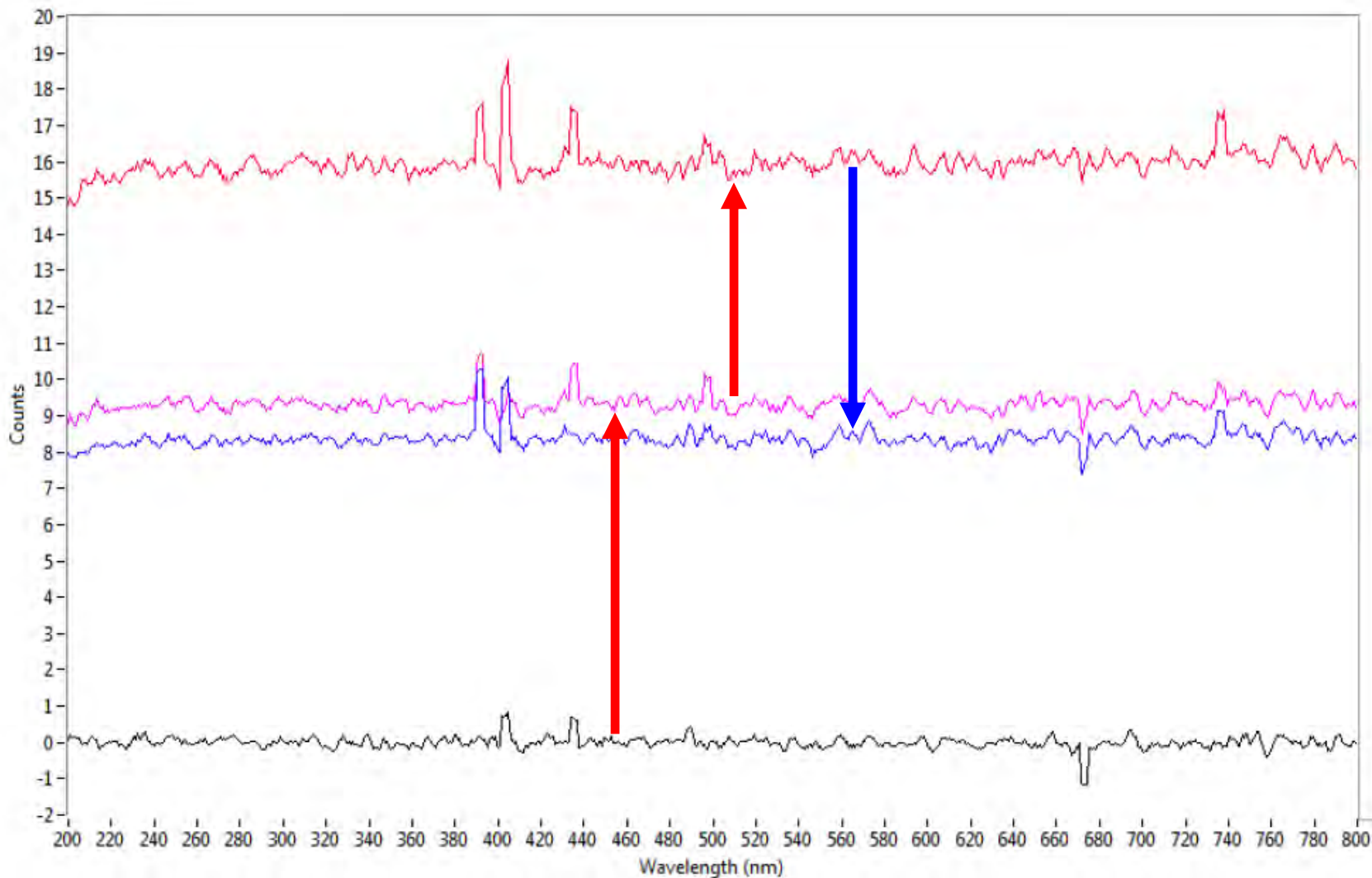


Figure 14. Comparison of background counts, relative to a dark scan collected at the beginning of the experiment, as the ambient room temperature rose from $\sim 23^{\circ}\text{C}$ (black) to $\sim 25^{\circ}\text{C}$ (red). Spectra were also collected at $\sim 24^{\circ}\text{C}$ during the warming (pink) and after the experiment as the room was cooling down (blue).

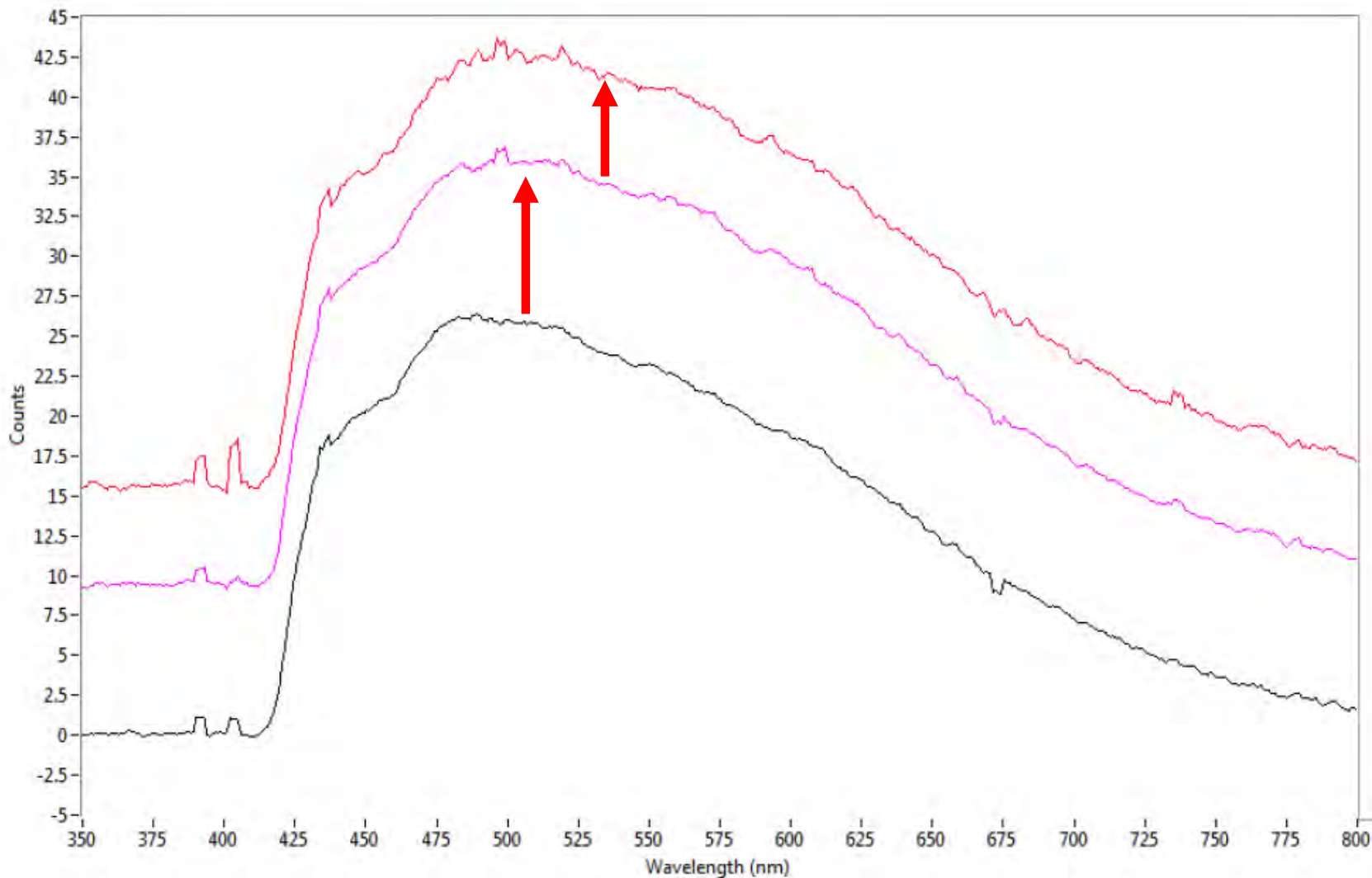


Figure 15. Comparison of MSF spectra collected from a weakly fluorescing sample, relative to a dark scan collected at the beginning of the experiment, as the ambient room temperature rose from ~ 23°C (black) to ~ 25°C (red). A spectrum was also collected at ~ 24°C during the warming (pink).

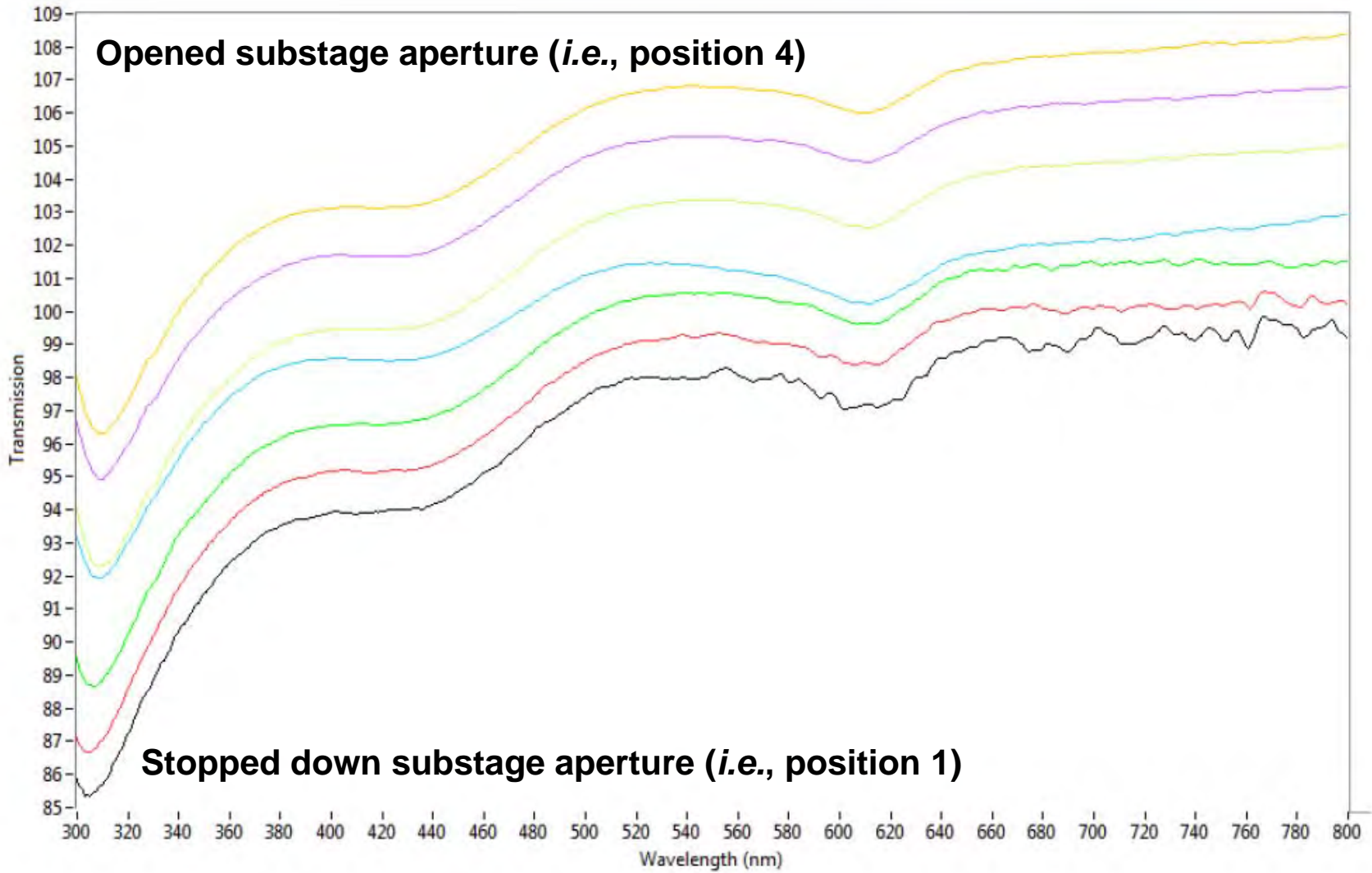


Figure 16. Spectral comparison of a light green bean shaped fiber at varying sub stage diaphragm positions (*i.e.*, from position 1 to 4 in half- interval steps). Shown with a ten percent spectral offset (stacked) for ease of viewing.

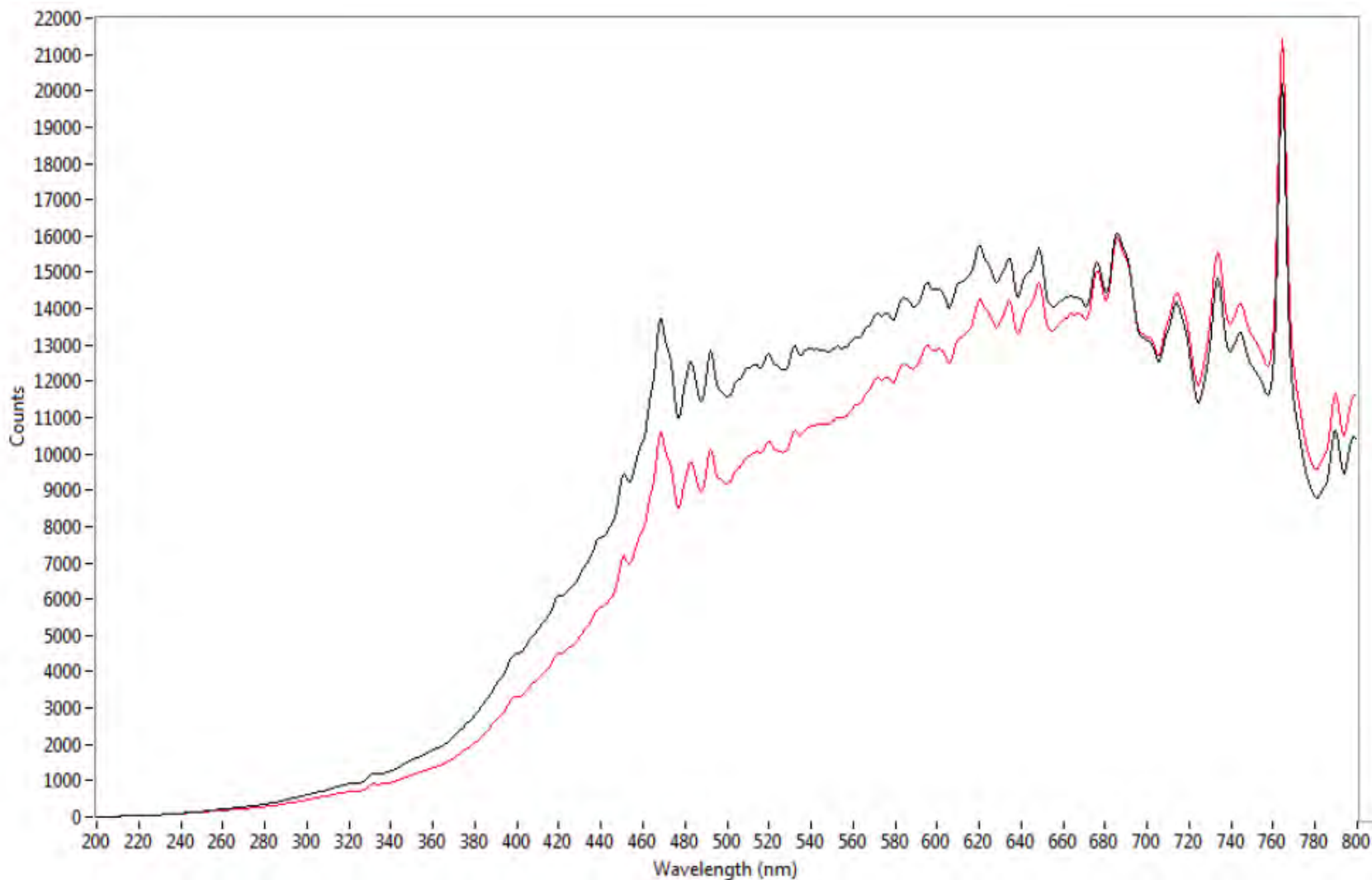


Figure 17. Relative intensity differences caused by lamp adjustments. The red spectrum has the highest counts at any particular wavelength, but the black spectrum has higher counts across the majority of the spectrum. This is especially significant at the lower end of the spectrum where there are fewer absolute counts.

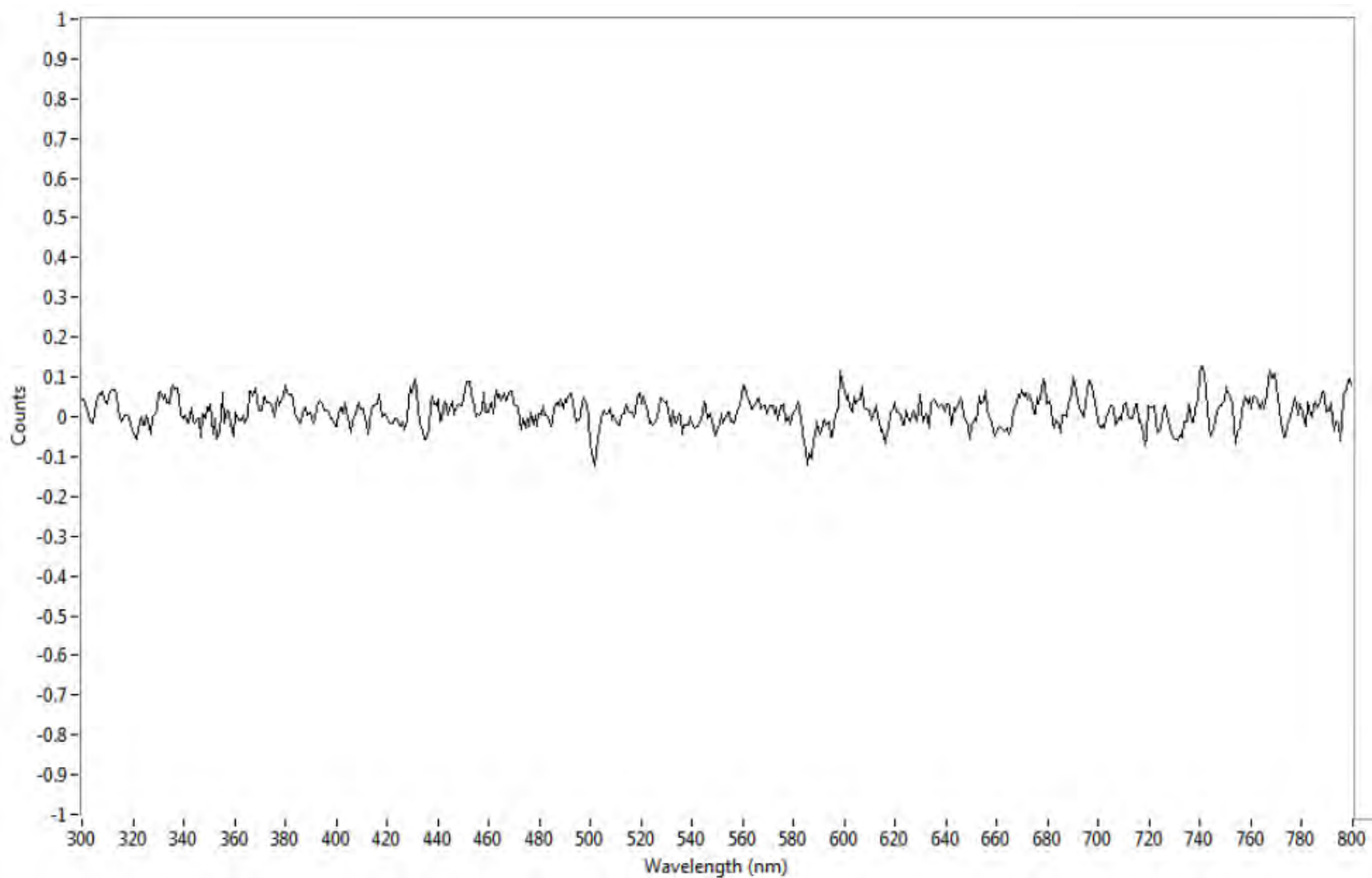


Figure 18. Spectrum collected with room lights on (beam splitter directing light to the oculars).

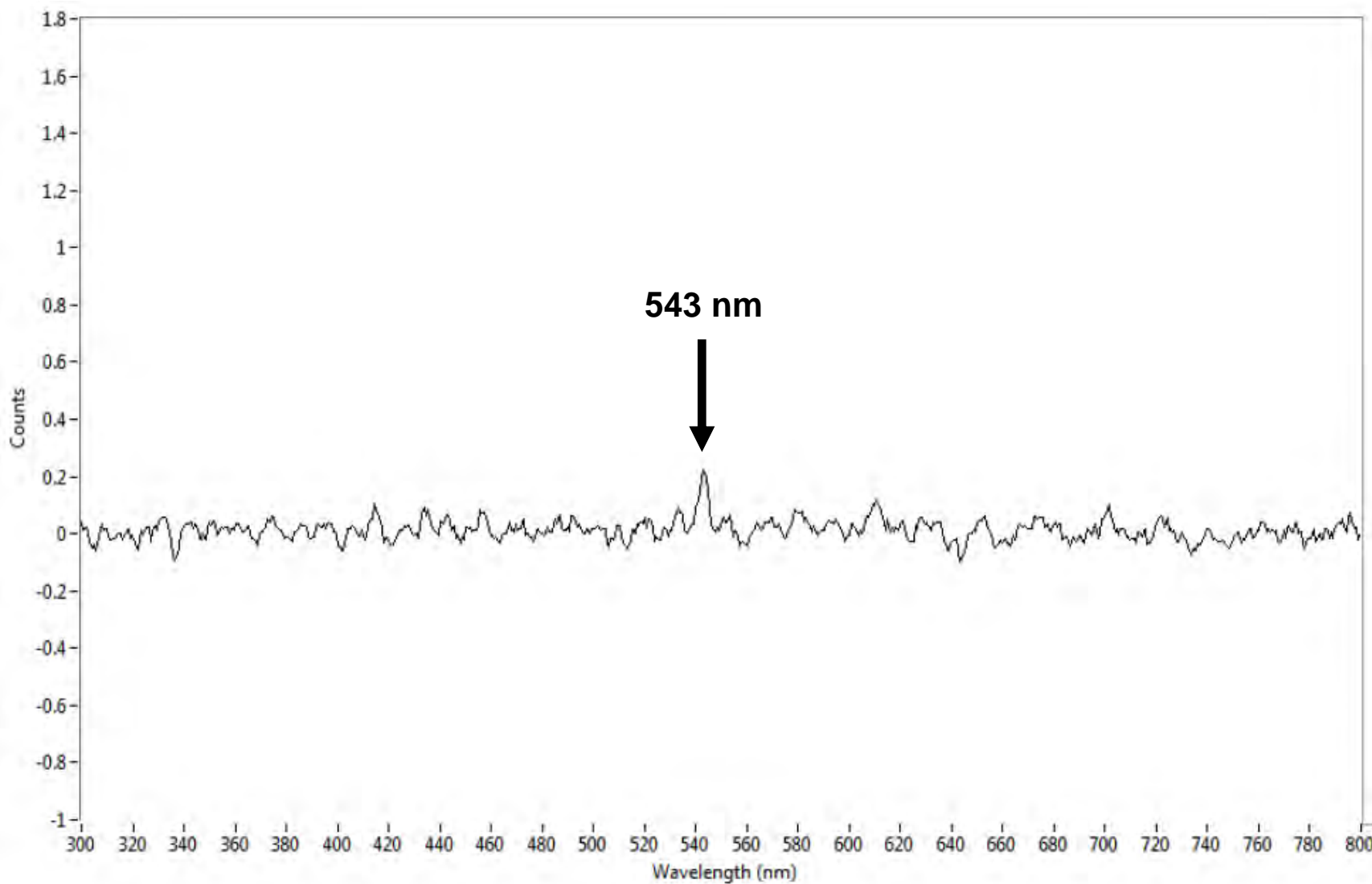


Figure 19. Spectrum collected with room lights on (beam splitter open – glass slide, aperture 1 (largest), 40X objective).

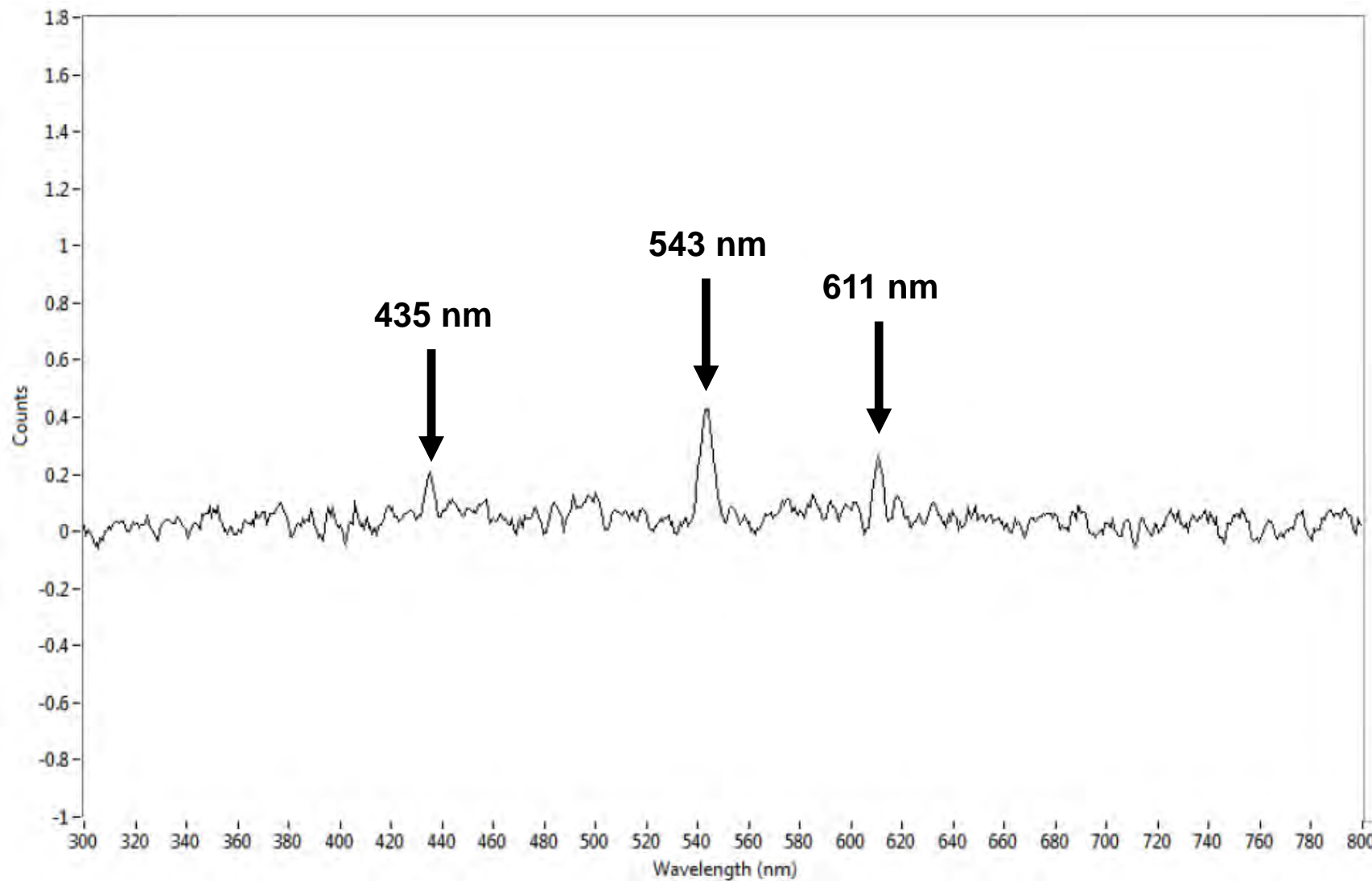


Figure 20. Spectrum collected with room lights on (beam splitter open – glass slide, aperture 1 (largest), 10X objective).

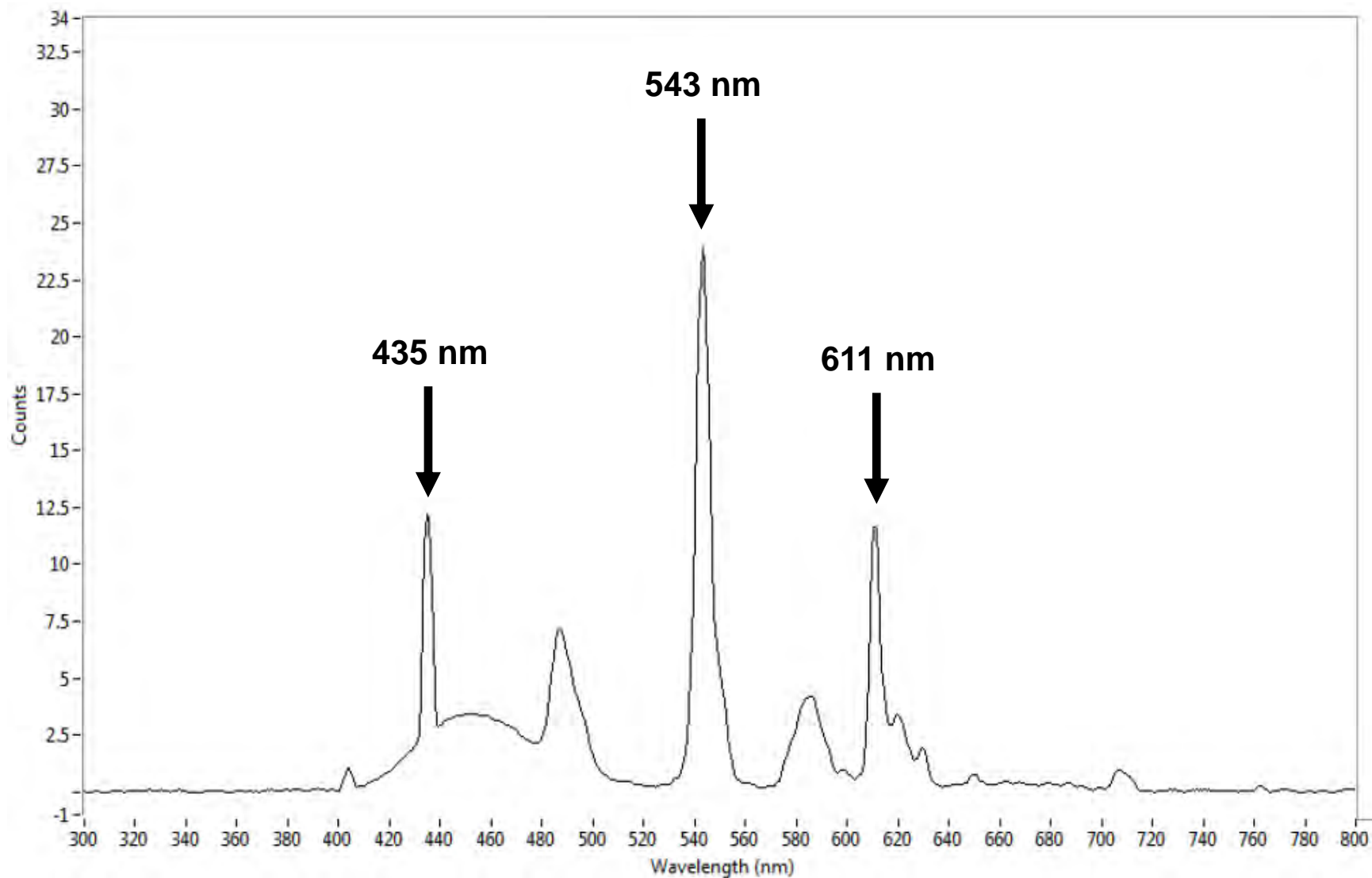


Figure 21. Spectrum collected with room lights on using an angled mirror to collect the light from the fluorescent overhead lights (beam splitter open – aperture 1 (largest), 10X objective).

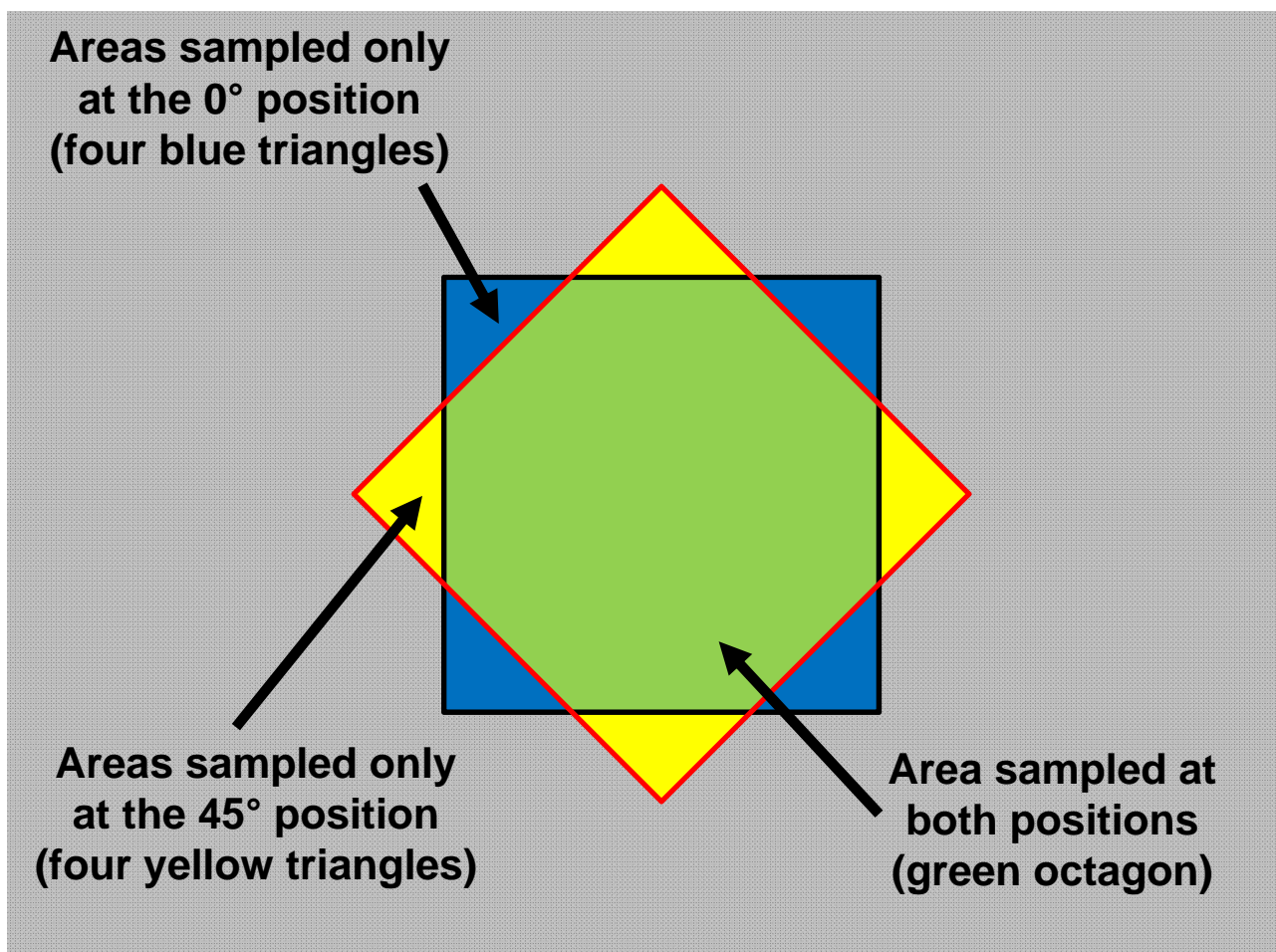


Figure 22. Aperture at original position (0° - black square) compared to the effective aperture position after the sample is rotated 45° - red square). While in reality the sample is rotated and the aperture is fixed, this diagram shows a fixed sample with a rotating aperture. The net effect, however, is the same.

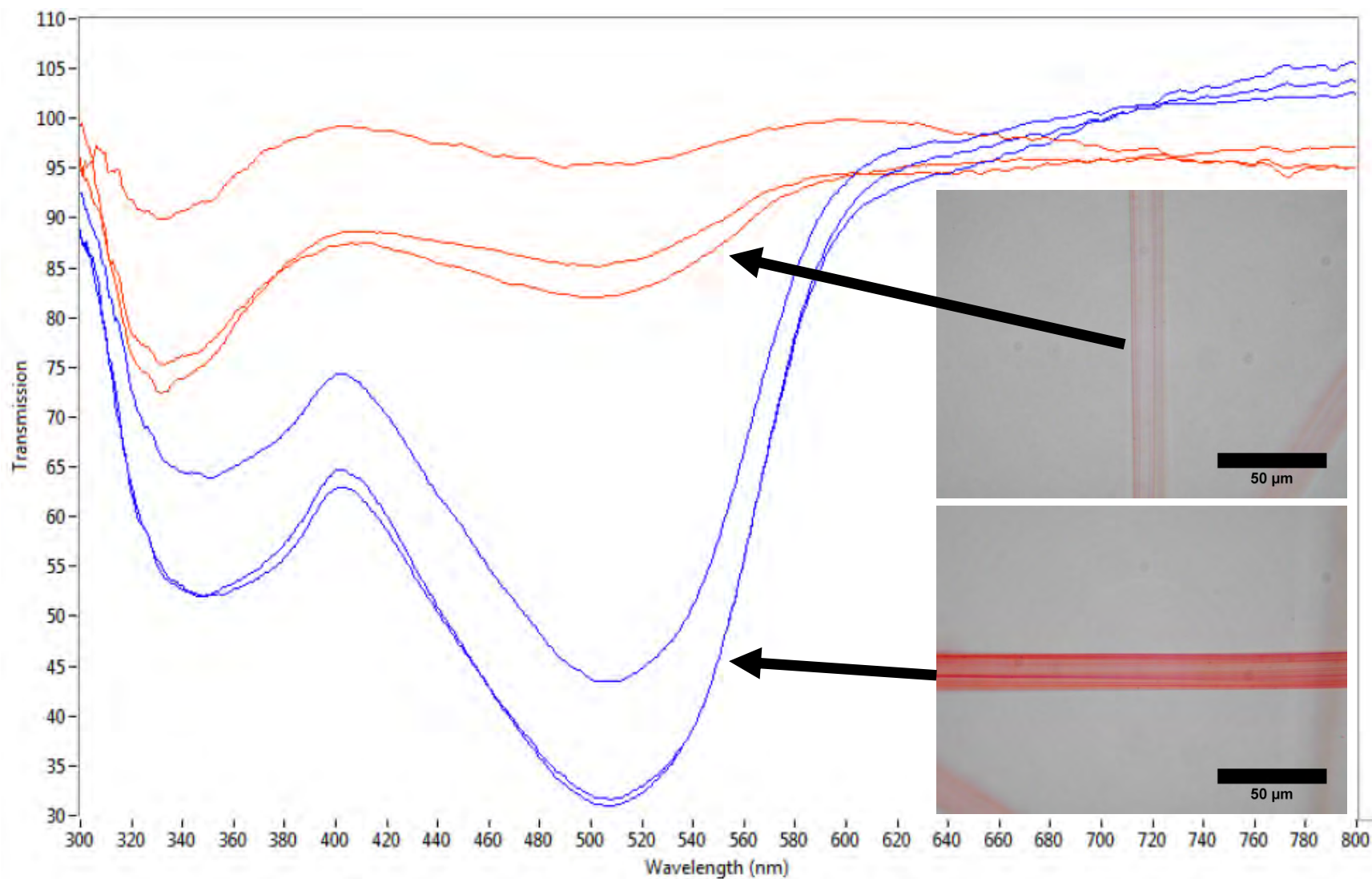


Figure 23. Spectra collected from three fibers dyed with Congo Red oriented parallel (blue) and perpendicular (red) to the preferential direction of a polarizer (mounted in glycerin). Photomicrograph insets show examples of the visible appearance of a fiber in these two orientations.

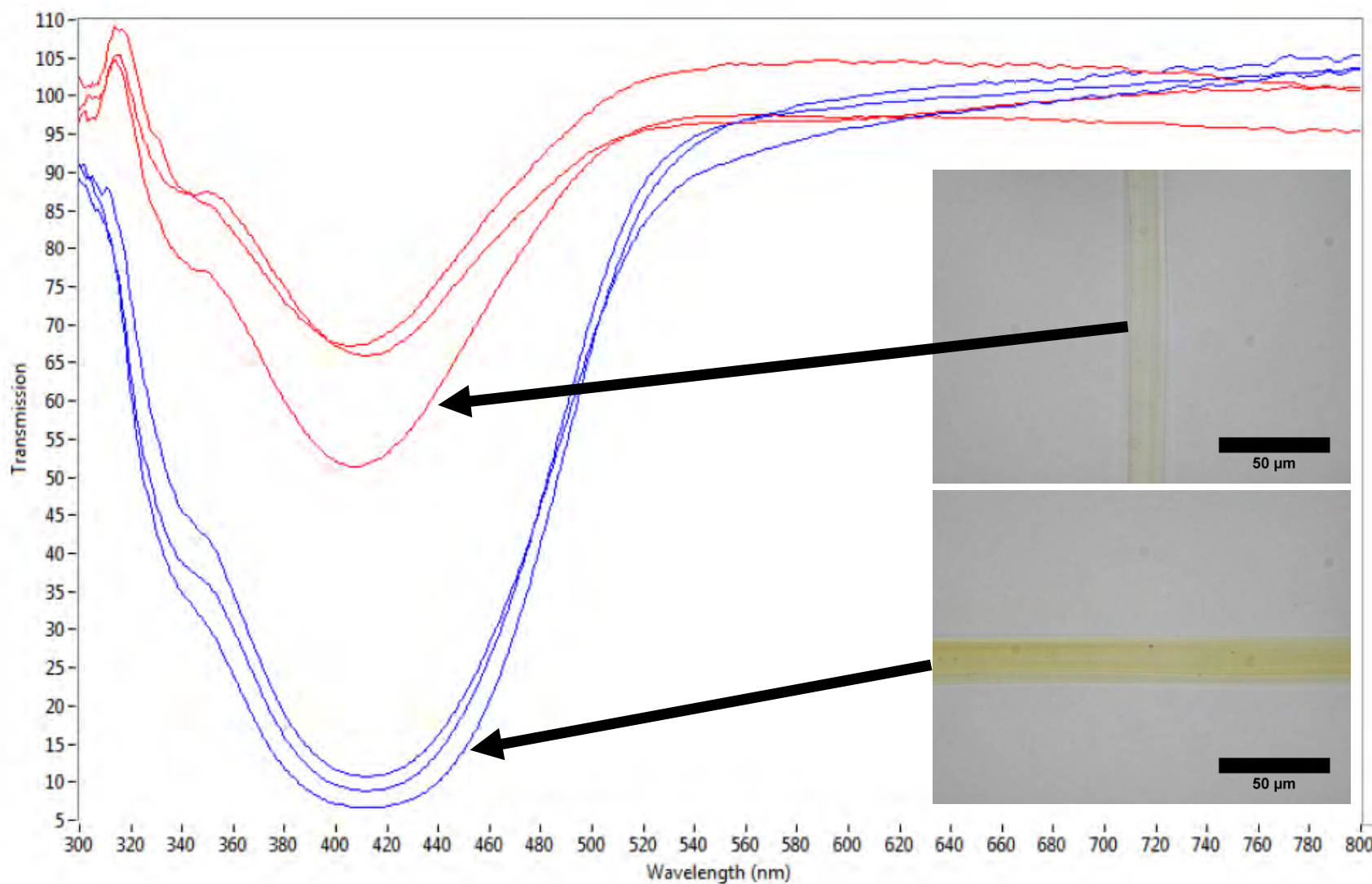


Figure 24. Spectra collected from three fibers dyed with CI Direct Yellow 12 oriented parallel (blue) and perpendicular (red) to the preferential direction of a polarizer (mounted in glycerin). Photomicrograph insets show examples of the visible appearance of a fiber in these two orientations.

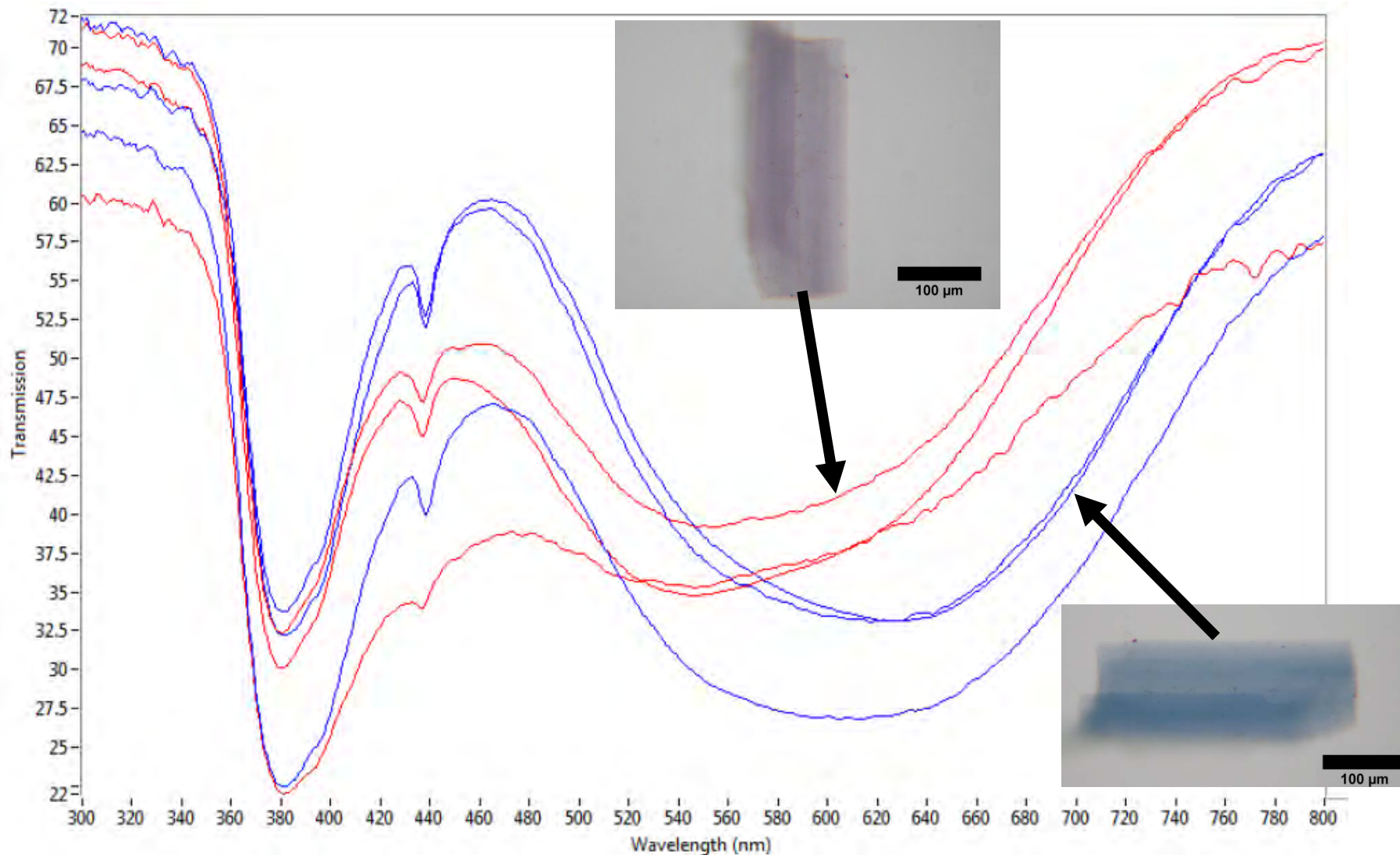


Figure 25. Spectra collected from three glaucophane grains oriented parallel (blue) and perpendicular (red) to the vibration direction of a polarizer (mounted in 1.662 Meltmount). Photomicrograph insets show examples of the visible appearance of a mineral grain in these two orientations.

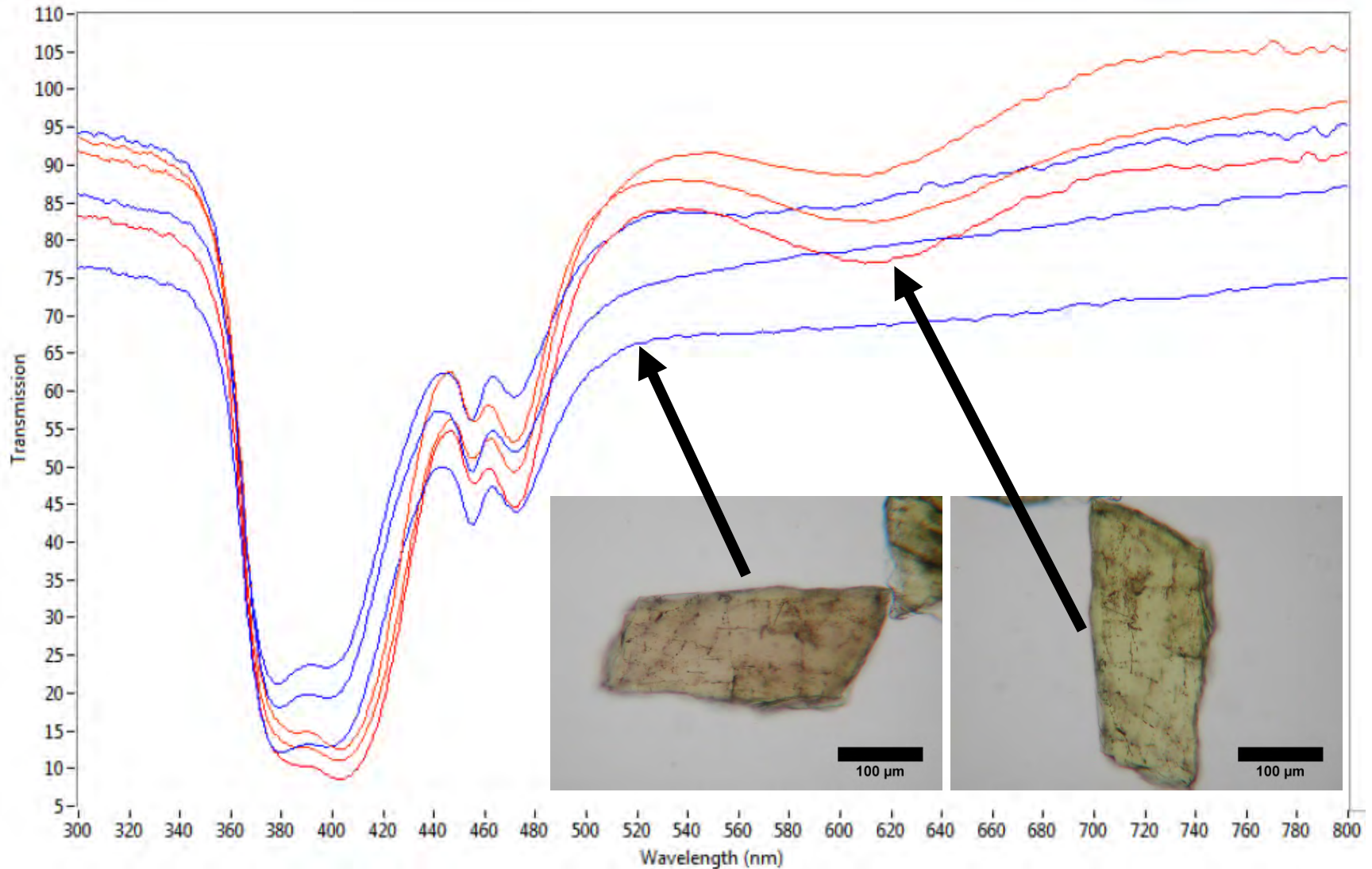


Figure 26. Spectra collected from three epidote grains oriented parallel (blue) and perpendicular (red) to the preferential direction of a polarizer (mounted in 1.662 Meltmount). Photomicrograph insets show examples of the visible appearance of a mineral grain in these two orientations.

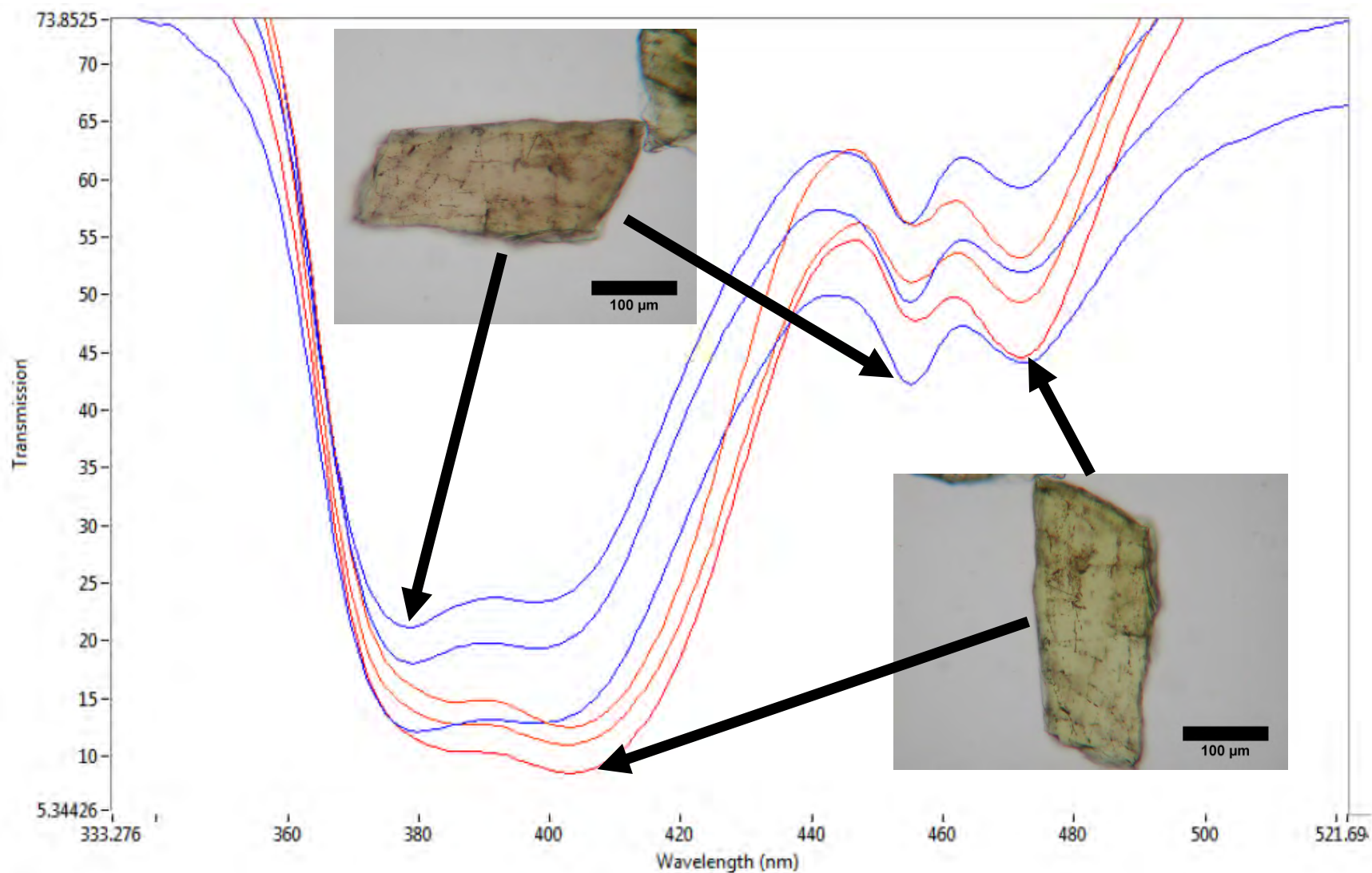


Figure 27. Close-up of spectra collected from three epidote grains oriented parallel (blue) and perpendicular (red) to the preferential direction of a polarizer (mounted in 1.662 Meltmount). Note the distinct doublet peak inversions at ~ 380 & 400 nm and 455 & 471 nm. The black arrows point to the dominant absorbance peaks in each of the doublets for the two orientations.

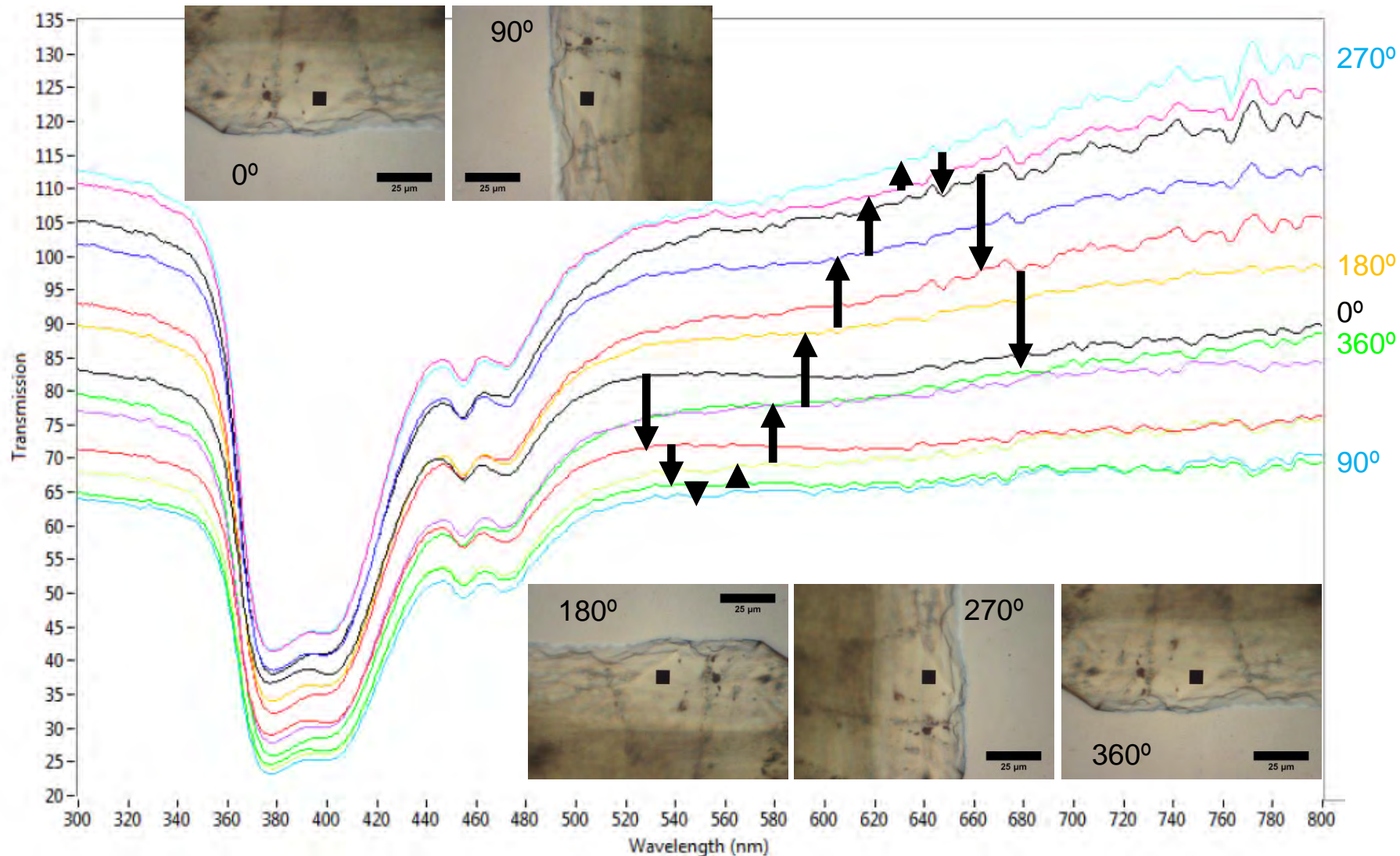


Figure 28. Spectra collected (shown in 30° increments) as an epidote mineral grain was rotated through 360° (mounted in 1.662 Meltmount). The spectra oscillate down, then up, and then down again as the rotation completes its circle (0° is represented by the black spectral trace in the middle of the plot and the arrows (read left to right) show the movement of the spectra as the grain is rotated). The photomicrographs show the grain and the instrument's aperture (the small black square) at the cardinal positions.

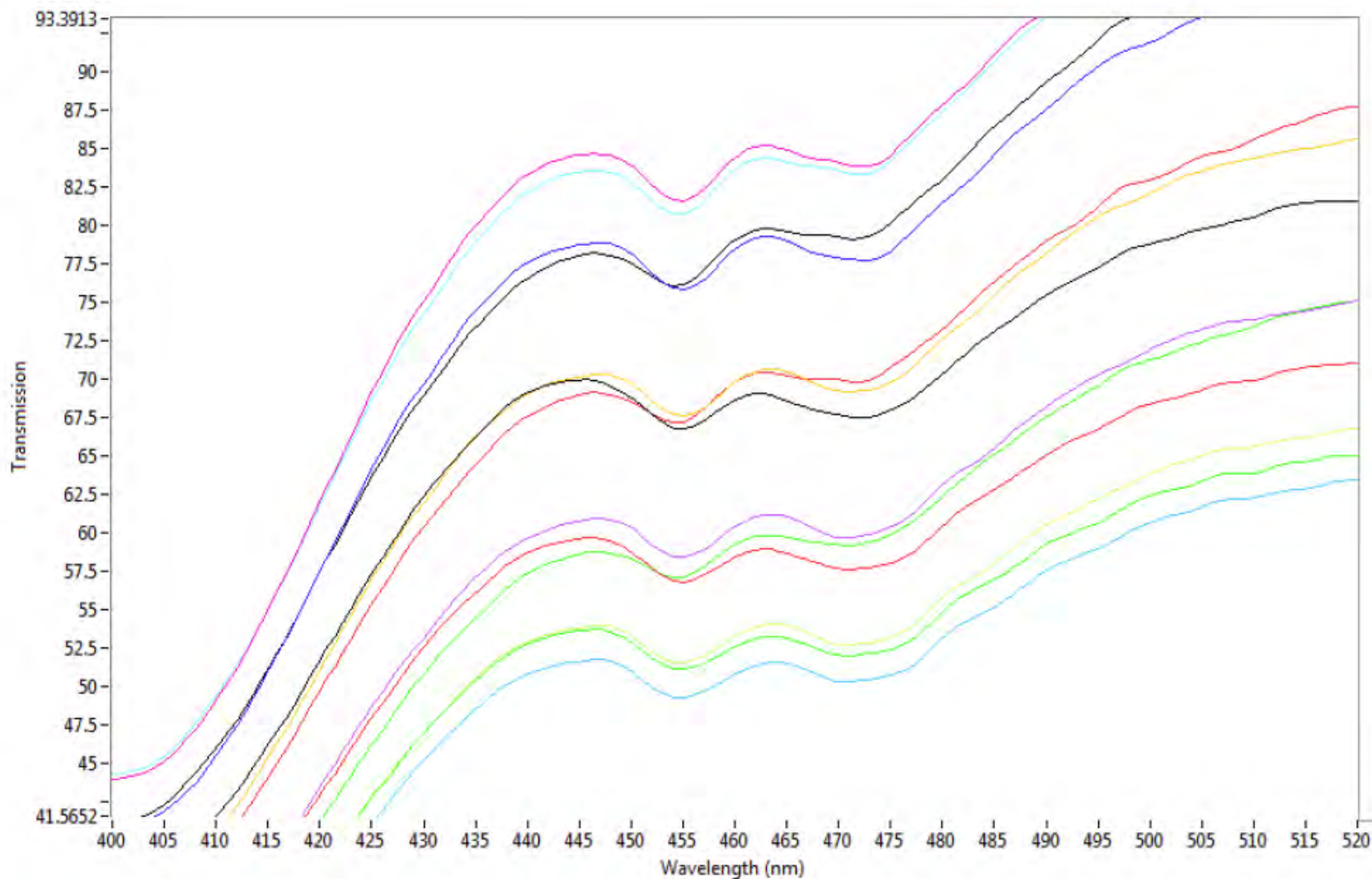


Figure 29. Close-up of a doublet in the spectra collected (shown in 30° increments) as an epidote mineral grain was rotated through 360° (mounted in 1.662 Meltmount).

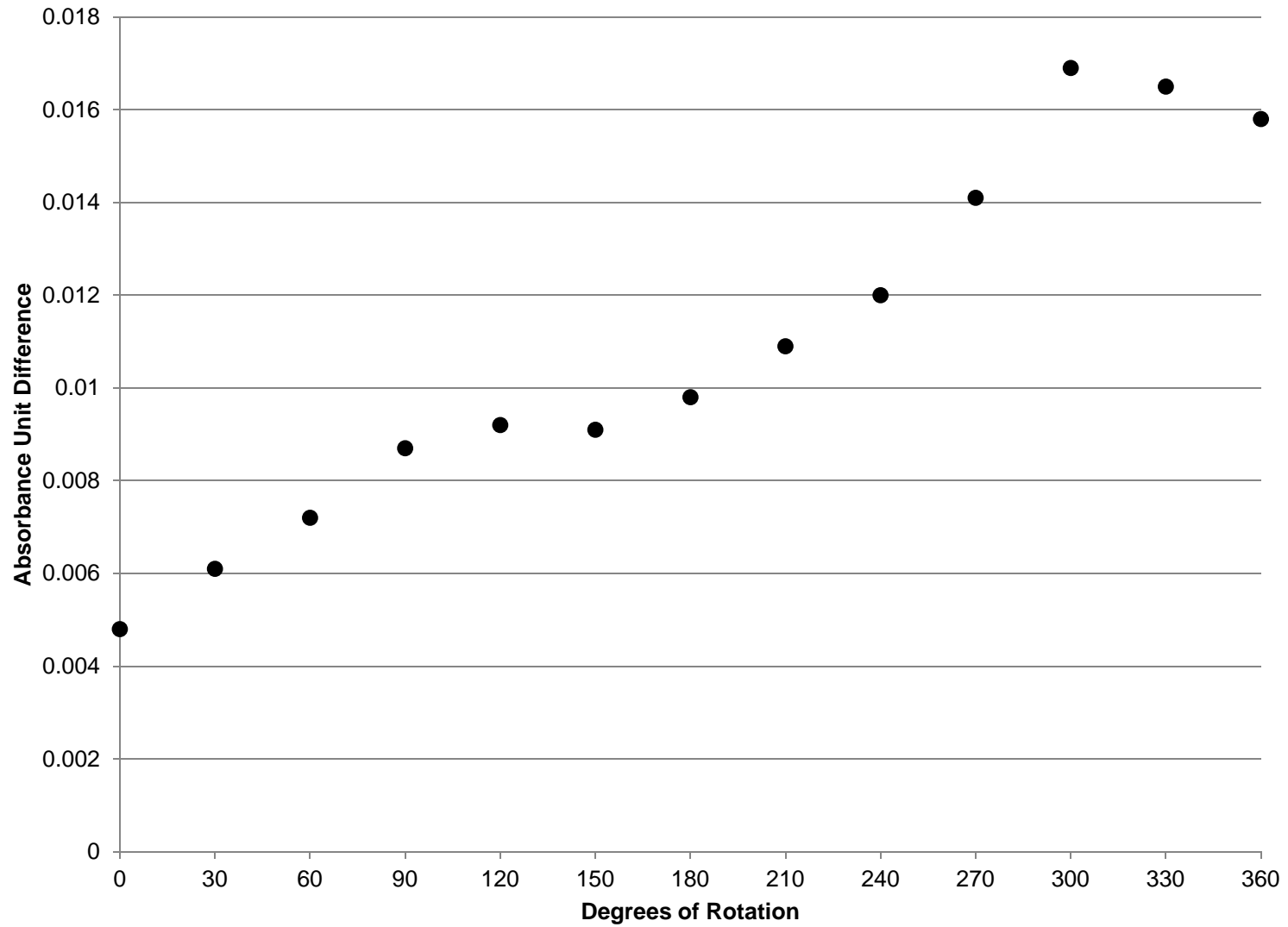


Figure 30. Difference between the intensity 455 nm and the 471 nm peak in the spectra of an epidote grain rotated 360°.

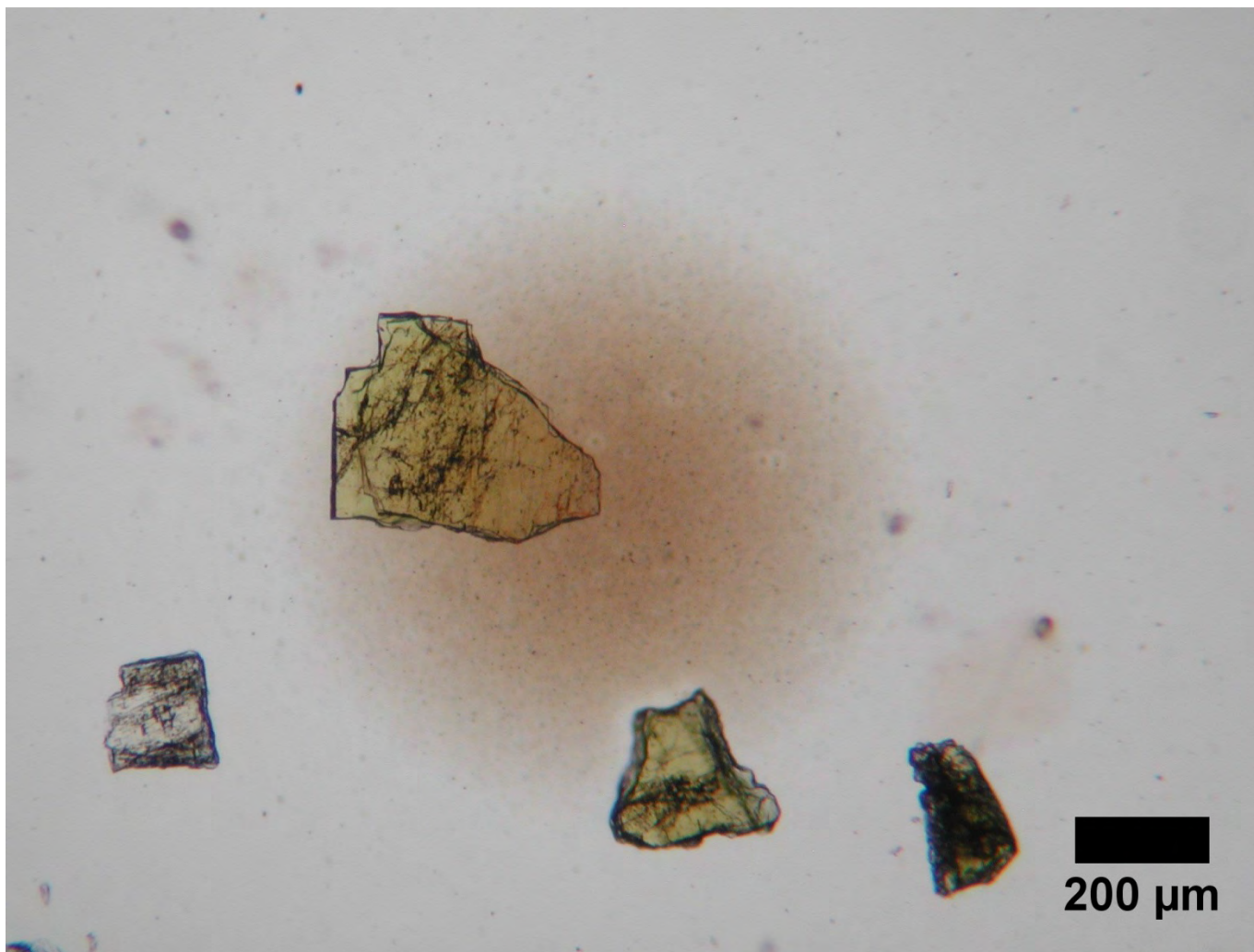


Figure 31. Epidote mineral grain used in the rotation experiments. The mounting medium (1.662 Meltmount) has been clearly discolored by the xenon illumination used during the course of the experiment.

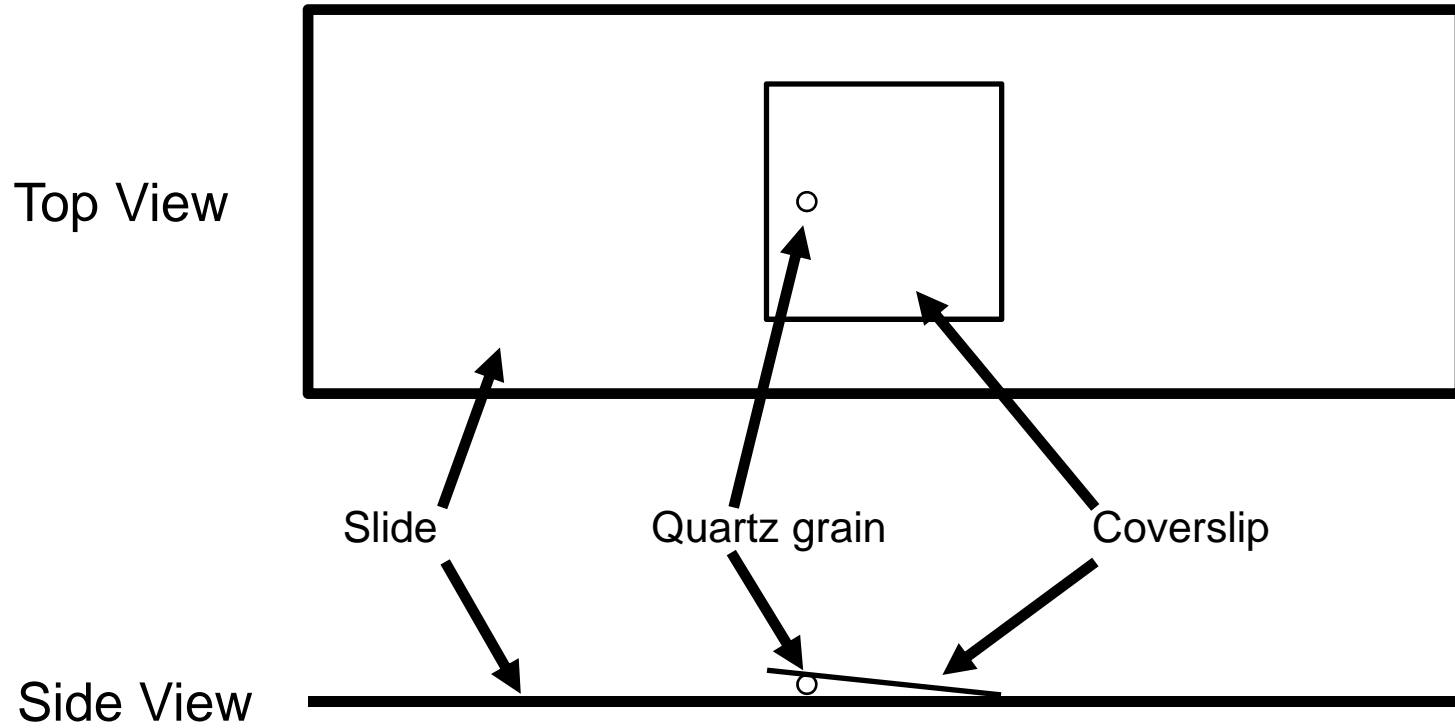


Figure 32. Setup of the tilted coverslip experiment.

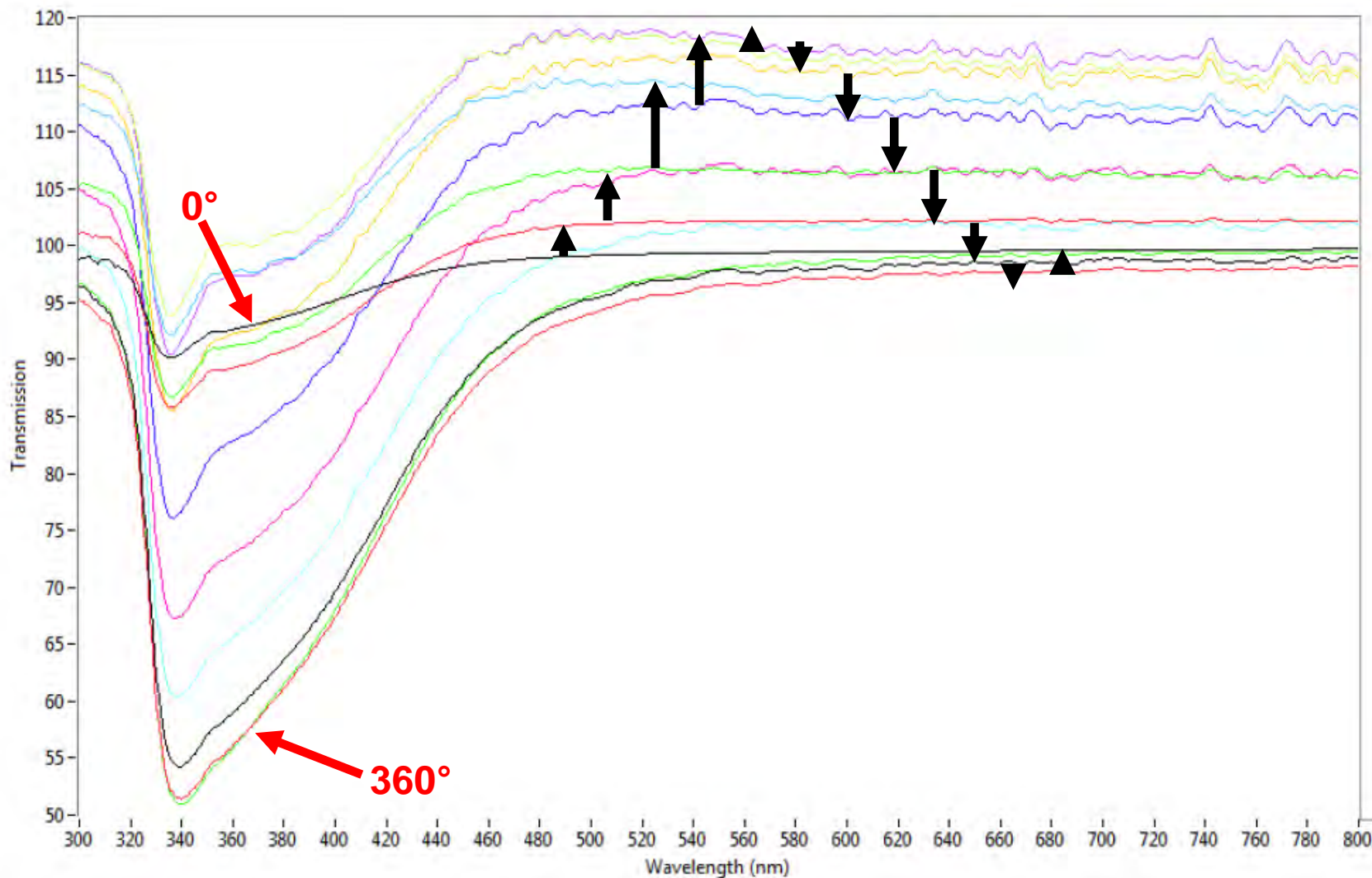


Figure 33. Spectra collected through a blank area of a slide with a tilted coverslip using 1.54 index of refraction oil as the mounting medium as it was rotated from 0° to 360° (shown in 30° increments) (xenon illumination).

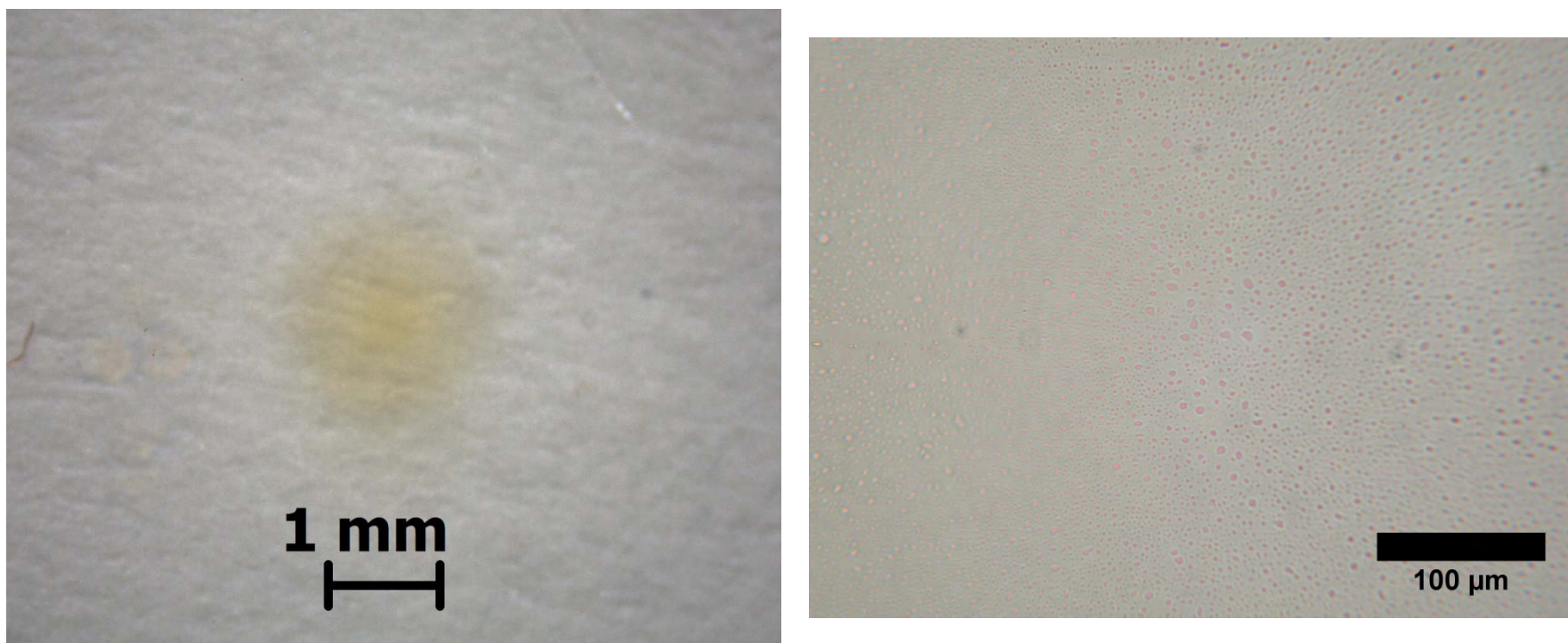


Figure 34. Photomicrograph taken using a stereomicroscope (left) of the area of the slide with 1.54 index of refraction oil that was exposed to prolonged xenon illumination. Image of the small liquid droplets on the underside of the coverslip which have separated out of the mounting medium (right - taken using a compound microscope).

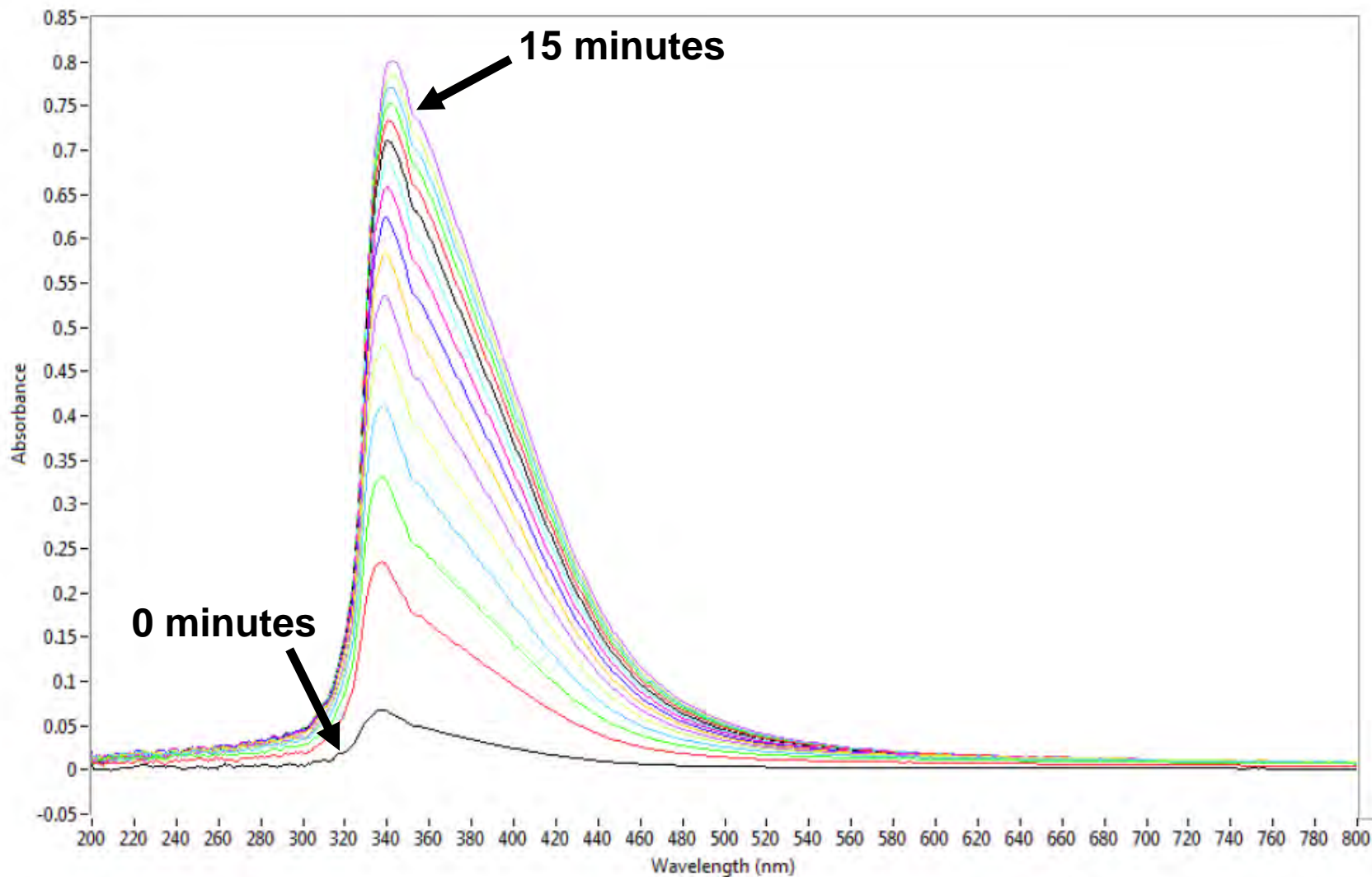


Figure 35. Spectra collected every minute for fifteen minutes through a blank area of a slide with a tilted coverslip using 1.54 index of refraction oil as the mounting medium (xenon illumination).

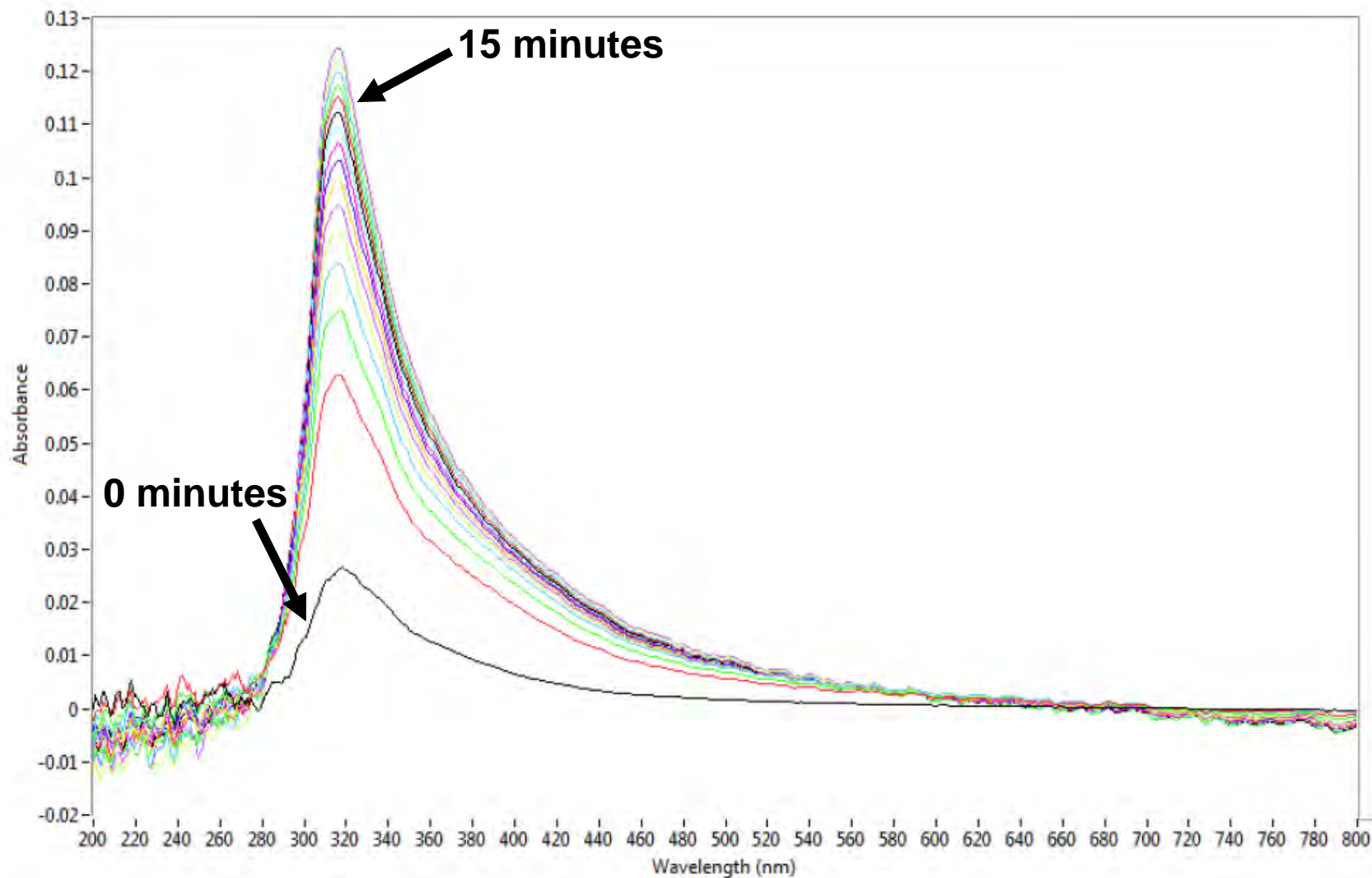


Figure 36. Spectra collected every minute for fifteen minutes through a blank area of a slide with a flat coverslip using 1.54 index of refraction oil as the mounting medium (xenon illumination).

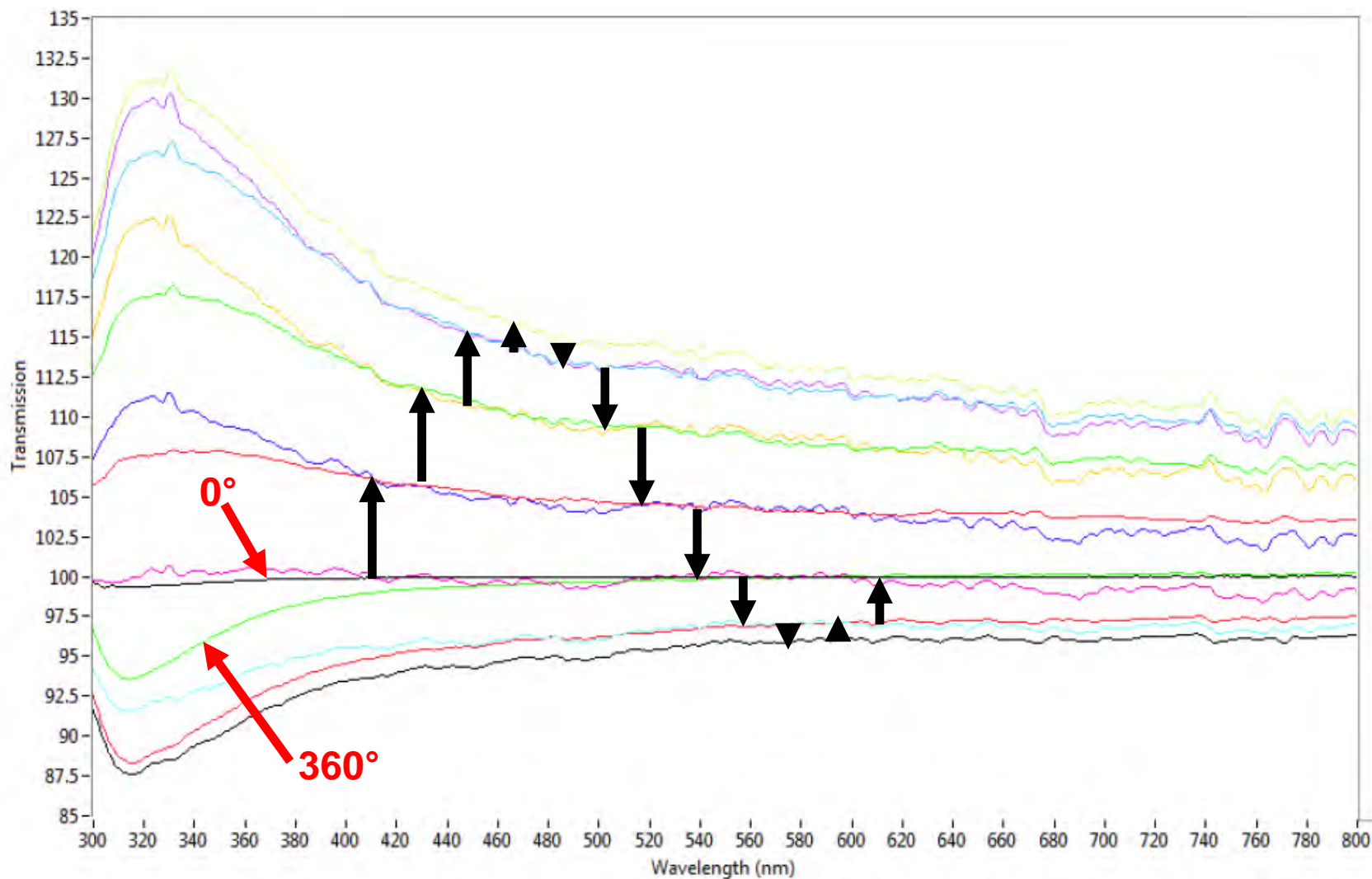


Figure 37. Spectra collected through a blank area of a slide with a tilted coverslip using glycerol as the mounting medium as it was rotated from 0° to 360° (shown in 30° increments) (xenon illumination).

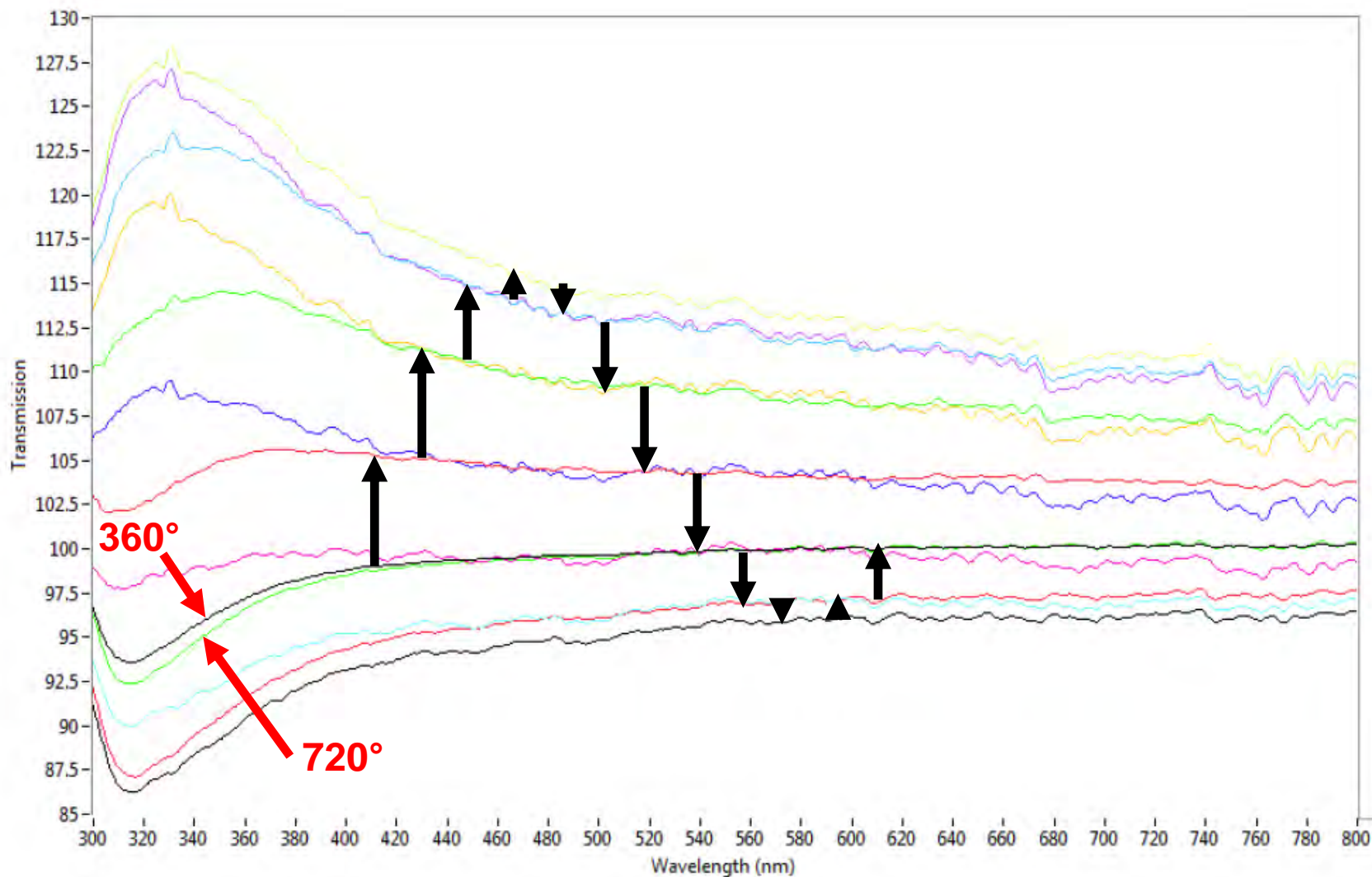


Figure 38. Spectra collected through a blank area of a slide with a tilted coverslip using glycerol as the mounting medium as it was rotated from 360° to 720° (shown in 30° increments) (xenon illumination). Note that the last spectrum collected (*i.e.*, 720° - green) is near the position of the first spectrum collected (*i.e.*, 360° - black) from this second rotation.

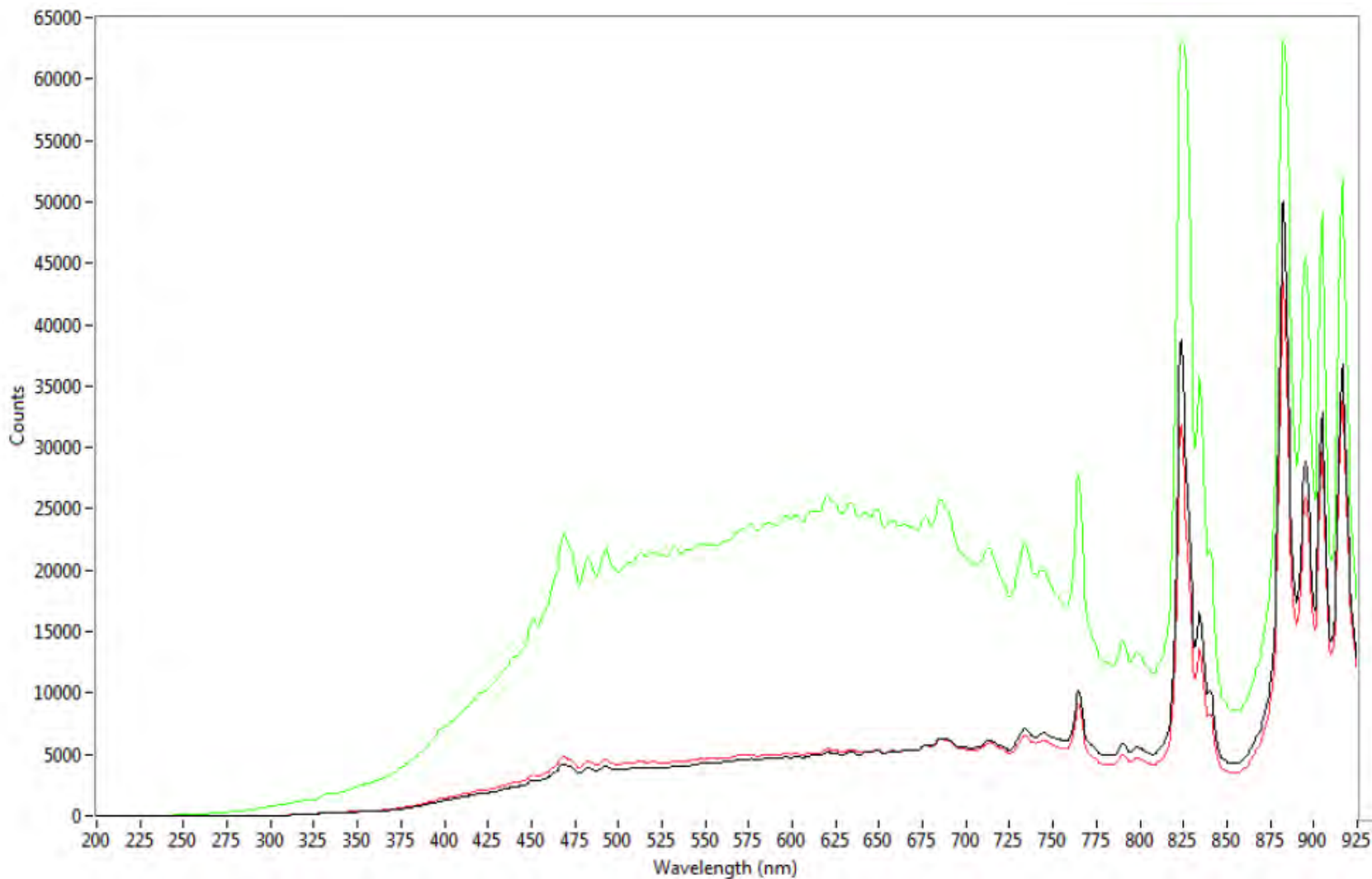


Figure 39. Light reaching the detector (in absolute counts) with no polarizer present (green) compared to when a polarizer is oriented east-west (black) and north-south (red) using xenon illumination.

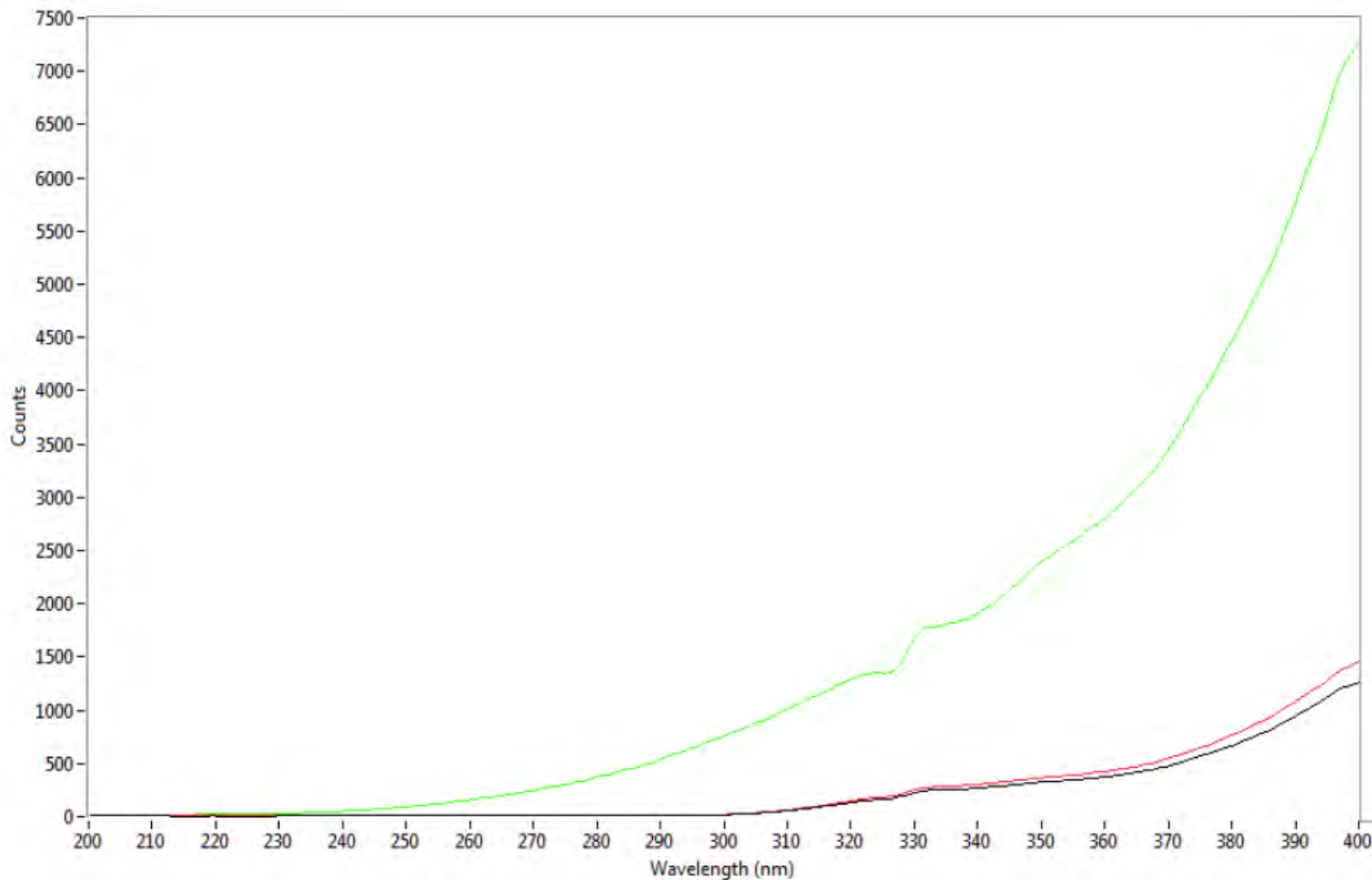


Figure 40. Close-up of the light reaching the detector (in absolute counts) with no polarizer present (green) compared to when a polarizer is oriented east-west (black) and north-south (red) using xenon illumination.

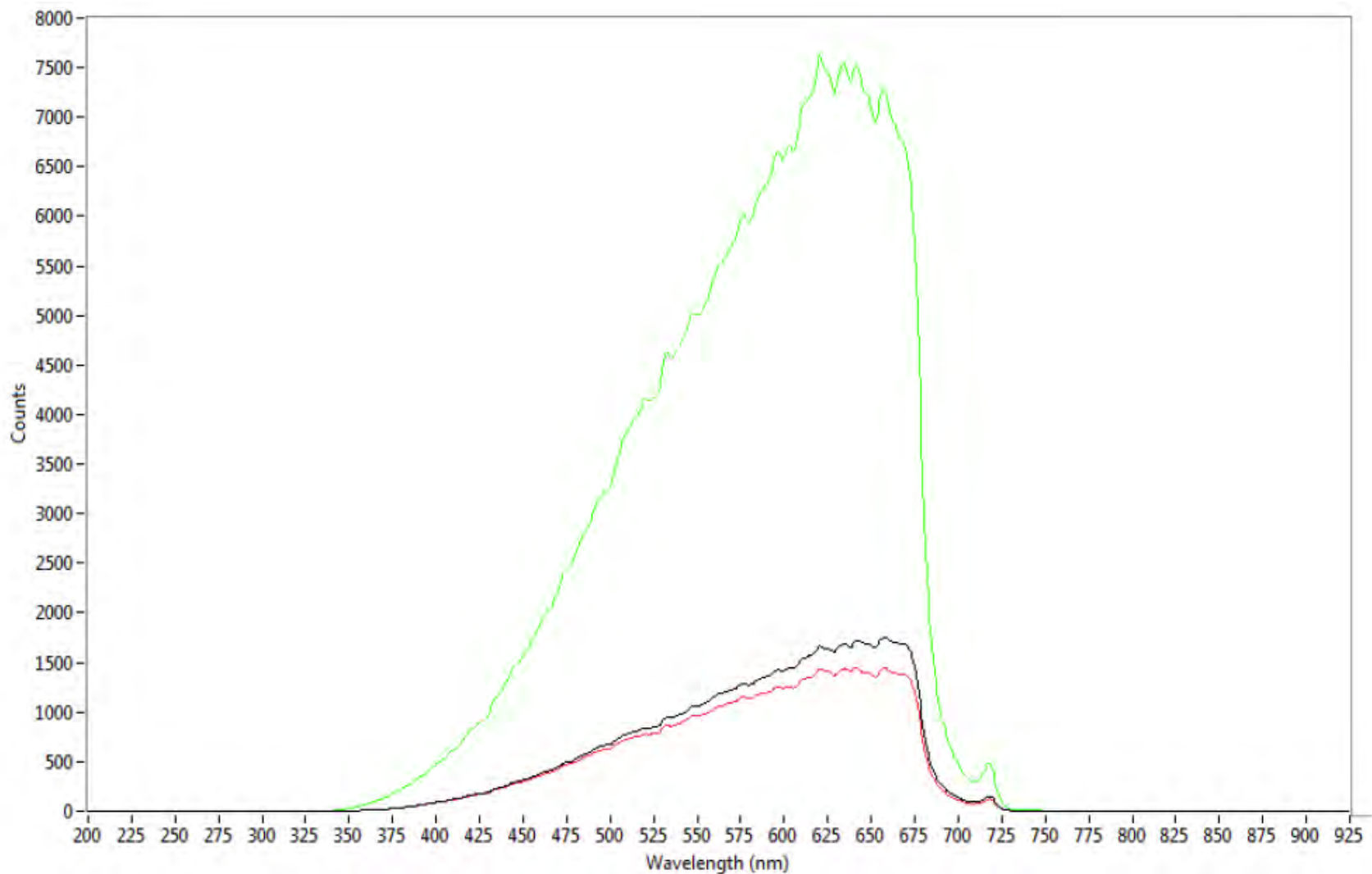


Figure 41. Light reaching the detector (in absolute counts) with no polarizer present (green) compared to when a polarizer is oriented east-west (black) and north-south (red) using tungsten halogen illumination.

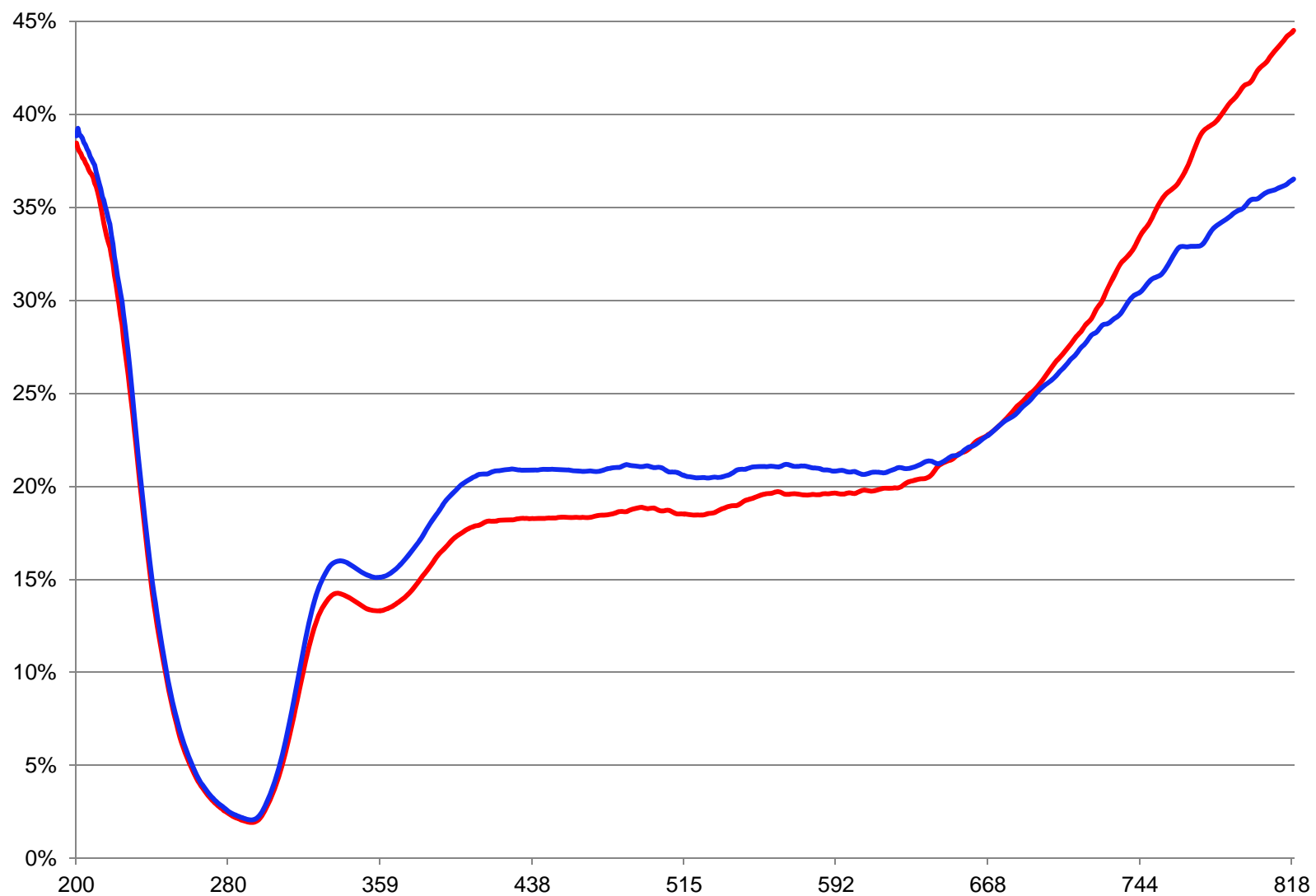


Figure 42. Percentage of light reaching the detector when a polarizer is oriented east-west (red) and north-south (blue) compared to when the polarizer is absent using xenon illumination.

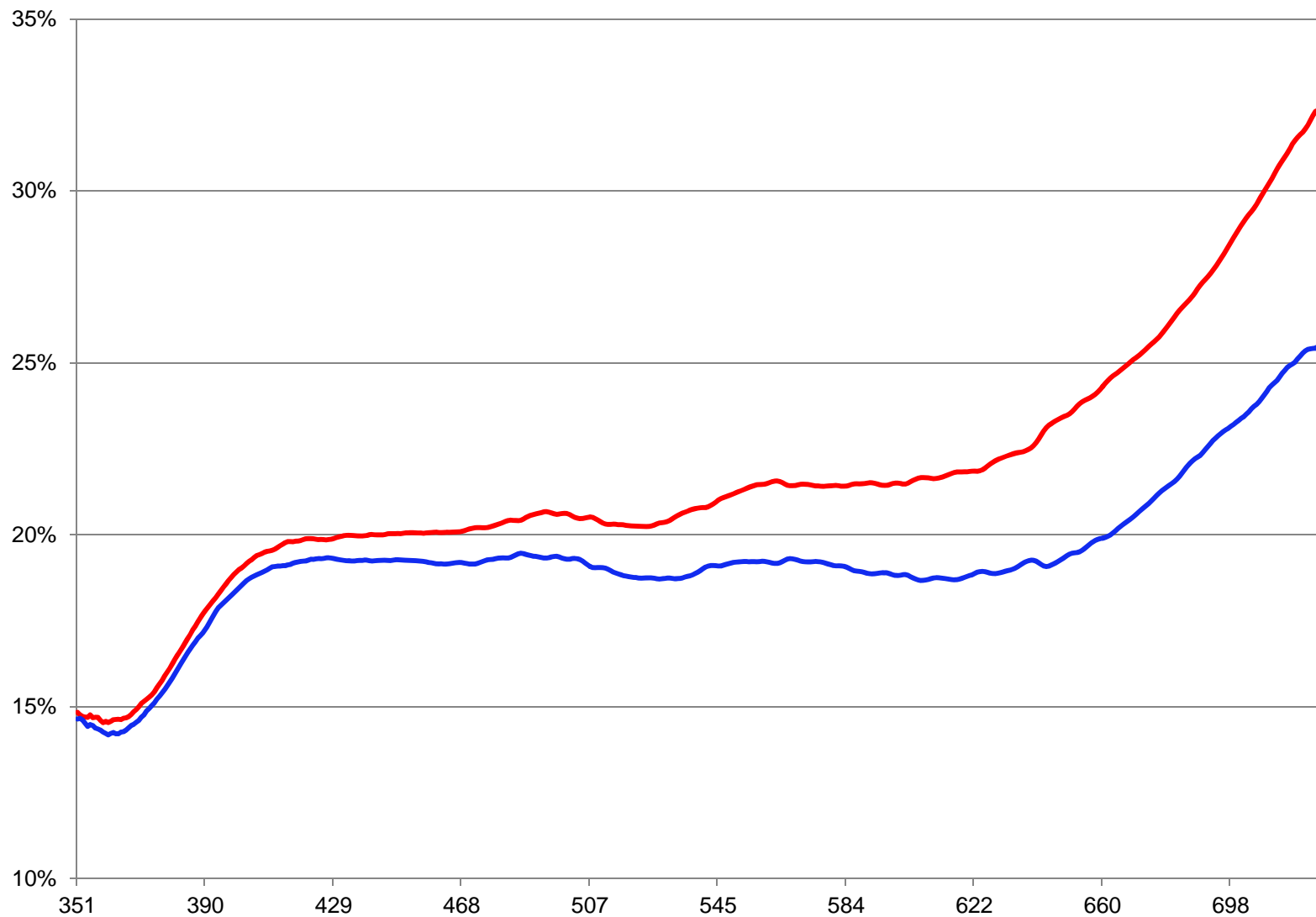


Figure 43. Percentage of light reaching the detector when a polarizer is oriented east-west (red) and north-south (blue) compared to when the polarizer is absent using tungsten halogen illumination.

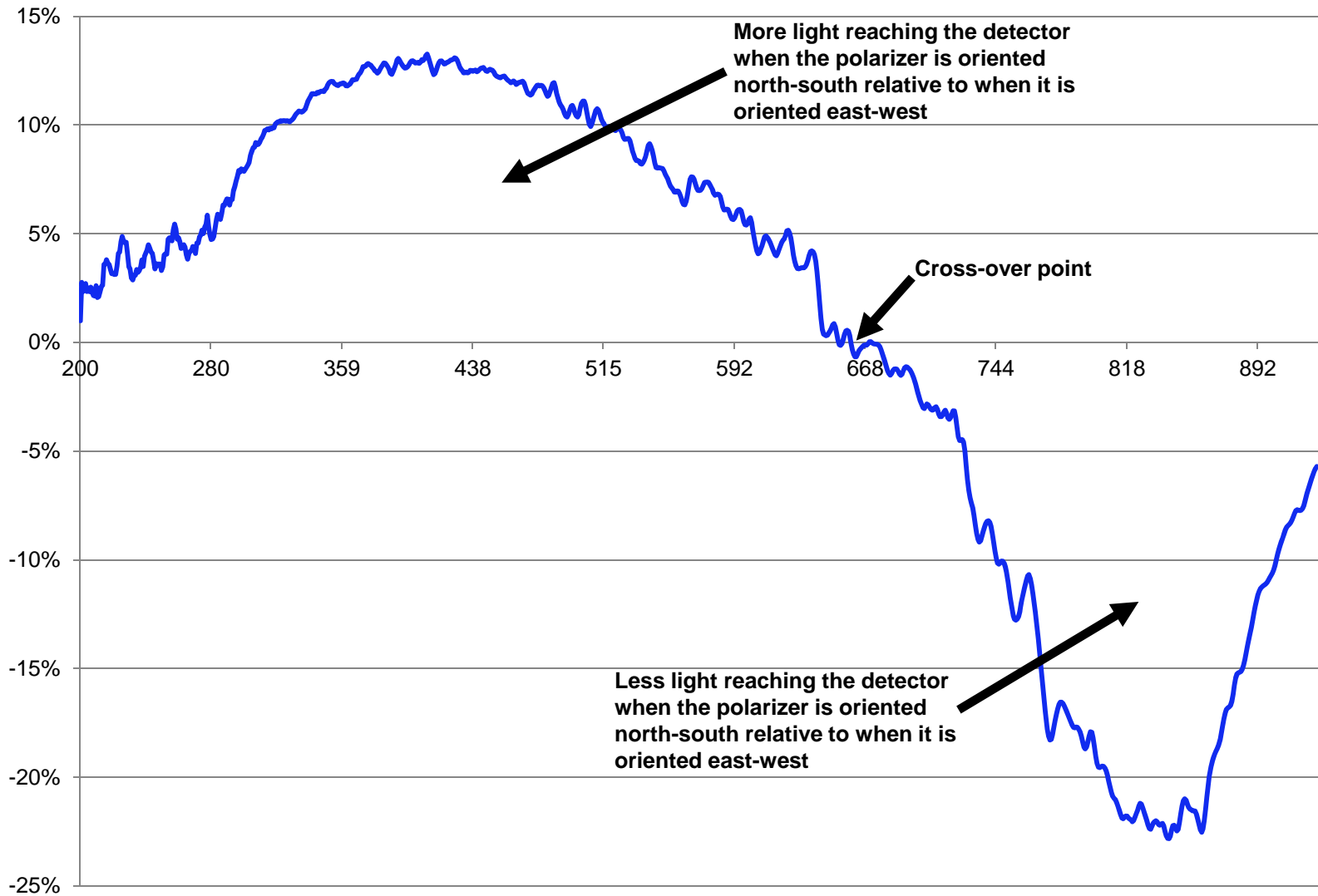


Figure 44. Percentage change in light reaching the detector when the polarizer is oriented north-south relative to when the polarizer is oriented east-west using xenon illumination.

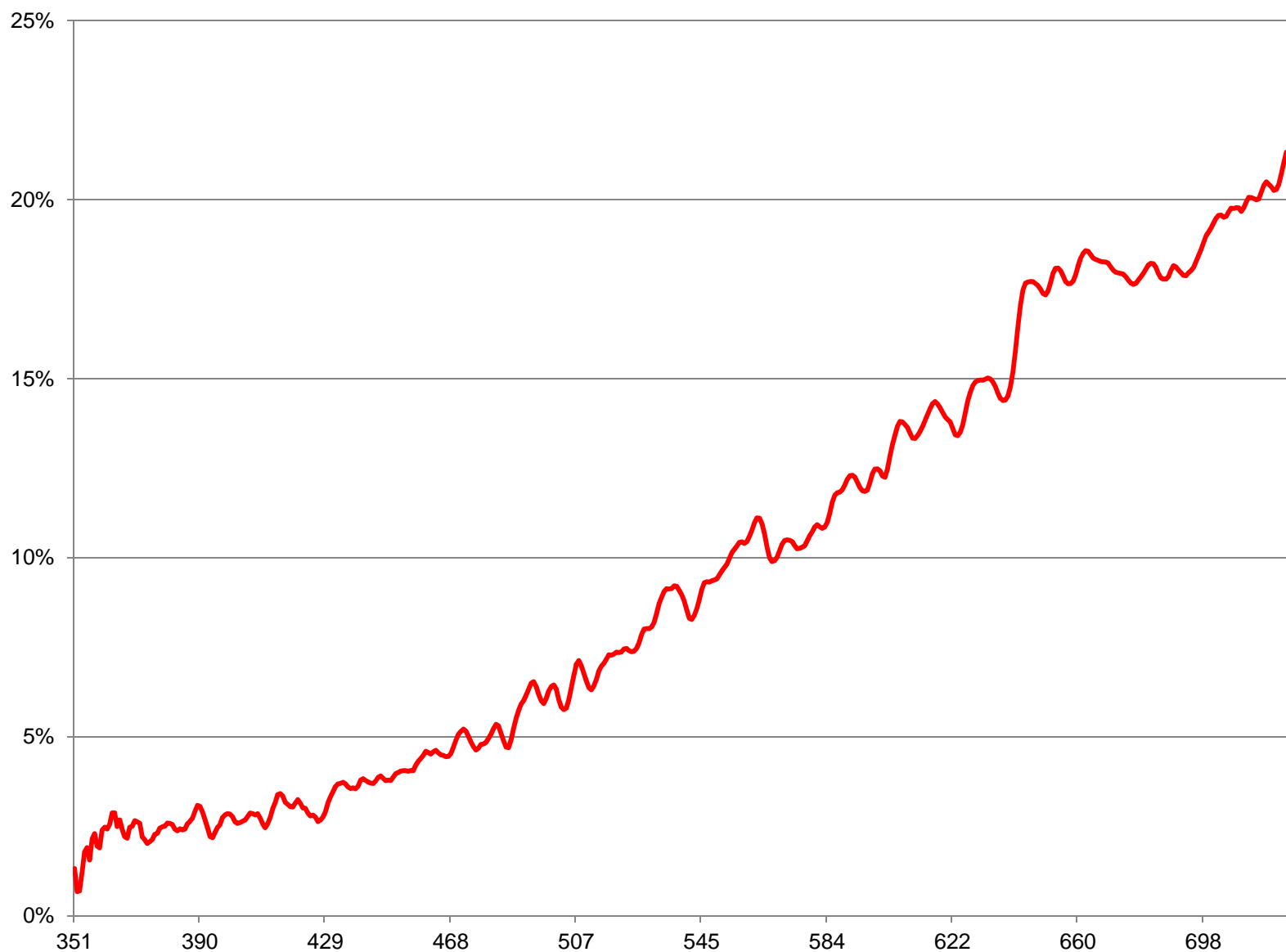


Figure 45. Percentage increase of light reaching the detector when the polarizer is oriented east-west relative to when the polarizer is oriented north-south using tungsten halogen illumination.

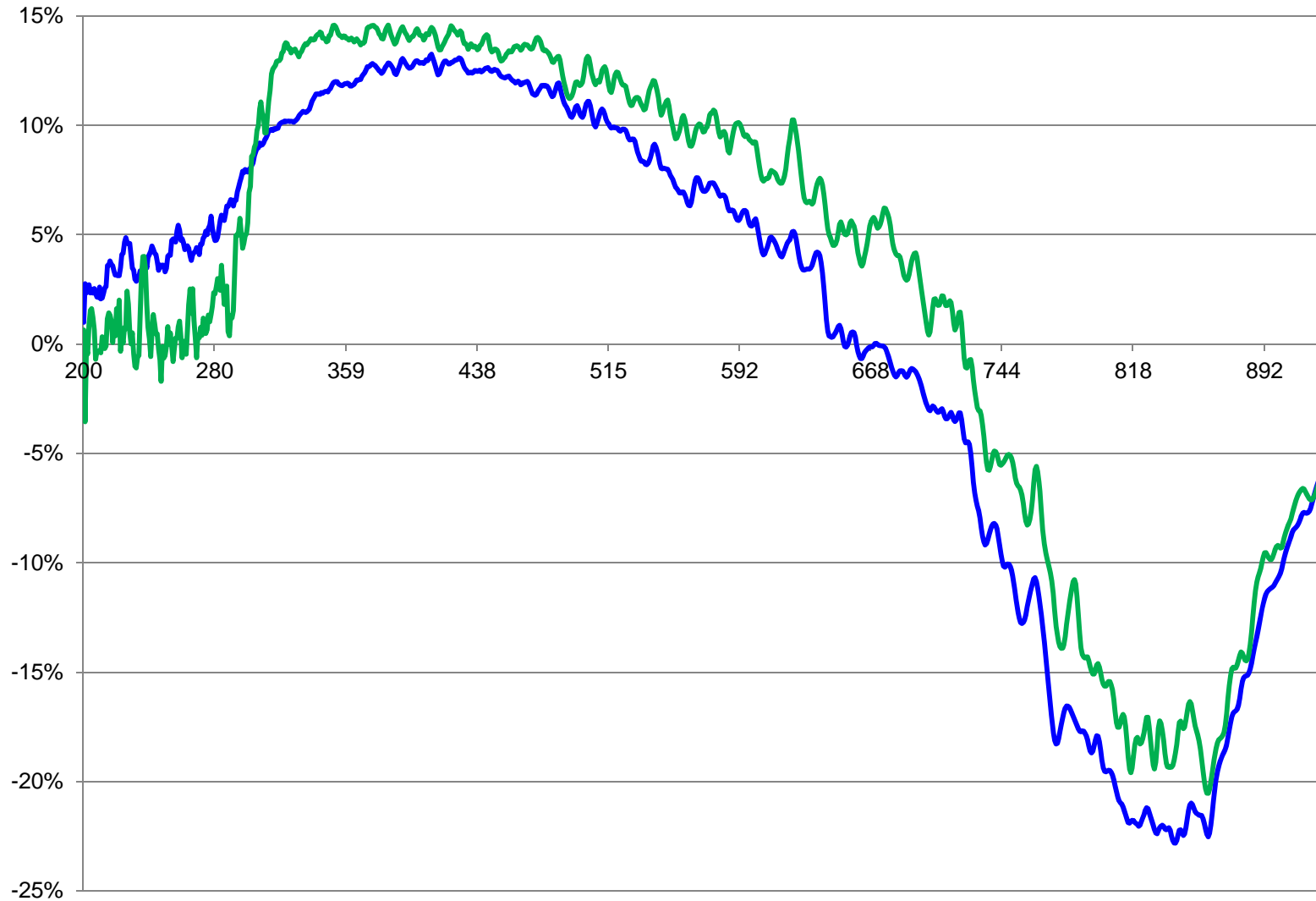


Figure 46. Percentage change in light reaching the detector when the polarizer is oriented north-south relative to when the polarizer is oriented east-west using xenon illumination. The blue plot represents the original data and the green plot was collected using the same polarizer approximately one month later.

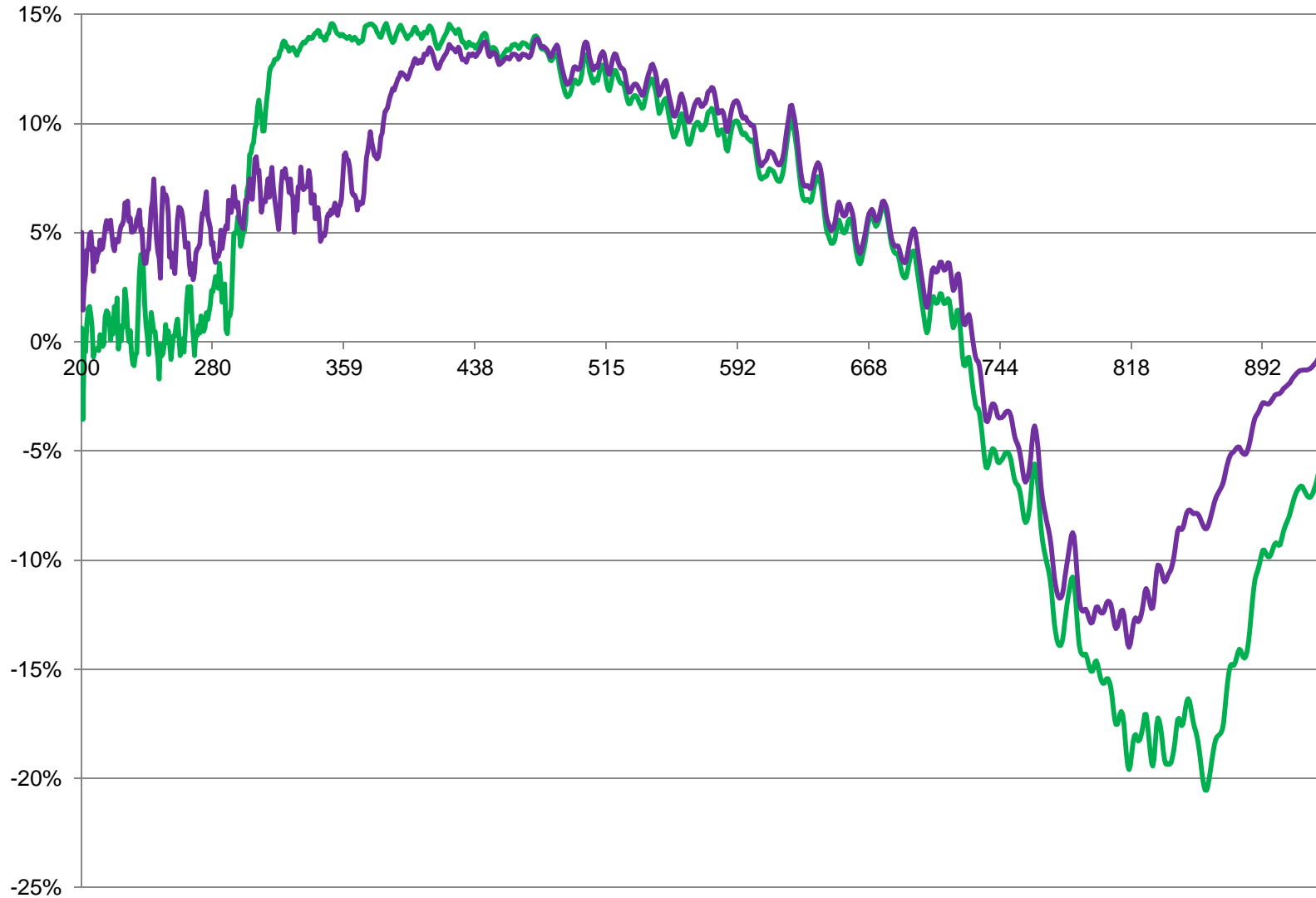


Figure 47. Percentage change in light reaching the detector when the polarizer is oriented north-south relative to when the polarizer is oriented east-west using xenon illumination. The green and purple plots were collected on the same day using different polarizing filters.

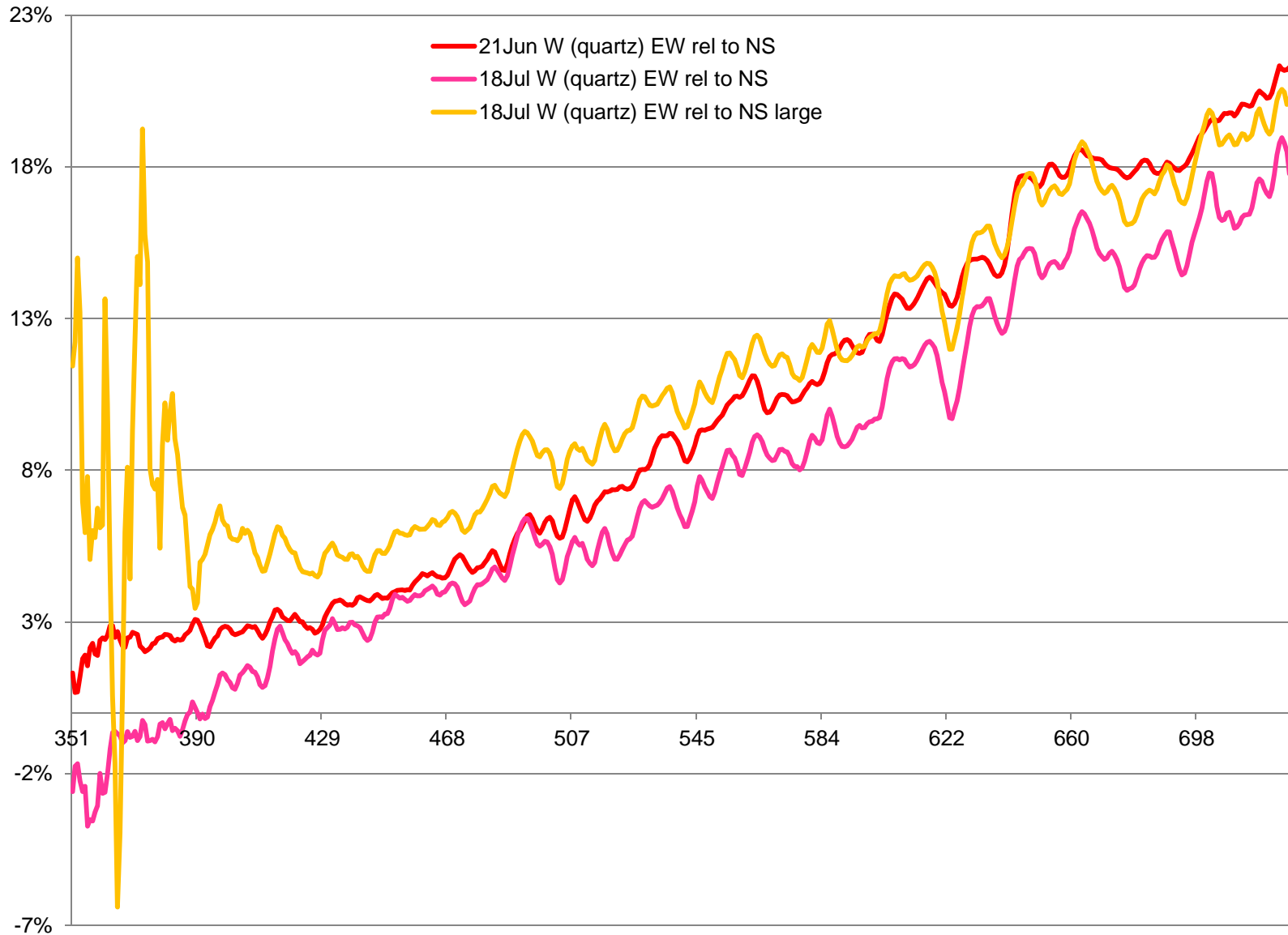


Figure 48. Percentage increase of light reaching the detector when the polarizer is oriented east-west relative to when the polarizer is oriented north-south using tungsten halogen illumination. The original data is plotted in red, the same filter was to collect the data shown in the pink plot a month later at which time a different filter was used to collect the data shown in the yellow plot.

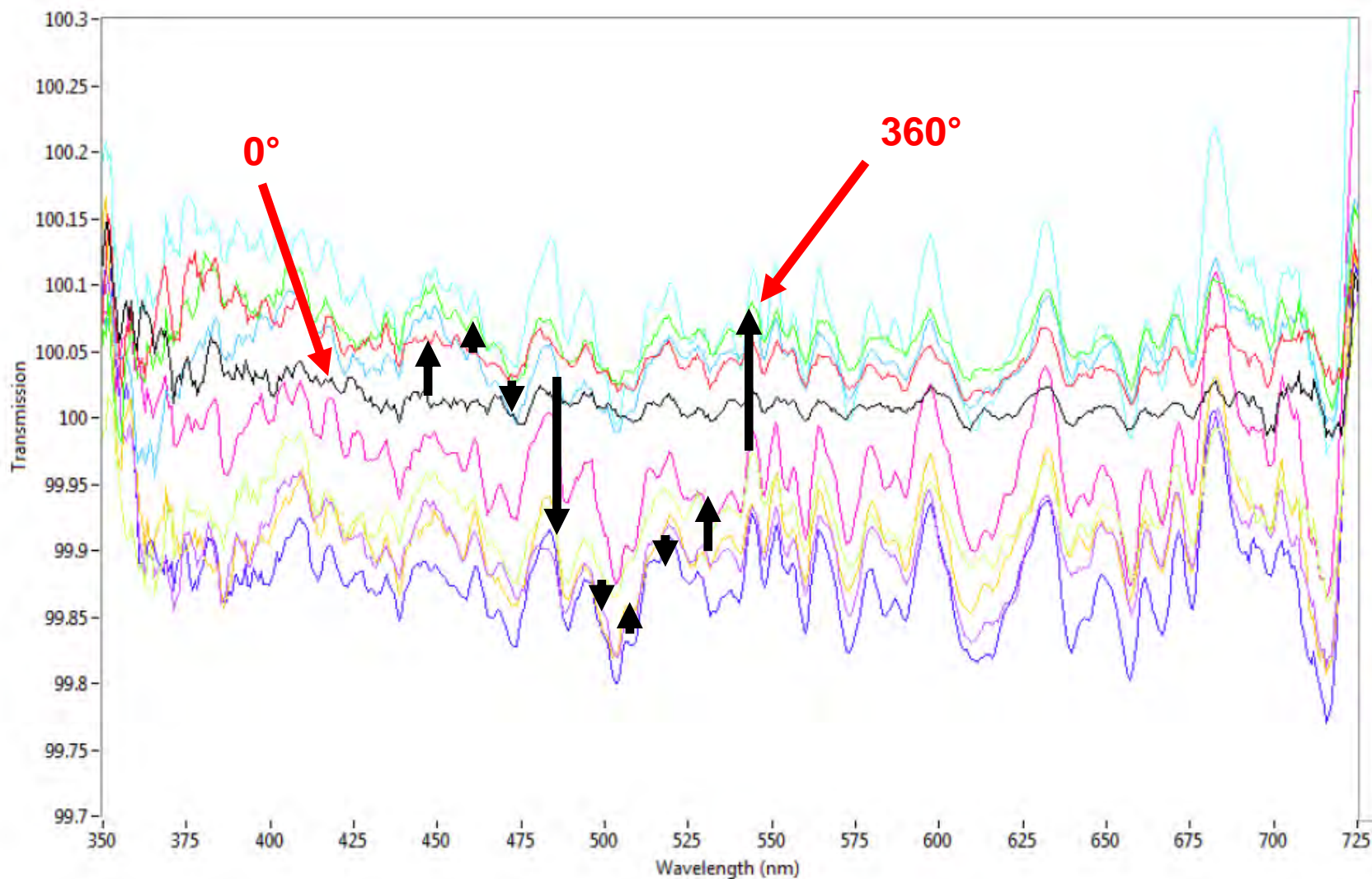


Figure 49. Spectra collected through a blank area of a slide (no sample or coverslip) as it was rotated from 0° to 360° (shown in 40° increments) (tungsten illumination).

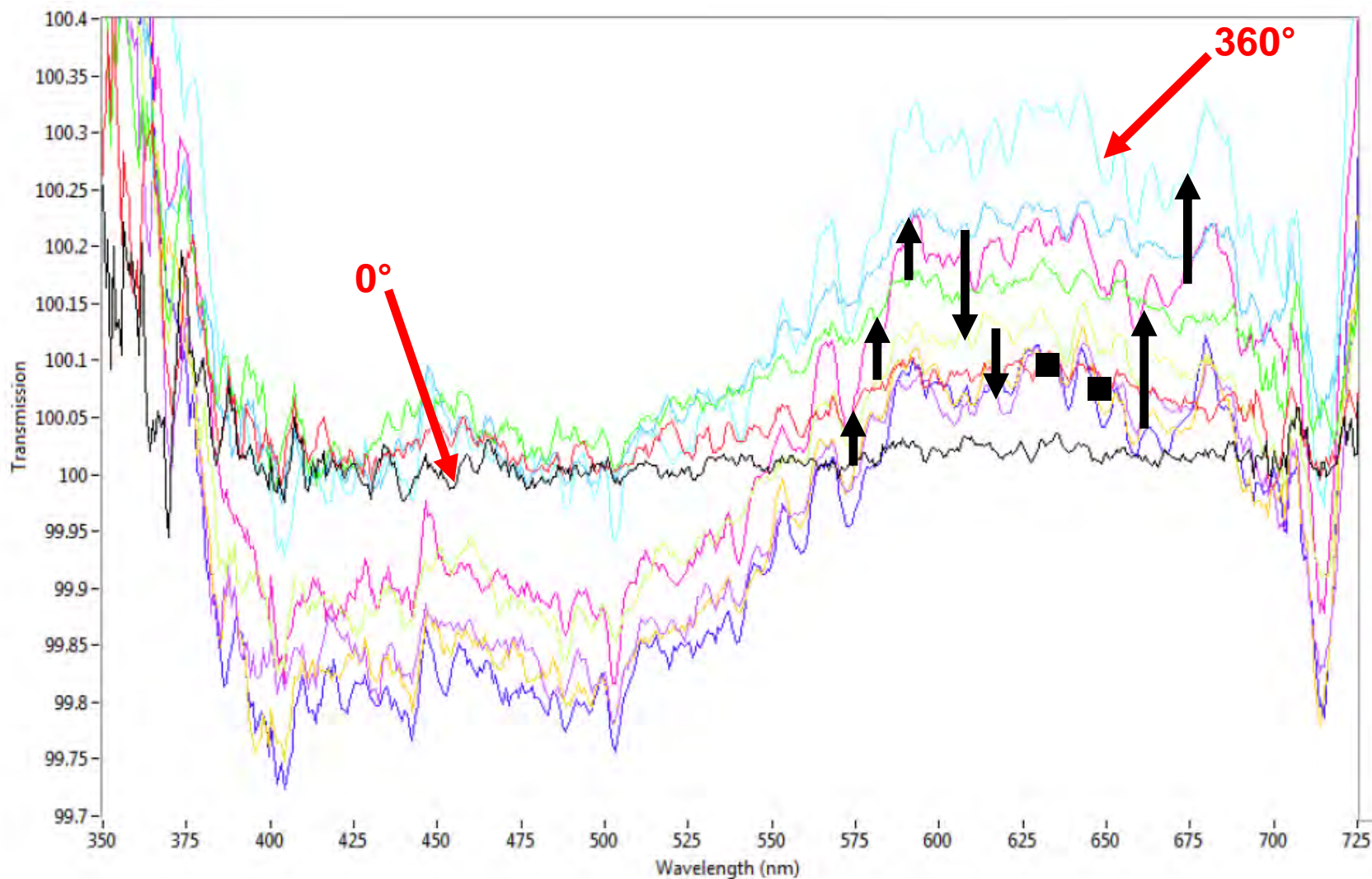


Figure 50. Spectra collected through a blank area of a slide (no sample or coverslip) as it was rotated from 0° to 360° (shown in 40° increments) (tungsten illumination). A polarizing filter was on the field diaphragm in a fixed east-west orientation throughout this experiment.

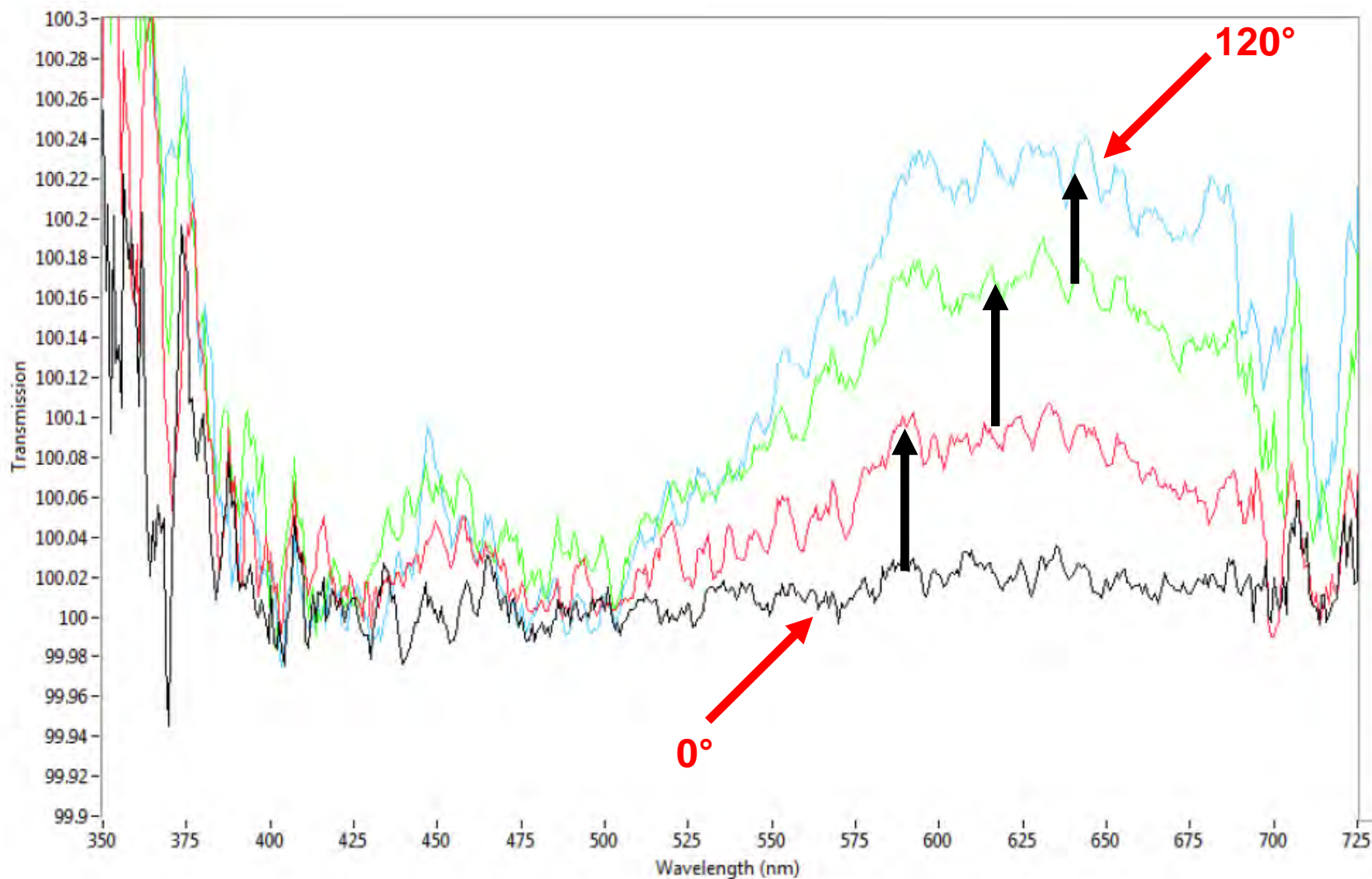


Figure 51. Spectra collected through a blank area of a slide (no sample or coverslip) as it was rotated from 0° to 120° (shown in 40° increments) (tungsten illumination). A polarizing filter was on the field diaphragm in a fixed east-west orientation throughout this experiment.

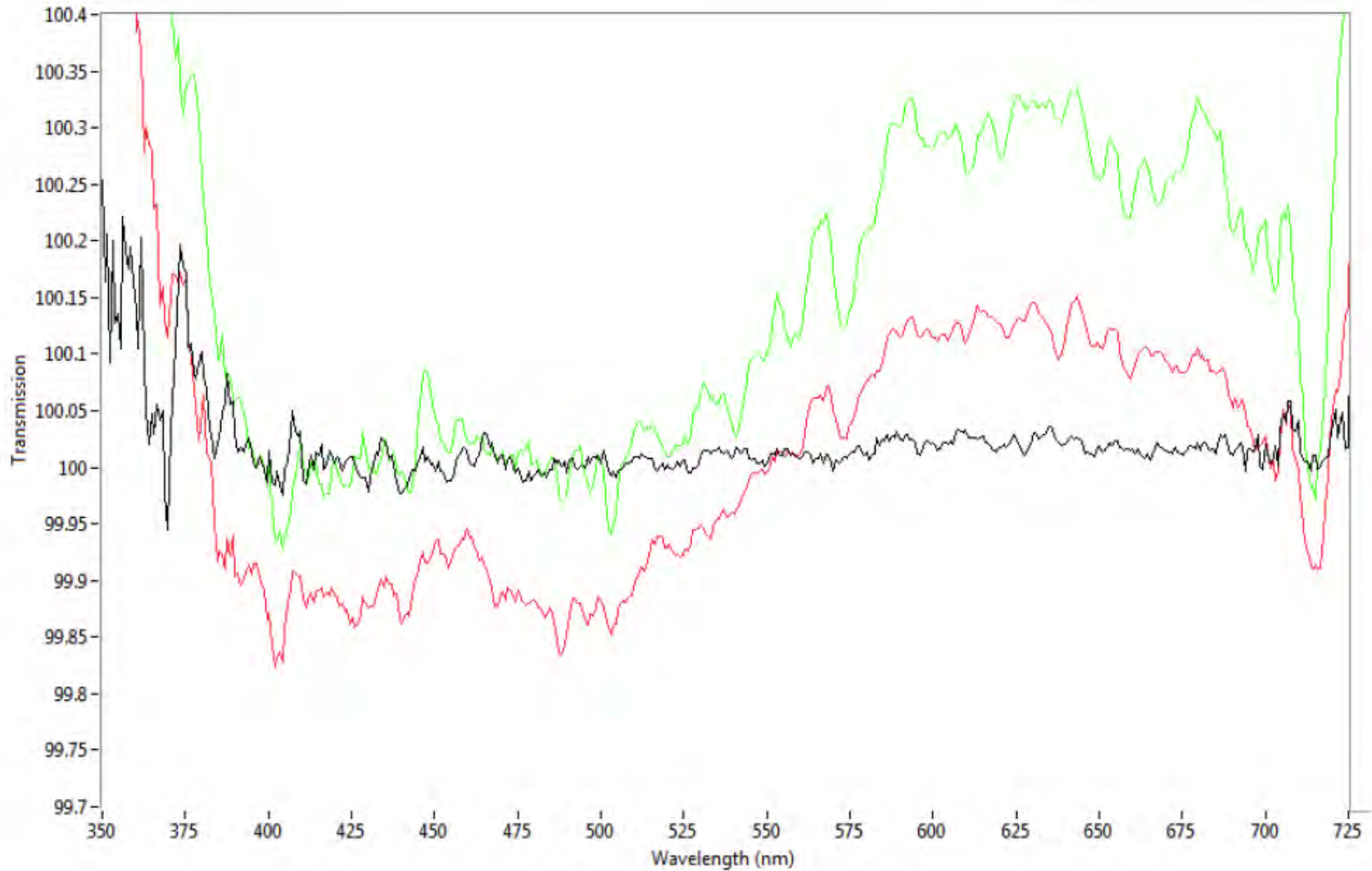


Figure 52. Spectra collected through a blank area of a slide (no sample or coverslip) as it was rotated from 0° (black), to 160° (red) and 360° (green) (tungsten illumination). A polarizing filter was on the field diaphragm in a fixed east-west orientation.

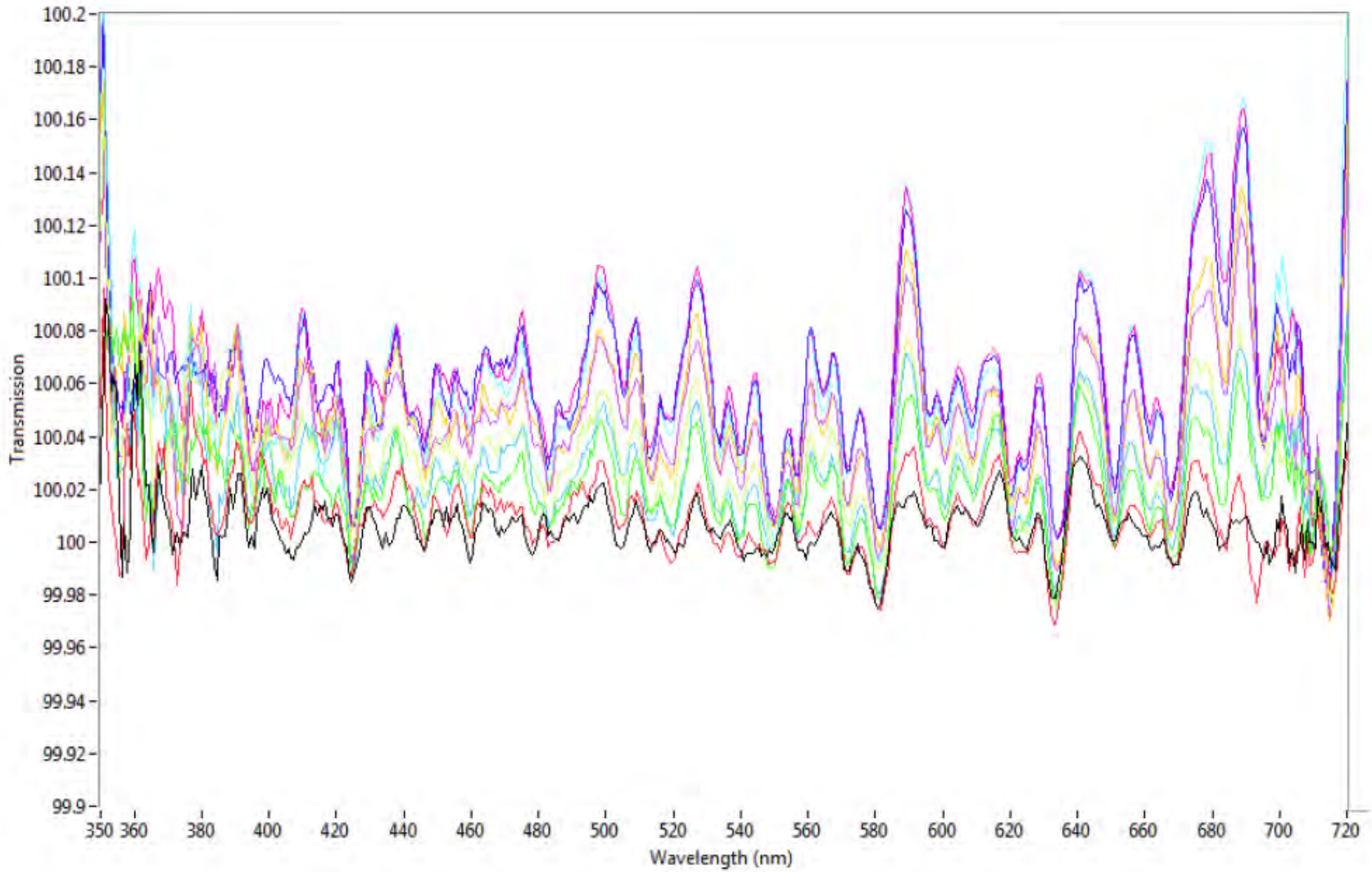


Figure 53. Spectra collected through a blank area of a slide (no sample or coverslip) every 30 seconds for 5 minutes (tungsten illumination).

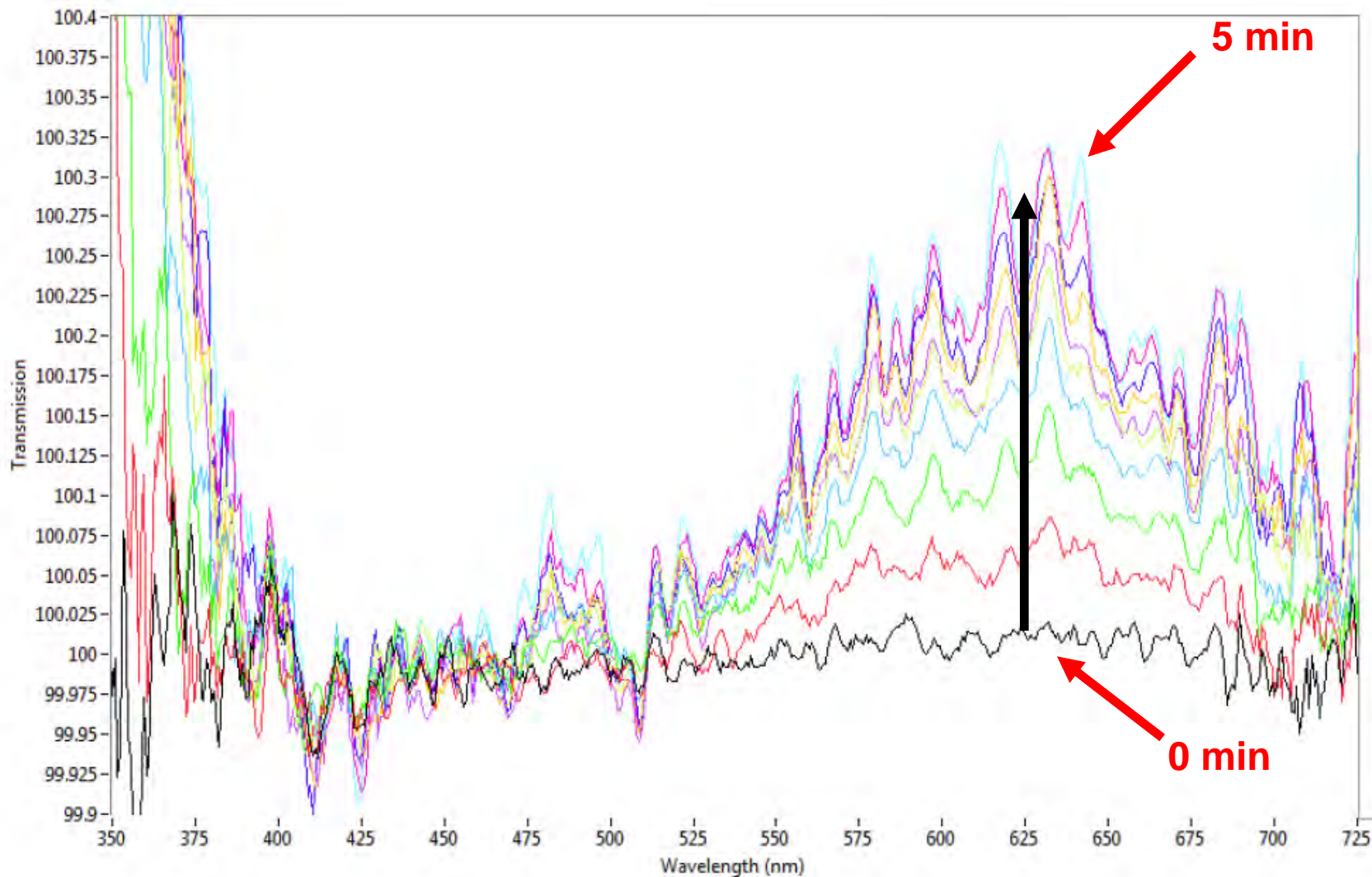


Figure 54. Spectra collected through a blank area of a slide (no sample or coverslip) every 30 seconds for 5 minutes (tungsten illumination). A polarizing filter was on the field diaphragm in a fixed east-west orientation.

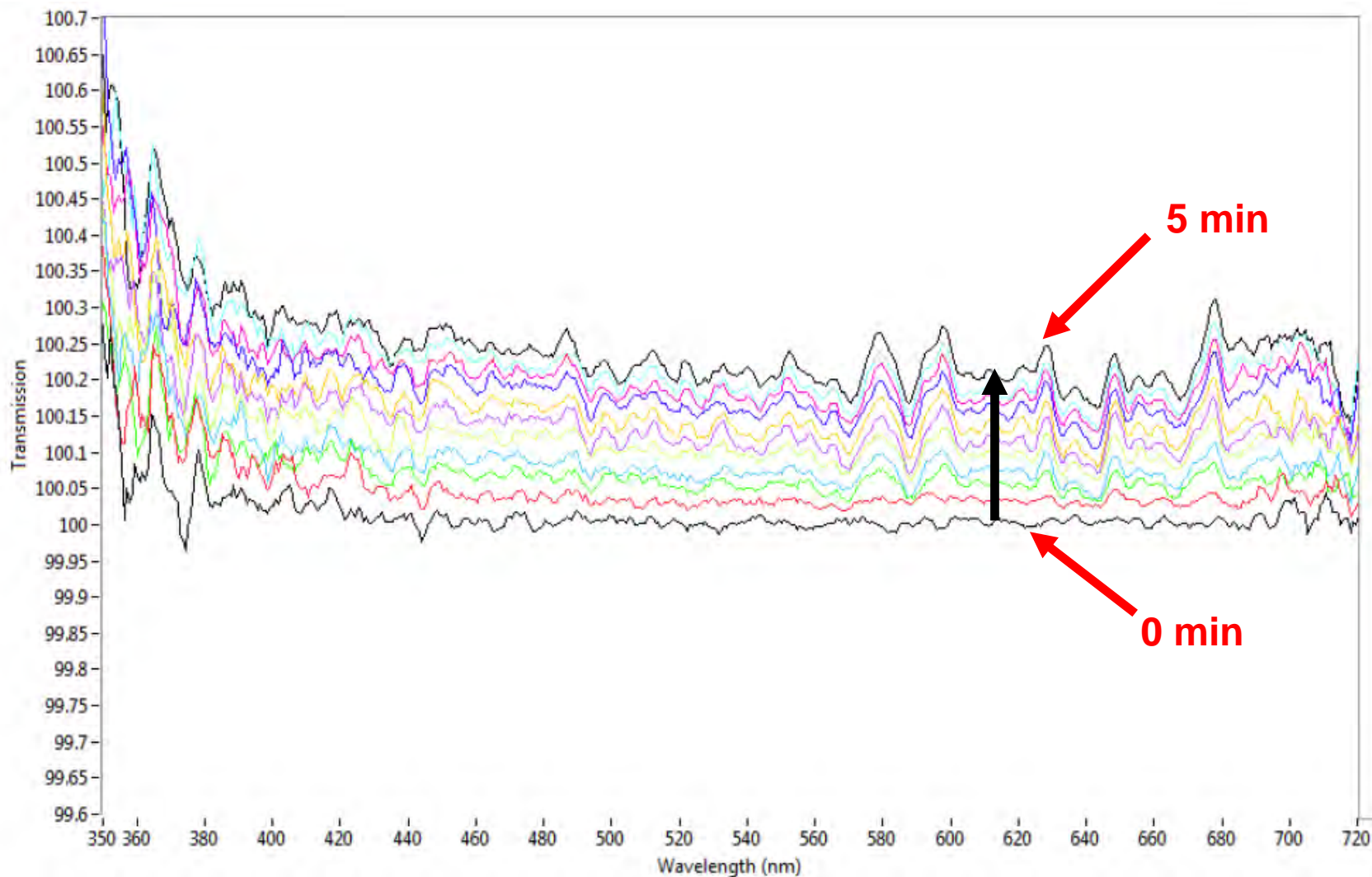


Figure 55. Spectra collected through a blank area (no slide, sample or coverslip) every 30 seconds for 5 minutes (tungsten illumination).

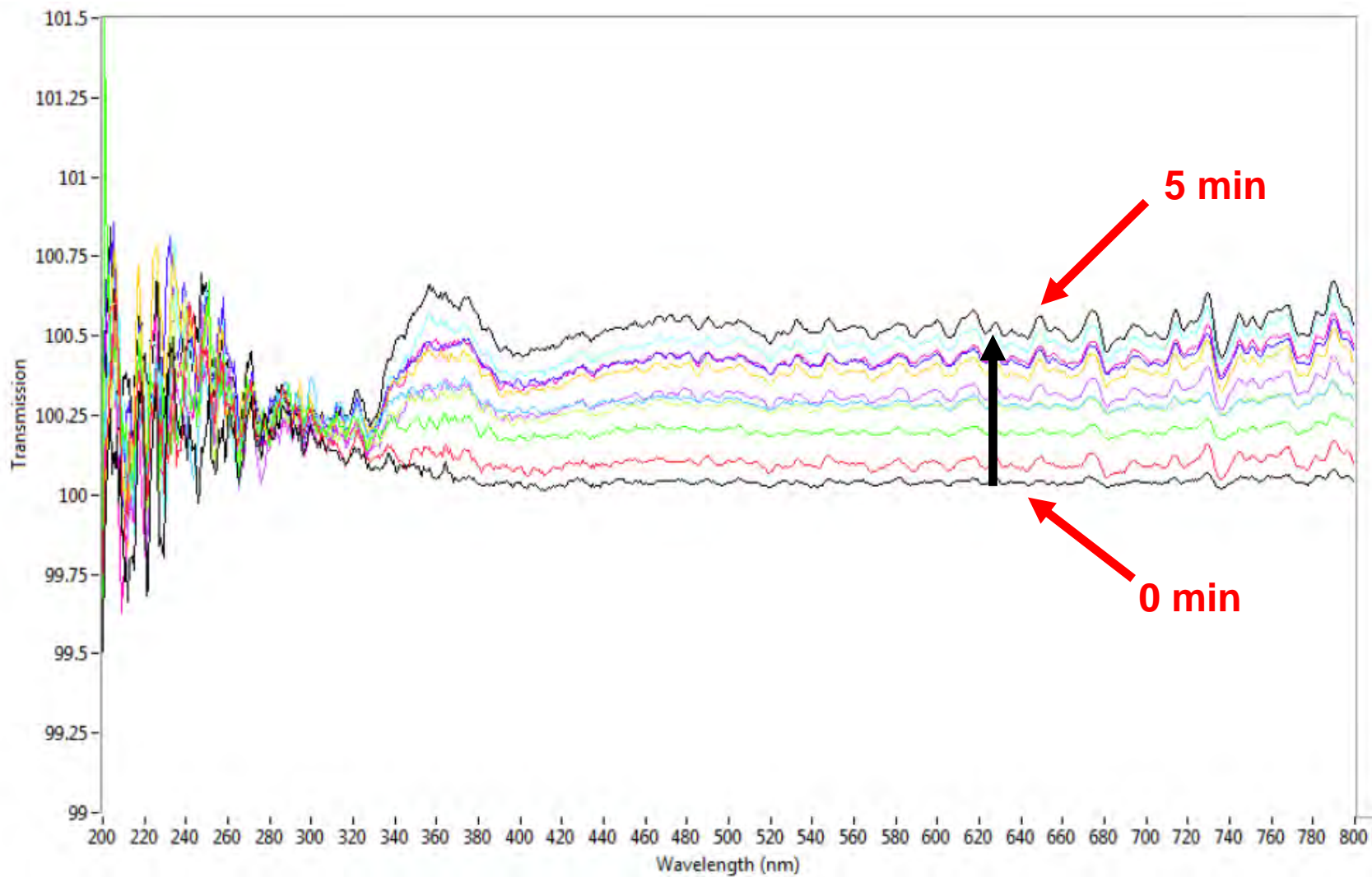


Figure 56. Spectra collected through a blank area (no slide, sample or coverslip) every 30 seconds for 5 minutes (xenon illumination).

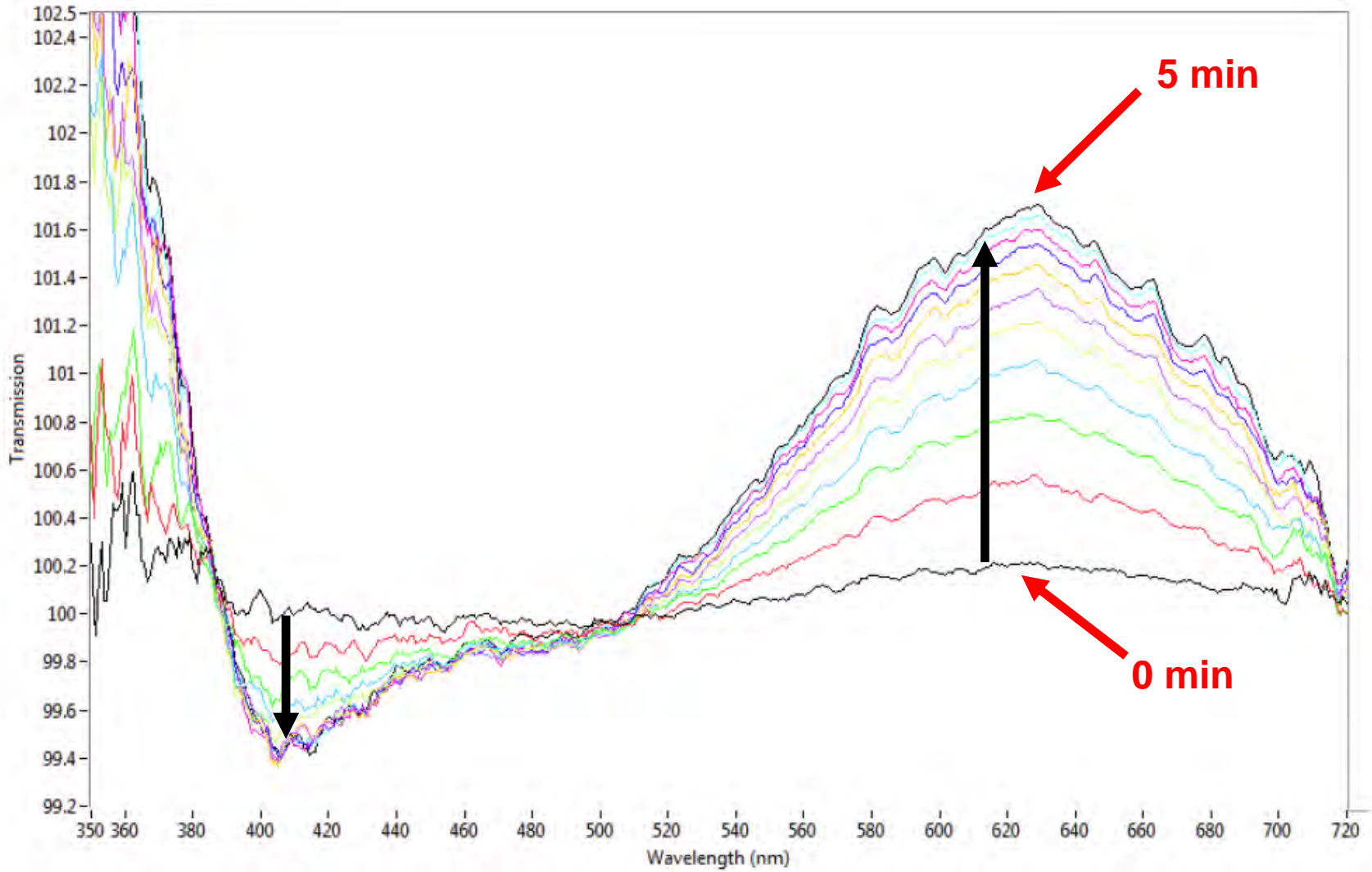


Figure 57. Spectra collected through a blank area (no slide, sample or coverslip) every 30 seconds for 5 minutes with Polarizer A oriented east-west (tungsten illumination).

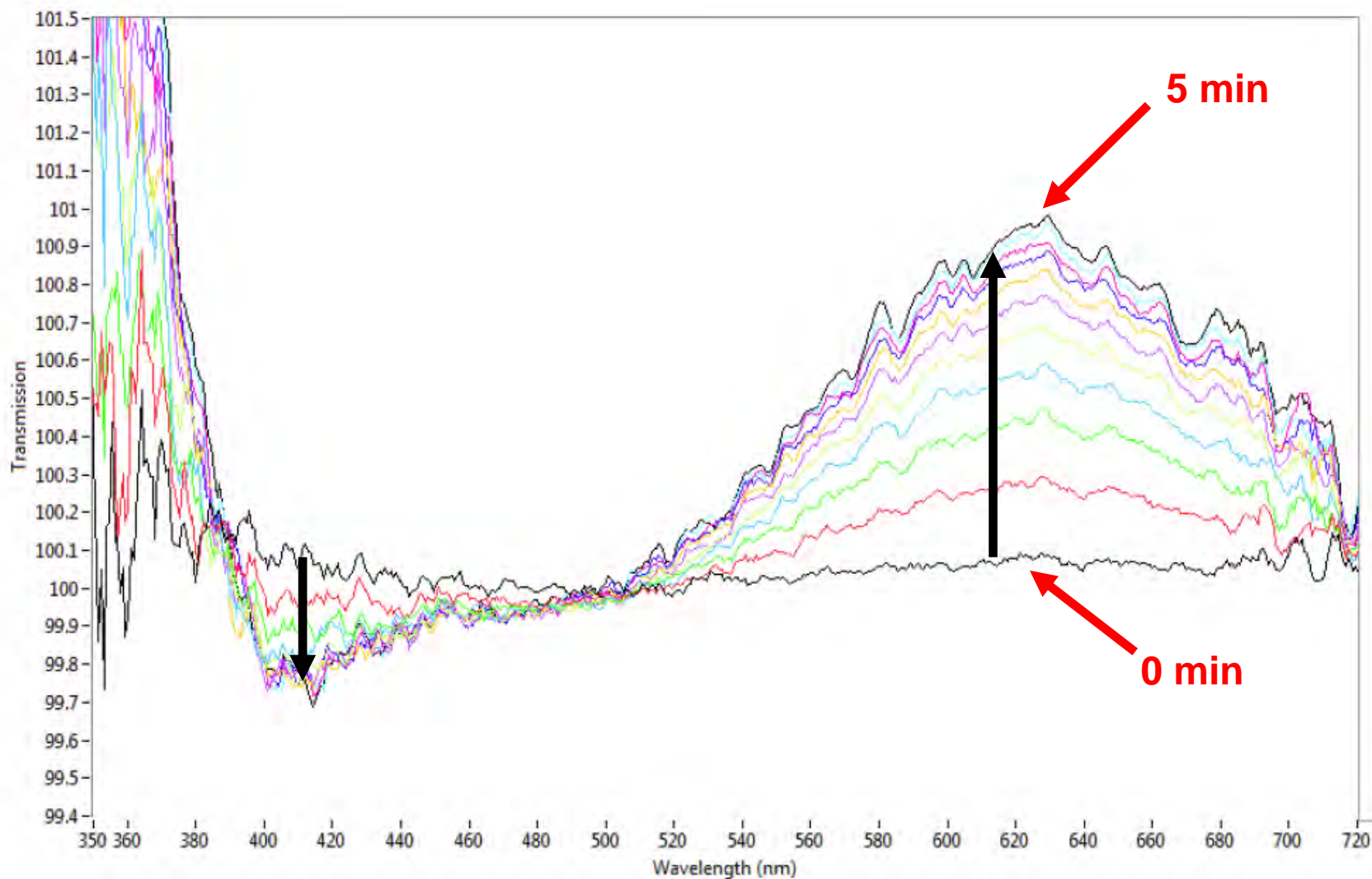


Figure 58. Spectra collected through a blank area (no slide, sample or coverslip) every 30 seconds for 5 minutes with Polarizer A oriented north-south (tungsten illumination).

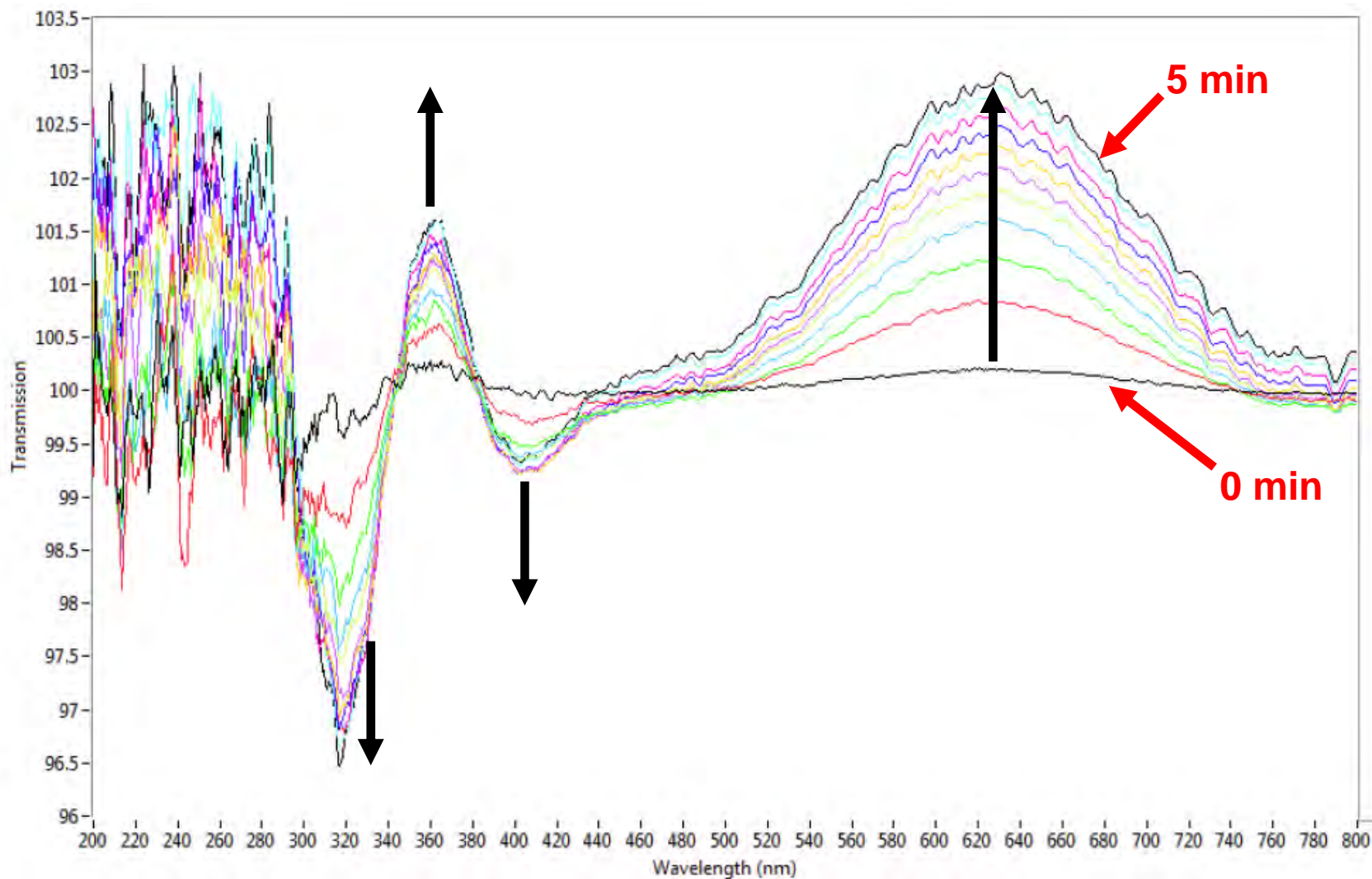


Figure 59. Spectra collected through a blank area (no slide, sample or coverslip) every 30 seconds for 5 minutes with Polarizer A oriented east-west (xenon illumination).

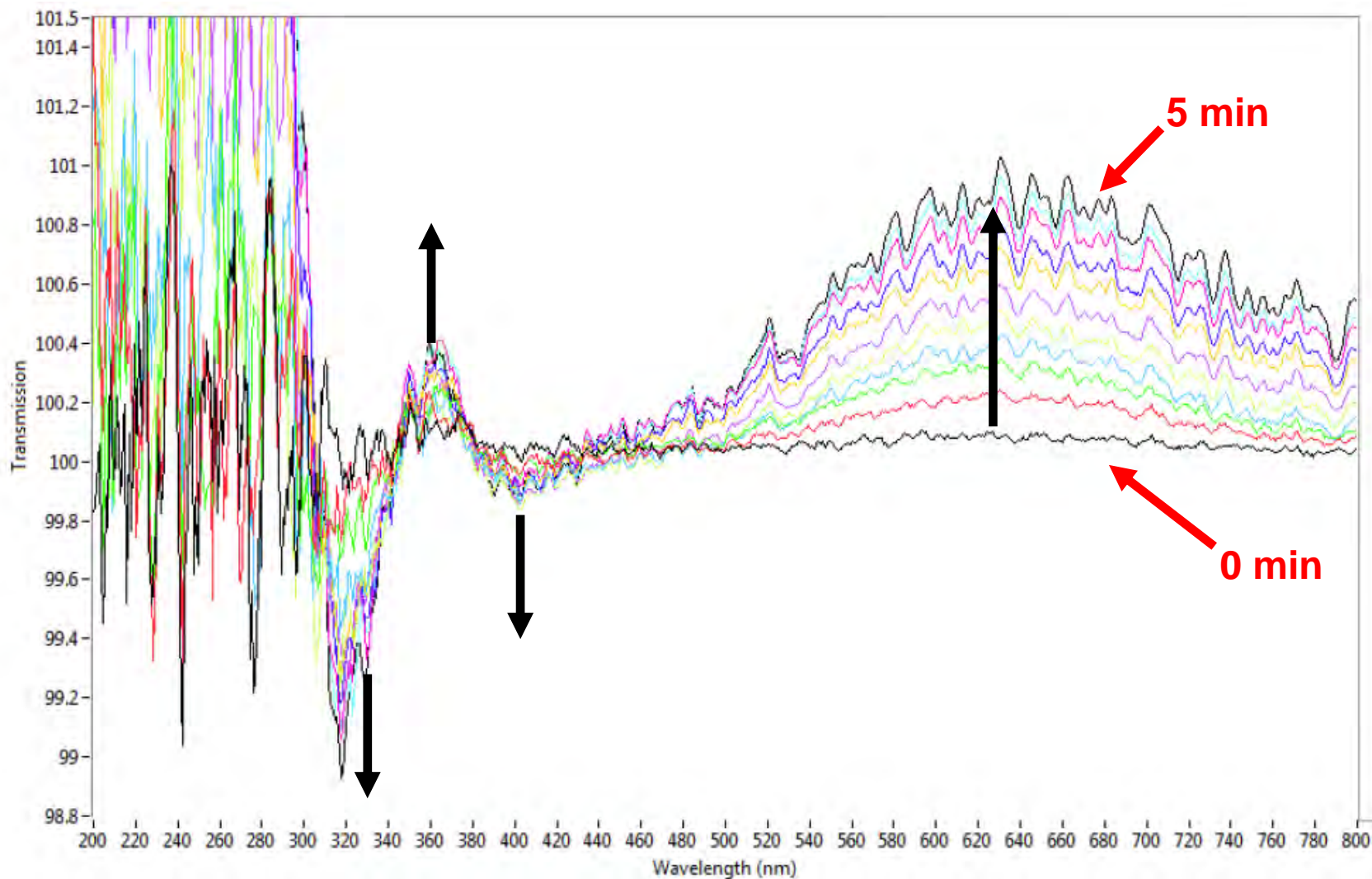


Figure 60. Spectra collected through a blank area (no slide, sample or coverslip) every 30 seconds for 5 minutes with Polarizer A oriented north-south (xenon illumination).

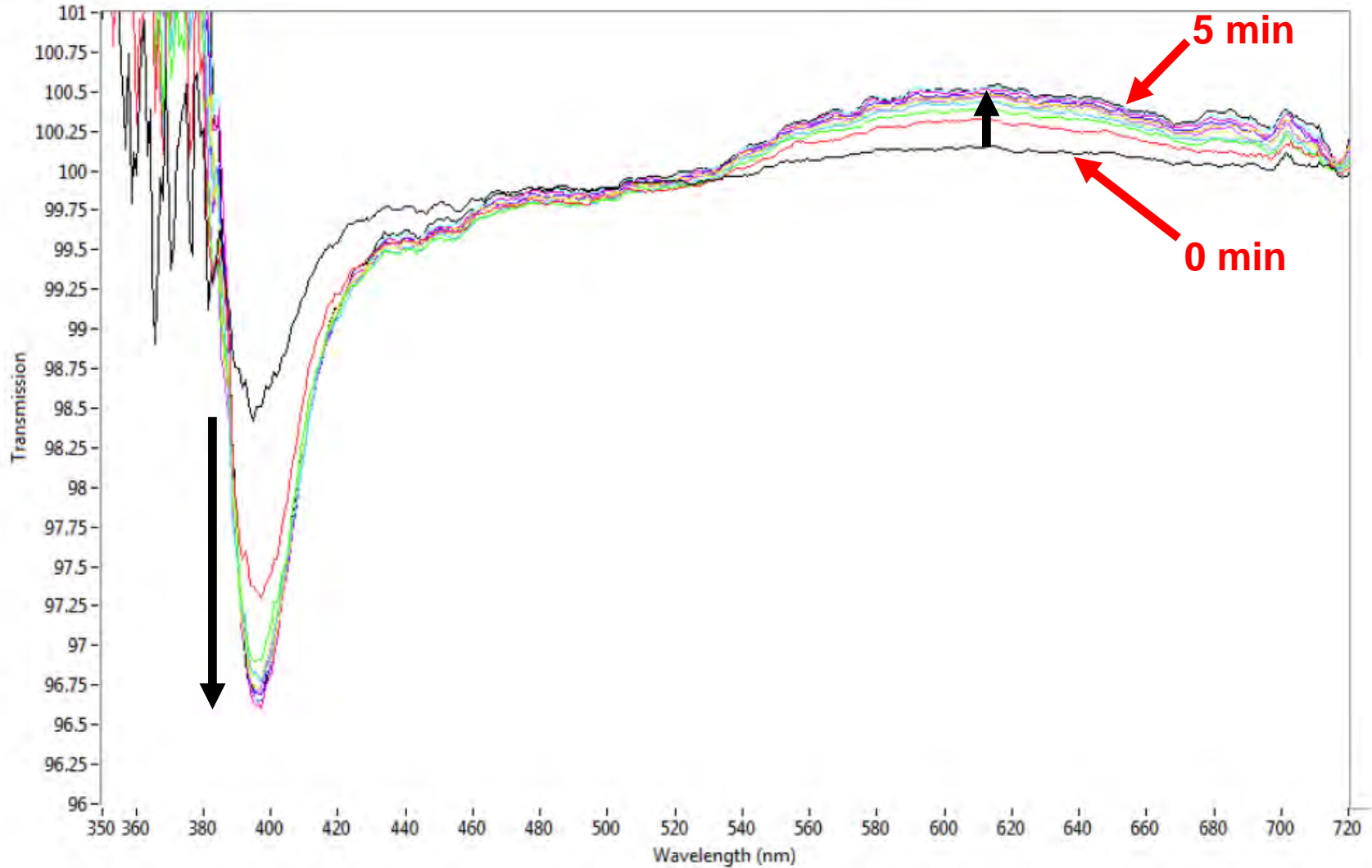


Figure 61. Spectra collected through a blank area (no slide, sample or coverslip) every 30 seconds for 5 minutes with Polarizer B oriented east-west (tungsten illumination).

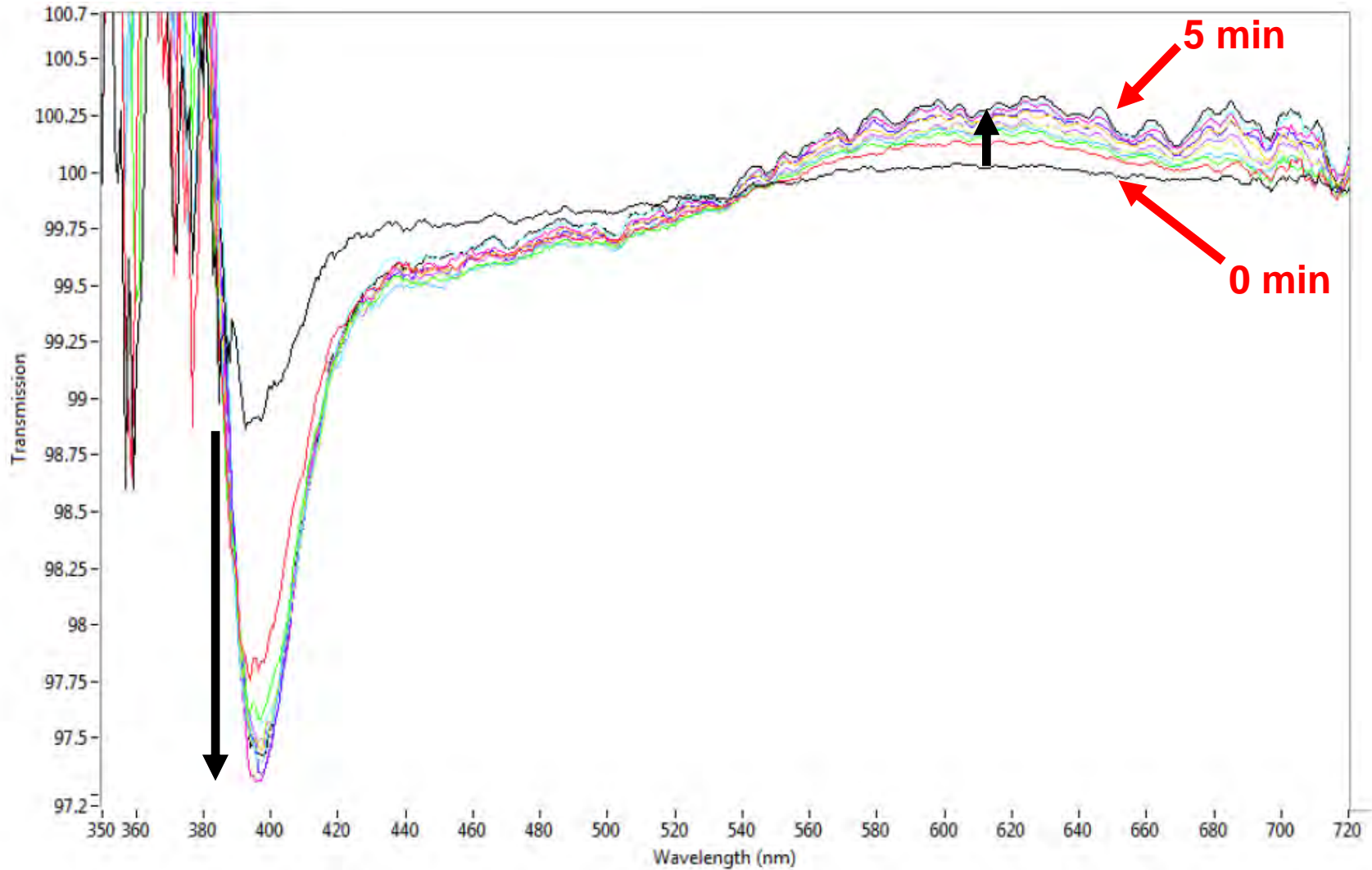


Figure 62. Spectra collected through a blank area (no slide, sample or coverslip) every 30 seconds for 5 minutes with Polarizer B oriented north-south (tungsten illumination).

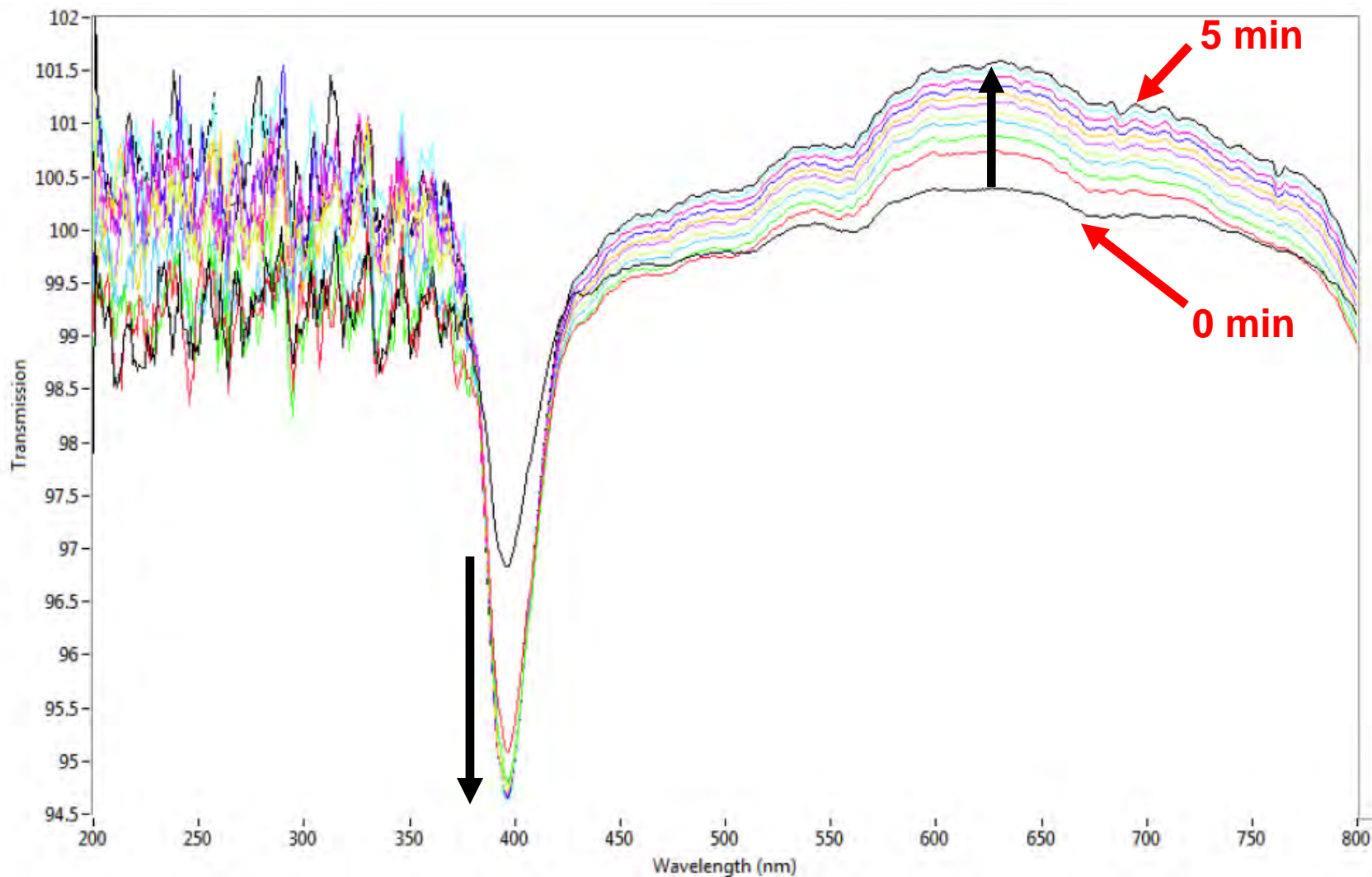


Figure 63. Spectra collected through a blank area (no slide, sample or coverslip) every 30 seconds for 5 minutes with Polarizer B oriented east-west (xenon illumination).

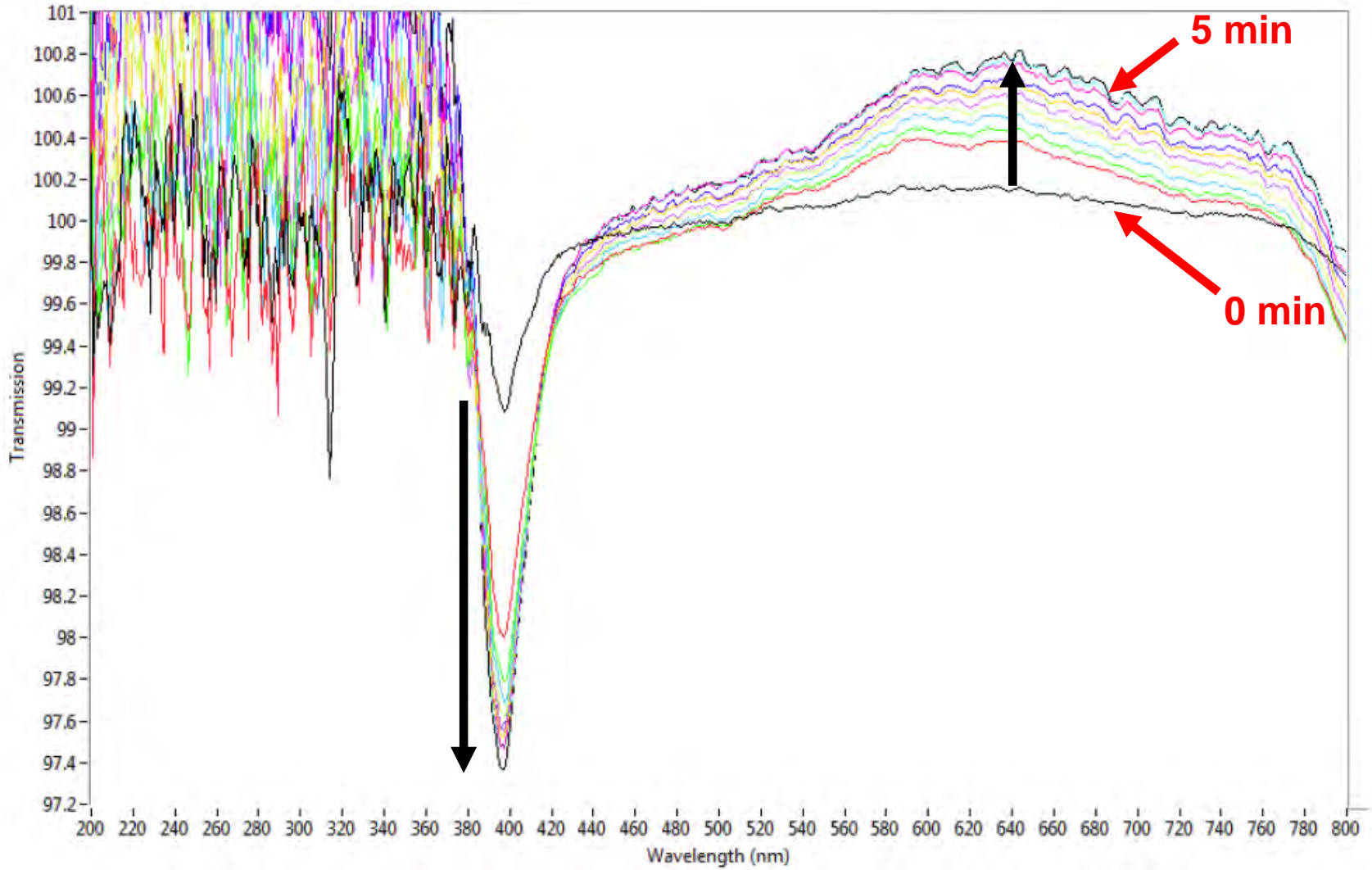


Figure 64. Spectra collected through a blank area (no slide, sample or coverslip) every 30 seconds for 5 minutes with Polarizer B oriented north-south (xenon illumination).

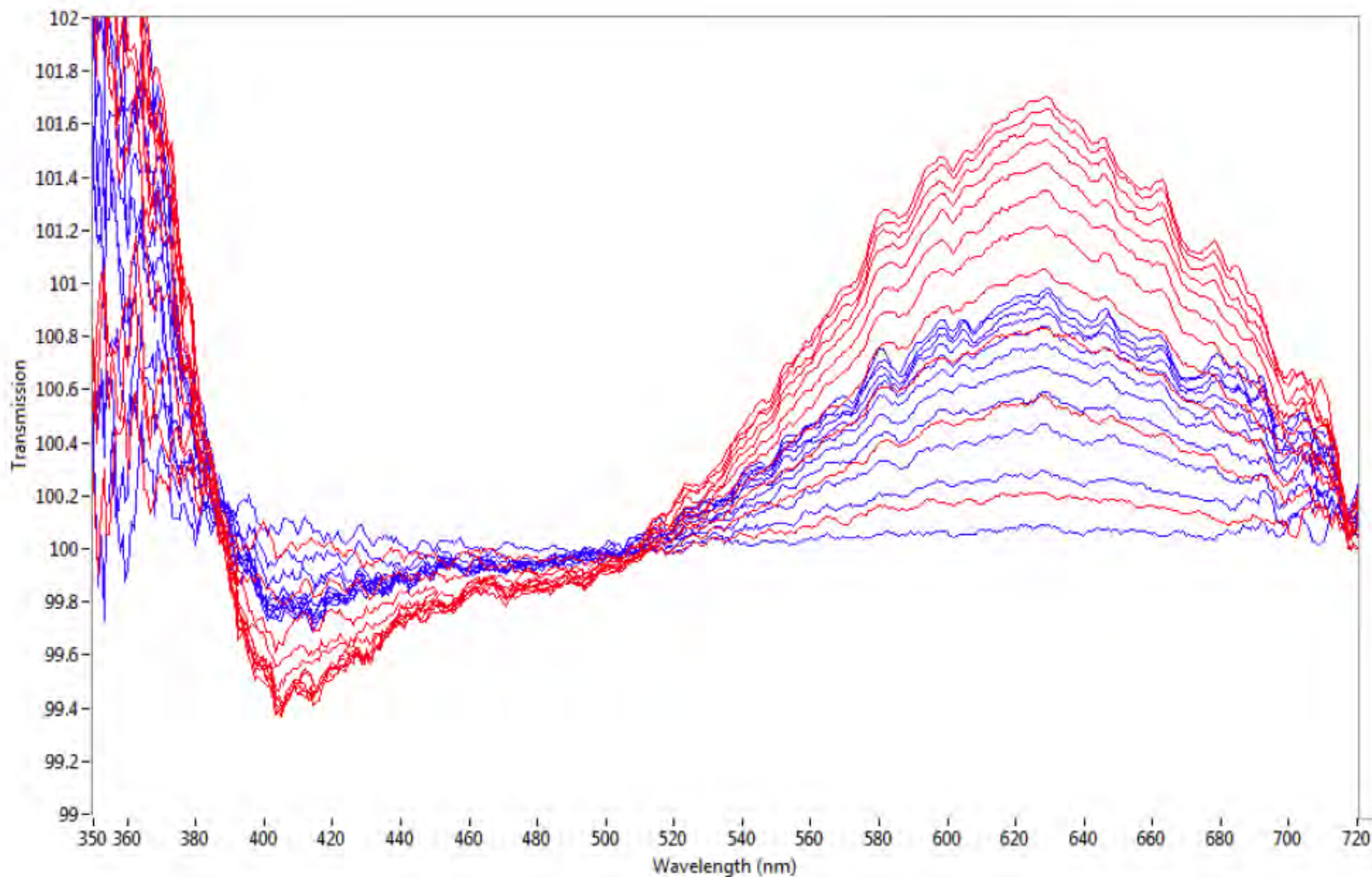


Figure 65. Comparison of spectra collected through a blank area (no slide, sample or coverslip) every 30 seconds for 5 minutes with Polarizer A oriented east-west (red) and then north-south (blue) (tungsten illumination).

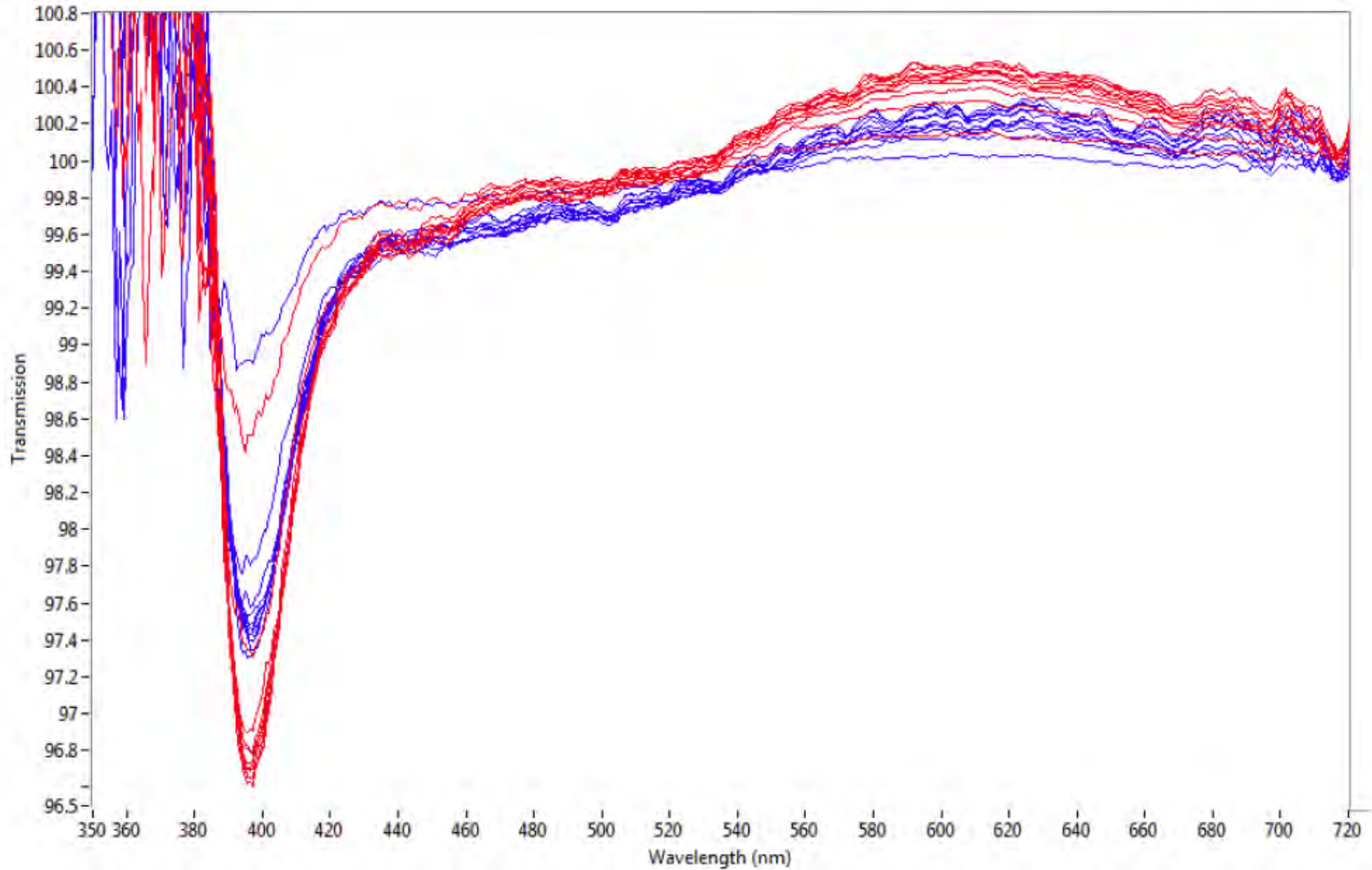


Figure 66. Comparison of spectra collected through a blank area (no slide, sample or coverslip) every 30 seconds for 5 minutes with Polarizer B oriented east-west (red) and then north-south (blue) (tungsten illumination).

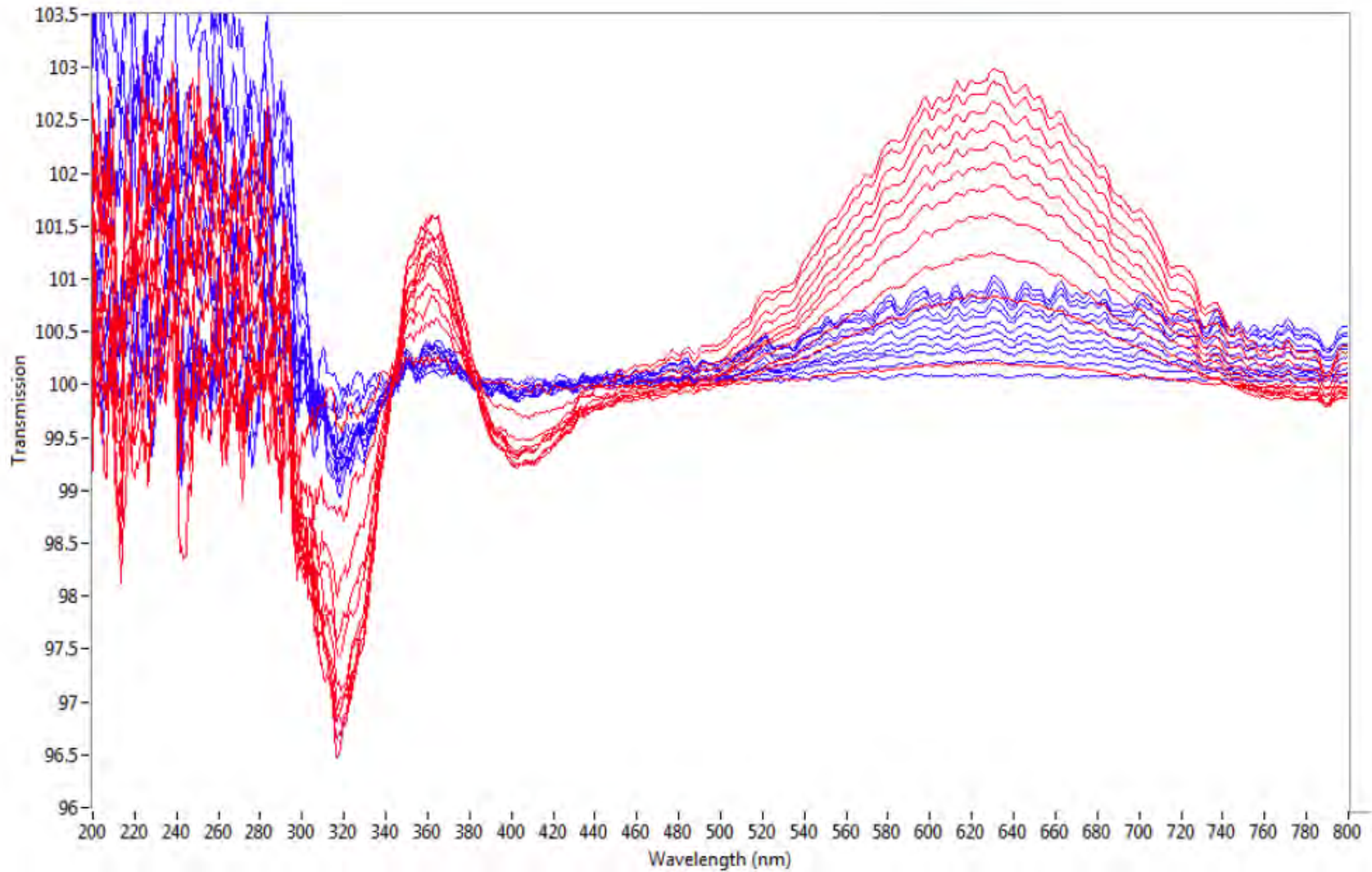


Figure 67. Comparison of spectra collected through a blank area (no slide, sample or coverslip) every 30 seconds for 5 minutes with Polarizer A oriented east-west (red) and then north-south (blue) (xenon illumination).

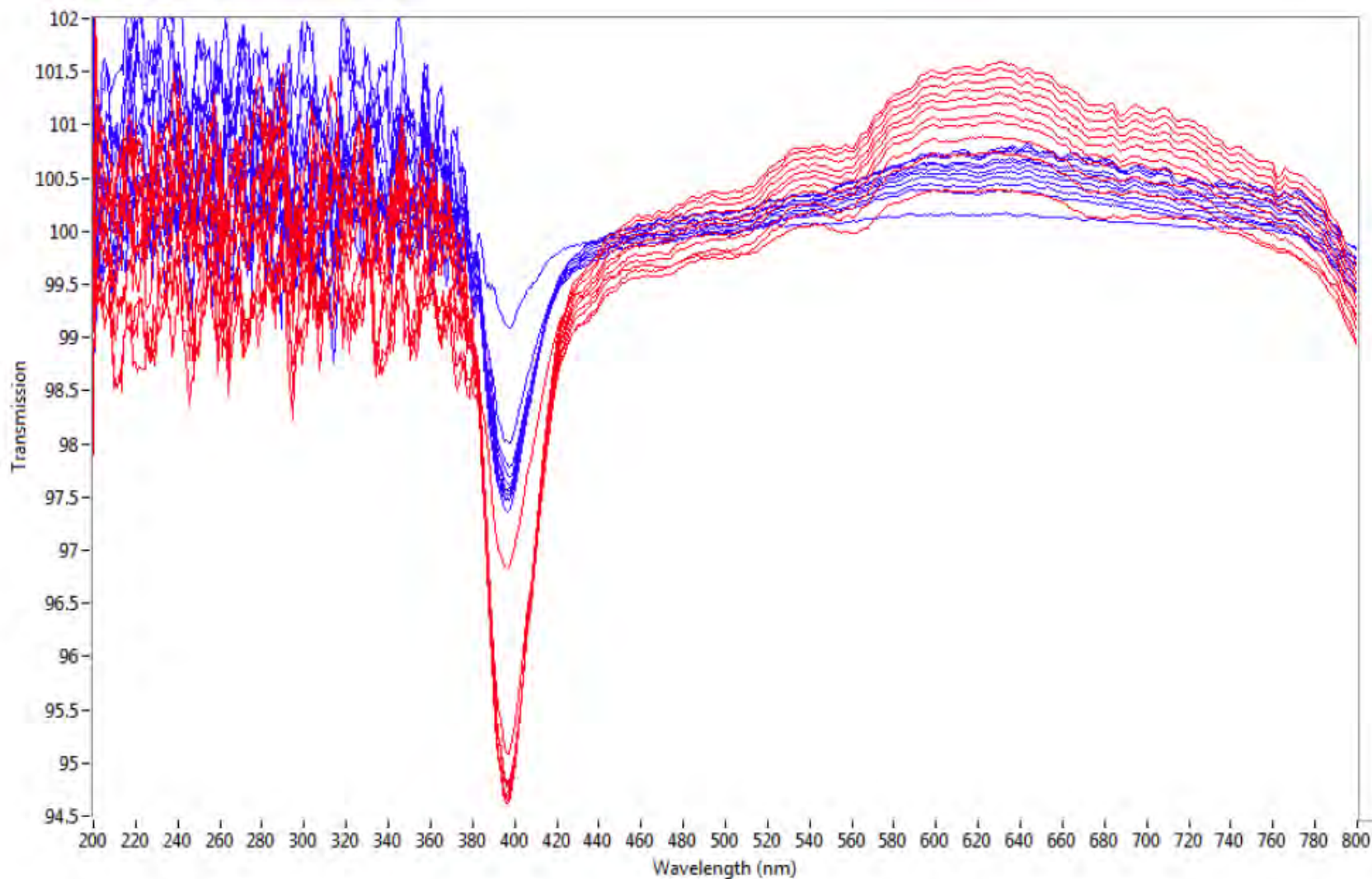


Figure 68. Comparison of spectra collected through a blank area (no slide, sample or coverslip) every 30 seconds for 5 minutes with Polarizer B oriented east-west (red) and then north-south (blue) (xenon illumination).

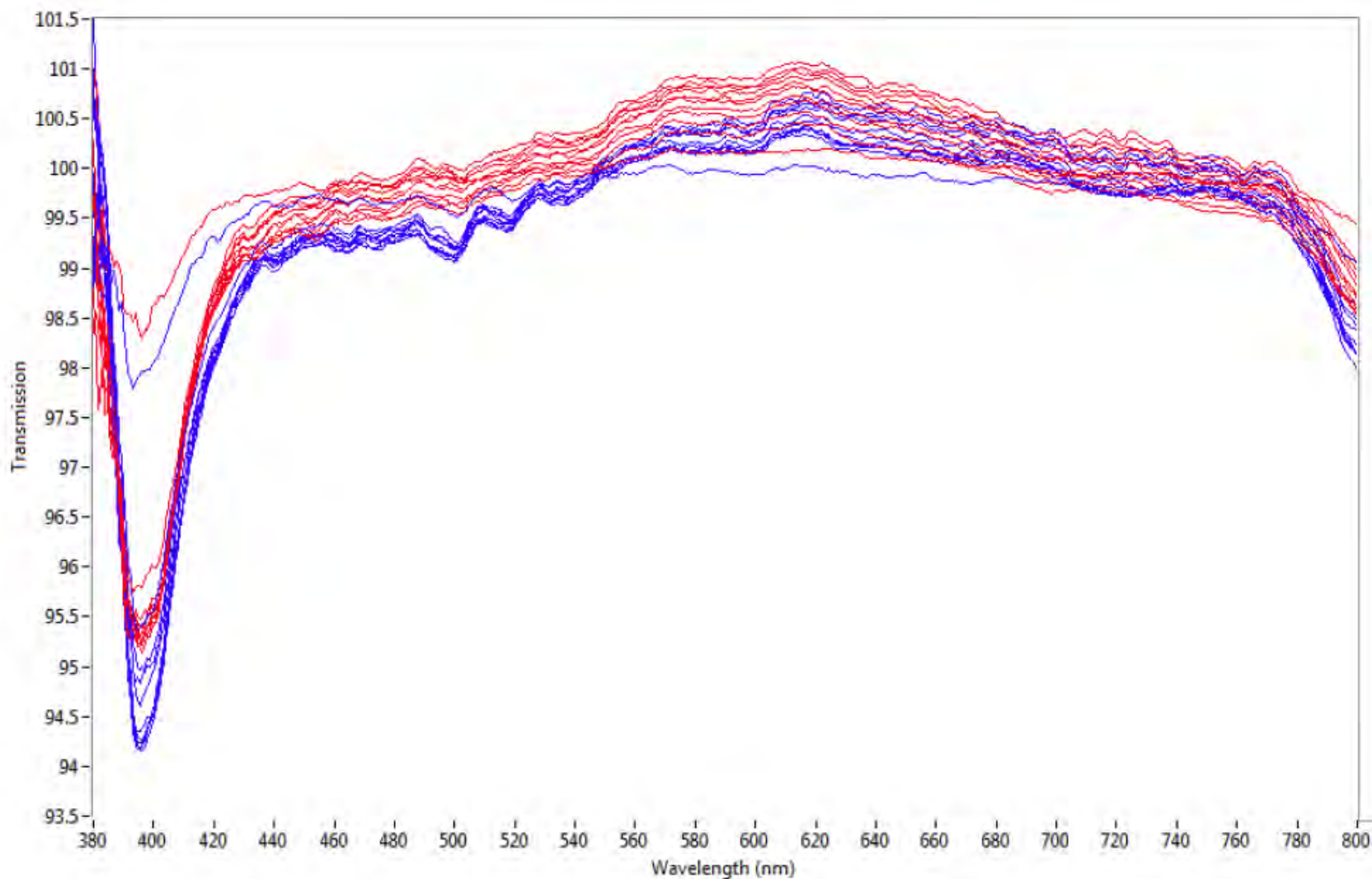


Figure 69. Comparison of spectra collected through a blank area (no slide, sample or coverslip) every 30 seconds for 5 minutes with Polarizer B oriented north-south (blue) and then east-west (red) (xenon illumination).

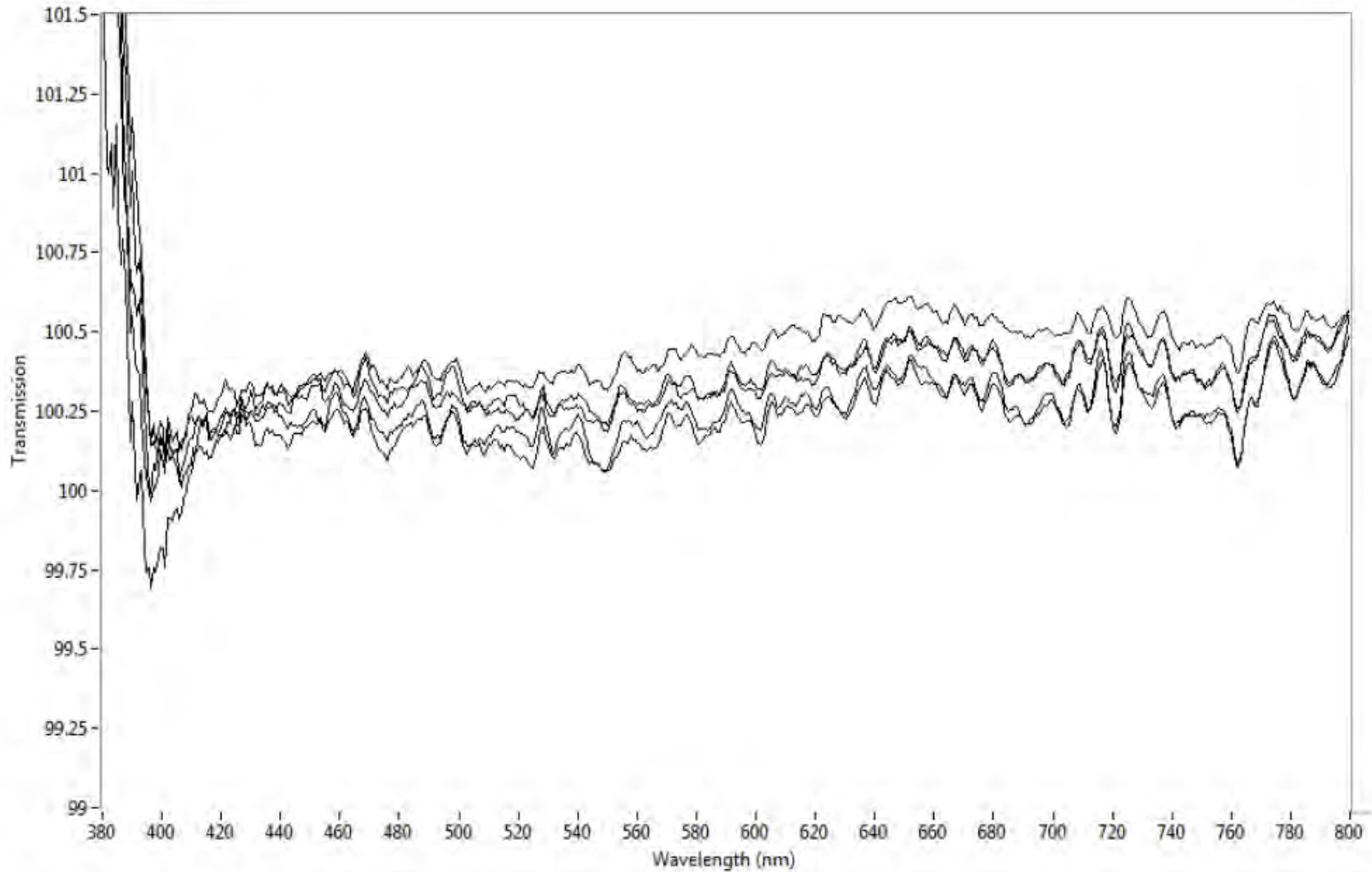


Figure 70. Spectra collected through a blank area (no slide, sample or coverslip) every 60 seconds for 5 minutes with Polarizer B oriented east-west (xenon illumination). The instrument's shutter was closed for sixty seconds prior to the collection of each of the above spectra.

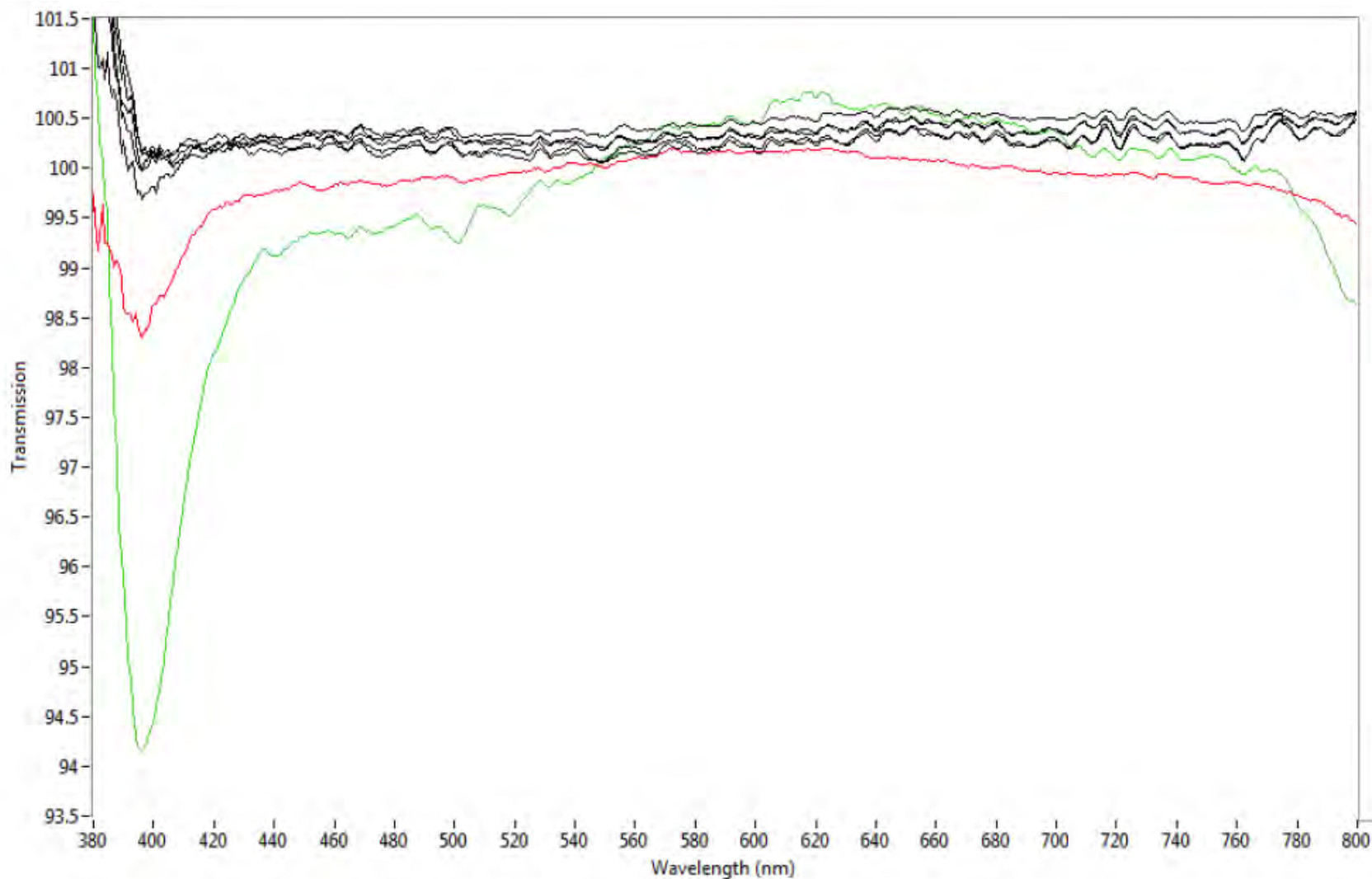


Figure 71. Comparison of spectra collected through a blank area (no slide, sample or coverslip) at the beginning (0 s - red) and end (300 s - green) of the initial time study and then every 60 seconds for 5 minutes thereafter (black) with Polarizer B oriented east-west (xenon illumination). The instrument's shutter was closed for sixty seconds prior to the collection of each of the above black spectra.

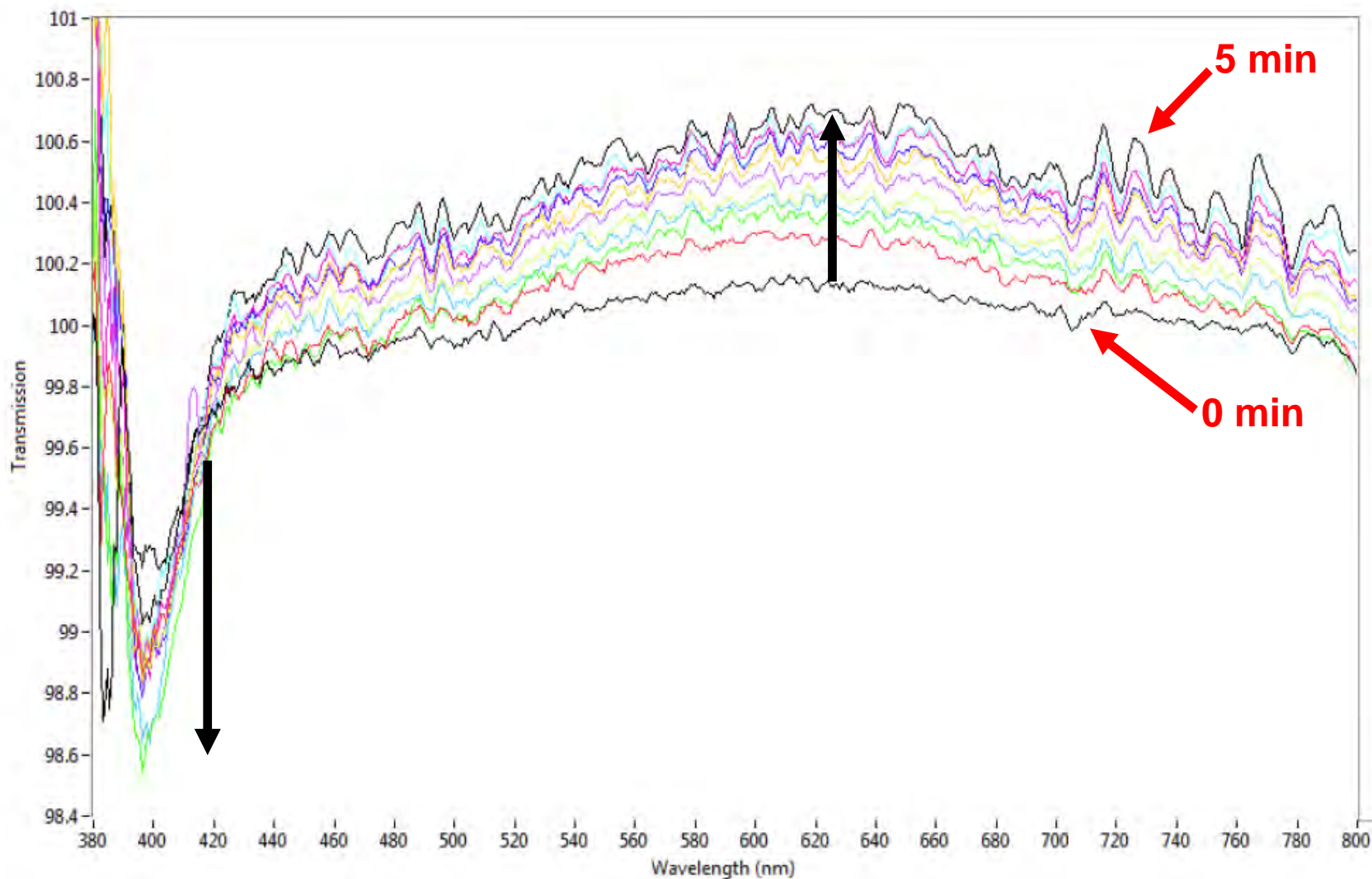


Figure 72. Spectra collected through a blank area (no slide, sample or coverslip) every 30 seconds for 5 minutes with Polarizer B oriented east-west after being continuously illuminated for more than two hours (xenon illumination).

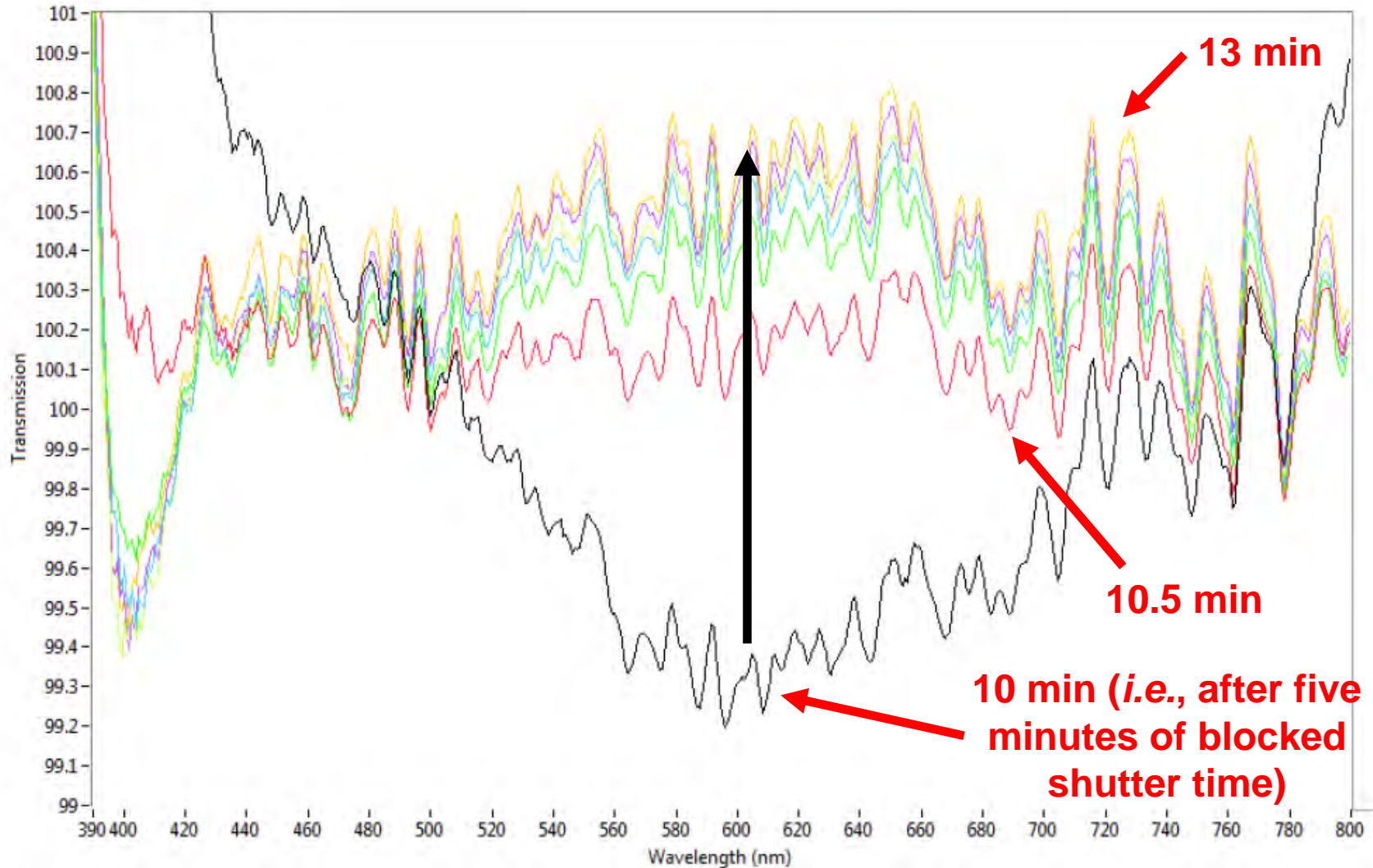


Figure 73. Spectra collected through a blank area (no slide, sample or coverslip) every 30 seconds for 3 minutes with Polarizer B oriented east-west after having a shutter block the light reaching the polarizer for five minutes. The polarizer had been previously continuously illuminated for more than two hours (xenon illumination).

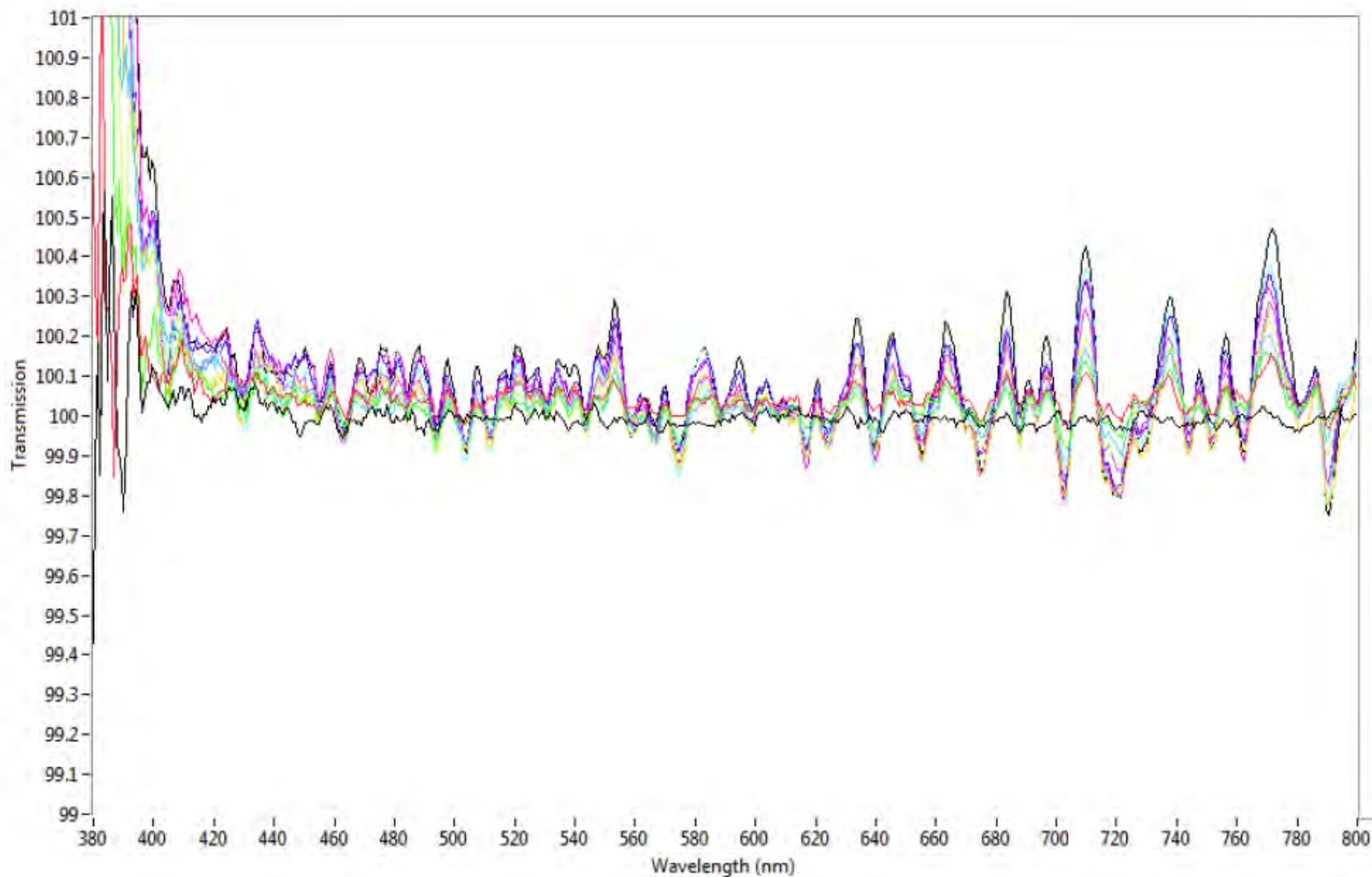


Figure 74. Spectra collected through a blank area (no slide, sample or coverslip) every 30 seconds for 5 minutes with Polarizer B oriented east-west after being continuously illuminated for more than three hours (xenon illumination).

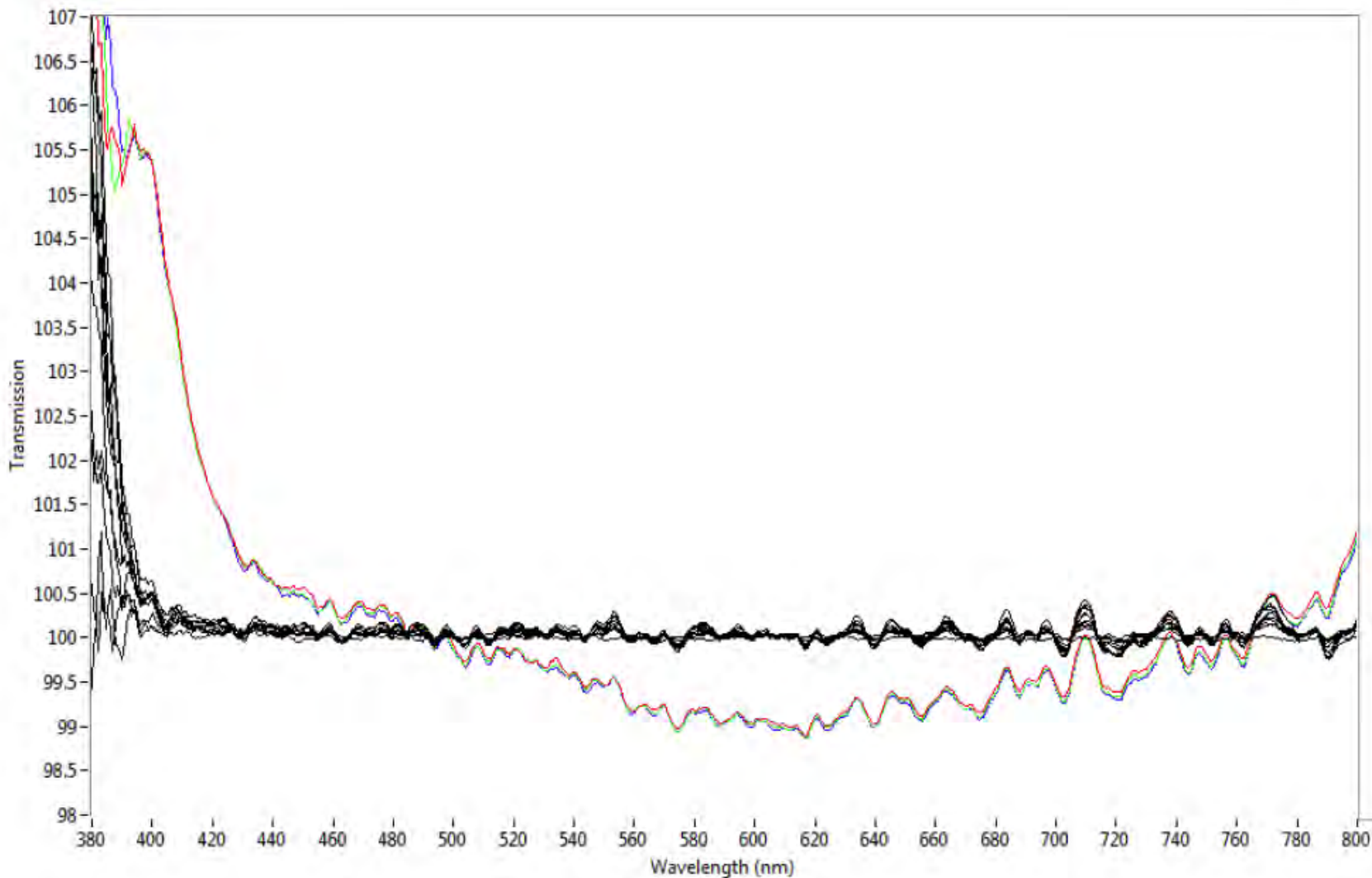


Figure 75. Spectra collected through a blank area (no slide, sample or coverslip) every 30 seconds for 5 minutes with Polarizer B oriented east-west after being continuously illuminated for more than three hours (xenon illumination)(black) compared to spectra collected after having the shutter block the light from reaching the polarizer for 1 minute (red) and 30 second intervals (blue and green).

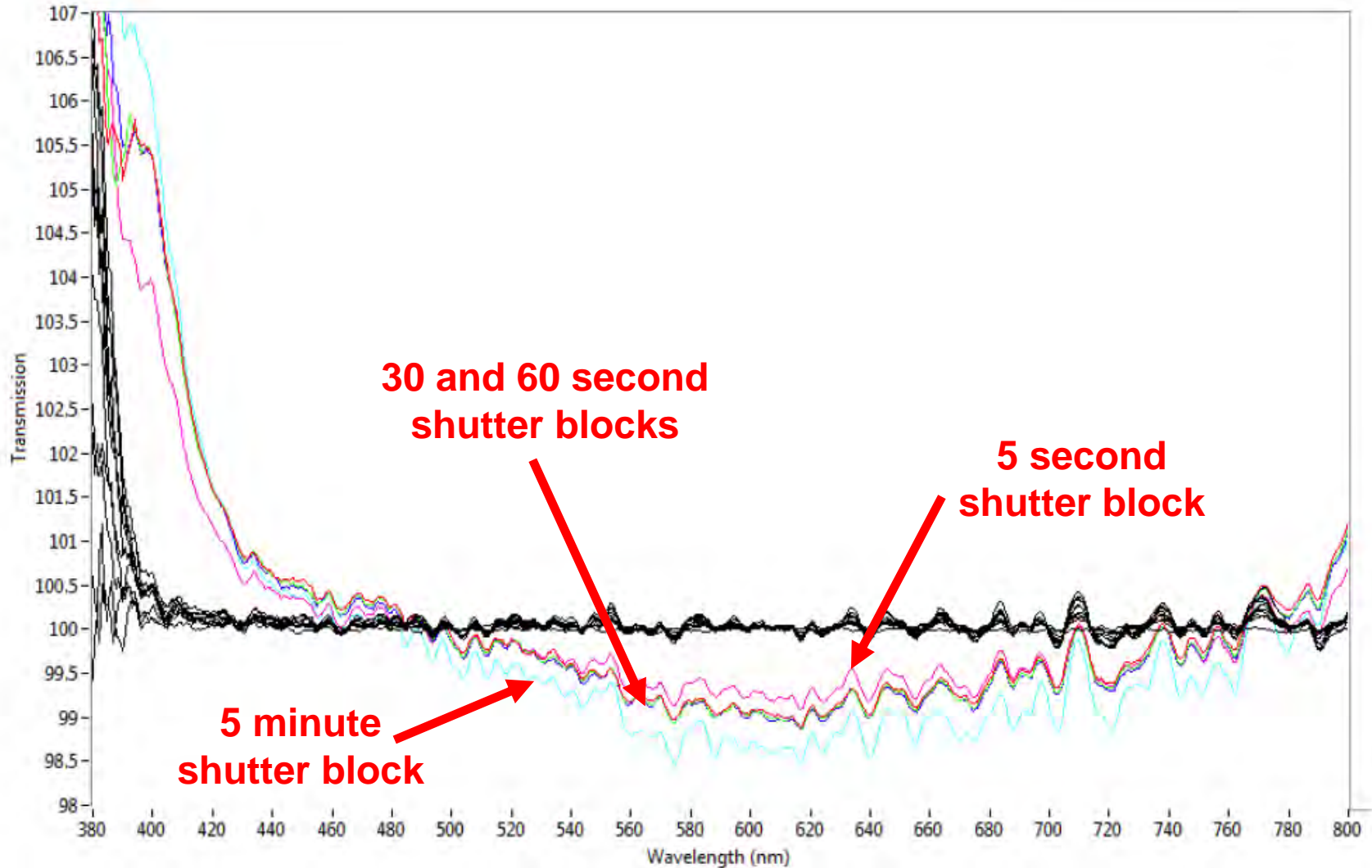


Figure 76. Spectra collected through a blank area (no slide, sample or coverslip) every 30 seconds for 5 minutes with Polarizer B oriented east-west after being continuously illuminated for more than three hours (xenon illumination)(black) compared to spectra collected after having the shutter block the light from reaching the polarizer for 5 minutes (light blue), 1 minute (red), 30 seconds (blue and green) and 5 seconds (pink) intervals.

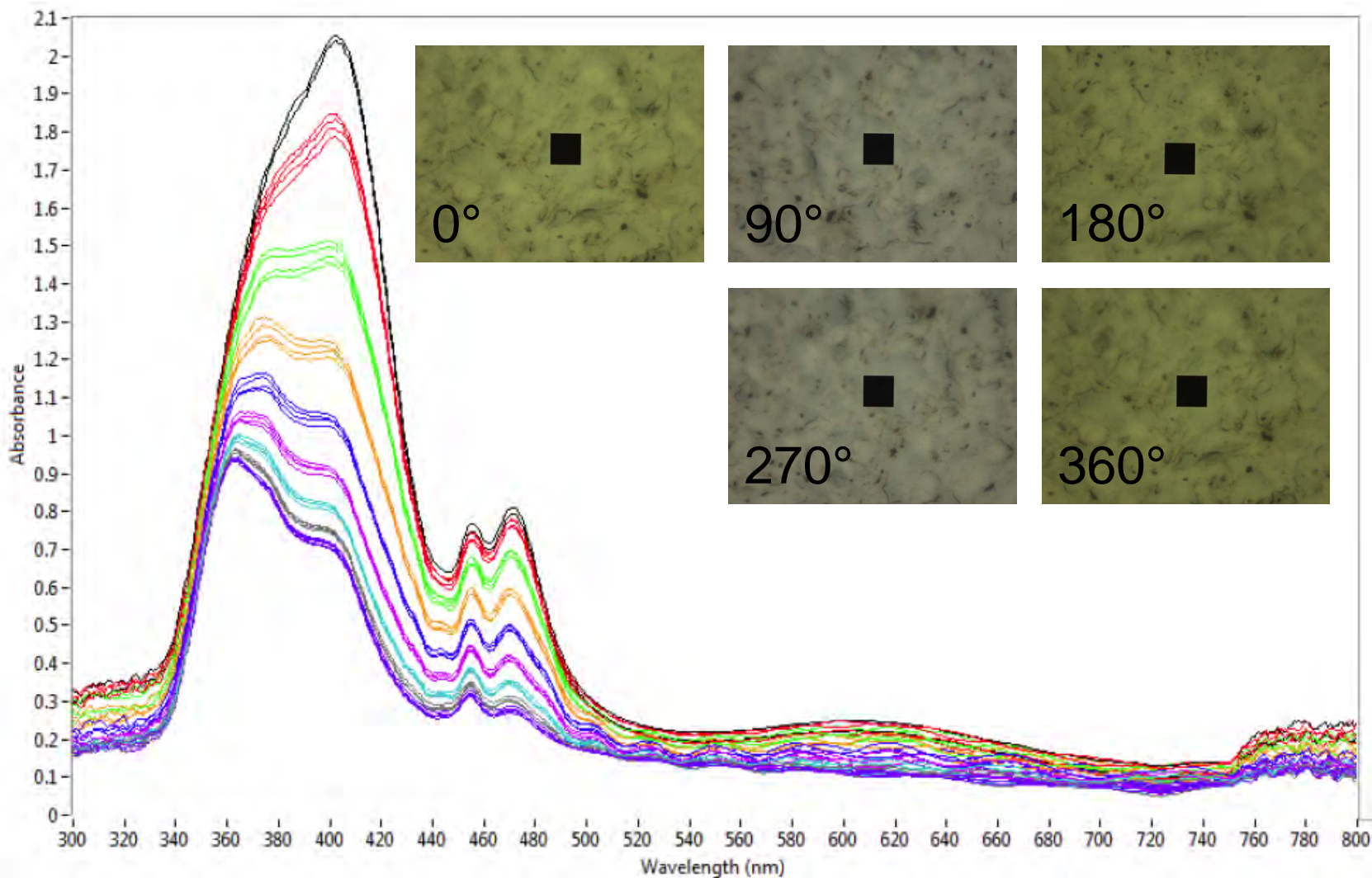


Figure 77. Spectra collected (10° increments) as a thin section of an epidote mineral grain was rotated through 360° using polarized light (mounted in Canada balsam). The spectra oscillate down and then up (twice) during the full rotation. The photomicrographs show the sample and the instrument's aperture (the small black square) at the 0° , 90° , 180° , 270° , and 360° positions.

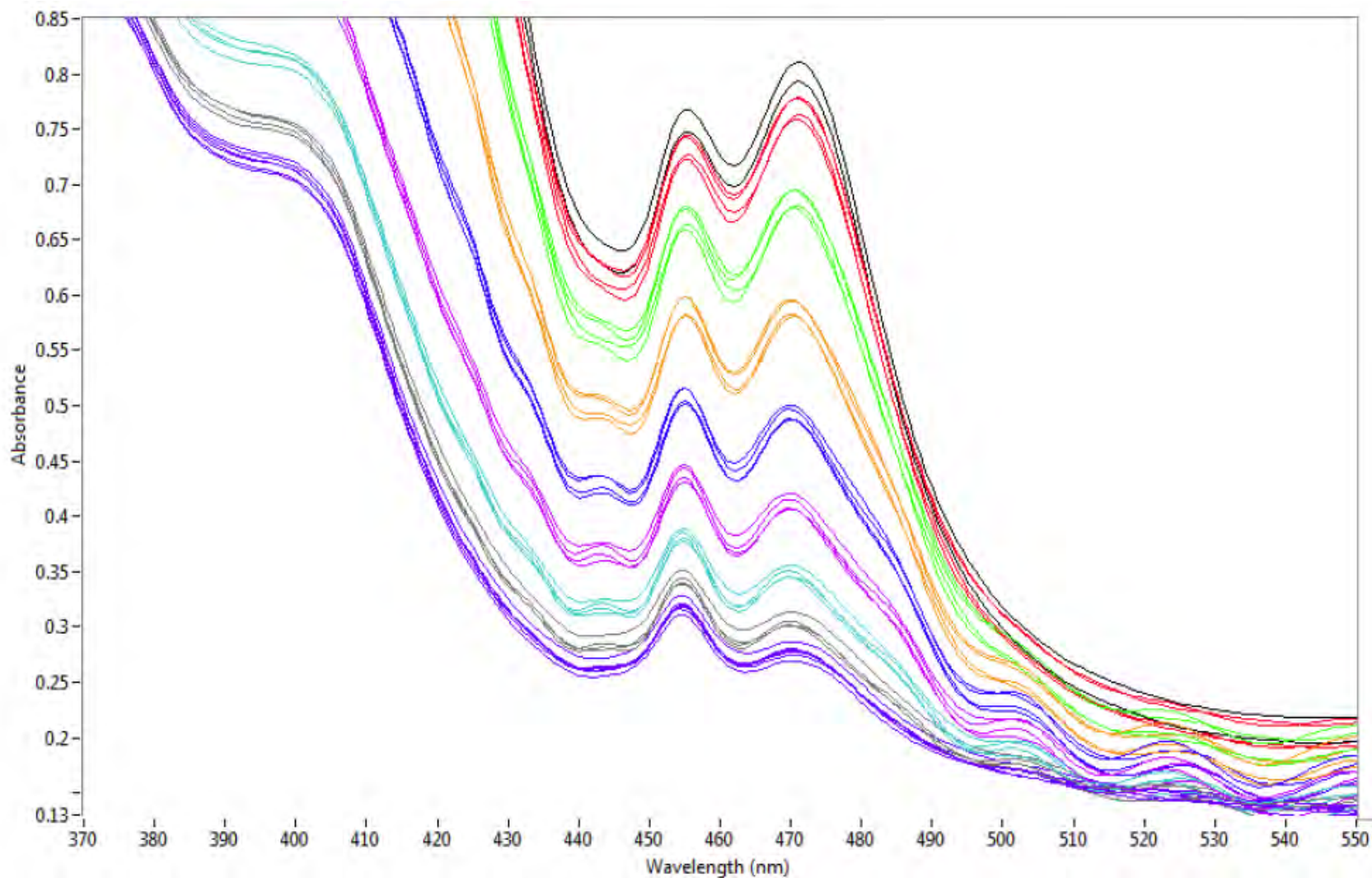


Figure 78. Close-up of the doublet at ~ 455 nm and 471 nm from the spectra collected (10° increments) as a thin section of an epidote mineral grain was rotated through 360° using polarized light. The spectra oscillate down and then up (twice) during the full rotation.

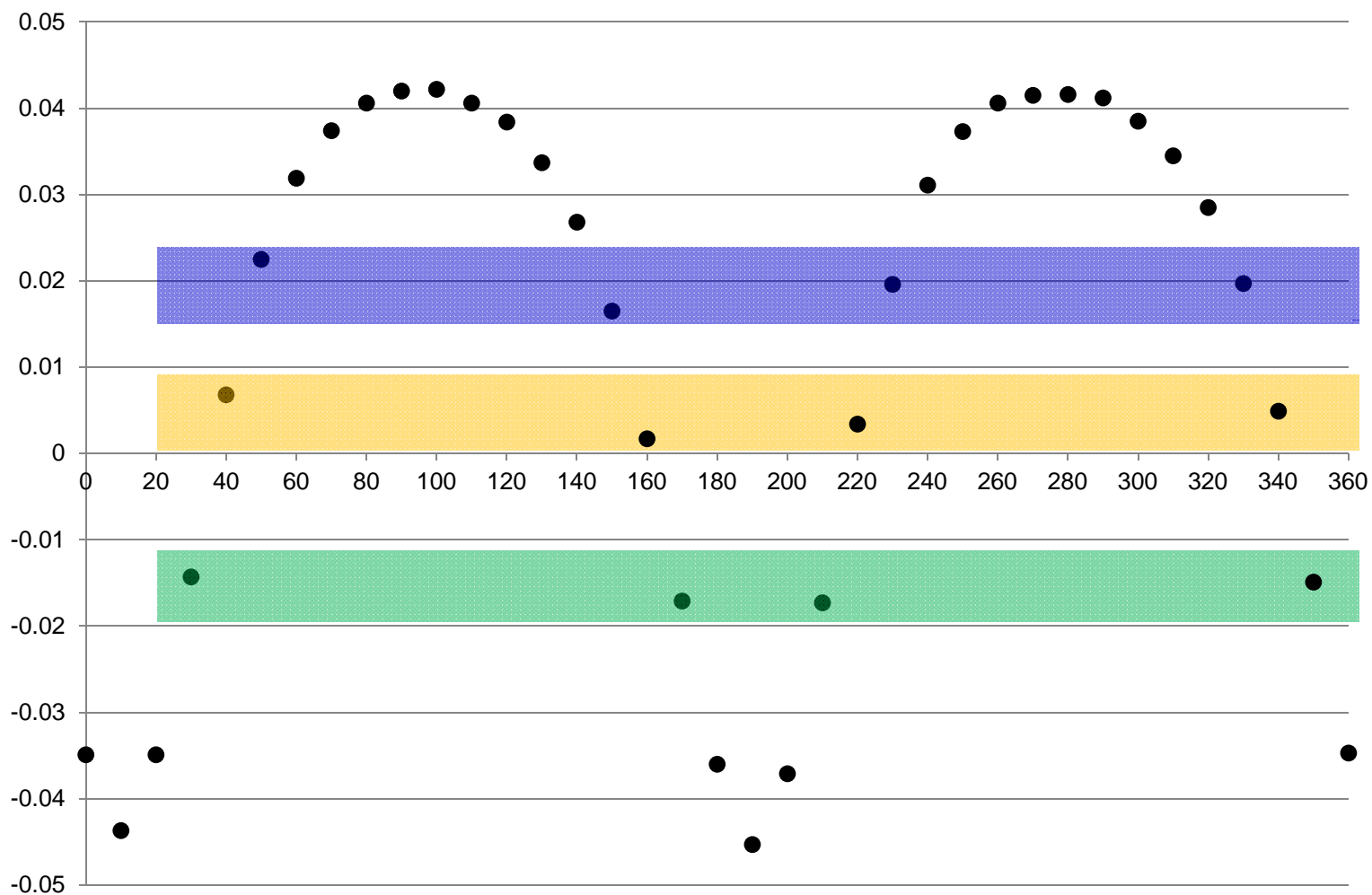


Figure 79. Absorbance difference between the peaks at ~ 455 nm and 471 nm from the spectra collected (10° increments) as a thin section of an epidote mineral grain was rotated through 360° using polarized light. The blue, orange, and green boxes correlate with the spectra of the same colors shown in Figure 78.

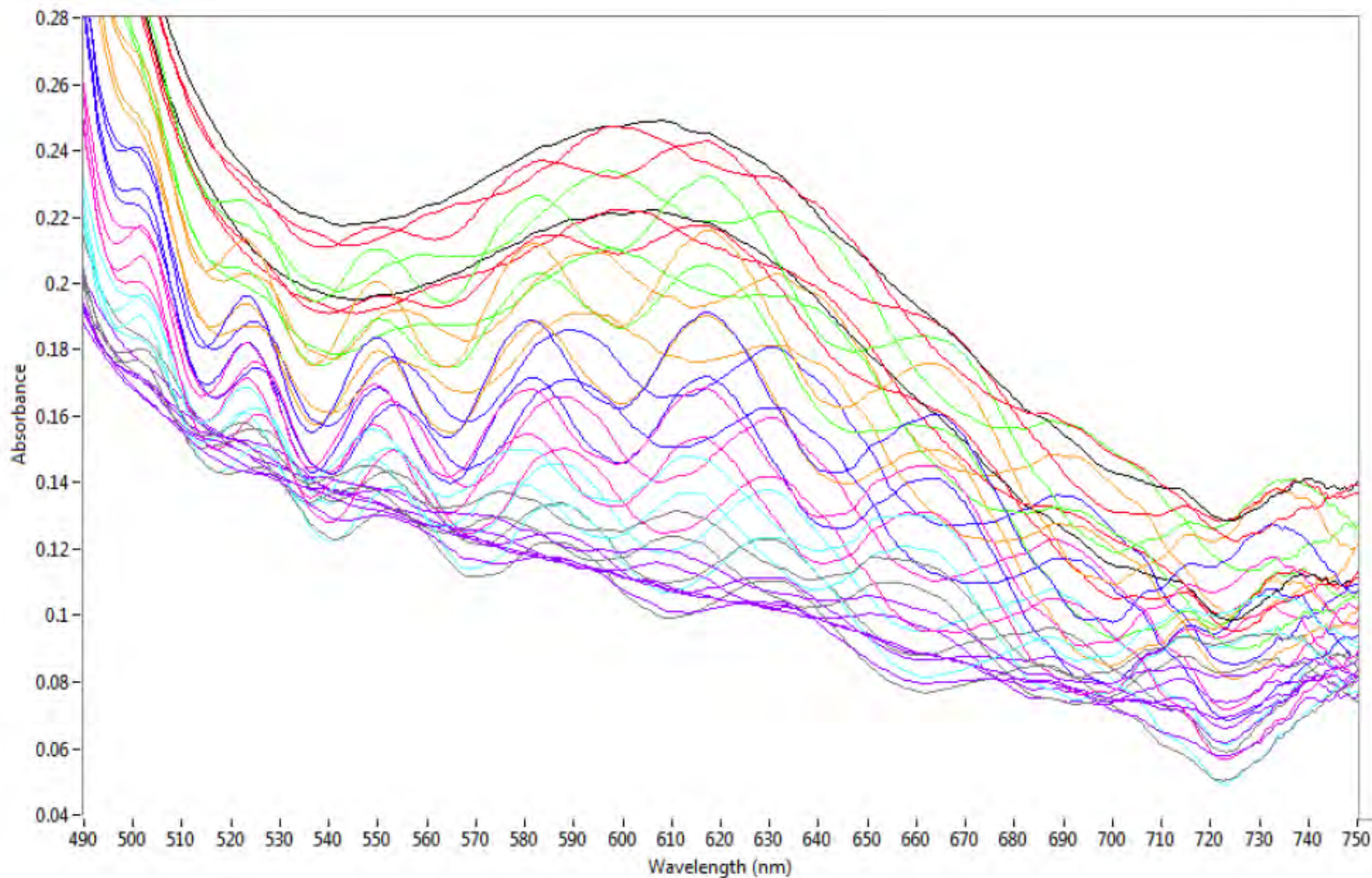


Figure 80. Close-up of the region between 490 nm and 750 nm from the spectra collected (10° increments) as a thin section of an epidote mineral grain was rotated through 360° illuminated by plane polarized light.

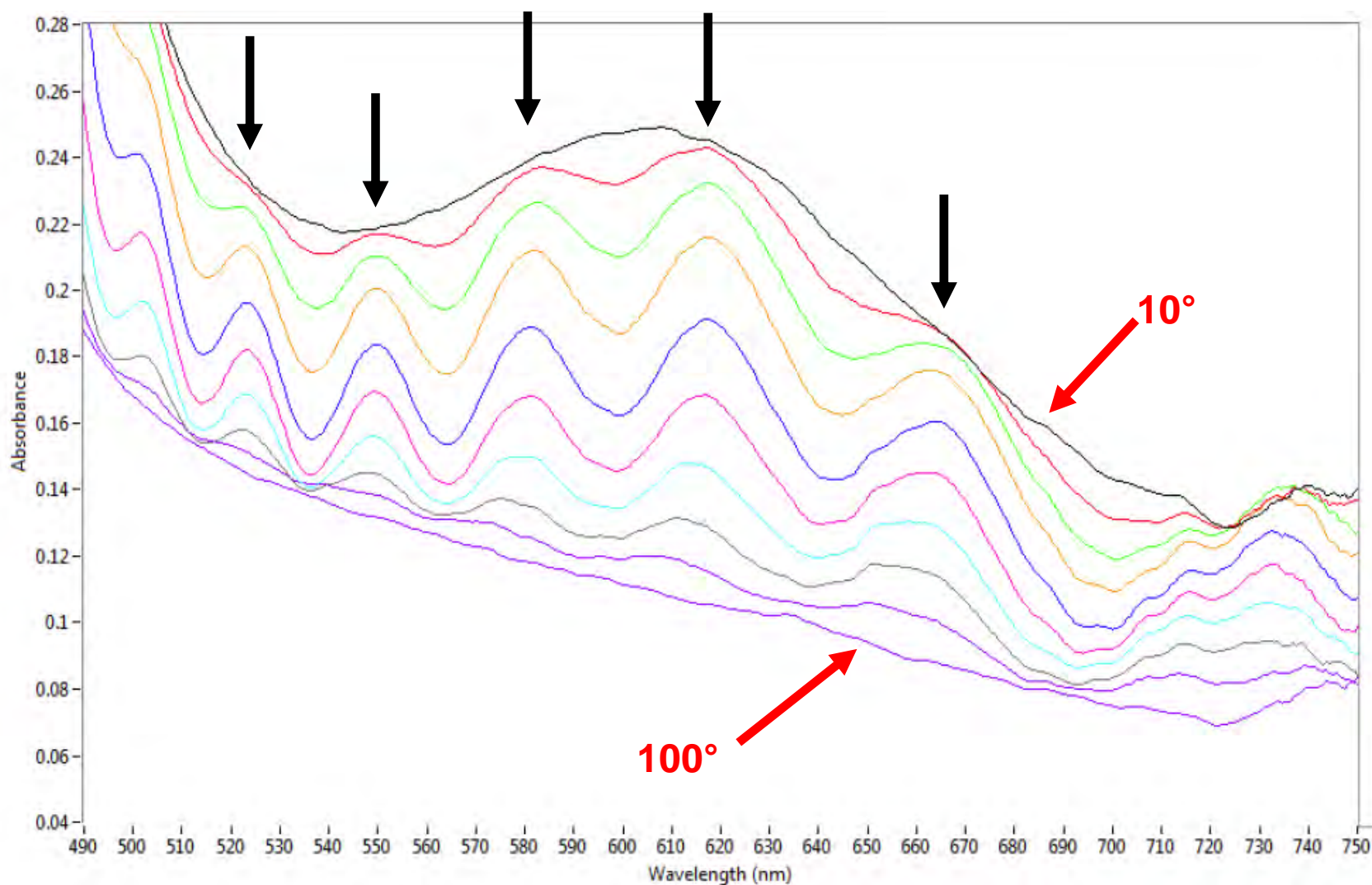


Figure 81. Close-up of the spectra between 490 nm and 750 nm collected as a thin section of an epidote mineral grain was rotated between 10° and 100° (10° increments) using polarized light. The black arrows mark the approximate positions of the artifactual “peaks.”

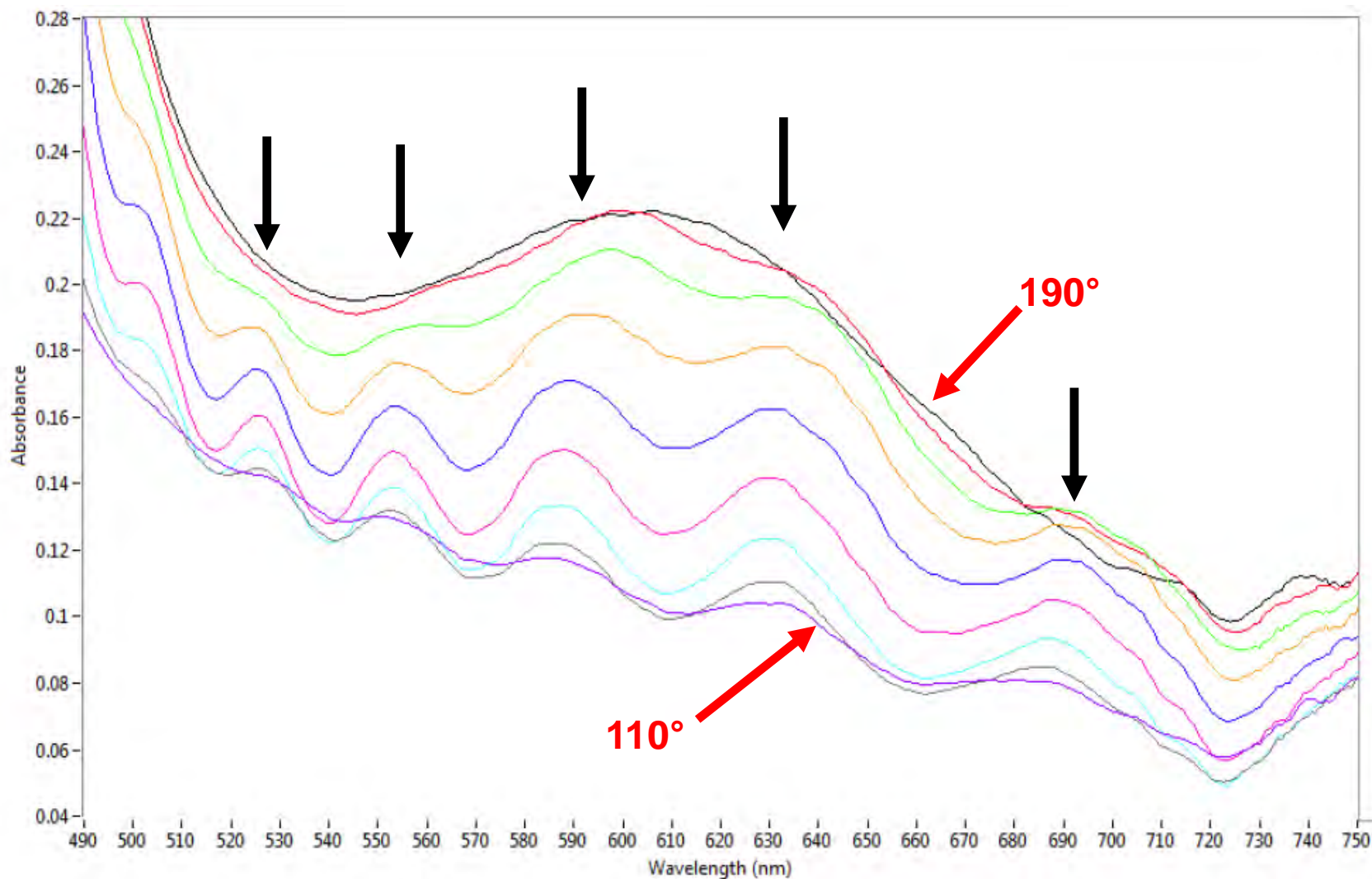


Figure 82. Close-up of the spectra between 490 nm and 750 nm collected as a thin section of an epidote mineral grain was rotated between 110° and 190° (10° increments) using polarized light. The black arrows mark the approximate positions of the artifactual “peaks.”

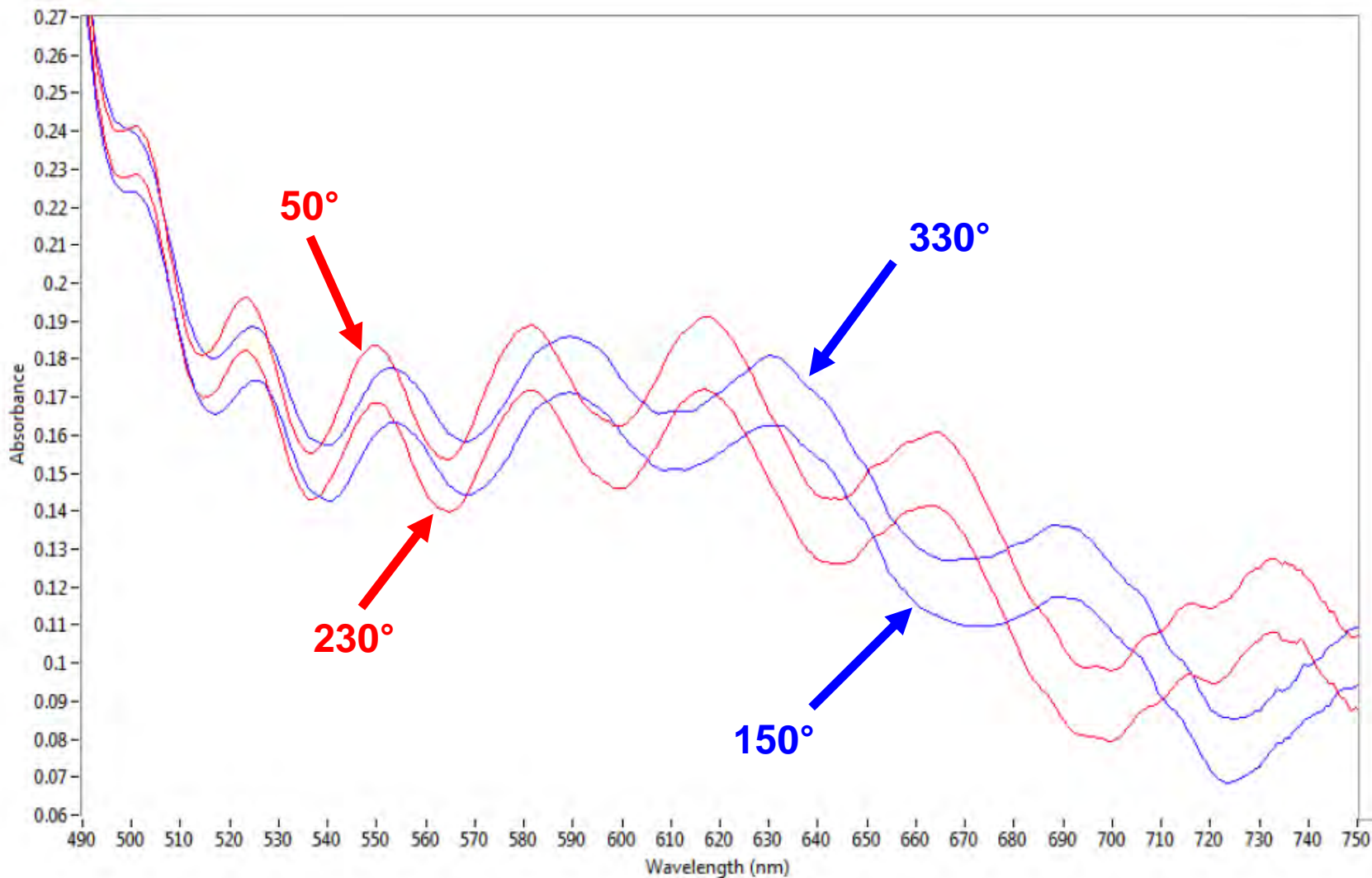


Figure 83. Close-up of the spectra between 490 nm and 750 nm collected at 50°, 150°, 230°, and 330° from a thin section of an epidote mineral grain using polarized light.

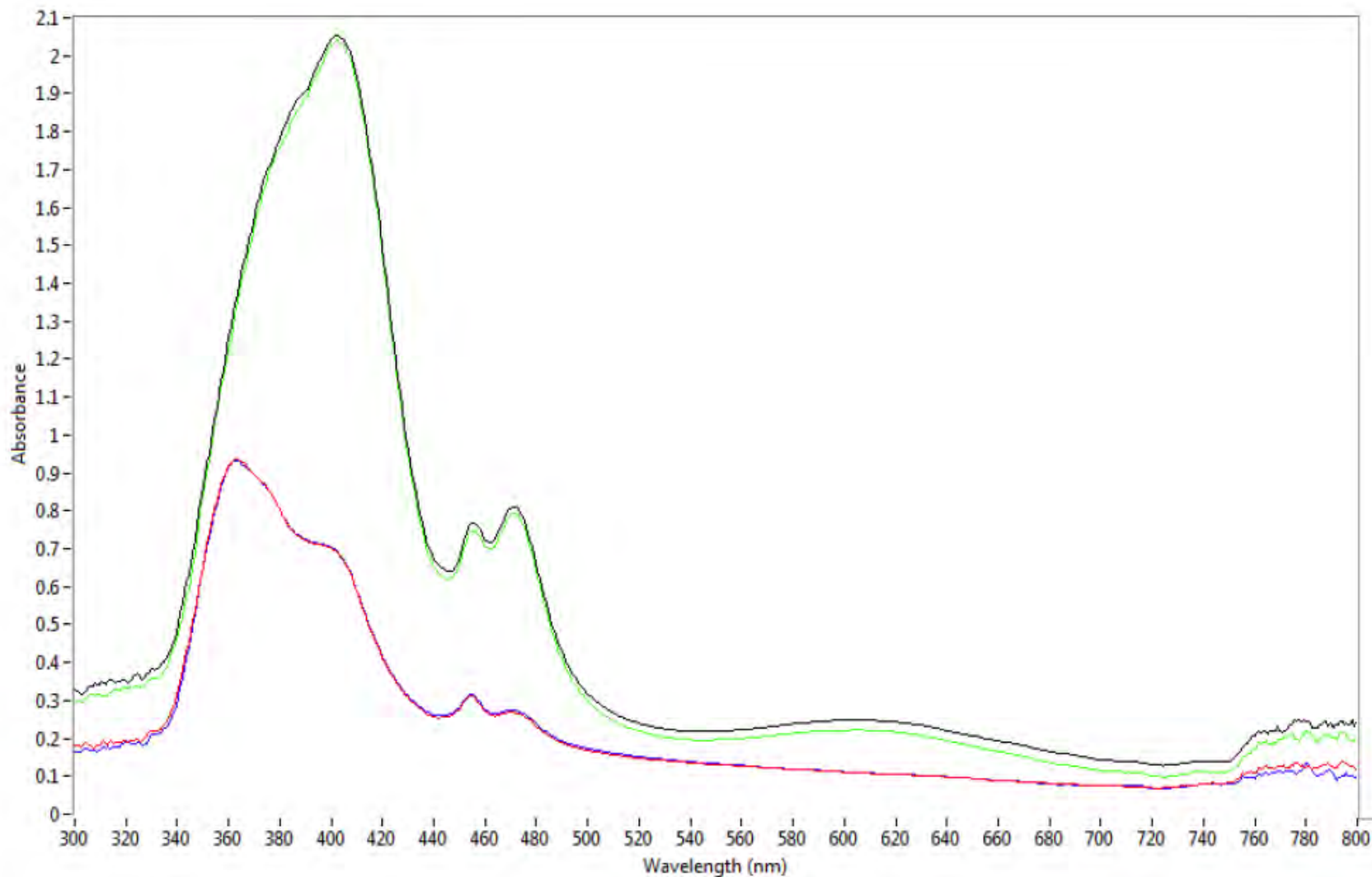


Figure 84. Spectra collected at 10° (black), 100° (red), 190° (green), and 270° (blue) from a thin section of an epidote mineral grain using polarized light.

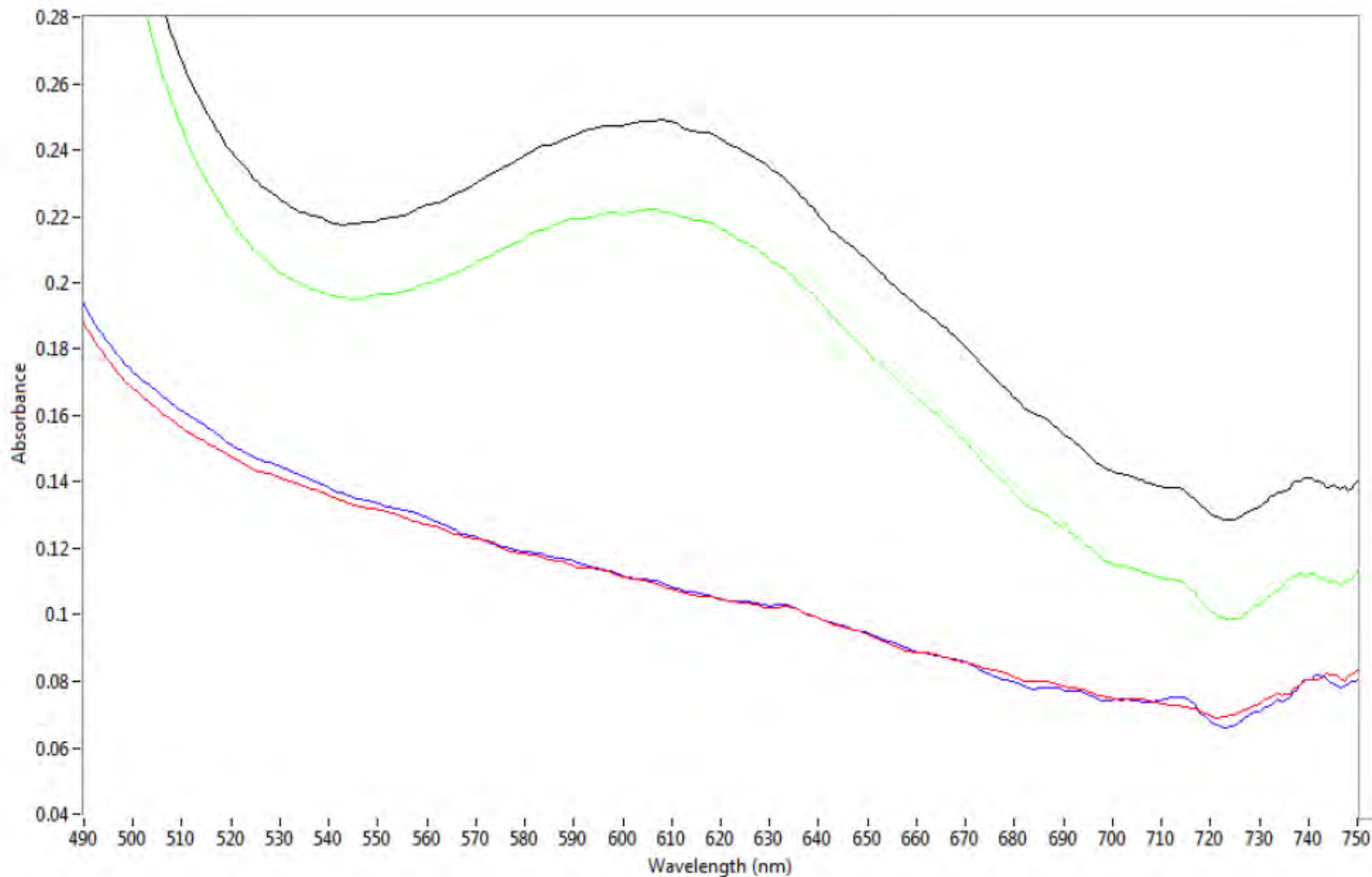


Figure 85. Close-up of the spectra between 490 nm and 750 nm collected at 10° (black), 100° (red), 190° green), and 270° (blue) from a thin section of an epidote mineral grain using polarized light.

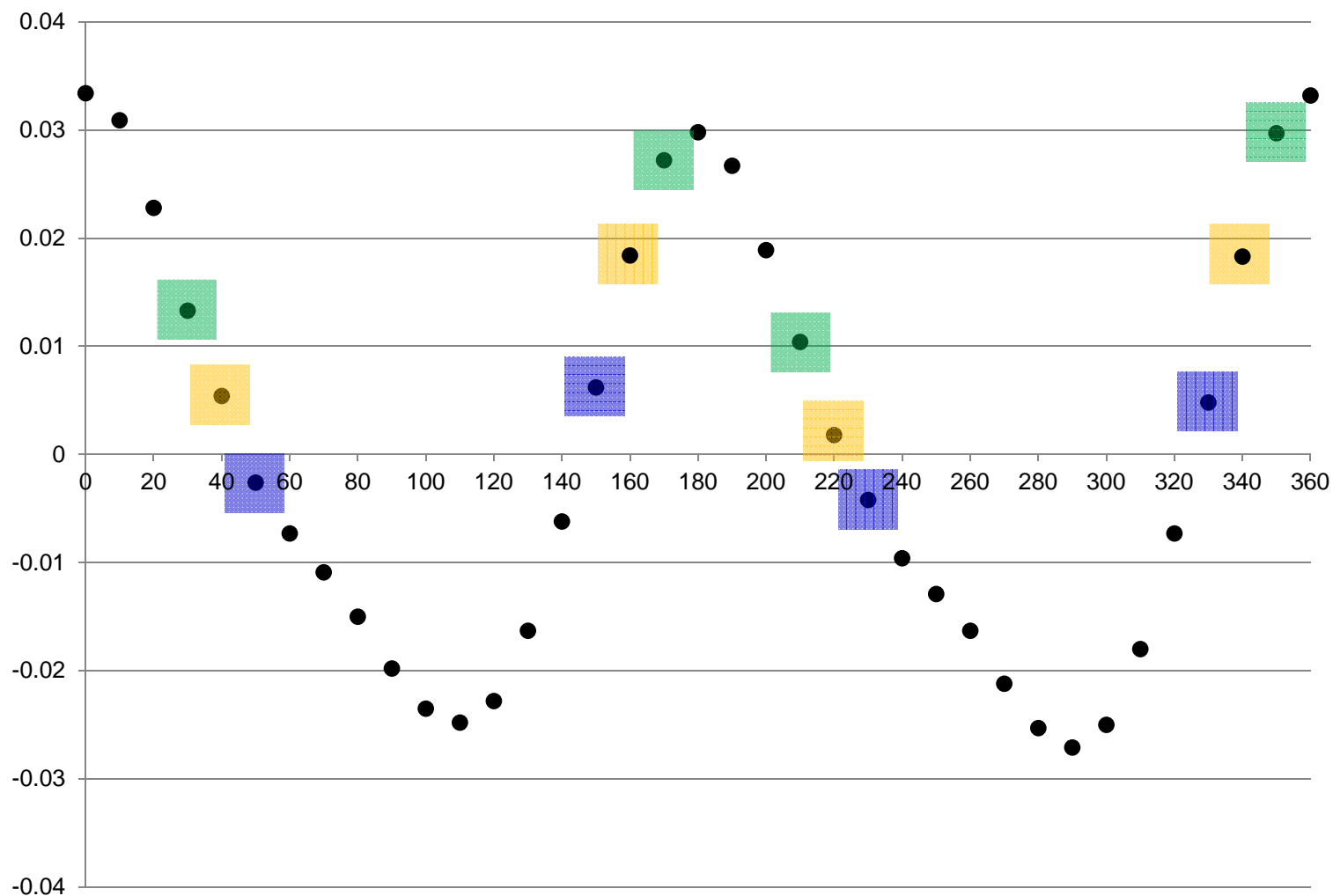


Figure 86. Absorbance difference between the peak at ~ 605 nm and 543 nm from the spectra collected (10° increments) as a thin section of an epidote mineral grain was rotated through 360° using polarized light. The blue, orange, and green boxes correlate with the spectra of the same colors shown in Figure 80.

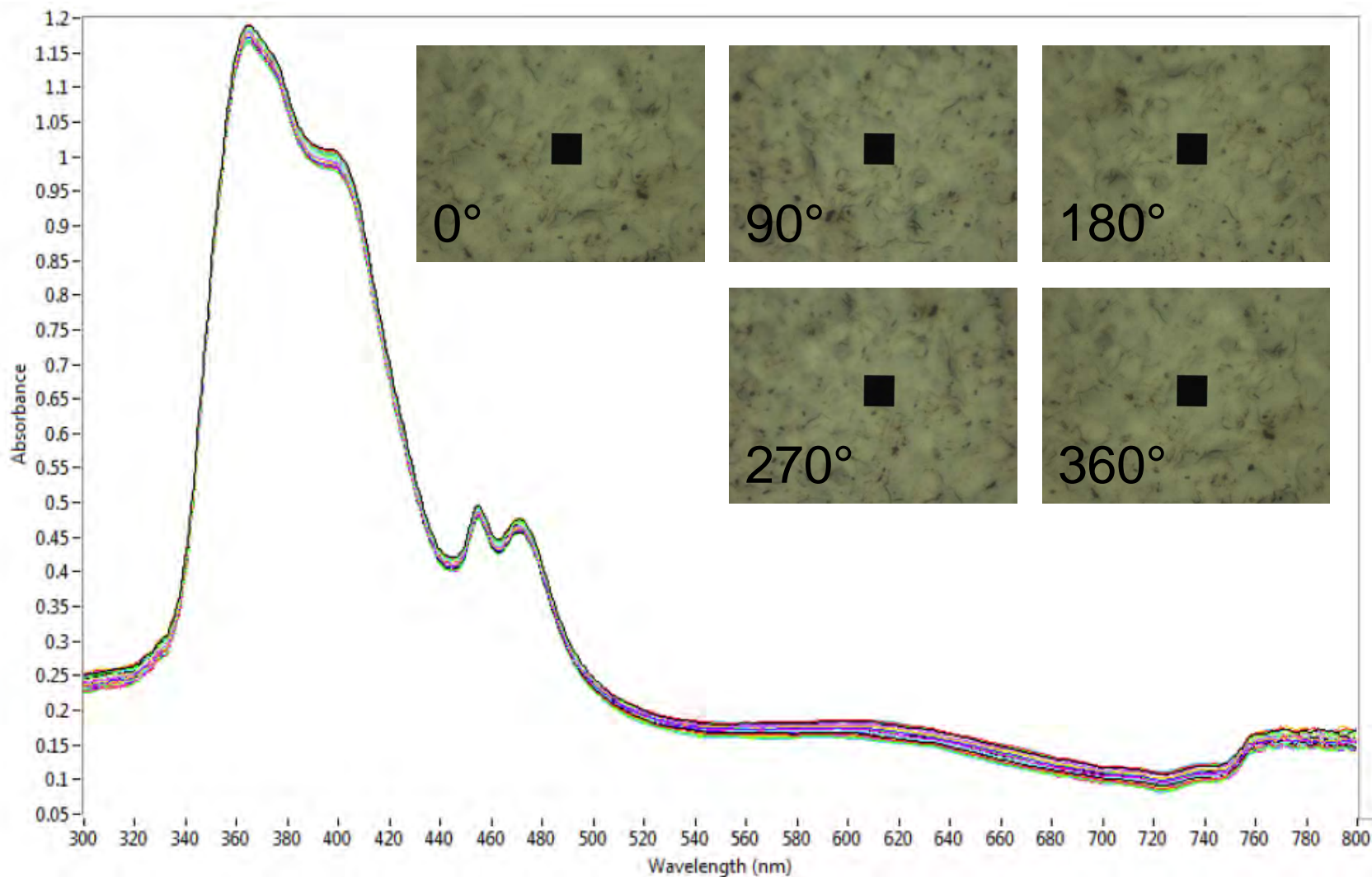


Figure 87. Spectra collected (10° increments) as a thin section of an epidote mineral grain was rotated through 360° (no polarizer). In general, the spectra are relatively stable throughout the full rotation. The photomicrographs show the sample and the instrument's aperture (the small black square) at the 0°, 90°, 180°, 270°, and 360° positions.

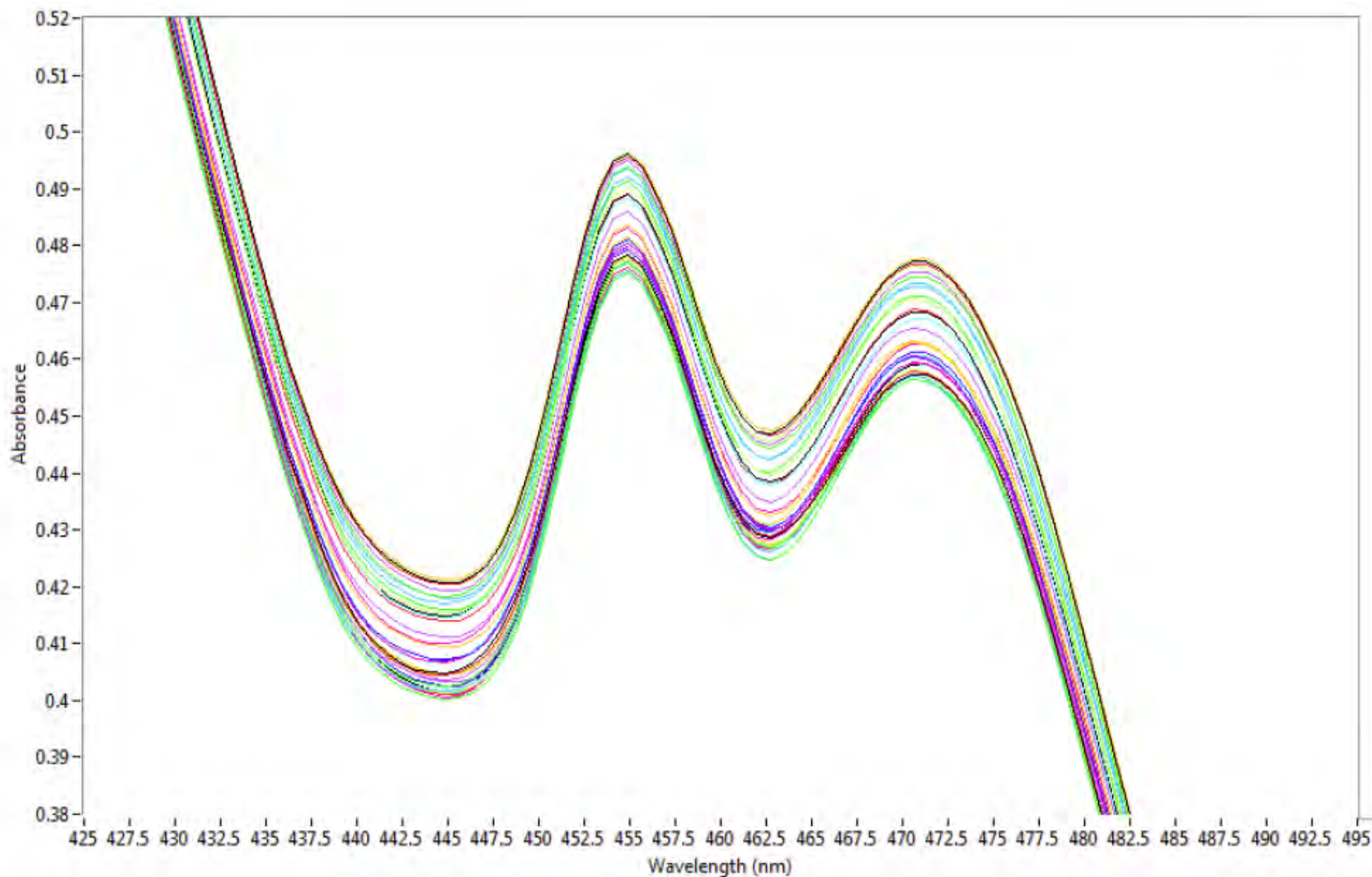


Figure 88. Close-up of the doublet at ~ 455 nm and 471 nm from the spectra collected (10° increments) as a thin section of an epidote mineral grain was rotated through 360° (no polarizer).

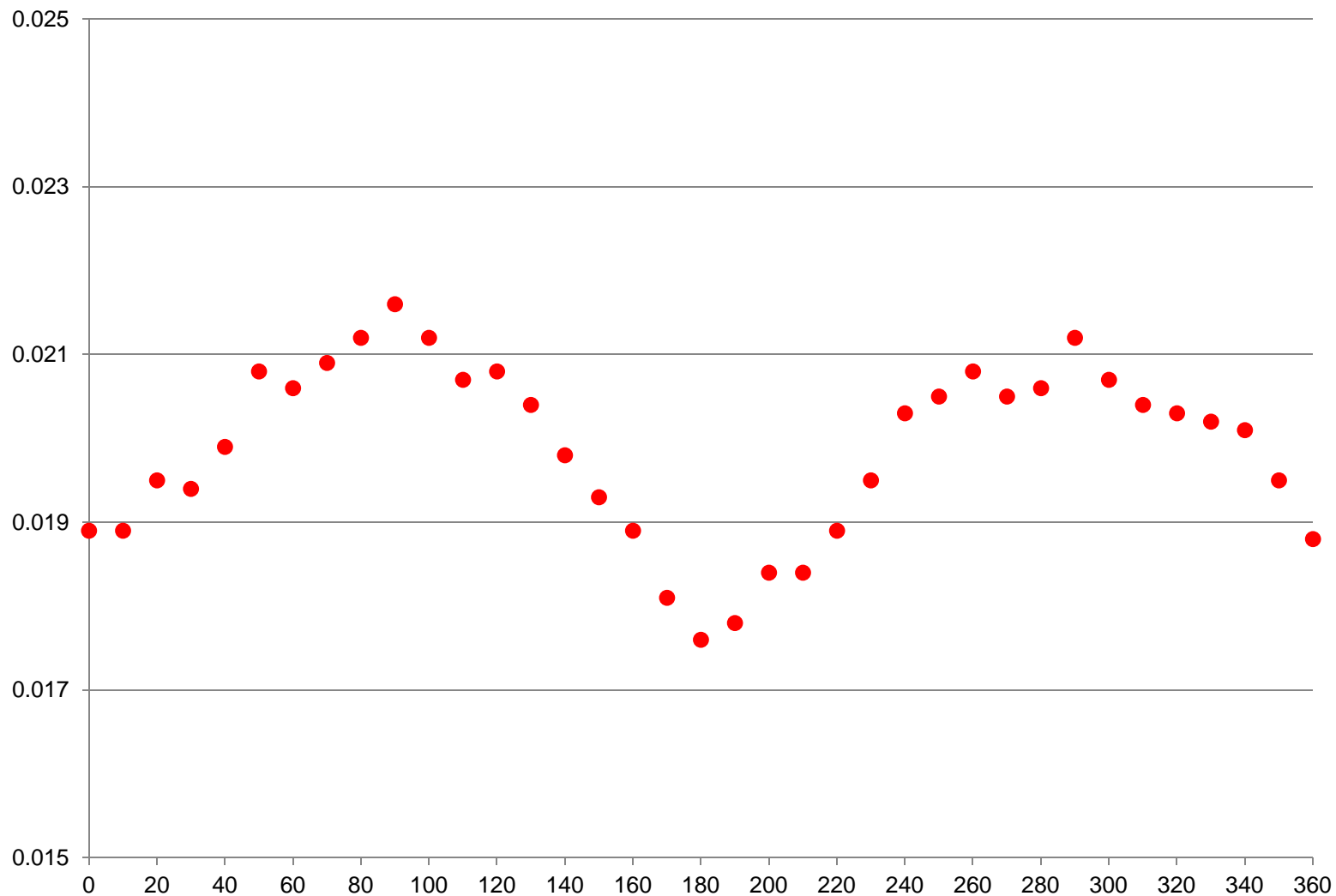


Figure 89. Absorbance difference between the peaks at ~ 455 nm and 471 nm from the spectra collected (10° increments) as a thin section of an epidote mineral grain was rotated through 360° (no polarizer).

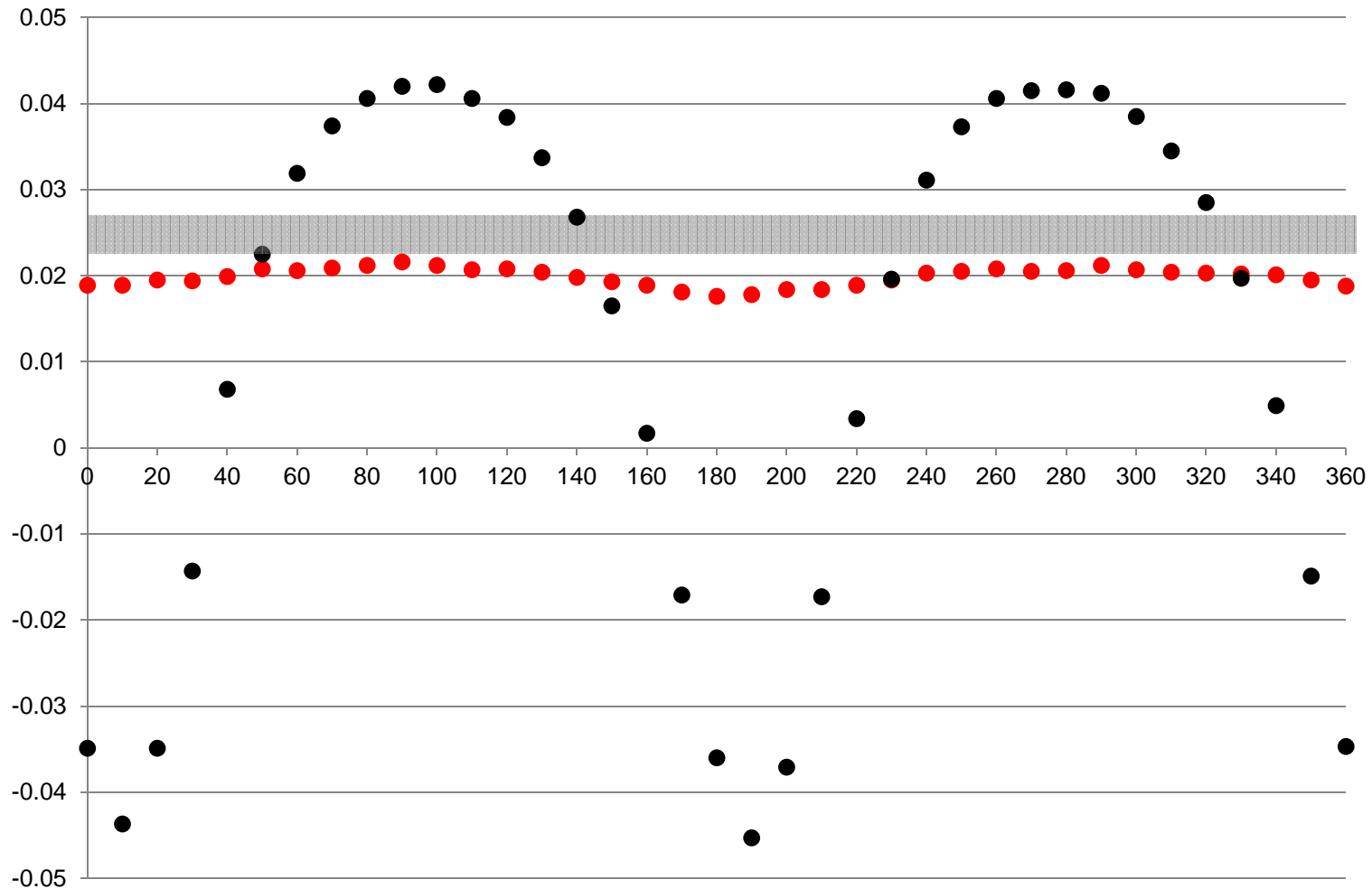


Figure 90. Comparison of the absorbance differences between the peaks at ~ 455 nm and 471 nm from the spectra collected (10° increments) as a thin section of an epidote mineral grain was rotated through 360° using polarized light (black) and without a polarizing filter (red). The gray box represents the approximate range where the absorbance difference would be located when the sample was rotated half-way between the “top” and “bottom” spectra (e.g., 55° , which is the rotational midpoint between 10° and 100°) using polarized light.

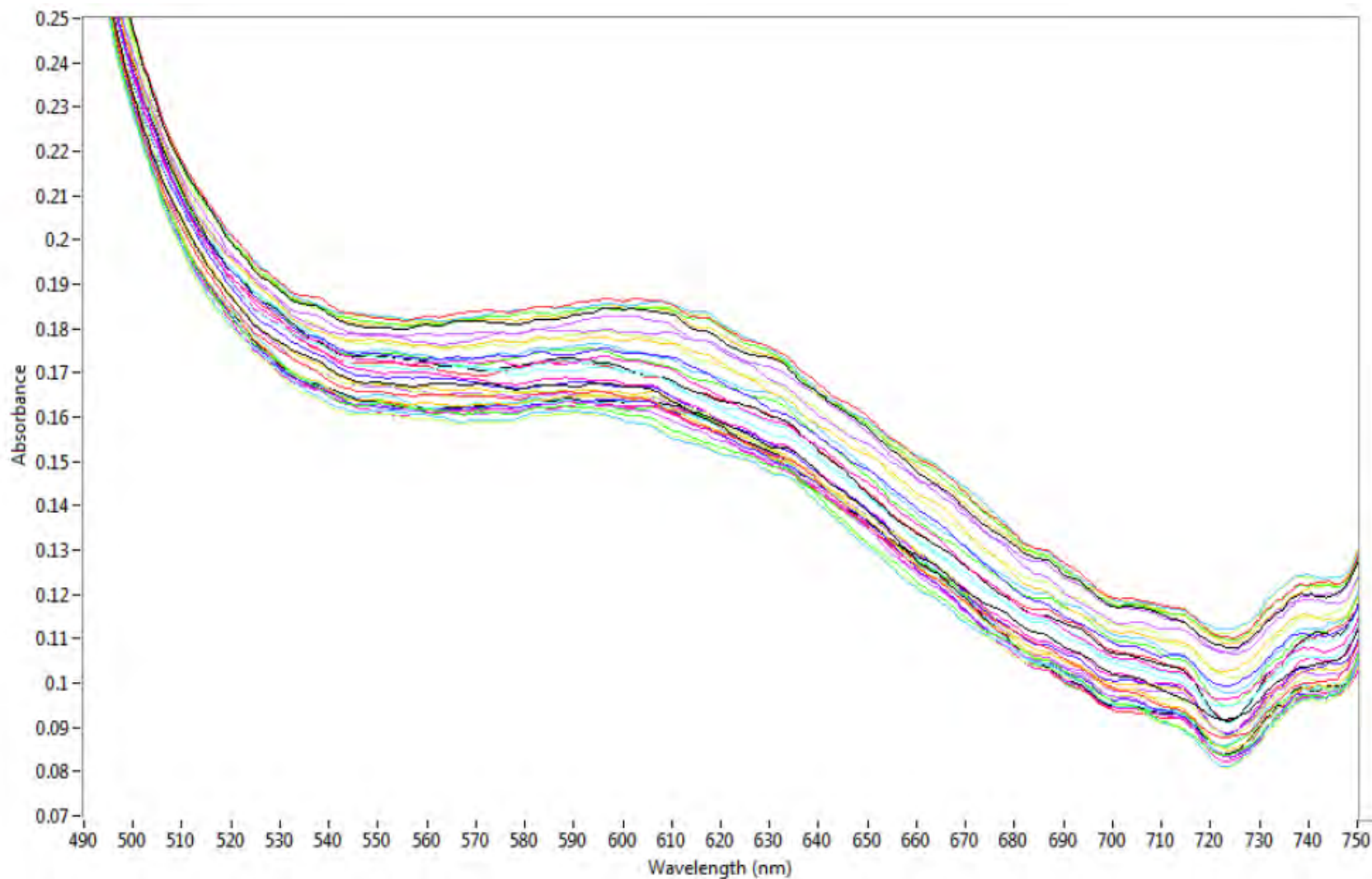


Figure 91. Close-up of the region between 490 nm and 750 nm from the spectra collected (10° increments) as a thin section of an epidote mineral grain was rotated through 360° (no polarizer).

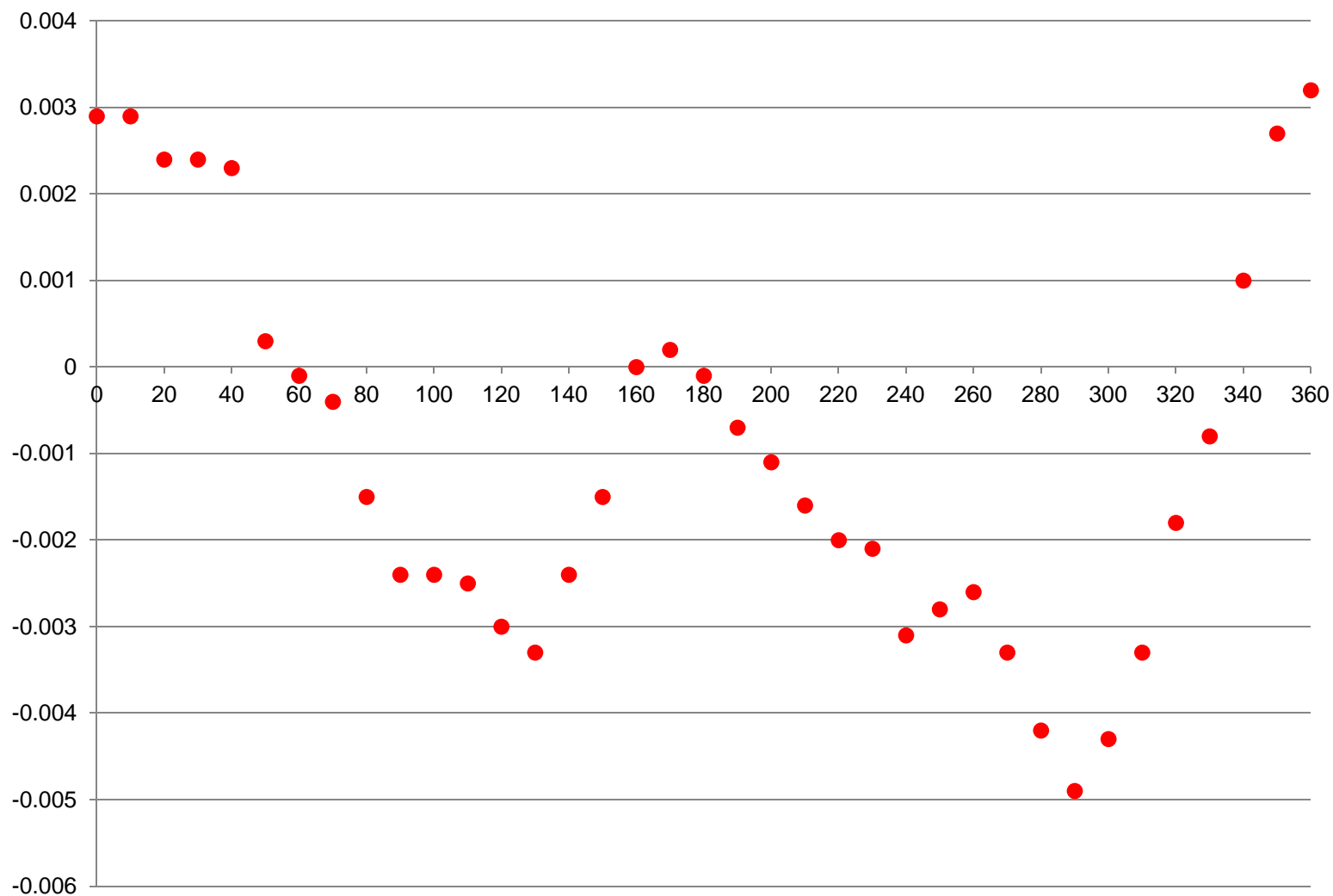


Figure 92. Absorbance difference between 605 nm and 543 nm from the spectra collected (10° increments) as a thin section of an epidote mineral grain was rotated through 360° (no polarizer).

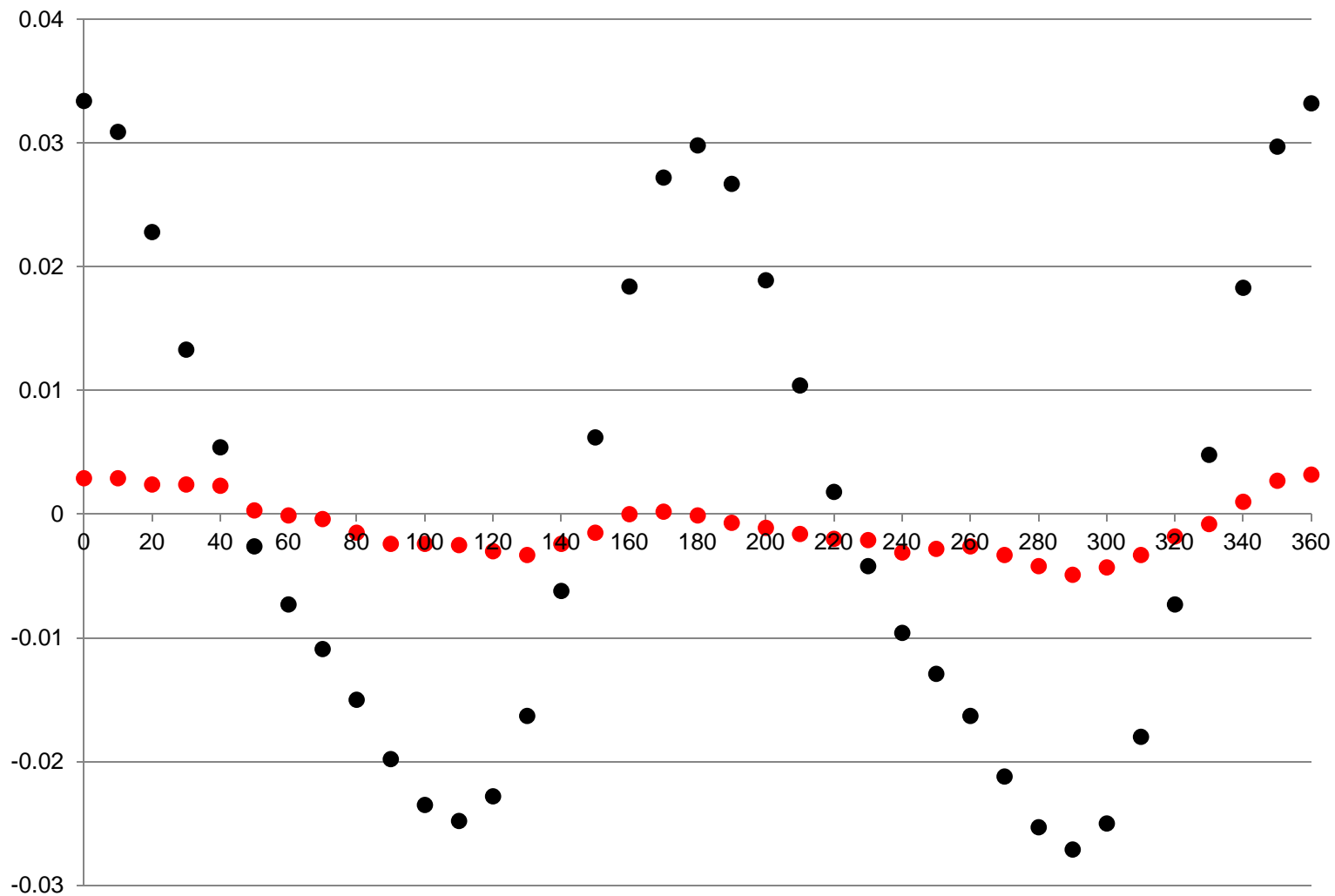


Figure 93. Comparison of the absorbance differences between the peaks at ~ 605 nm and 543 nm from the spectra collected (10° increments) as a thin section of an epidote mineral grain was rotated through 360° using polarized light (black) and without a polarizing filter (red).

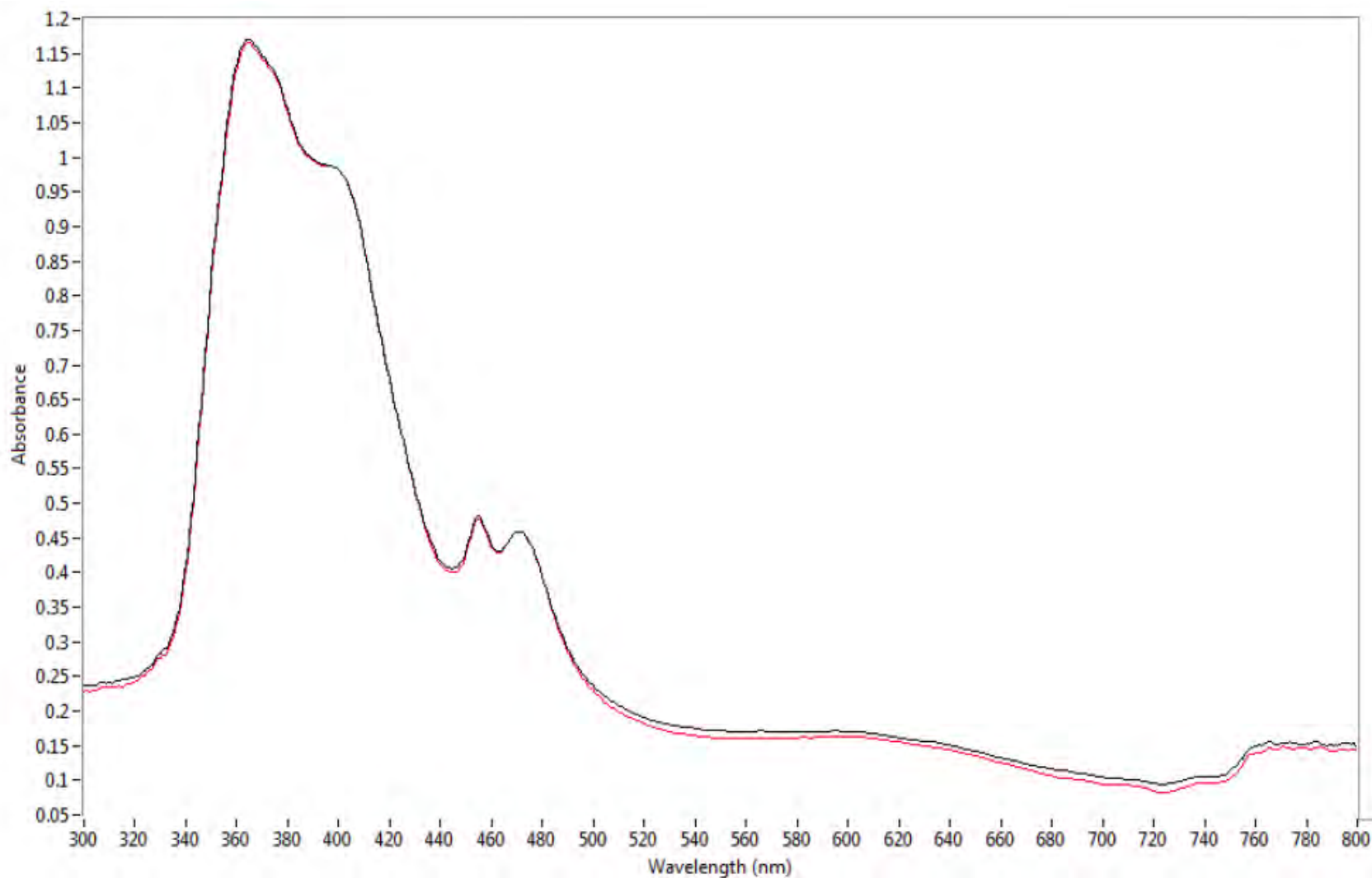


Figure 94. Spectra collected at the 90° (black) and 180° (red) positions from a thin section of an epidote mineral grain (no polarizer).

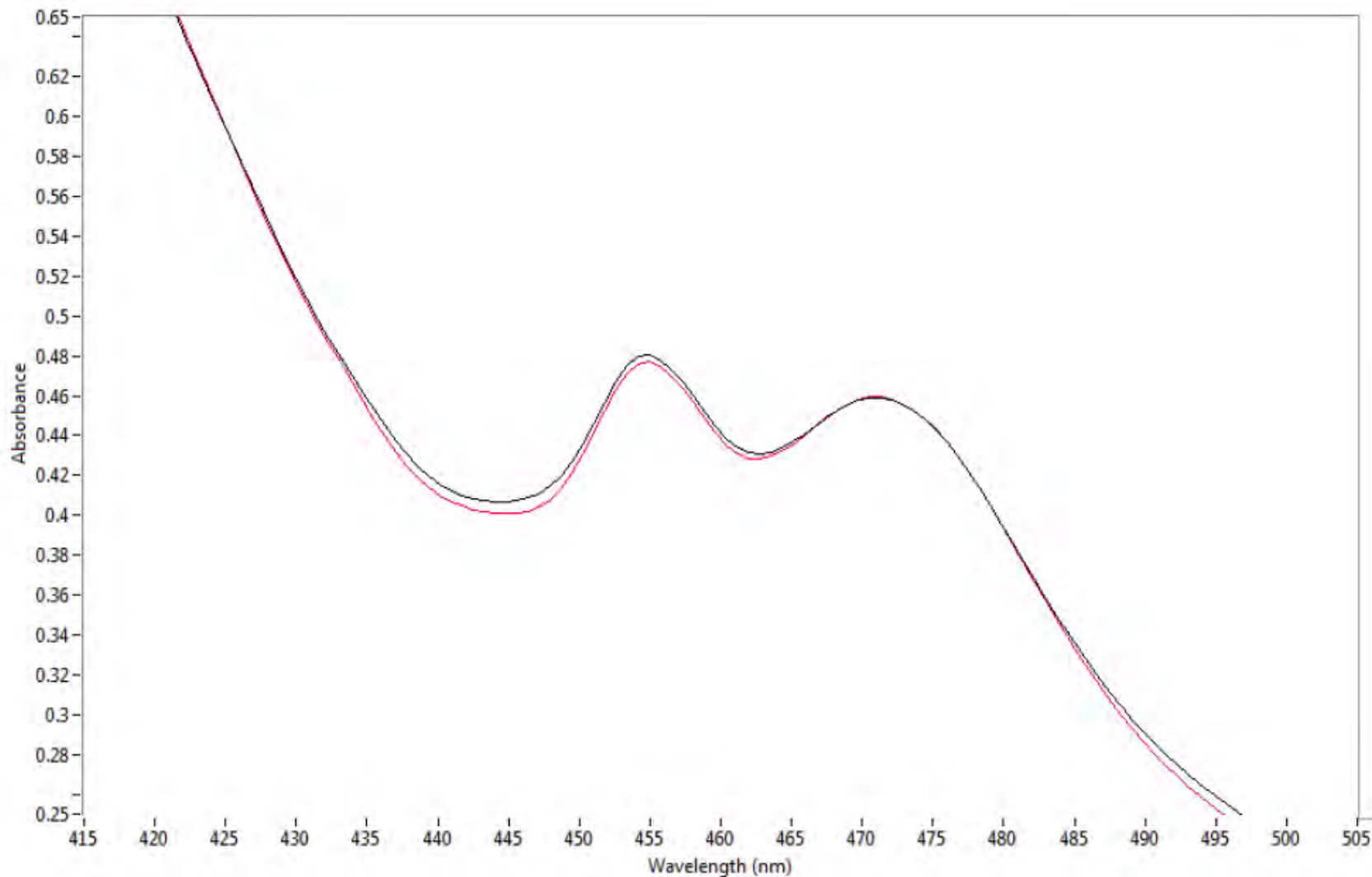


Figure 95. Close-up of the doublet at ~ 455 nm and 471 nm of a thin section of an epidote mineral grain (no polarizer): 90° (black) and 180° (red).

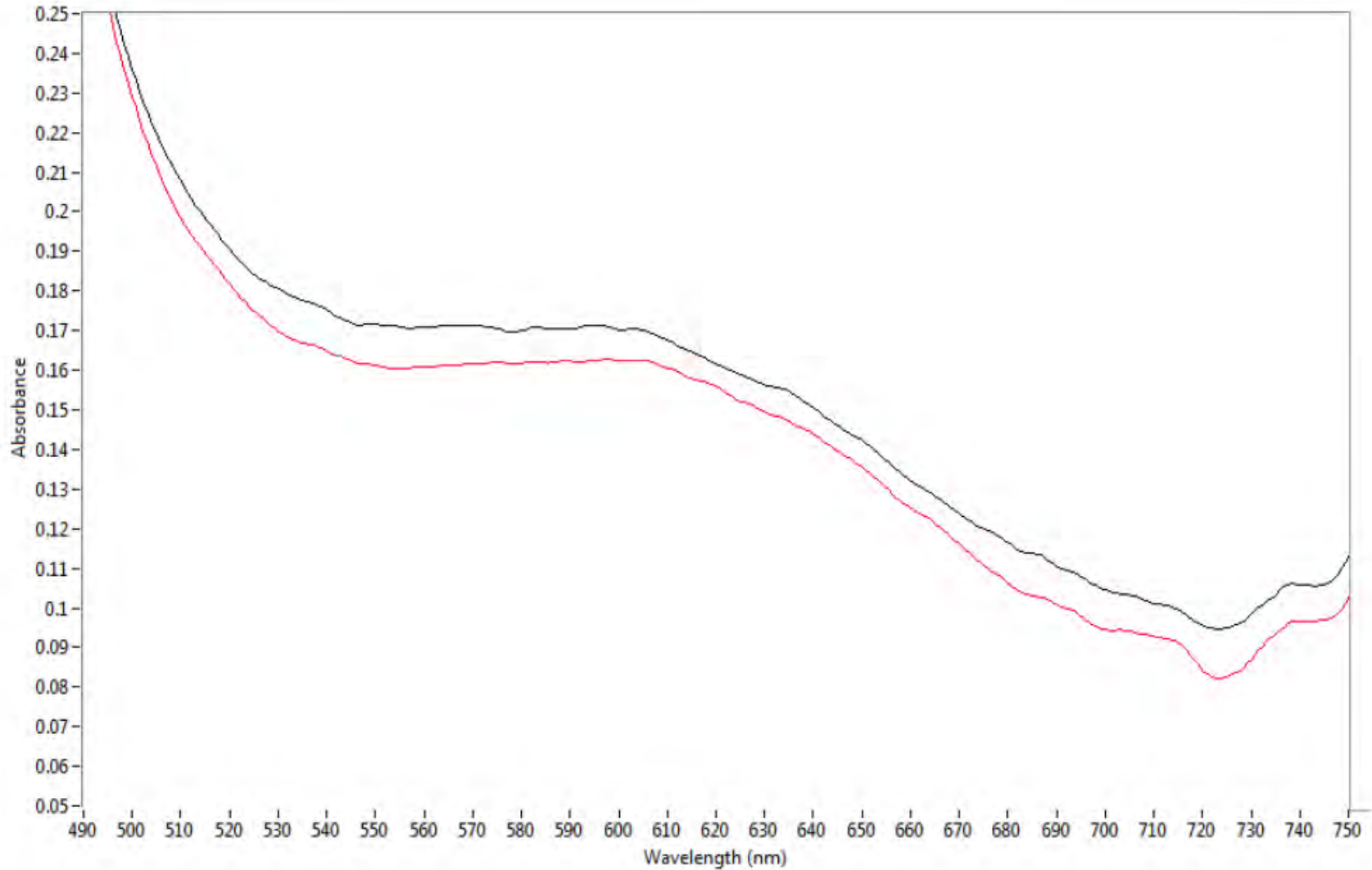


Figure 96. Close-up of the region between 490 nm and 750 nm of a thin section of an epidote mineral grain (no polarizer): 90° (black) and 180° (red).

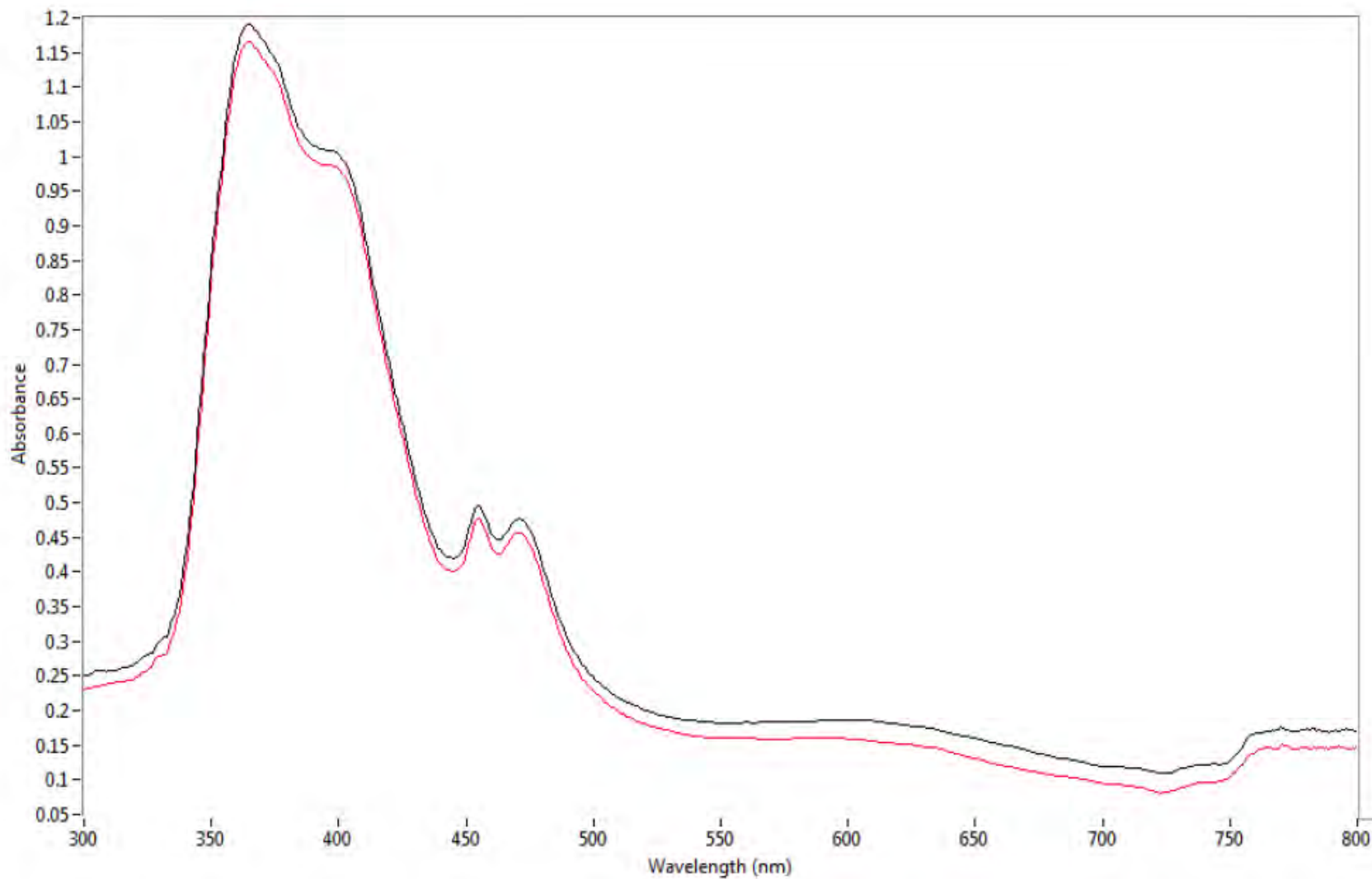


Figure 97. Spectra collected at the 10° (black) and 130° (red) positions from a thin section of an epidote mineral grain (no polarizer).

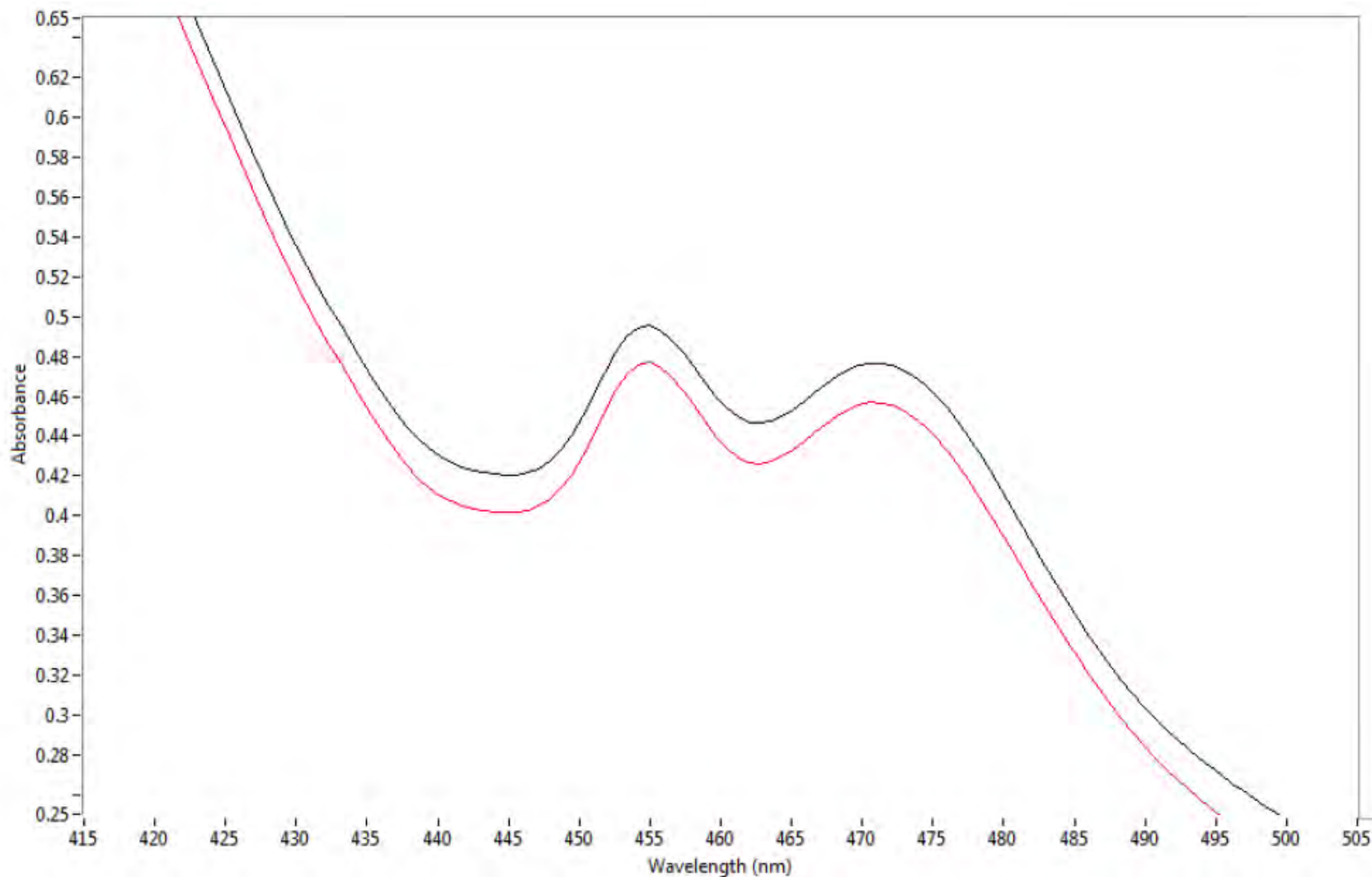


Figure 98. Close-up of the doublet at ~ 455 nm and 471 nm of a thin section of an epidote mineral grain (no polarizer): 10° (black) and 130° (red).

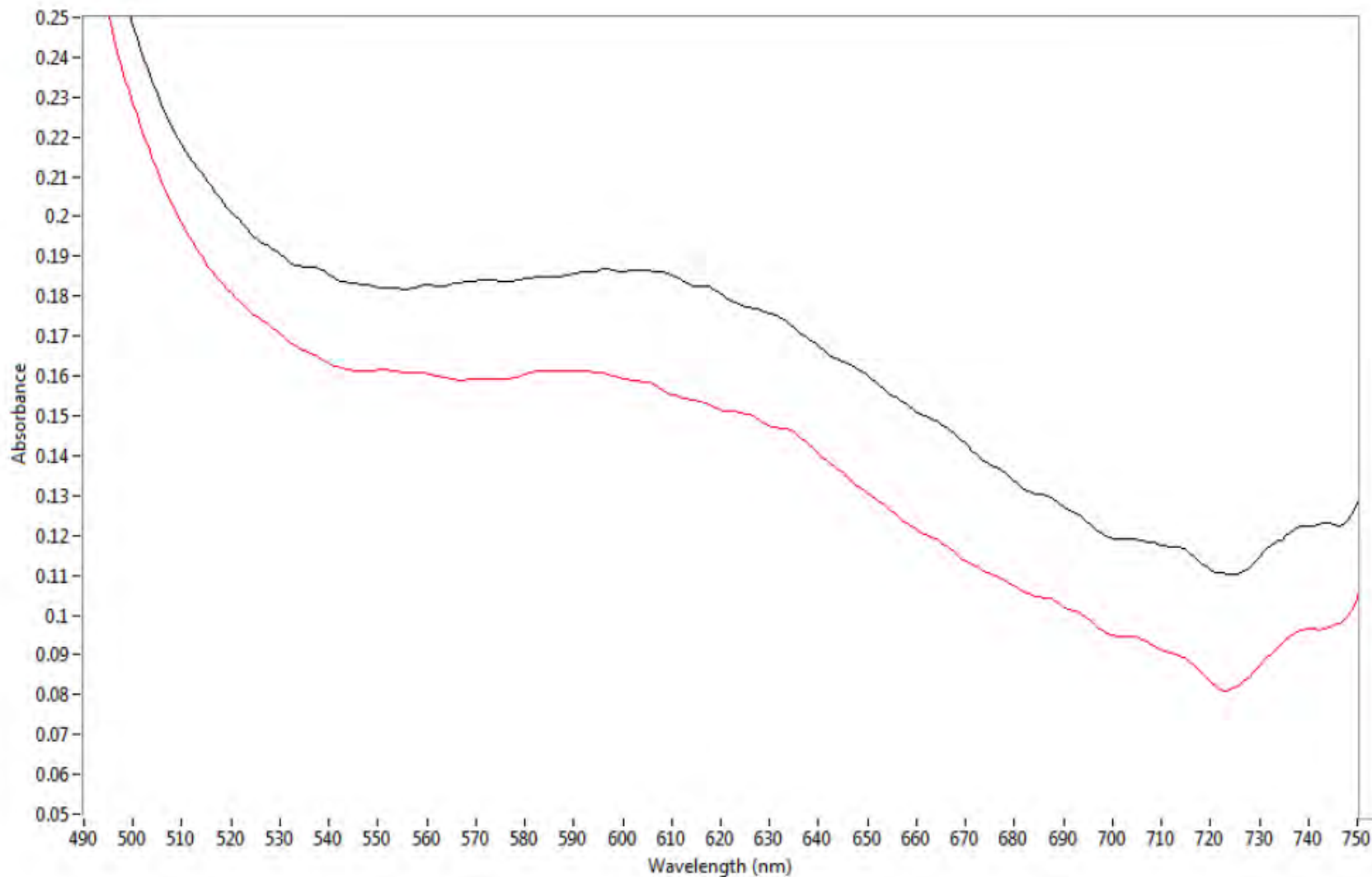


Figure 99. Close-up of the region between 490 nm and 750 nm of a thin section of an epidote mineral grain (no polarizer): 10° (black) and 130° (red).

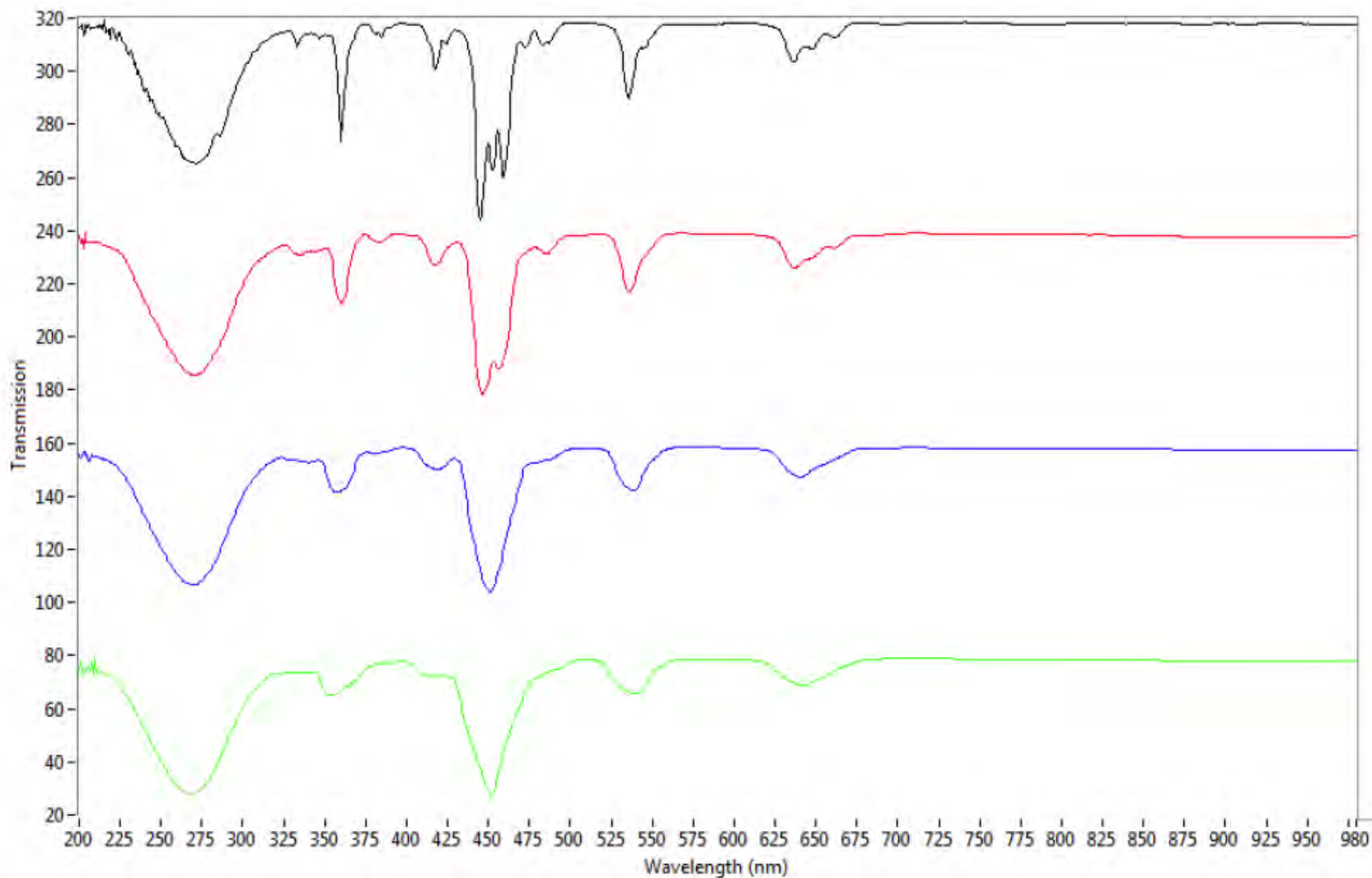


Figure 100. Spectra of holmium oxide collected using resolution factors of: 0 (black), 5 (red), 10 (blue), and 15 (green). The spectra are stacked for ease of viewing.

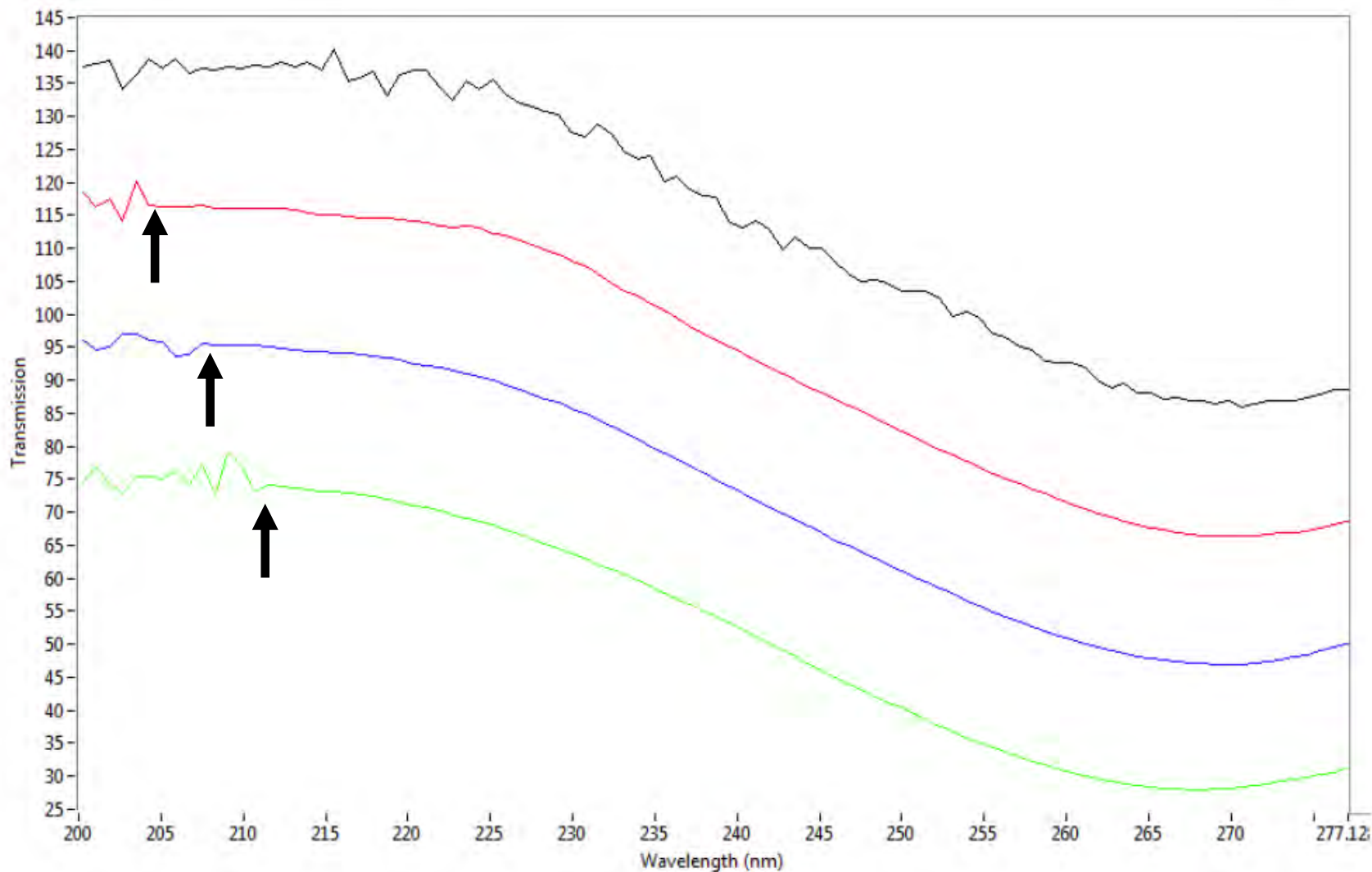


Figure 101. Close-up view of the spectra of holmium oxide collected using resolution factors of: 0 (black), 5 (red), 10 (blue), and 15 (green). The spectra are stacked for ease of viewing and the black arrows mark the approximate position of the boundary of the artifact peaks.

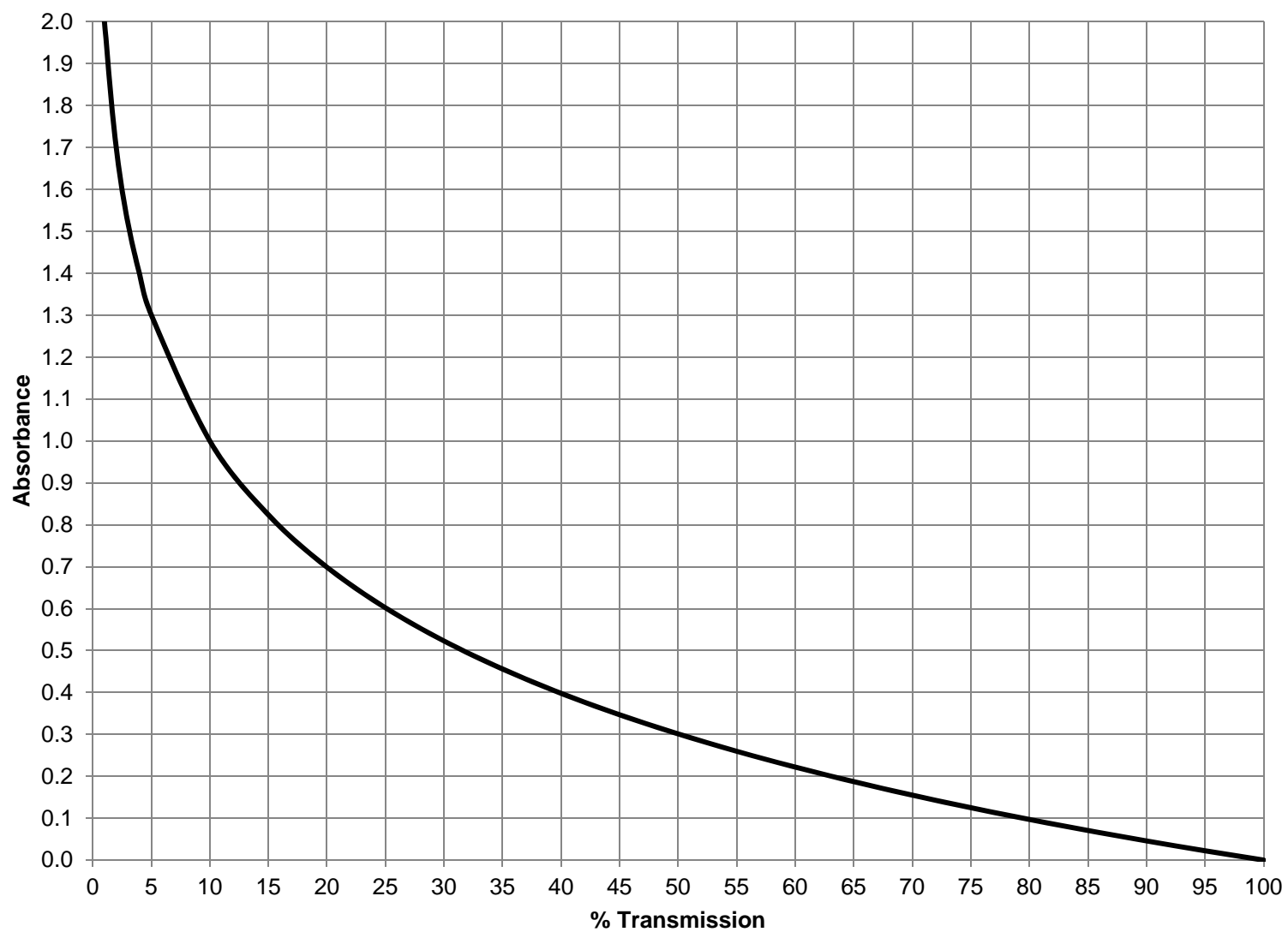


Figure 102. Plot showing the correlation between absorbance and transmittance

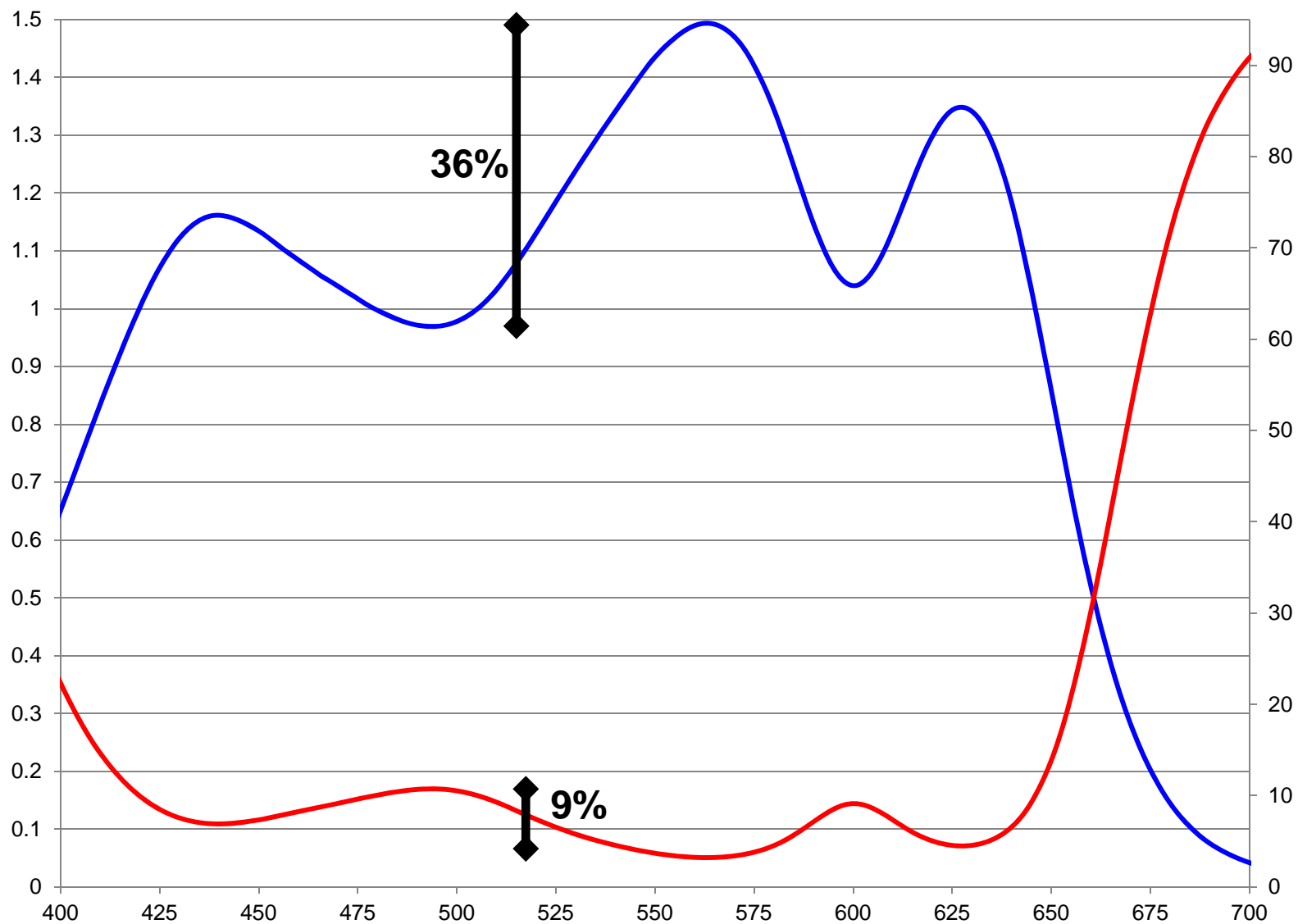


Figure 103. MSP spectra of a black fiber plotted in both absorbance (blue) and transmission (red) on two independent axes.

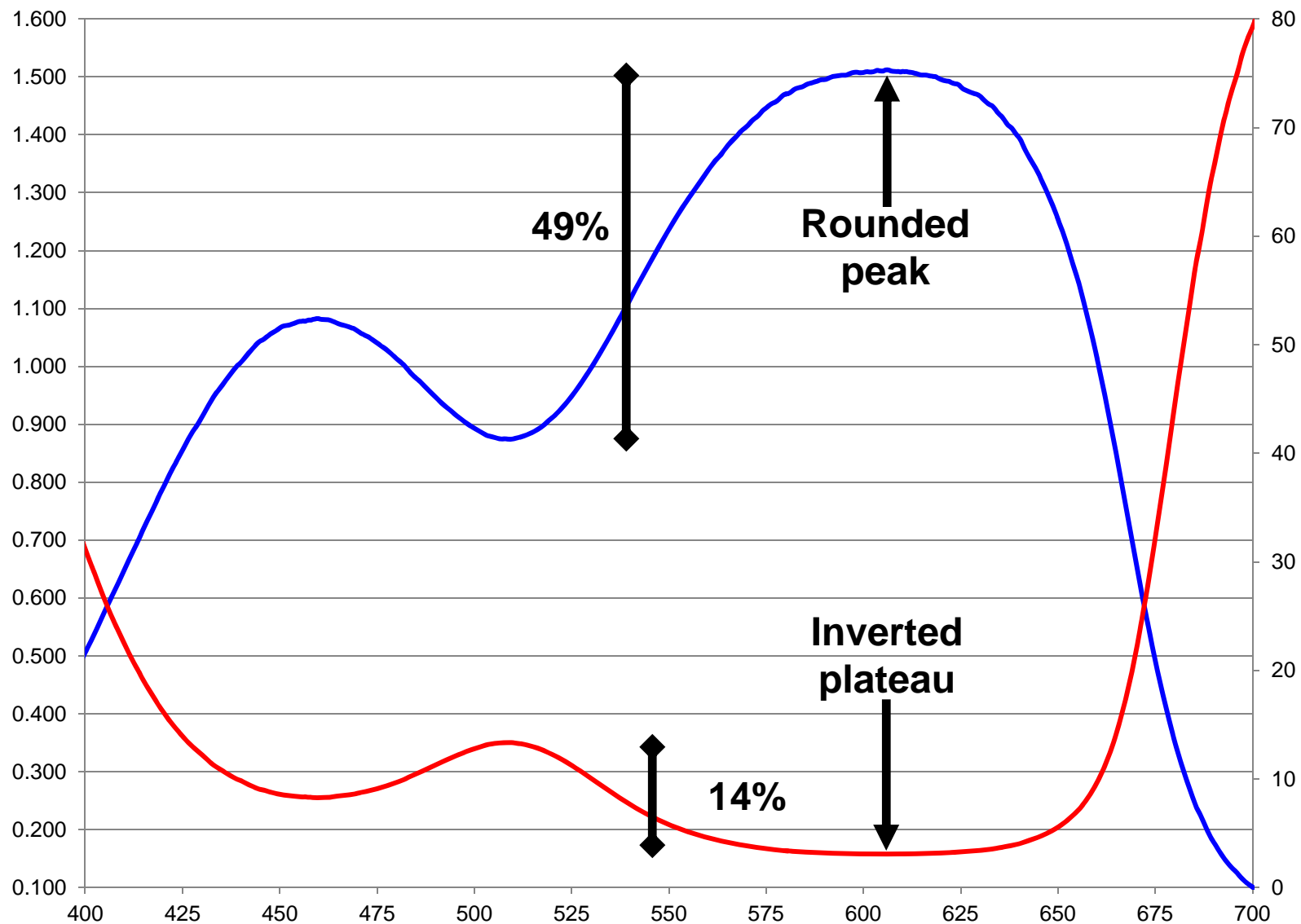


Figure 104. MSP spectra of a black fiber plotted in both absorbance (blue) and transmission (red) on two independent axes. Note the rounded absorbance peak compared to the more inverted plateau-like transmission peak.

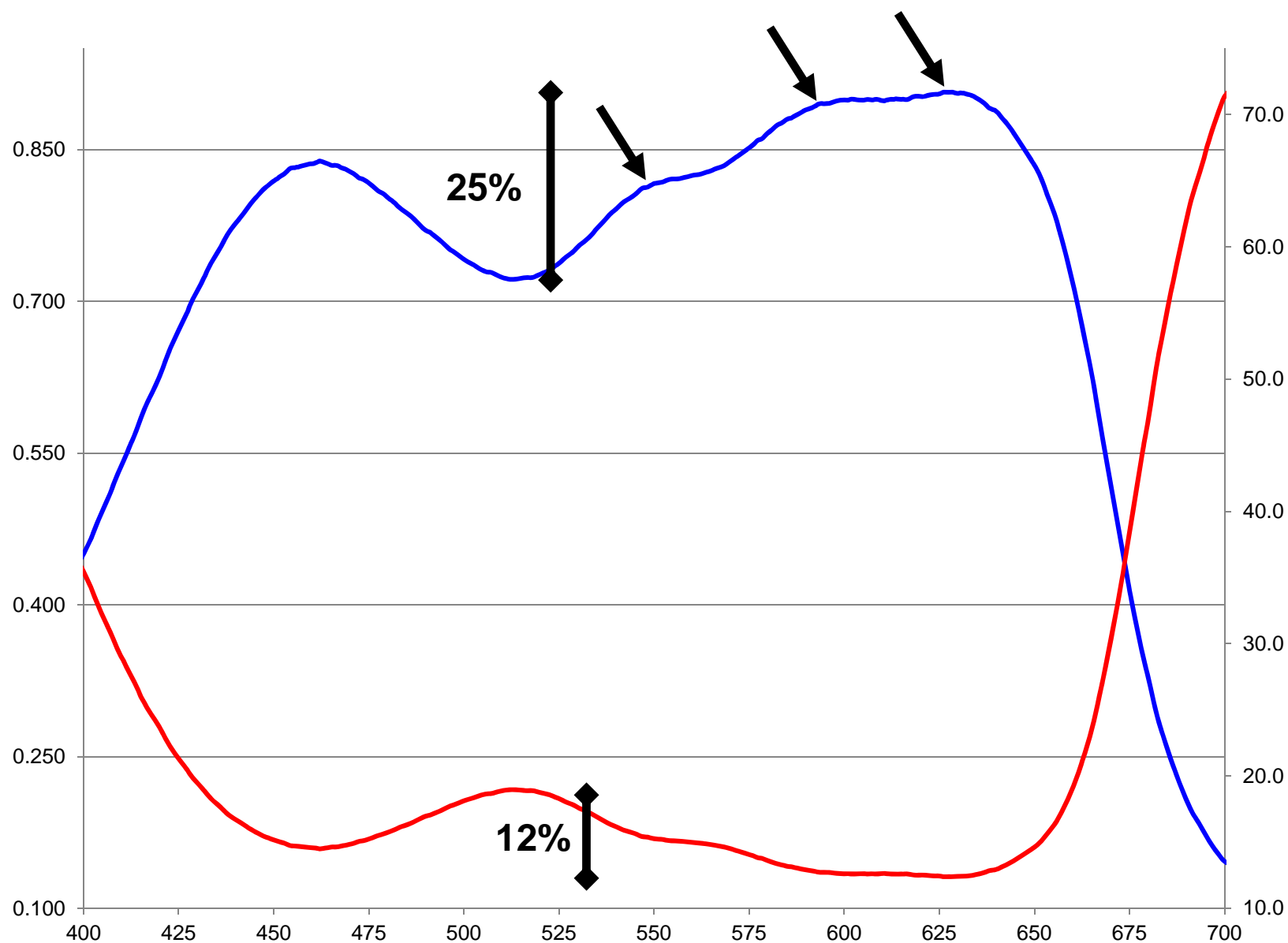


Figure 105. MSP spectra of a black fiber plotted in both absorbance (blue) and transmission (red) on two independent axes. Note that the subtle spectral features (marked by arrows) are easier to observe in the absorbance plot.

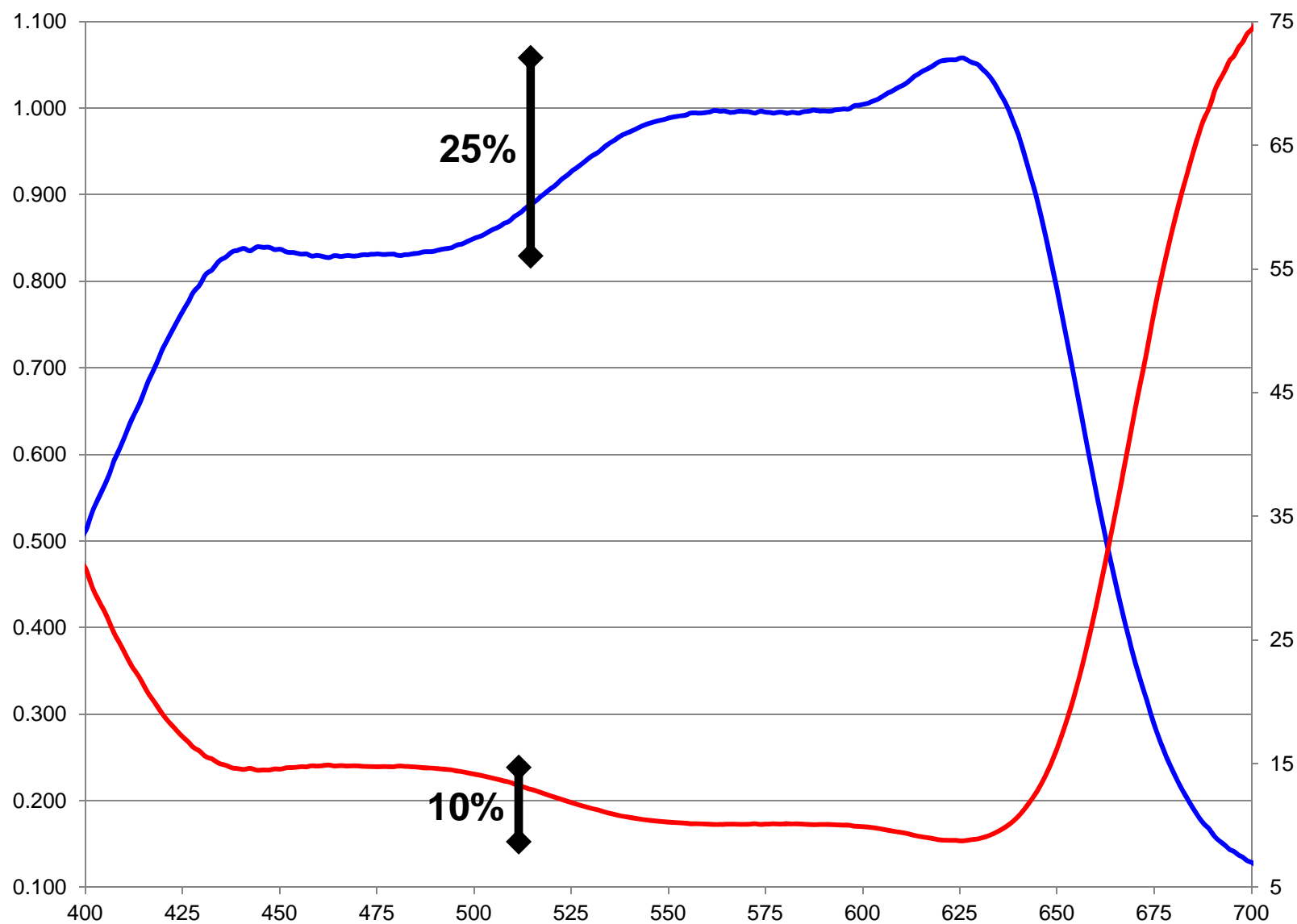


Figure 106. MSP spectra of a black fiber plotted in both absorbance (blue) and transmission (red) on two independent axes. Note the apparent ordinate expansion of the spectral features in the absorbance plot.

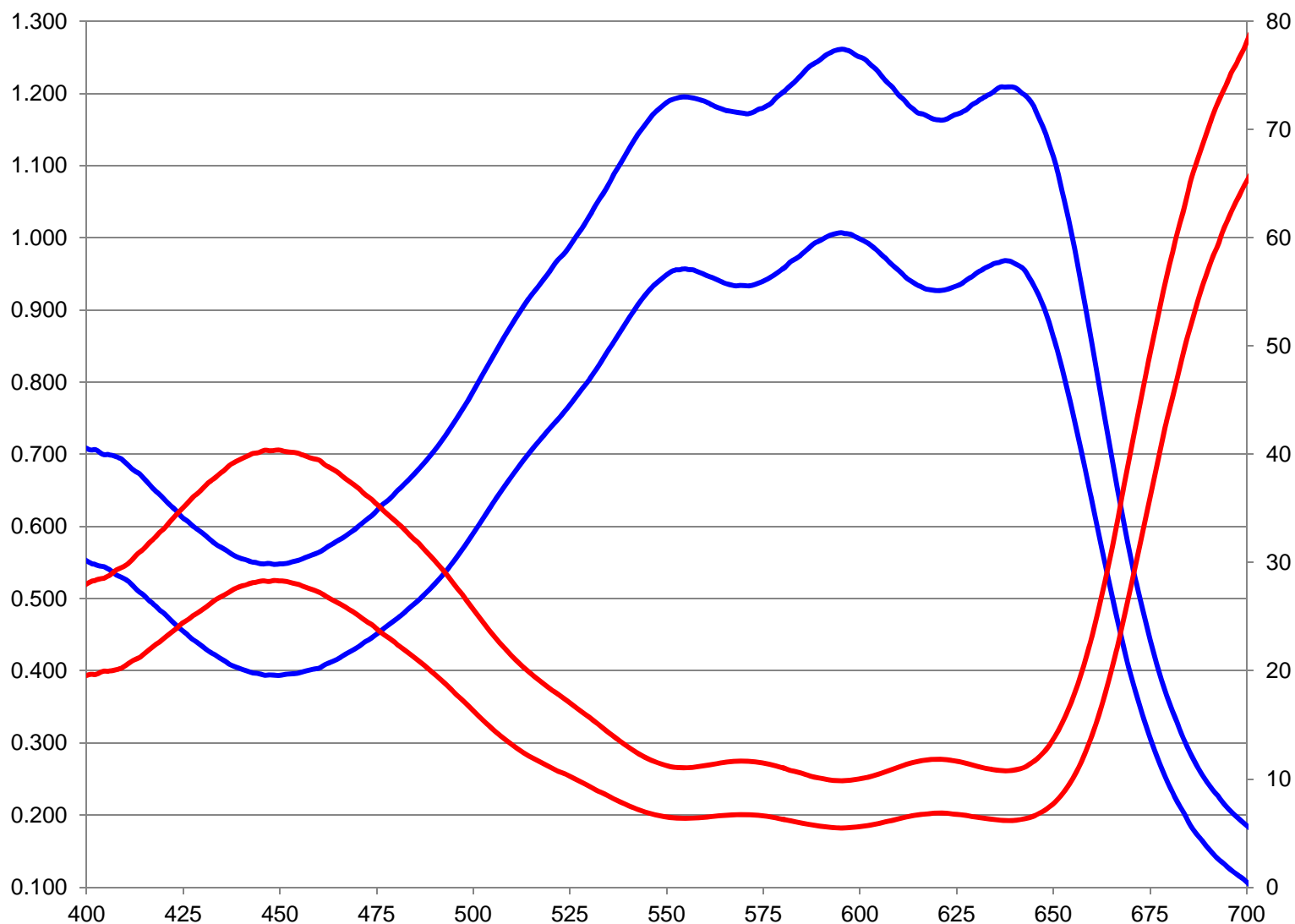


Figure 107. MSP spectra of two dark blue fibers plotted in both absorbance (blue) and transmission (red) on two independent axes. Note the two transmission spectra appear closer together between ~550 and 650 nm compared to their absorbance spectra.

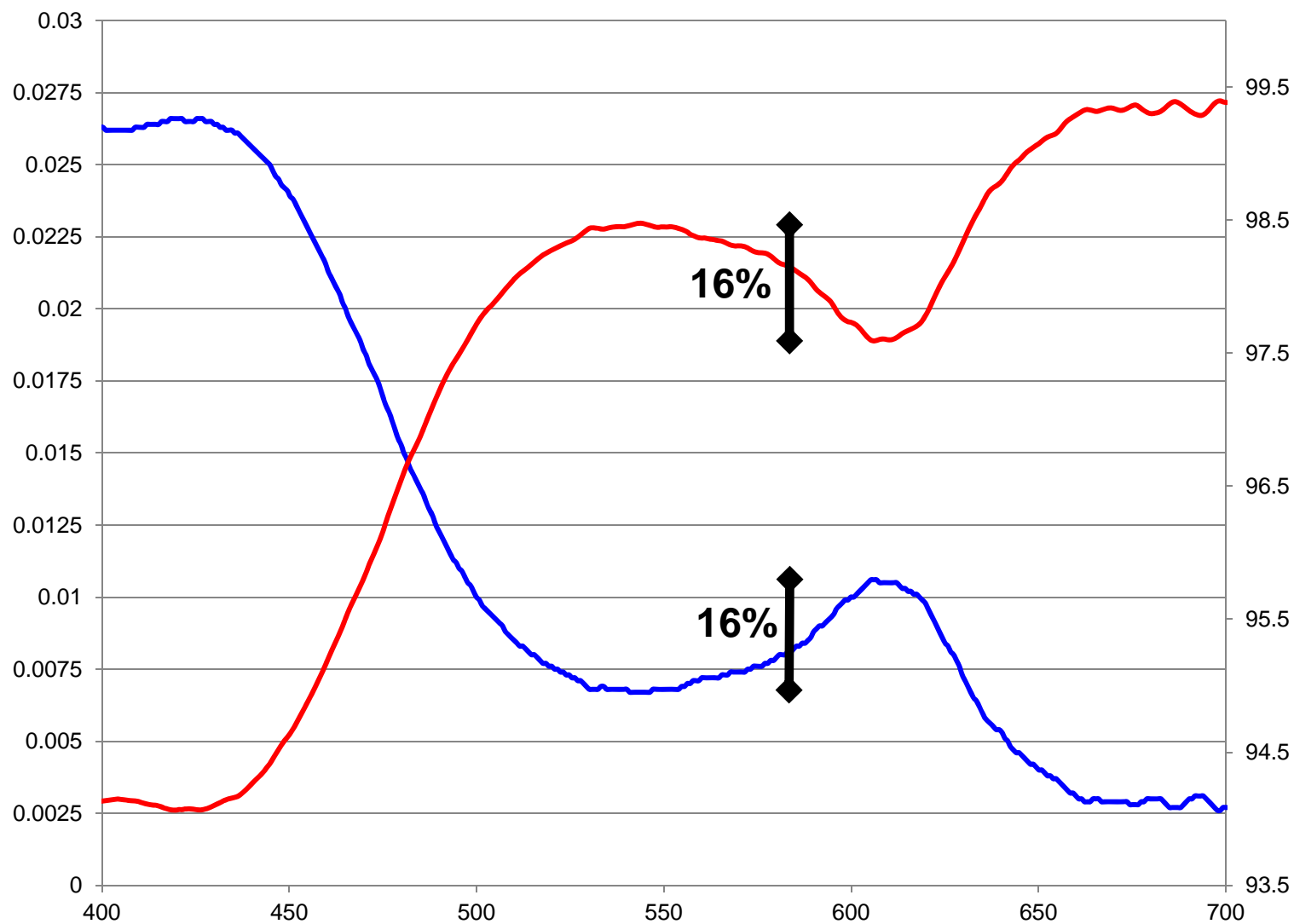


Figure 108. MSP spectra of a light green fiber plotted in both absorbance (blue) and transmission (red) on two independent axes.

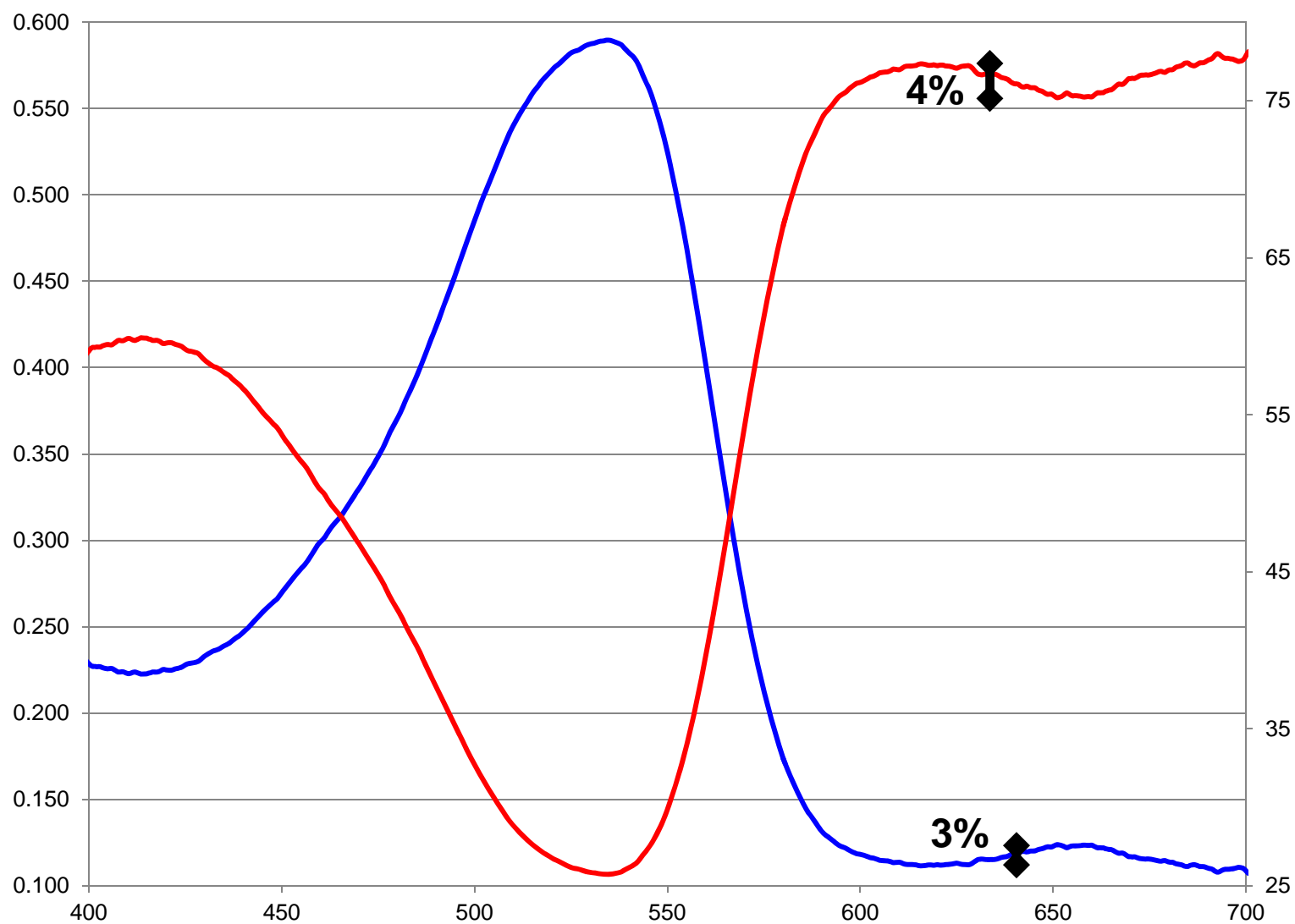


Figure 109. MSP spectra of a red fiber plotted in both absorbance (blue) and transmission (red) on two independent axes.

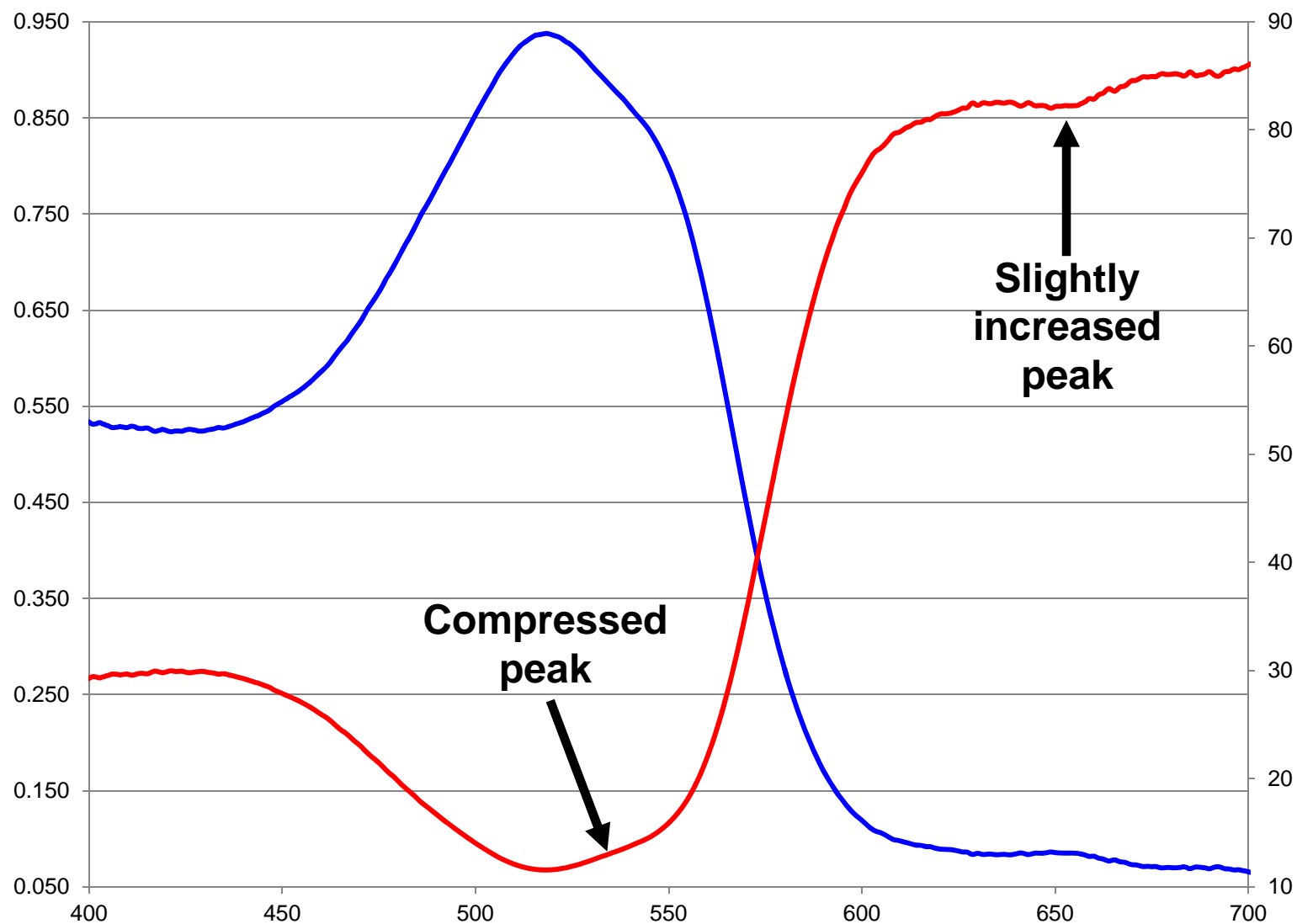


Figure 110. MSP spectra of a red fiber plotted in both absorbance (blue) and transmission (red) on two independent axes.

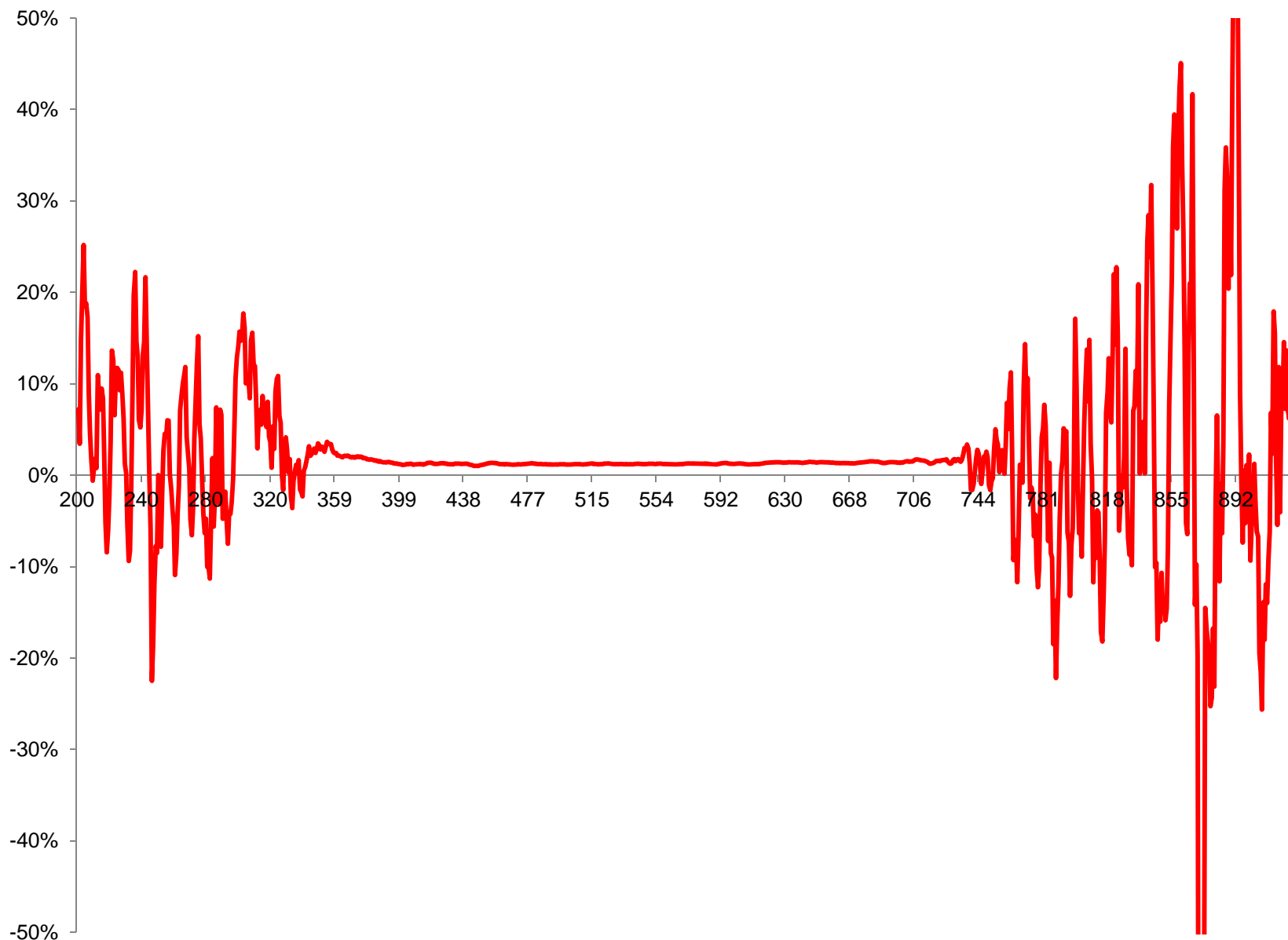


Figure 111. Percent increase in the intensity of the emission of a tungsten halogen bulb passing through a quartz slide relative to the emission passing through a glass slide.

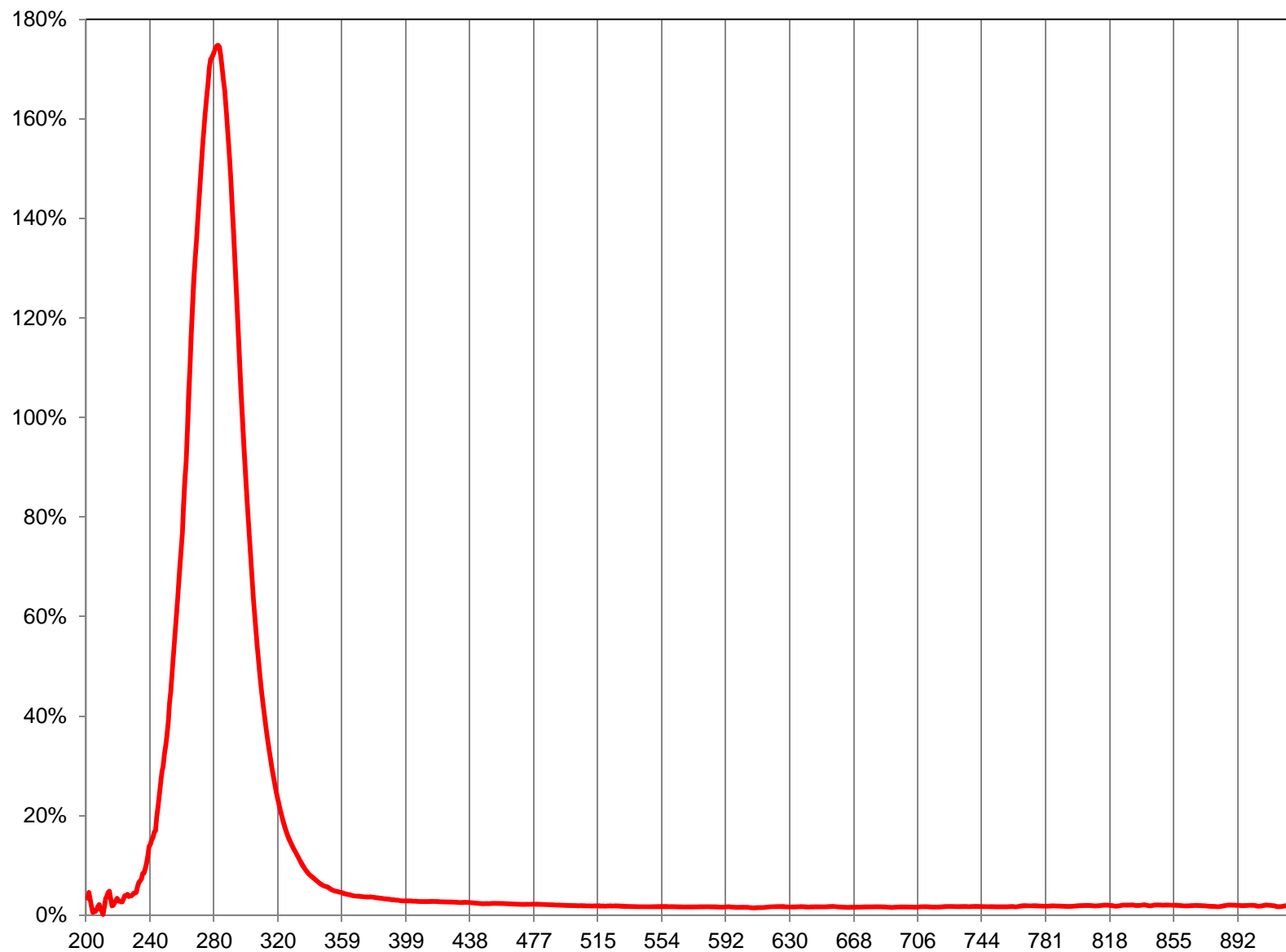


Figure 112. Percent increase in the intensity of the emission of a xenon bulb passing through a quartz slide relative to the emission passing through a glass slide.

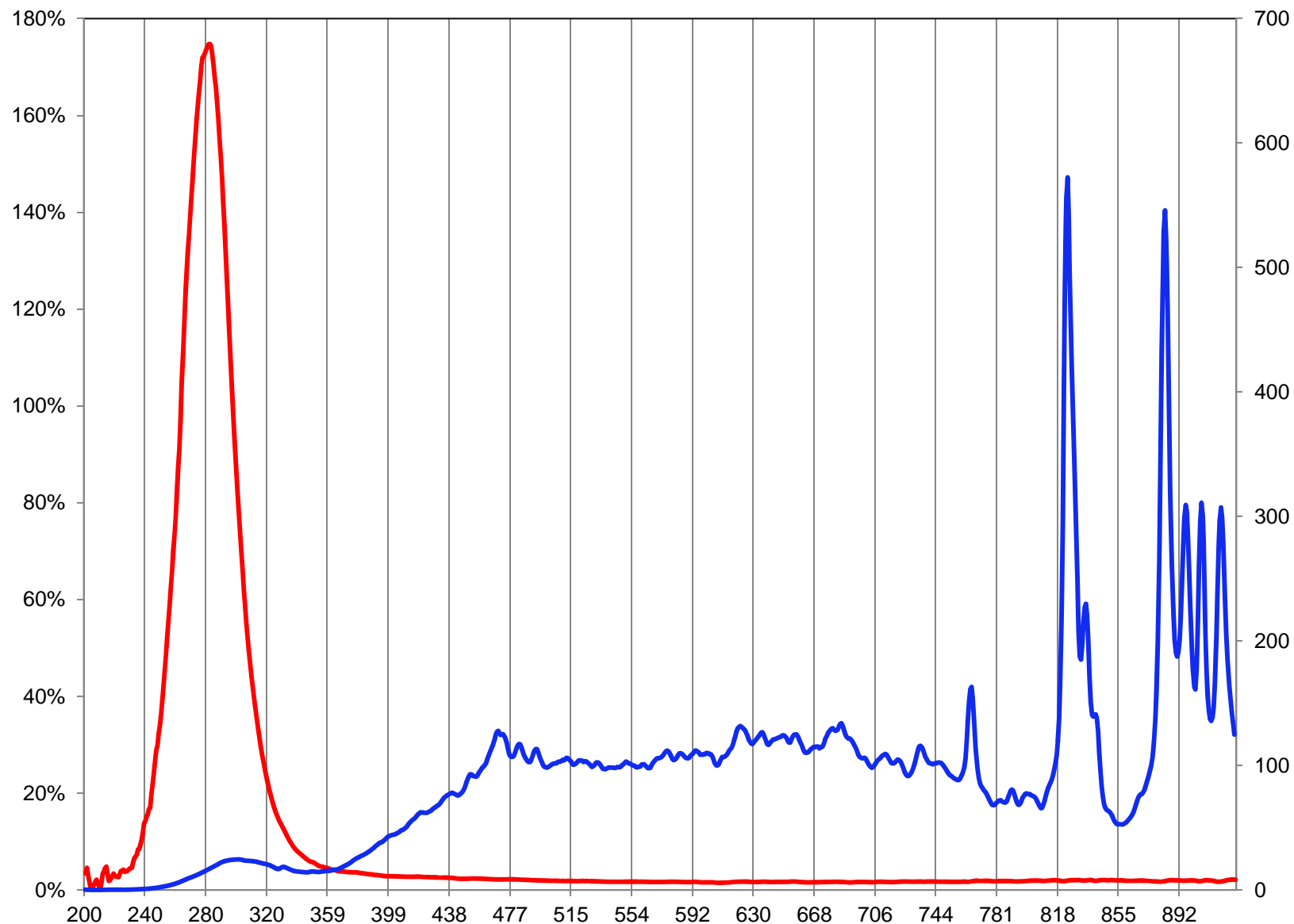


Figure 113. Percent increase in the intensity of the emission of a xenon bulb passing through a quartz slide relative to the emission passing through a glass slide (red – left axis) compared to the difference, in absolute counts, of the emission passing through the quartz and glass slides (blue - plotted on the secondary [right] axis).

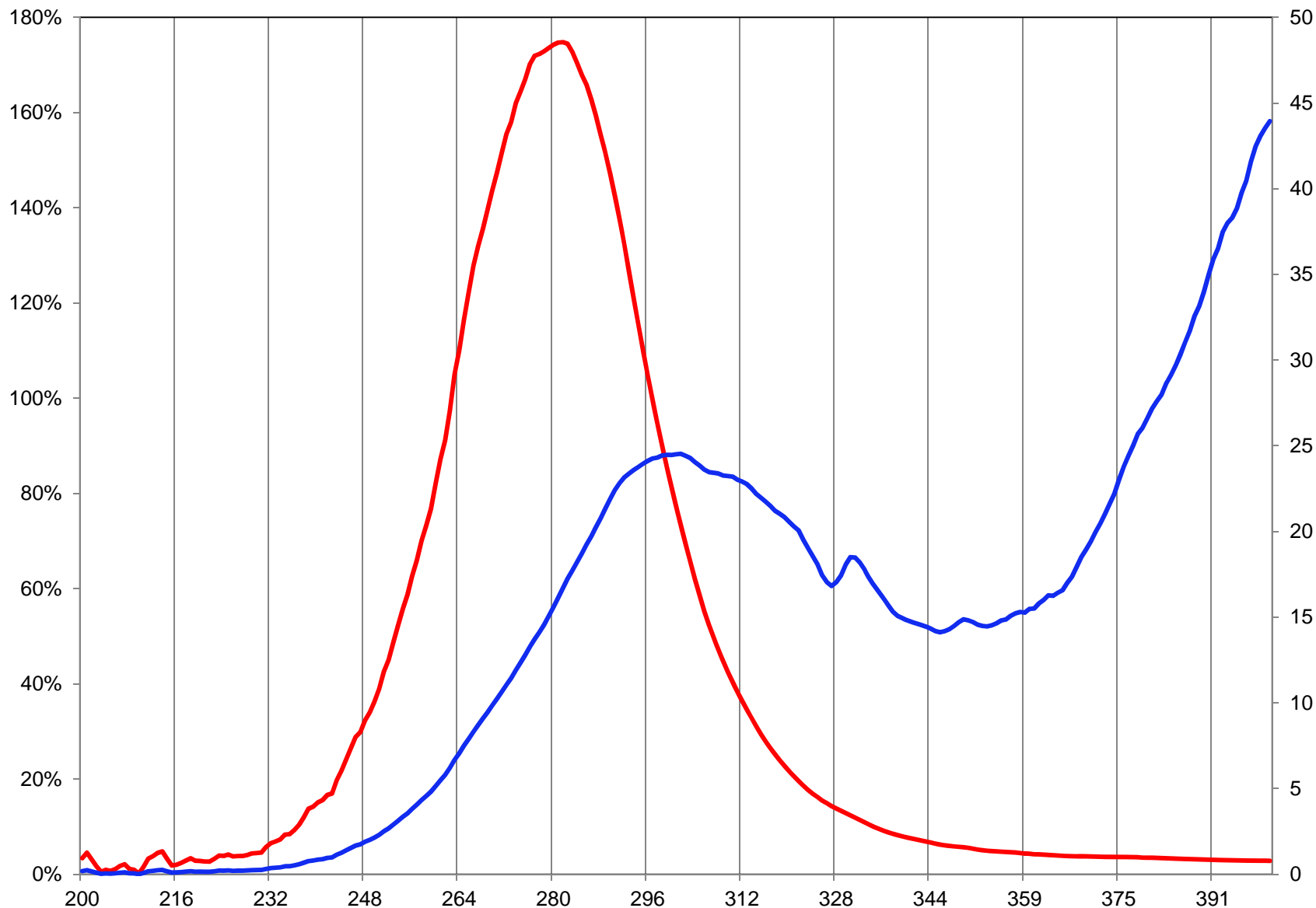


Figure 114. Percent increase in the intensity of the emission of a xenon bulb passing through a quartz slide relative to the emission passing through a glass slide (red – left axis) compared to the difference, in absolute counts, of the emission passing through the quartz and glass slides (blue - plotted on the secondary [right] axis).

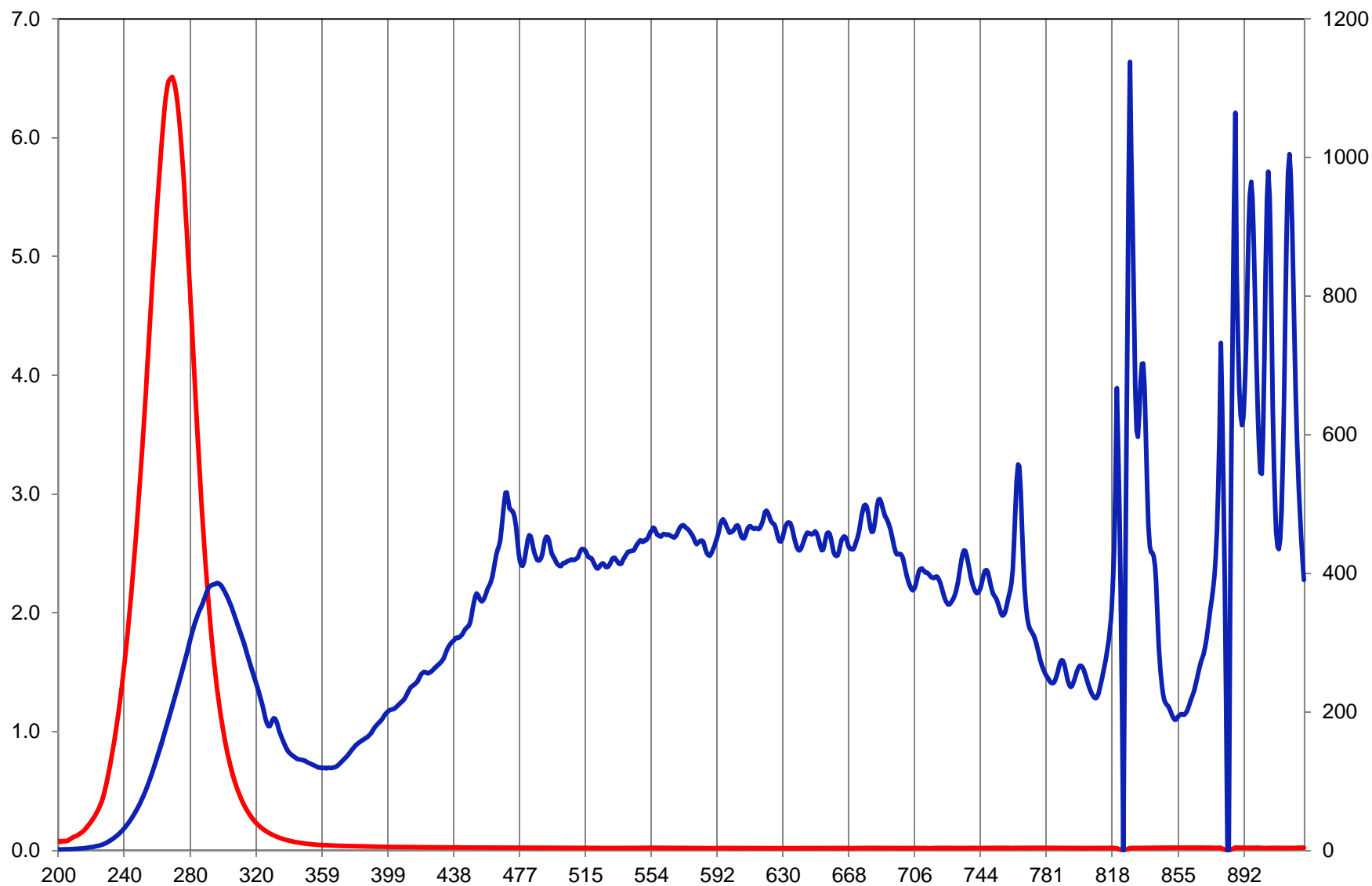


Figure 115. Percent increase in the intensity of the emission of a xenon bulb passing through a quartz slide relative to the emission passing through a glass slide (red – left axis) compared to the difference, in absolute counts, of the emission passing through the quartz and glass slides (blue - plotted on the secondary [right] axis). Collected using different parameters compared to the previous figures.

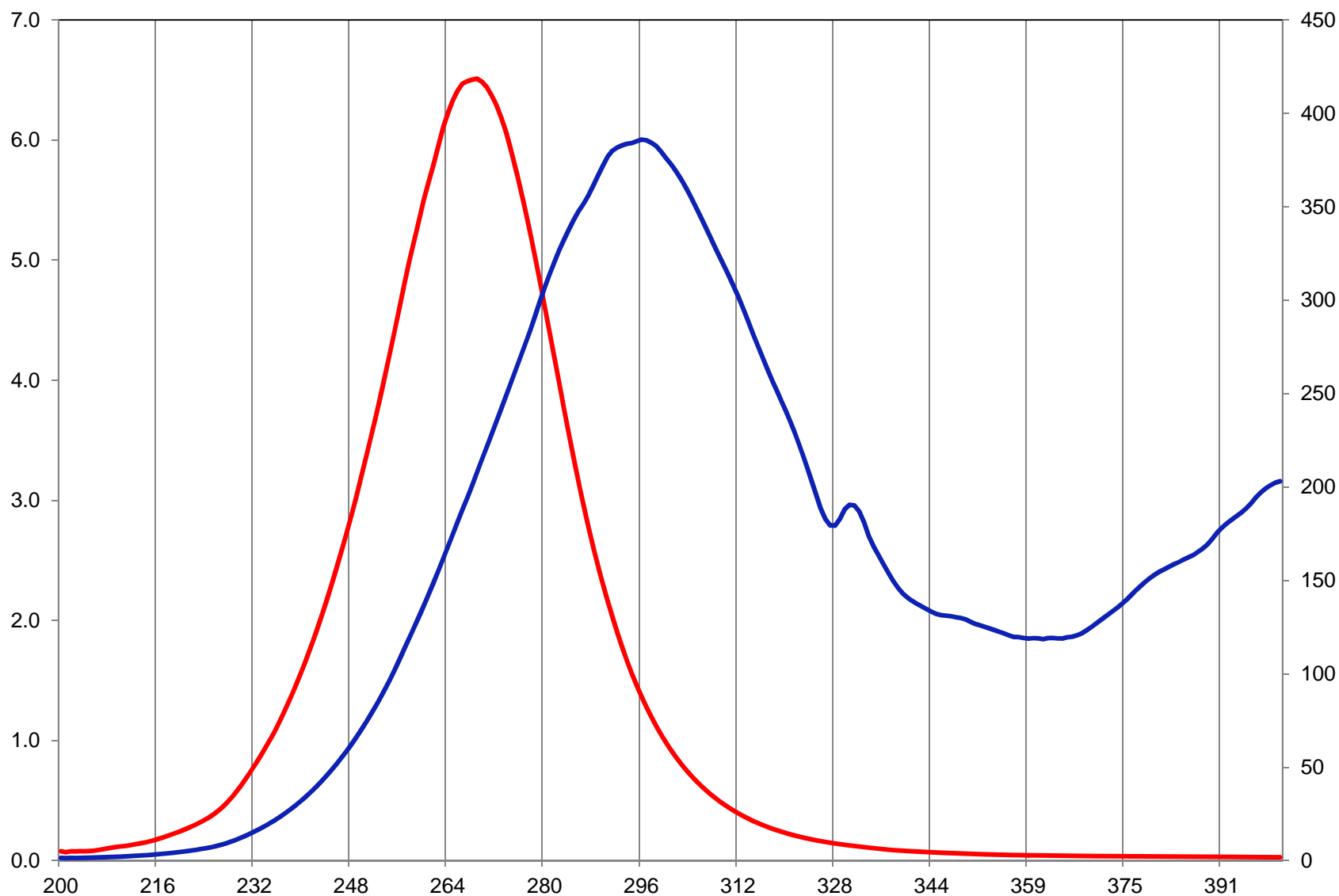


Figure 116. Percent increase in the intensity of the emission of a xenon bulb passing through a quartz slide relative to the emission passing through a glass slide (red – left axis) compared to the difference, in absolute counts, of the emission passing through the quartz and glass slides (blue - plotted on the secondary [right] axis). Collected using different parameters compared to the previous figures.

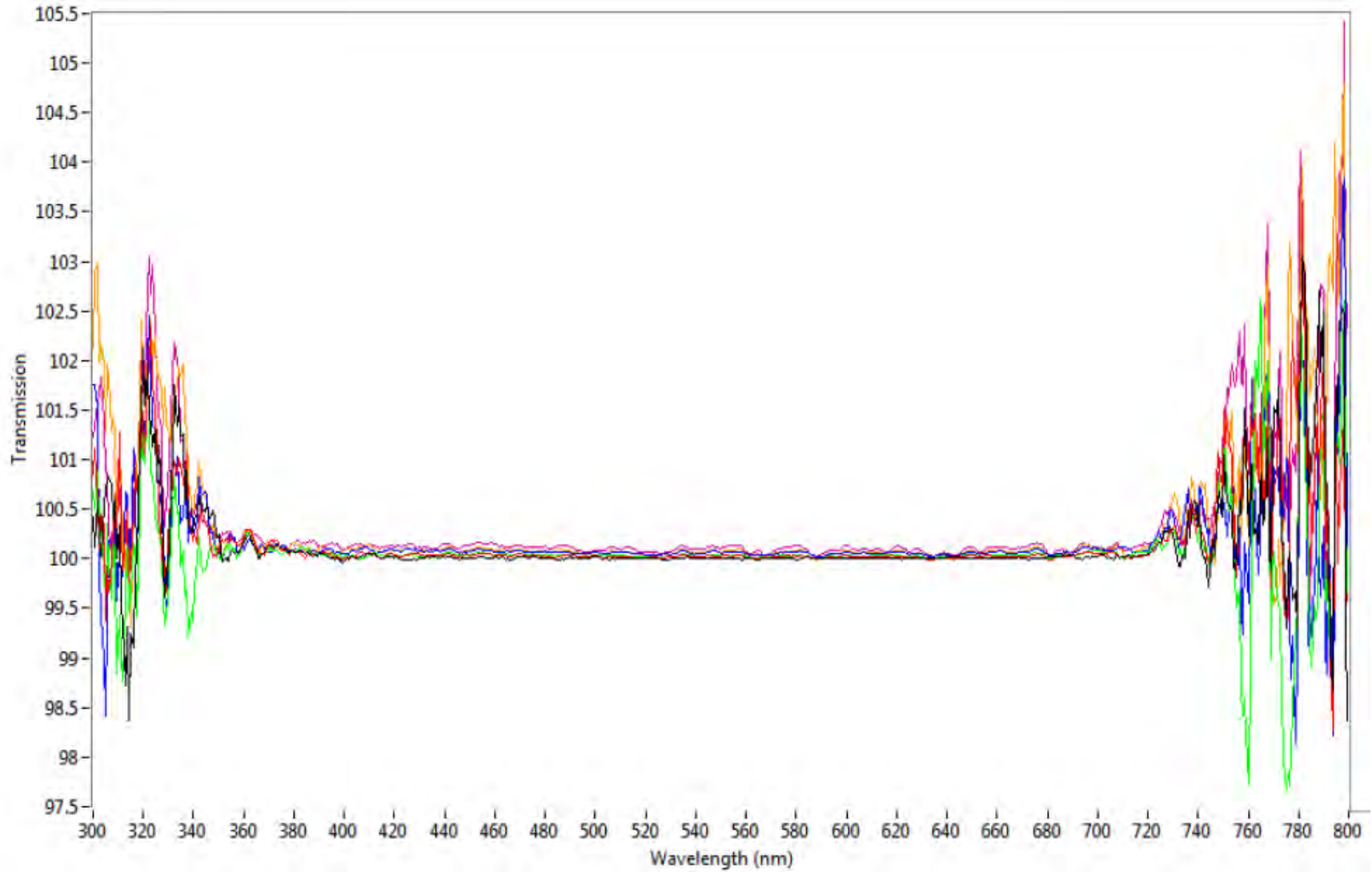


Figure 117. Spectra collected every minute for five minutes through a quartz slide using tungsten halogen illumination.

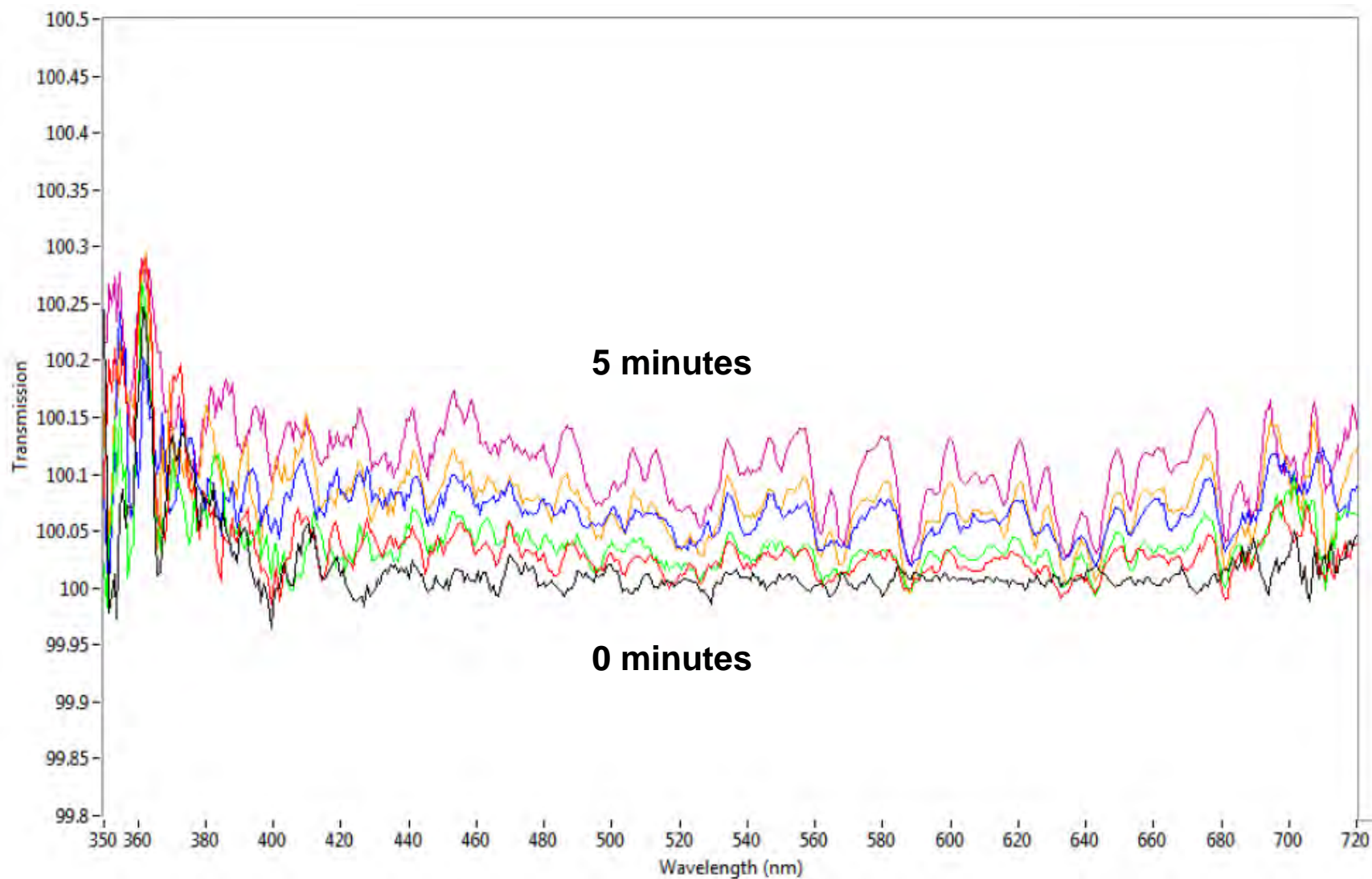


Figure 118. Close-up of spectra collected every minute for five minutes through a quartz slide using tungsten halogen illumination.

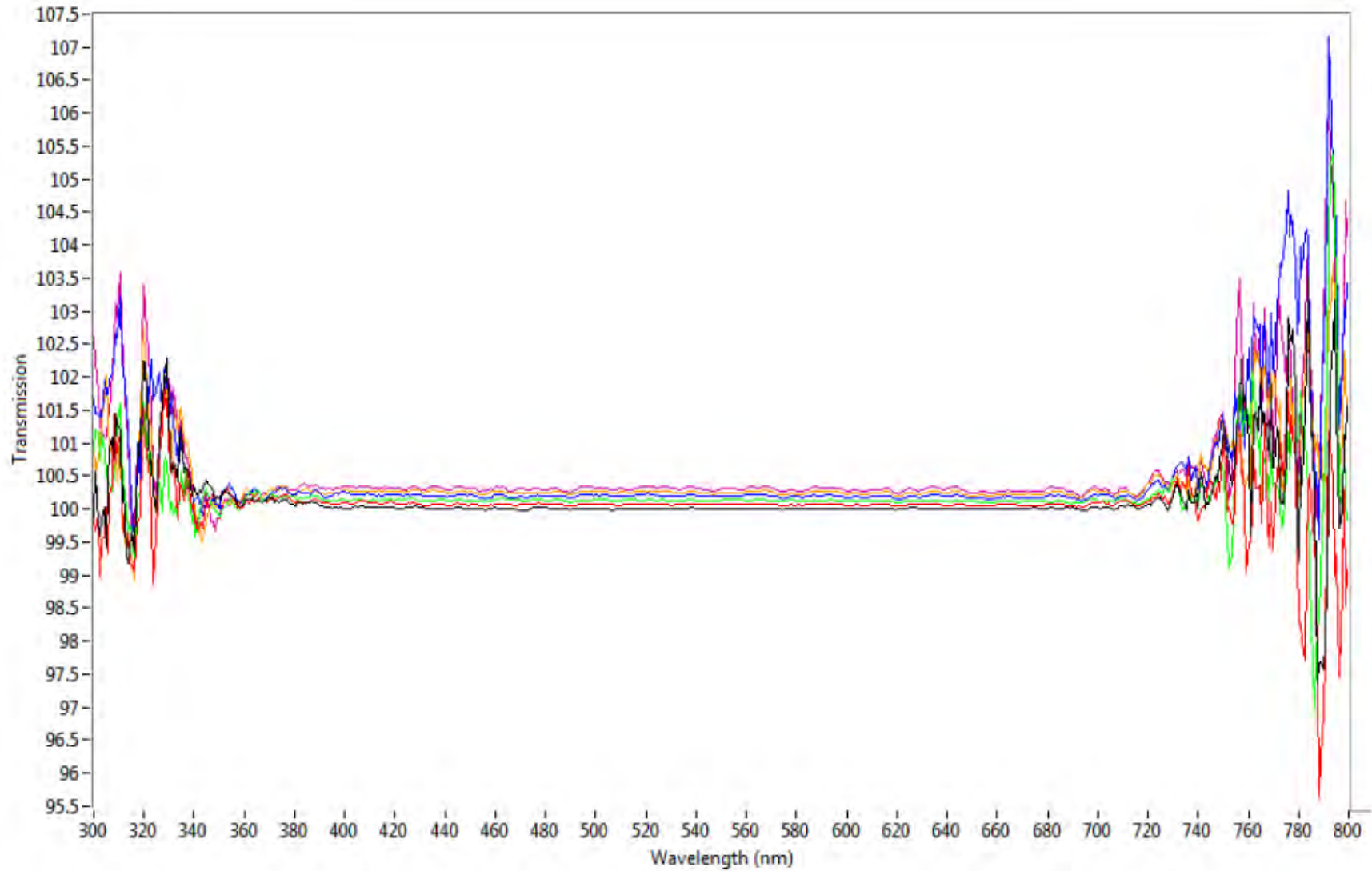


Figure 119. Spectra collected every minute for five minutes through a glass slide using tungsten halogen illumination.

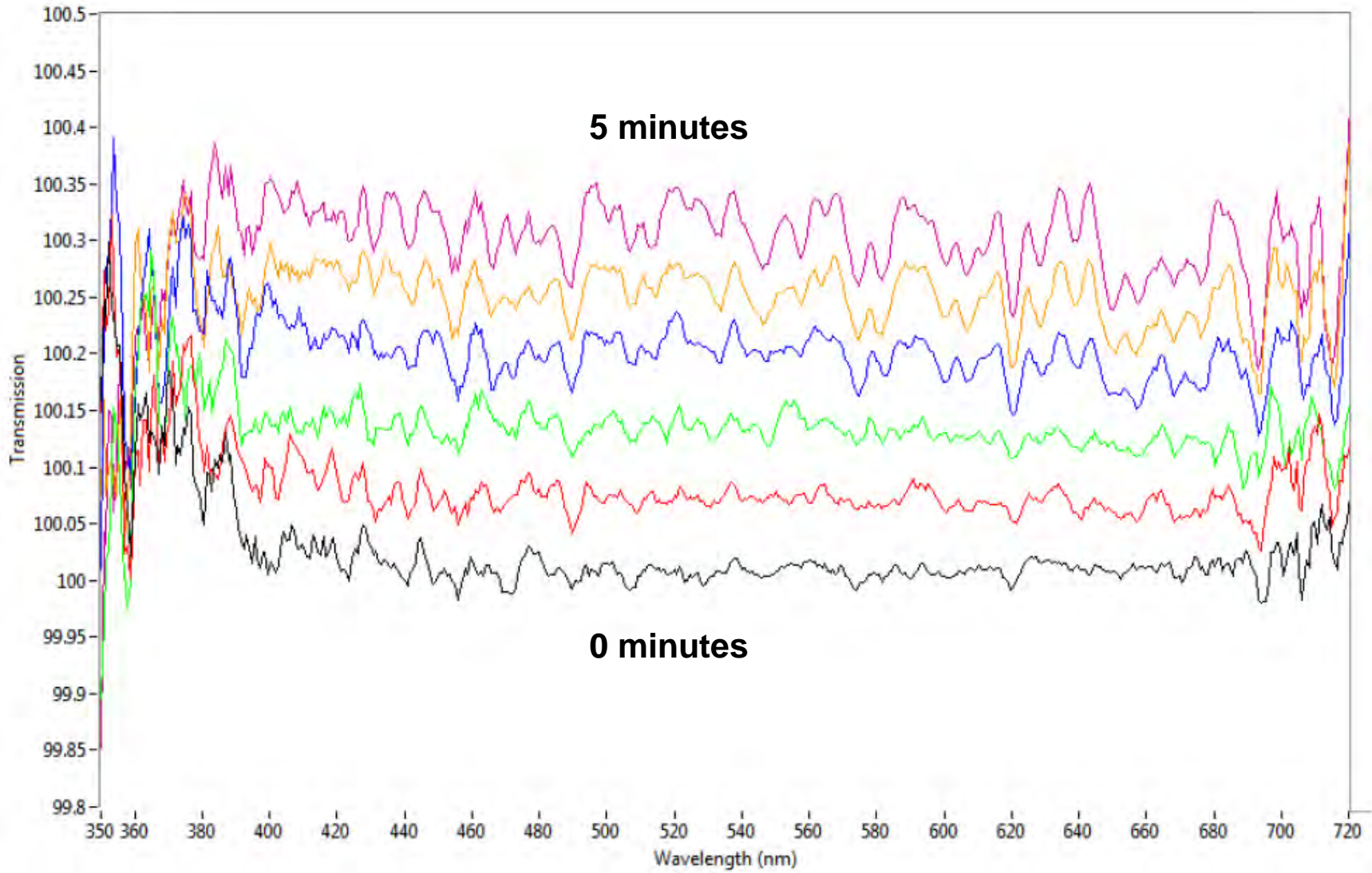


Figure 120. Close-up of spectra collected every minute for five minutes through a glass slide using tungsten halogen illumination.

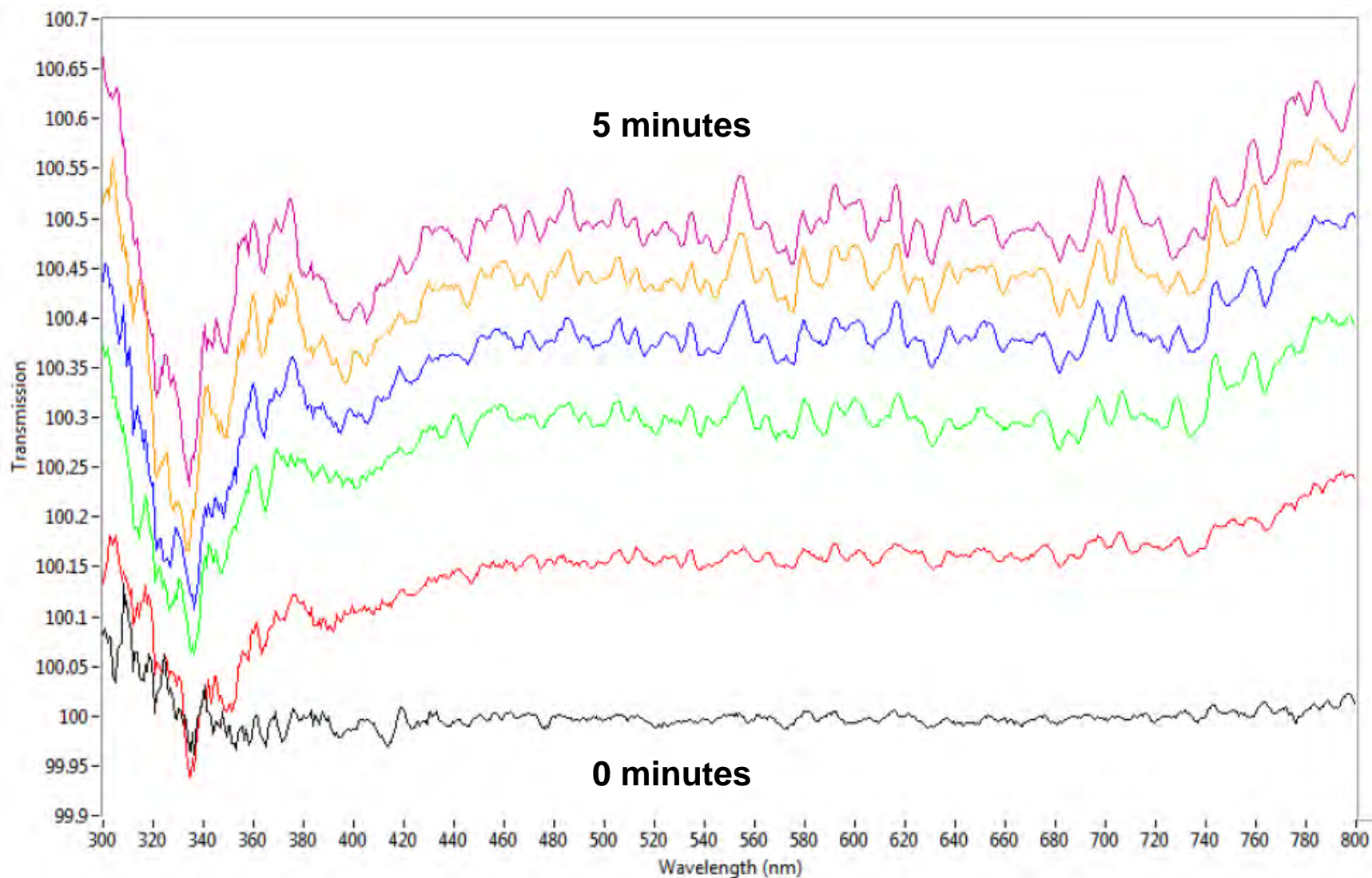


Figure 121. Spectra collected every minute for five minutes through a quartz slide using xenon illumination.

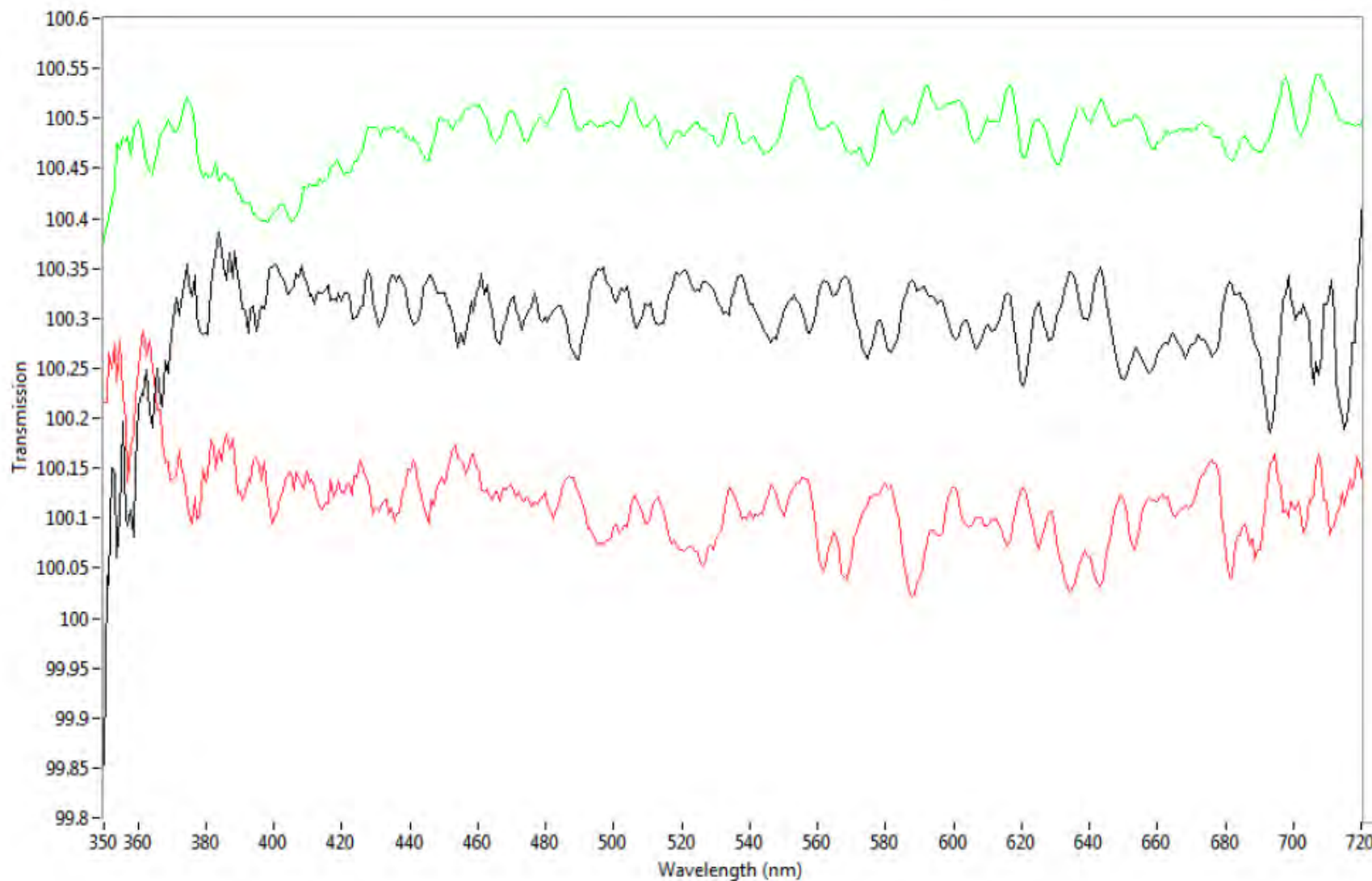


Figure 122. Spectra collected after five minutes of elapsed time with xenon illumination through a quartz slide (top), and tungsten halogen illumination through quartz (bottom) and glass (middle) slides.

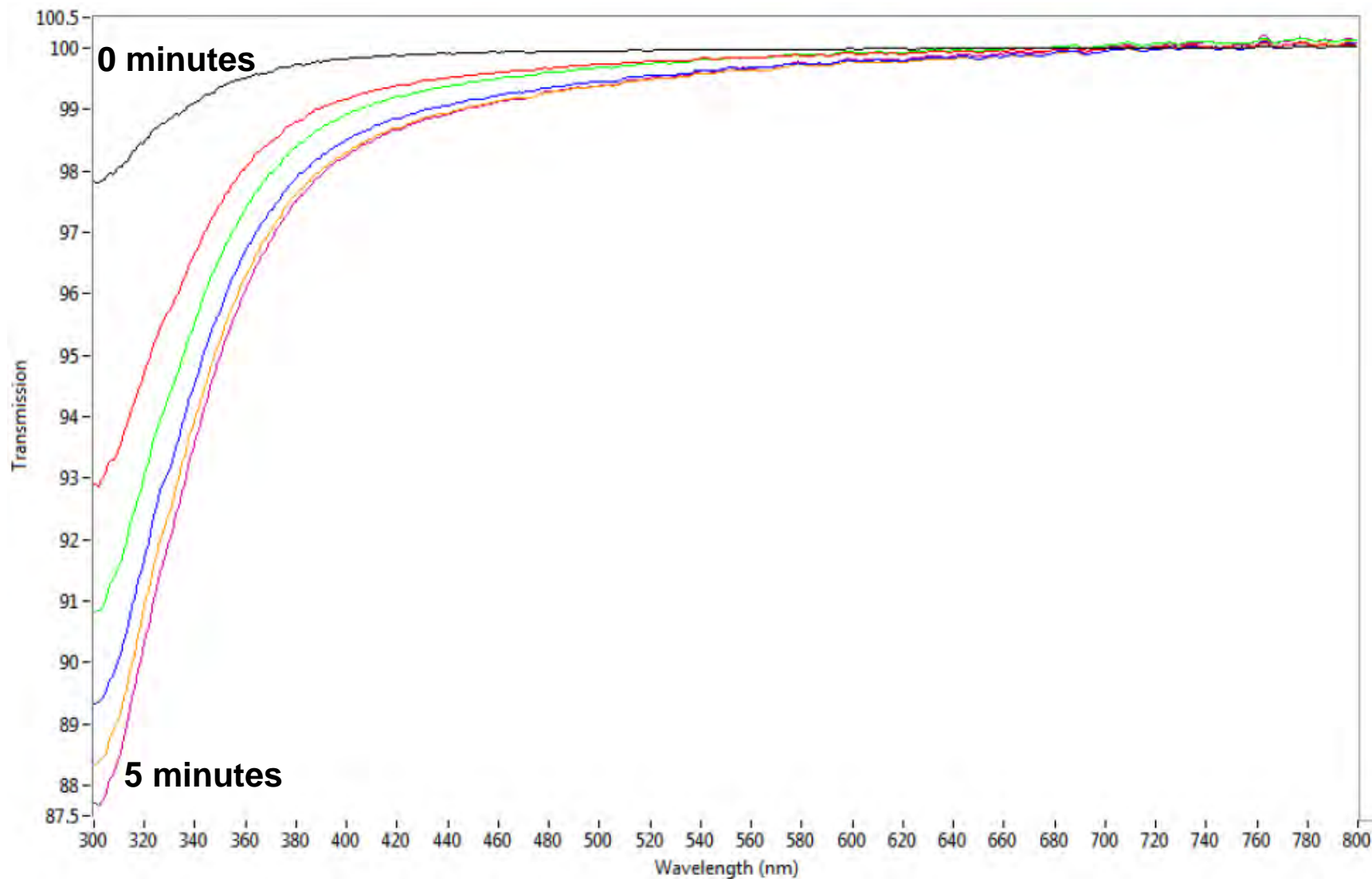


Figure 123. Spectra collected every minute for five minutes through a glass slide using xenon illumination.

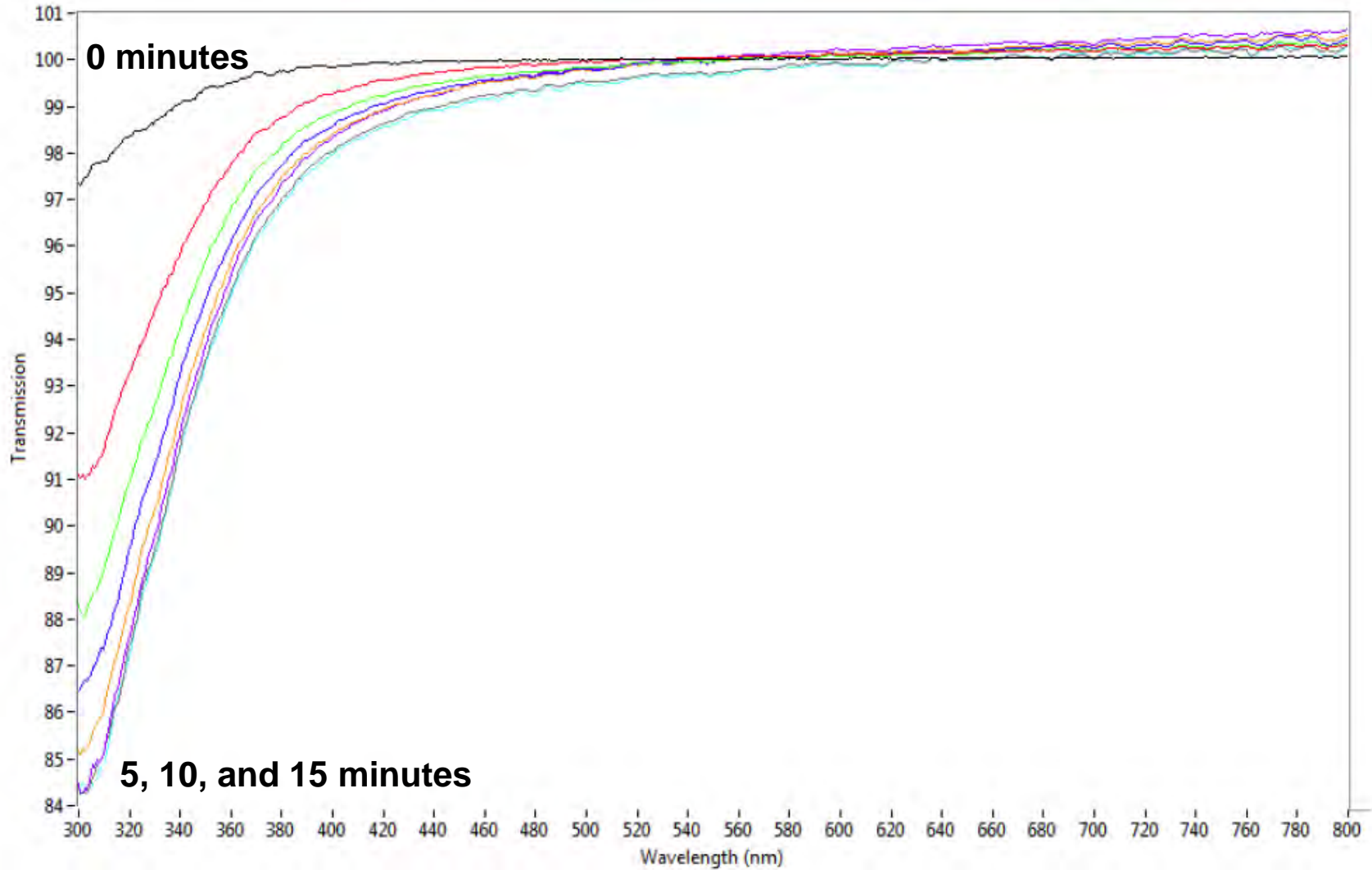


Figure 124. Spectra collected every minute for five minutes through a glass slide using xenon illumination (black, red, green, dark blue, orange, and purple) compared to spectra collected after five minutes (gray) and ten minutes (light blue) without illumination.

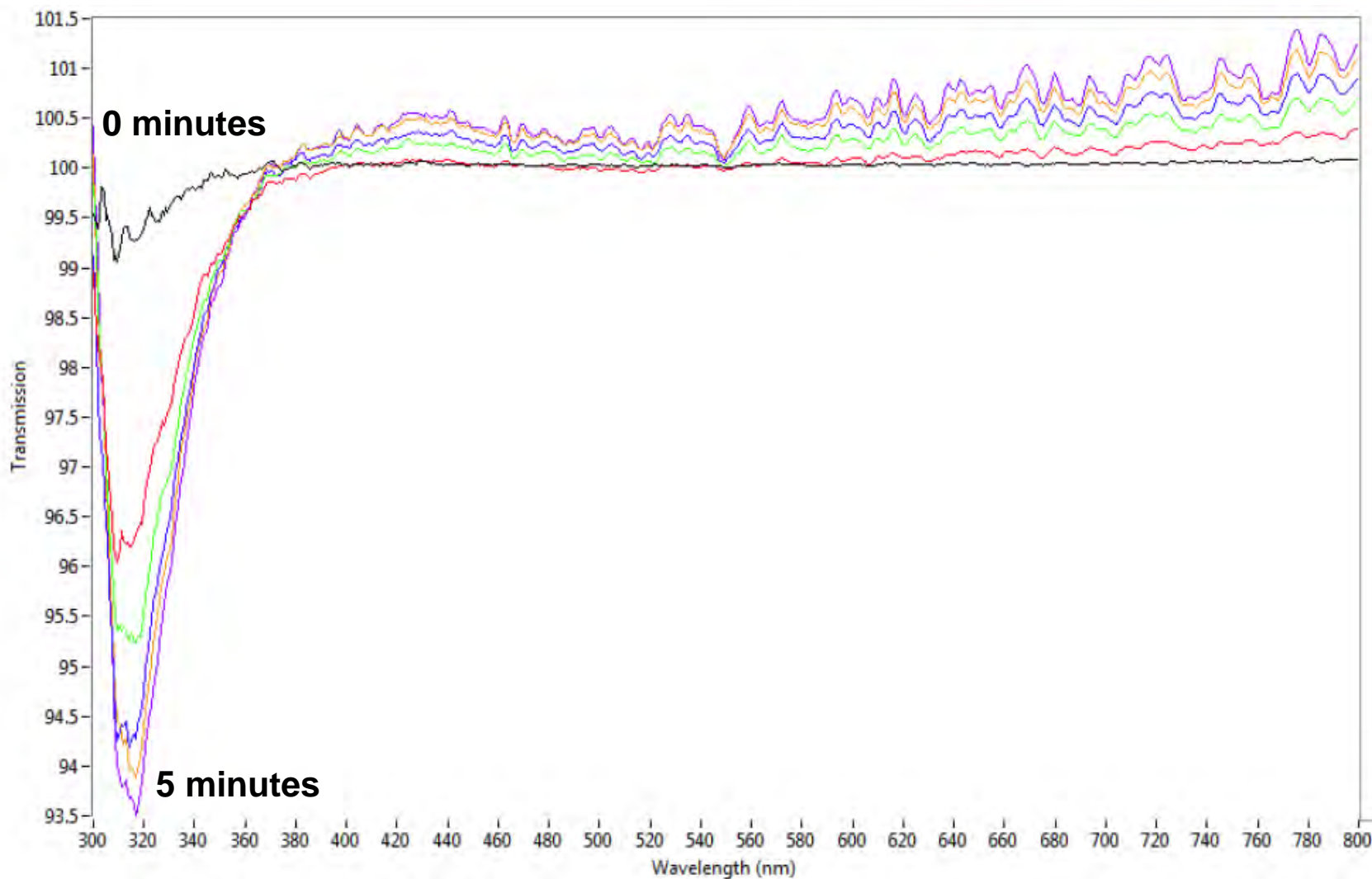


Figure 125. Spectra collected every minute for five minutes through a glass slide using xenon illumination (Karter brand).

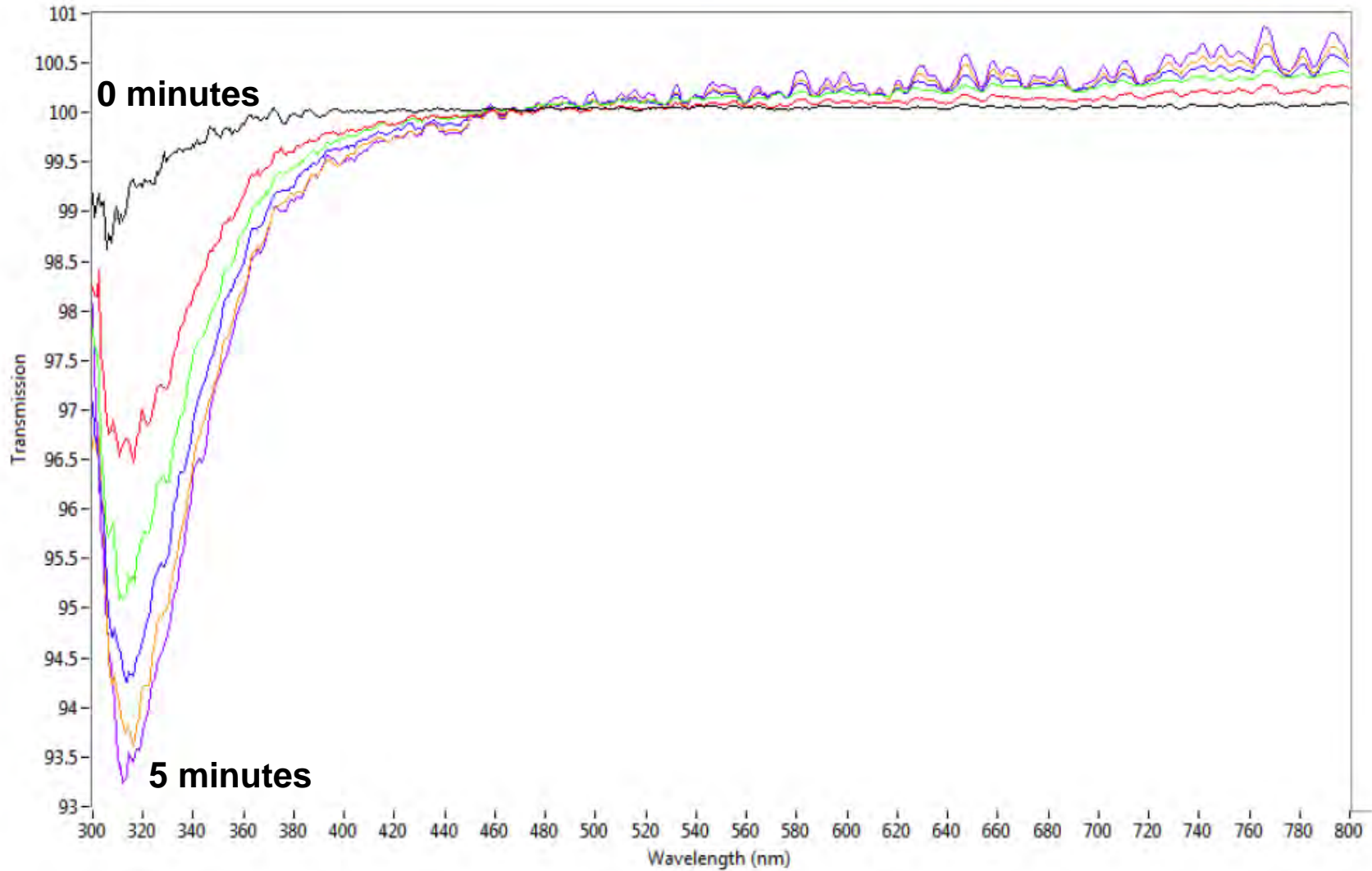


Figure 126. Spectra collected every minute for five minutes through a glass slide using xenon illumination (Fisher brand – thick slides).

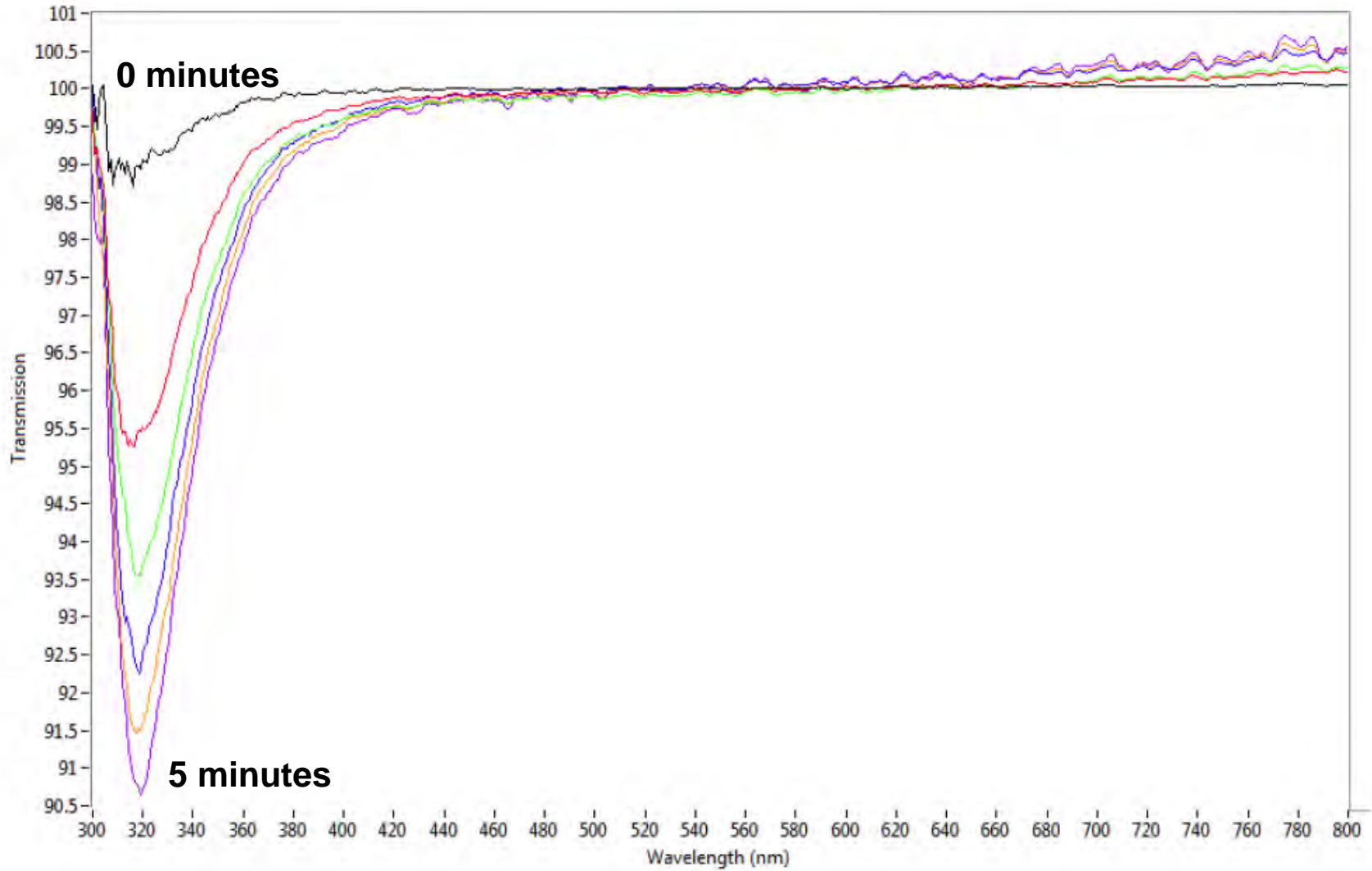


Figure 127. Spectra collected every minute for five minutes through a glass slide using xenon illumination (Fisher brand).

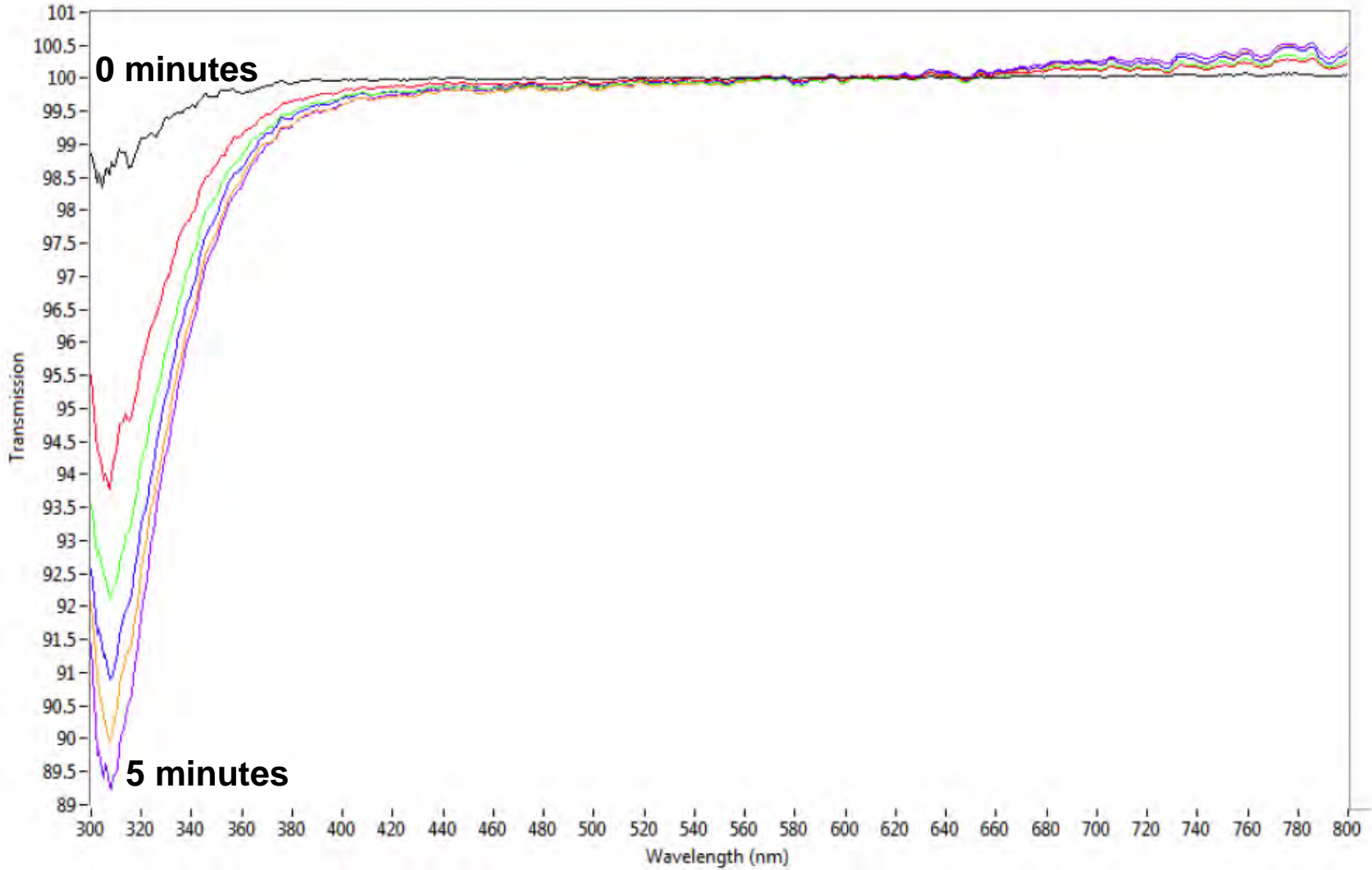


Figure 128. Spectra collected every minute for five minutes through a glass slide using xenon illumination (Goldstar brand).

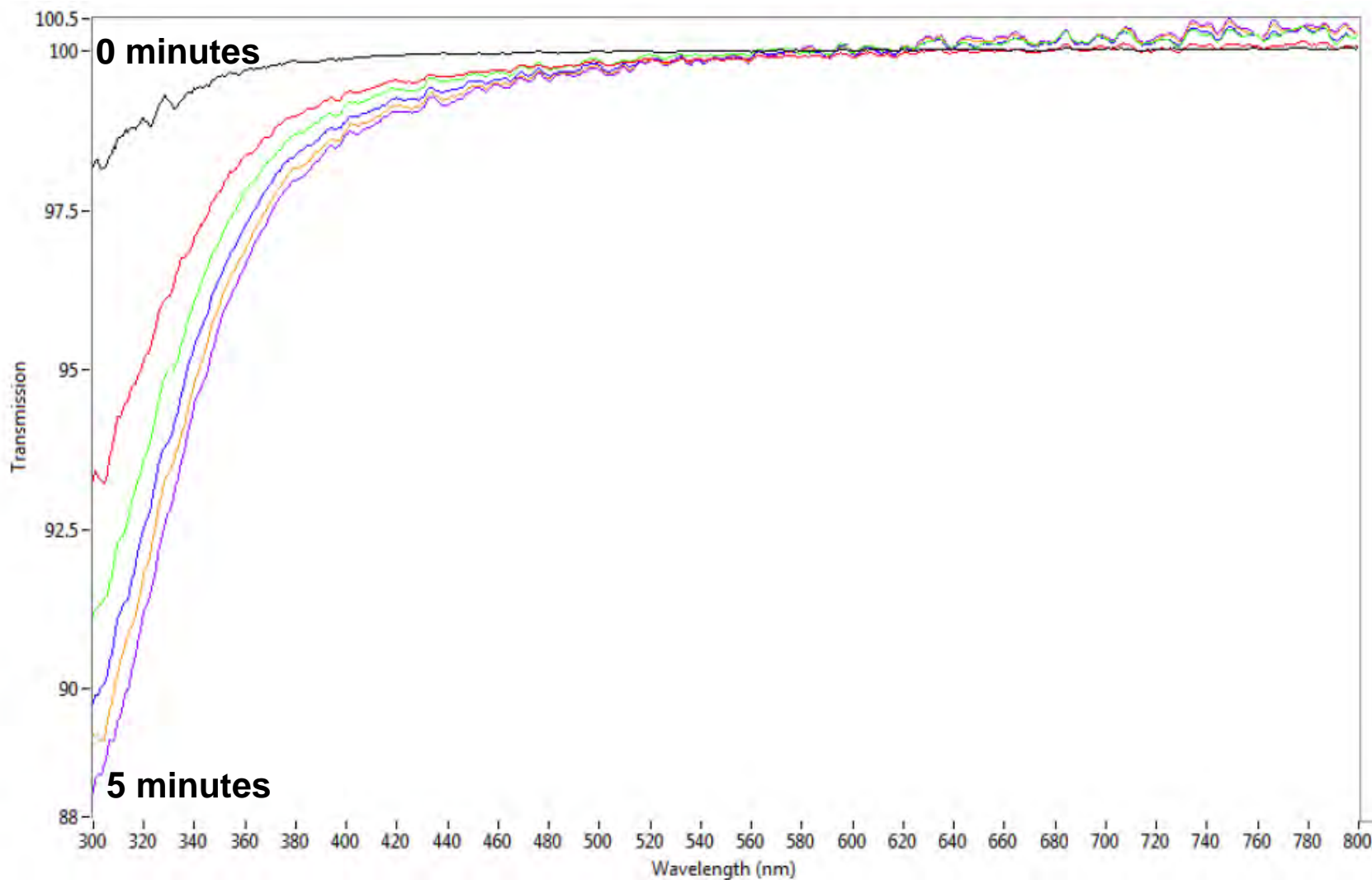


Figure 129. Spectra collected every minute for five minutes through a glass slide using xenon illumination (Corning brand – new slides).

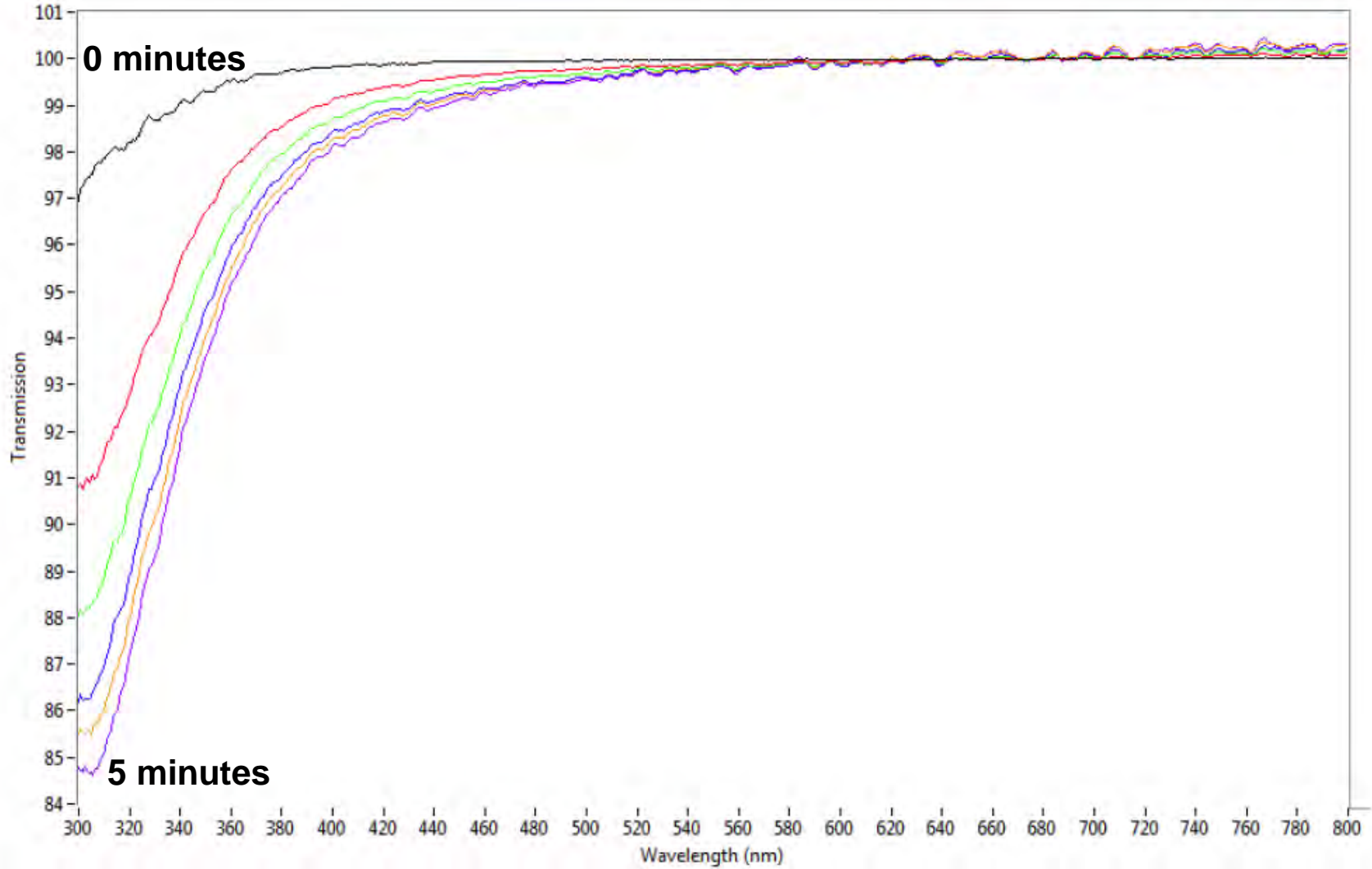


Figure 130. Spectra collected every minute for five minutes through a glass slide using xenon illumination (Corning brand – old slides).

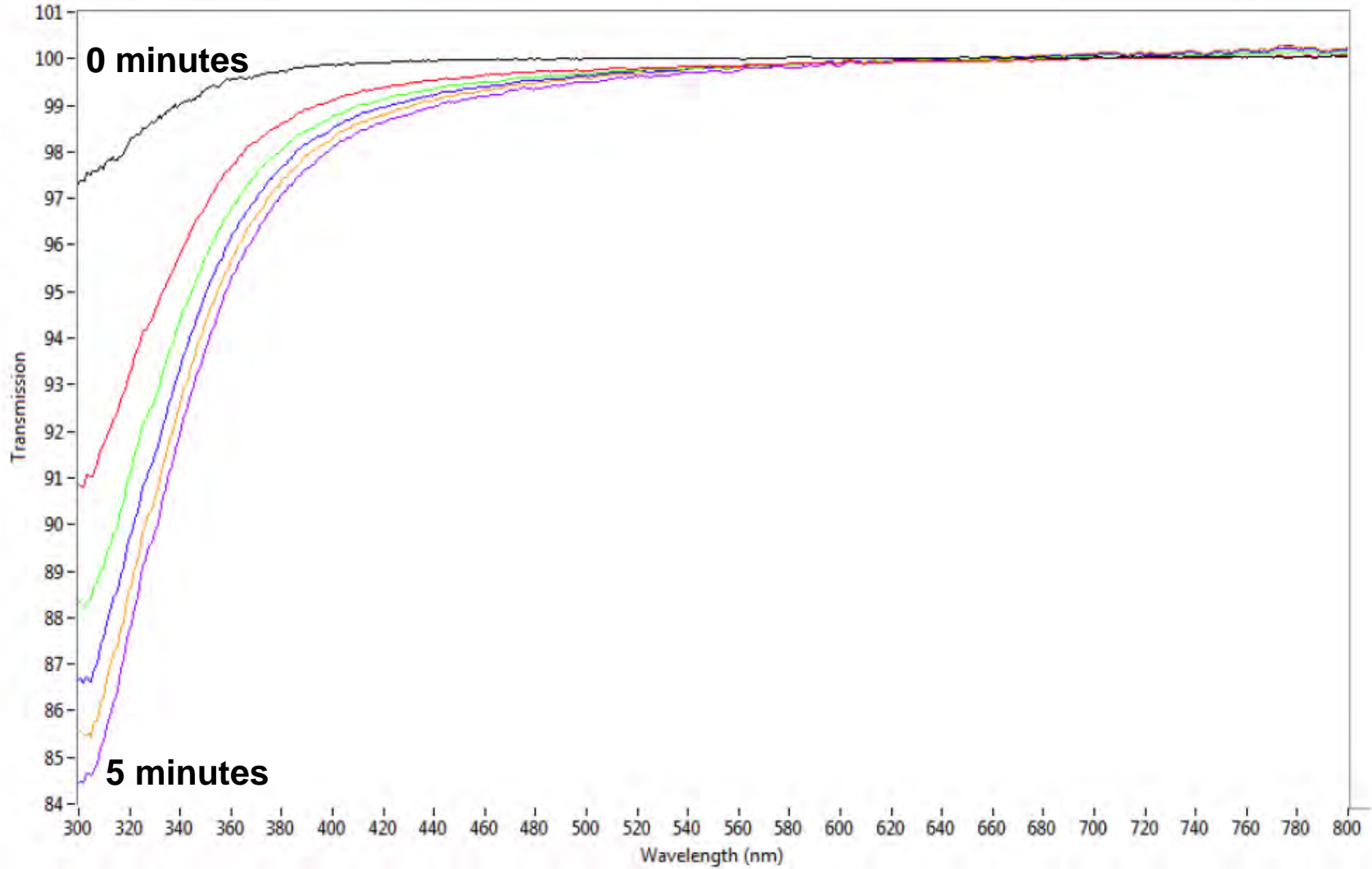


Figure 131. Spectra collected every minute for five minutes through a glass slide using xenon illumination (Esco brand).

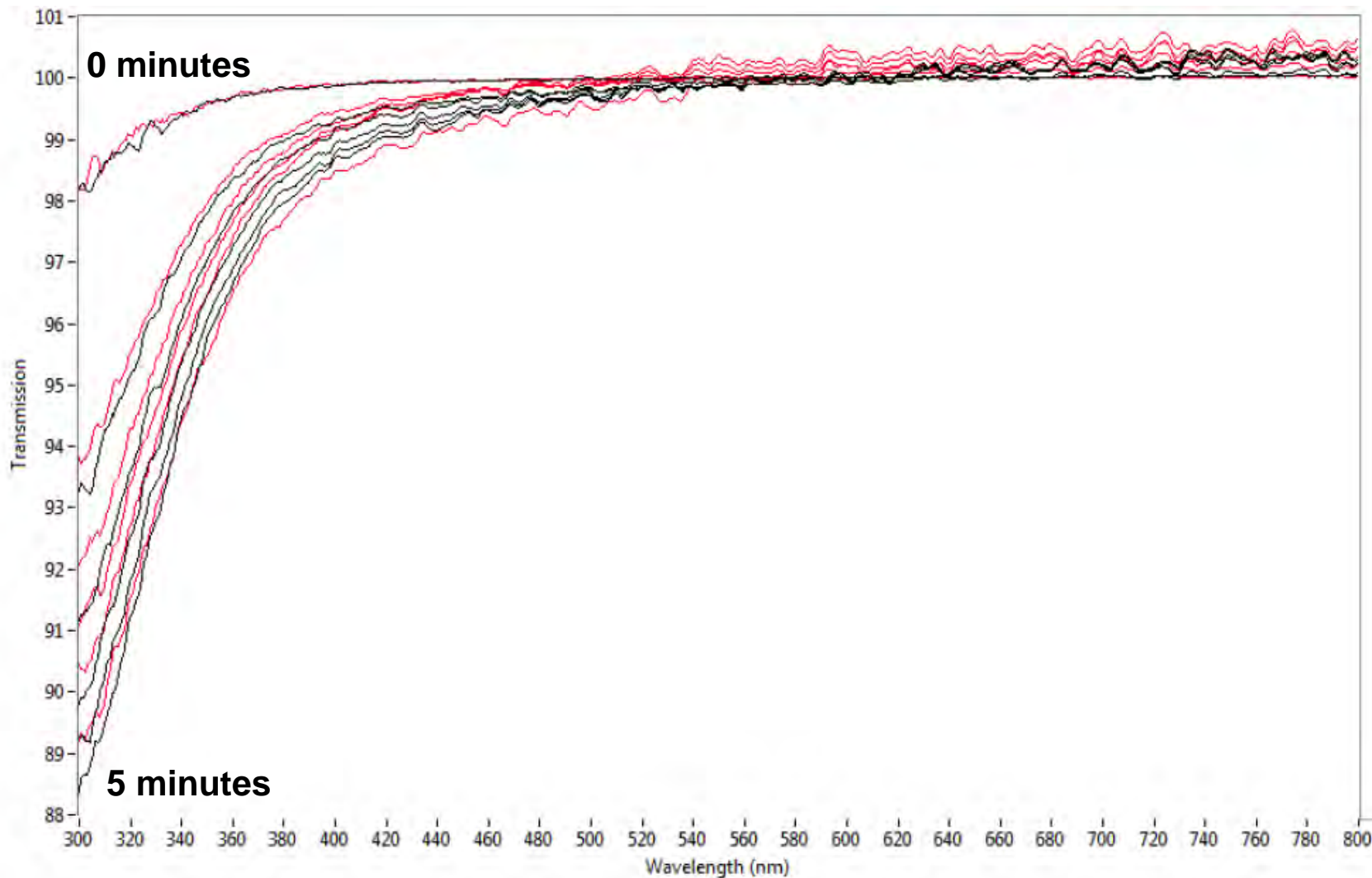


Figure 132. Spectra collected every minute for five minutes through both unwashed (black) and sulfuric acid-hydrogen peroxide washed (red) glass slides (Corning band – new slides) using xenon illumination.

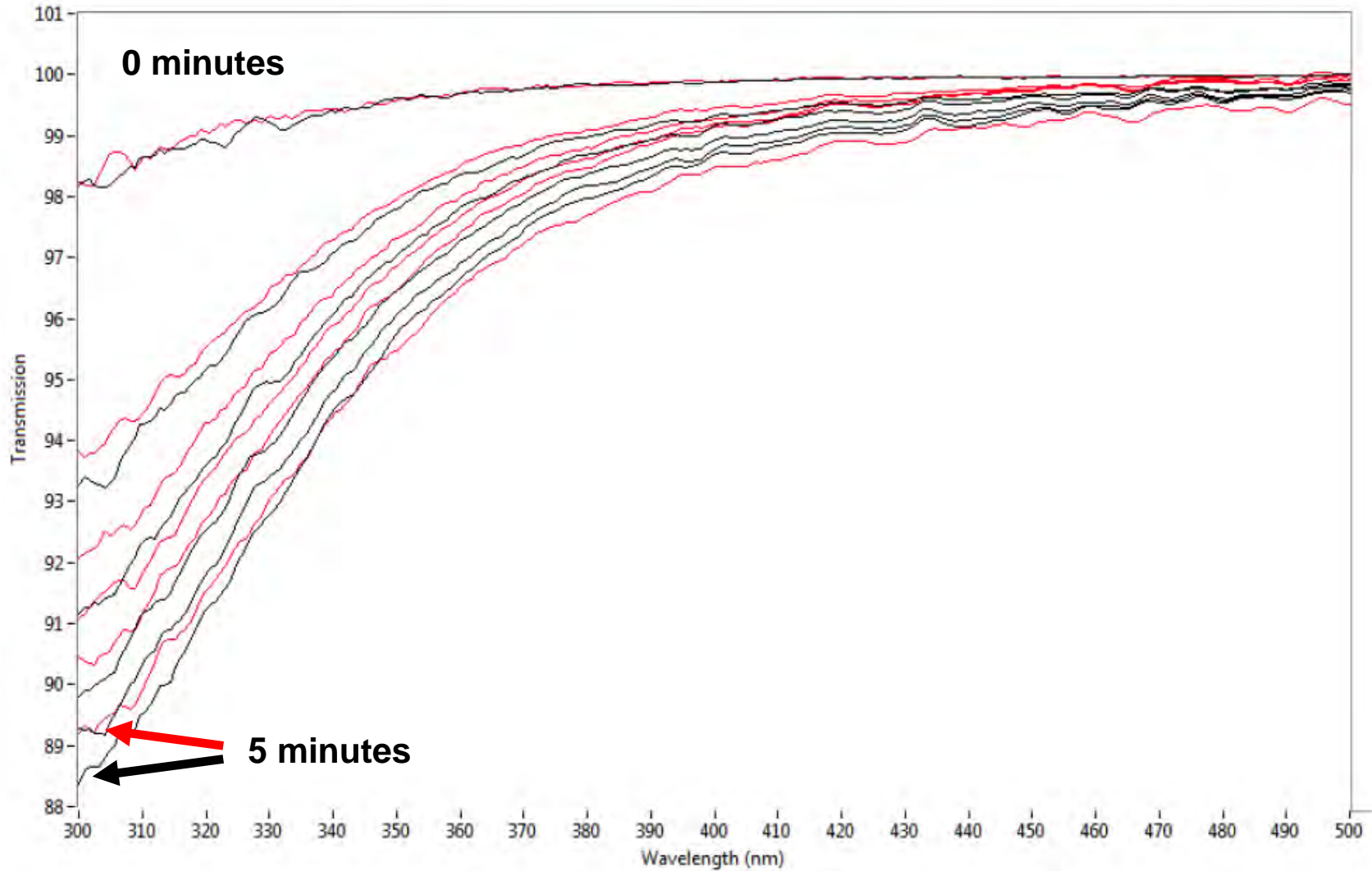


Figure 133. Close-up view of spectra collected every minute for five minutes through both unwashed (black) and sulfuric acid-hydrogen peroxide washed (red) glass slides (Corning band – new slides) using xenon illumination. It is clear the harsh cleaning has not significantly affected the change in absorption.

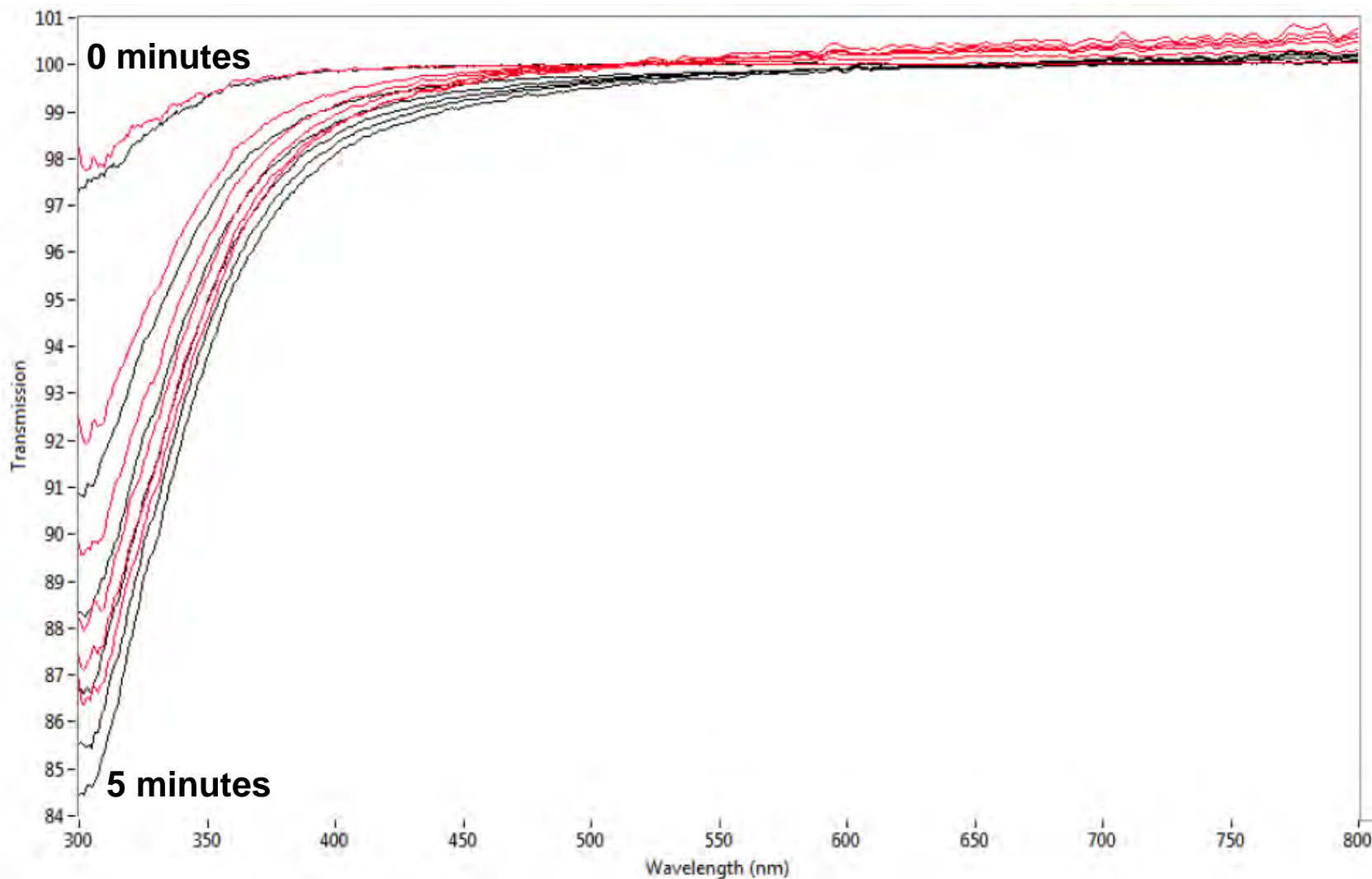


Figure 134. Spectra collected every minute for five minutes through both unashed (black) and plasma ashed (red) glass slides (Esco band) using xenon illumination.

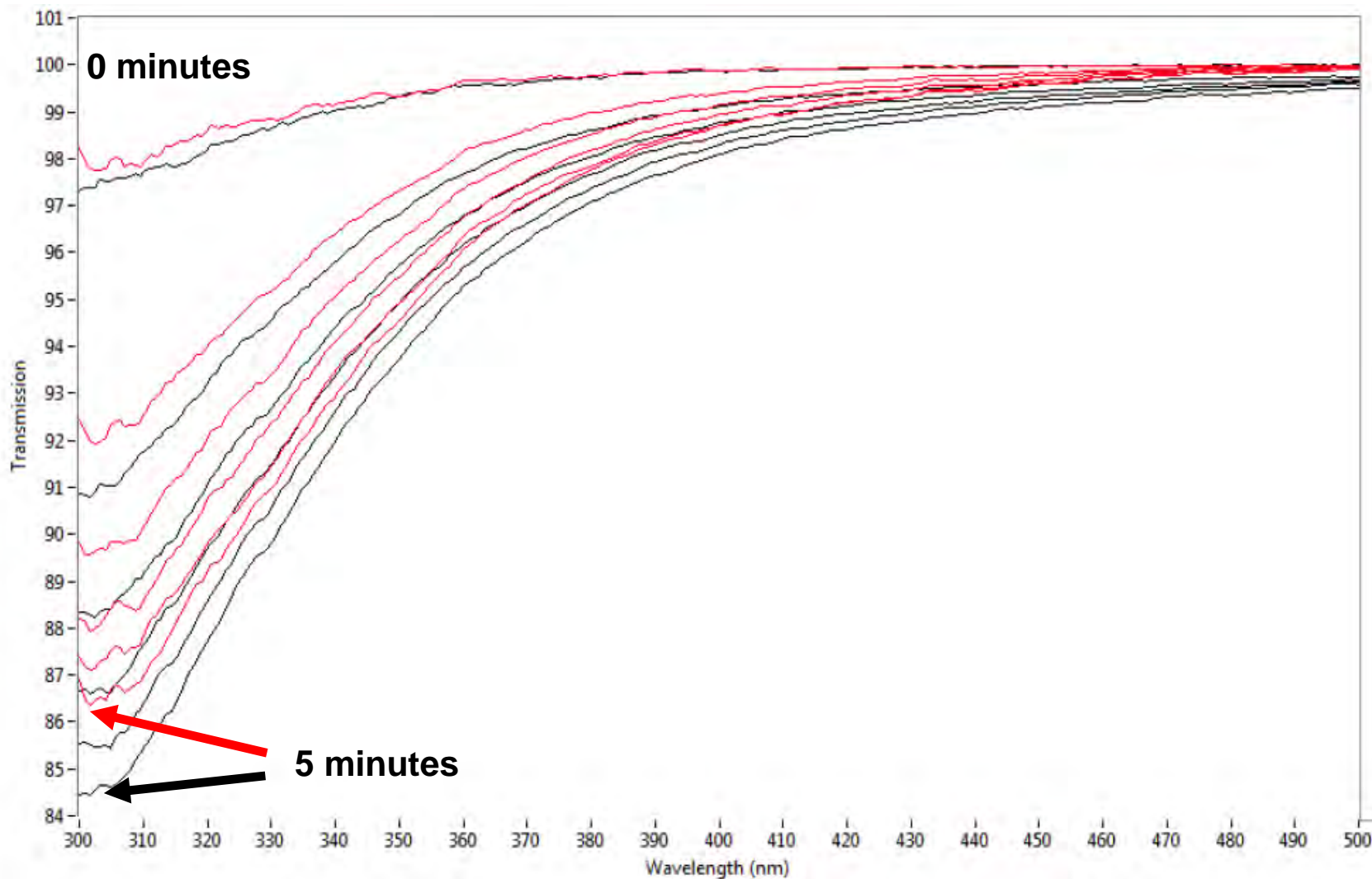


Figure 135. Close-up view of spectra collected every minute for five minutes through both unashed (black) and plasma ashed (red) glass slides (Esco band) using xenon illumination.

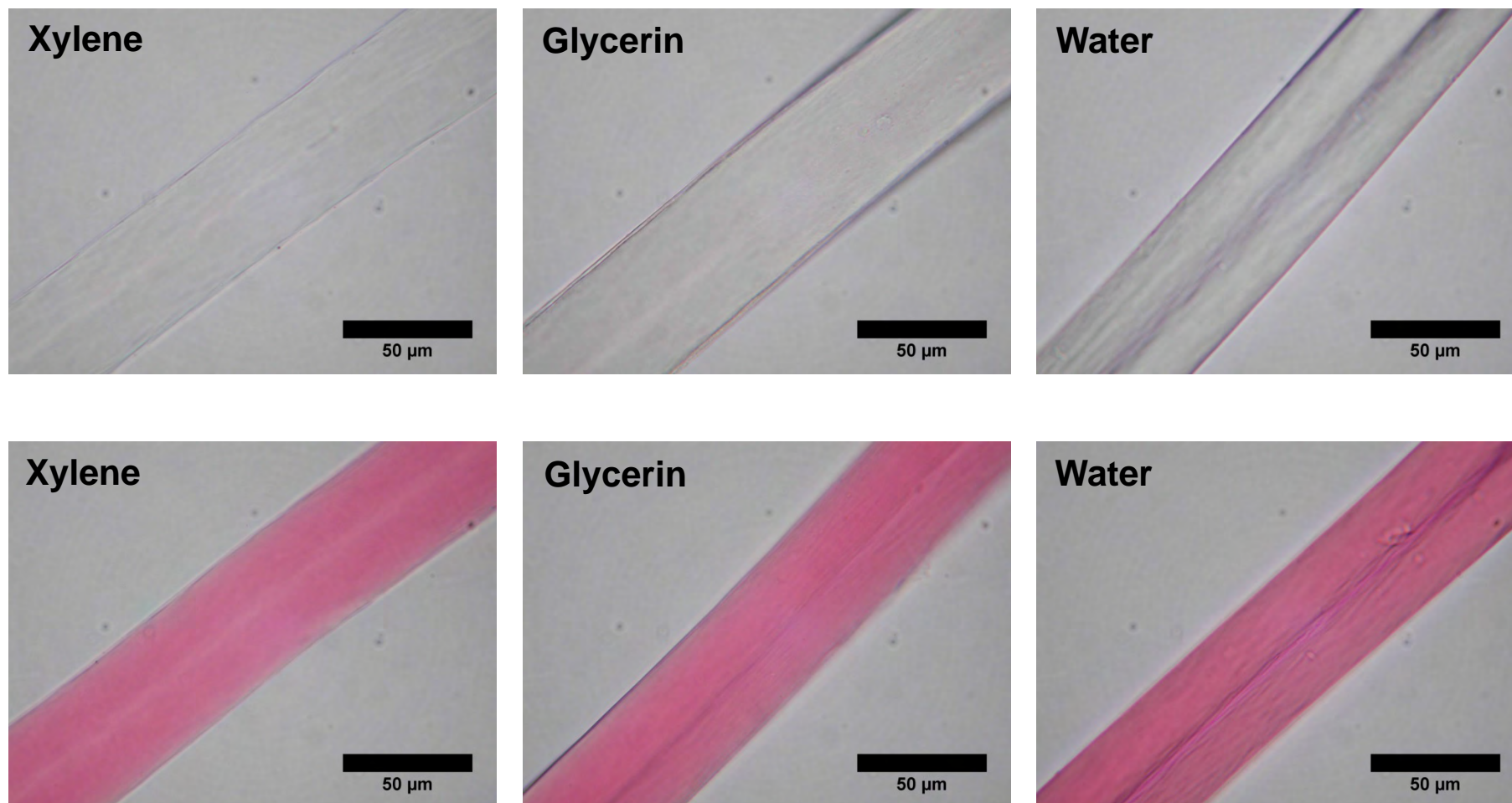


Figure 136. Light (top) and dark (bottom) red colored PAN fibers mounted in xylene, glycerin, and water (viewed using transmitted light).

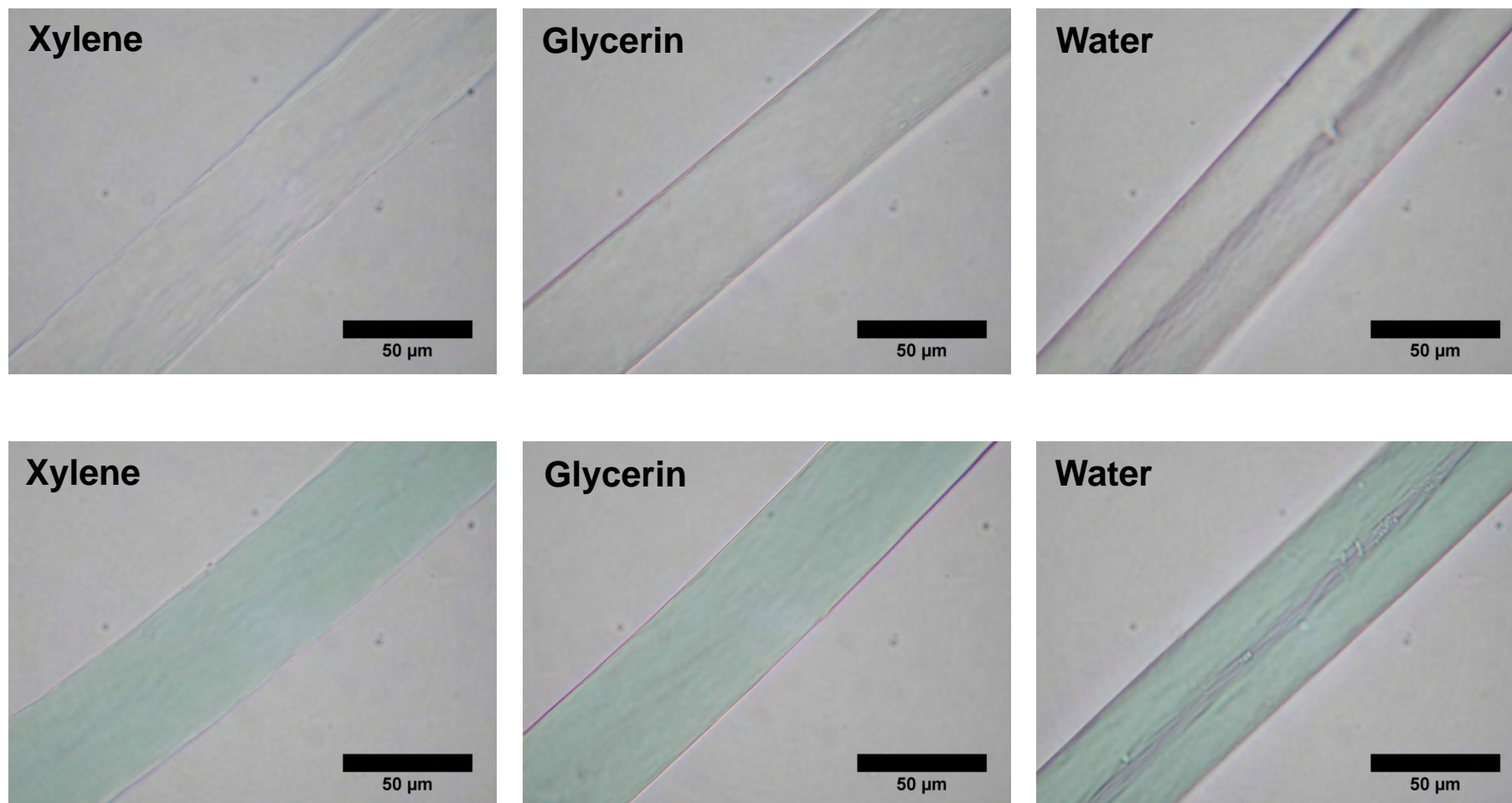


Figure 137. Light (top) and dark (bottom) green colored PAN fibers mounted in xylene, glycerin, and water (viewed using transmitted light).

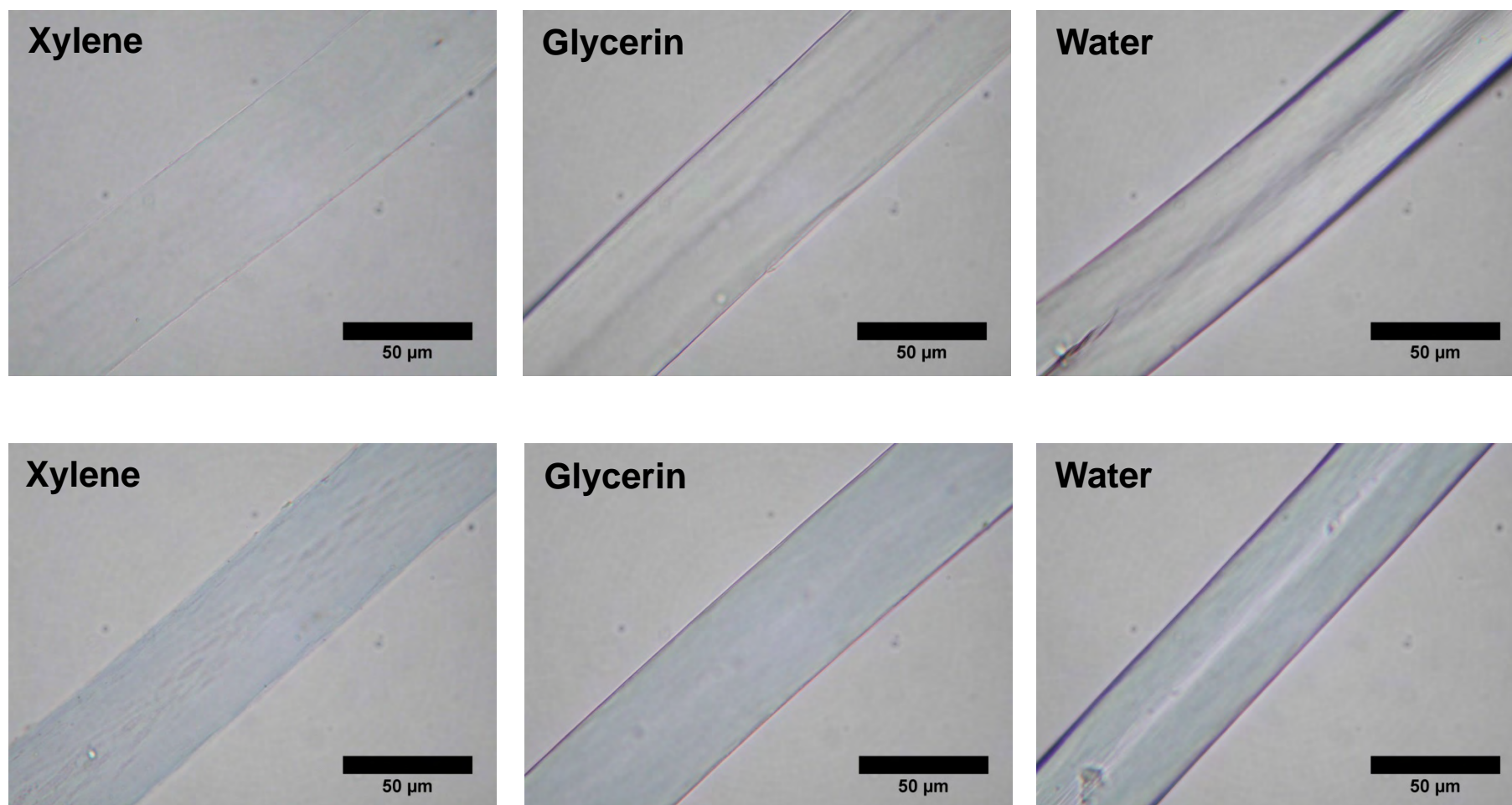


Figure 138. Light (top) and dark (bottom) blue colored PAN fibers mounted in xylene, glycerin, and water (viewed using transmitted light).

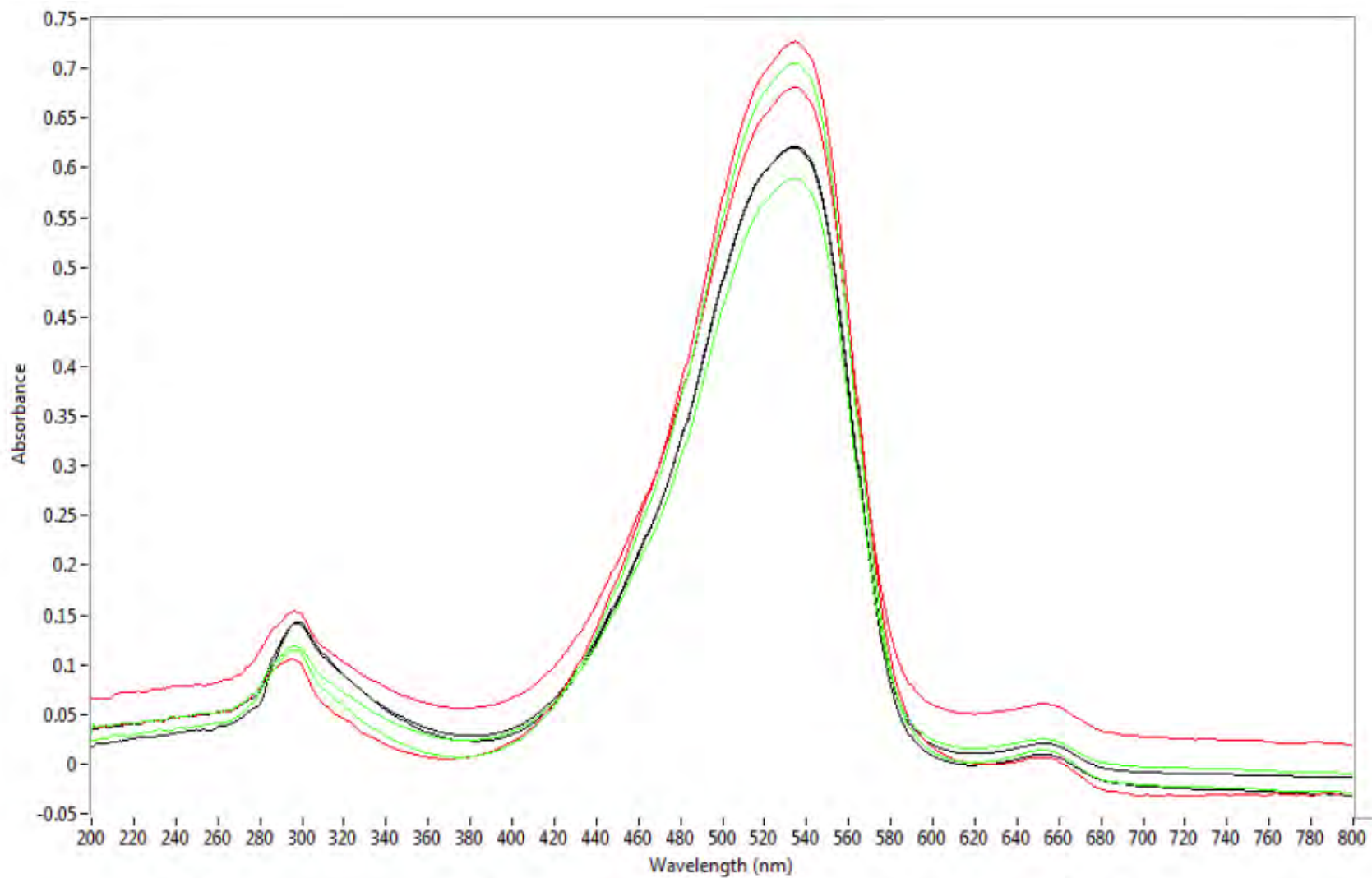


Figure 139. MSP collected through dark red acrylic fibers mounted in xylene (black), glycerin (green), and water (red).

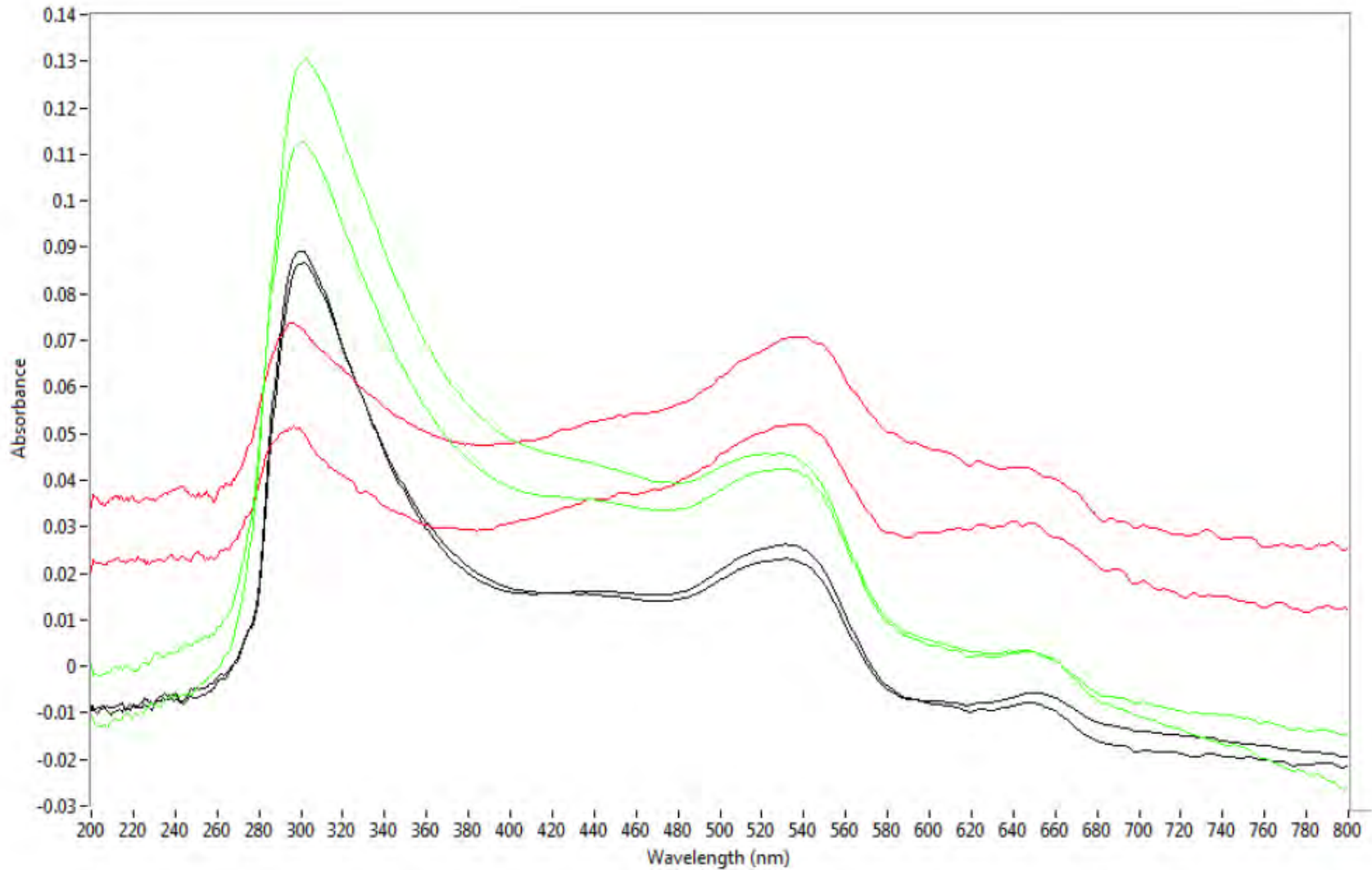


Figure 140. MSP collected through light red acrylic fibers mounted in xylene (black), glycerin (green), and water (red).

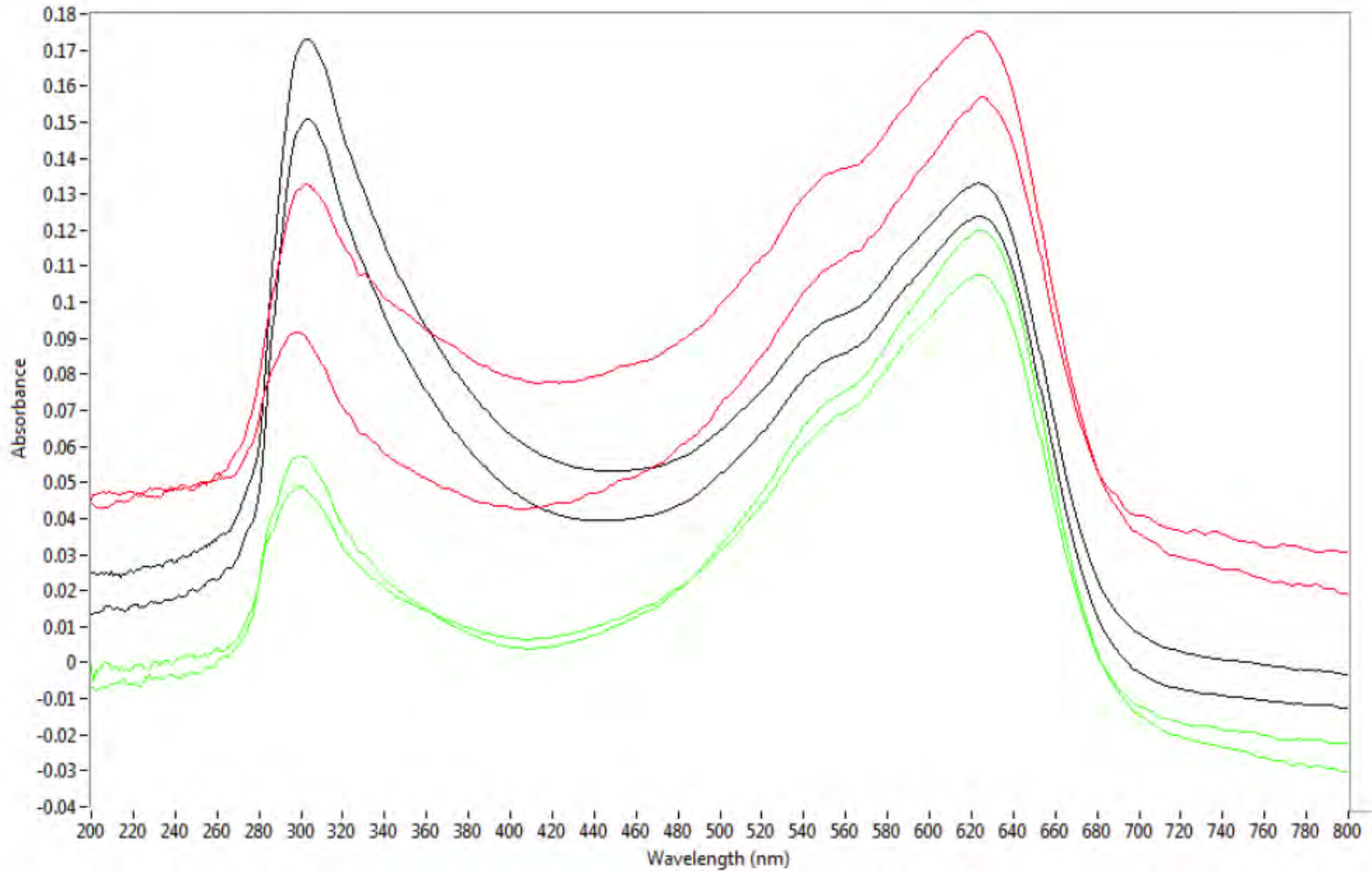


Figure 141. MSP collected through dark blue acrylic fibers mounted in xylene (black), glycerin (green), and water (red).

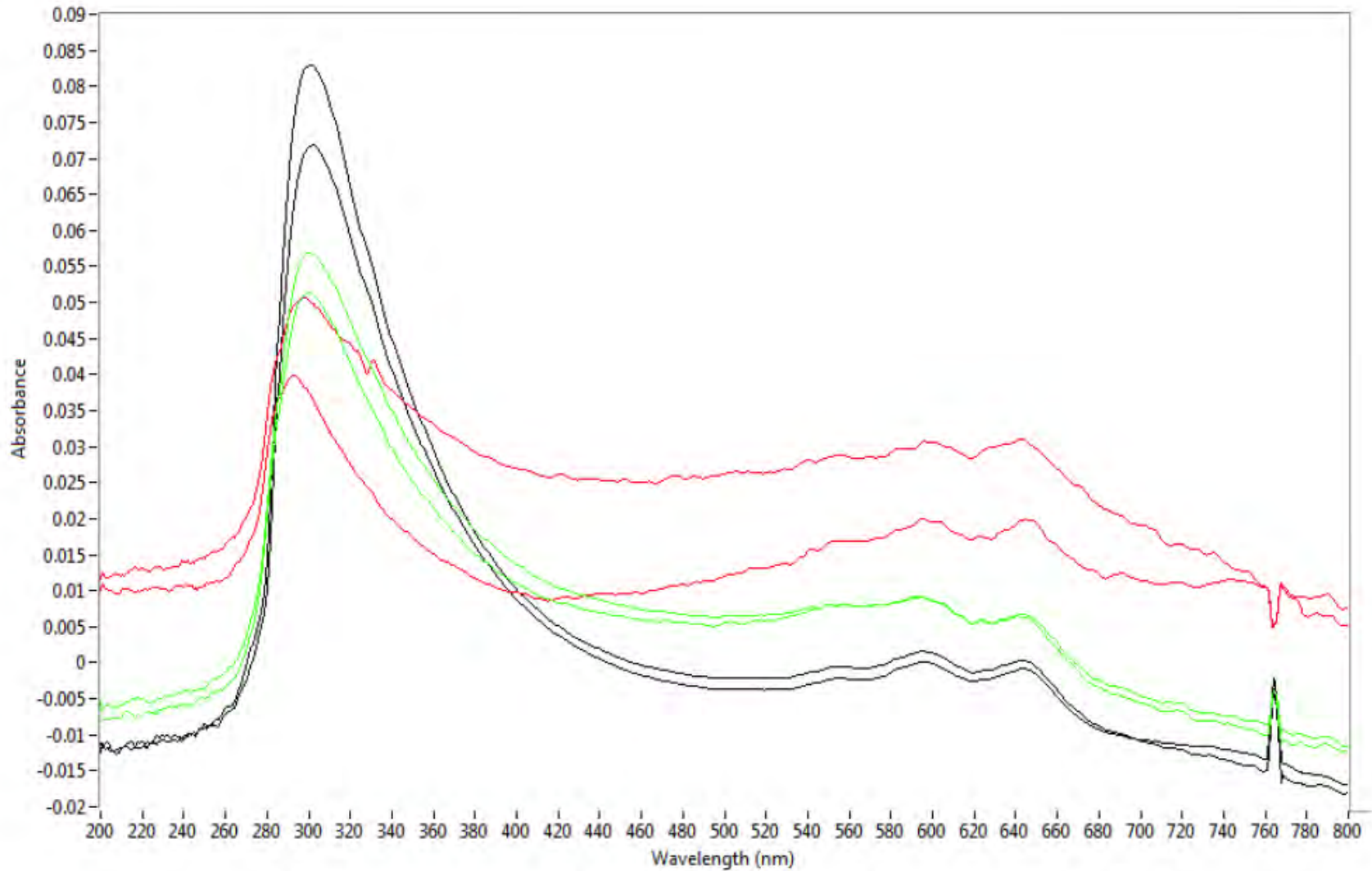


Figure 142. MSP collected through light blue acrylic fibers mounted in xylene (black), glycerin (green), and water (red).

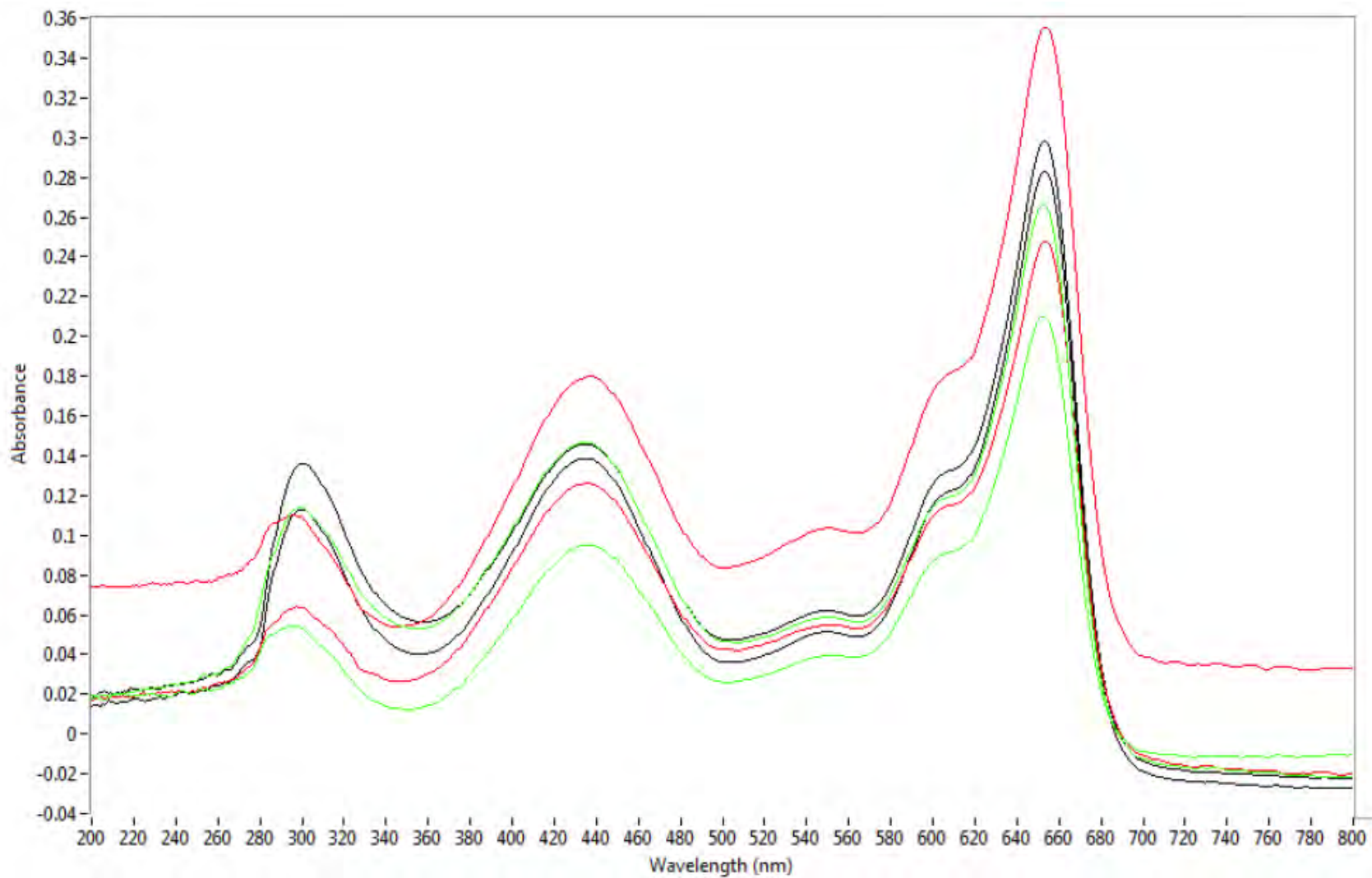


Figure 143. MSP collected through dark green acrylic fibers mounted in xylene (black), glycerin (green), and water (red).

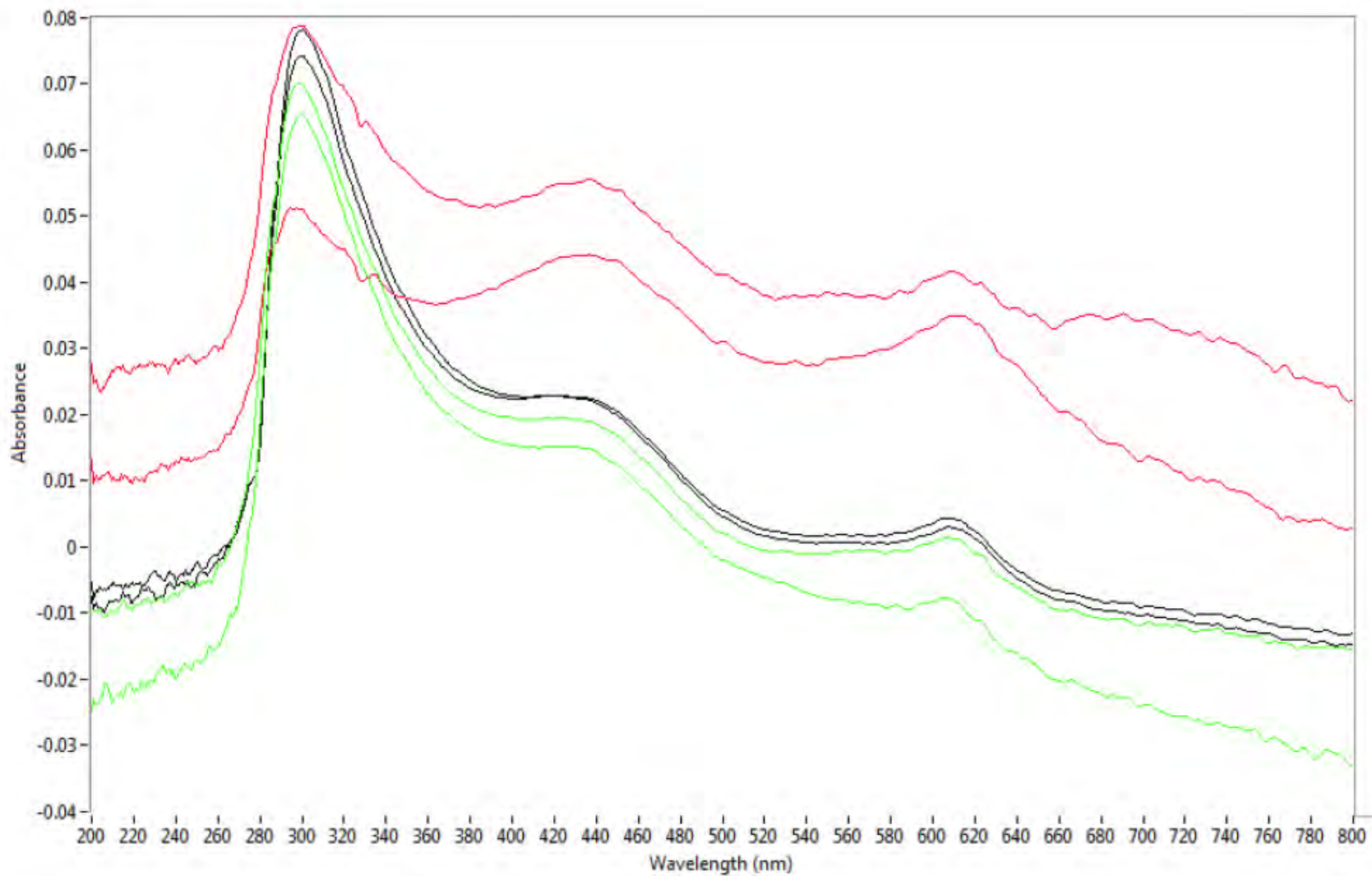


Figure 144. MSP collected through light green acrylic fibers mounted in xylene (black), glycerin (green), and water (red).

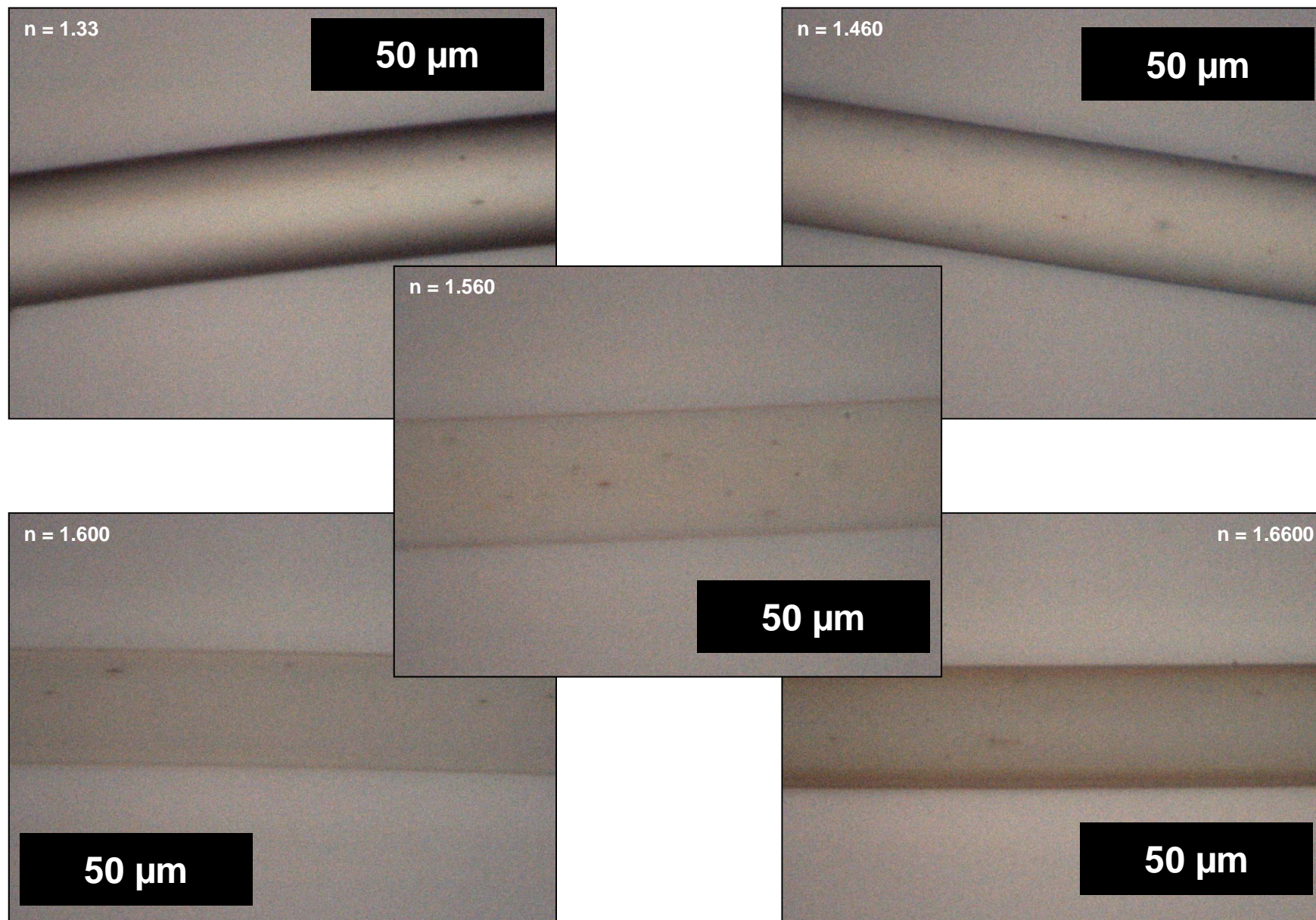


Figure 145. Nylon fiber mounted in five media with different refractive indices.

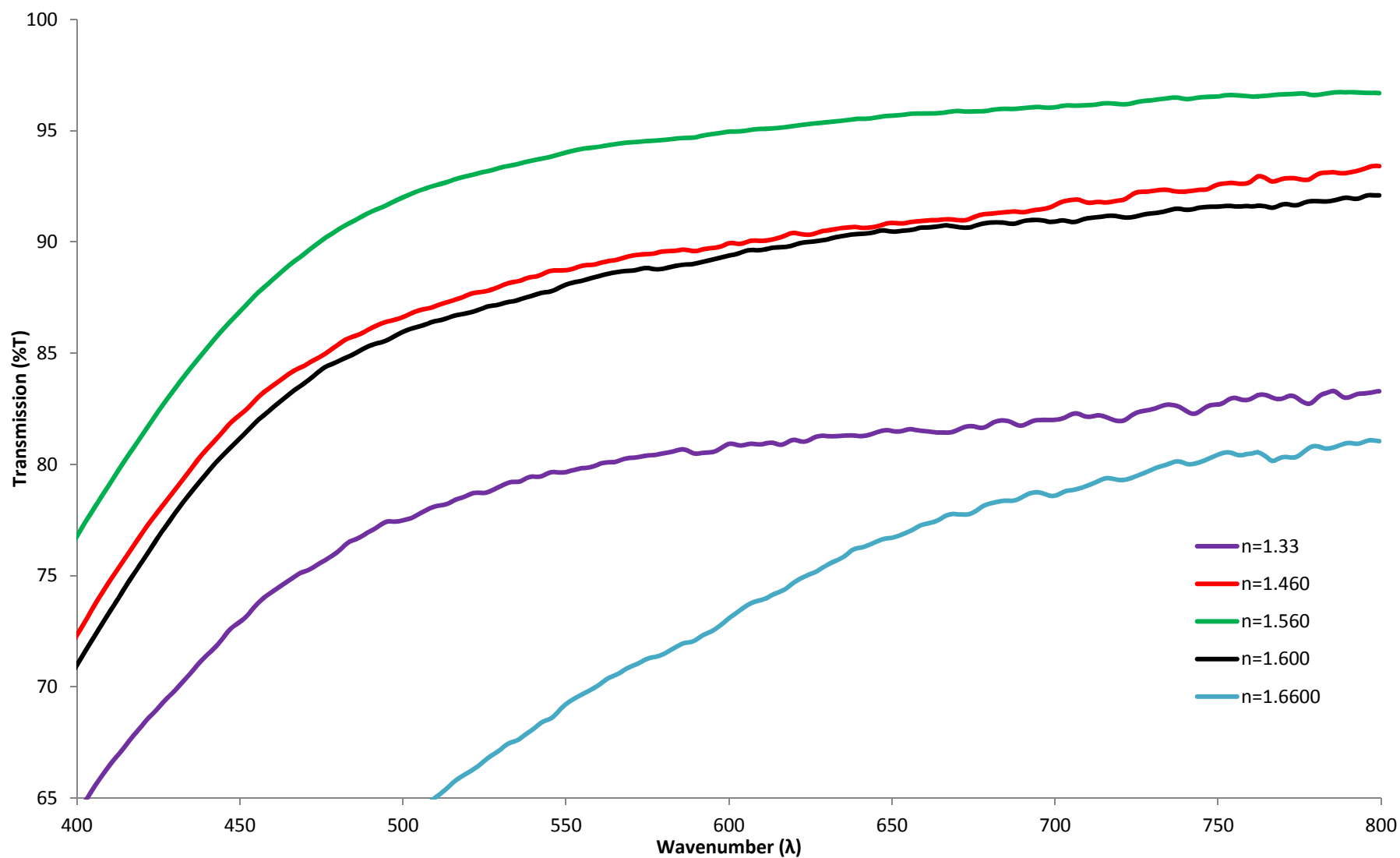


Figure 146. Spectral overlay of averaged data for N-0081 at each analyzed refractive index.

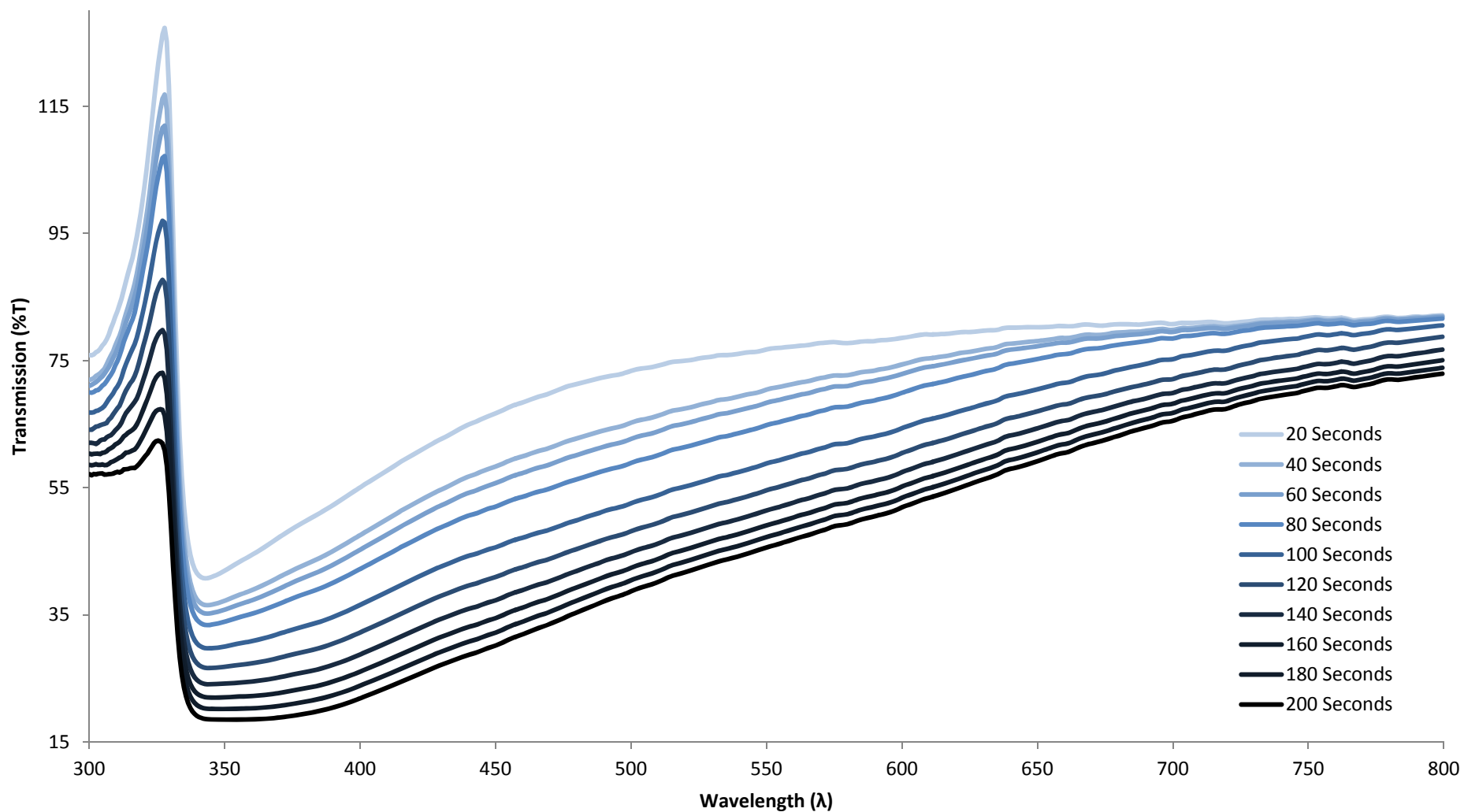


Figure 147. Spectra collected every twenty seconds from the same area of a nylon fiber mounted in 1.660 index of refraction oil over the course of three minutes of continual illumination with a xenon bulb.

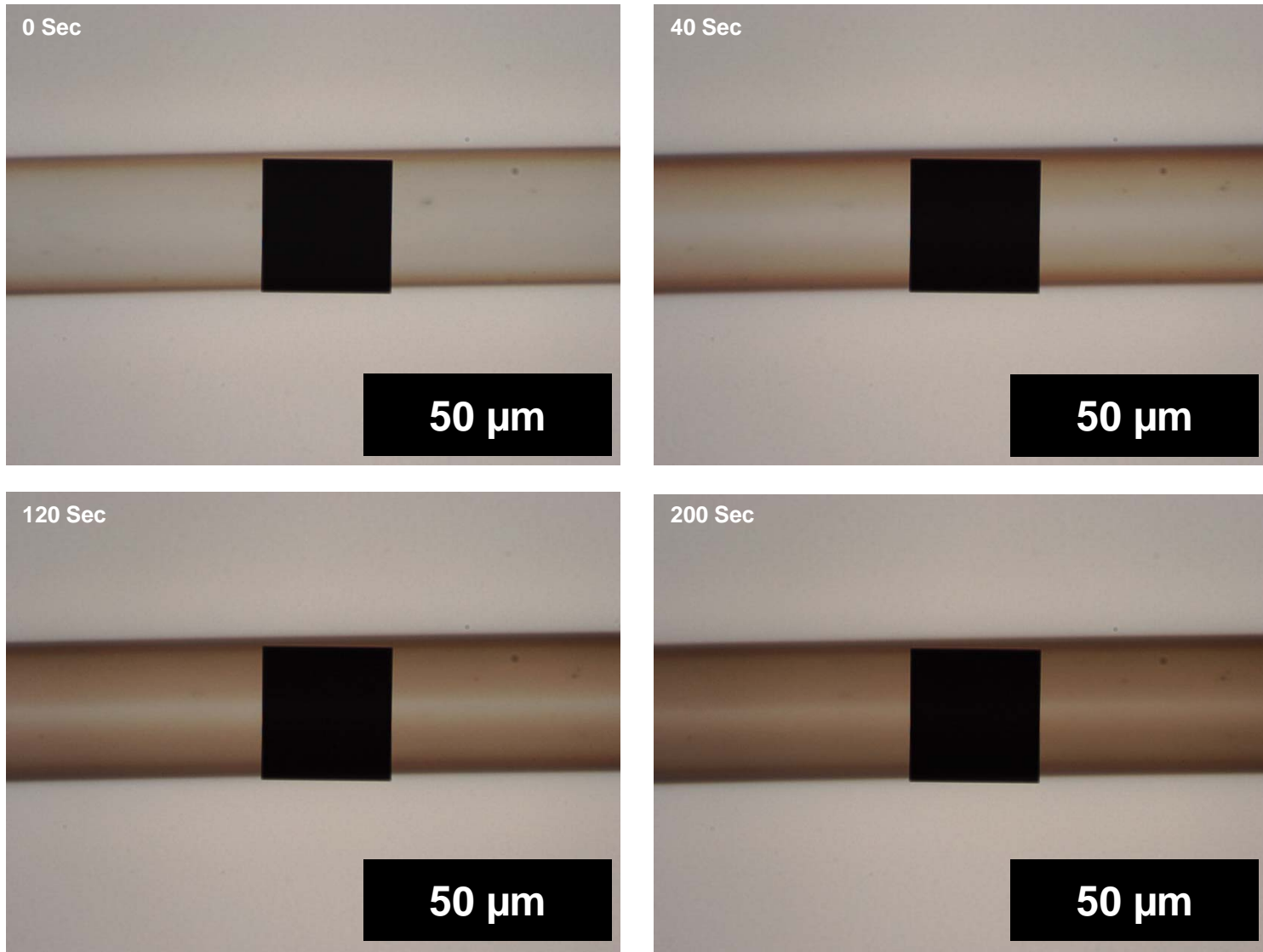


Figure 148. Photomicrographs of a nylon fiber mounted in 1.660 index of refraction oil collected over the course of approximately three minutes of continual illumination from a xenon bulb.

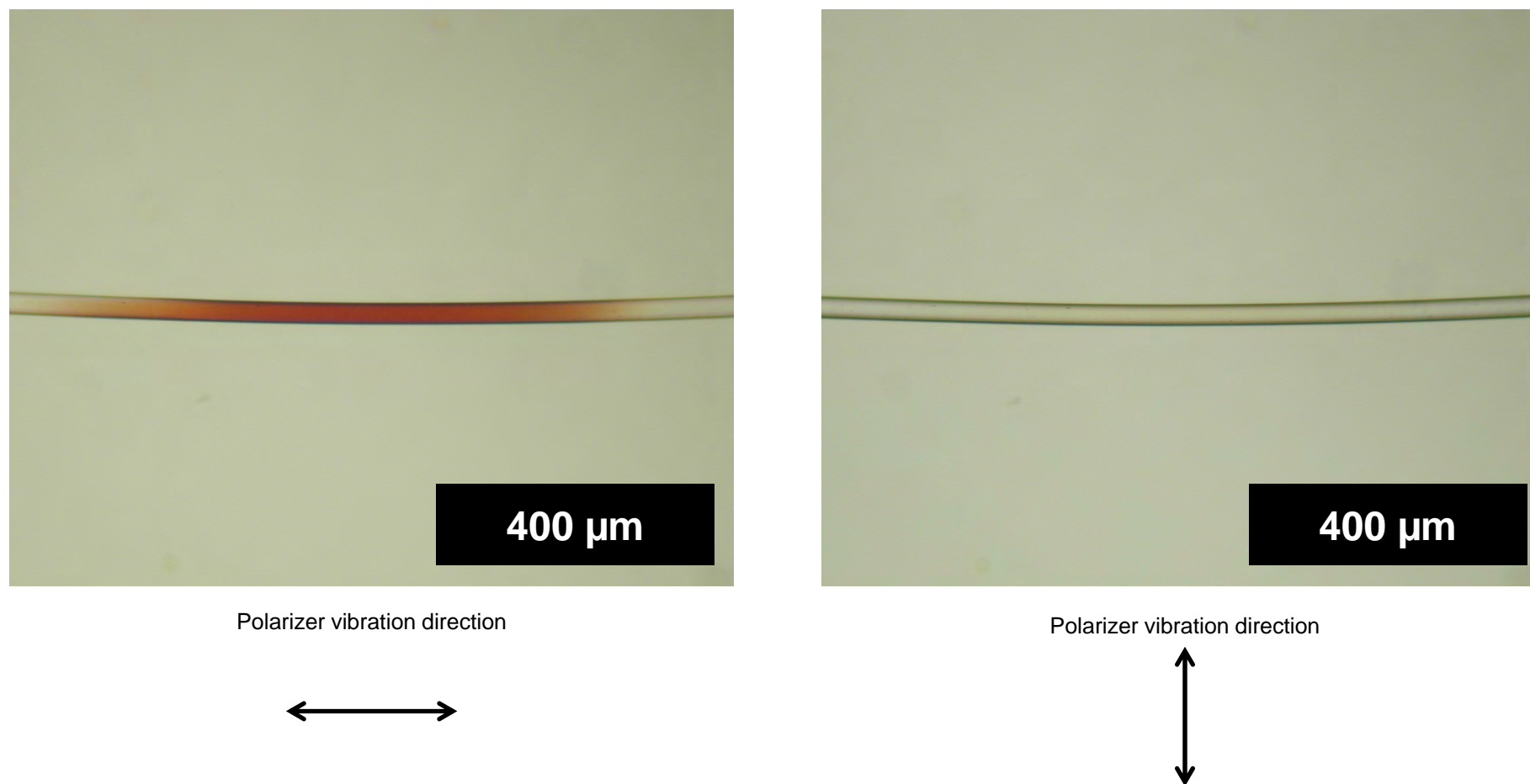


Figure 149. The nylon fiber mounted in 1.660 index of refraction oil exposed to approximately three minutes of continual illumination from a xenon bulb (viewed using plane polarized light with the polarizer orientated east-west (left) and north-south (right)).

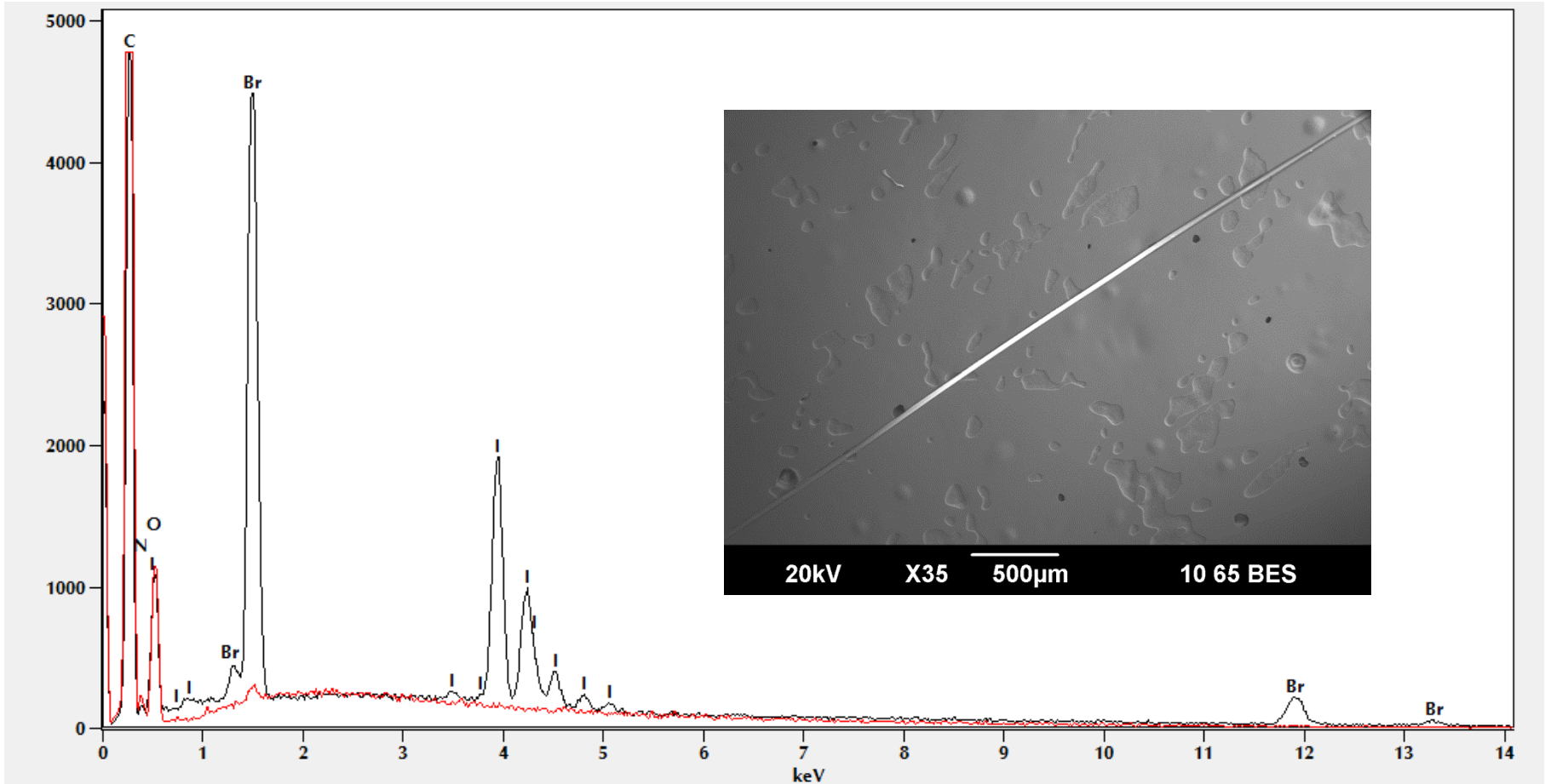


Figure 150. EDS spectra collected from the discolored (black) and control (red) areas of the fiber. The discolored area appears brighter in the inset SEM image because the adsorbed/absorbed iodine and bromine have increased the average atomic number of the fiber in that area.

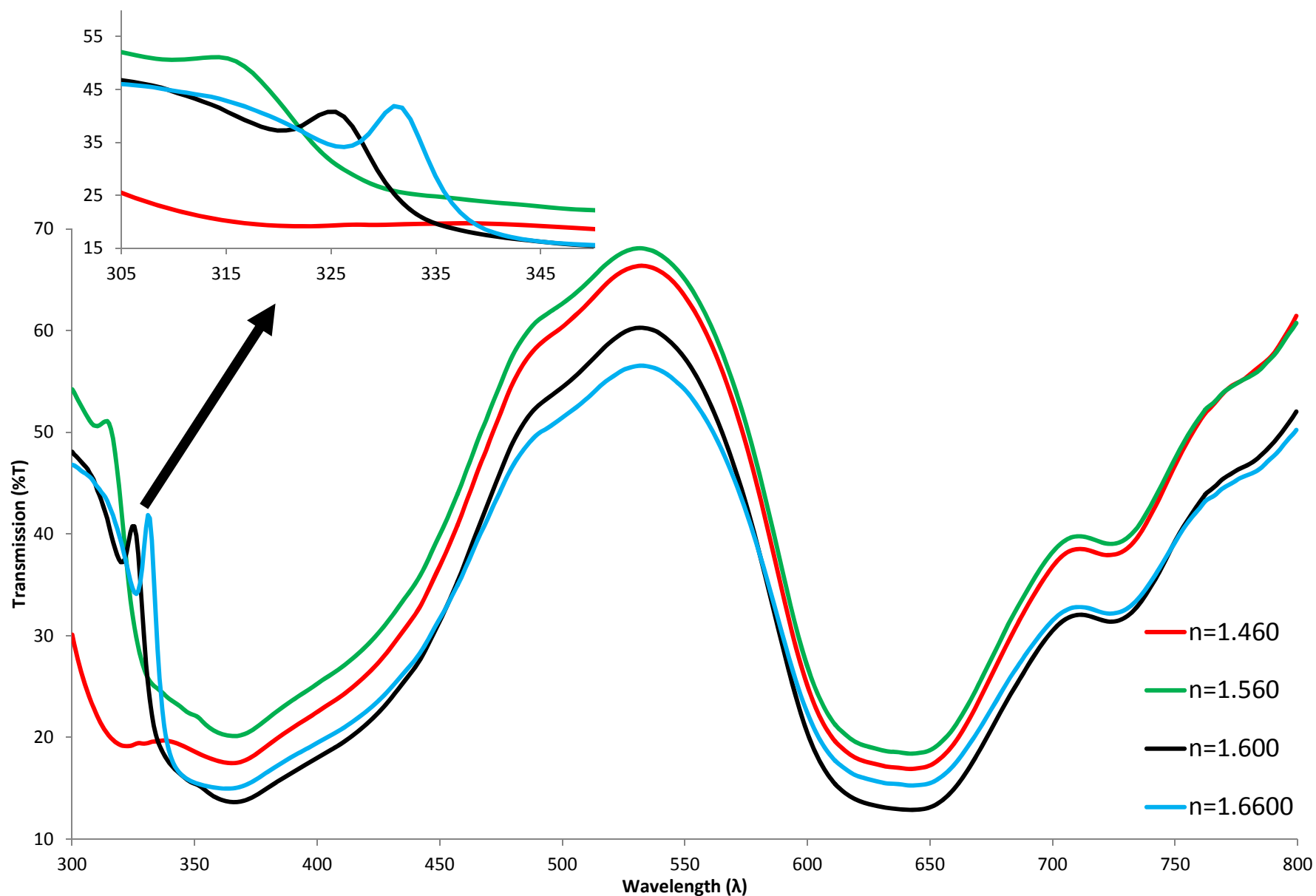


Figure 151. MSP spectra collected from a polyolefin fiber mounted in a variety of refractive index oils. An inset details the spectral artifacts observed at low wavelengths.

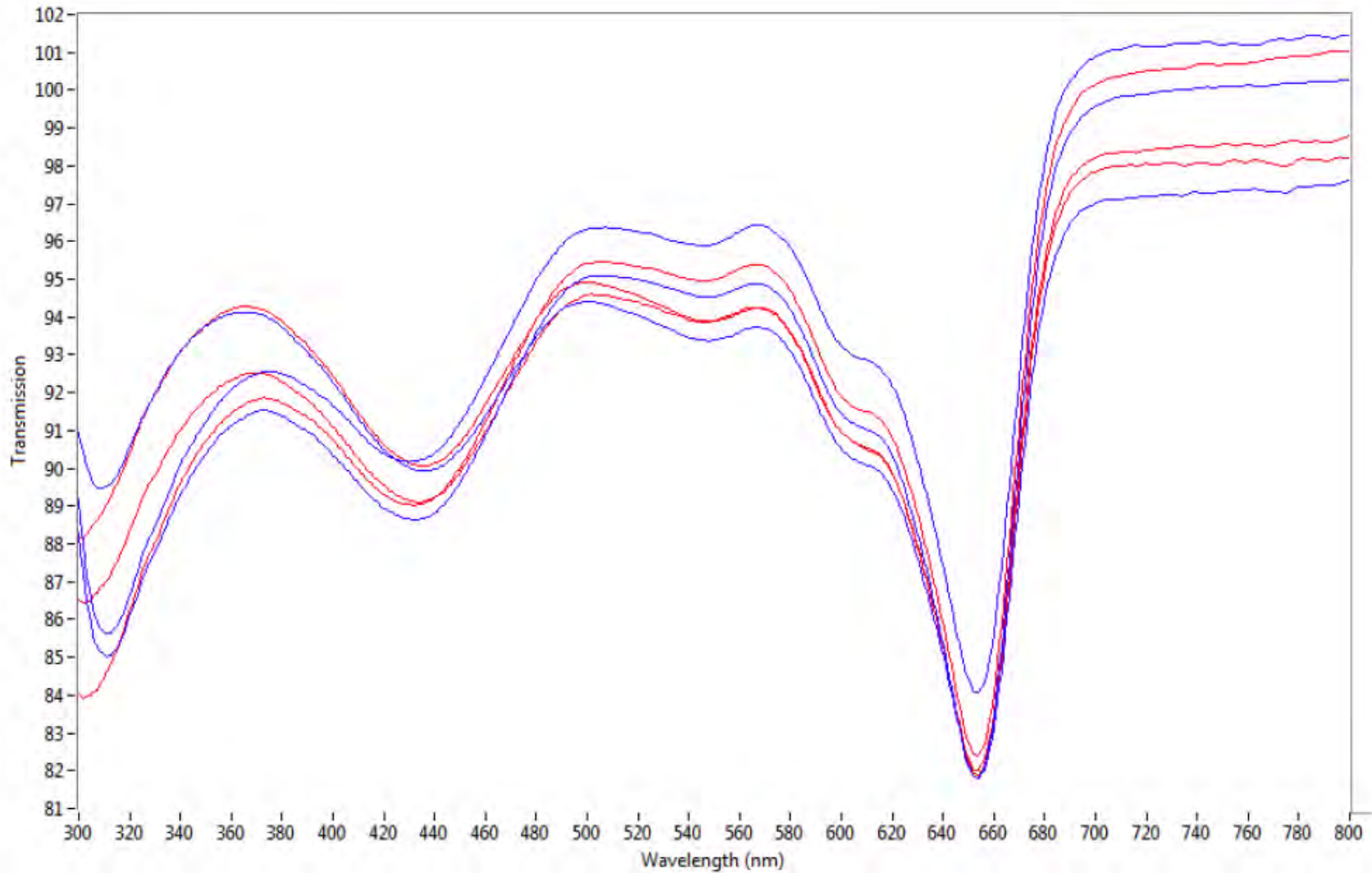


Figure 152. MSP spectra of fibers from the same source collected with a No. 1 cover slip (red) compared to those collected with a No. 1 ½ cover slip (blue).

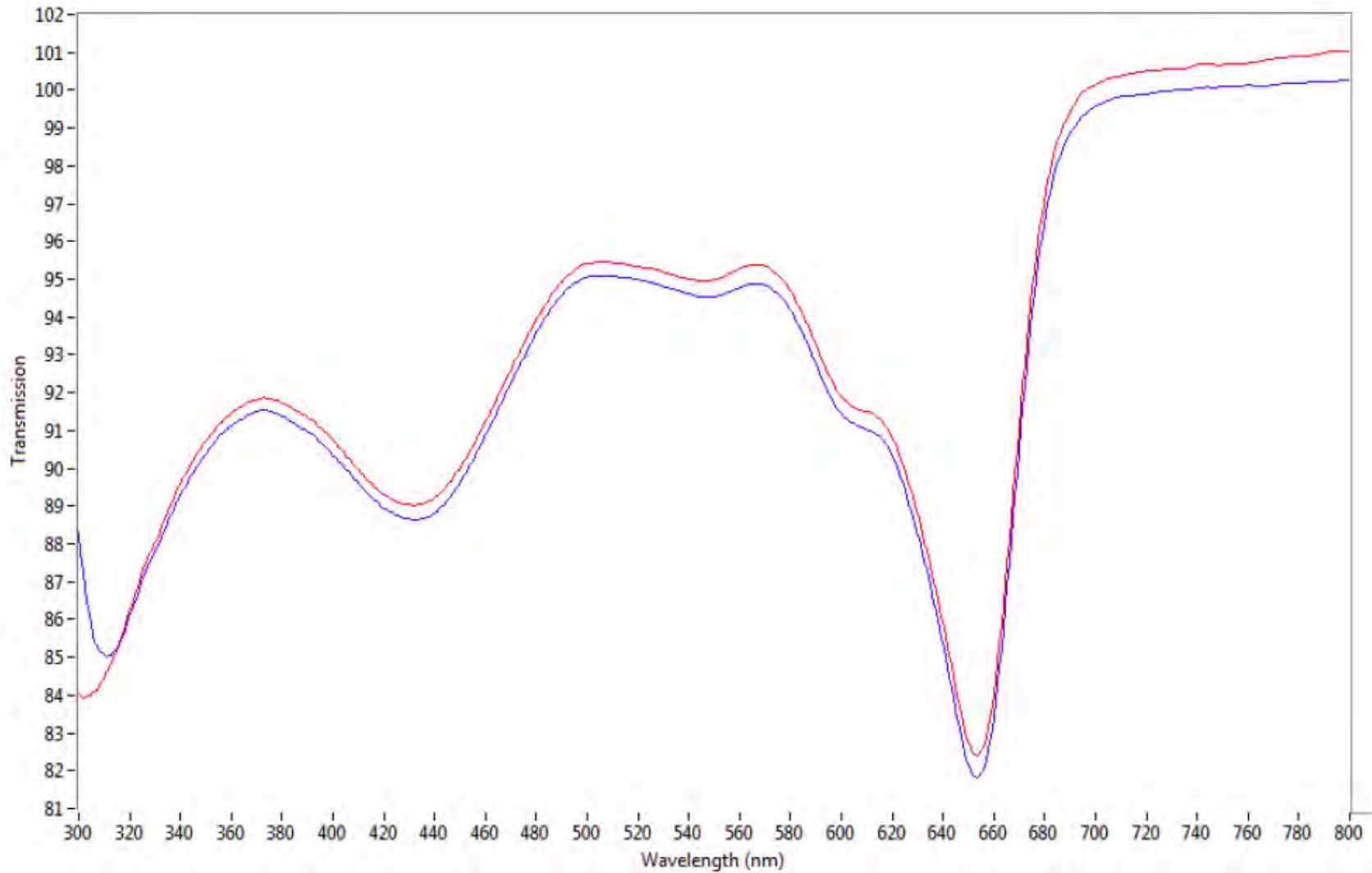


Figure 153. MSP spectra of fibers from the same source collected with a No. 1 cover slip (red) compared to those collected with a No. 1 ½ cover slip (blue).

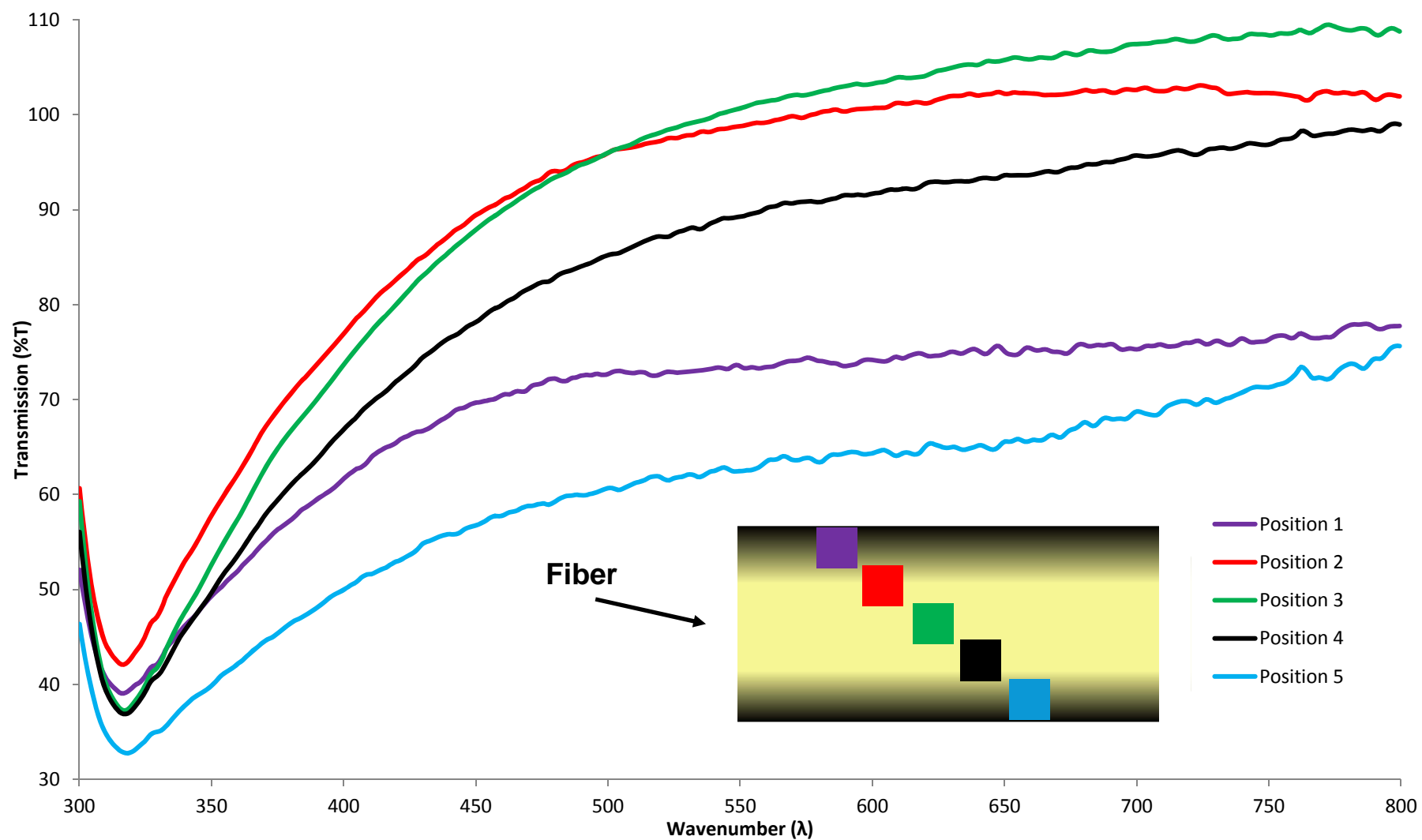


Figure 154. MSP spectra collected from five areas across the width of a nylon fiber mounted in 1.460 index of refraction oil.

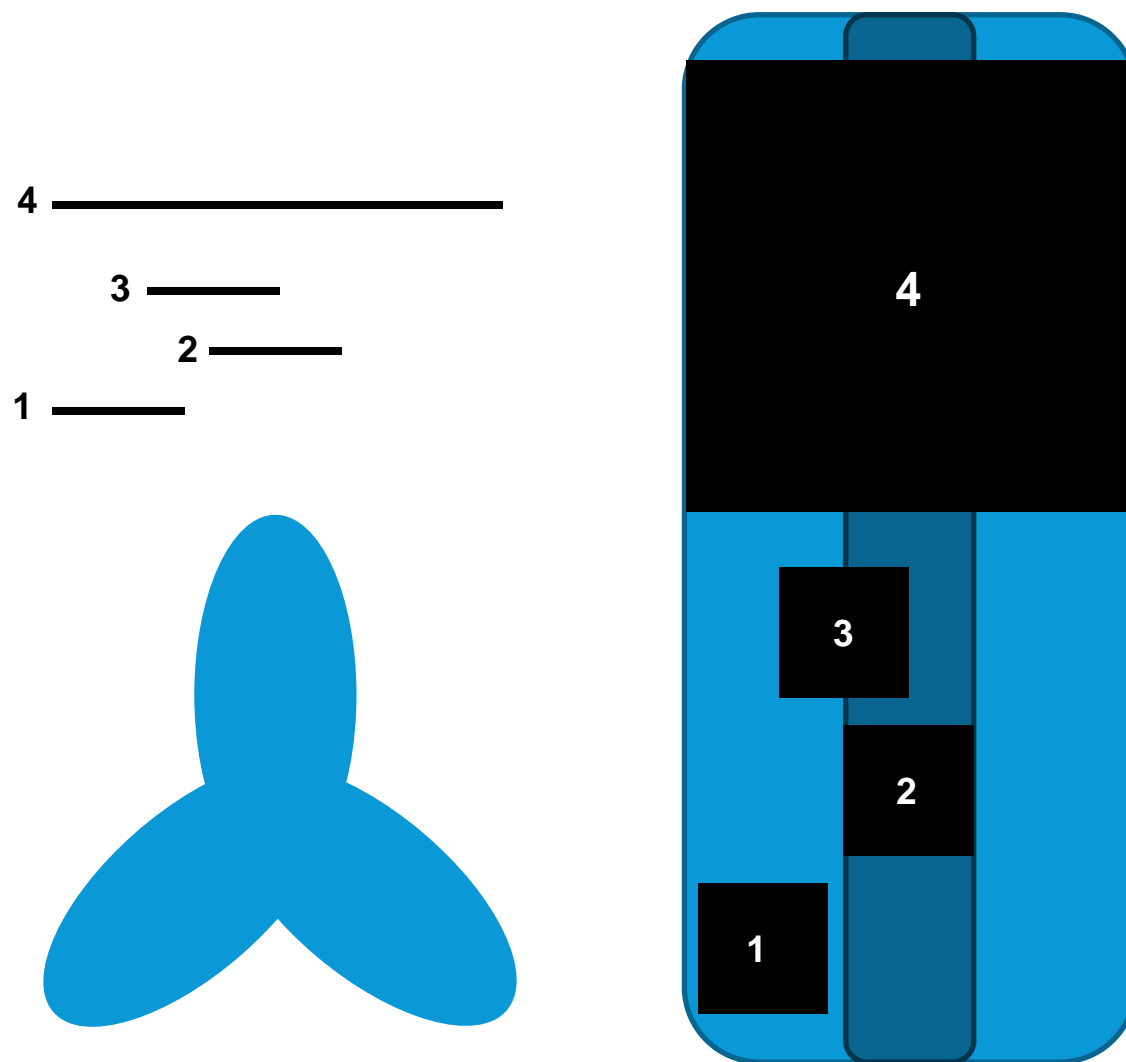


Figure 155. Pictorial representations of the four collection areas used during the examination of nylon fiber with a trilobal cross section (left = cross section view; right = top view).

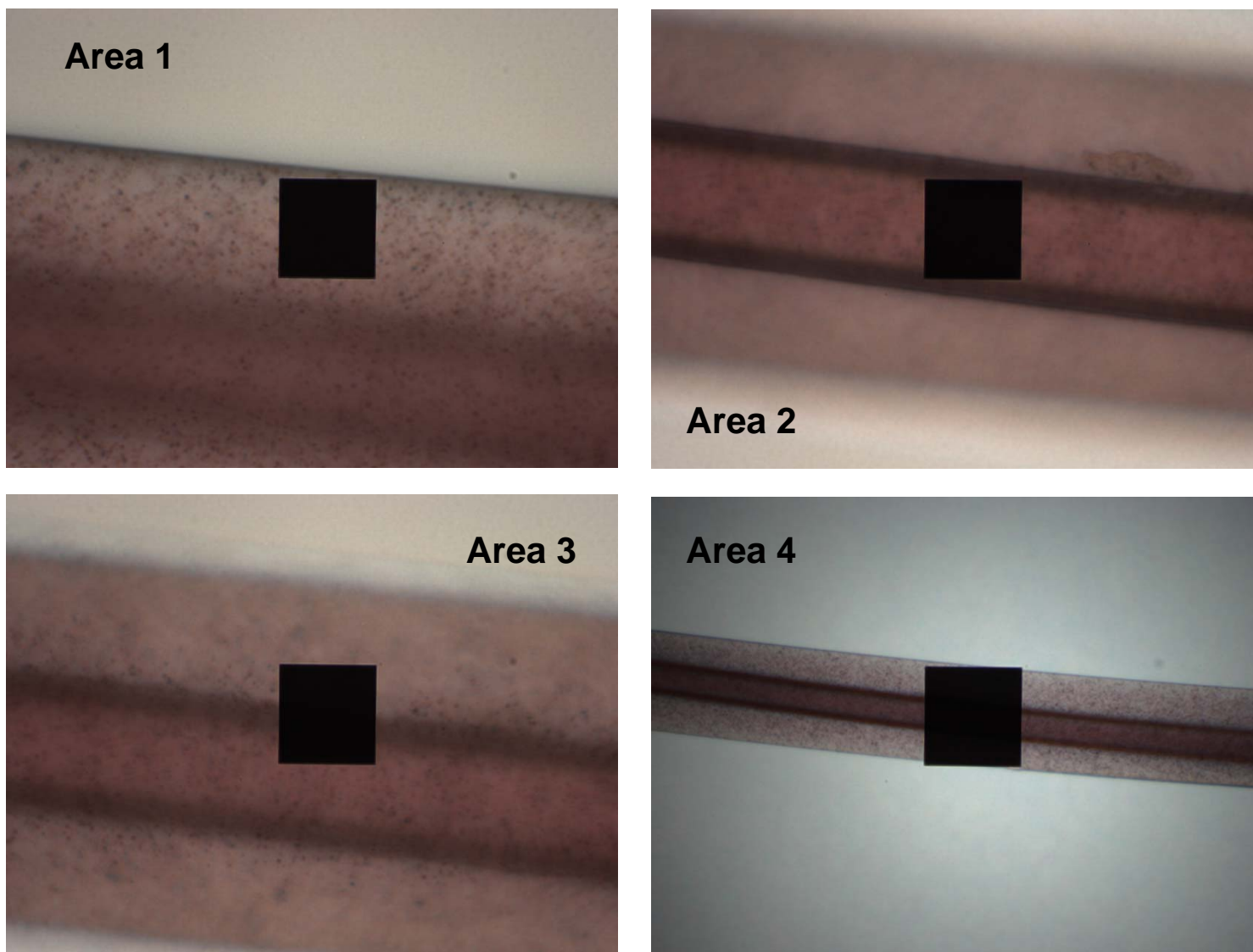


Figure 156. Photomicrographs showing the trilobal nylon fiber and the four positions of the collection aperture.

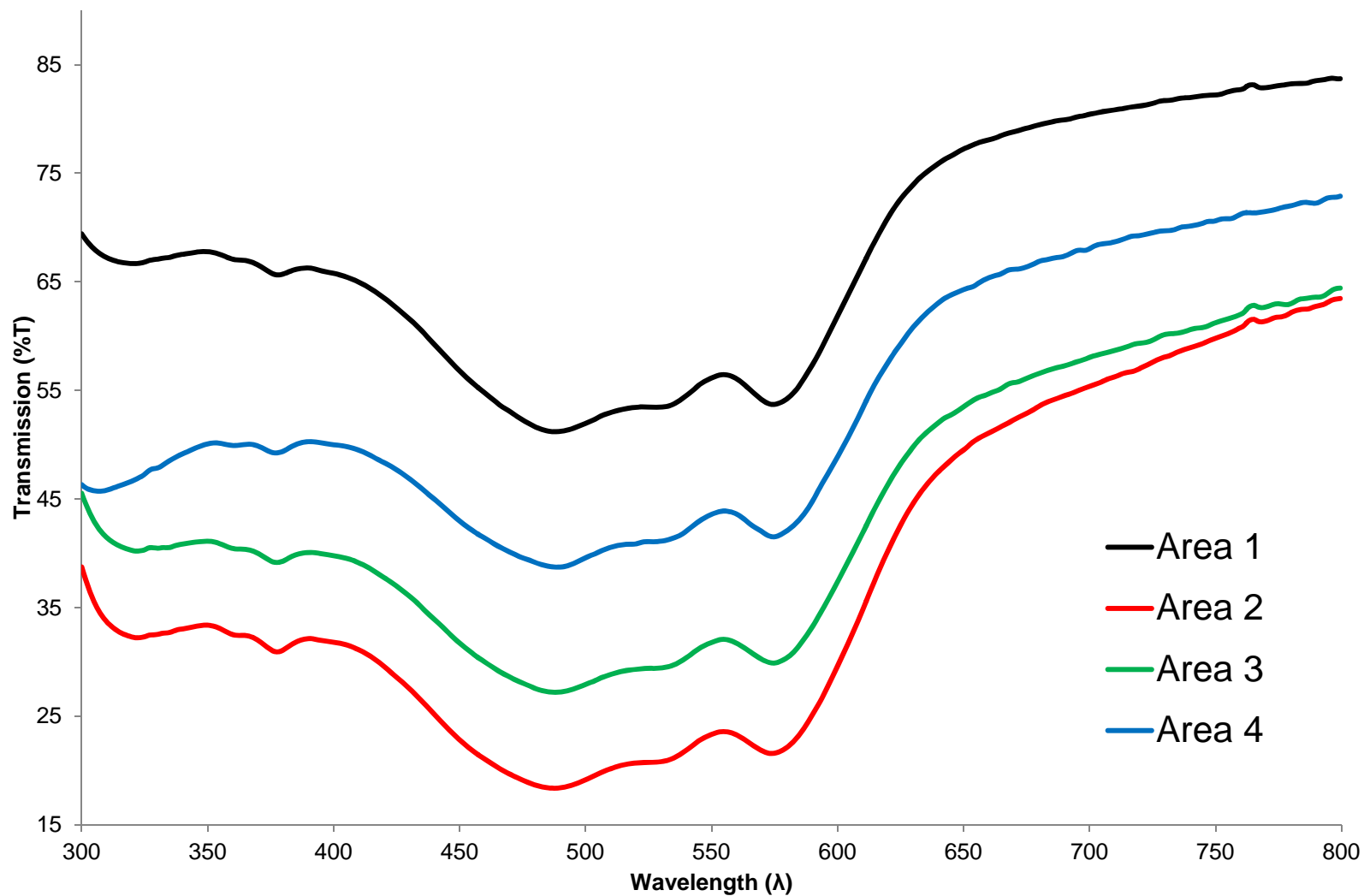


Figure 157. MSP spectra collected from different areas of the same nylon trilobal fiber.

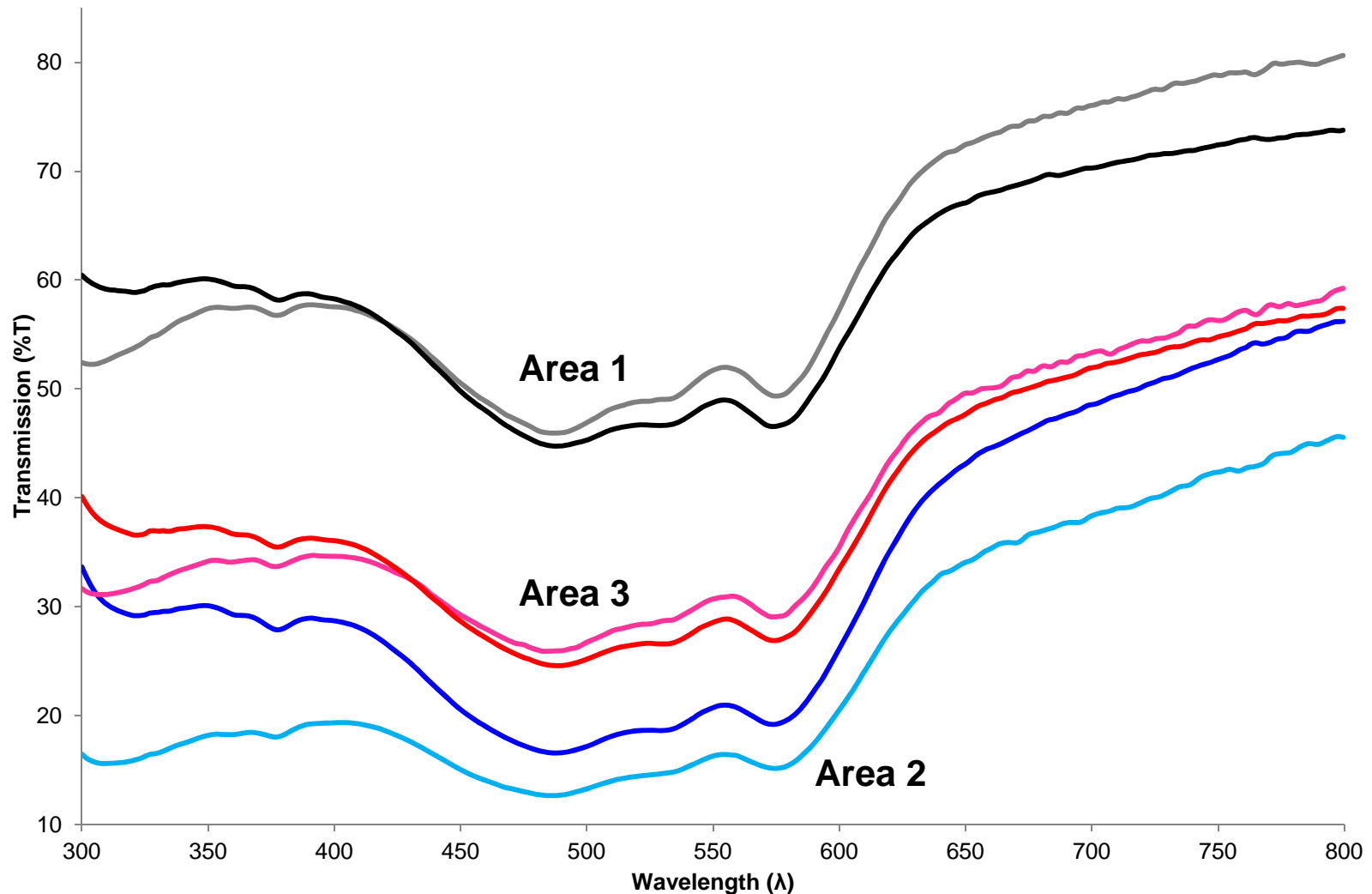


Figure 158. MSP spectra of a trilobal nylon fiber through area 1 (black/gray), area 2 (blue, light blue), and area 3 (red, pink). The black, blue and red spectra were collected using a 40X objective while the other three were collected using a 10X objective. The spectra collected using the 10X objective all exhibit a “dip” below ~ 400 nm compared to their respective spectra collected using a 40X objective.

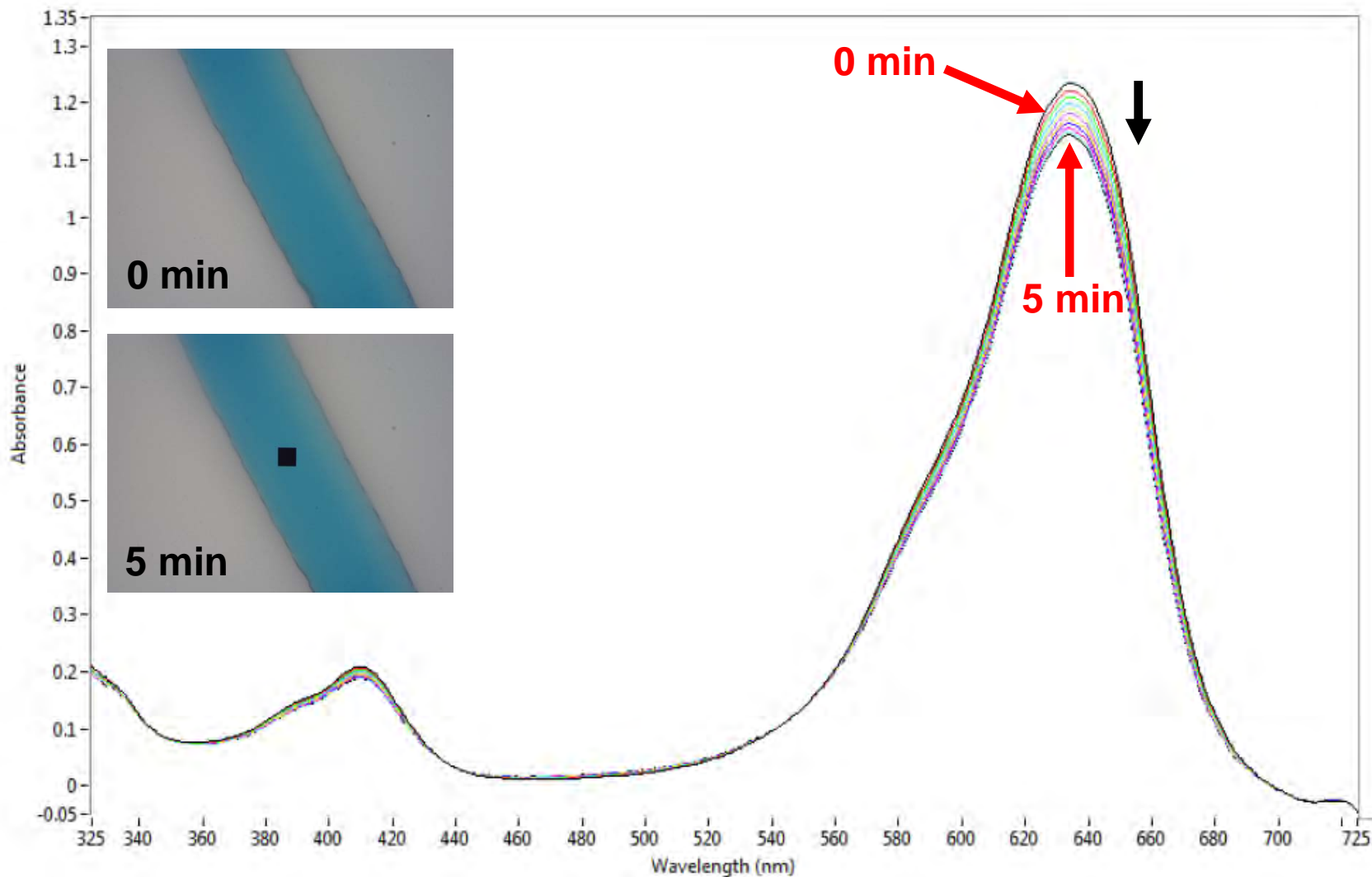


Figure 159. MSP spectra collected every 30 seconds for 5 minutes through a wool fiber dyed with Acid Blue 9 using tungsten illumination (mounted on a quartz slide with a quartz coverslip). Photomicrographs show the fiber at the beginning and end of the experiment.

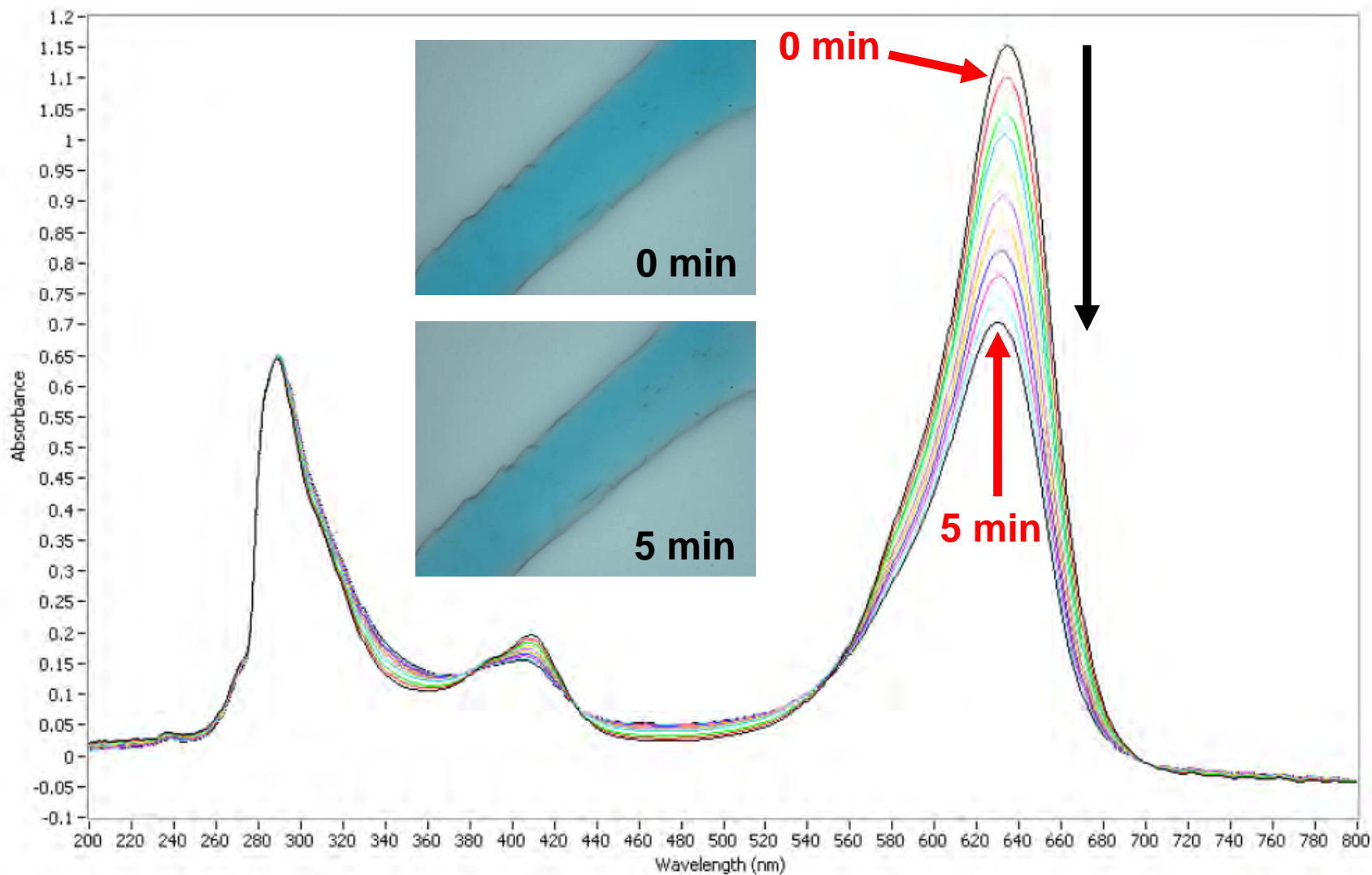


Figure 160. MSP spectra collected every 30 seconds for 5 minutes through a wool fiber dyed with Acid Blue 9 using xenon illumination (mounted on a quartz slide with a quartz coverslip). Photomicrographs show the fiber at the beginning and end of the experiment.

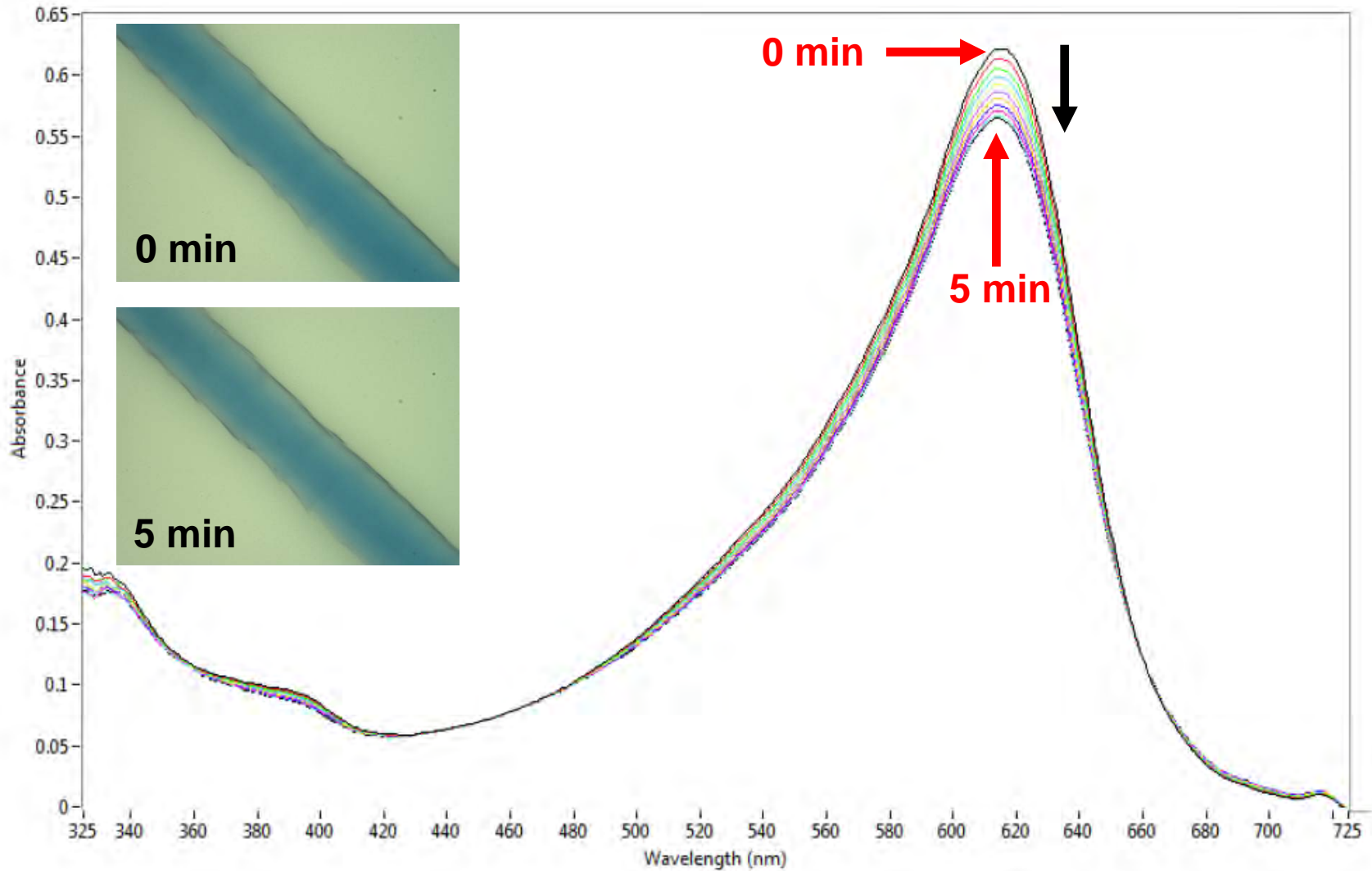


Figure 161. MSP spectra collected every 30 seconds for 5 minutes through a wool fiber dyed with Acid Blue 13 using tungsten illumination (mounted on a quartz slide with a quartz coverslip). Photomicrographs show the fiber at the beginning and end of the experiment.

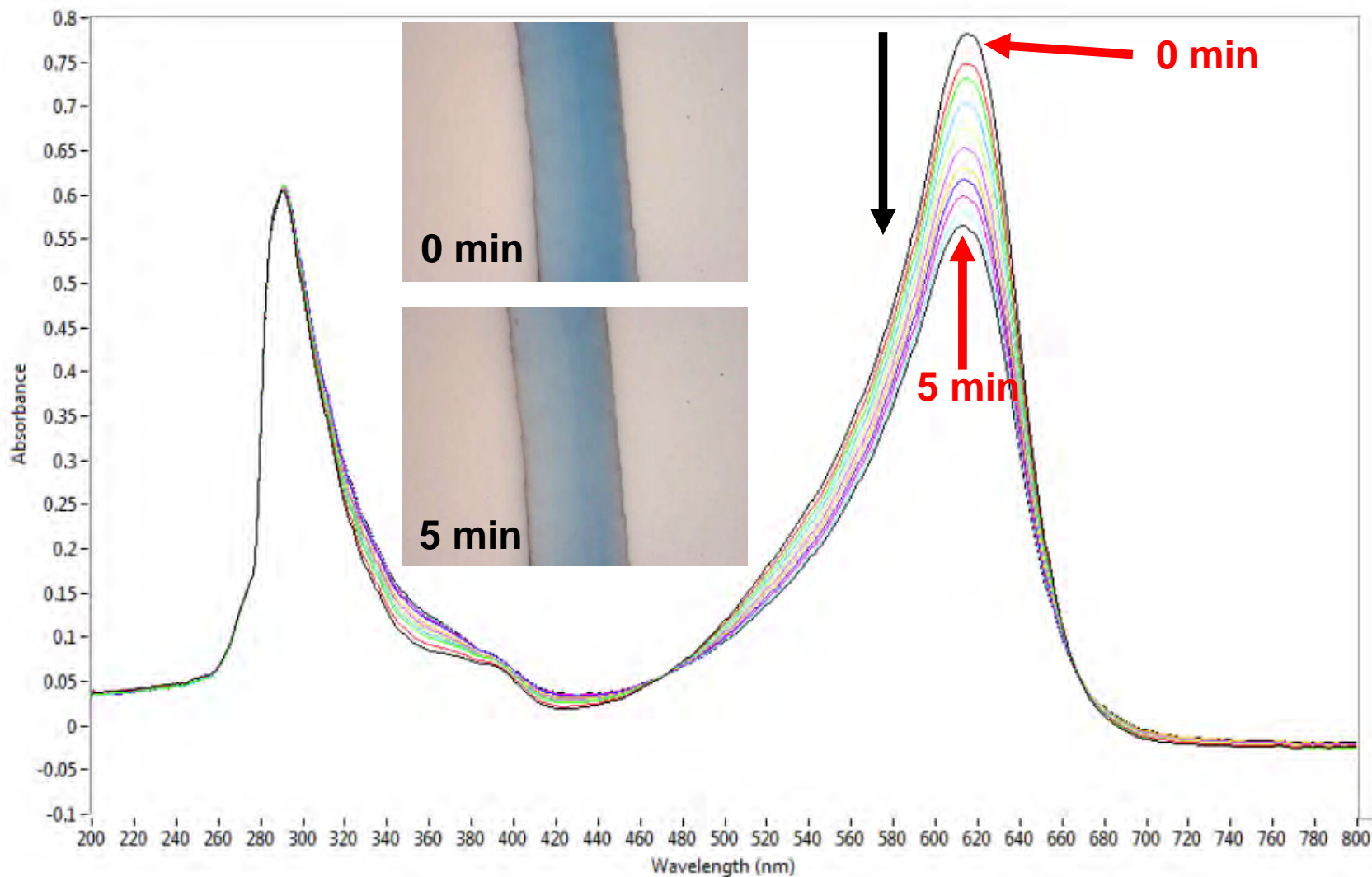


Figure 162. MSP spectra collected every 30 seconds for 5 minutes through a wool fiber dyed with Acid Blue 13 using xenon illumination (mounted on a quartz slide with a quartz coverslip). Photomicrographs show the fiber at the beginning and end of the experiment.

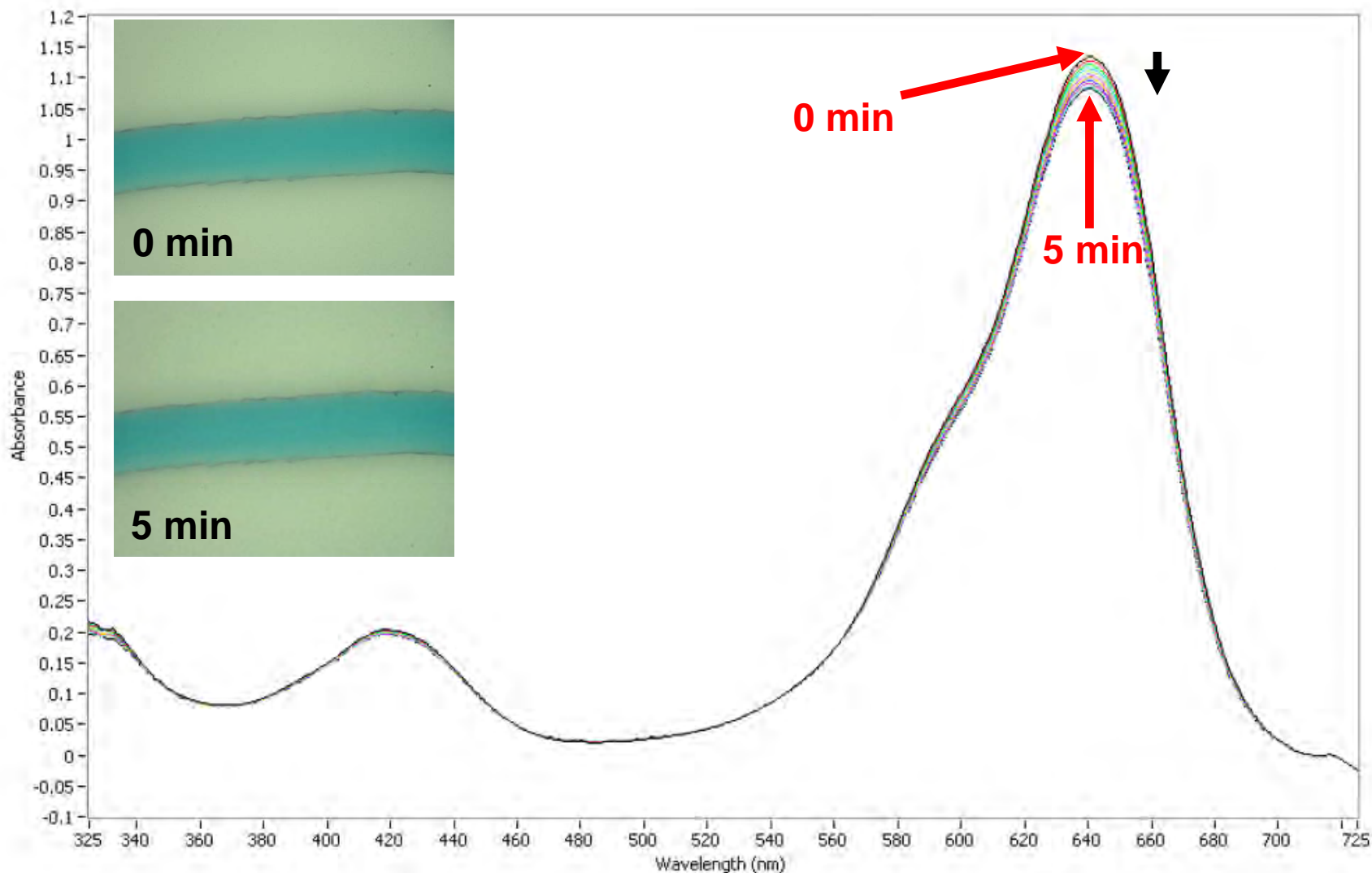


Figure 163. MSP spectra collected every 30 seconds for 5 minutes through a wool fiber dyed with Acid Green 7 using tungsten illumination (mounted on a quartz slide with a quartz coverslip). Photomicrographs show the fiber at the beginning and end of the experiment.

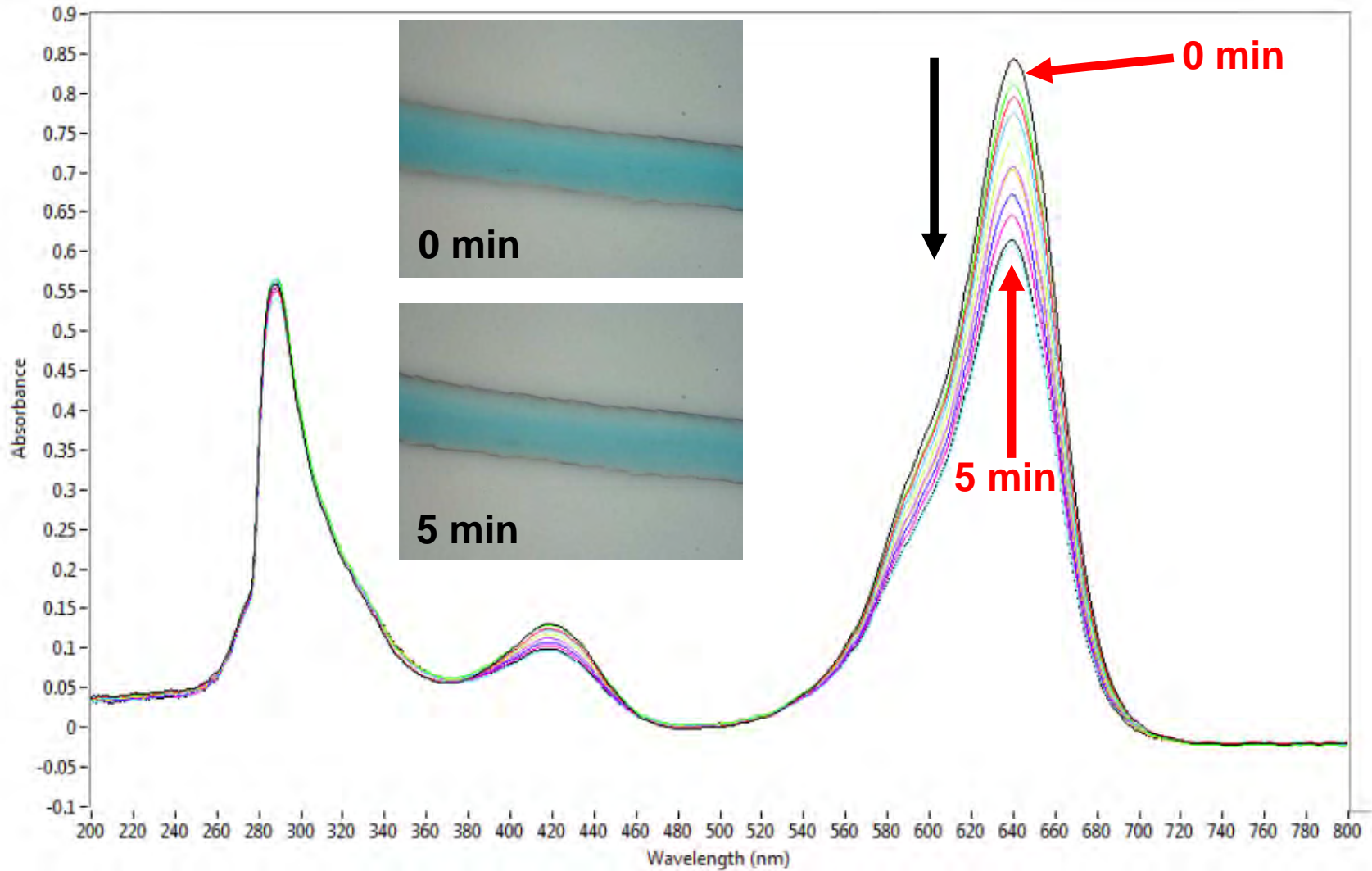


Figure 164. MSP spectra collected every 30 seconds for 5 minutes through a wool fiber dyed with Acid Green 7 using xenon illumination (mounted on a quartz slide with a quartz coverslip). Photomicrographs show the fiber at the beginning and end of the experiment.

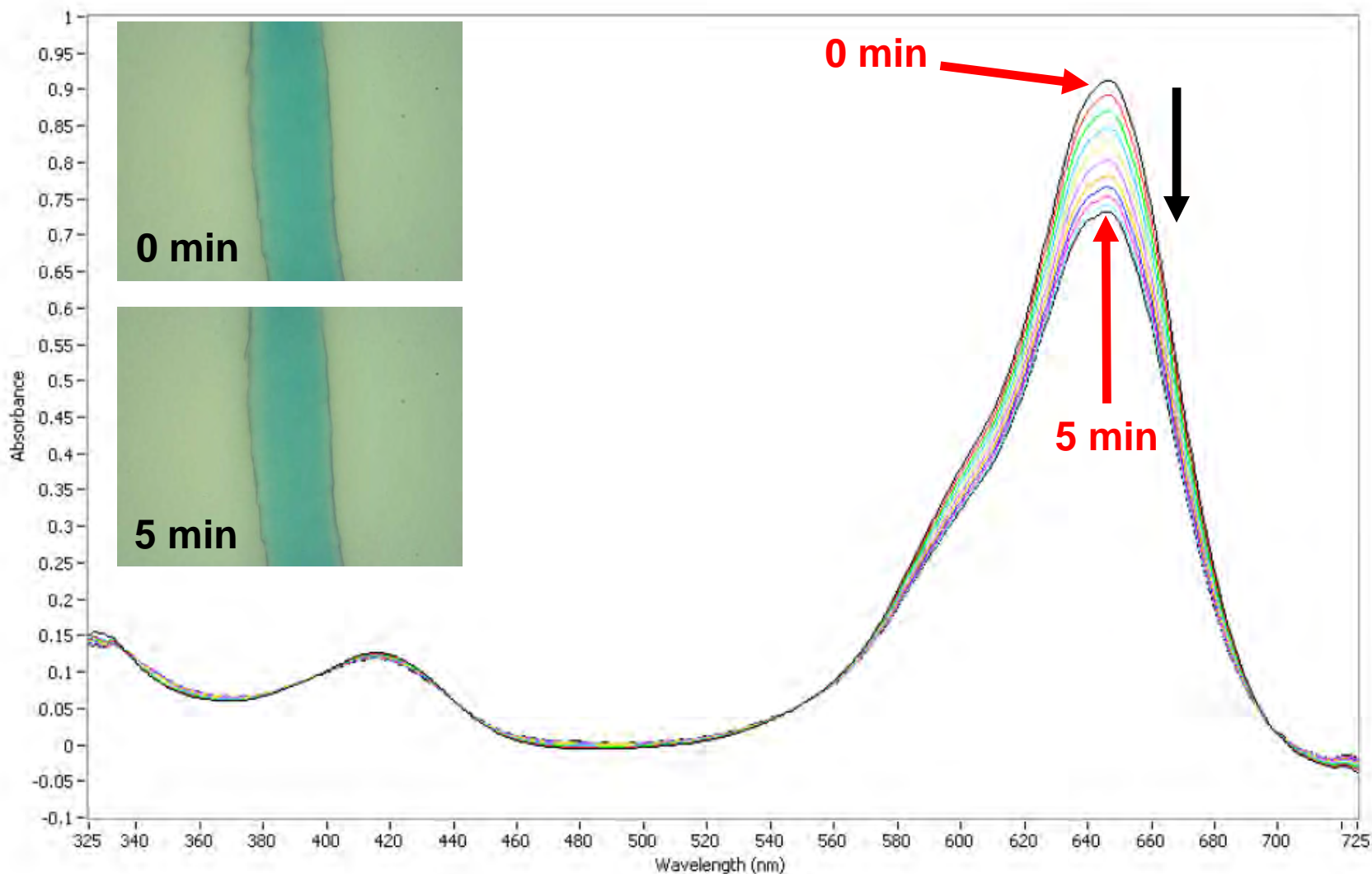


Figure 165. MSP spectra collected every 30 seconds for 5 minutes through a wool fiber dyed with Acid Green 9 using tungsten illumination (mounted on a quartz slide with a quartz coverslip). Photomicrographs show the fiber at the beginning and end of the experiment.

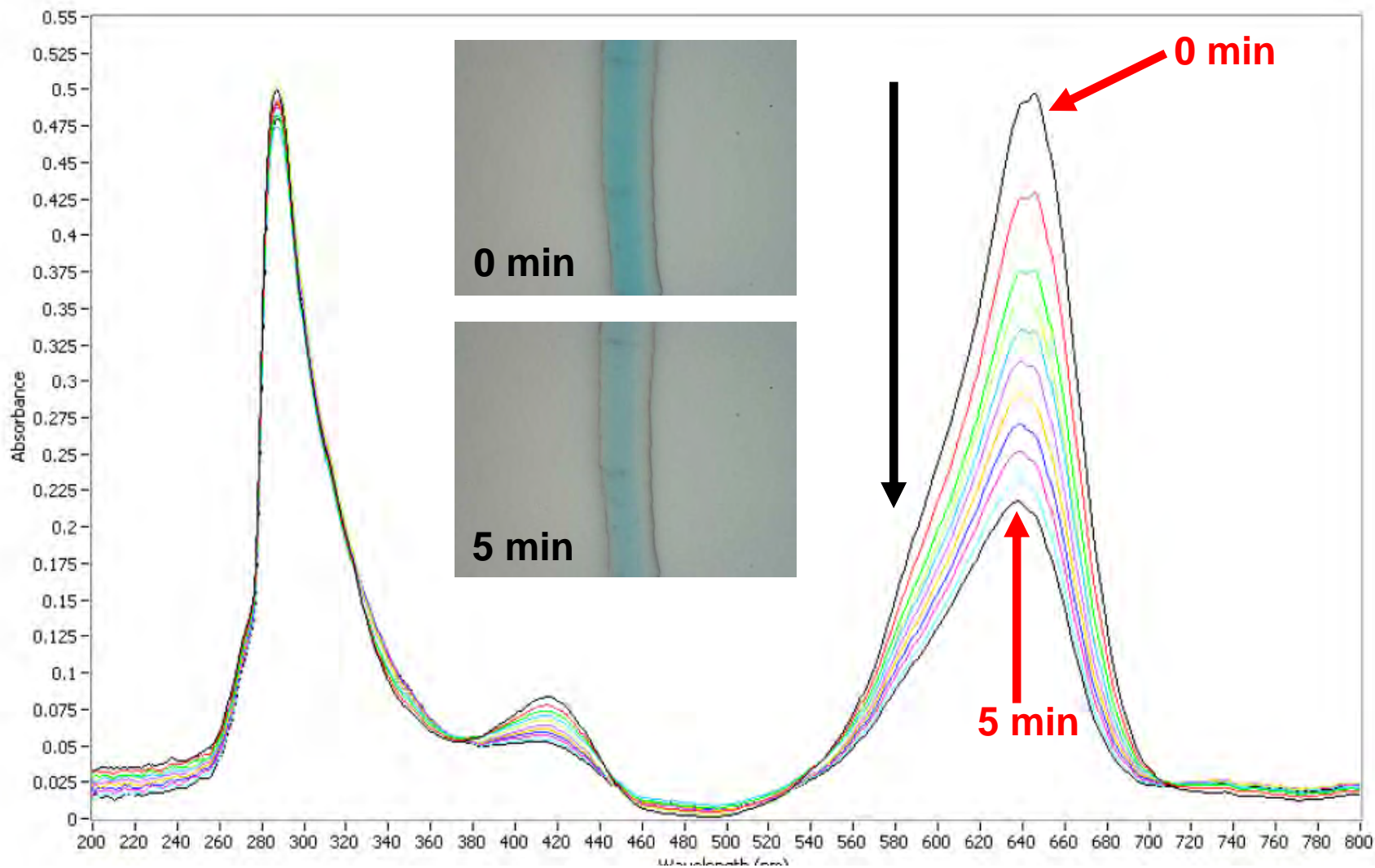


Figure 166. MSP spectra collected every 30 seconds for 5 minutes through a wool fiber dyed with Acid Green 9 using xenon illumination (mounted on a quartz slide with a quartz coverslip). Photomicrographs show the fiber at the beginning and end of the experiment.

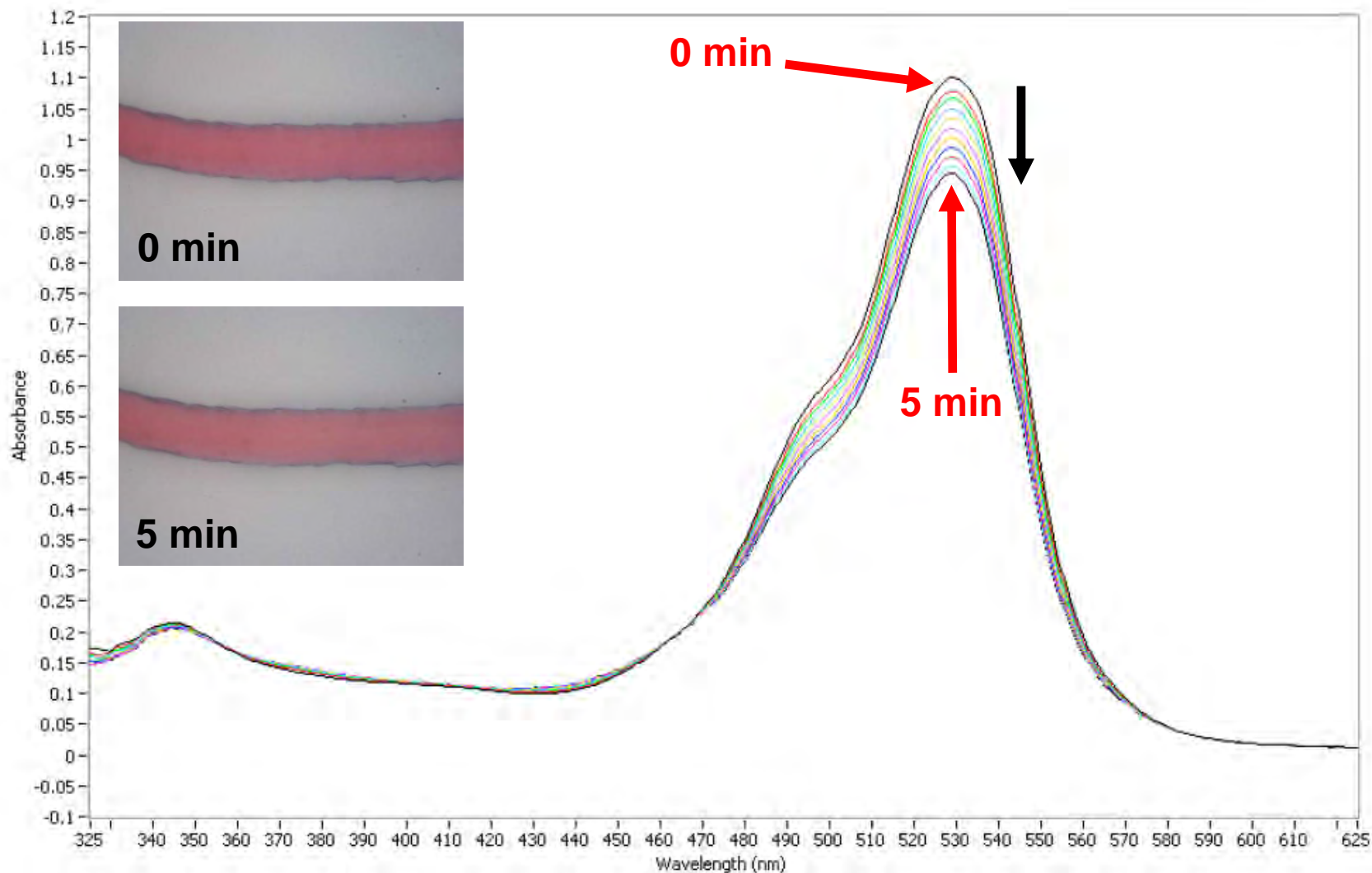


Figure 167. MSP spectra collected every 30 seconds for 5 minutes through a wool fiber dyed with Acid Red 51 using tungsten illumination (mounted on a quartz slide with a quartz coverslip). Photomicrographs show the fiber at the beginning and end of the experiment.

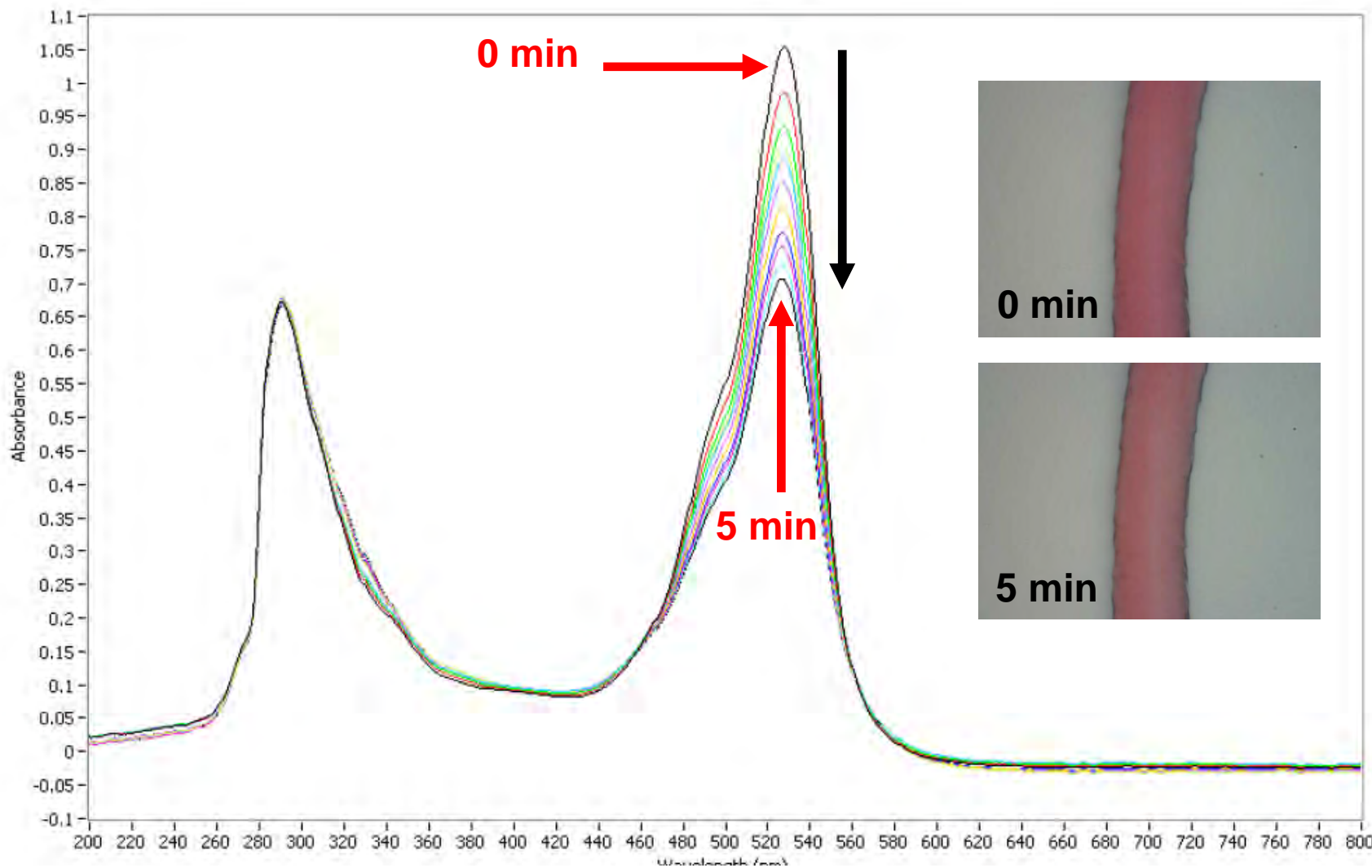


Figure 168. MSP spectra collected every 30 seconds for 5 minutes through a wool fiber dyed with Acid Red 51 using xenon illumination (mounted on a quartz slide with a quartz coverslip). Photomicrographs show the fiber at the beginning and end of the experiment.

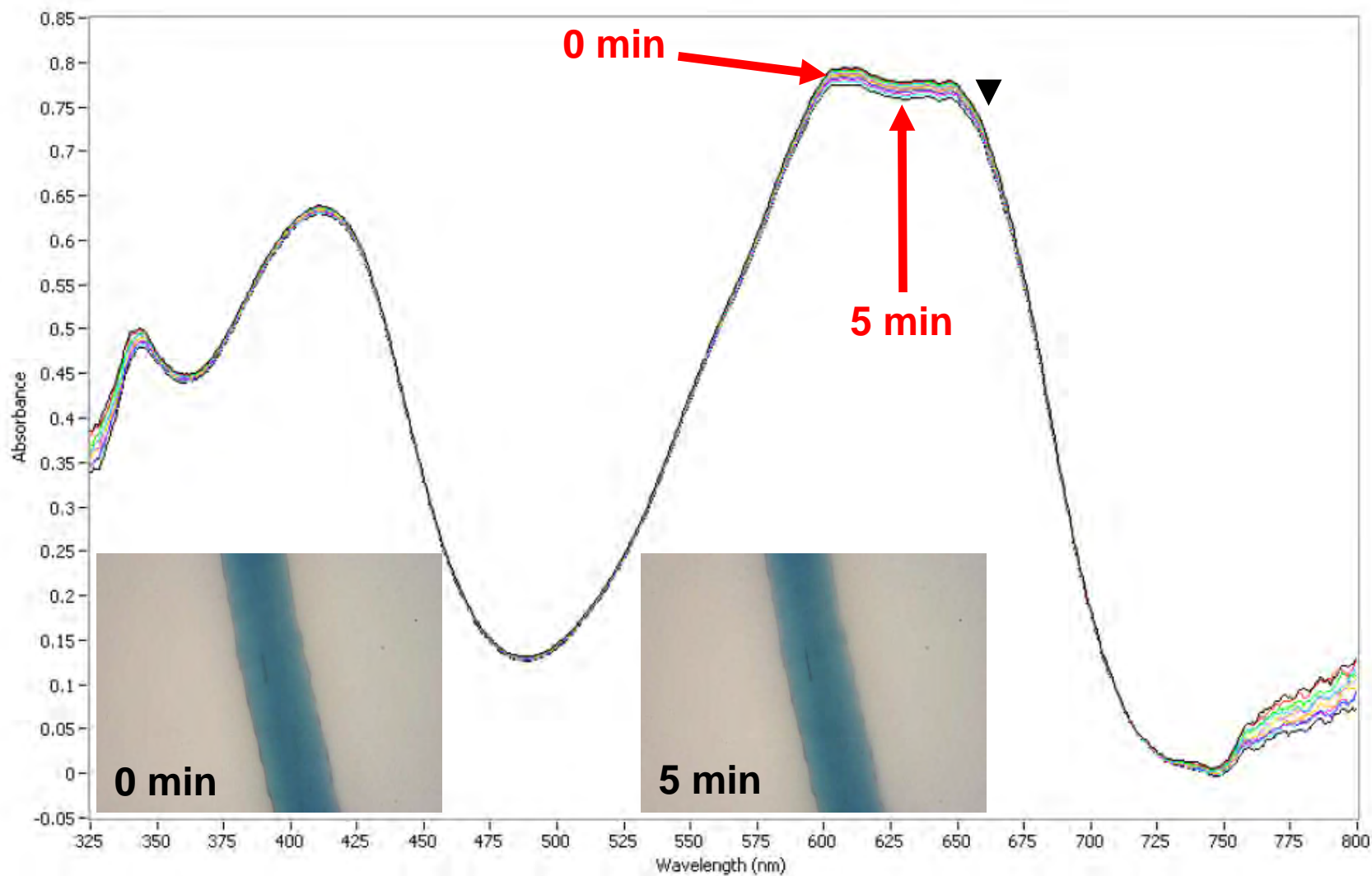


Figure 169. MSP spectra collected every 30 seconds for 5 minutes through a wool fiber dyed with Acid Green 25 using tungsten illumination (mounted on a quartz slide with a quartz coverslip). Photomicrographs show the fiber at the beginning and end of the experiment.

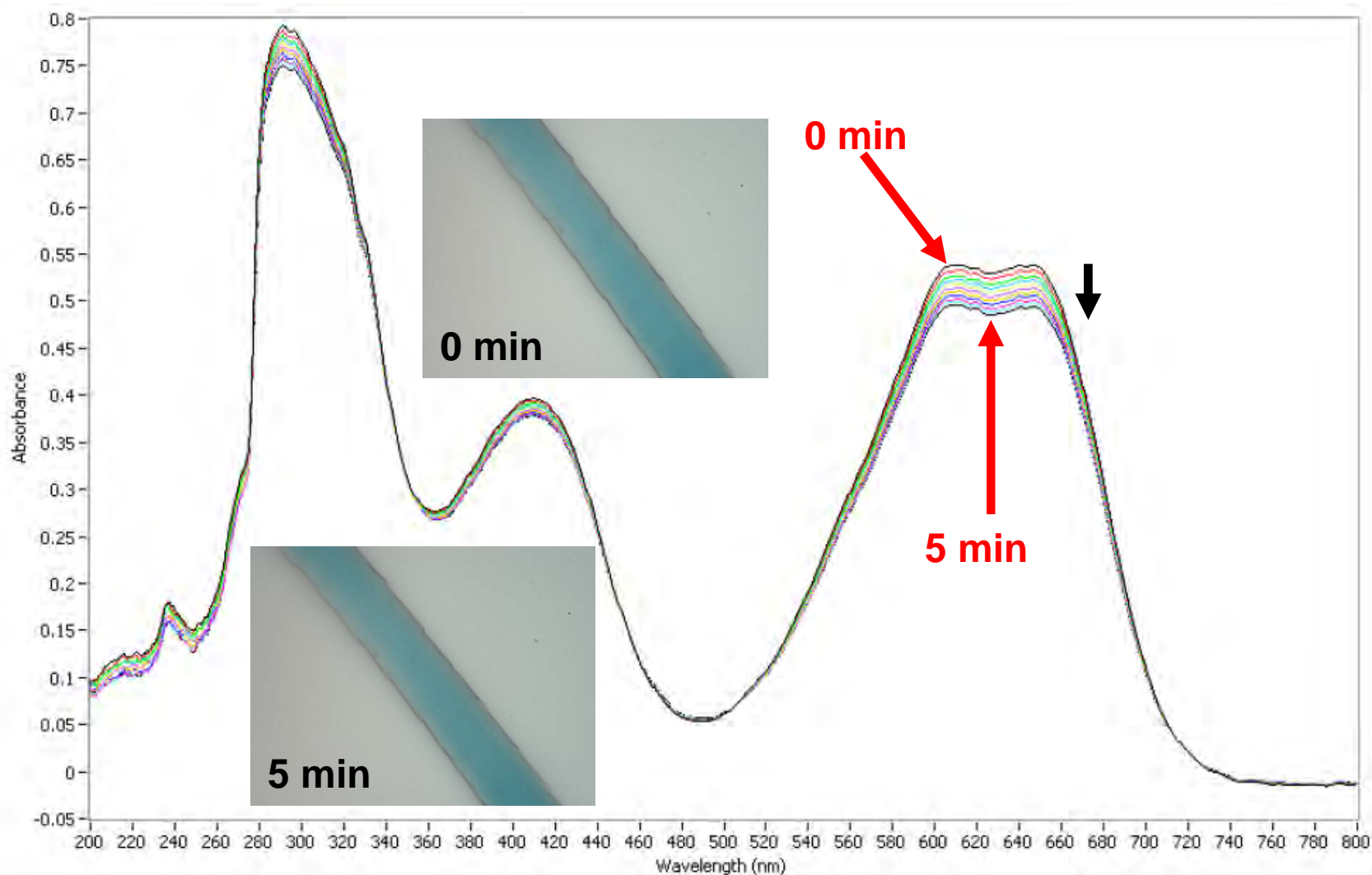


Figure 170. MSP spectra collected every 30 seconds for 5 minutes through a wool fiber dyed with Acid Green 25 using xenon illumination (mounted on a quartz slide with a quartz coverslip). Photomicrographs show the fiber at the beginning and end of the experiment.

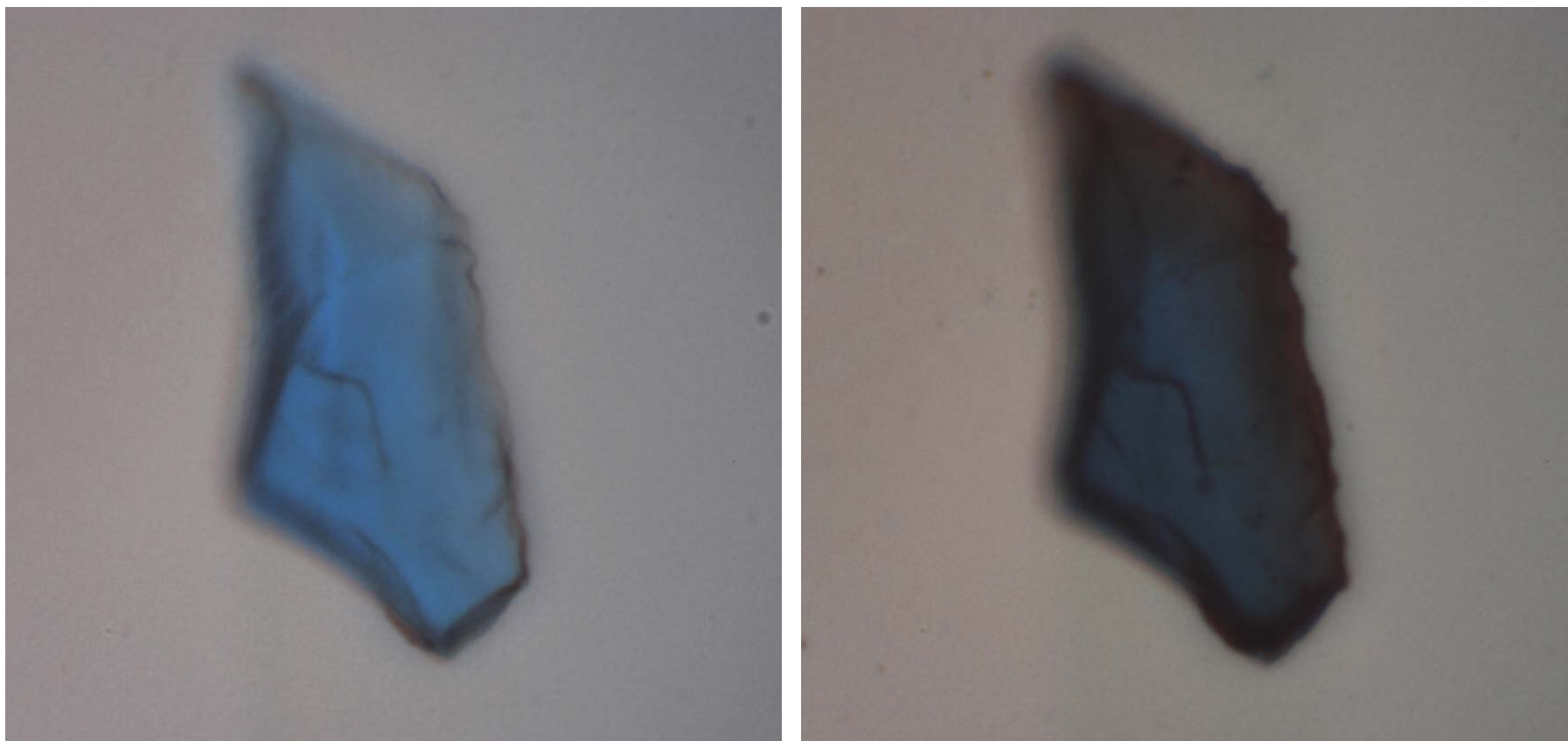


Figure 171. PB30 grain mounted in 1.662 Meltmount at time zero (left) and after five minutes of continual exposure from xenon illumination.

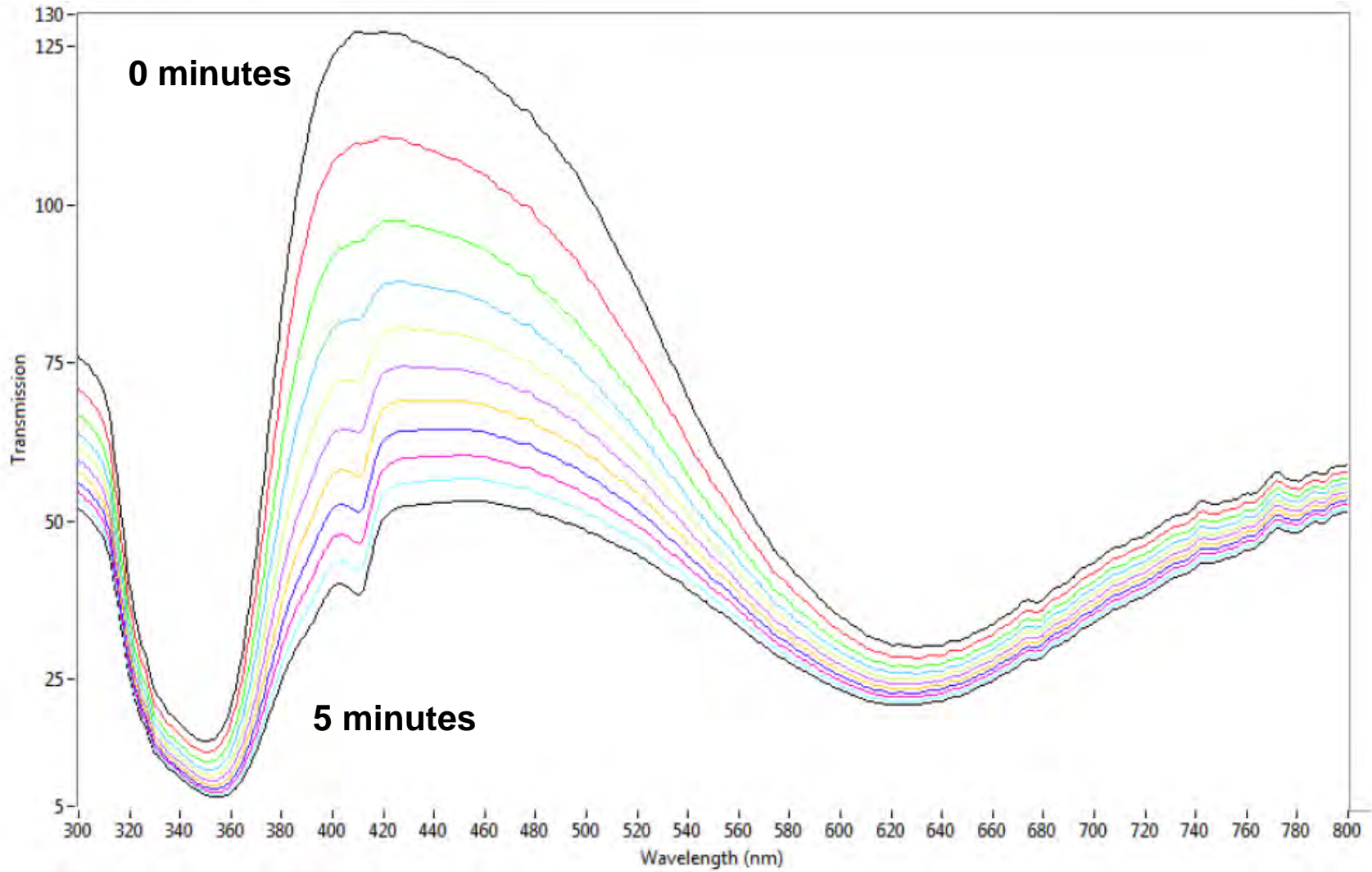


Figure 172. Spectra collected every thirty seconds from a PB30 grain mounted in 1.662 Meltmount with continual exposure from xenon illumination.

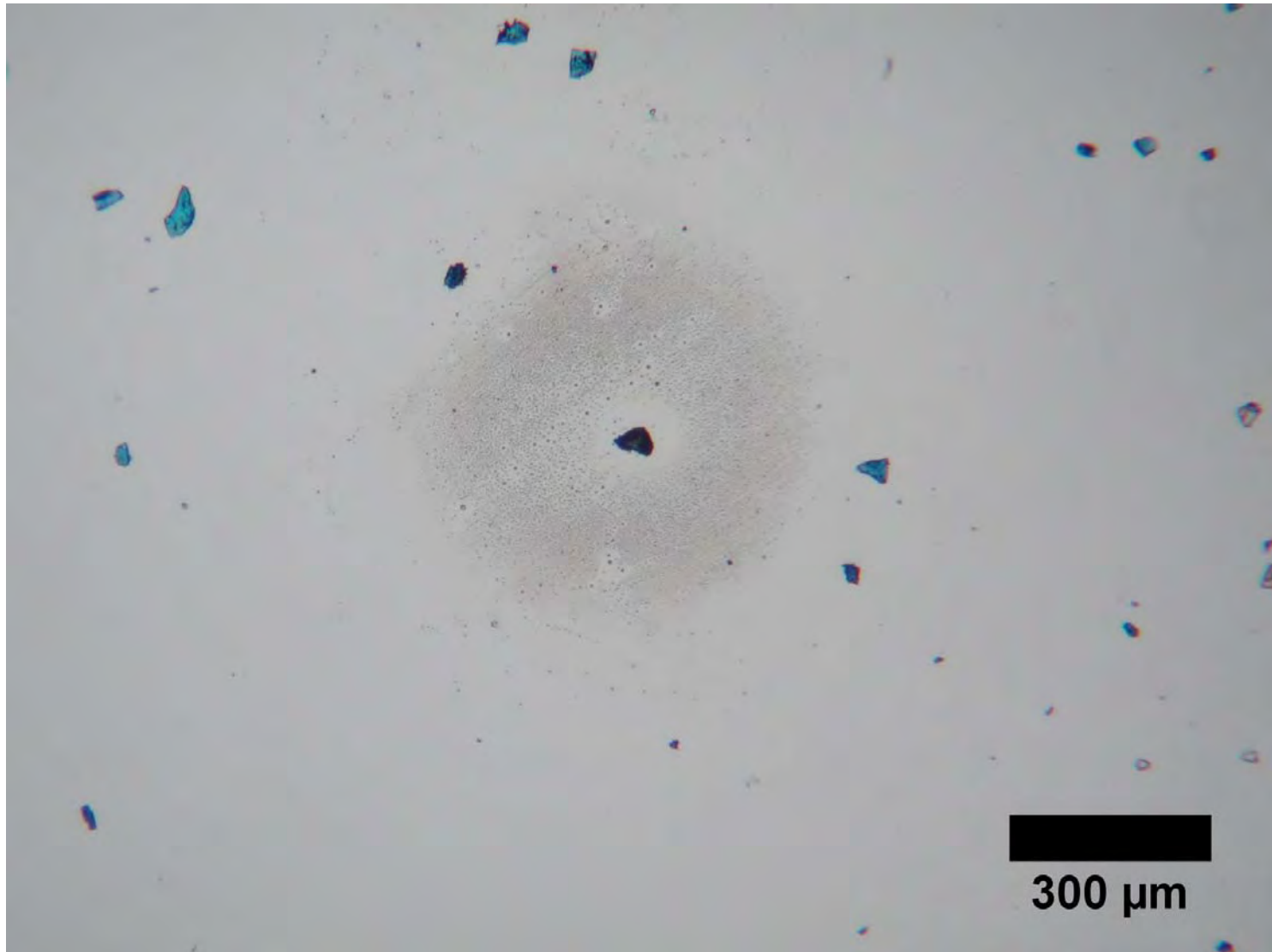


Figure 173. Low magnification view of PB30 grains mounted in 1.662 Meltmount. The central grain has been exposed to several minutes of continual exposure from xenon illumination using a higher powered objective. Note the darkened color of the grain and the surrounding mounting media, which correlates to the area illuminated using the higher powered objective.

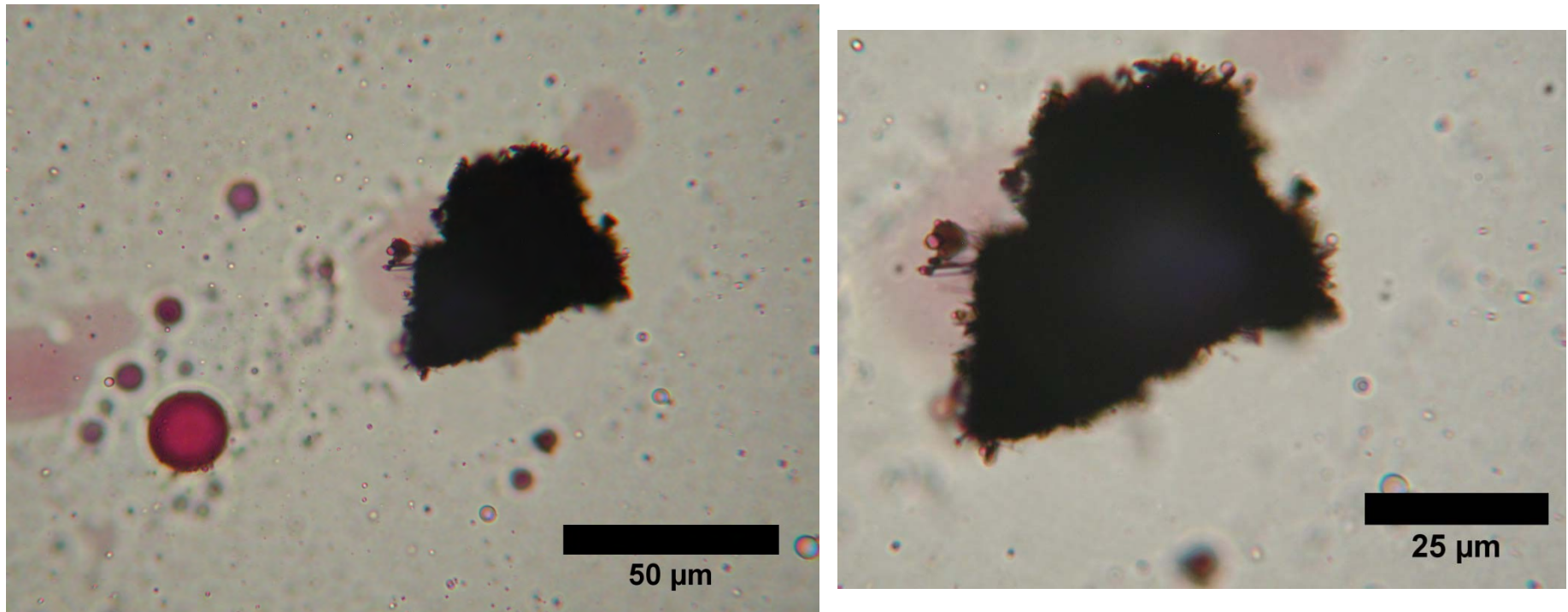


Figure 174. PB30 grain mounted in 1.662 Meltmount a few months after it was subjected to several minutes of continual exposure to xenon illumination.

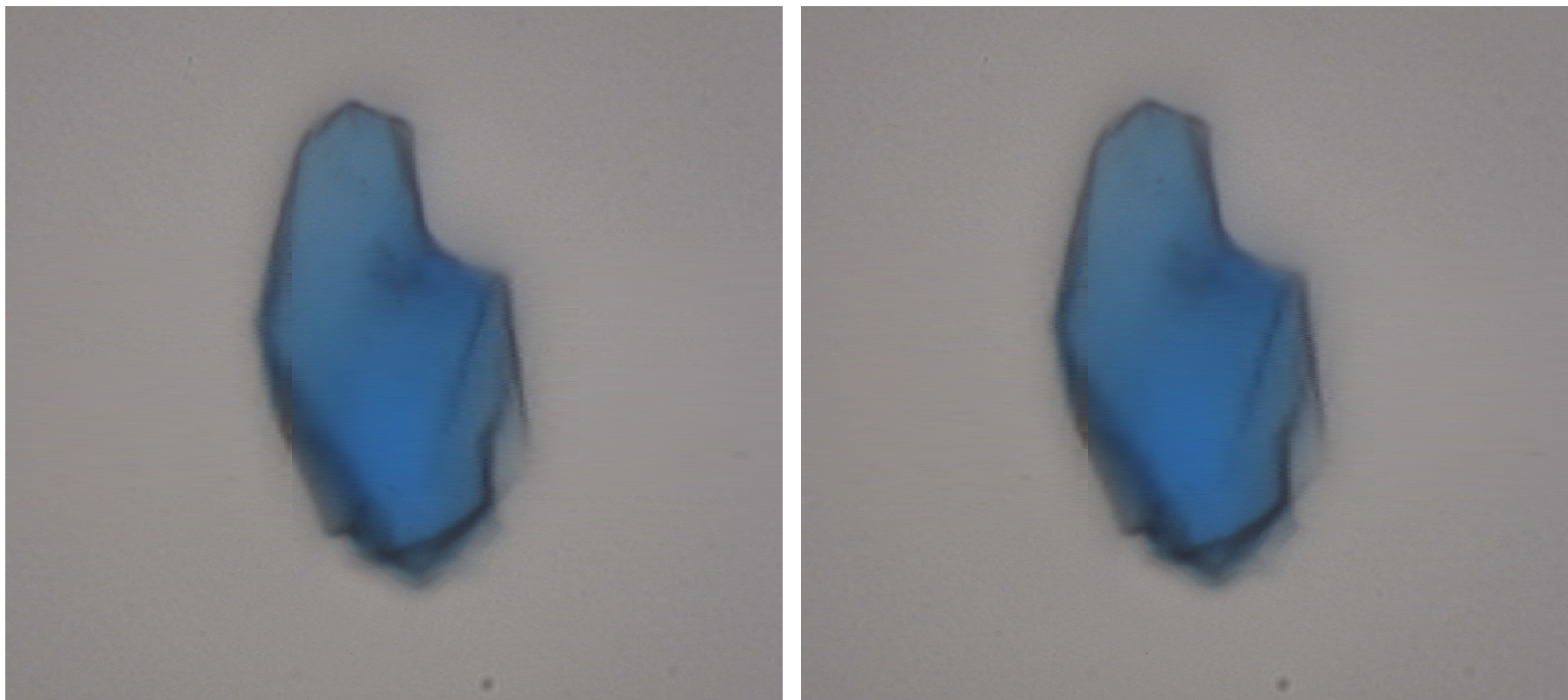


Figure 175. PB30 grain mounted in 1.662 Meltmount at time zero (left) and after five minutes of continual exposure from tungsten halogen illumination.

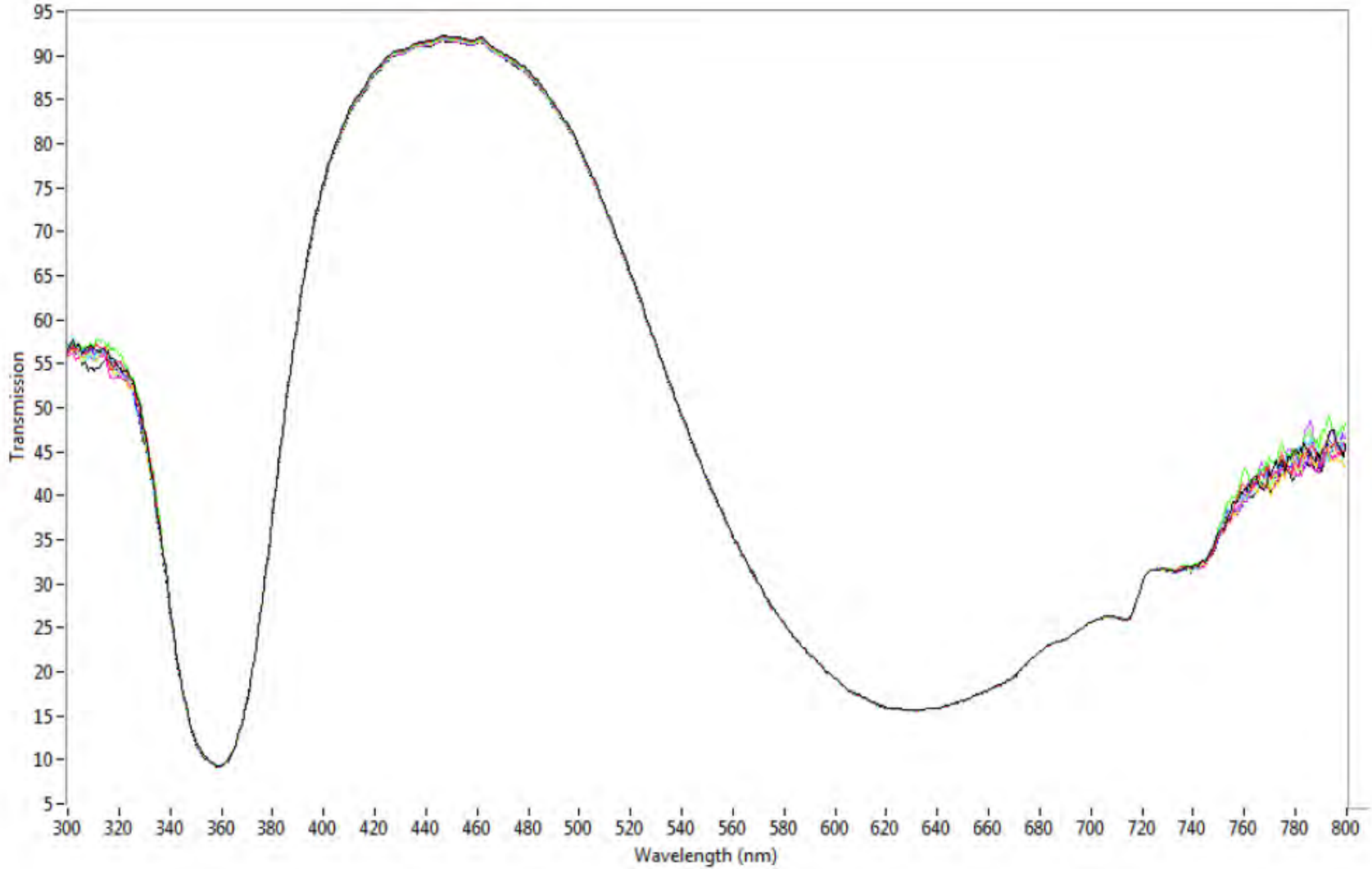


Figure 176. Spectra collected every thirty seconds from a PB30 grain mounted in 1.662 Meltmount with continual exposure from tungsten halogen illumination.

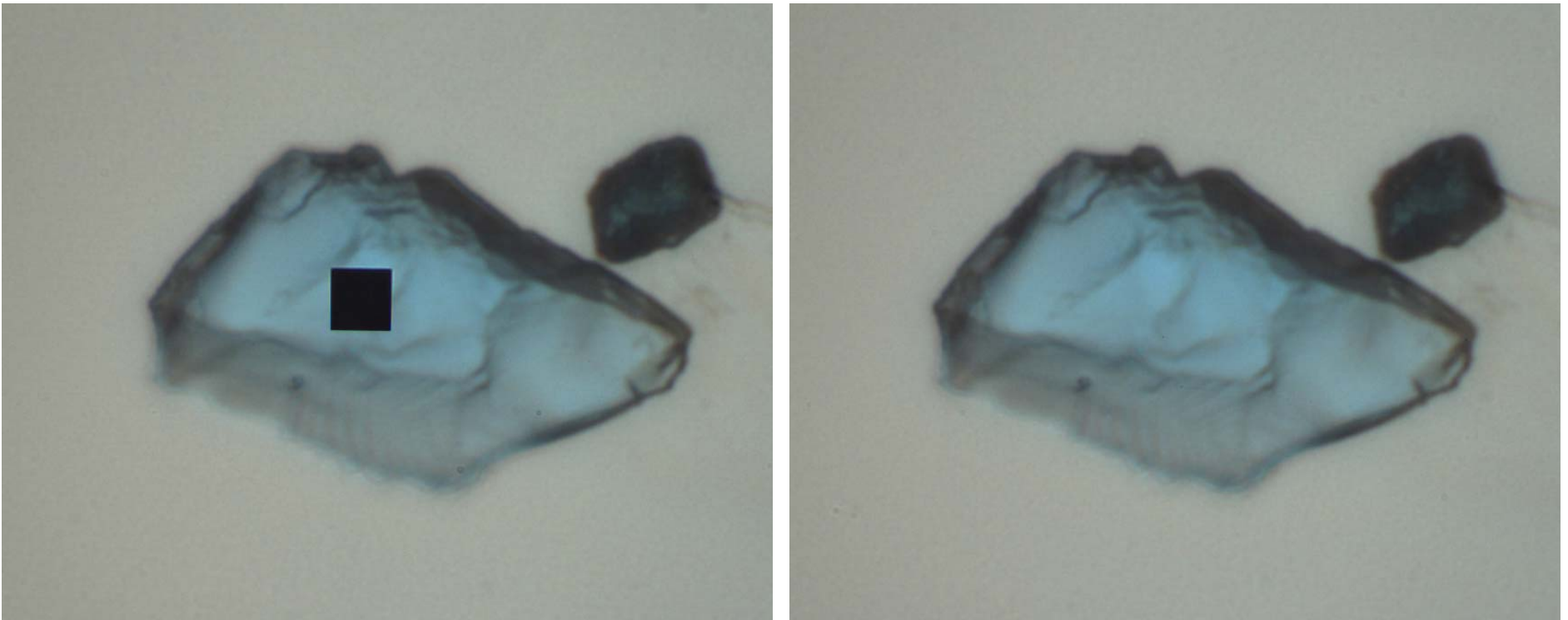


Figure 177. PB30 grain mounted in water at time zero (left) and after five minutes of continual exposure from xenon illumination. The black square in the left image is the collection aperture used to generate the spectra.

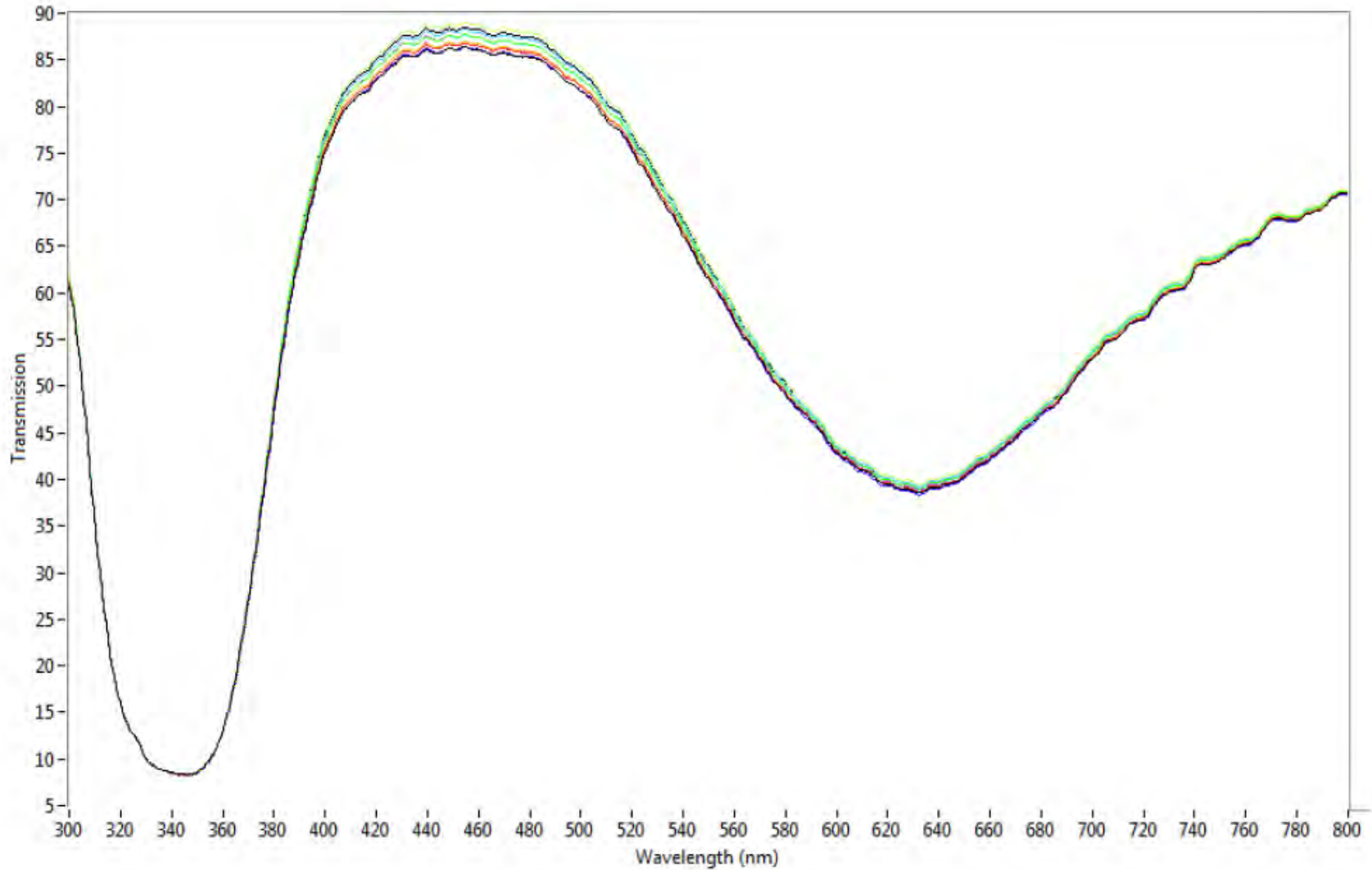


Figure 178. Spectra collected every thirty seconds from a PB30 grain mounted in water with continual exposure from xenon illumination.

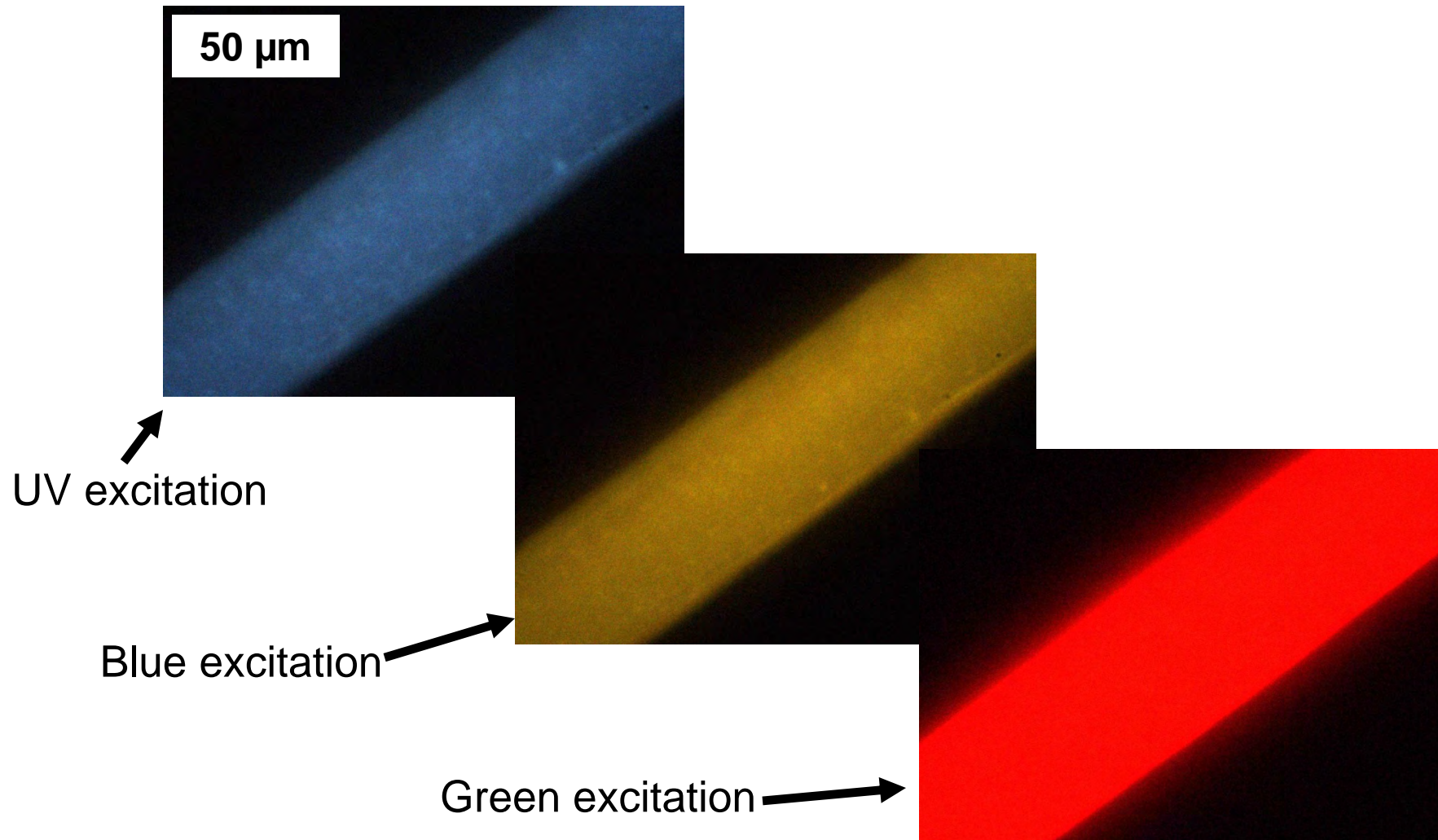


Figure 179. Photomicrographs exhibiting the different fluorescence colors observed when the same green fiber is illuminated with UV, blue, and green light.

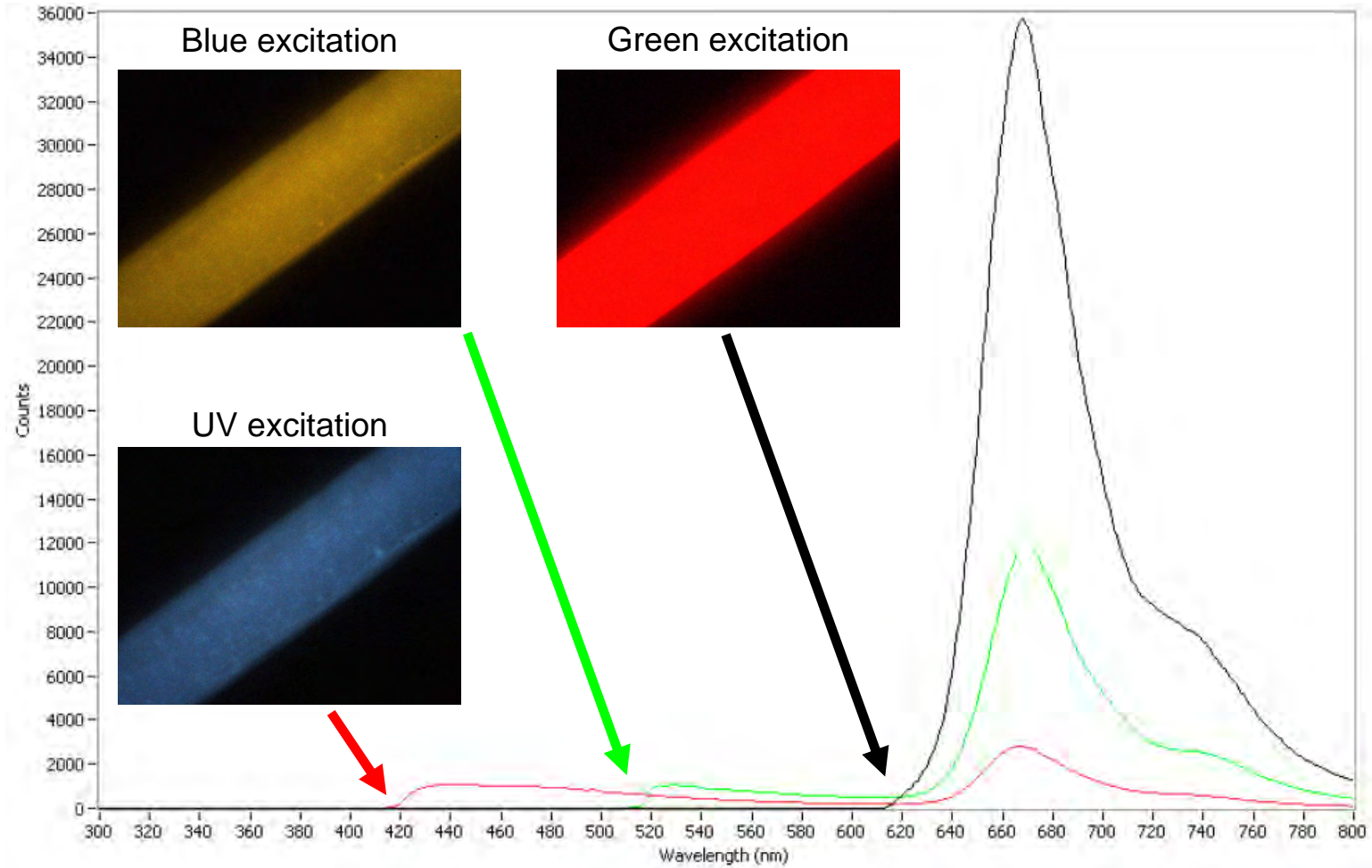


Figure 180. MSF spectra and photomicrographs comparing the fluorescence observed when the same green fiber is illuminated with UV (red), blue (green), and green (black) light. The arrows mark the approximate cutoff locations of the emission filters.

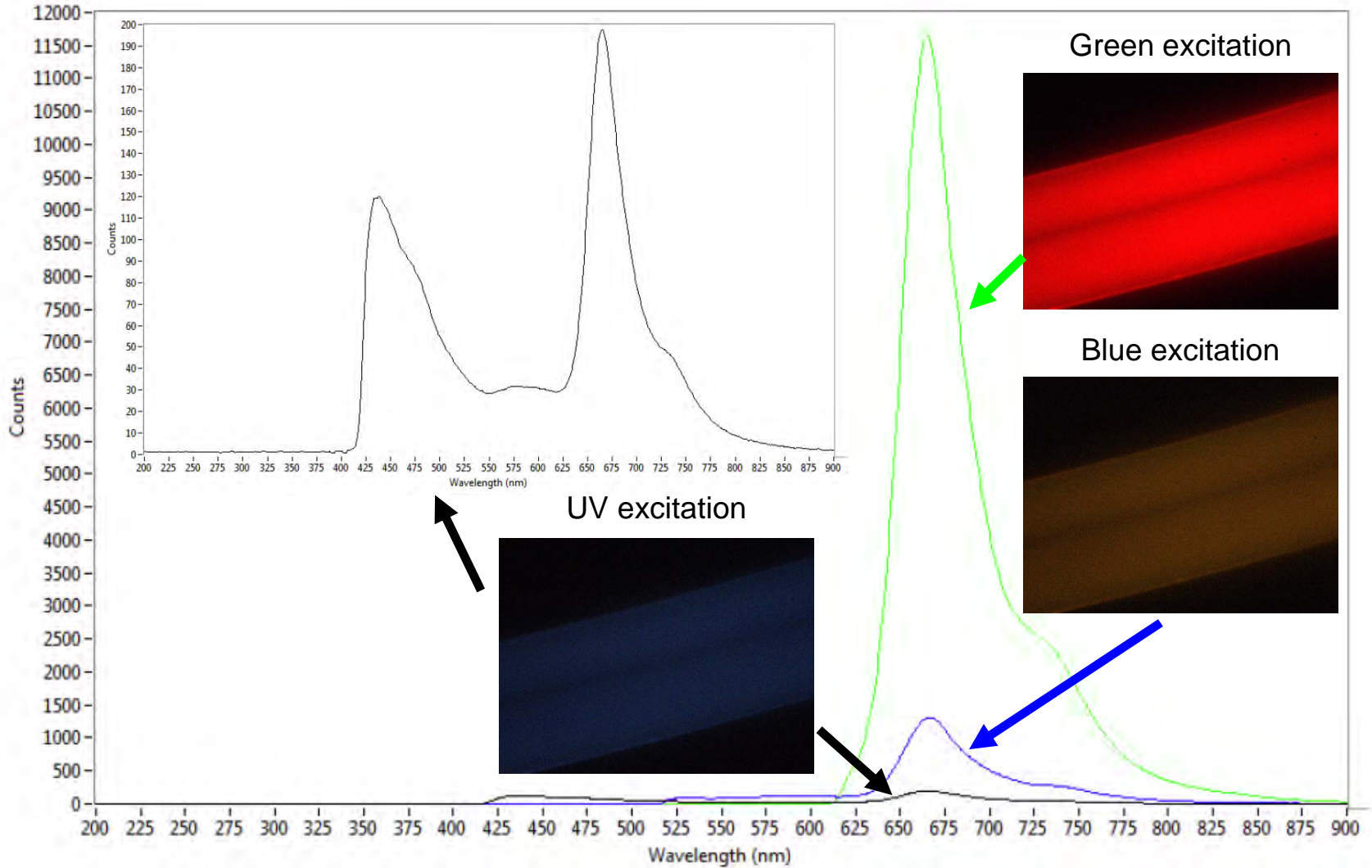


Figure 181. MSF spectra and photomicrographs comparing the fluorescence observed when the same red fiber is illuminated with UV (black), blue (blue), and green (green) light. An ordinate expanded inset of the fiber illuminated with UV light is also shown.

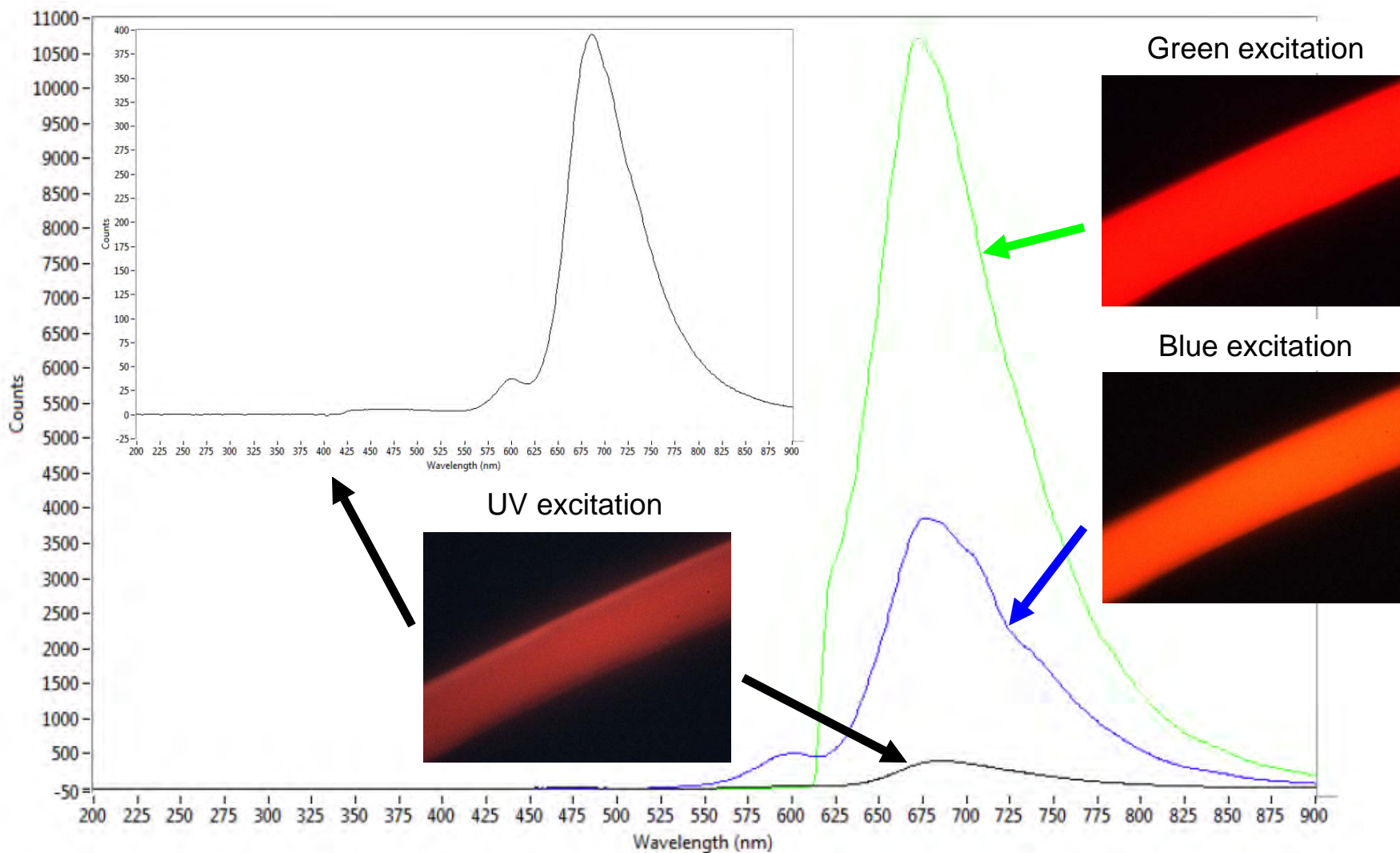


Figure 182. MSF spectra and photomicrographs comparing the fluorescence observed when the same black fiber is illuminated with UV (black), blue (blue), and green (green) light. An ordinate expanded inset of the fiber illuminated with UV light is also shown.

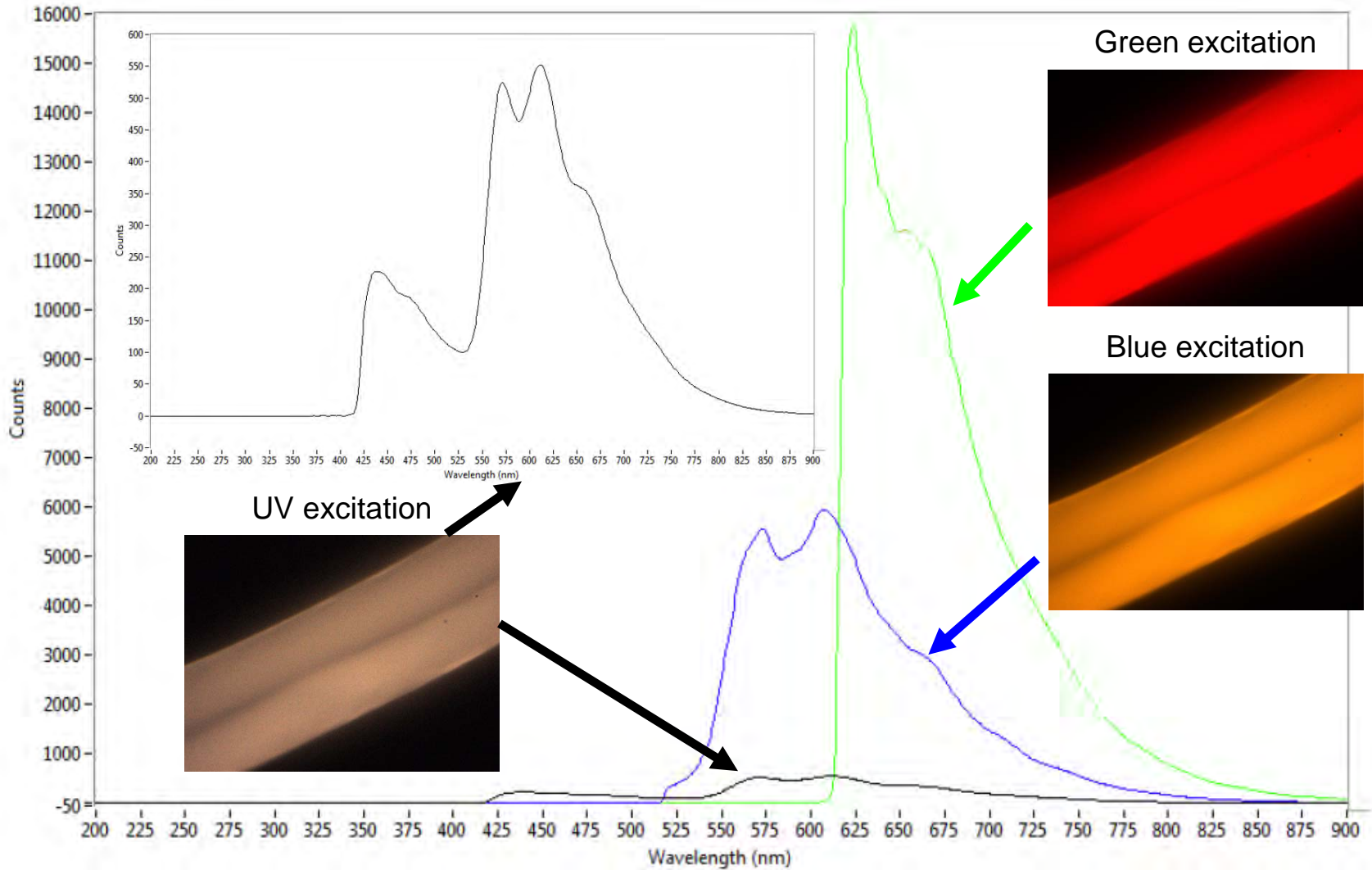


Figure 183. MSF spectra and photomicrographs comparing the fluorescence observed when the same purple fiber is illuminated with UV (black), blue (blue), and green (green) light. An ordinate expanded inset of the fiber illuminated with UV light is also shown.

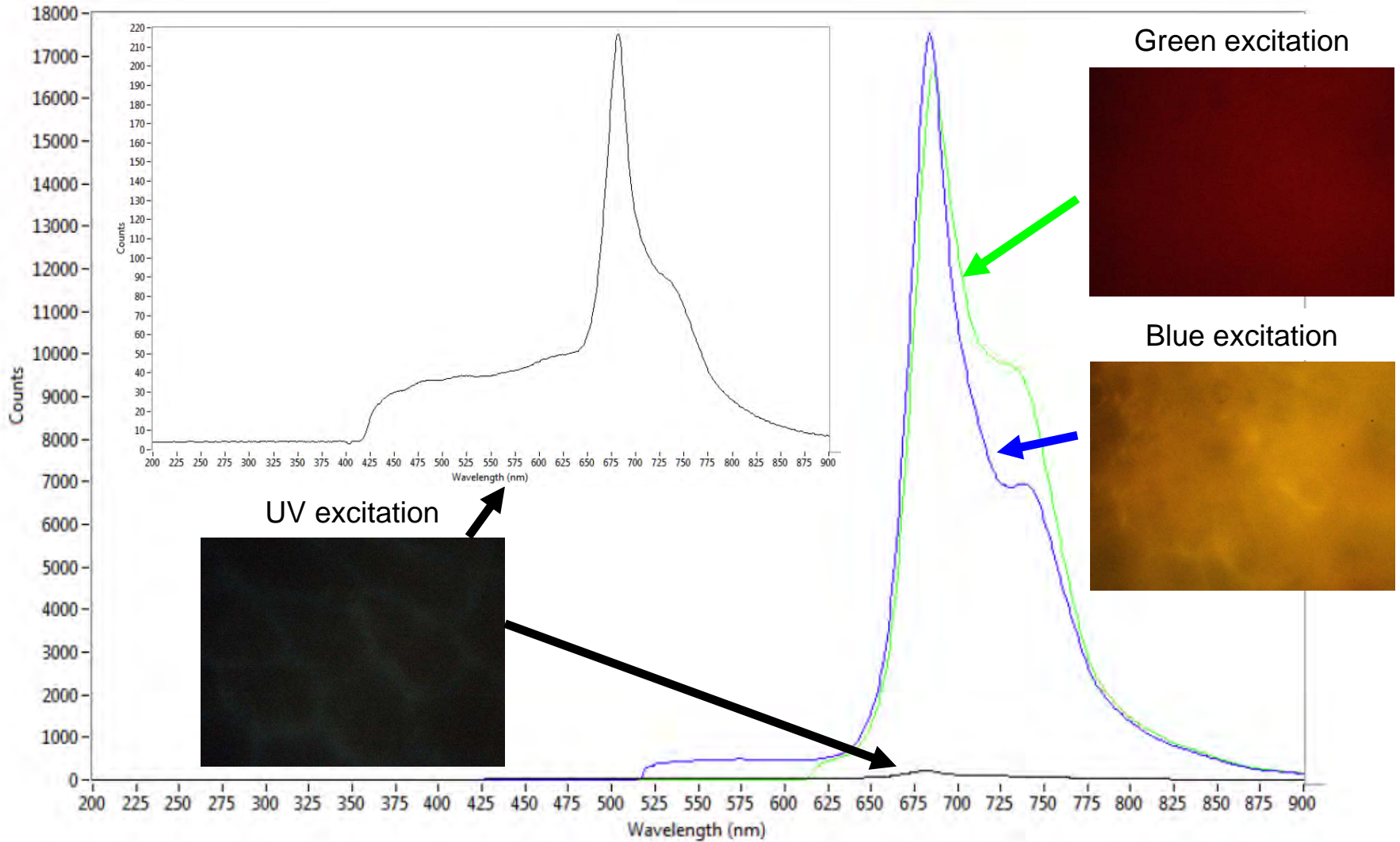


Figure 184. MSF spectra and photomicrographs comparing the fluorescence observed when the a leaf fragment is illuminated with UV (black), blue (blue), and green (green) light. An ordinate expanded inset of the sample illuminated with UV light is also shown (the fluorescence is caused by the chlorophyll in the leaf tissue).

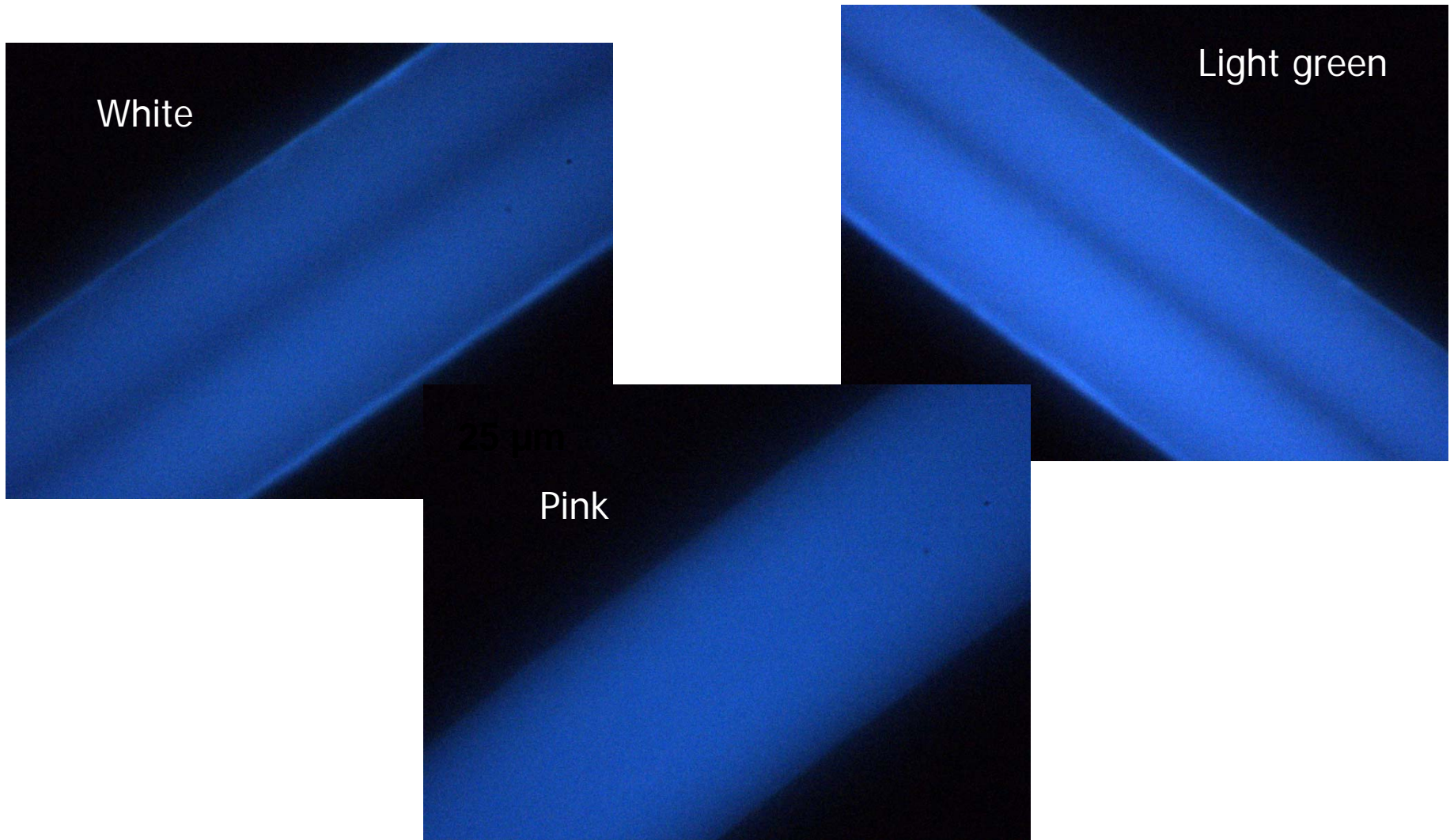


Figure 185. Photomicrographs comparing the fluorescence observed when white, pink and light green fibers are illuminated with UV light.

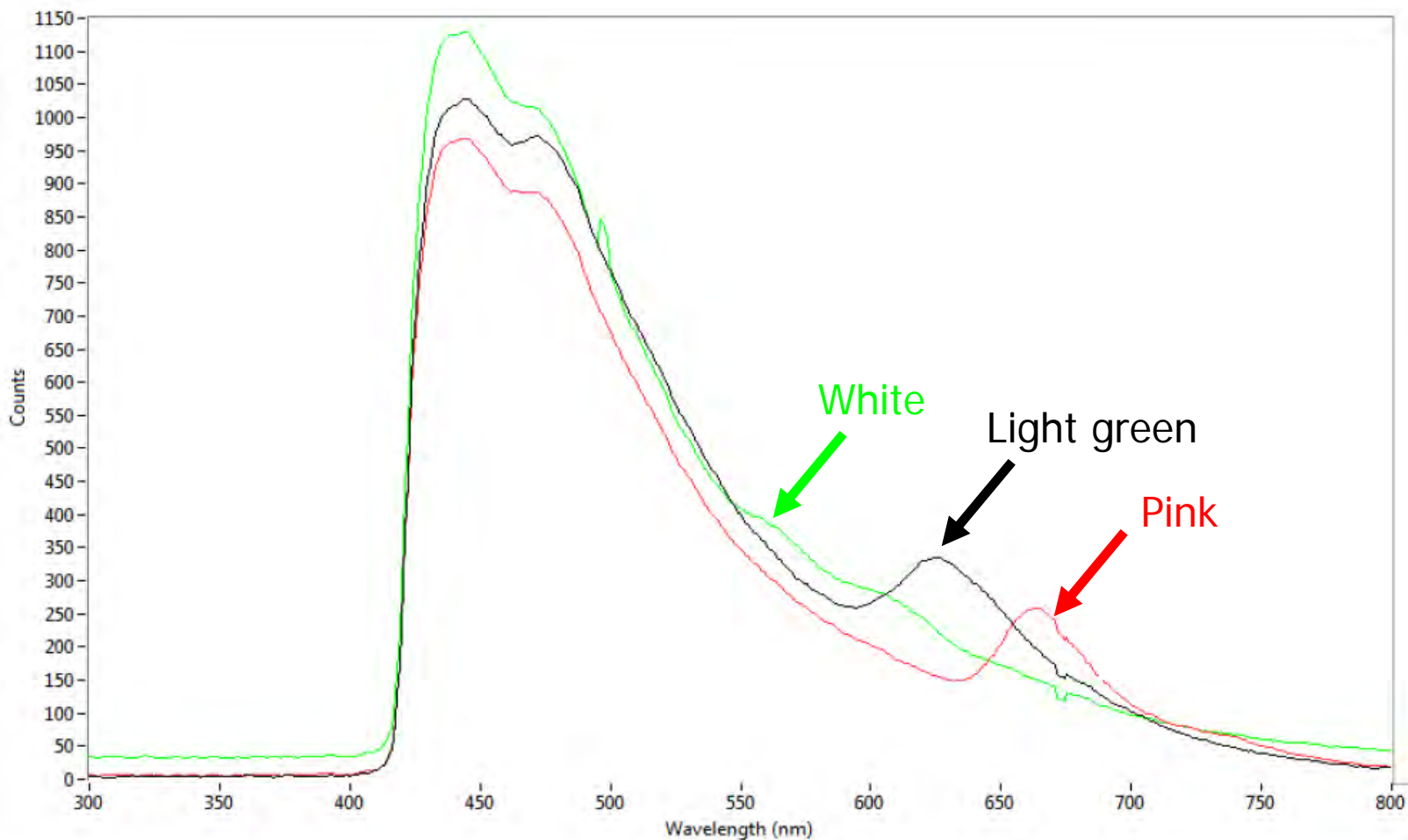


Figure 186. MSF spectra collected the white (green), pink (red), and light green (black) fibers are illuminated with UV light.

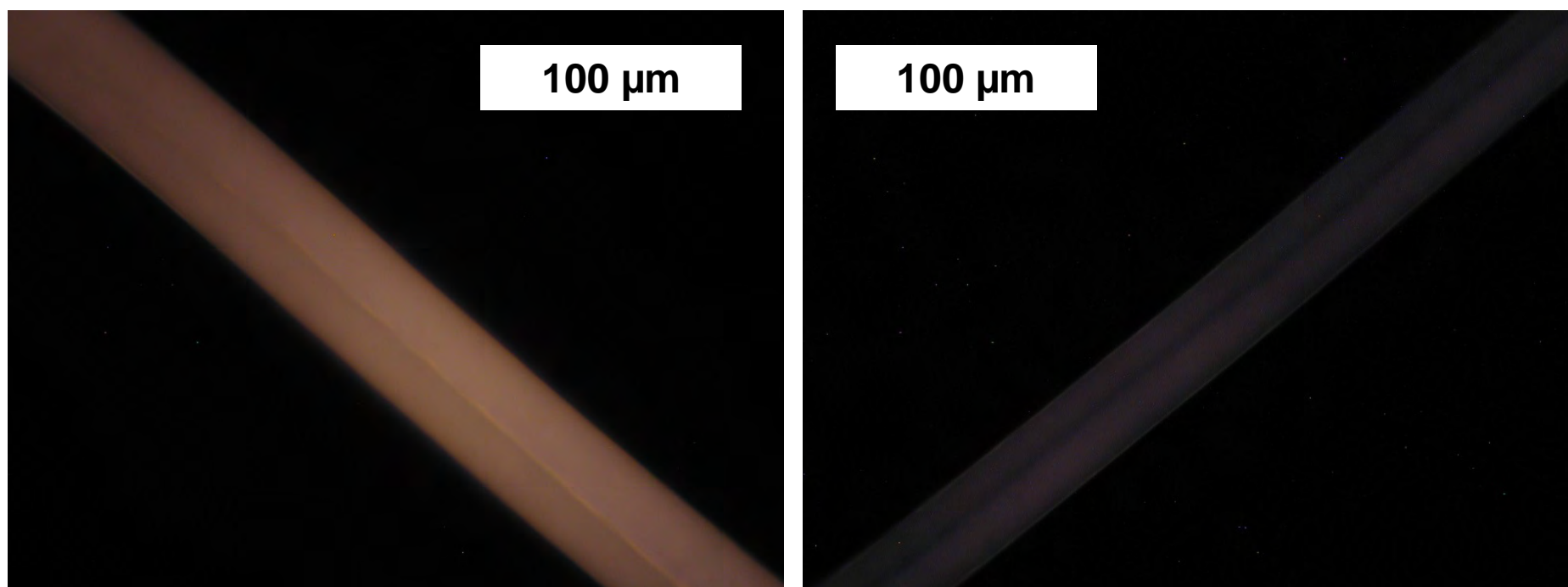


Figure 187. Photomicrographs comparing the fluorescence observed from relatively thick (~45 μm) and thin (~30 μm), mauve colored fibers from the same source (illuminated with UV light).

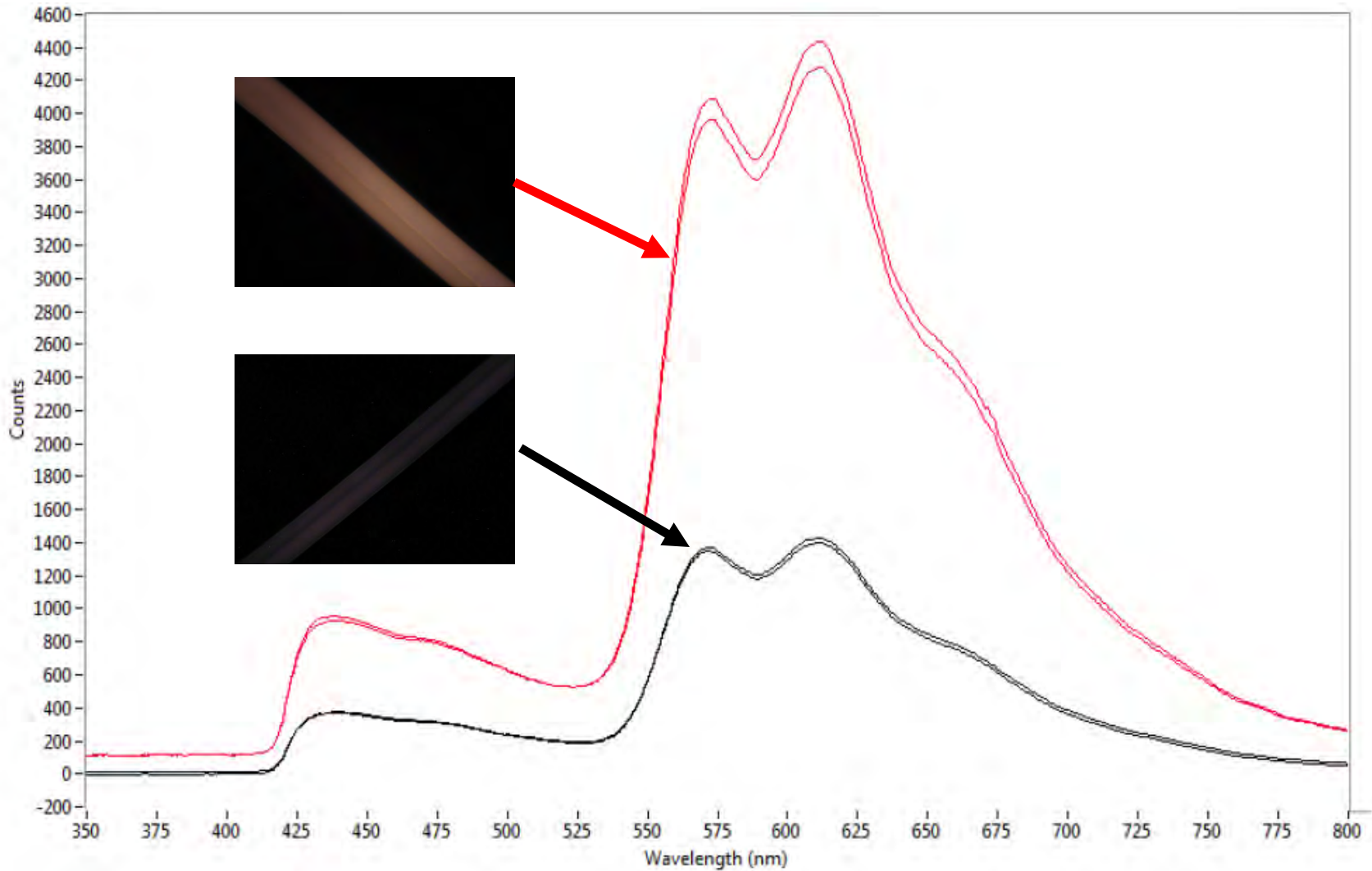


Figure 188. Representative MSF spectra collected from the relatively thick (~45 μm - red) and thin (~30 μm - black) mauve colored fibers illuminated with UV light.

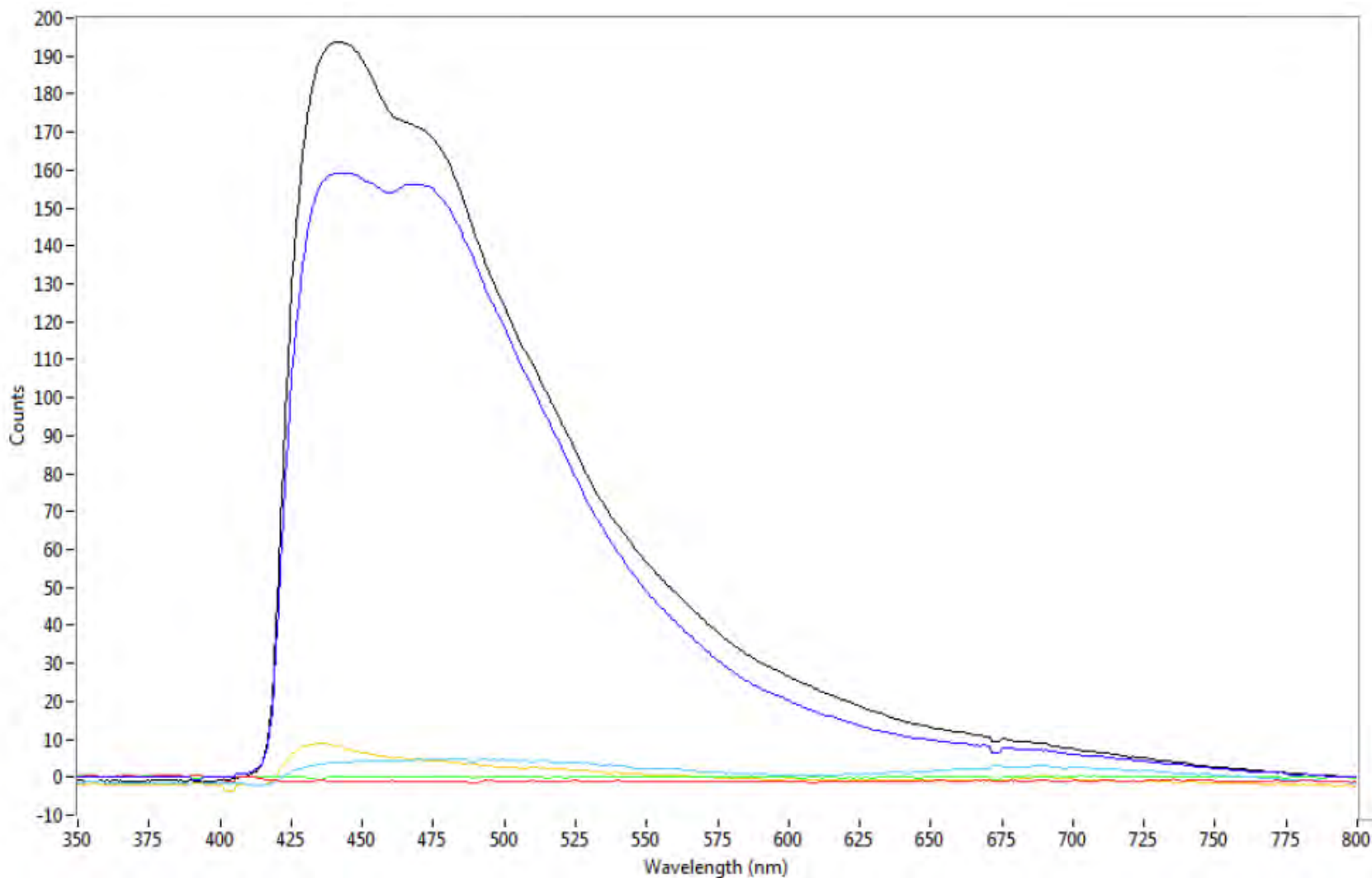


Figure 189. MSF spectra collected from xylene (orange), glycerol (light blue), air (red), water (green), Permout™ (black), and Cargille 1.520 index of refraction oil (blue) using UV excitation.

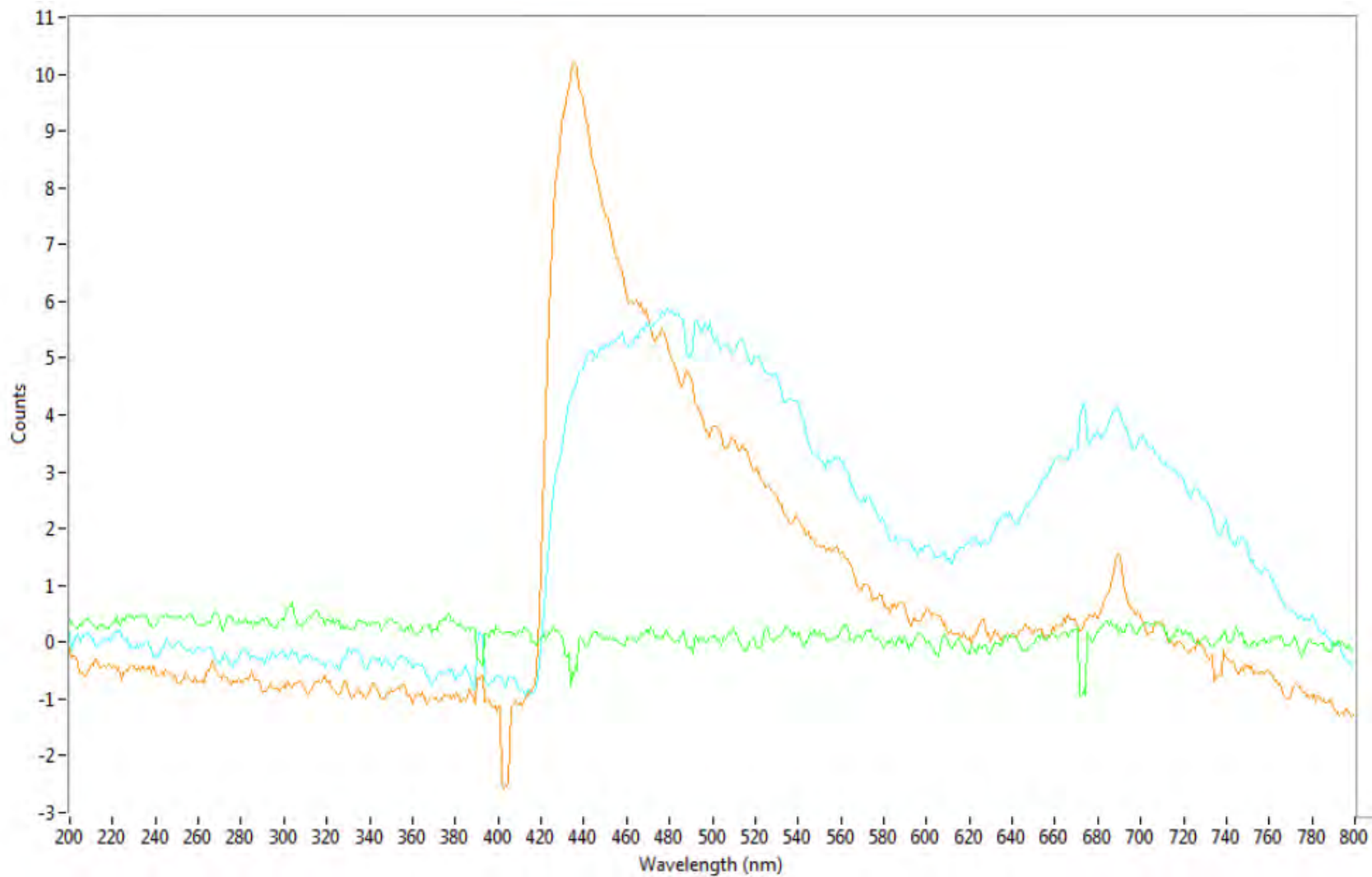


Figure 190. MSF spectra collected from xylene (orange), glycerol (light blue), and water (green) using UV excitation.

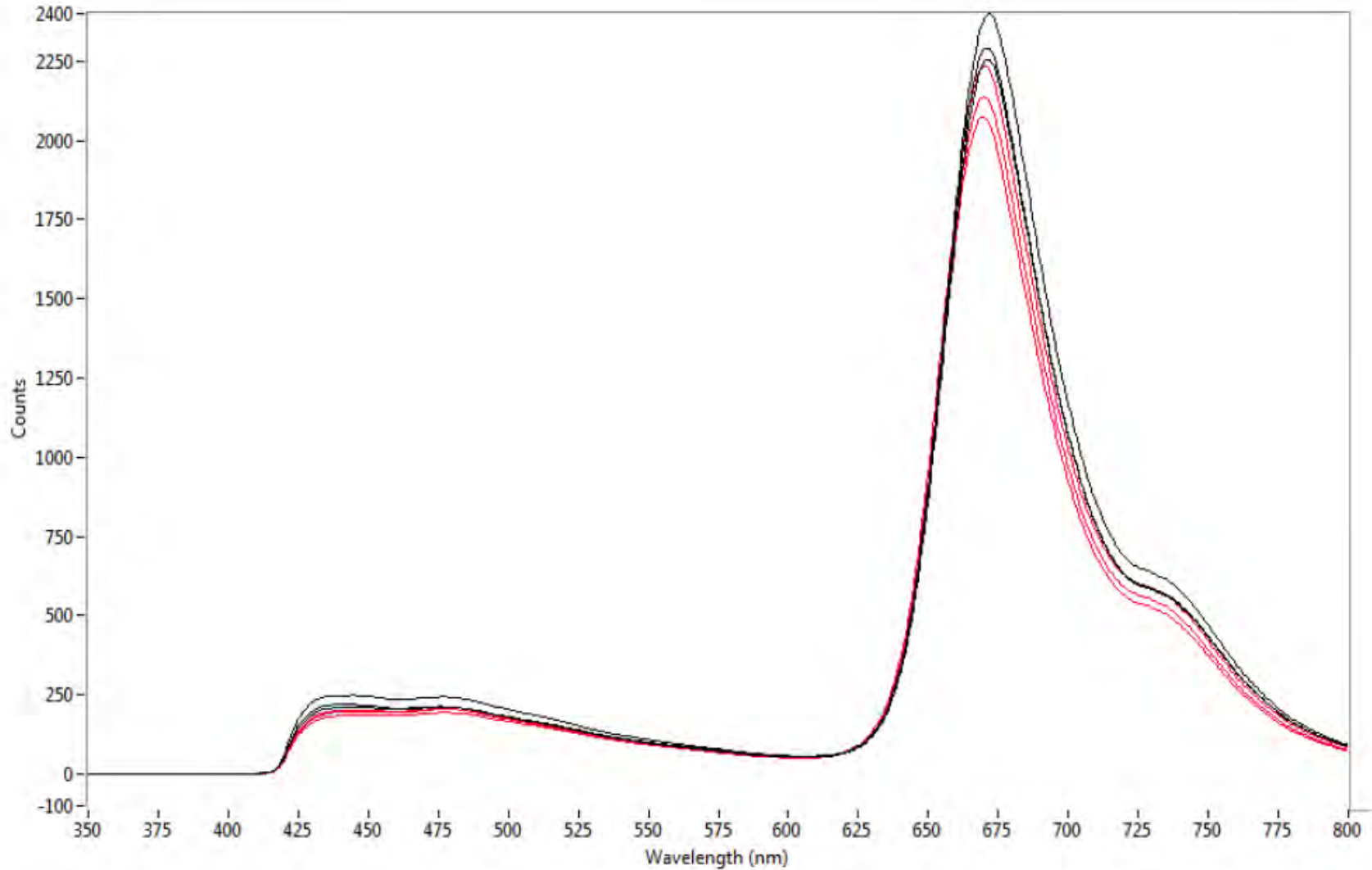


Figure 191. MSF spectra dark green fibers mounted in water (black) and xylene (red). The position of the main peak (~ 670 nm) is located at slightly higher wavelengths when the fibers are mounted in water compared to xylene.

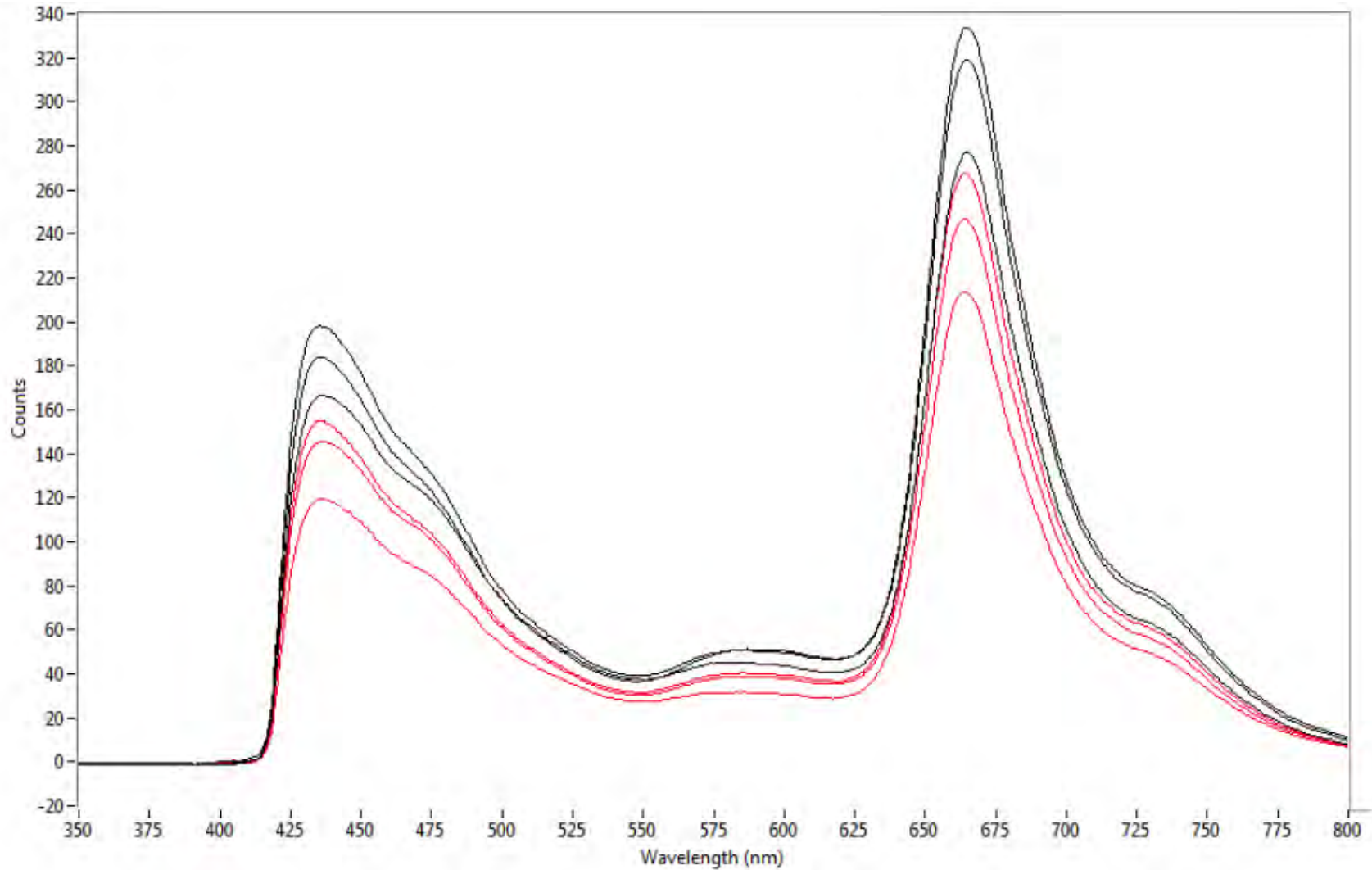


Figure 192. MSF spectra dark red fibers mounted in water (black) and xylene (red). The position of the main peak (~ 665 nm) is located at slightly higher wavelengths when the fibers are mounted in water compared to xylene.

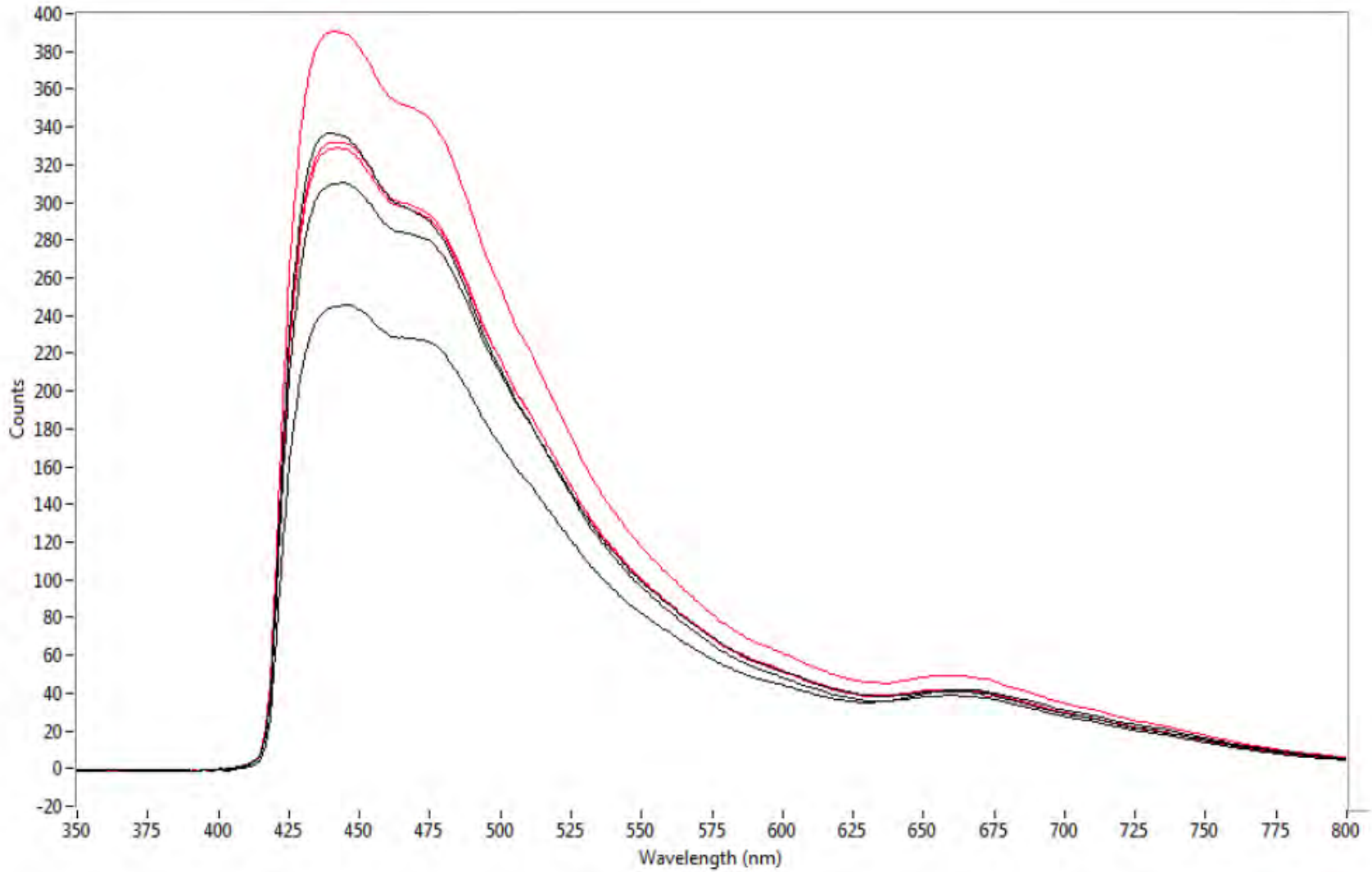


Figure 193. MSF spectra from dark blue fibers mounted in water (black) and xylene (red).

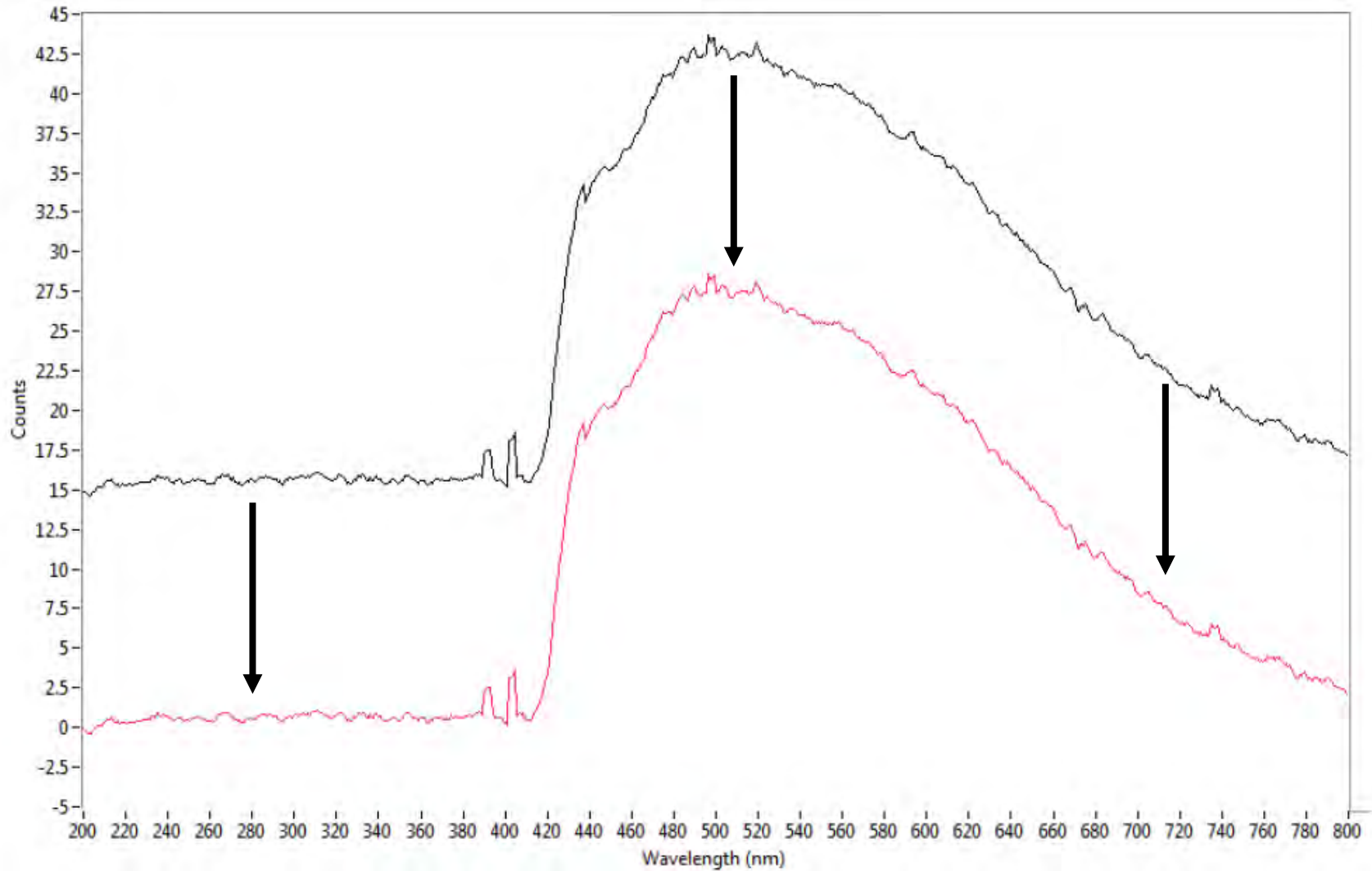


Figure 194. Resultant MSF spectrum (red) after 15 counts were subtracted from the originally collected spectrum (black) in an effort to compensate for dark scan drift.

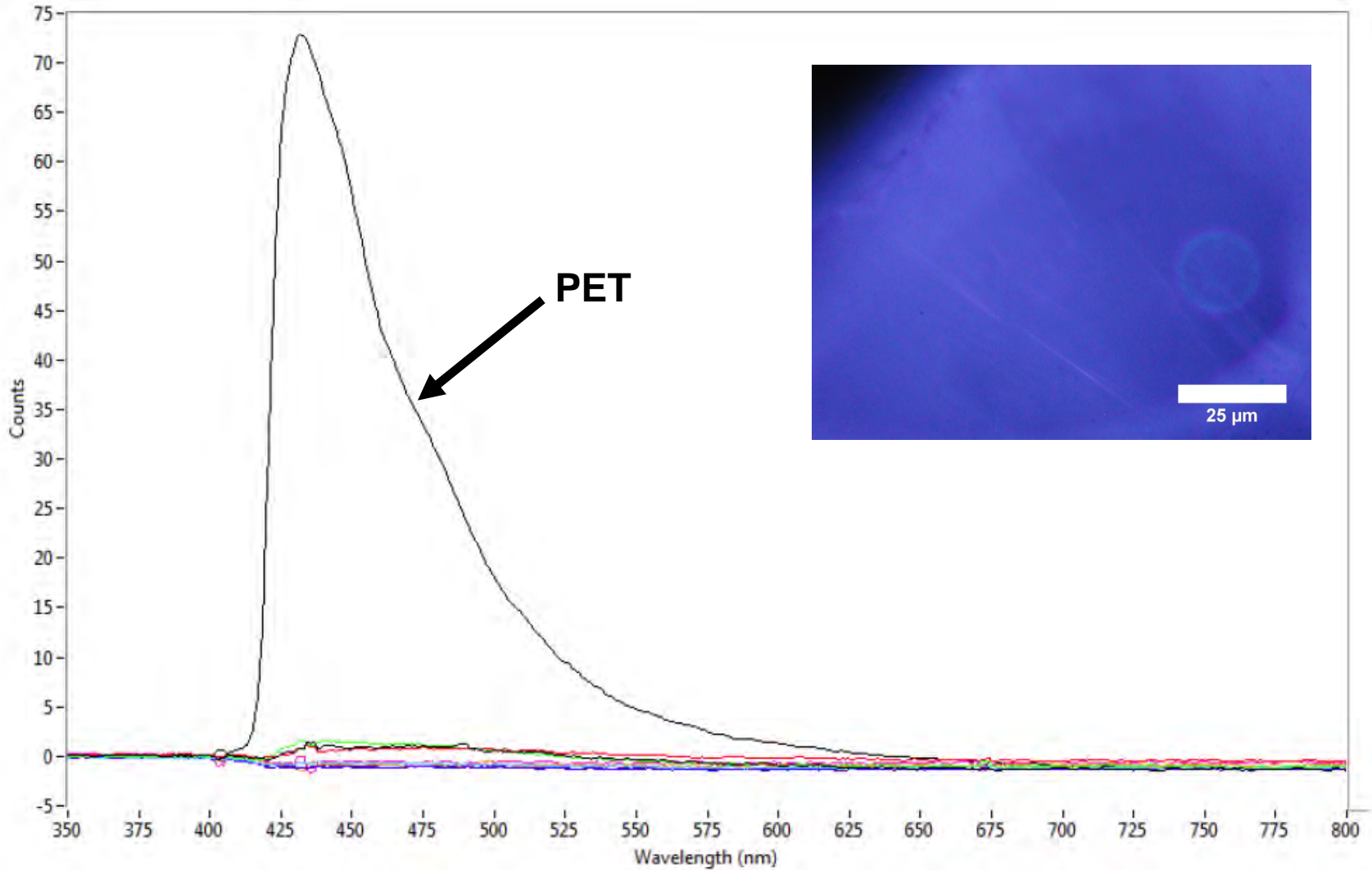


Figure 195. MSF spectrum of PET compared to the MSF spectra collected from the other polymers (UV excitation). A photomicrograph illustrates the color observed when PET is viewed using UV excitation.

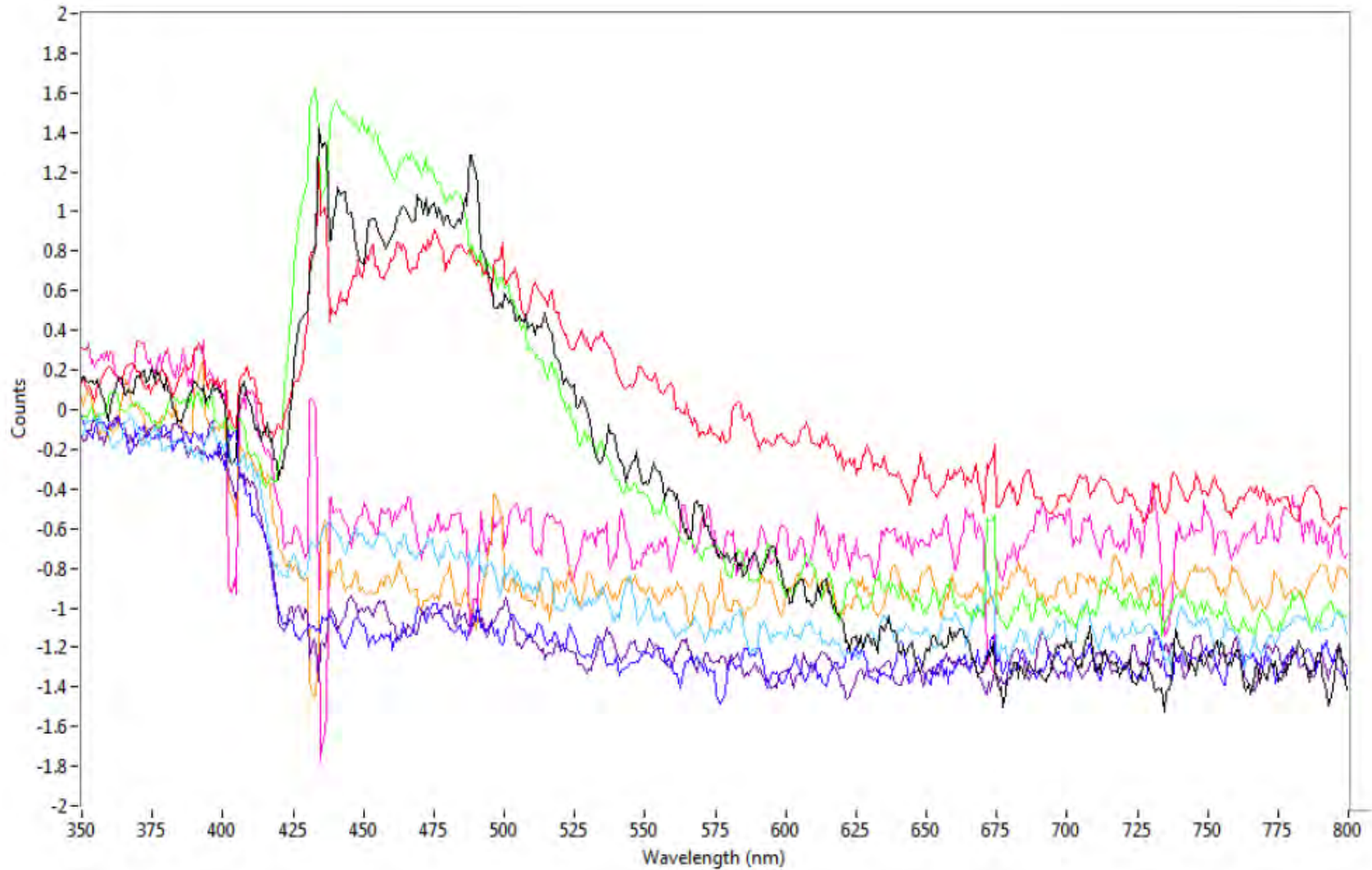


Figure 196. MSF spectra of known cellulose acetate (black), CTA (red), nylon 6 (green), nylon 6/6 (light blue), HDPE (blue), LDPW (purple), PMMA (orange), PP (pink) using UV excitation.

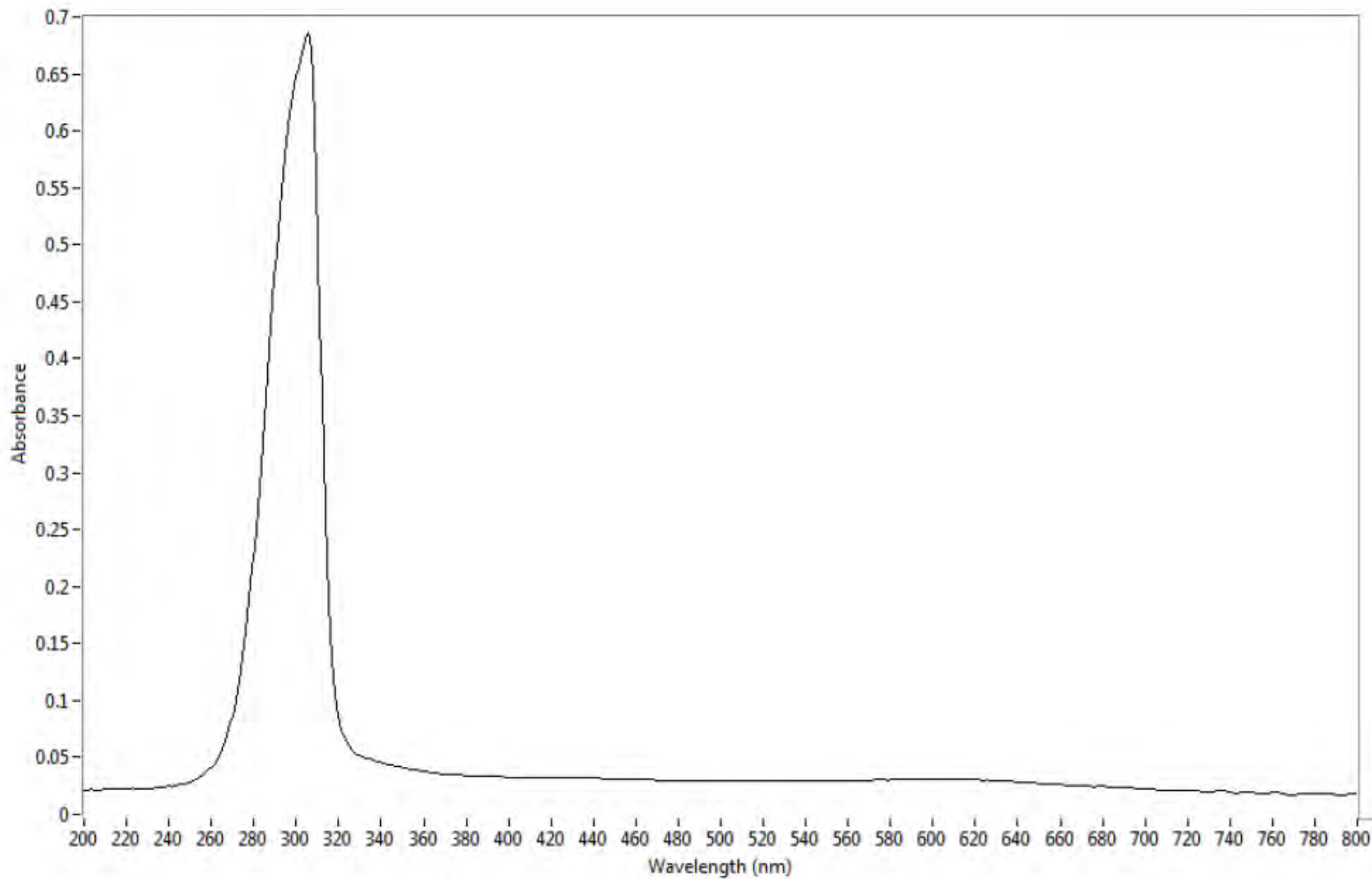


Figure 197. MSP spectrum of known PET.

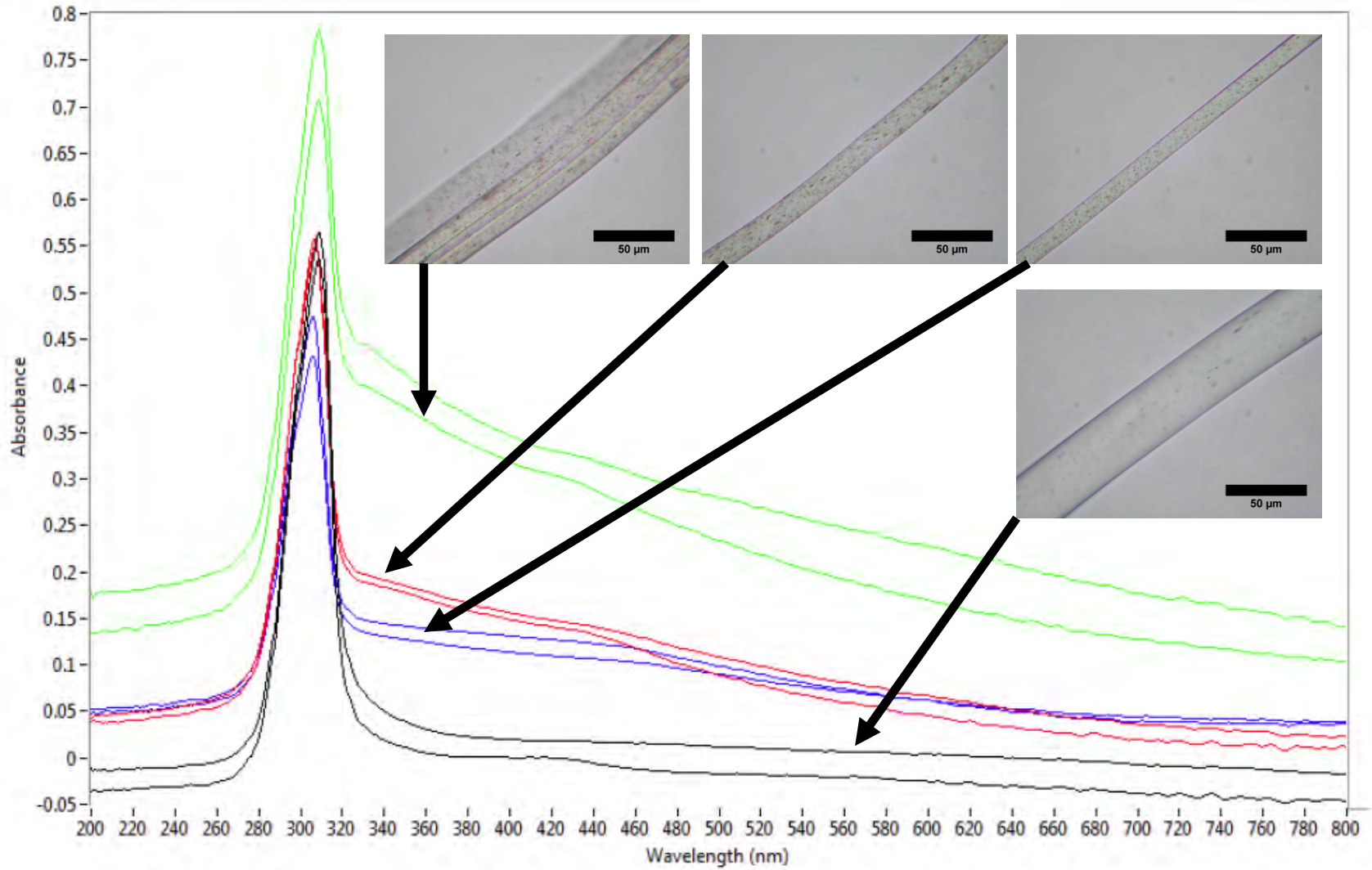


Figure 198. MSP spectra (averages from two fibers) and photomicrographs from four different colorless PET fiber types.

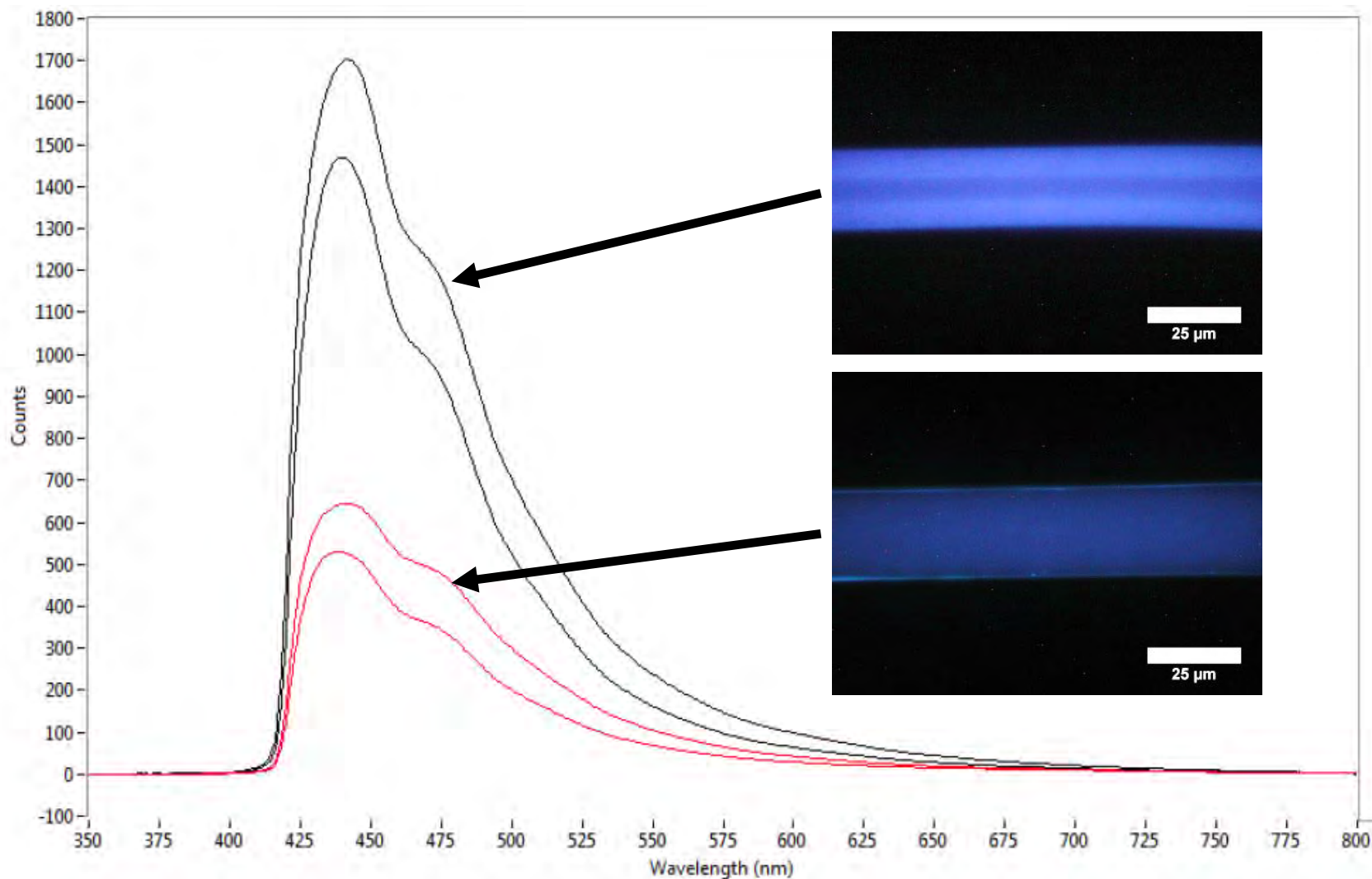


Figure 199. MSF spectra (averages from two fibers) and photomicrographs from the two thicker colorless PET fiber types. All of the spectra and photomicrographs were collected using the same parameters.

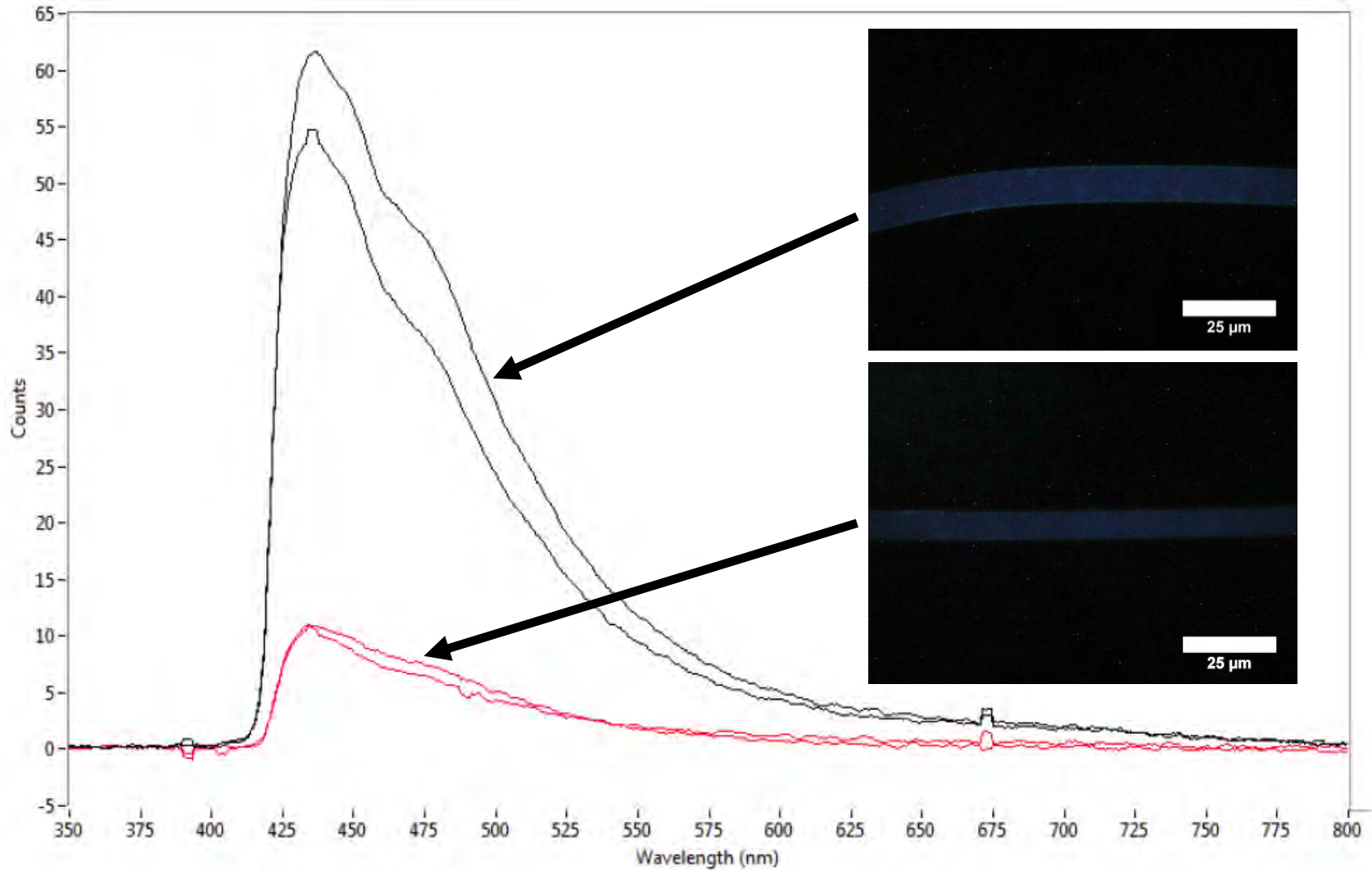


Figure 200. MSF spectra (averages from two fibers) and photomicrographs from the two thinner colorless PET fiber types. All of the spectra and photomicrographs were collected using the same parameters.

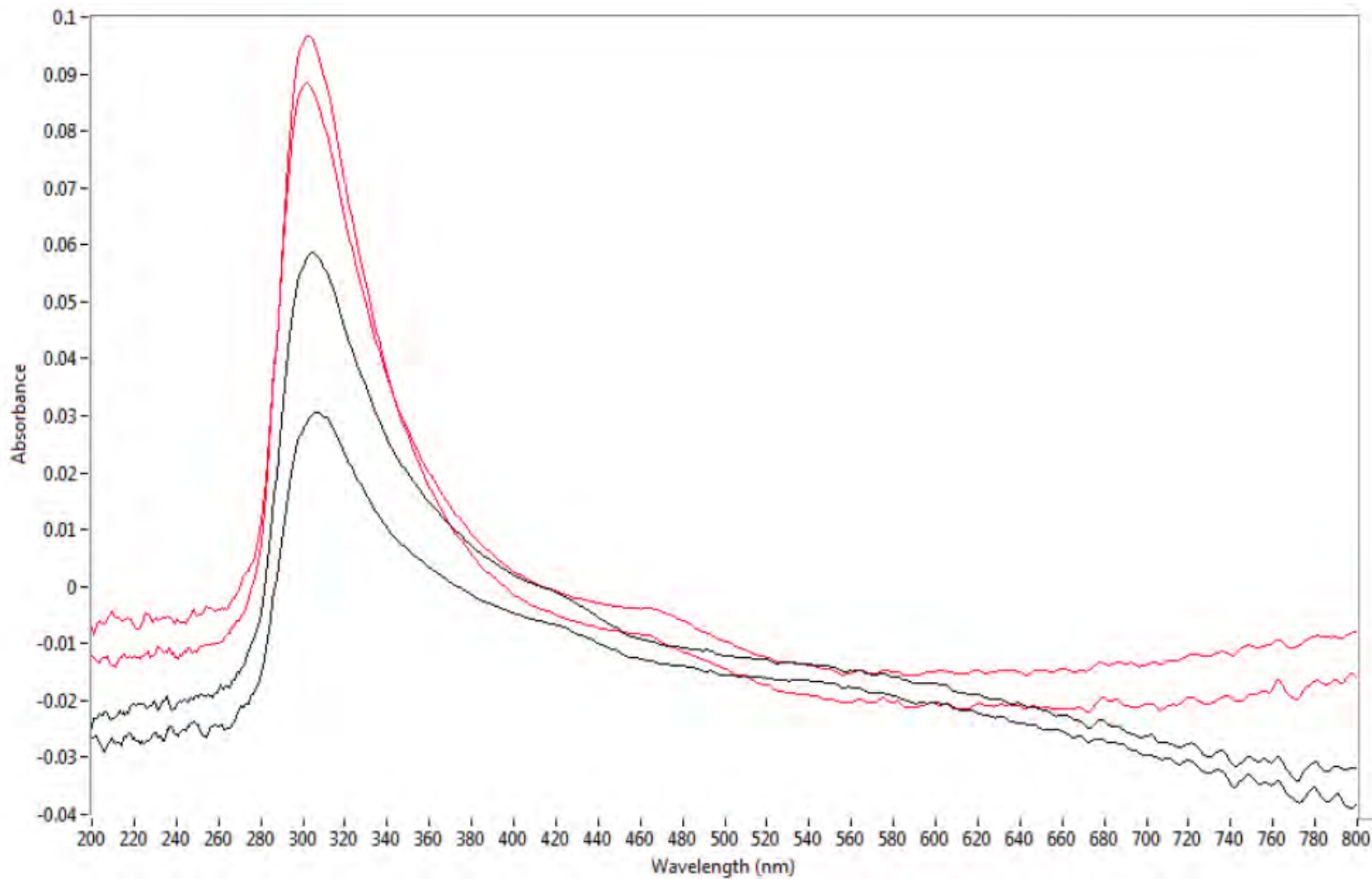


Figure 201. MSP spectra (averages from two fibers) from two different colorless acrylic fiber types.

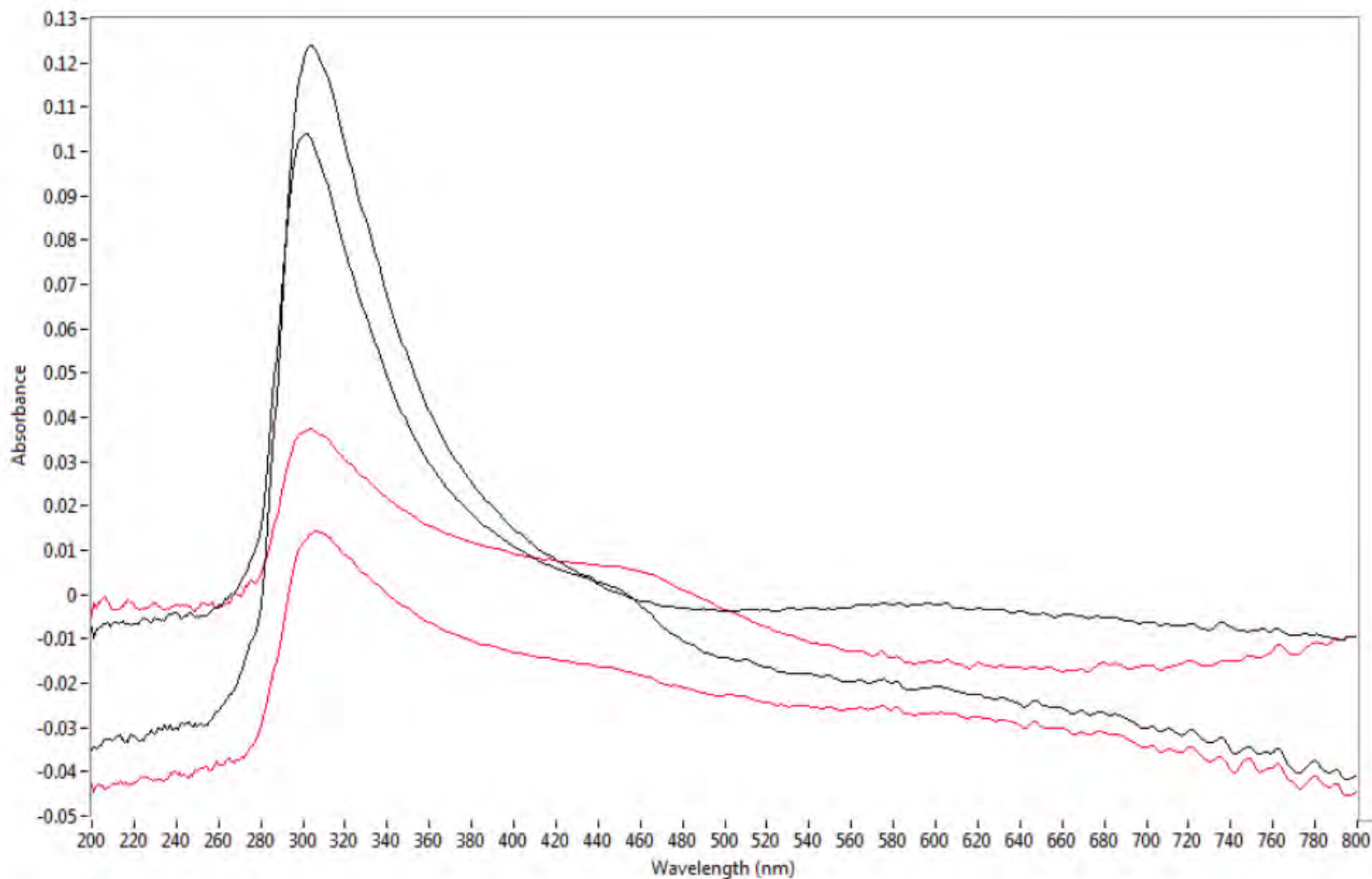


Figure 202. MSP spectra (averages from two fibers) from two different colorless modacrylic fiber types.

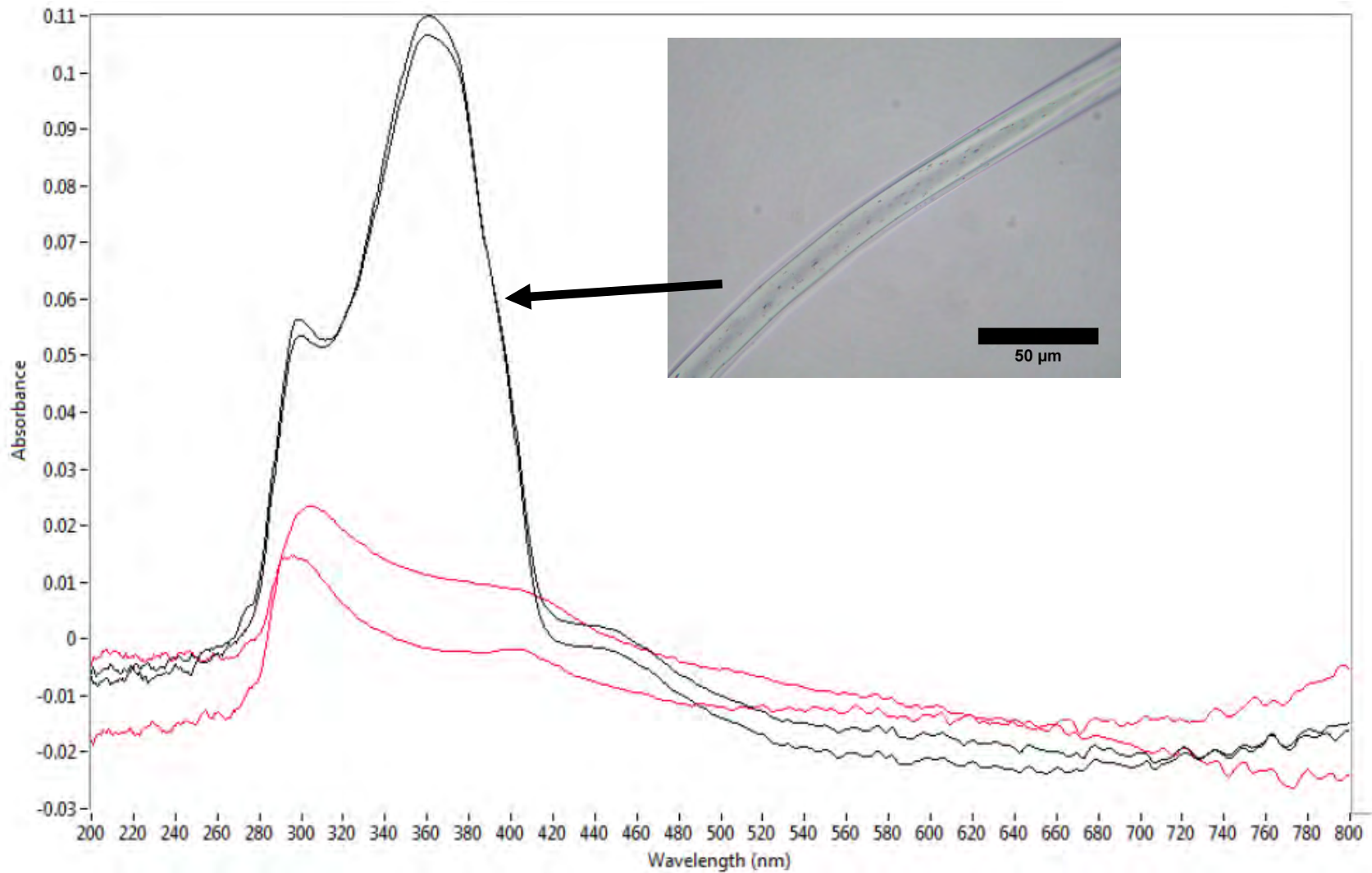


Figure 203. MSP spectra (averages from two fibers) from two different colorless nylon fiber types. A photomicrograph inset is shown of one of the nylon fibers which has an unexplained absorbance at ~ 360 nm.

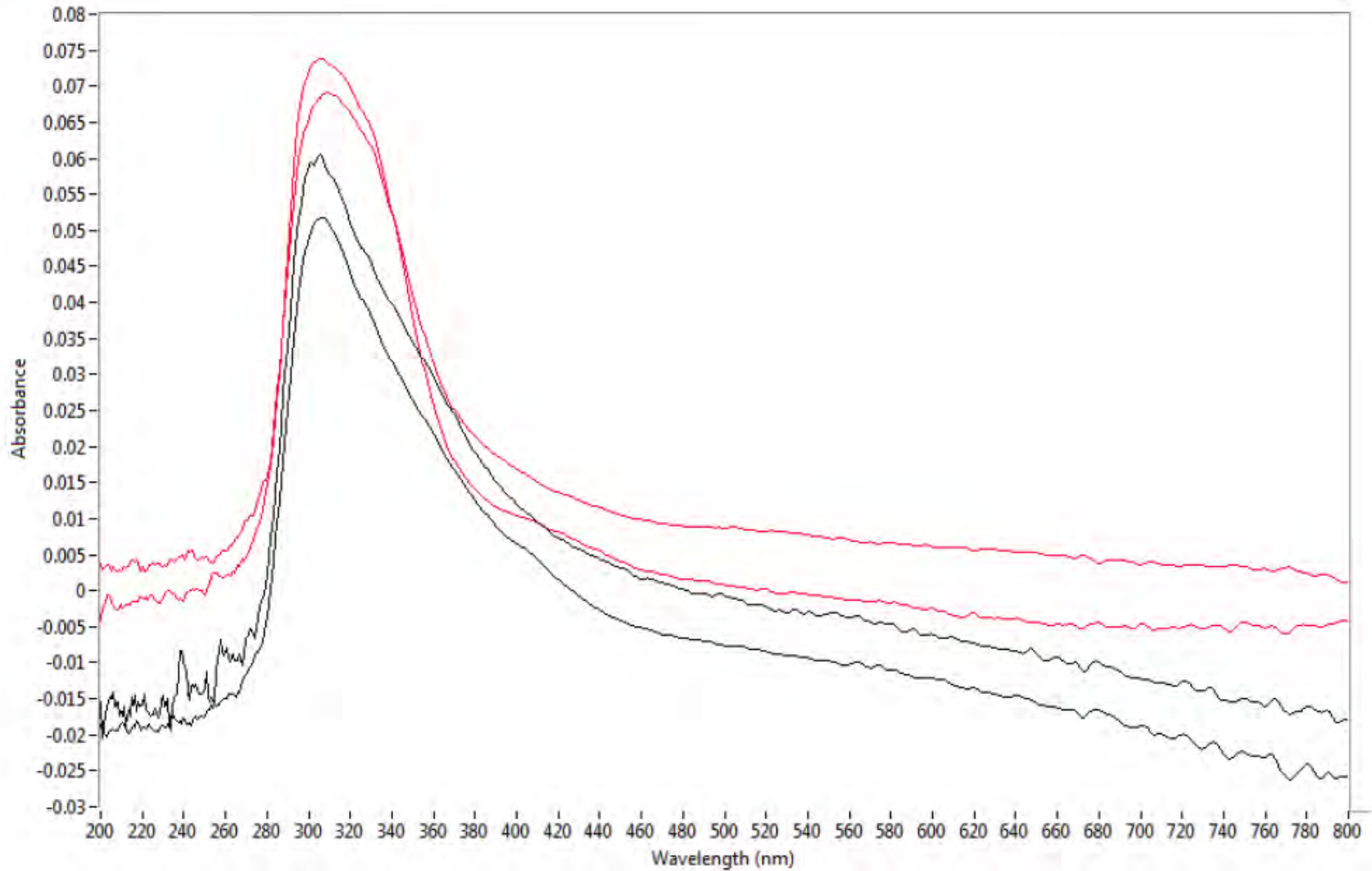


Figure 204. MSP spectra (averages from two fibers) from two different colorless polypropylene fiber types.

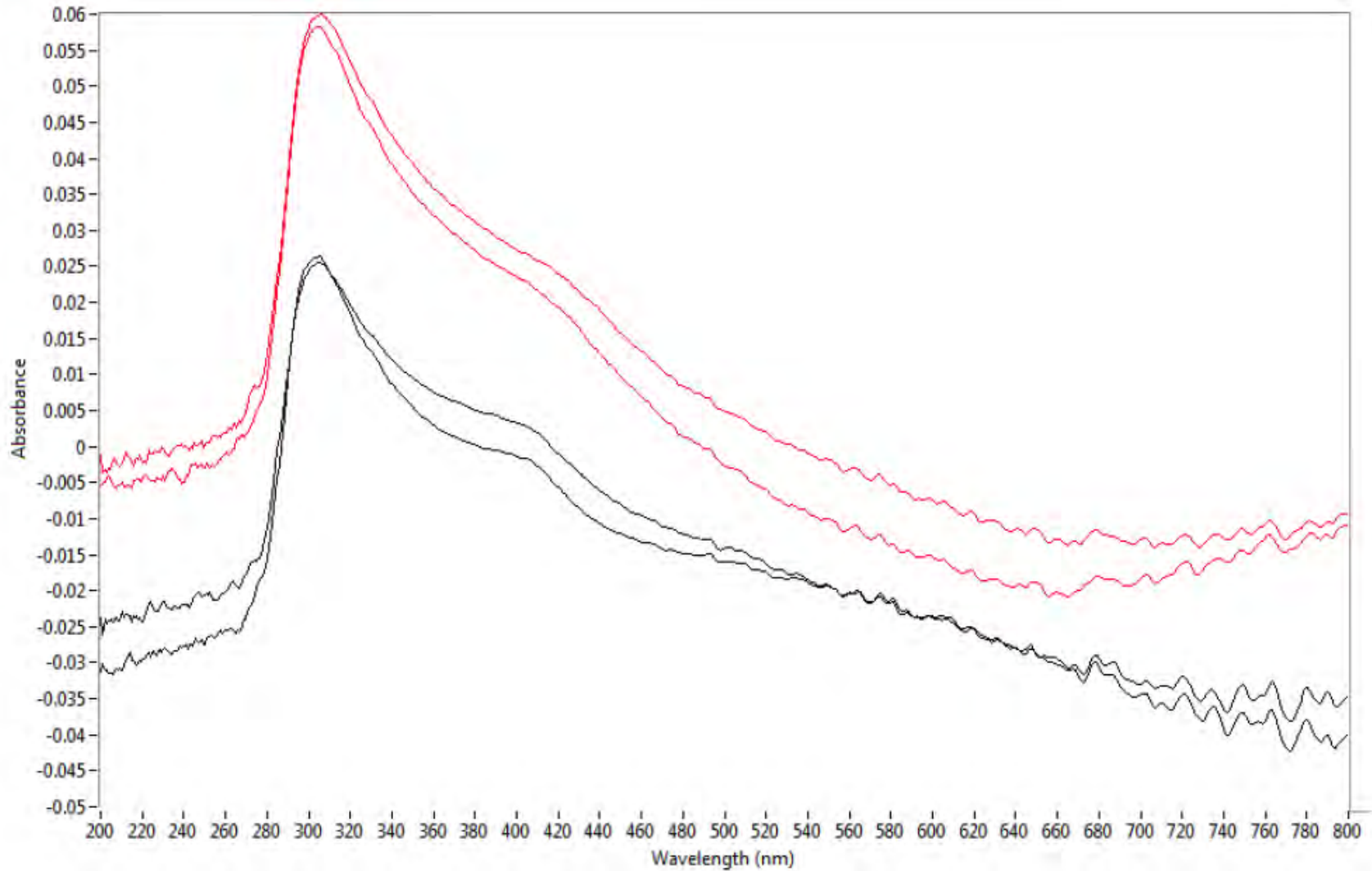


Figure 205. MSP spectra (averages from two fibers) from two different colorless rayon fiber types.

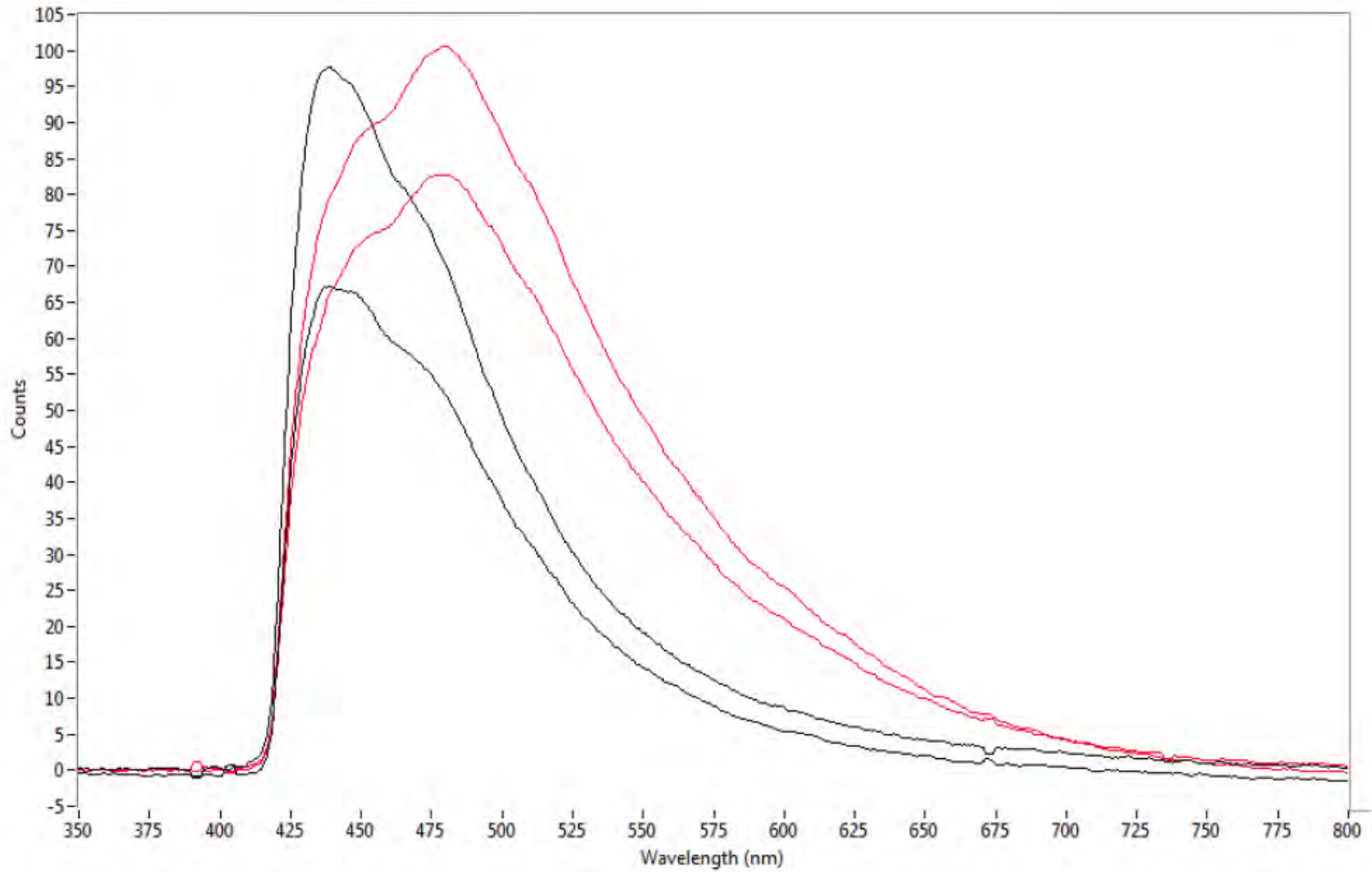


Figure 206. MSF spectra (averages from two fibers) from two different colorless acrylic fiber types.

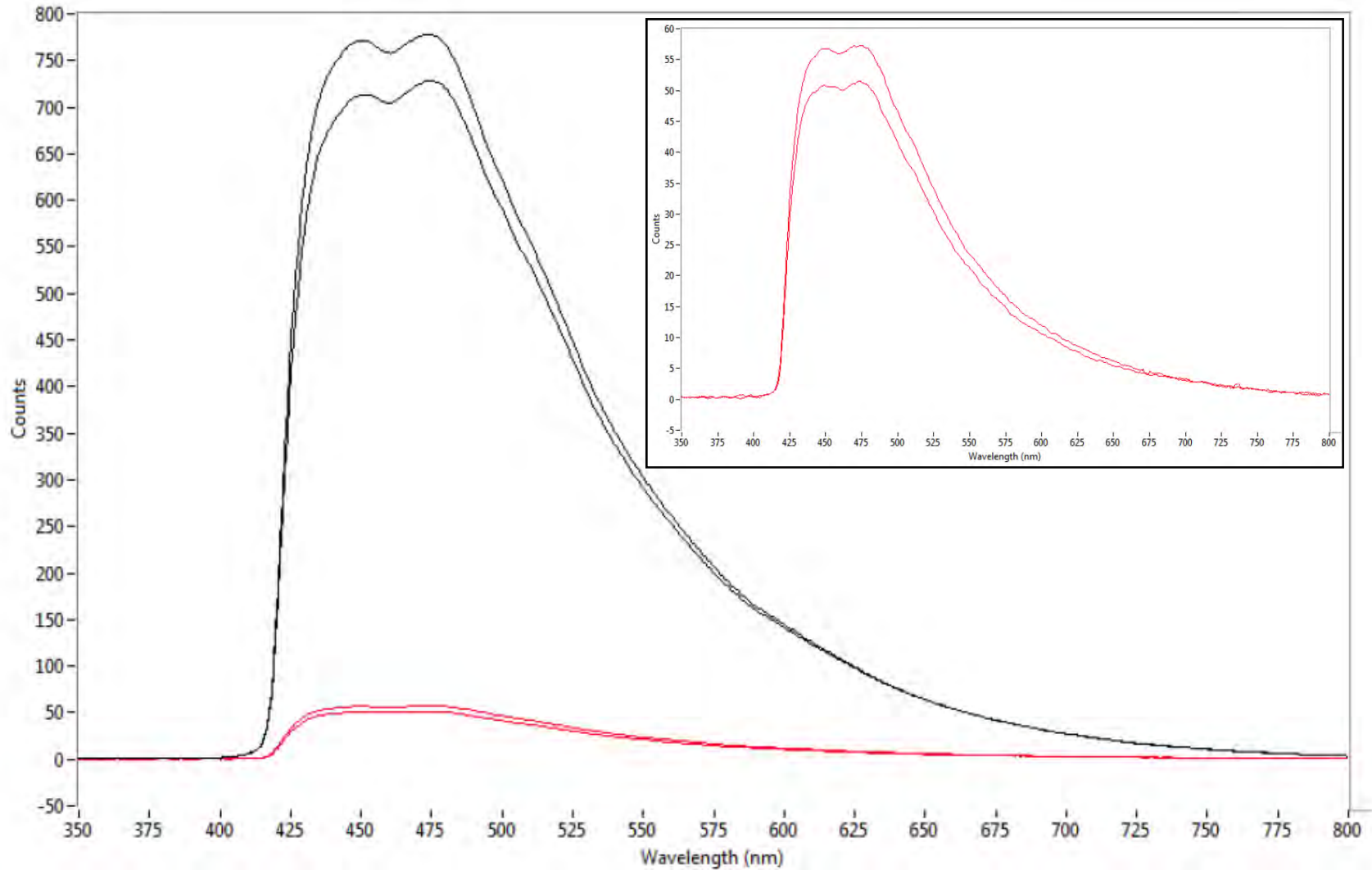


Figure 207. MSF spectra (averages from two fibers) from two different colorless modacrylic fiber types. An inset shows a close-up view of the fibers with lower fluorescence.

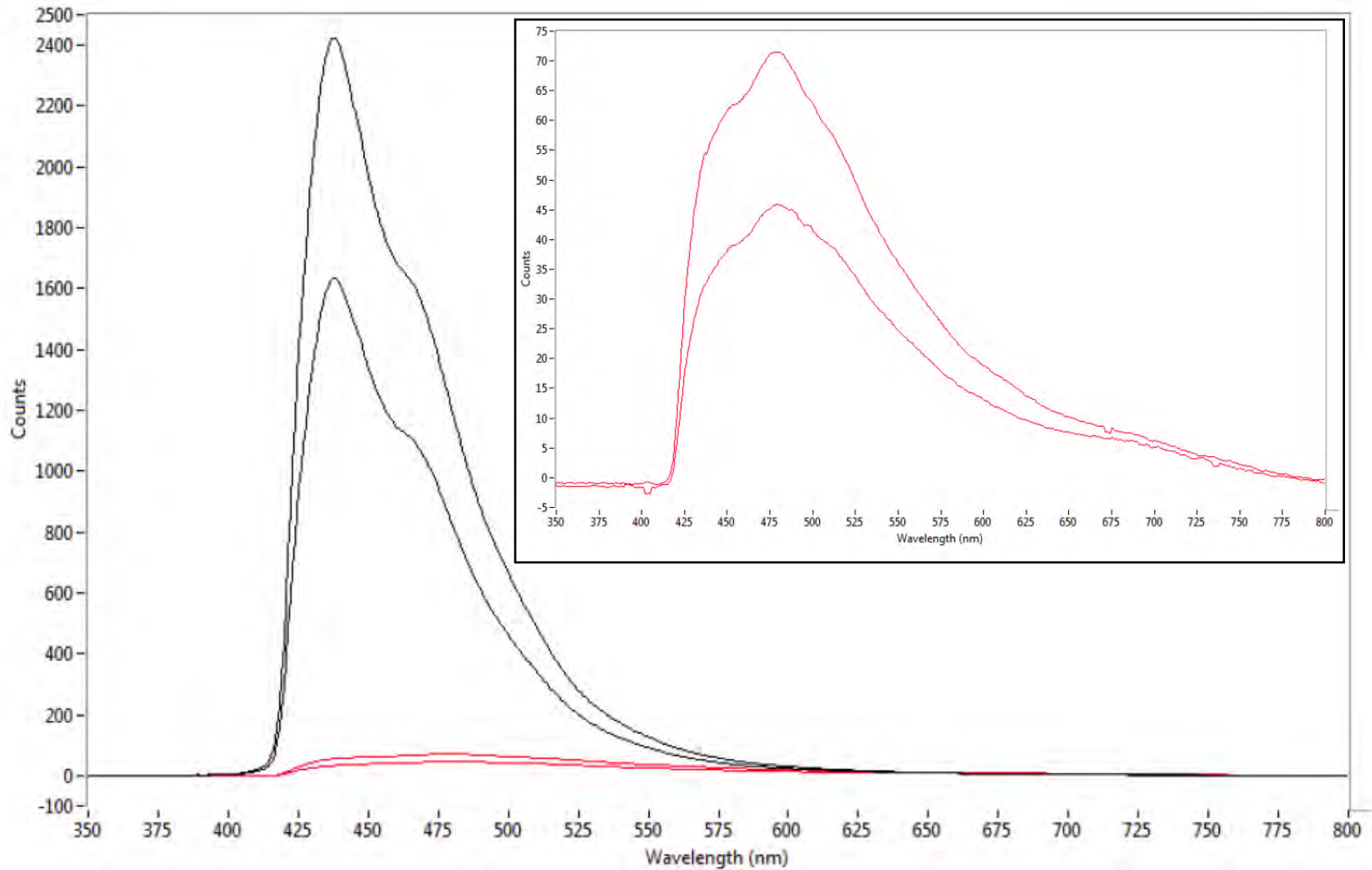


Figure 208. MSF spectra (averages from two fibers) from two different colorless nylon fiber types. An inset shows a close-up view of the fibers with lower fluorescence.

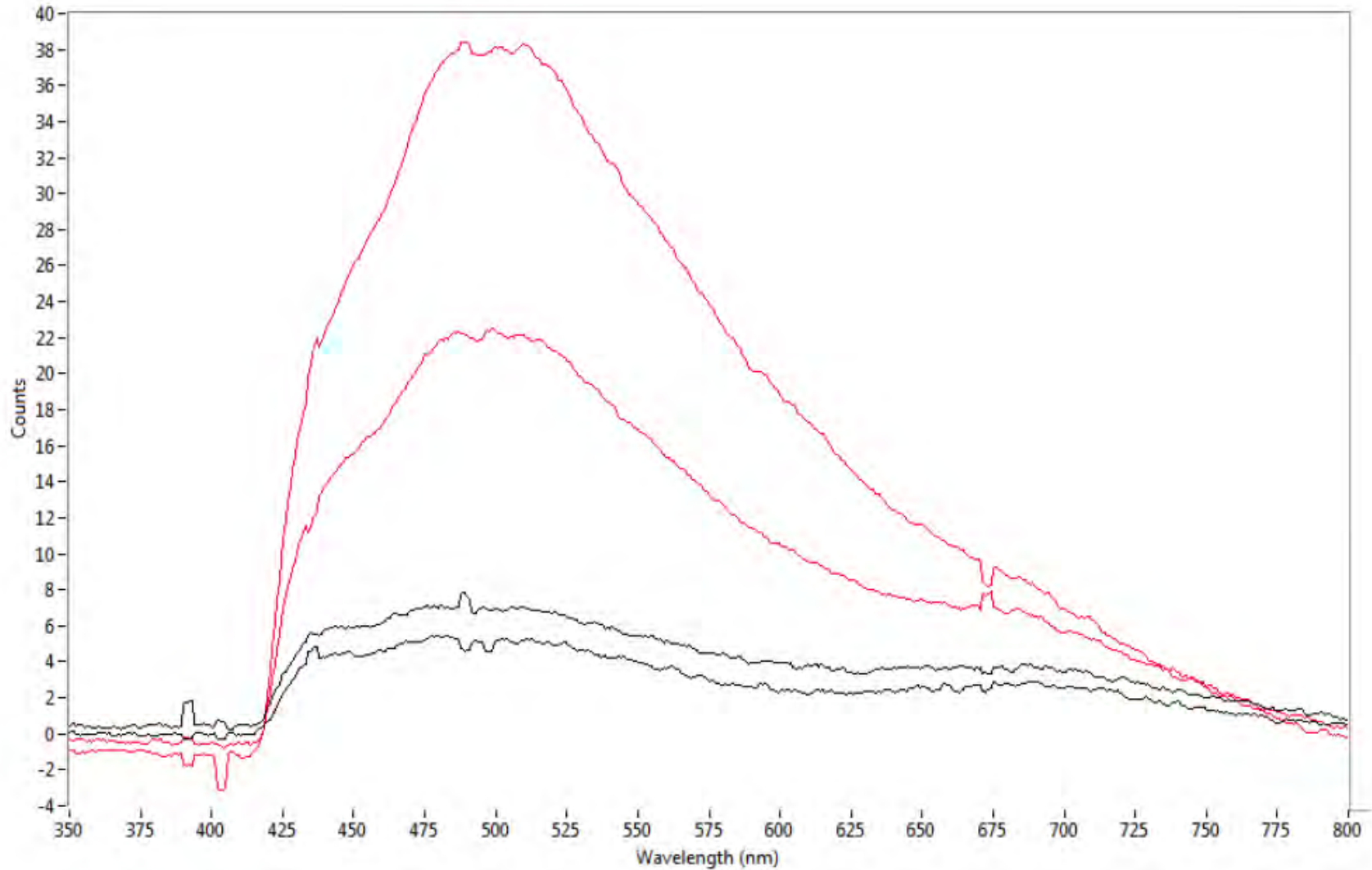


Figure 209. MSF spectra (averages from two fibers) from two different colorless polypropylene fiber types.

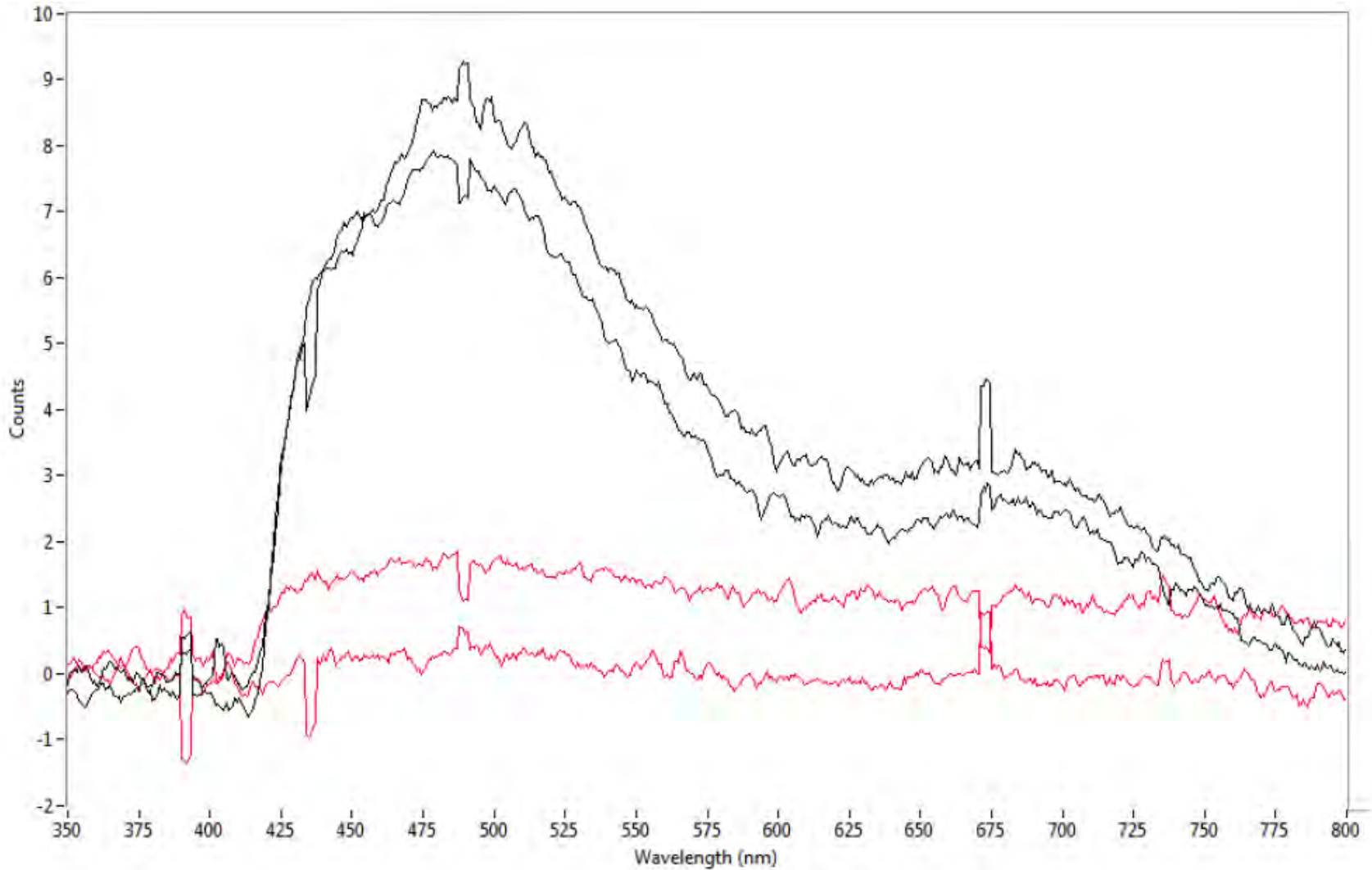


Figure 210. MSF spectra (averages from two fibers) from two different colorless rayon fiber types.

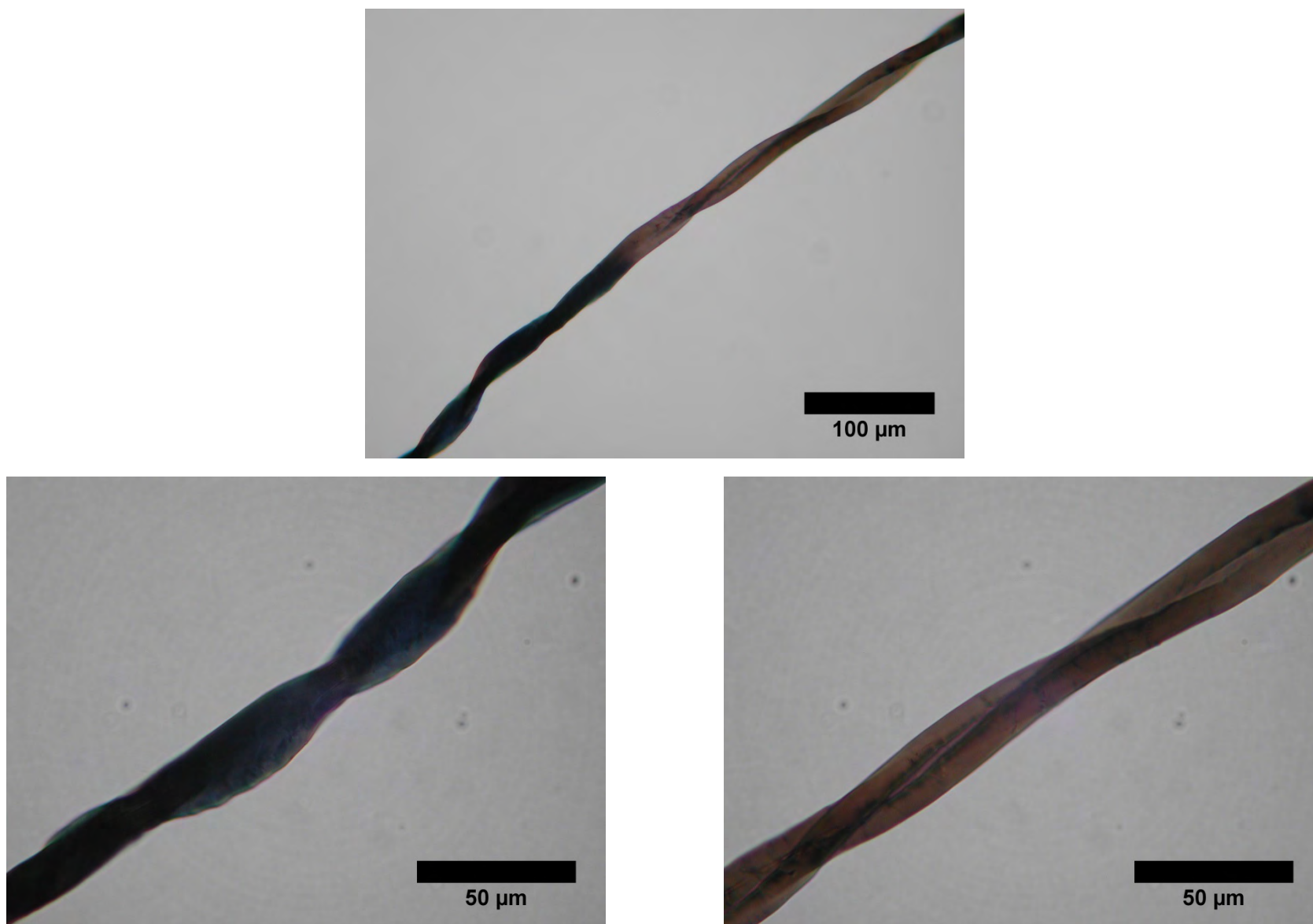


Figure 211. Photomicrographs of the differentially dyed cotton fiber (center) with close-up images of the deep blue (left) and brown (right) areas) (mounted in xylene and viewed using transmitted light).

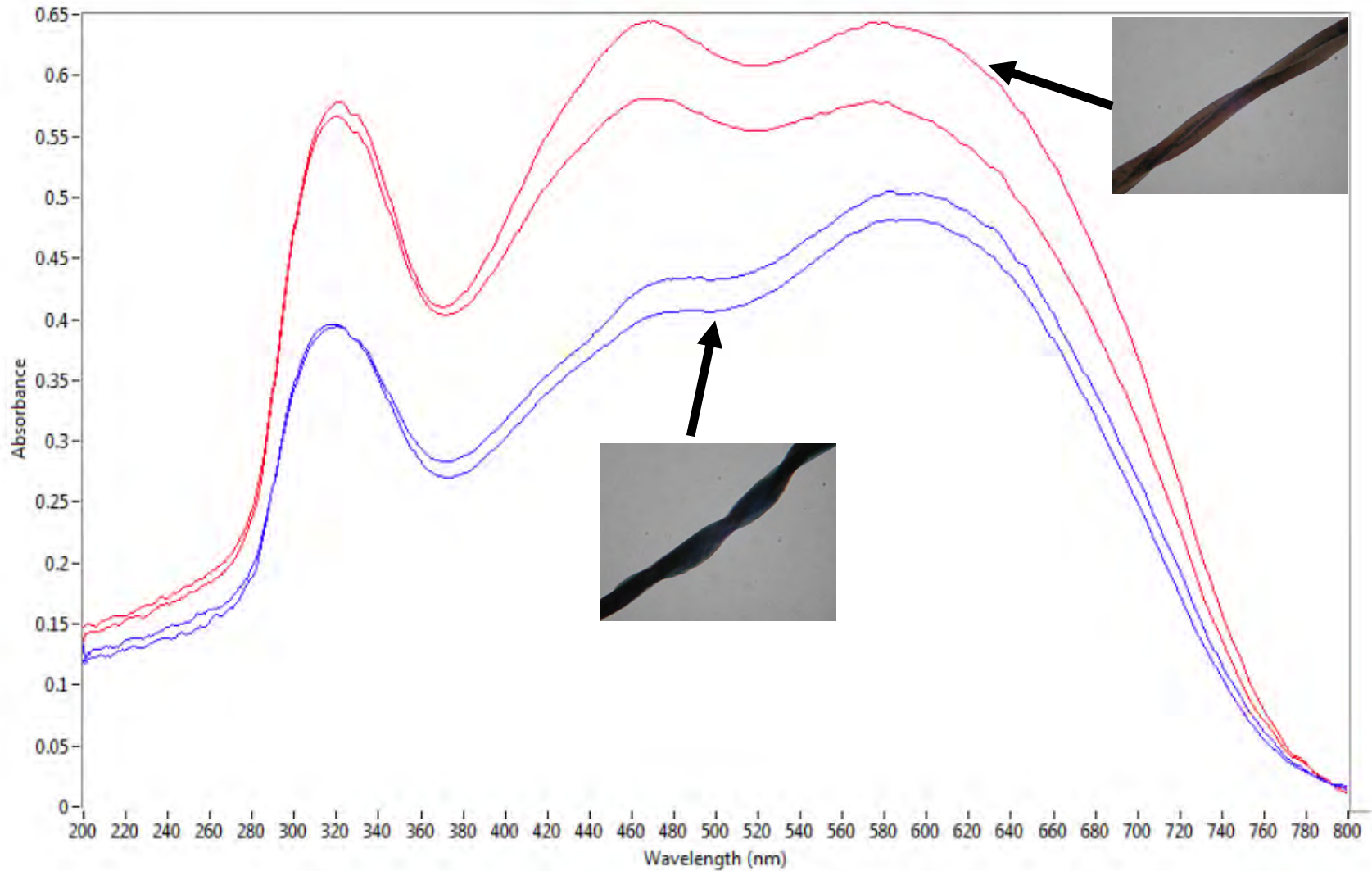


Figure 212. MSP spectra collected from the deep blue (blue) and brown (red) areas of the same two cotton fibers.



Figure 213. Tuft of heterogeneously dyed carpet fibers (left) and a single isolated fiber (right).

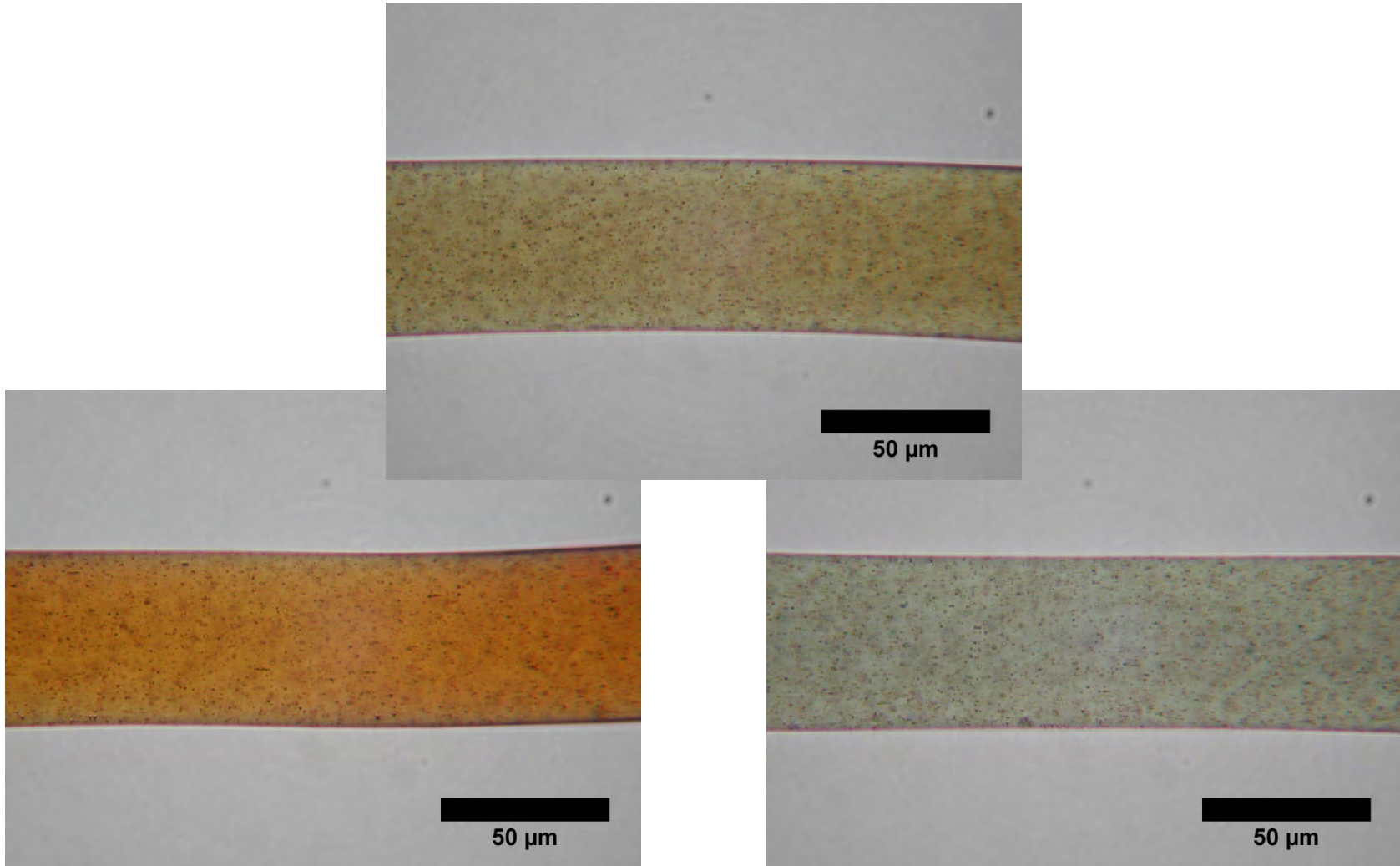


Figure 214. Photomicrographs of the orange (left), transition (center), and green (right) areas of the same carpet fiber (mounted in xylene and viewed using transmitted light).

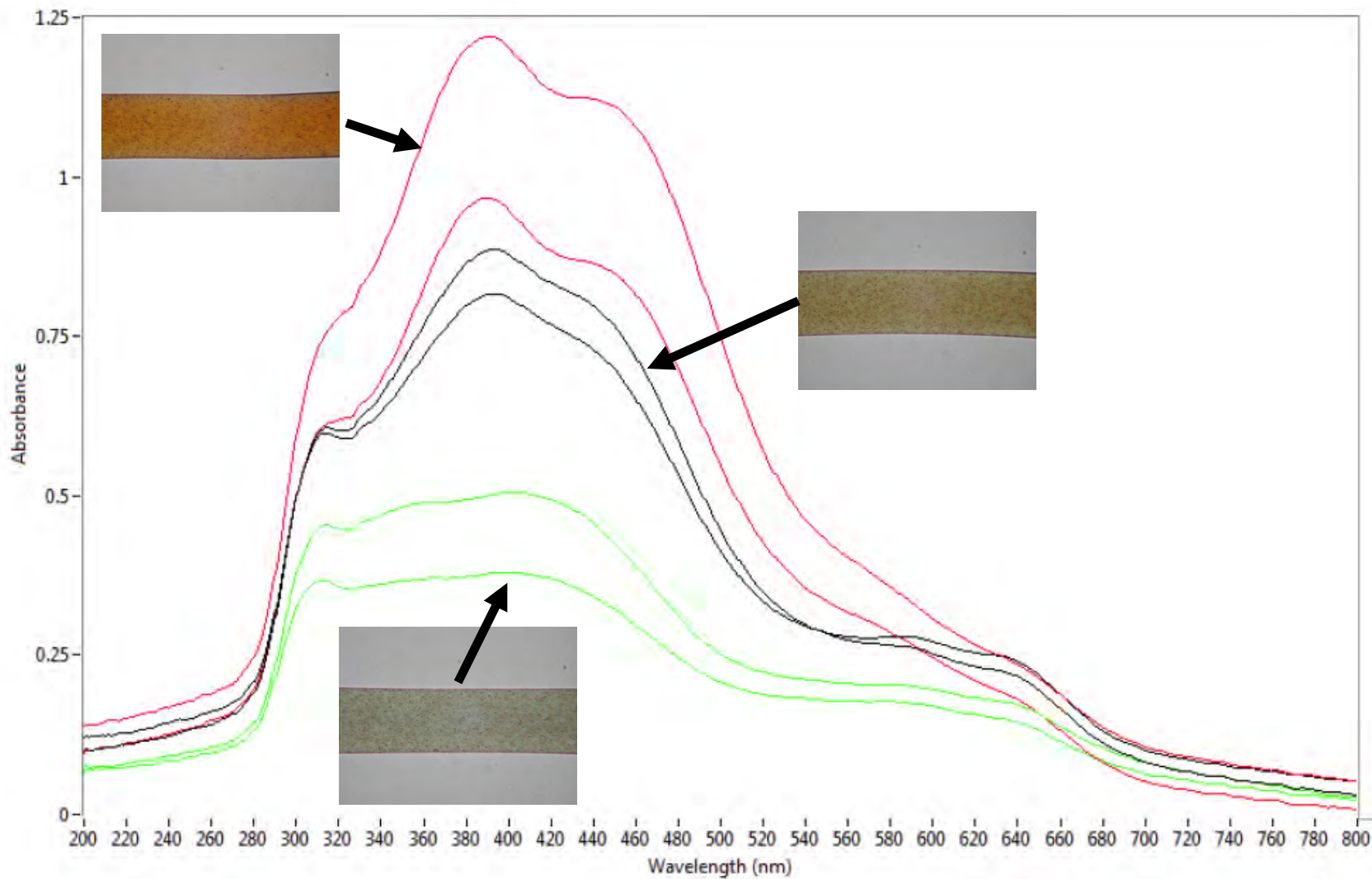


Figure 215. MSP spectra collected from the orange (red), transition (black), and green (green) areas of the same two carpet fibers.

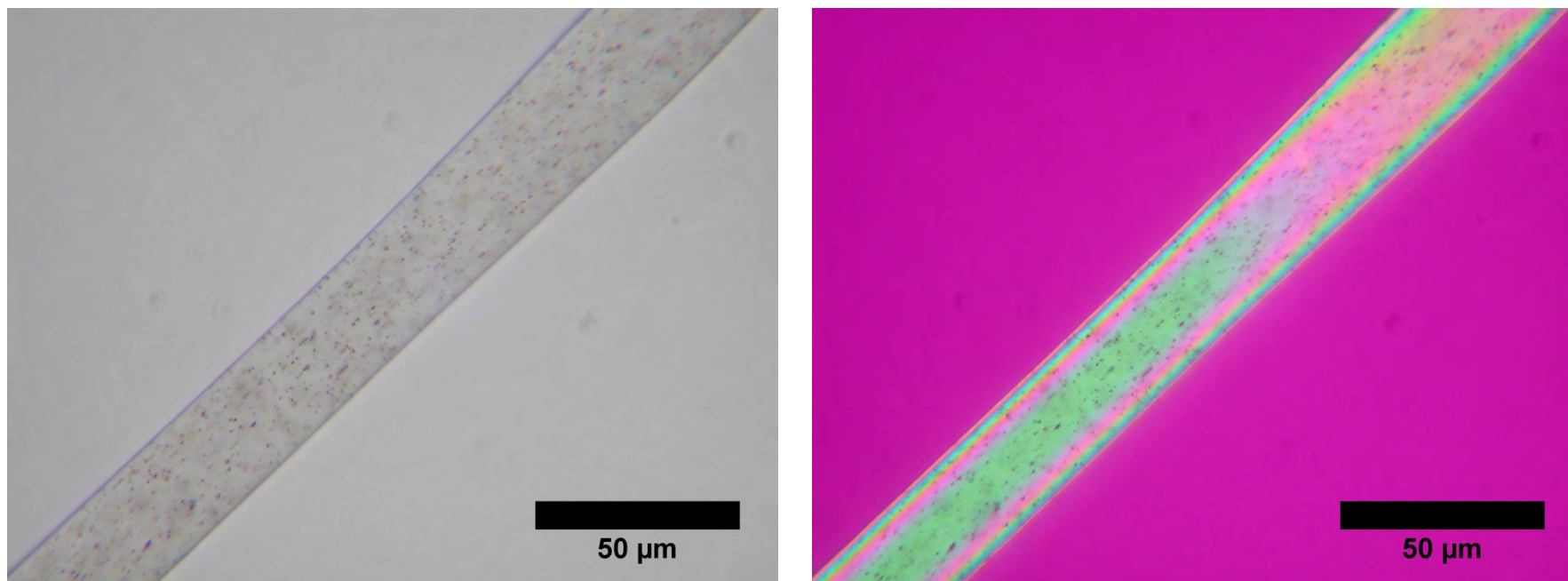


Figure 216. Colorless man-made fiber with titanium dioxide delustrant particles viewed using plane polarized transmitted light (left) and between crossed polars with a first order red compensator inserted (right).

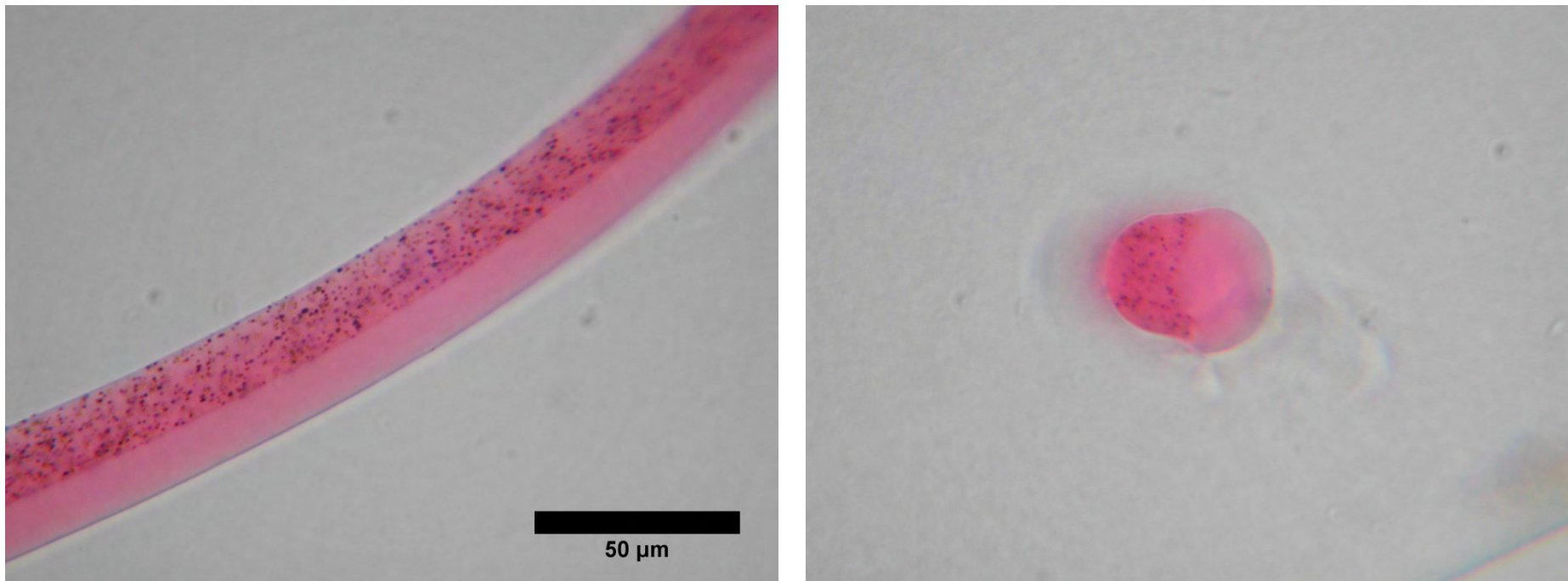


Figure 217. Dark red bicomponent acrylic fiber containing delustrant particles in only one-half (whole mount [left] and cross-section [right]). If the cross-section is considered to be mushroom shaped, it will be noted that the delustrant is confined to the stem while the cap is bright (*i.e.*, without delustrant).

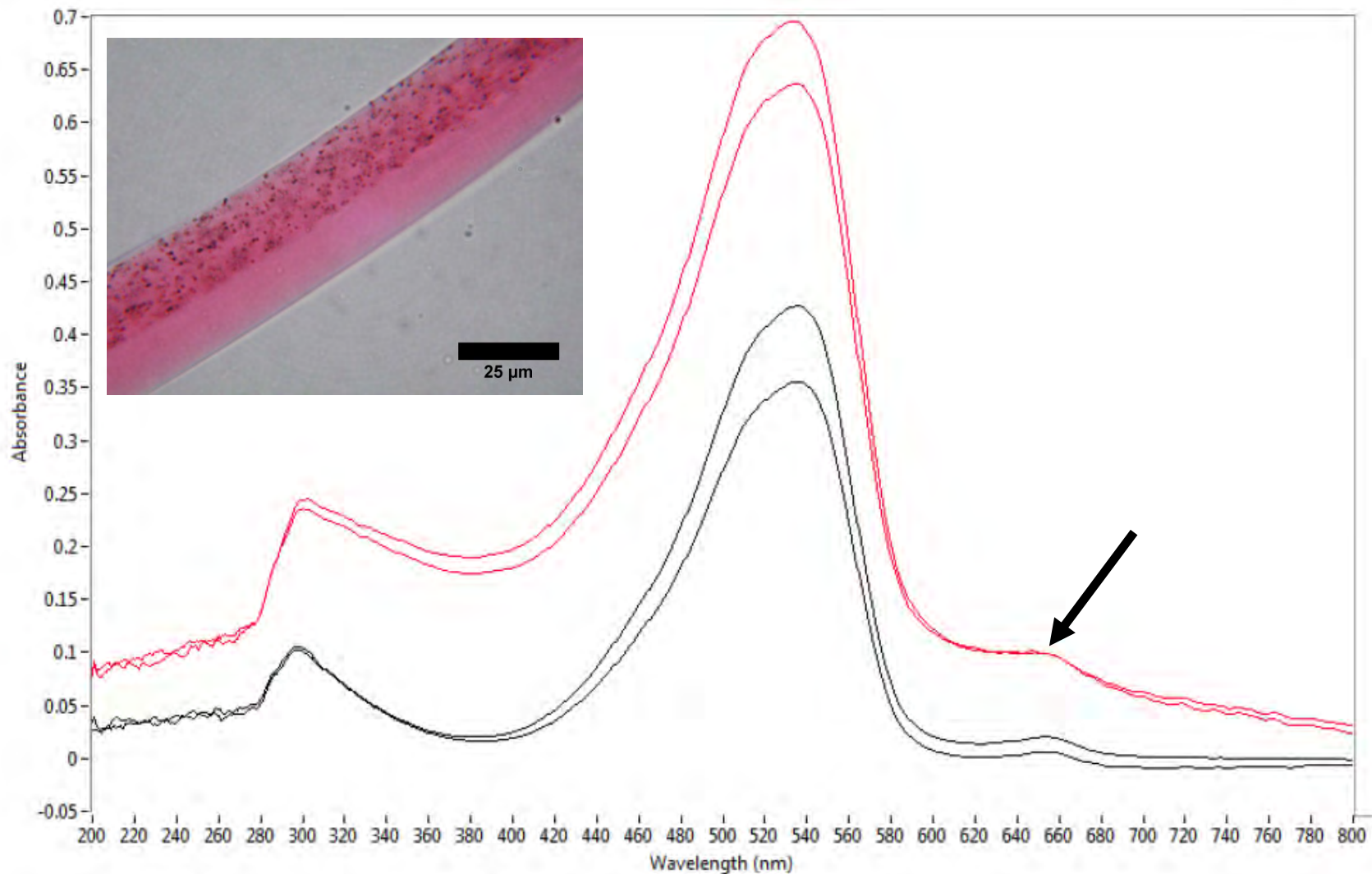


Figure 218. Comparison of MSP spectra collected from two dark red bicomponent acrylic fibers through areas with (red) and without (black) delustrant particles. The black arrow marks a shoulder which appears as a more distinct peak in the spectra collected through a non-delustrated area.

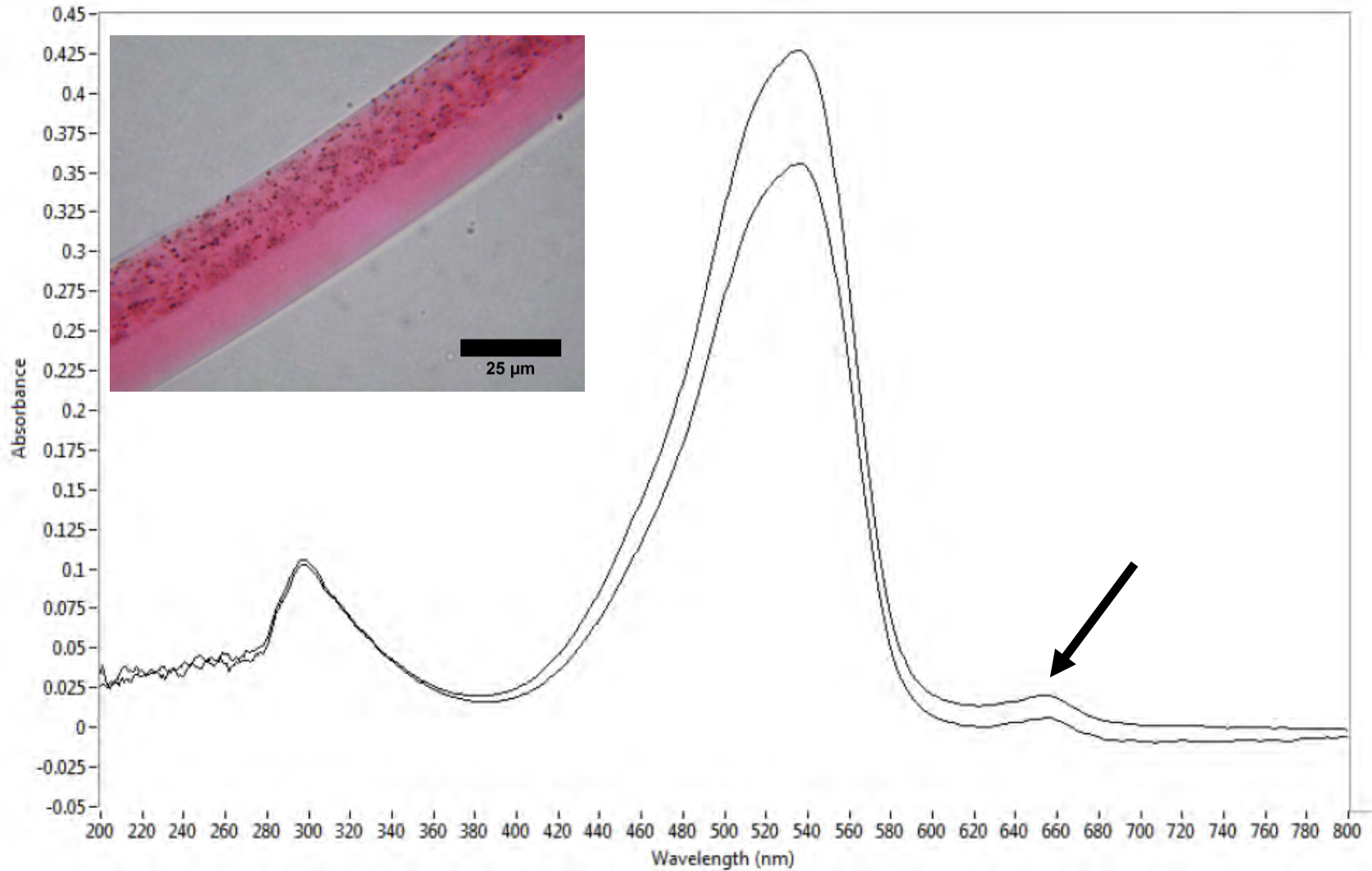


Figure 219. MSP spectra collected from two dark red bicomponent acrylic fibers through areas without delustrant particles. Note the presence of a small, but distinct peak when the spectra are collected through a non-delustered area.

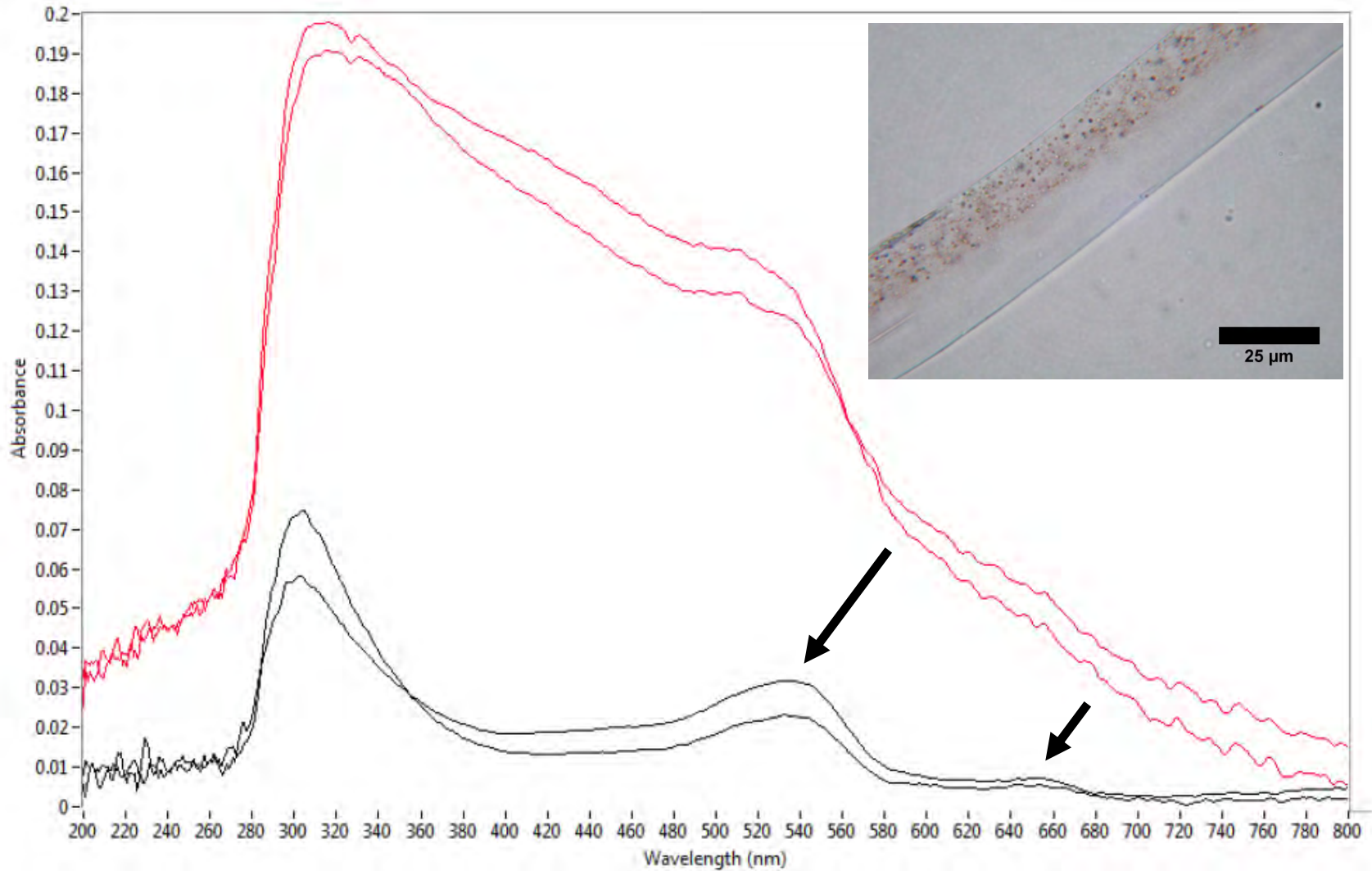


Figure 220. Comparison of MSP spectra collected from two light red bicomponent acrylic fibers through areas with (red) and without (black) delustrant particles. The black arrows mark spectral features which are better defined in the spectra collected through a non-delustrated area compared to a delustrated area.

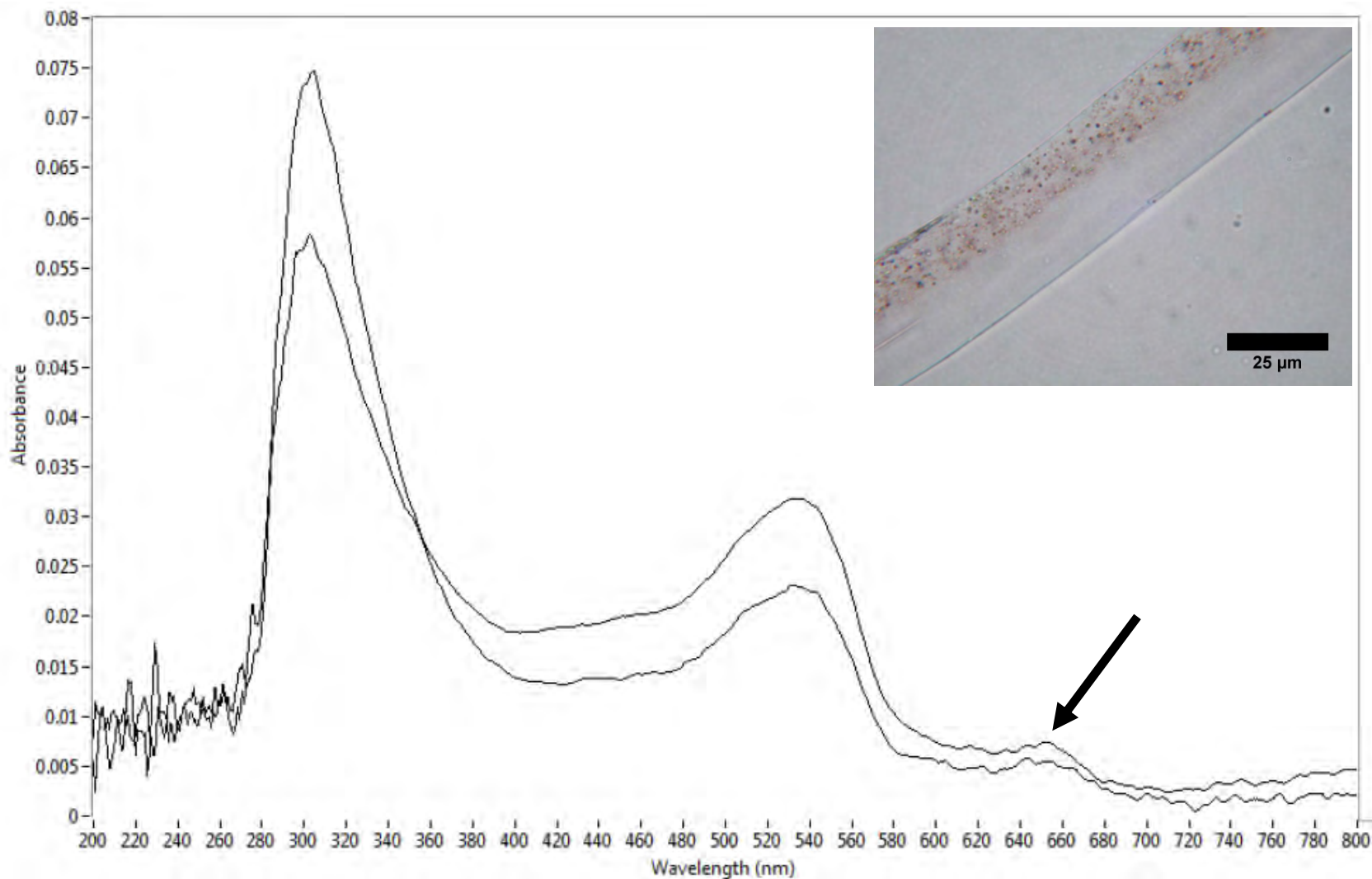


Figure 221. MSP spectra collected from two light red bicomponent acrylic fibers through areas without delustrant particles. Note the presence of a small, but distinct peak when the spectra are collected through a non-delustered area.

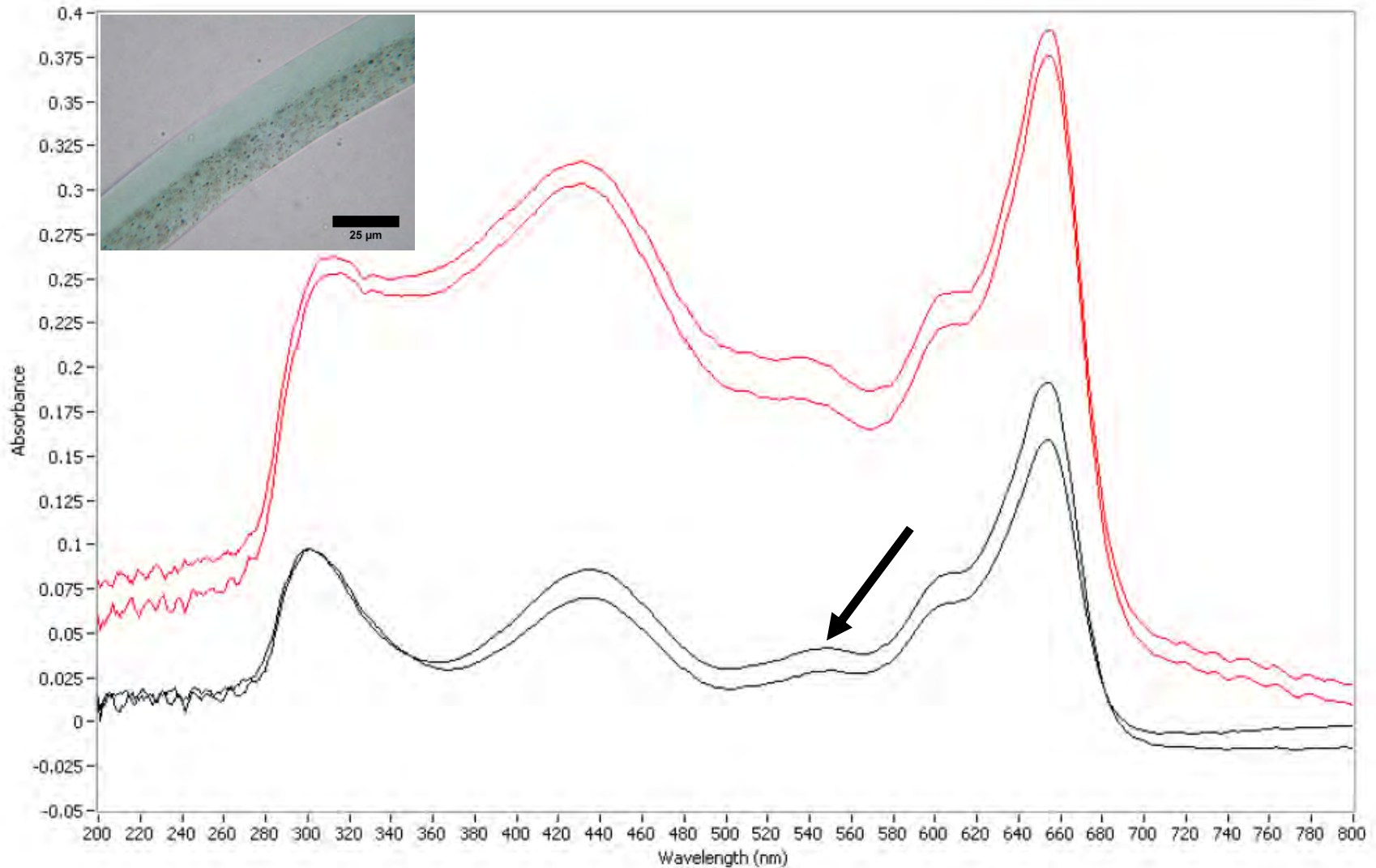


Figure 222. Comparison of MSP spectra collected from two dark green bicomponent acrylic fibers through areas with (red) and without (black) delustrant particles. The black arrow marks a spectral feature which is better defined in the spectra collected through a non-delustrated area compared to a delustrated area.

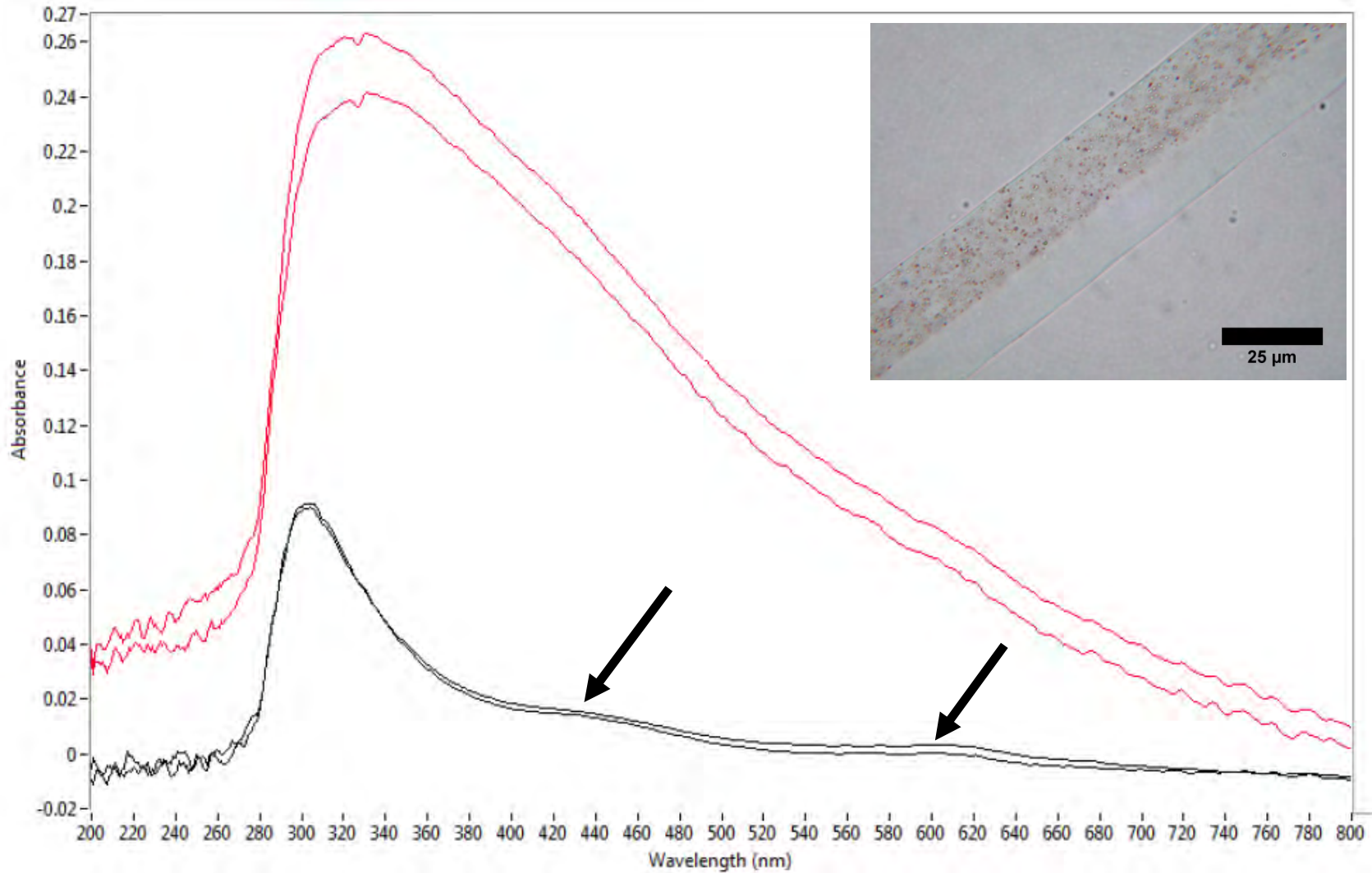


Figure 223. Comparison of MSP spectra collected from two light green bicomponent acrylic fibers through areas with (red) and without (black) delustrant particles. The black arrows mark spectral features which are better defined in the spectra collected through a non-delustered area compared to a delustered area.

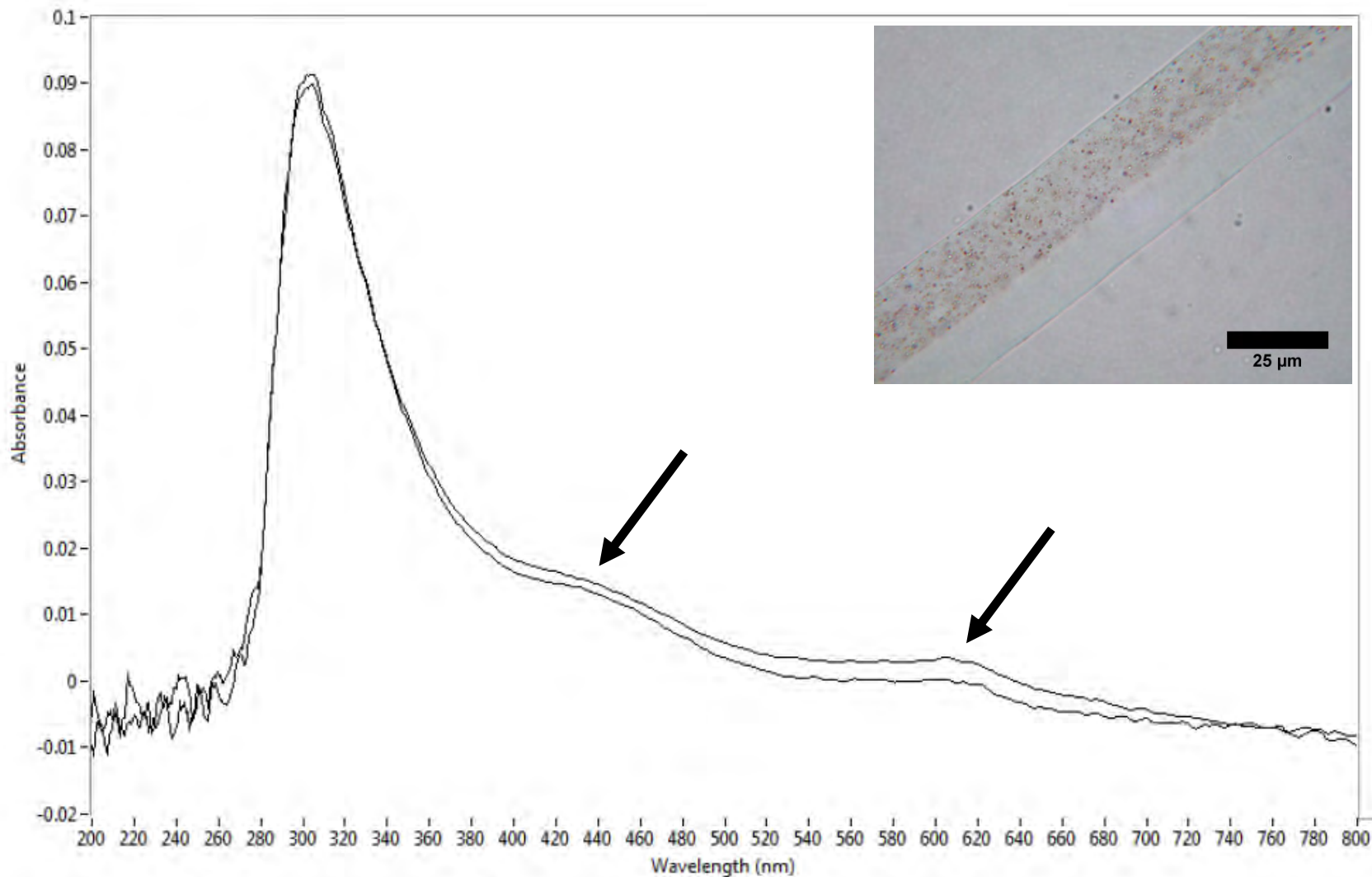


Figure 224. MSP spectra collected from two light green bicomponent acrylic fibers through areas without delustrant particles. Note the presence of subtle spectral features when the data is collected through a non-delustered area.

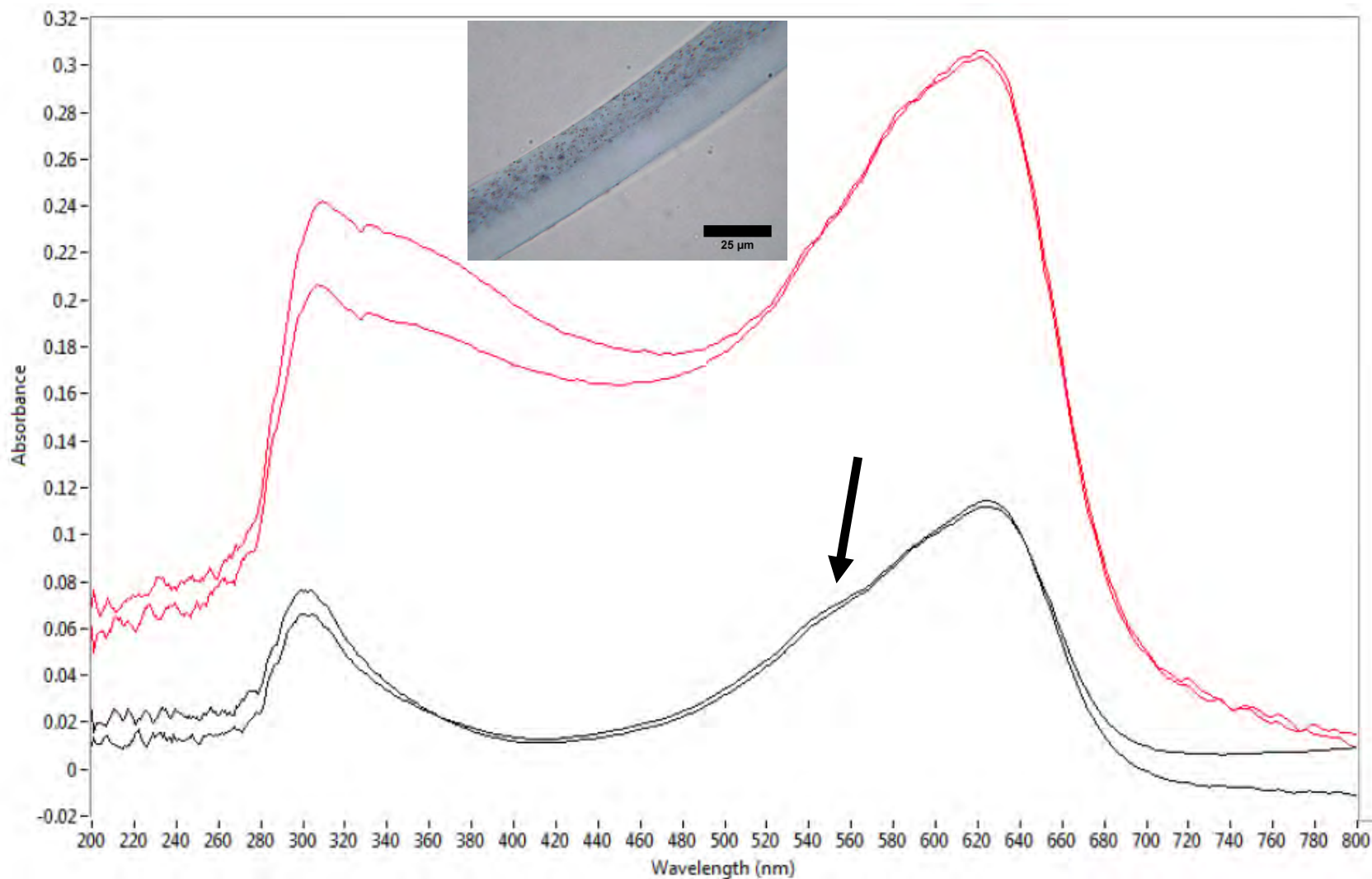


Figure 225. Comparison of MSP spectra collected from two dark blue bicomponent acrylic fibers through areas with (red) and without (black) delustrant particles. The black arrow marks a spectral feature which is better defined in the spectra collected through a non-delustrated area compared to a delustrated area.

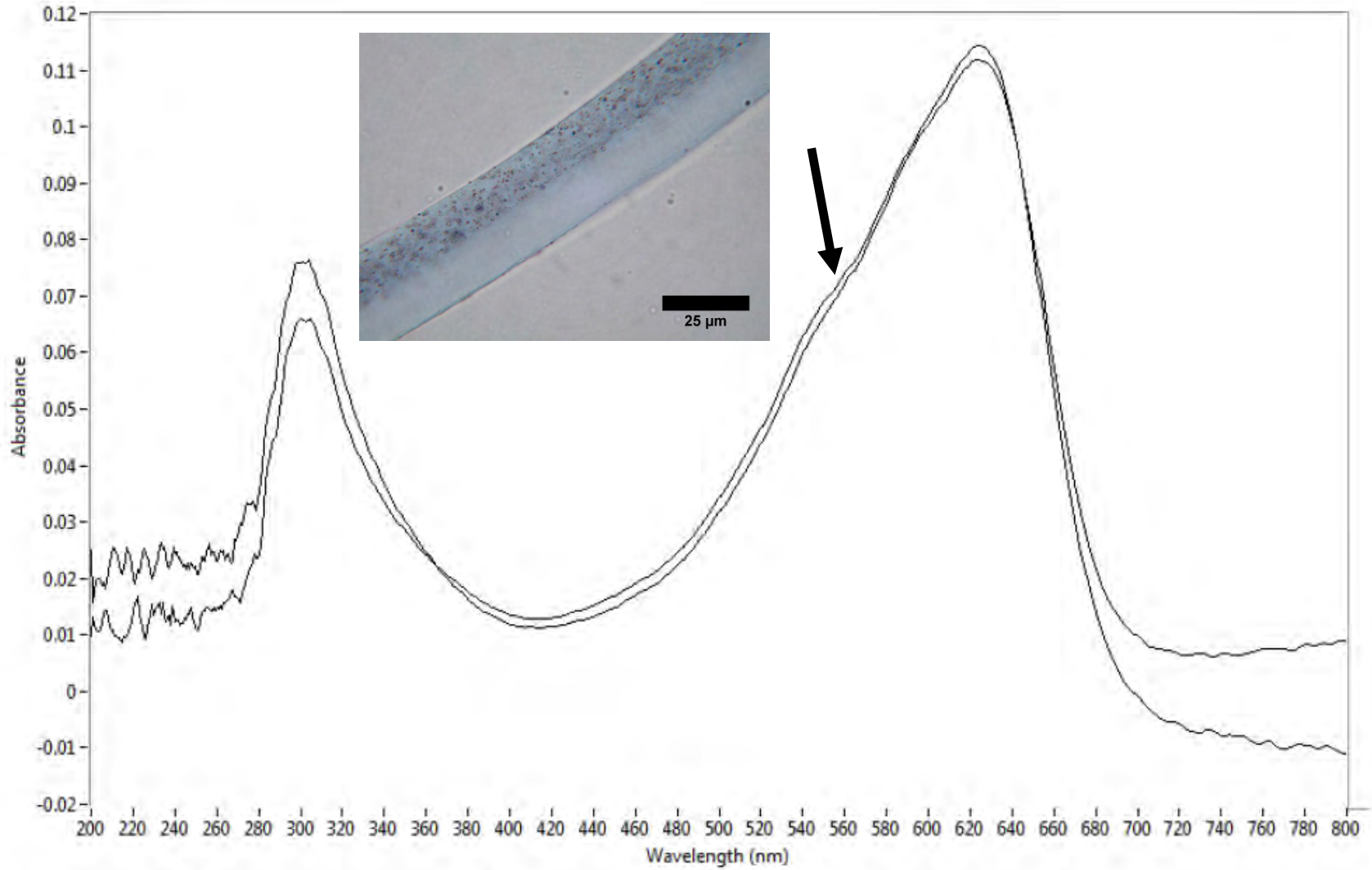


Figure 226. MSP spectra collected from two dark blue bicomponent acrylic fibers through areas without delustrant particles. Note the presence of a subtle spectral feature when the data is collected through a non-delustered area.

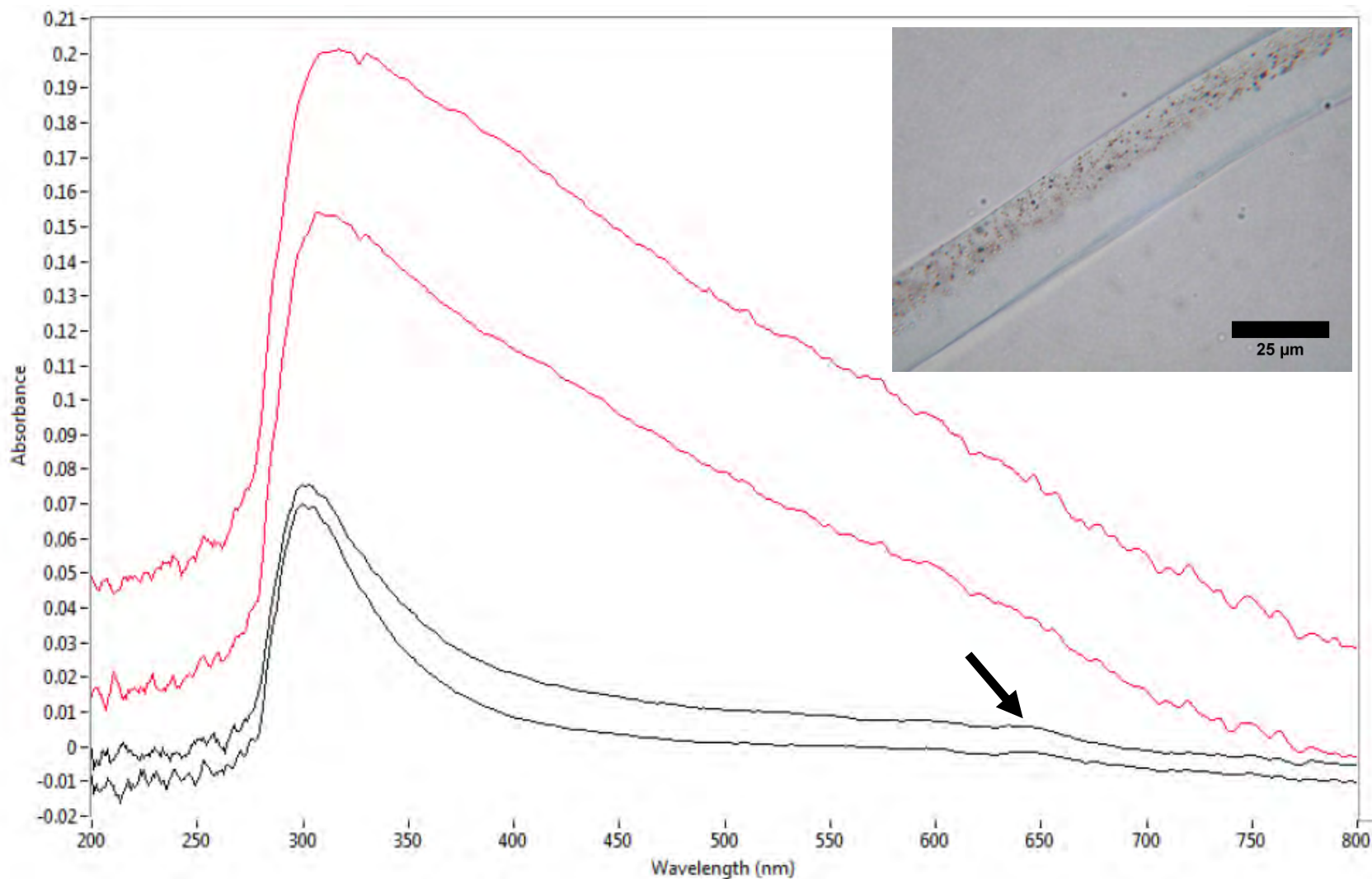


Figure 227. Comparison of MSP spectra collected from two light blue bicomponent acrylic fibers through areas with (red) and without (black) delustrant particles. The black arrow marks a spectral feature which is better defined in the spectra collected through a non-delustrated area compared to a delustrated area.

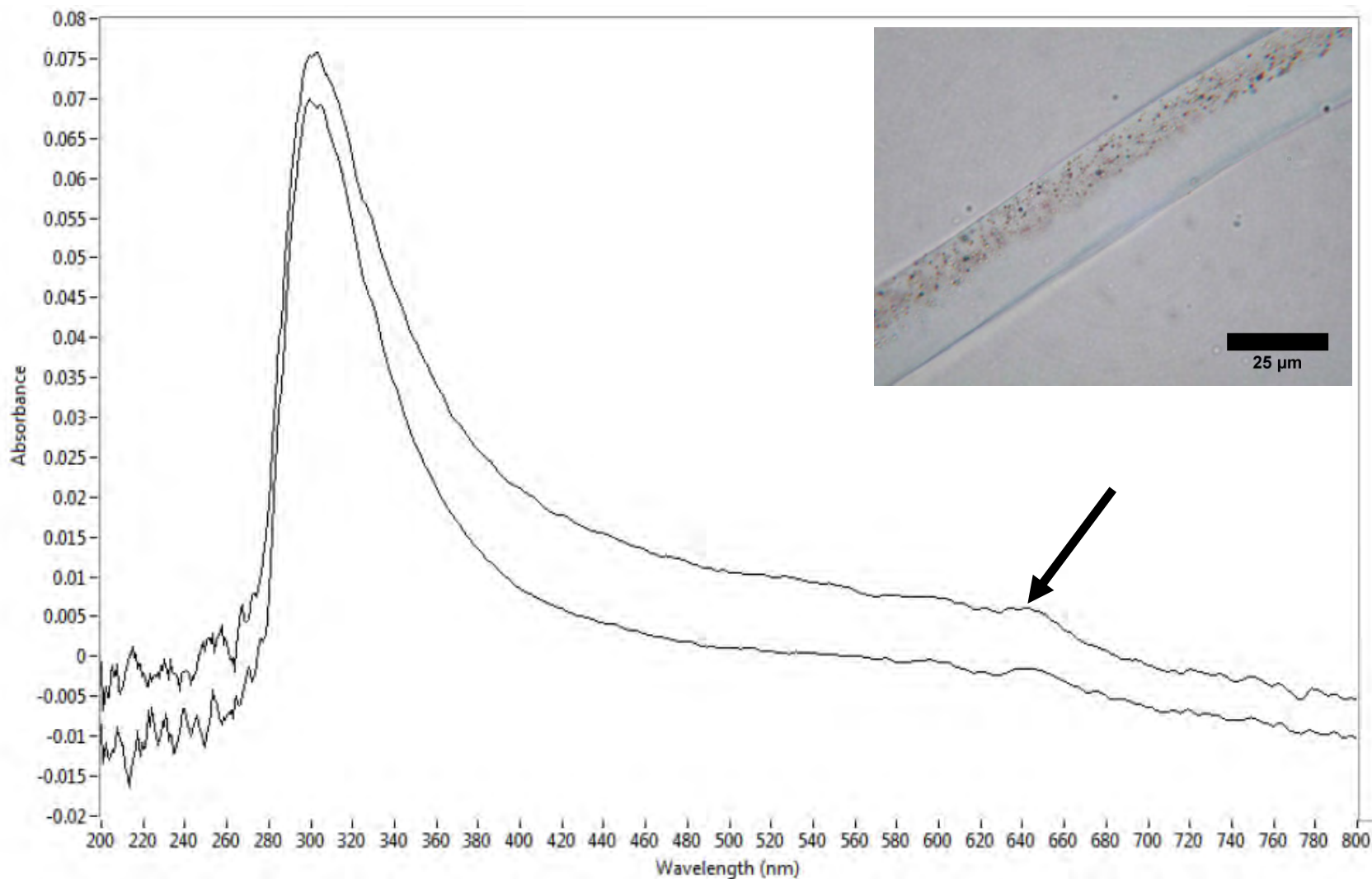


Figure 228. MSP spectra collected from two light blue bicomponent acrylic fibers through areas without delustrant particles. Note the presence of a subtle spectral feature when the data is collected through a non-delustered area.

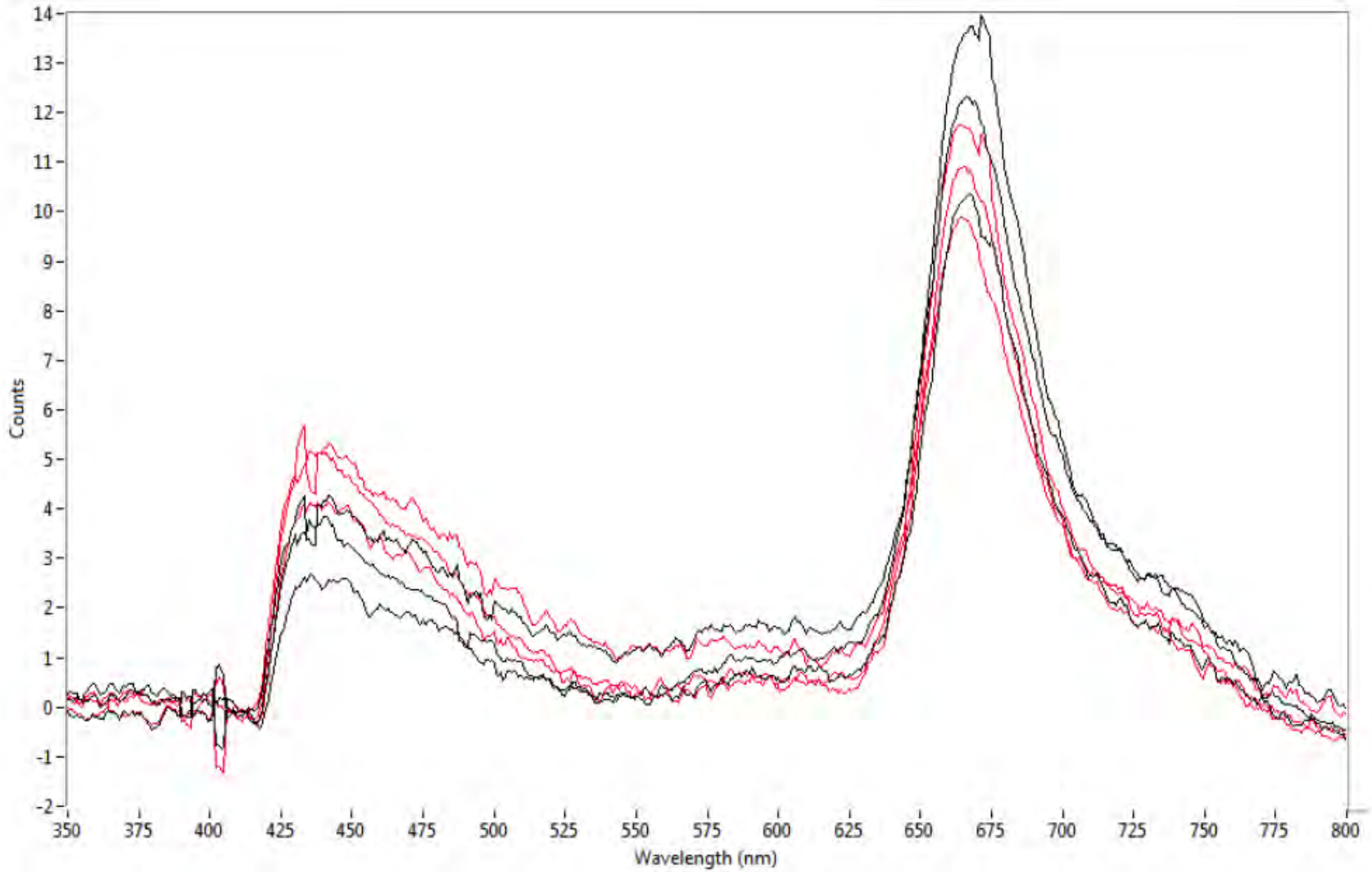


Figure 229. MSF spectra collected from the delustered (black) and non delustered (red) regions of bicomponent dark red fibers (UV excitation).

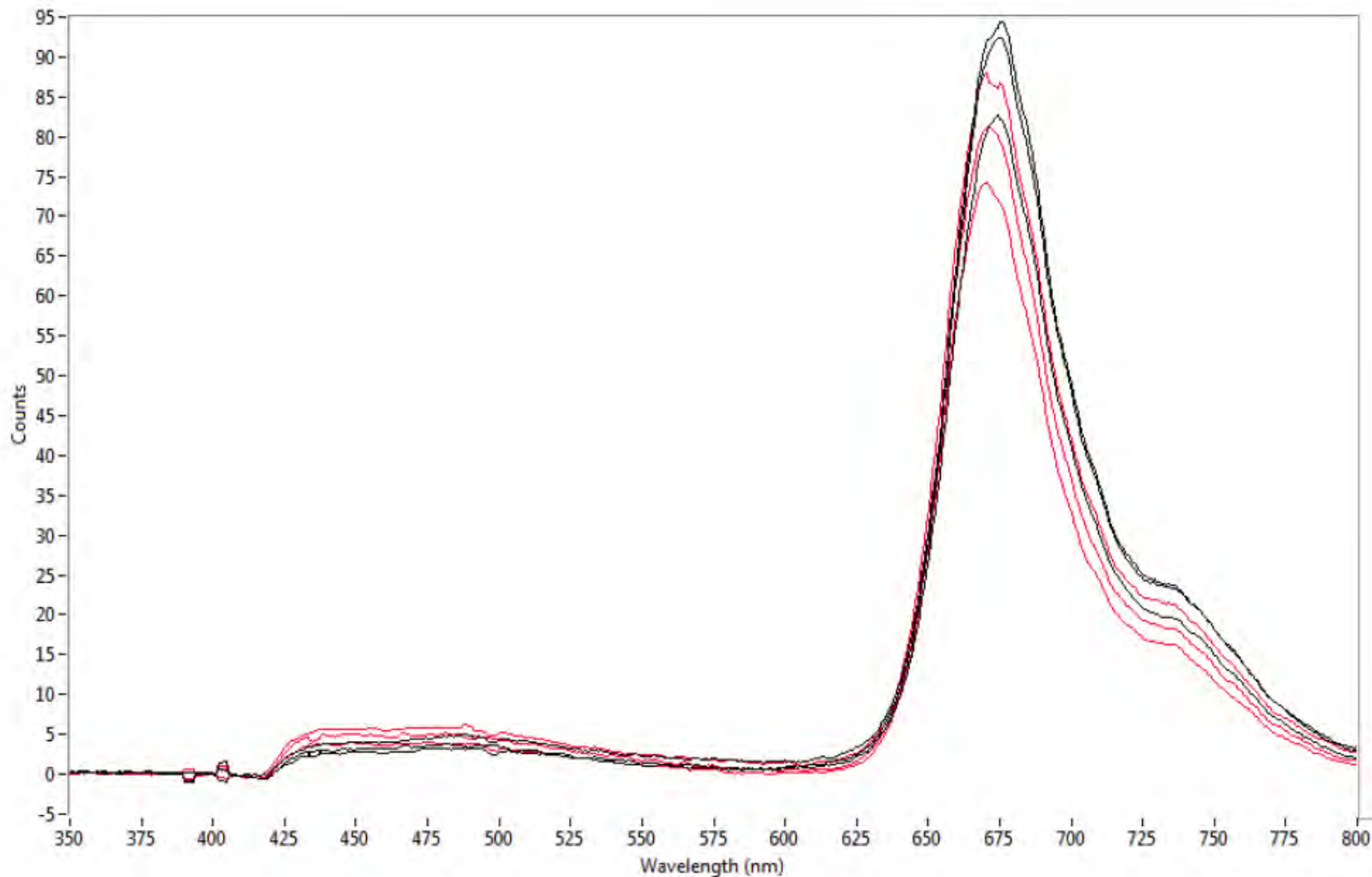


Figure 230. MSF spectra collected from the delustered (black) and non delustered (red) regions of bicomponent dark green fibers (UV excitation).

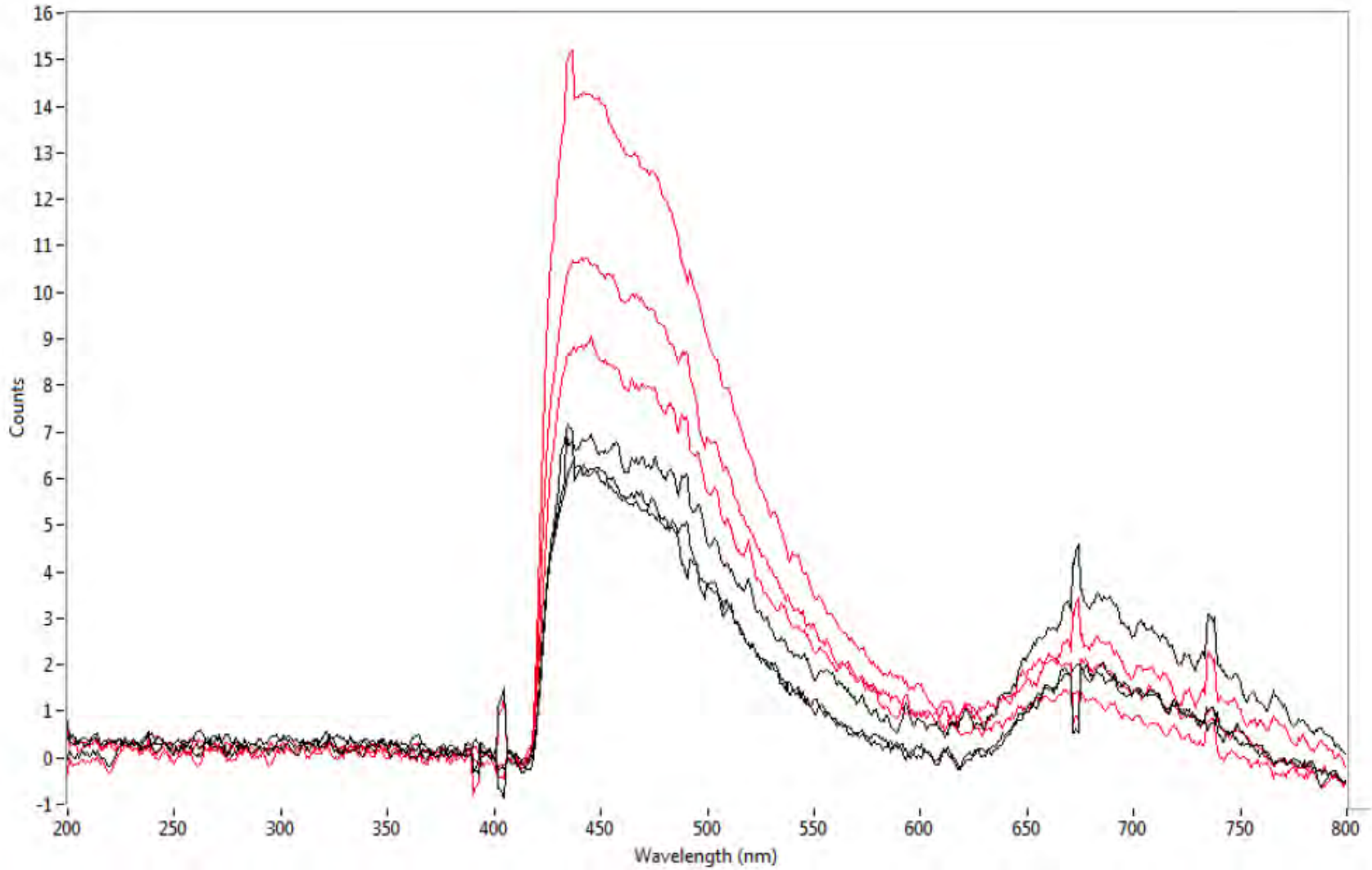


Figure 231. MSF spectra collected from the delustered (black) and non delustered (red) regions of bicomponent dark blue fibers (UV excitation).

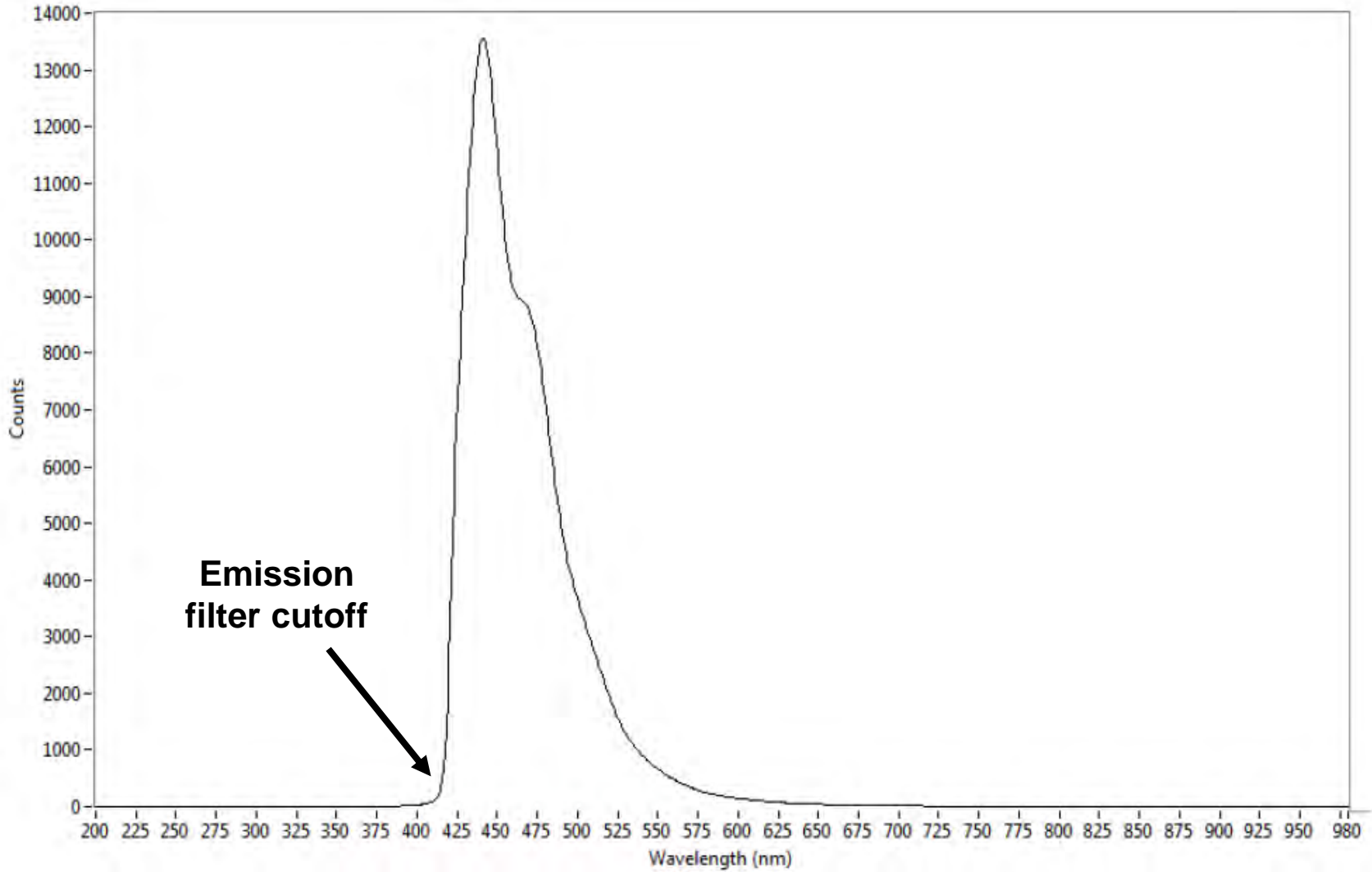


Figure 232. Typical MSF spectrum of a cotton fabric washed in a commercial detergent containing an optical brightener (UV excitation).

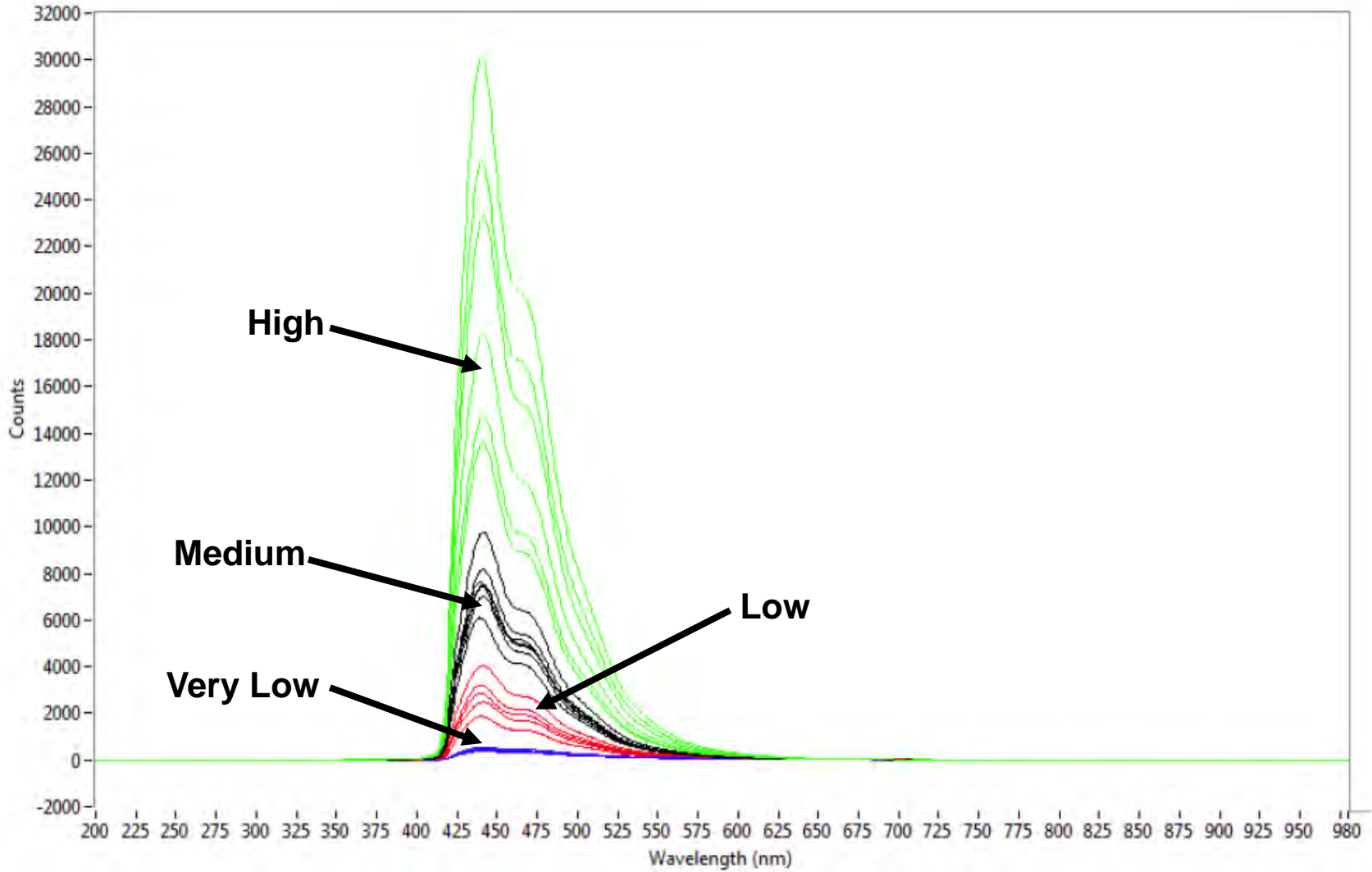


Figure 233. MSF spectra of the cotton fabric swatches washed with twenty-two commercial detergents (UV excitation).

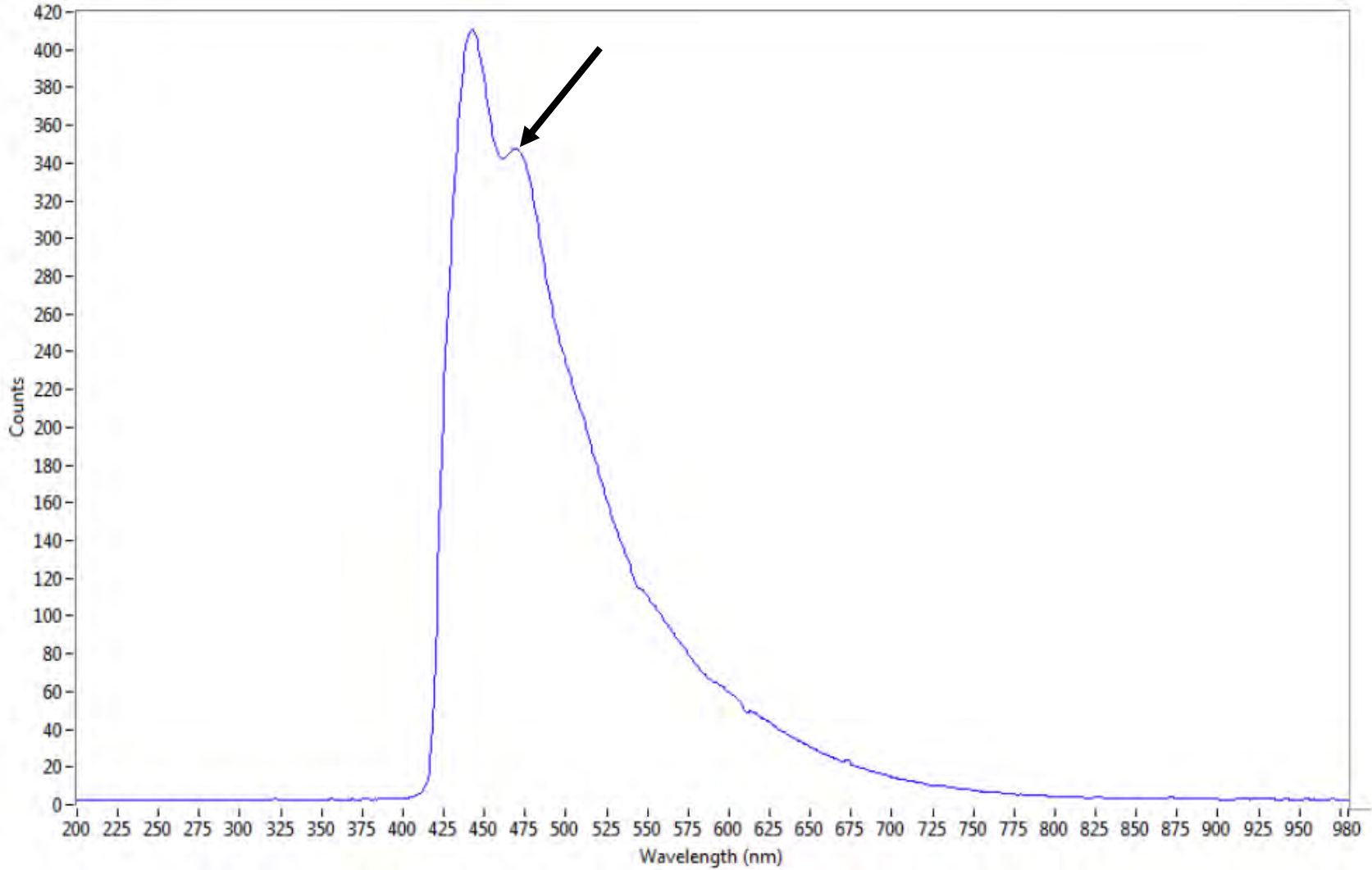


Figure 234. Typical MSF spectrum of a fabric with “very low” fluorescence (note the distinct minor peak at ~ 468 nm).

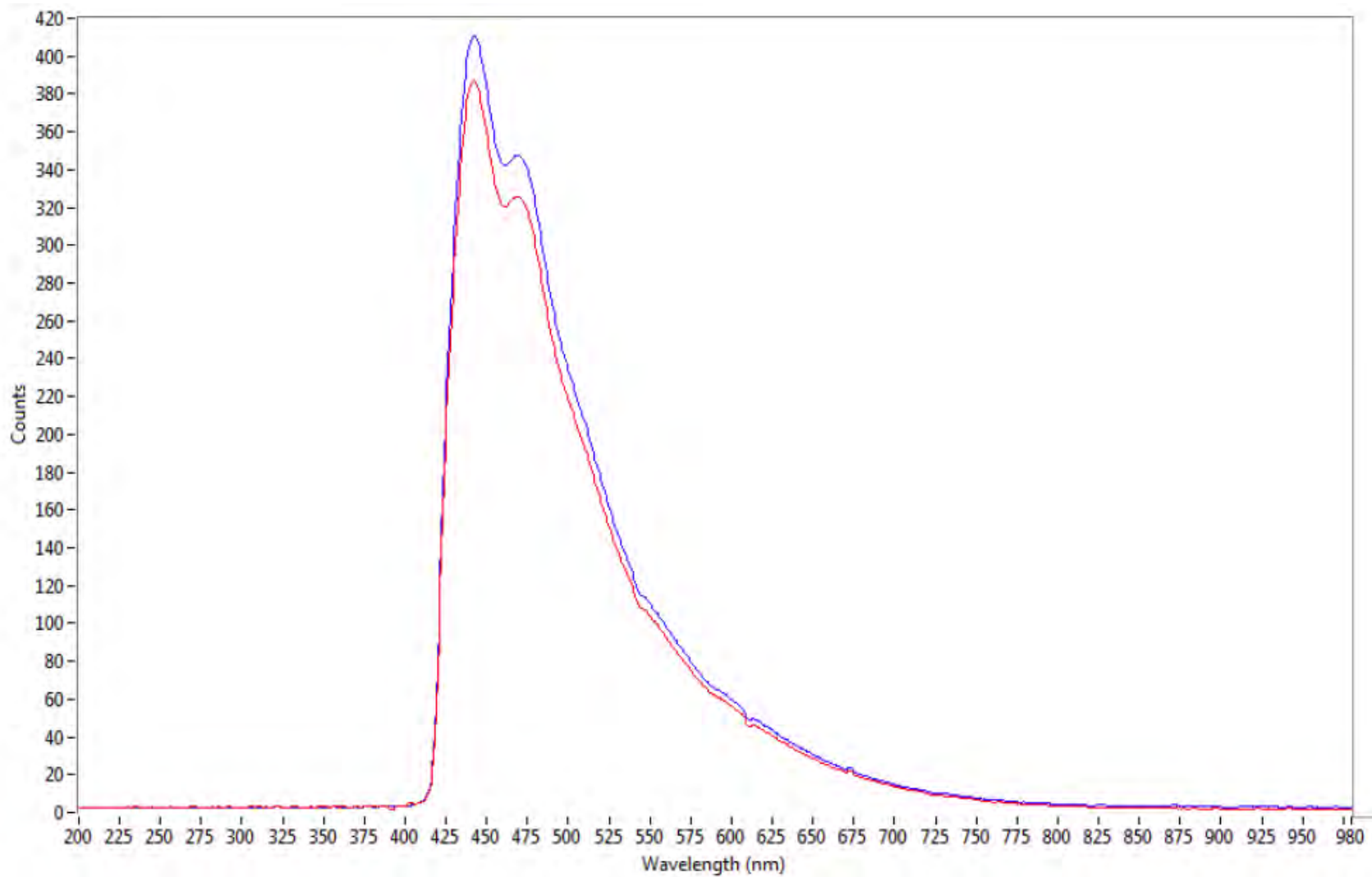


Figure 235. Typical MSF spectrum of a fabric with “very low” fluorescence (blue) compared to the spectrum of the control (*i.e.*, unwashed) cotton fabric (red).

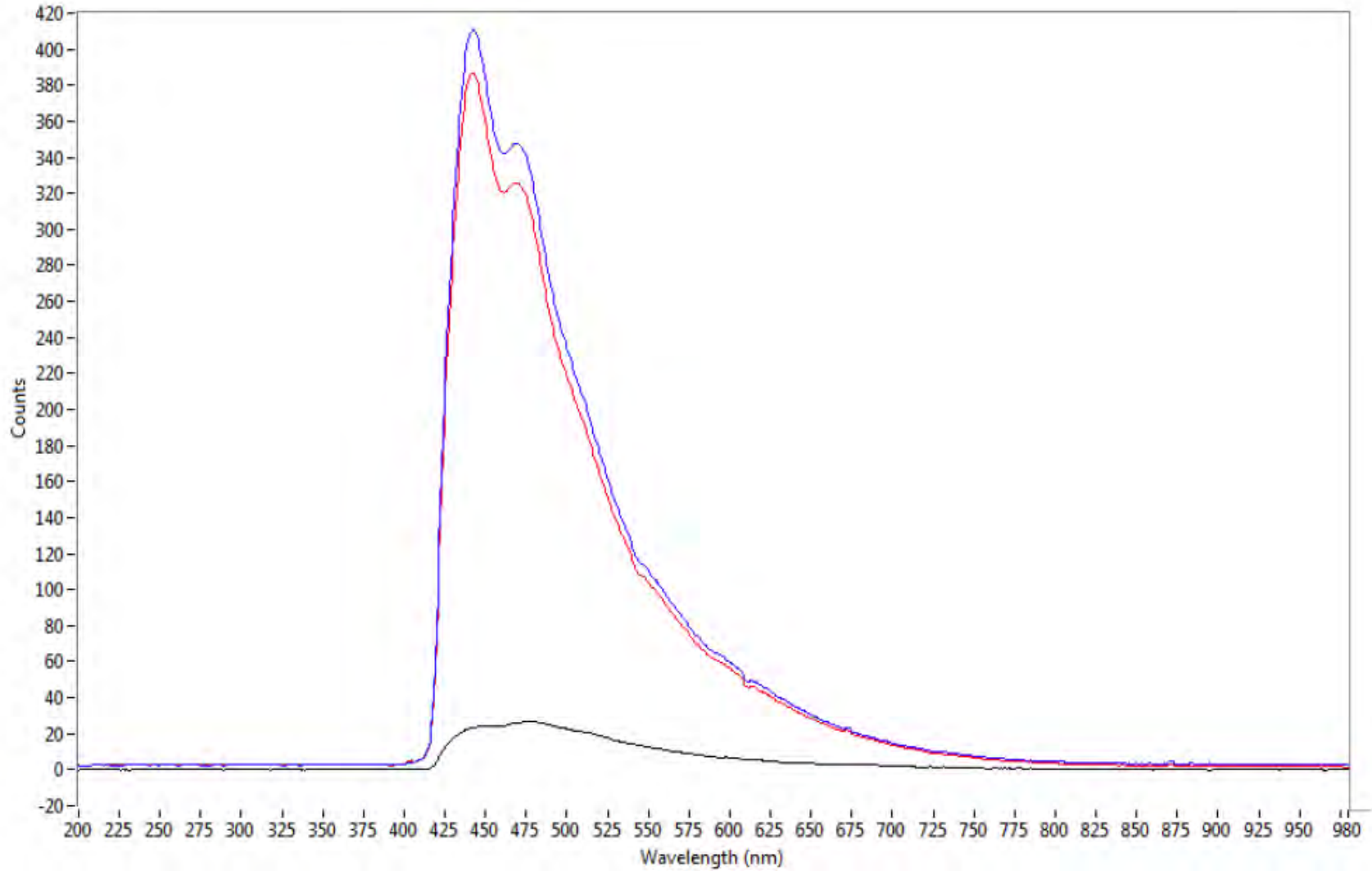


Figure 236. Typical MSF spectrum of a fabric with “very low” fluorescence (blue) compared to spectra of the control (*i.e.*, unwashed) cotton fabric (red) and a cotton ball (black).

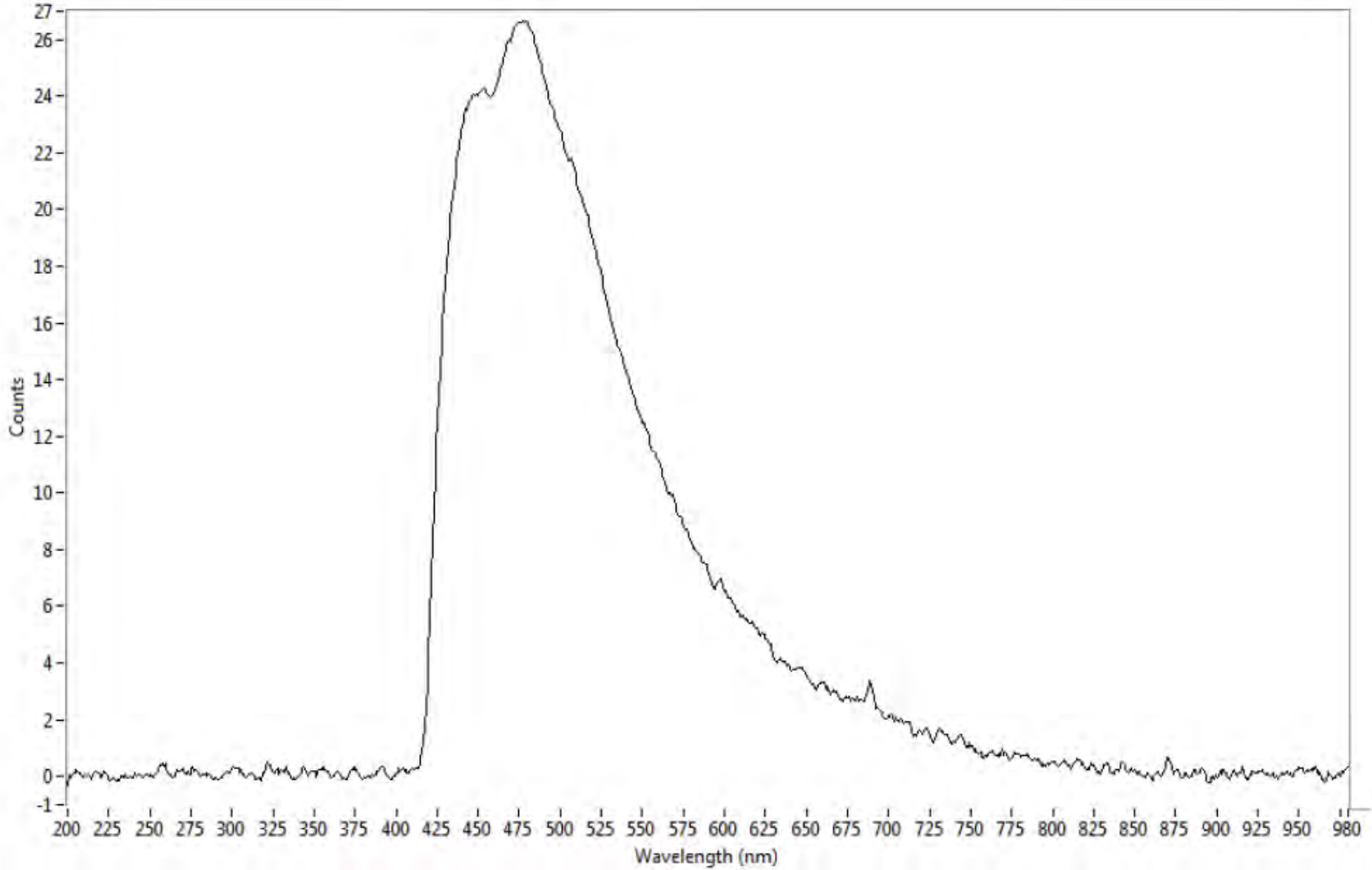


Figure 237. MSF spectrum of a mass of fibers from a cotton ball.

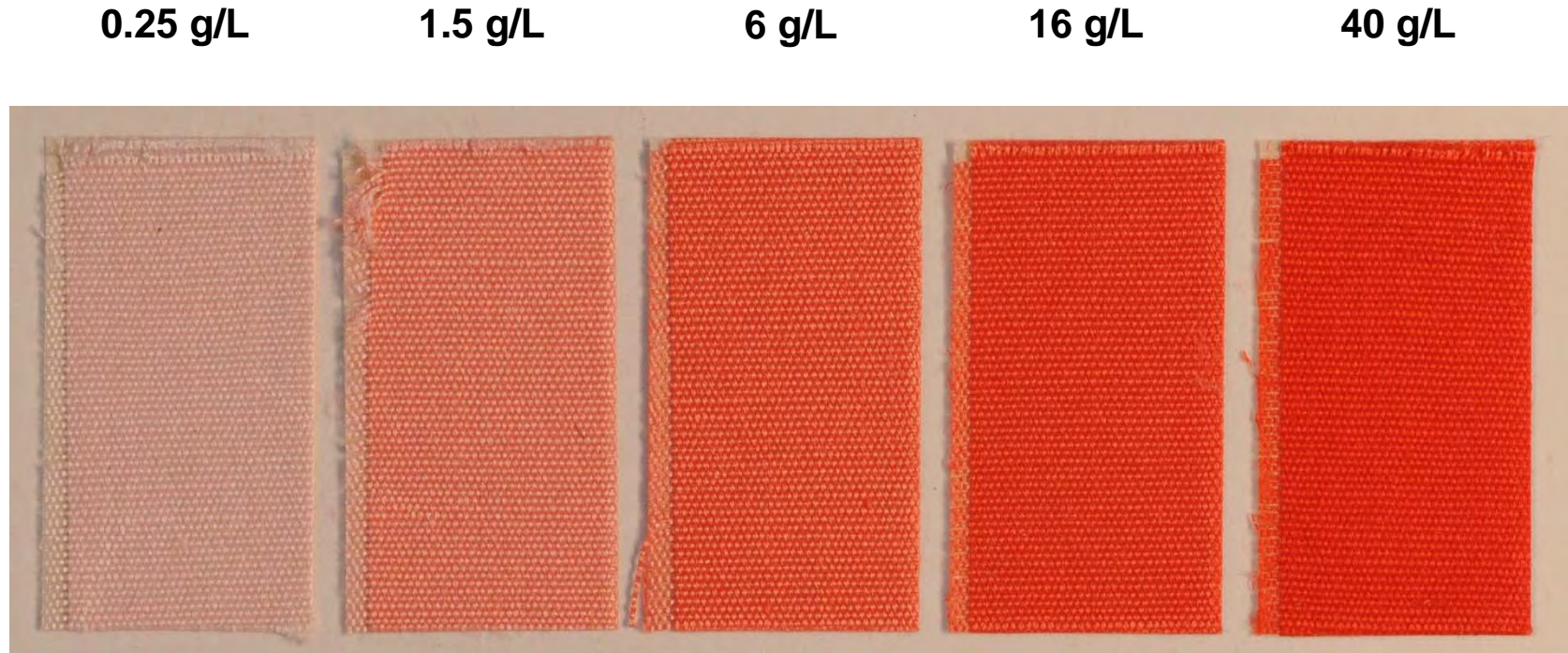


Figure 238. Five swatches of cotton dyed with varying concentrations of Reactive Red 43.

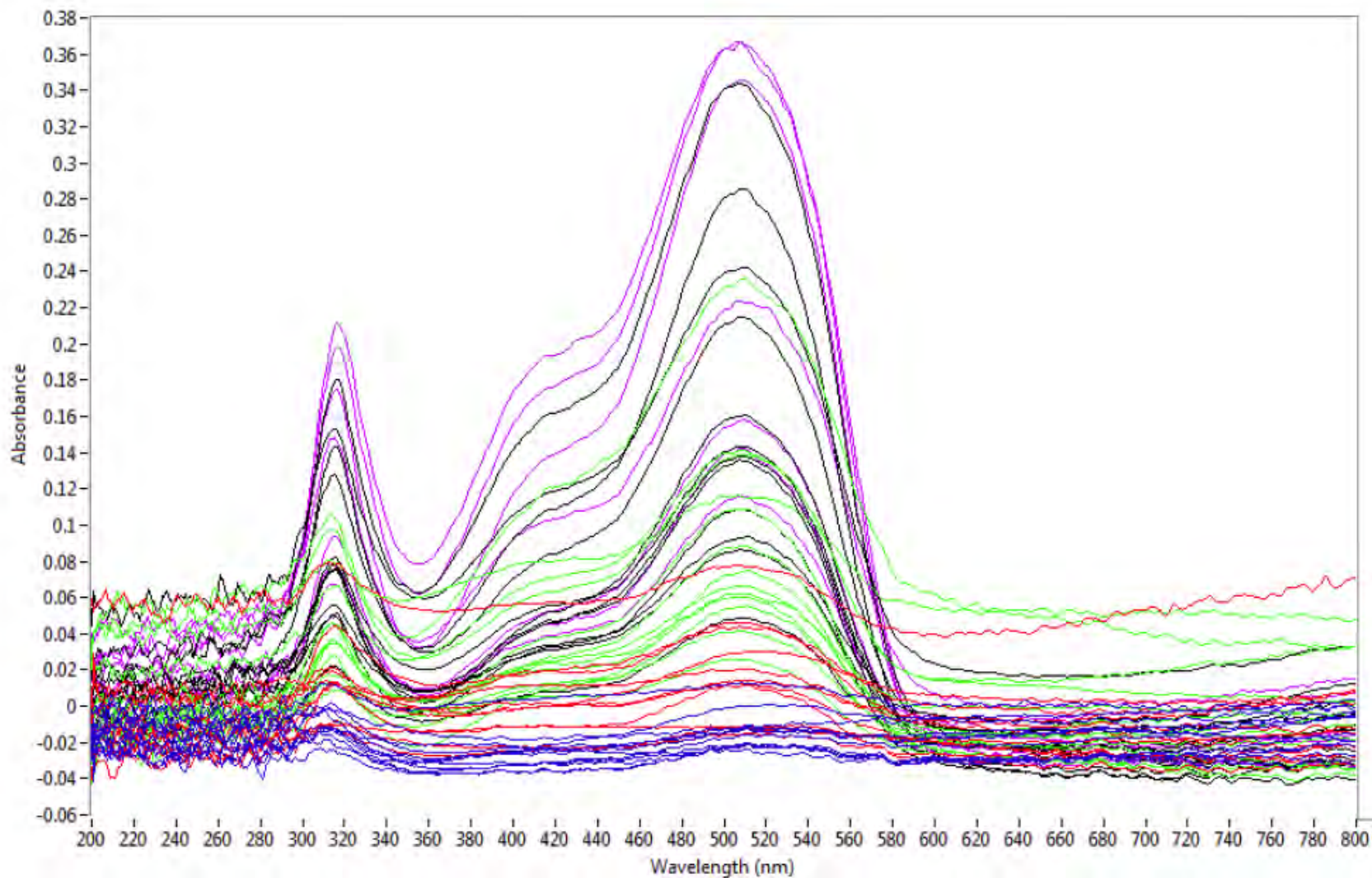


Figure 239. Spectra collected from cotton fibers dyed with five different concentrations of Reactive Red 33 (blue = 0.25 g/L, red = 1.5 g/L, green = 6 g/L, black = 16 g/L, purple = 40 g/L). Some of the deepest absorbing fibers dyed at 40 g/L (*i.e.*, purple have been omitted to allow for scaling purposes).

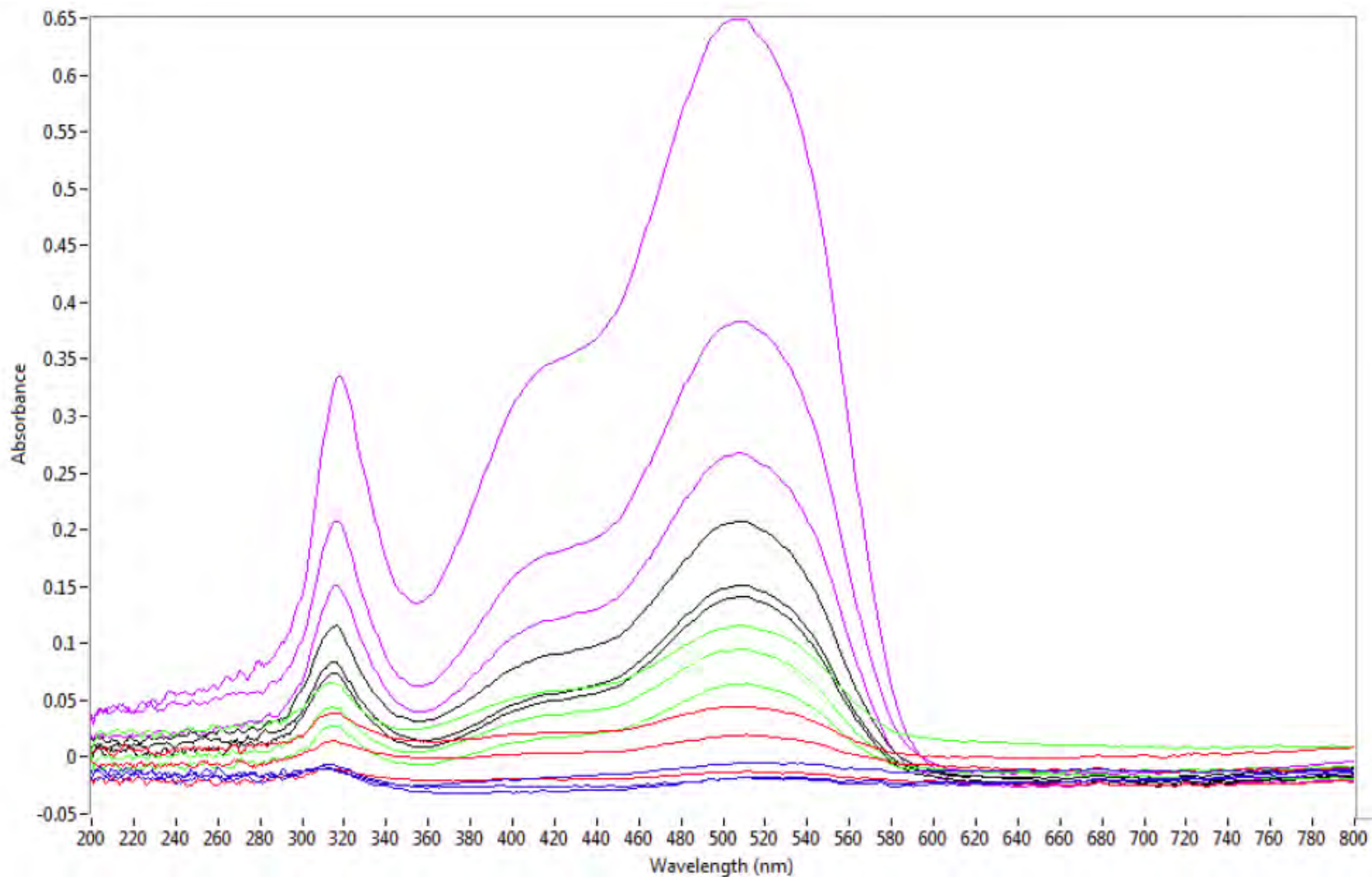


Figure 240. Spectra, averaged from individual fibers, collected from cotton fibers dyed with five different concentrations of Reactive Red 43 (blue = 0.25 g/L, red = 1.5 g/L, green = 6 g/L, black = 16 g/L, purple = 40 g/L).

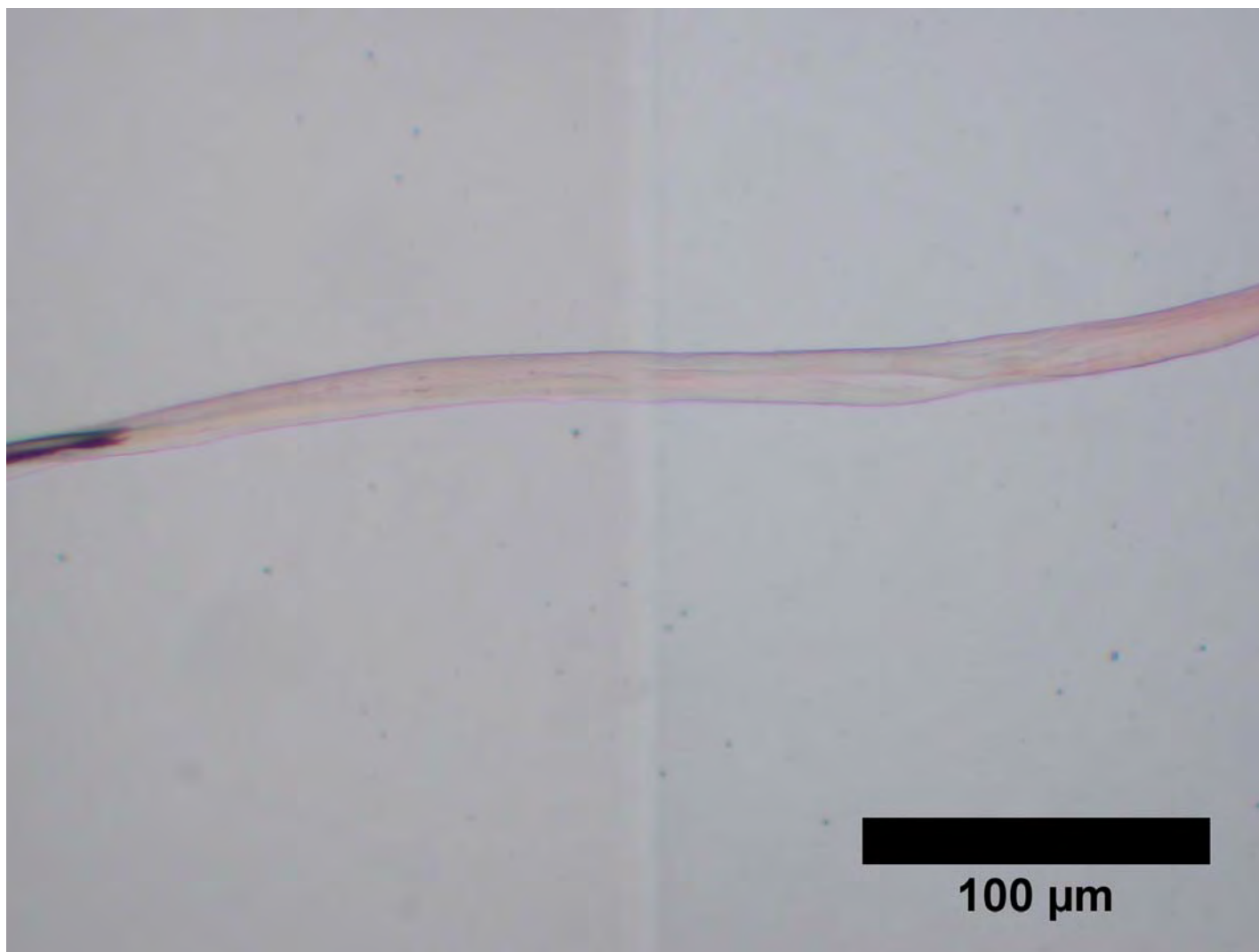


Figure 241. Photomicrograph of a cotton fiber dyed with Reactive Red 43 at a concentration of 6 g/L (left) compared to one dyed at a concentration of 16 g/L (right).

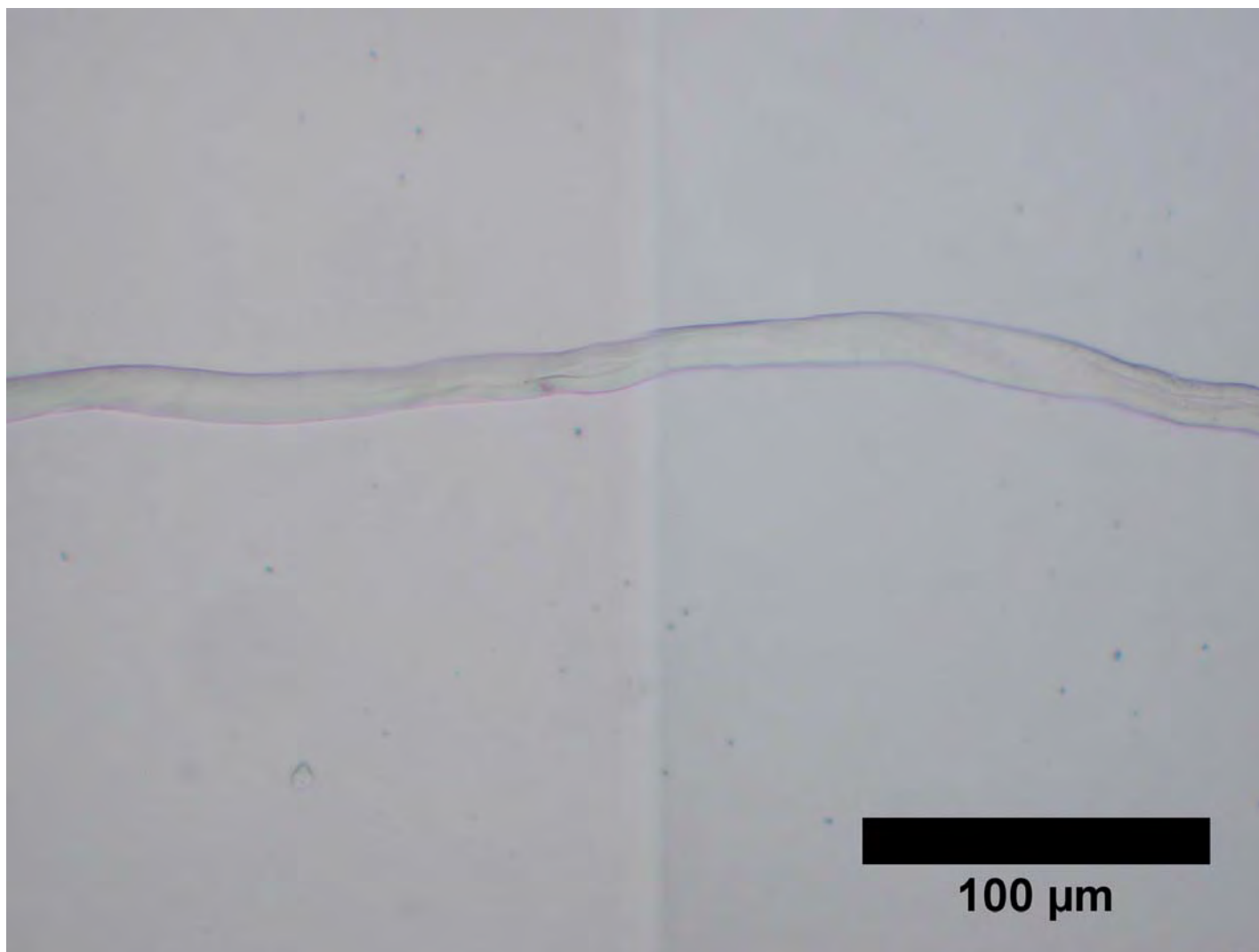


Figure 242. Photomicrograph of a cotton fiber dyed with Reactive Red 43 at a concentration of 0.25 g/L (left) compared to one dyed at a concentration of 1.5 g/L (right).

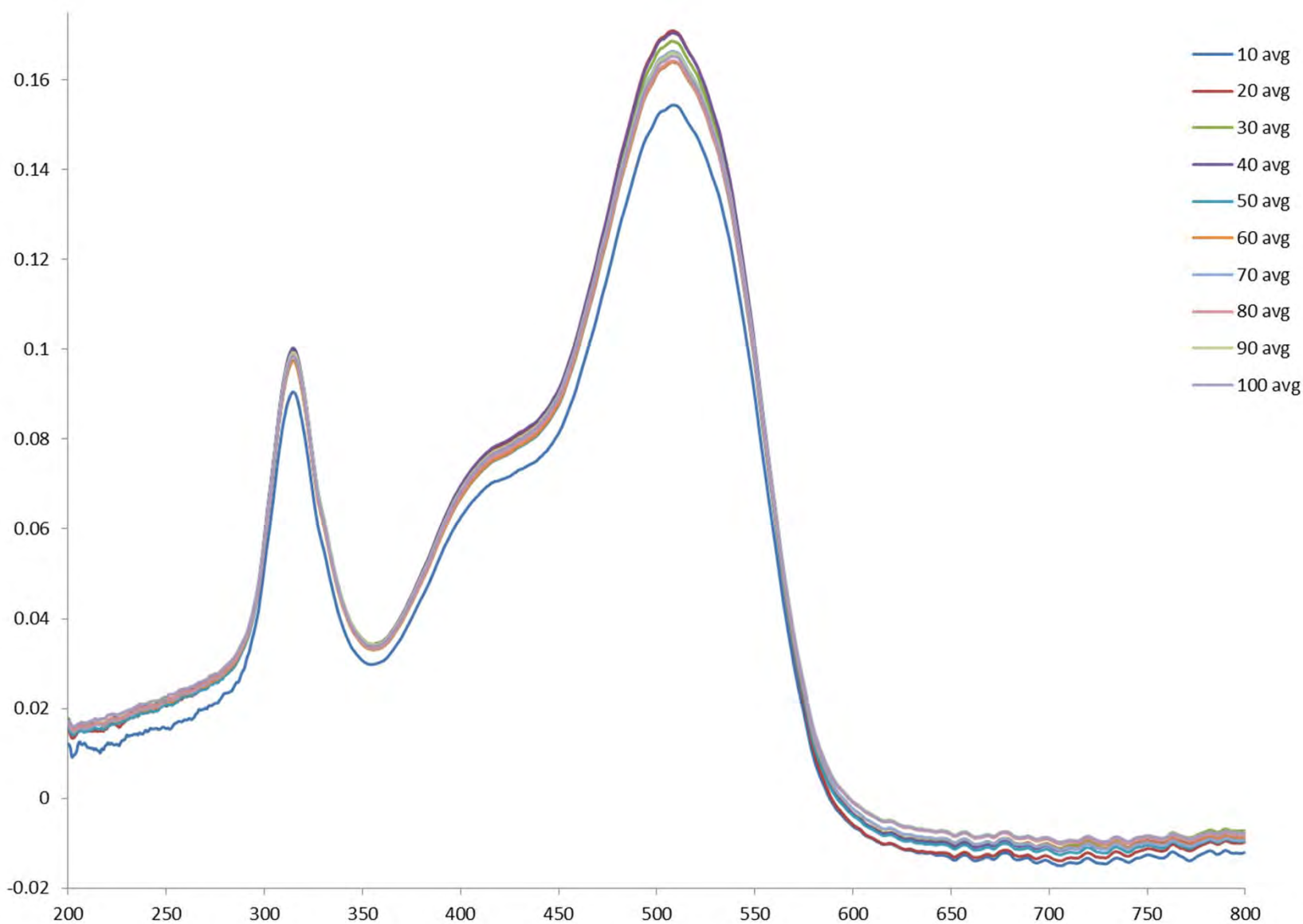


Figure 243. Change in the average spectrum of one-hundred cotton fibers dyed with Reactive Red 43 in ten fiber intervals (*i.e.*, “10 avg” represents the average of the first ten fibers (thirty spectra), “20 avg” represents the average of the first twenty fibers (sixty spectra), *etc.*).

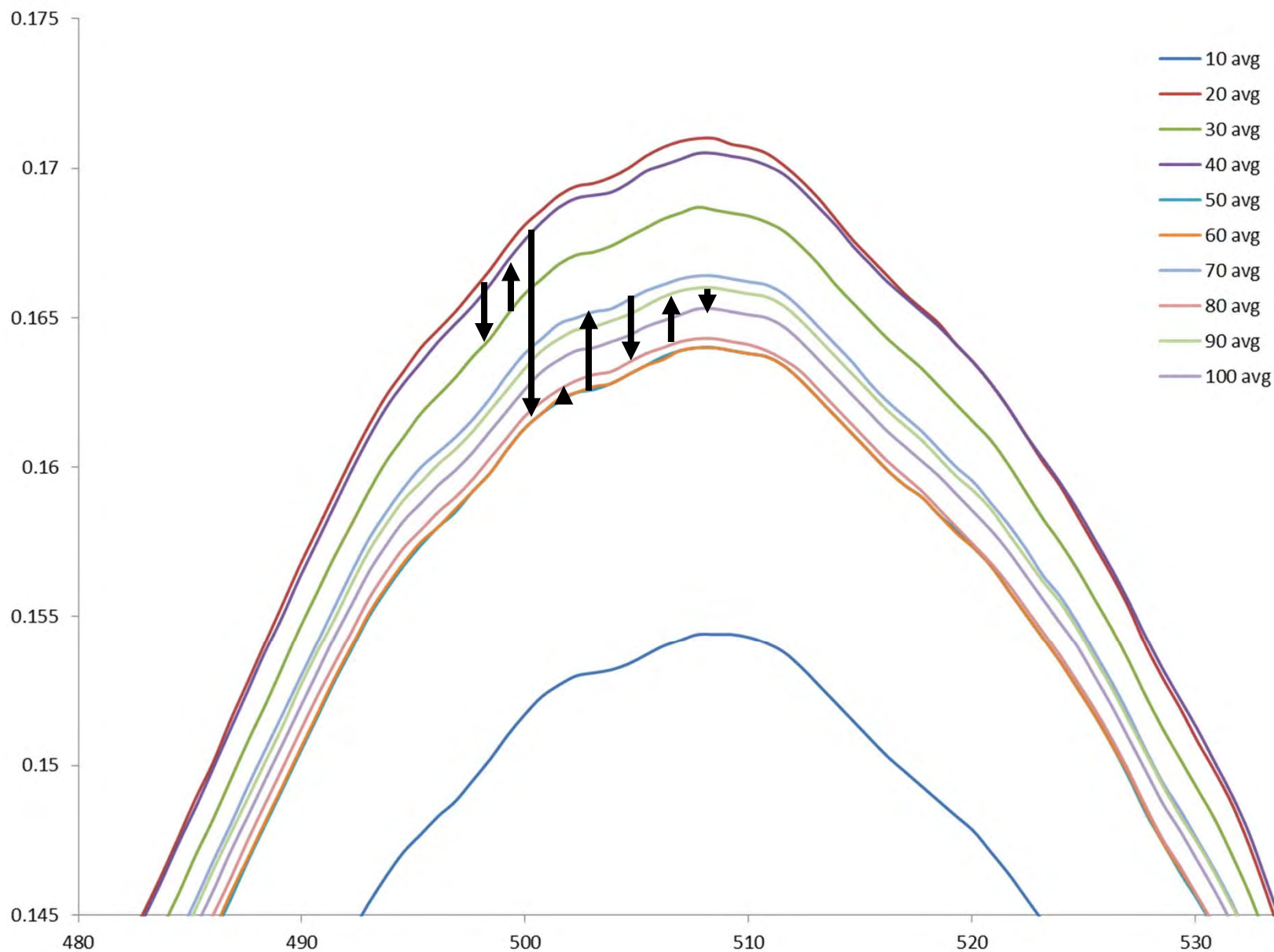


Figure 244. Change in the average spectrum of one-hundred cotton fibers dyed with Reactive Red 39 in ten fiber intervals (*i.e.*, “10 avg” represents the average of the first ten fibers (thirty spectra), “20 avg” represents the average of the first twenty fibers (sixty spectra), *etc.*). Black arrows (read from left to right) indicate how the average fluctuates as more fibers are averaged.

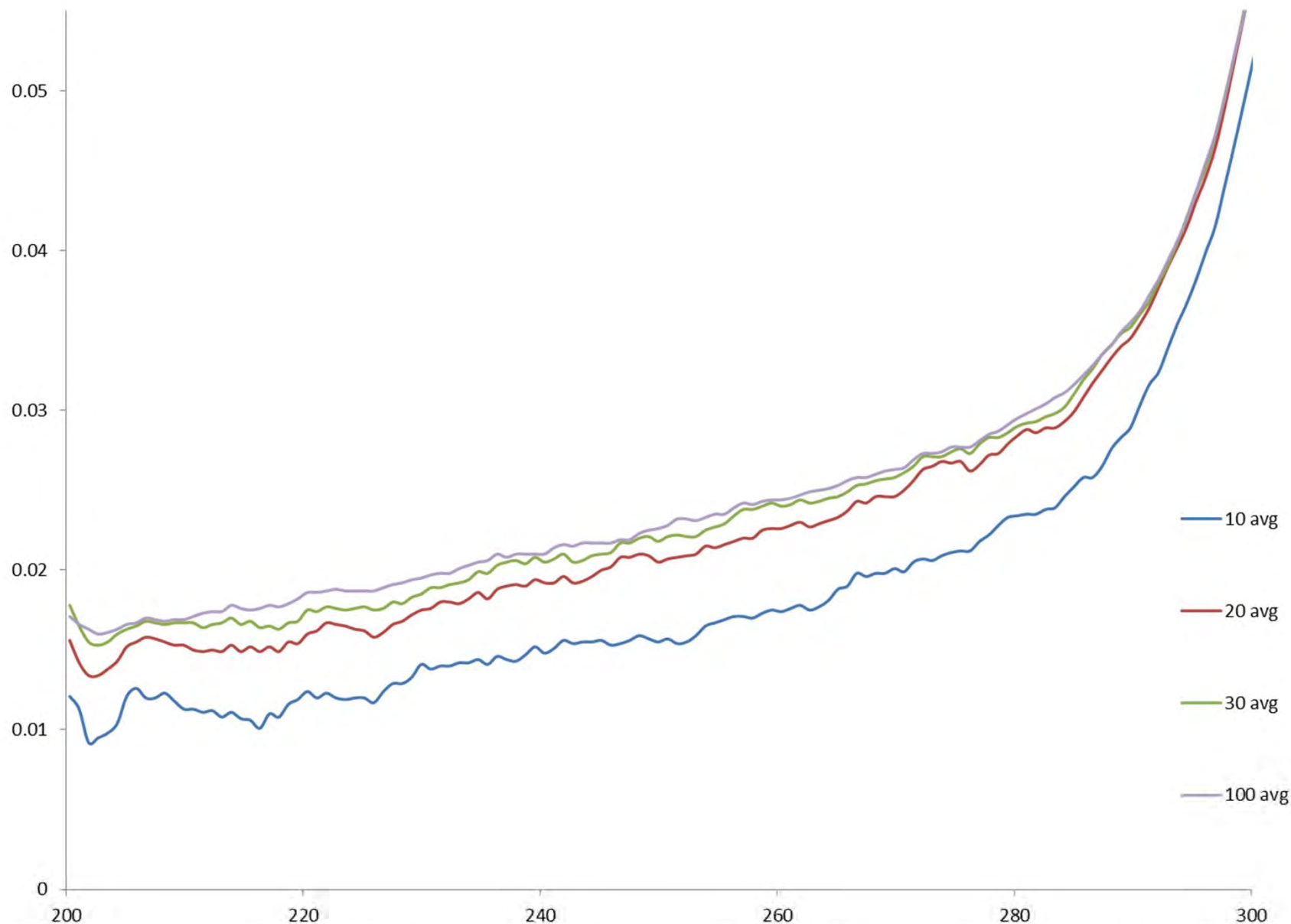


Figure 245. Change in the average spectrum of one-hundred cotton fibers dyed with Reactive Red 43 in ten fiber intervals (*i.e.*, “10 avg” represents the average of the first ten fibers (thirty spectra), “20 avg” represents the average of the first twenty fibers (sixty spectra), *etc.* with averages of 40 – 90 fibers omitted for clarity). Note the significant decrease in the amplitude of the noise in this region.

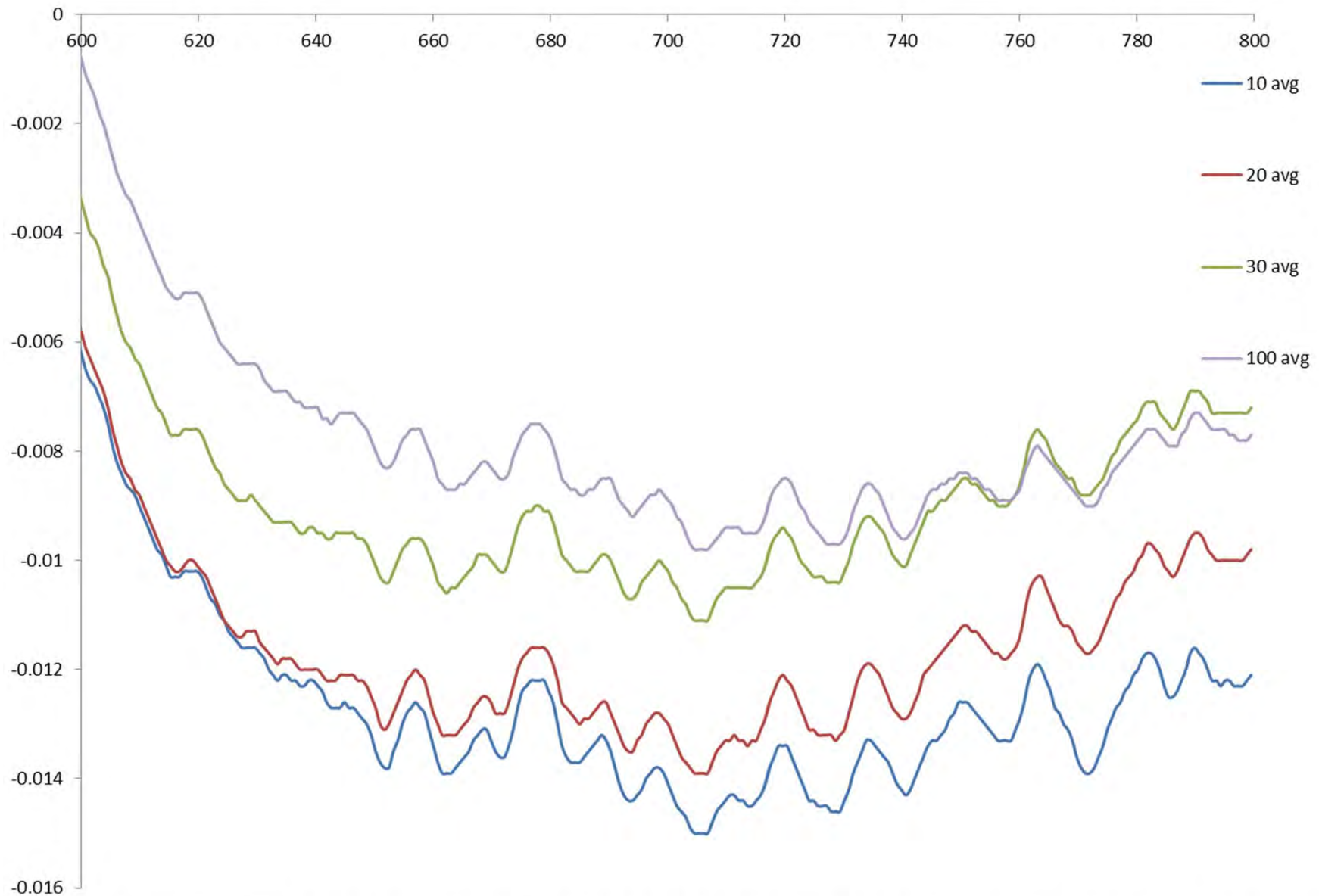


Figure 246. Change in the average spectrum of one-hundred cotton fibers dyed with Reactive Red 43 in ten fiber intervals (*i.e.*, “10 avg” represents the average of the first ten fibers (thirty spectra), “20 avg” represents the average of the first twenty fibers (sixty spectra), *etc.* with averages of 40 – 90 fibers omitted for clarity). Note that there is minimal decrease in the amplitude of the fluctuations in this region.

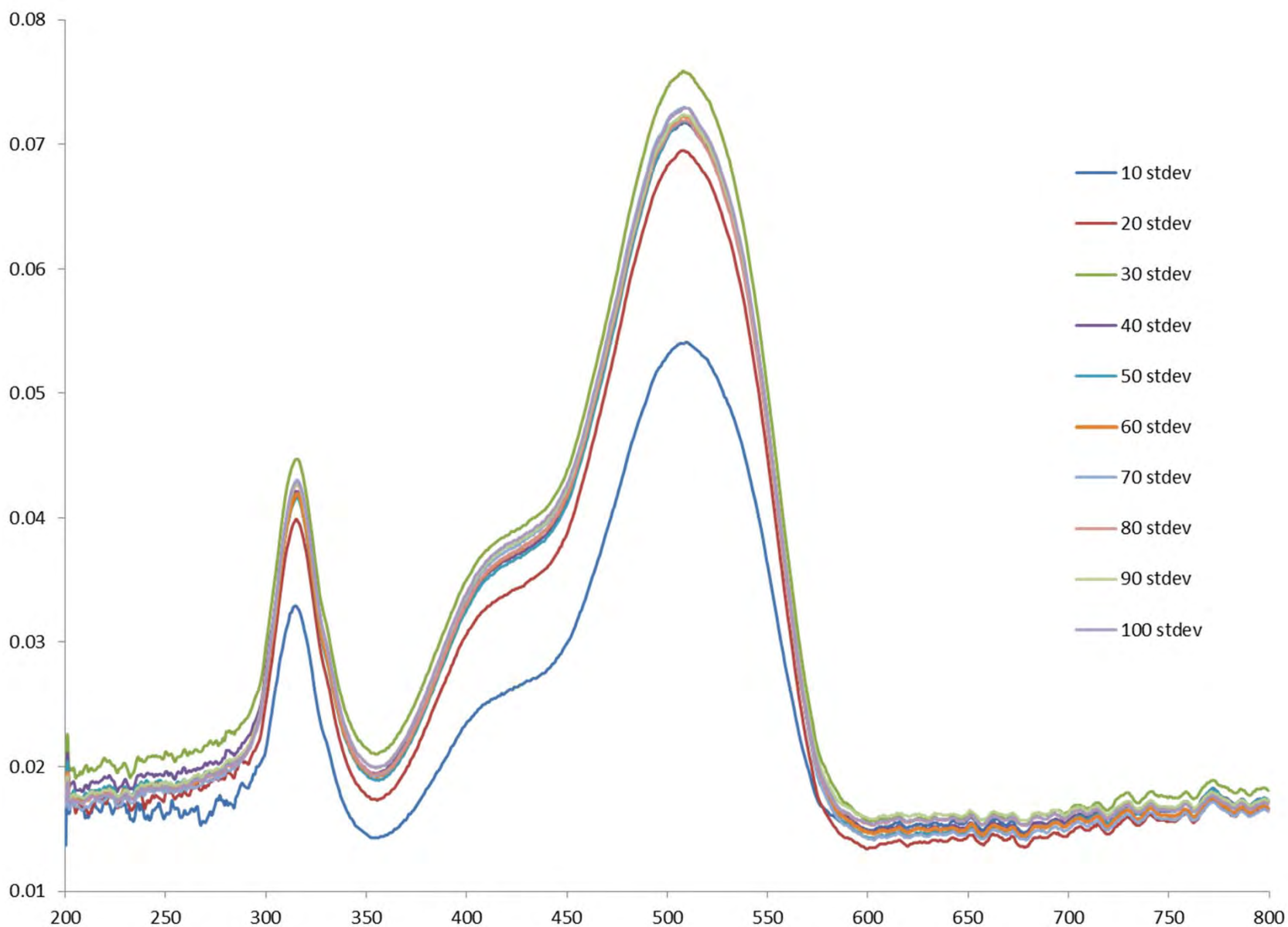


Figure 247. Change in the standard deviation of one-hundred cotton fibers dyed with Reactive Red 43 in ten fiber intervals (*i.e.*, “10 stdev” represents the standard deviation of the first ten fibers (thirty spectra), “20 stdev” represents the standard deviation of the first twenty fibers (sixty spectra), *etc.*).

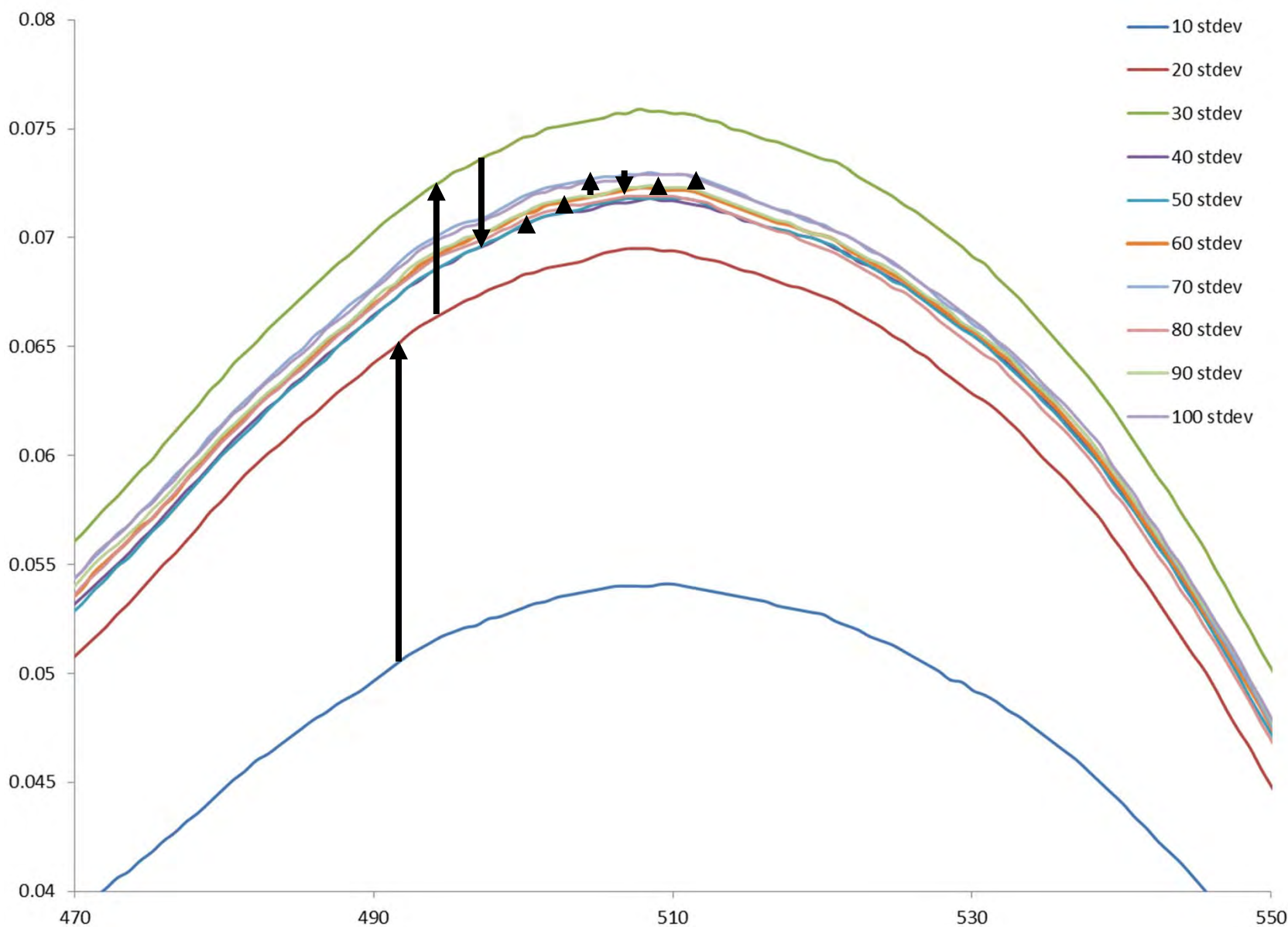


Figure 248. Change in the standard deviation of one-hundred cotton fibers dyed with Reactive Red 43 in ten fiber intervals (*i.e.*, “10 stdev” represents the standard deviation of the first ten fibers (thirty spectra), “20 stdev” represents the standard deviation of the first twenty fibers (sixty spectra), *etc.*). Black arrows (read from left to right) indicate how the standard deviation fluctuates as more fibers are averaged.

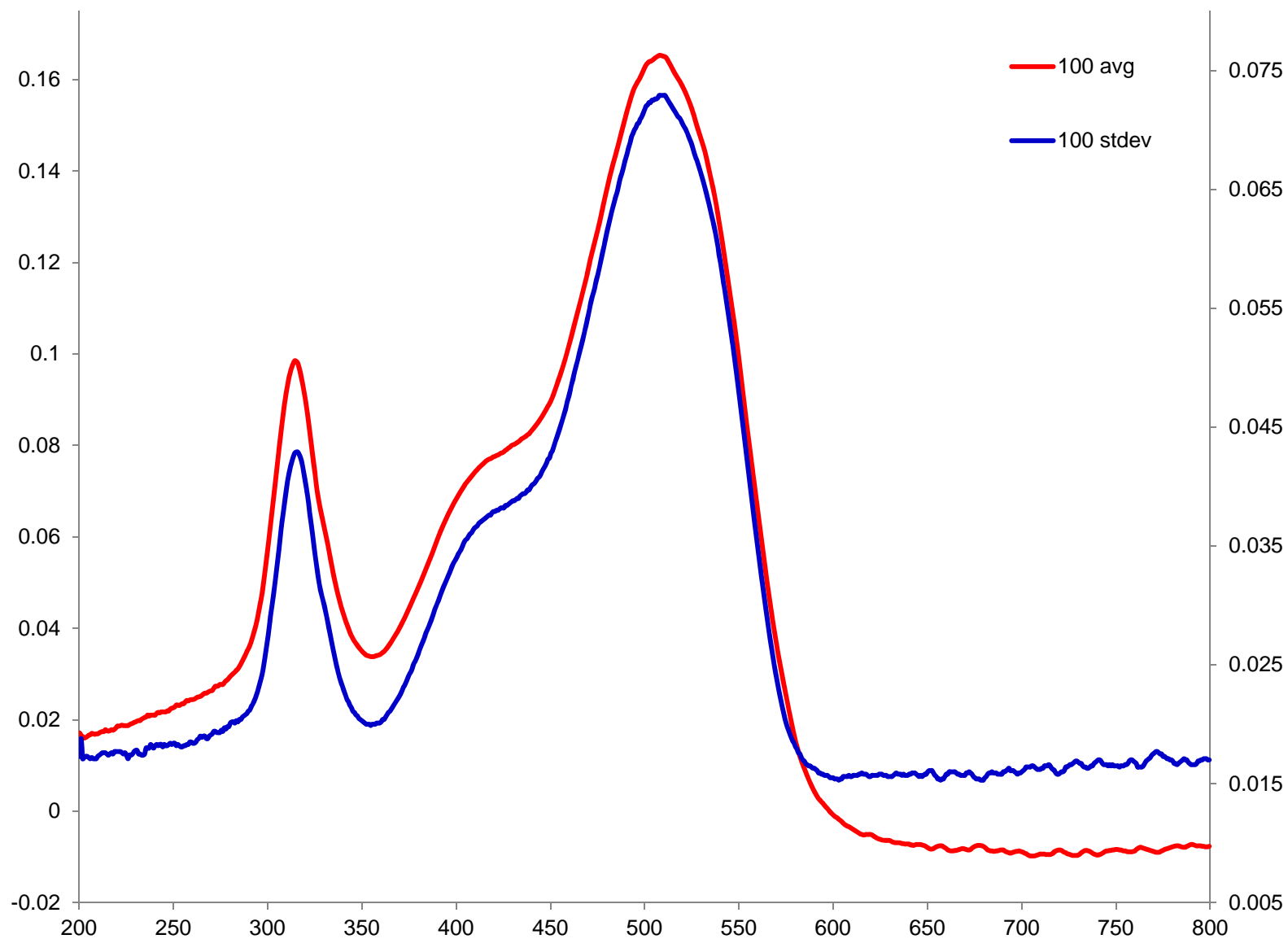


Figure 249. Average spectrum of 100 Reactive Red fibers (300 spectra) (red – left axis) compared to the standard deviation of the same spectra (blue – right axis).

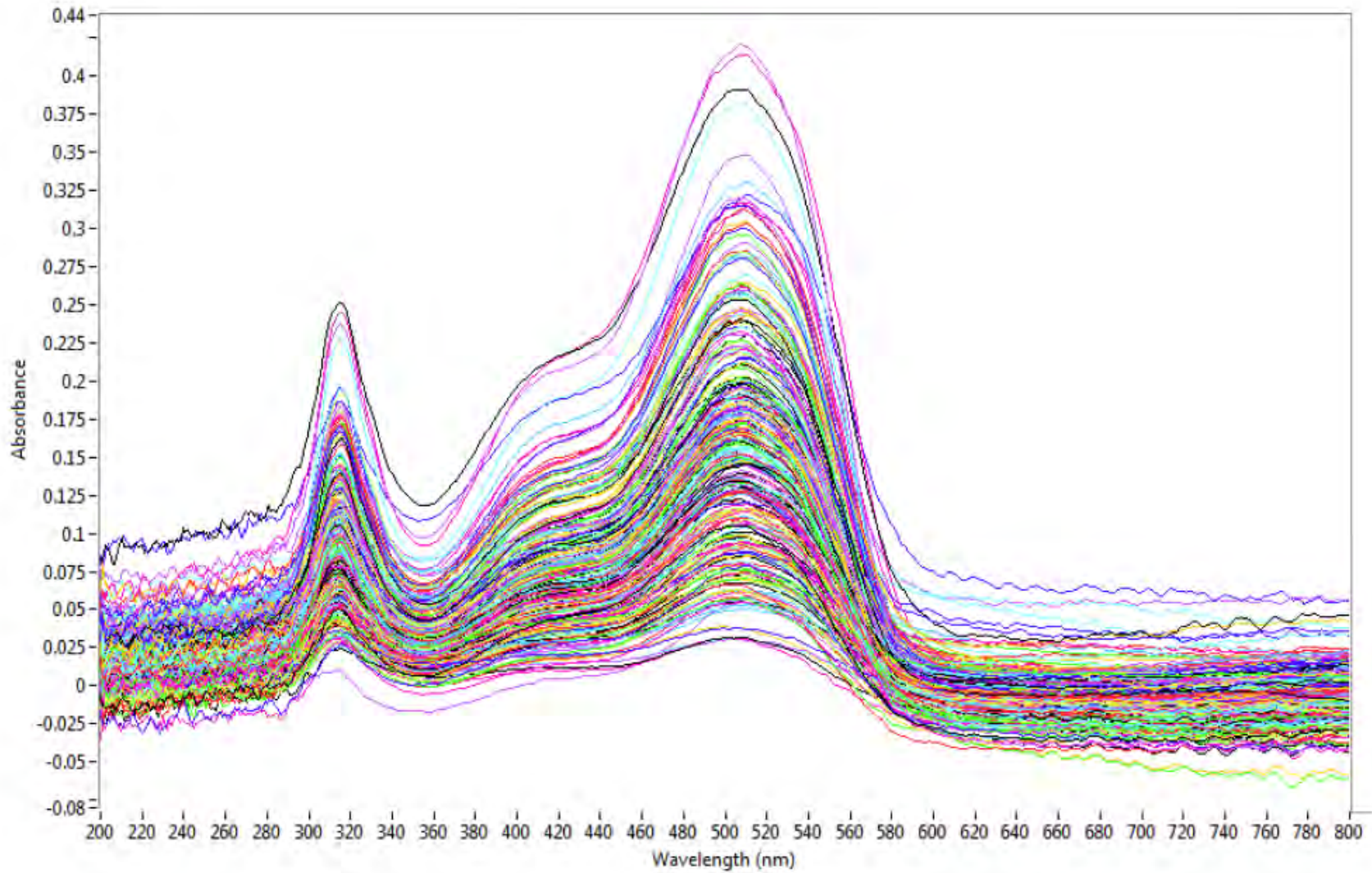


Figure 250. Three-hundred individual spectra collected from one-hundred Reactive Red fibers.

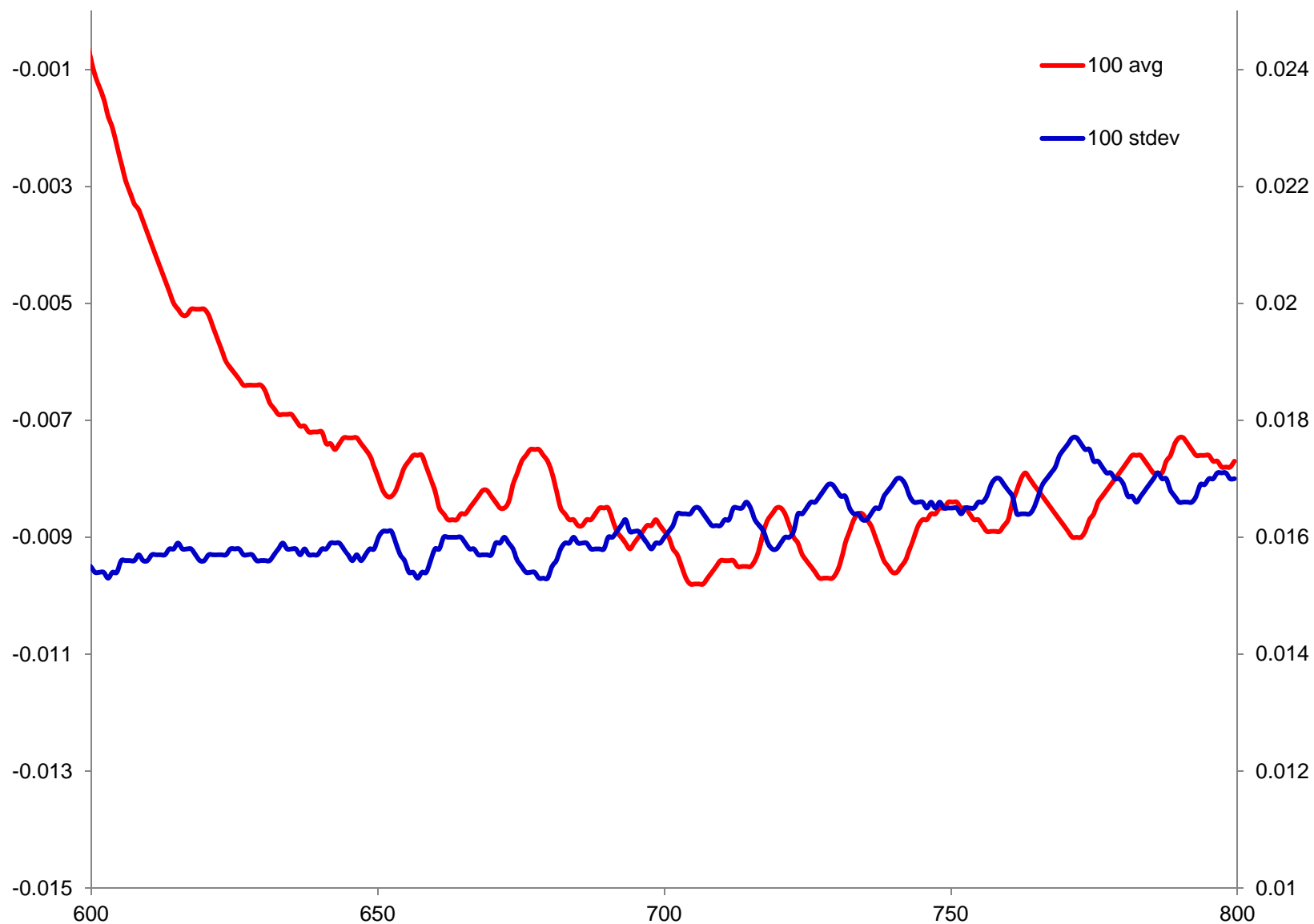


Figure 251. Average spectrum of 100 Reactive Red fibers (300 spectra) (red – left axis) compared to the standard deviation of the same spectra (blue – right axis).

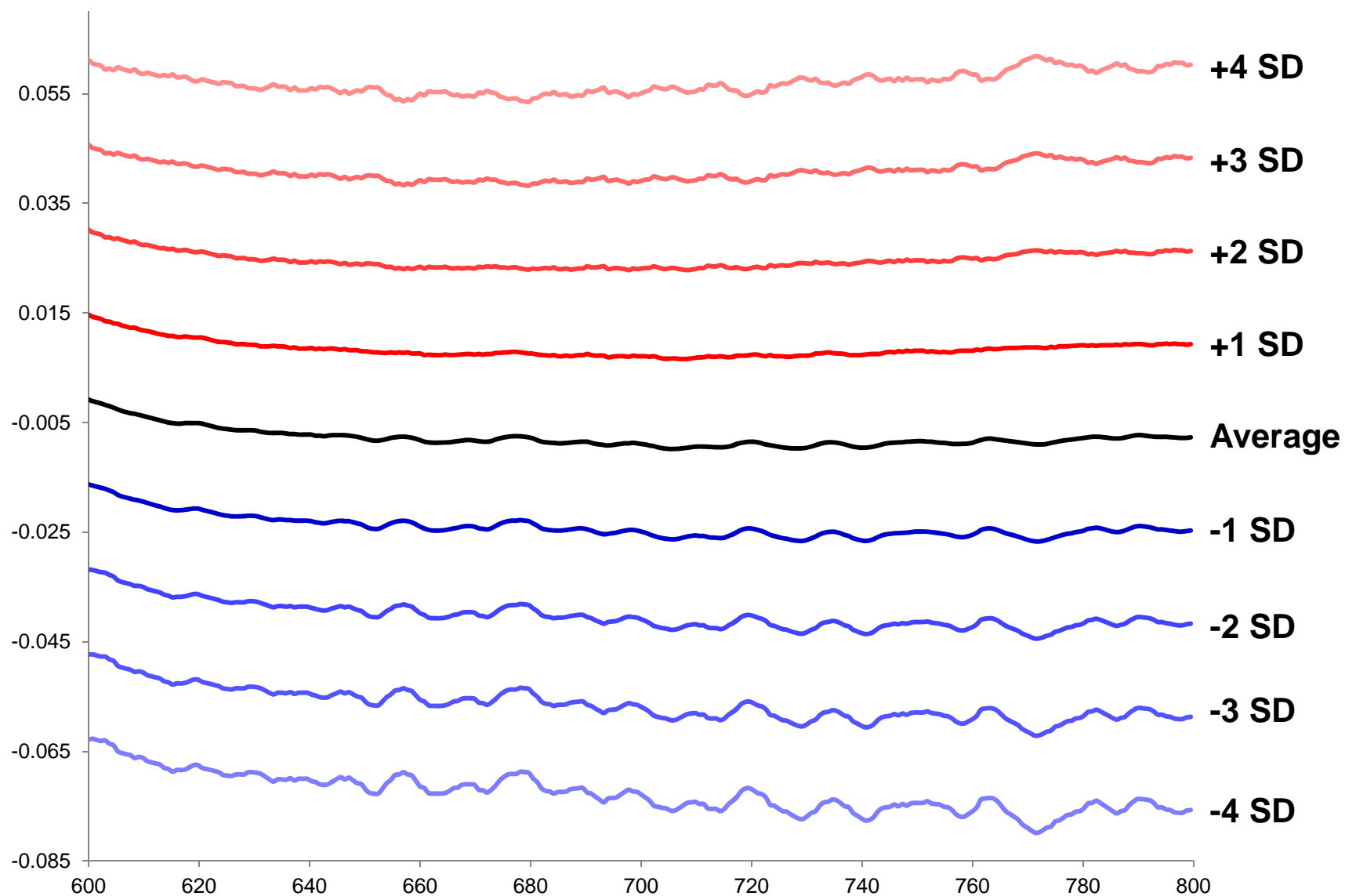


Figure 252. Average spectrum of 100 Reactive Red fibers (300 spectra) (black) with plots where the standard deviation had been added (red) and subtracted (blue).

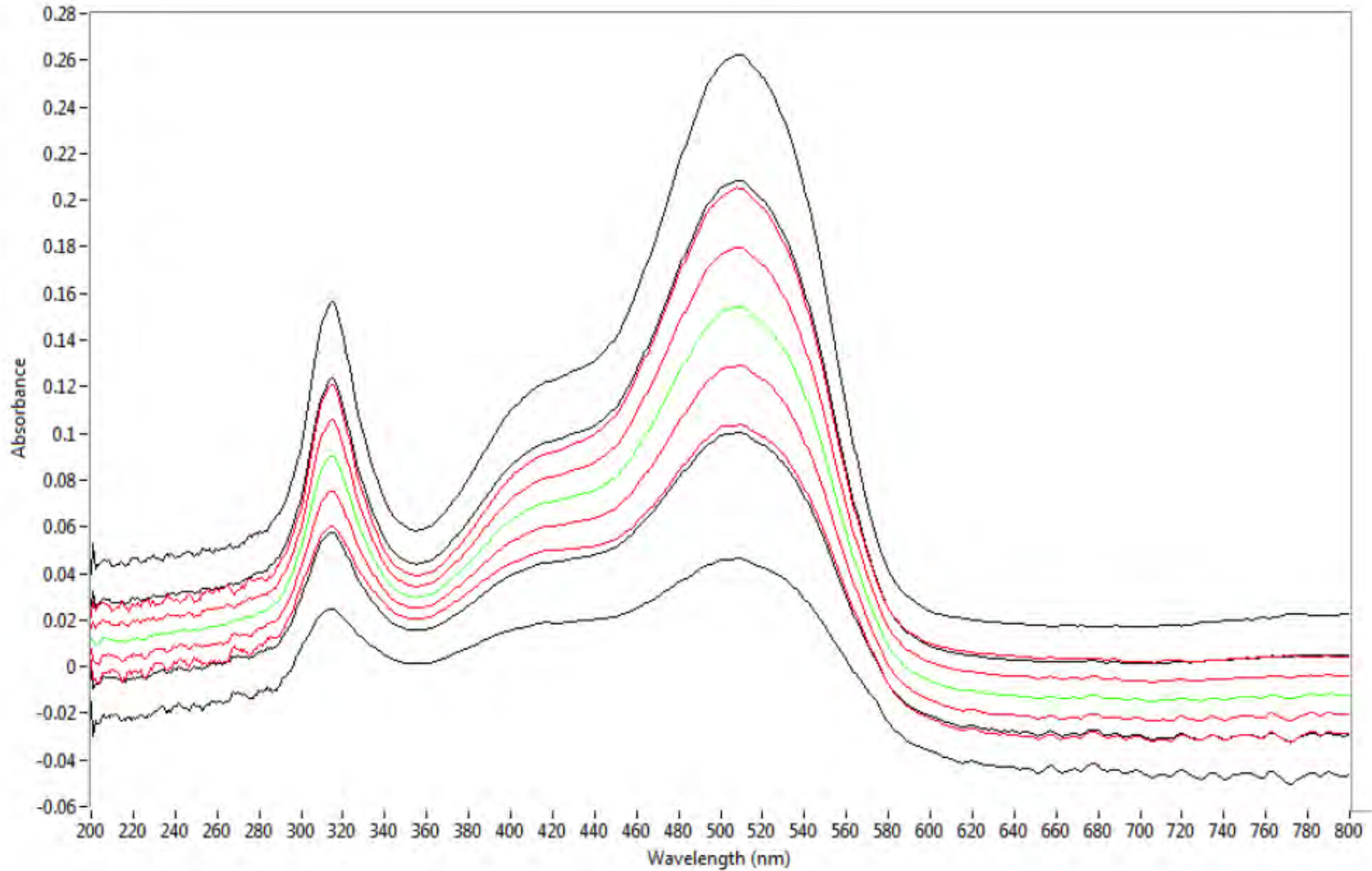


Figure 253. Average spectrum of ten fibers dyed with Reactive Red 43 (green) compared to ± 1 and 2σ calculated using the original individual thirty spectra (black) and ± 1 and 2σ calculated using the sub-averaged spectra (ten spectra each an average of three spectra) (red).

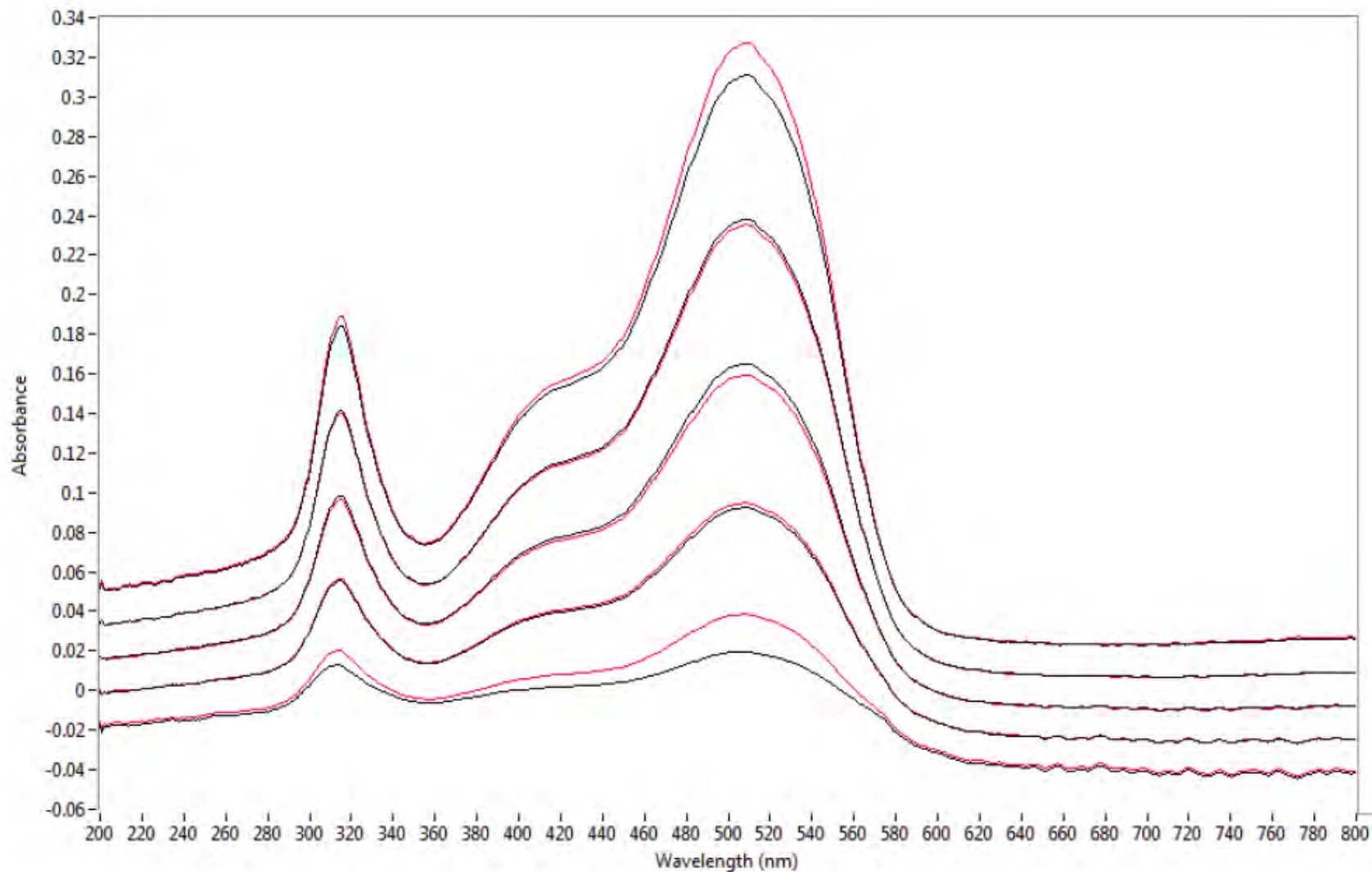


Figure 254. Average and ± 1 and 2σ spectra calculated using absorbance (black) and transmission (red) data from the 100 cotton fibers dyed with Reactive Red 43 (300 spectra). The spectra calculated using transmission data were converted to absorbance after the calculations were performed.

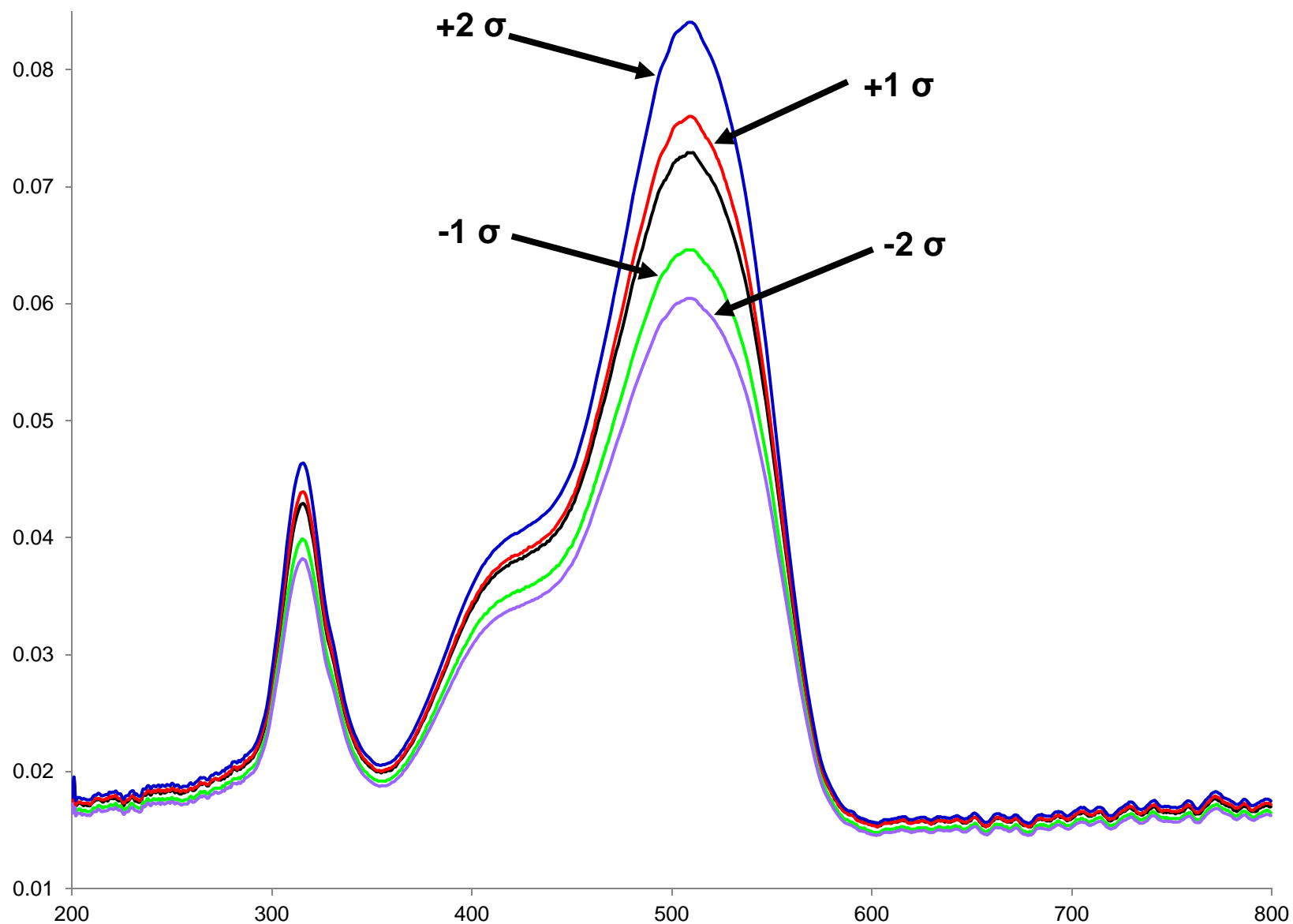


Figure 255. Absolute value of the standard deviation calculated using absorbance (black) compared to the absolute values of ± 1 and 2σ calculated using transmission data (and then plotted in absorbance units).

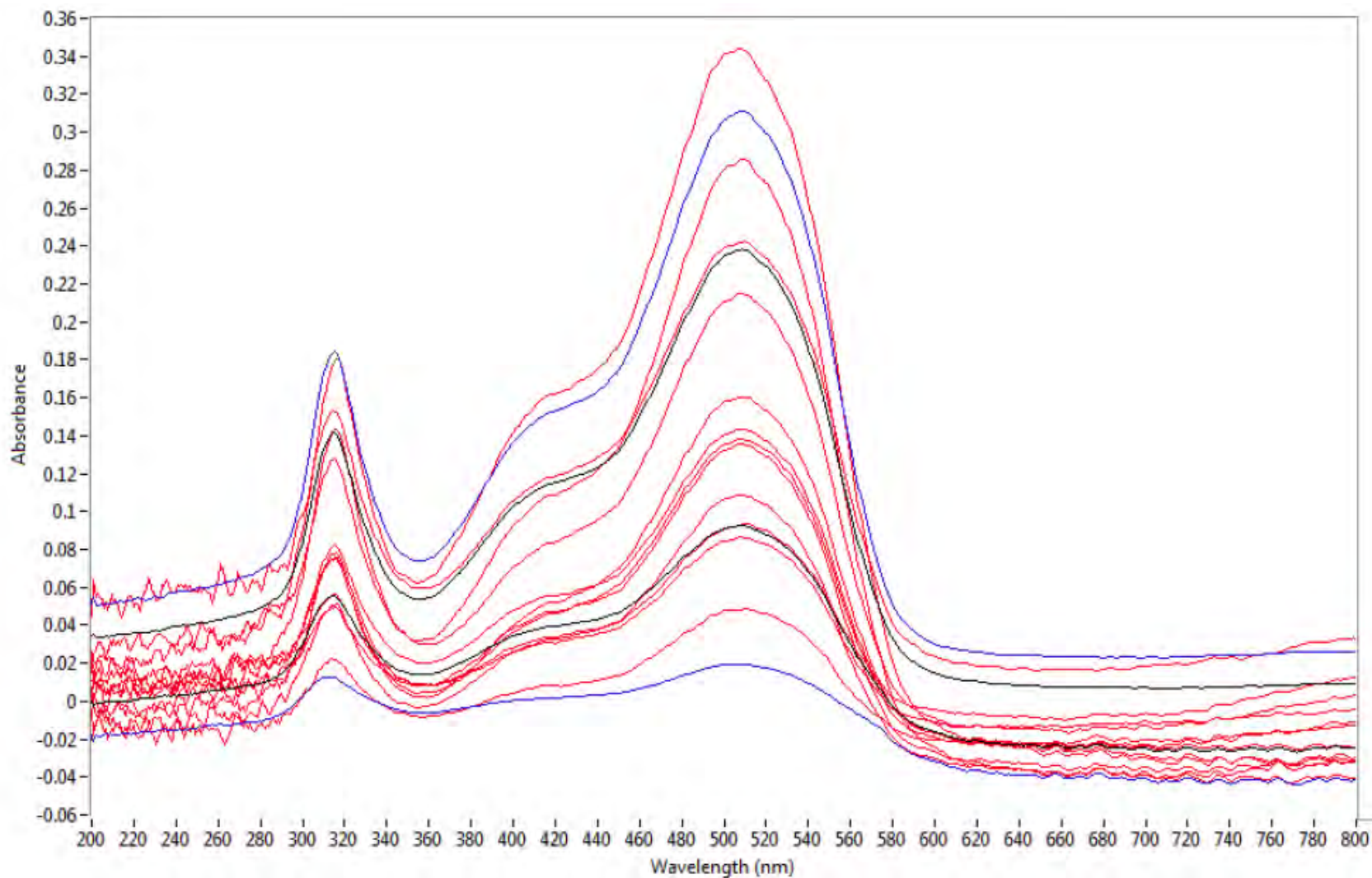


Figure 256. Plus and minus one (black) and two (blue) standard deviations calculated from the three-hundred individual spectra collected from one-hundred cotton fibers dyed with Reactive Red 43 at a concentration of 16 g/L compared to twelve spectra collected from four different cotton fibers dyed at the same concentration.

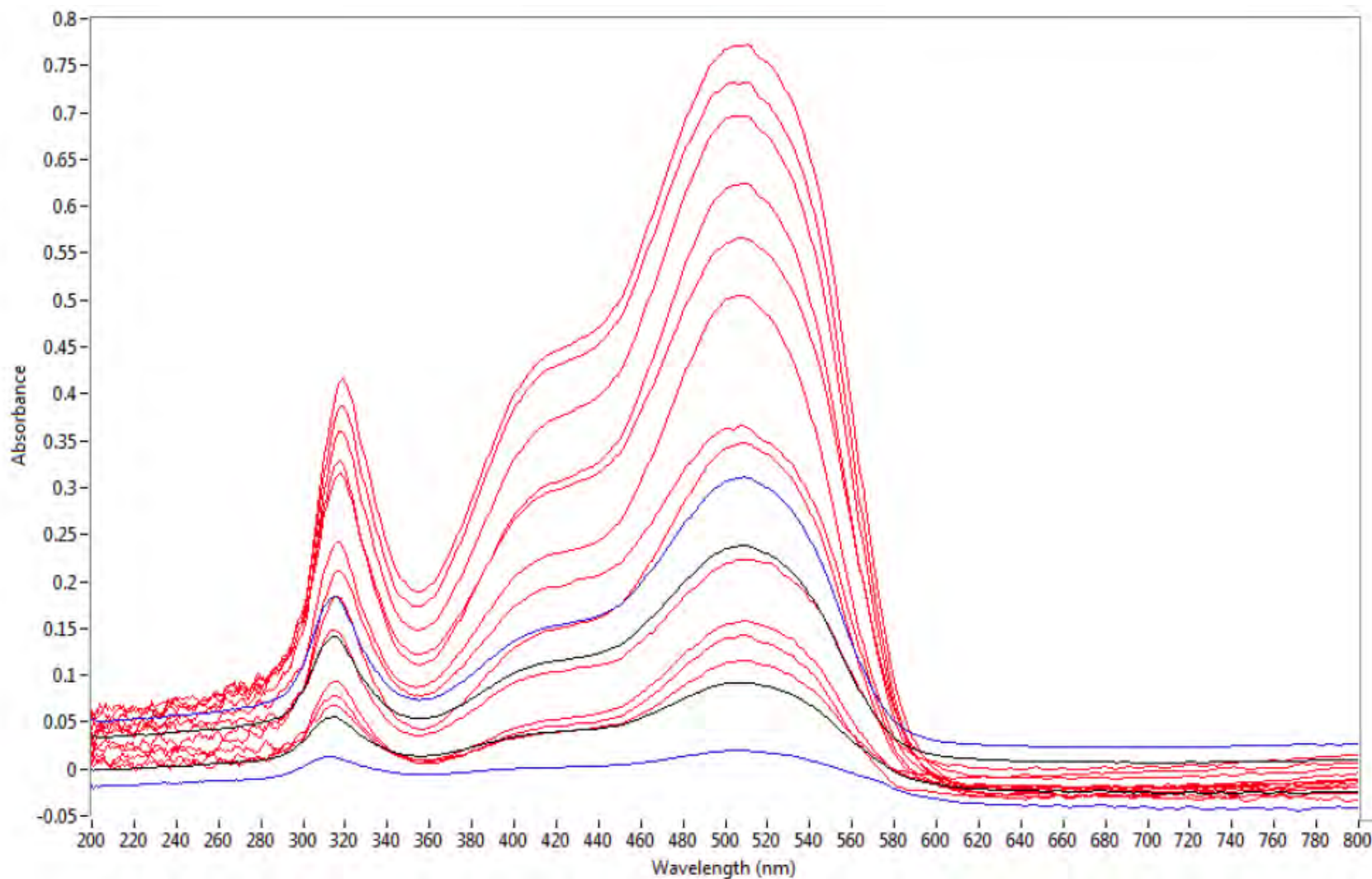


Figure 257. Plus and minus one (black) and two (blue) standard deviations calculated from the three-hundred individual spectra collected from one-hundred cotton fibers dyed with Reactive Red 43 at a concentration of 16 g/L compared to twelve spectra collected from four cotton fibers dyed at a higher concentration (40 g/L).

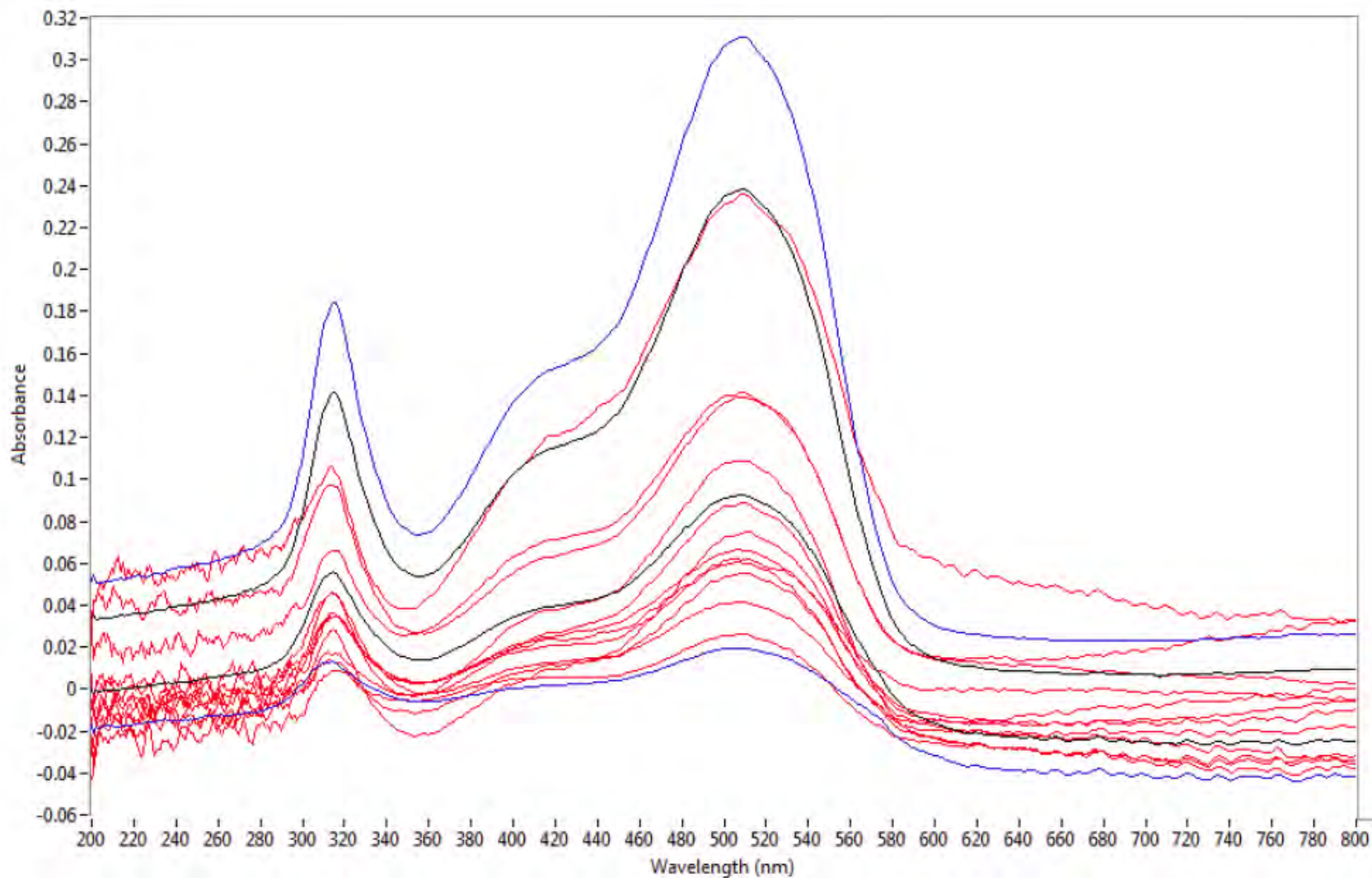


Figure 258. Plus and minus one (black) and two (blue) standard deviations calculated from the three-hundred individual spectra collected from one-hundred cotton fibers dyed with Reactive Red 43 at a concentration of 16 g/L compared to twelve spectra collected from four cotton fibers dyed at a lower concentration (6 g/L).

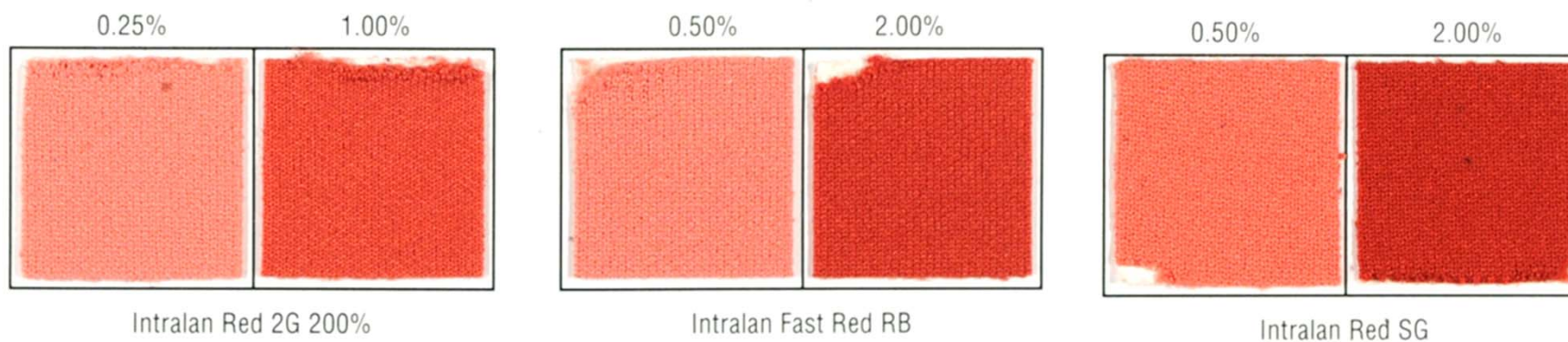


Figure 259. Six Intralan fabric swatches selected for examination.

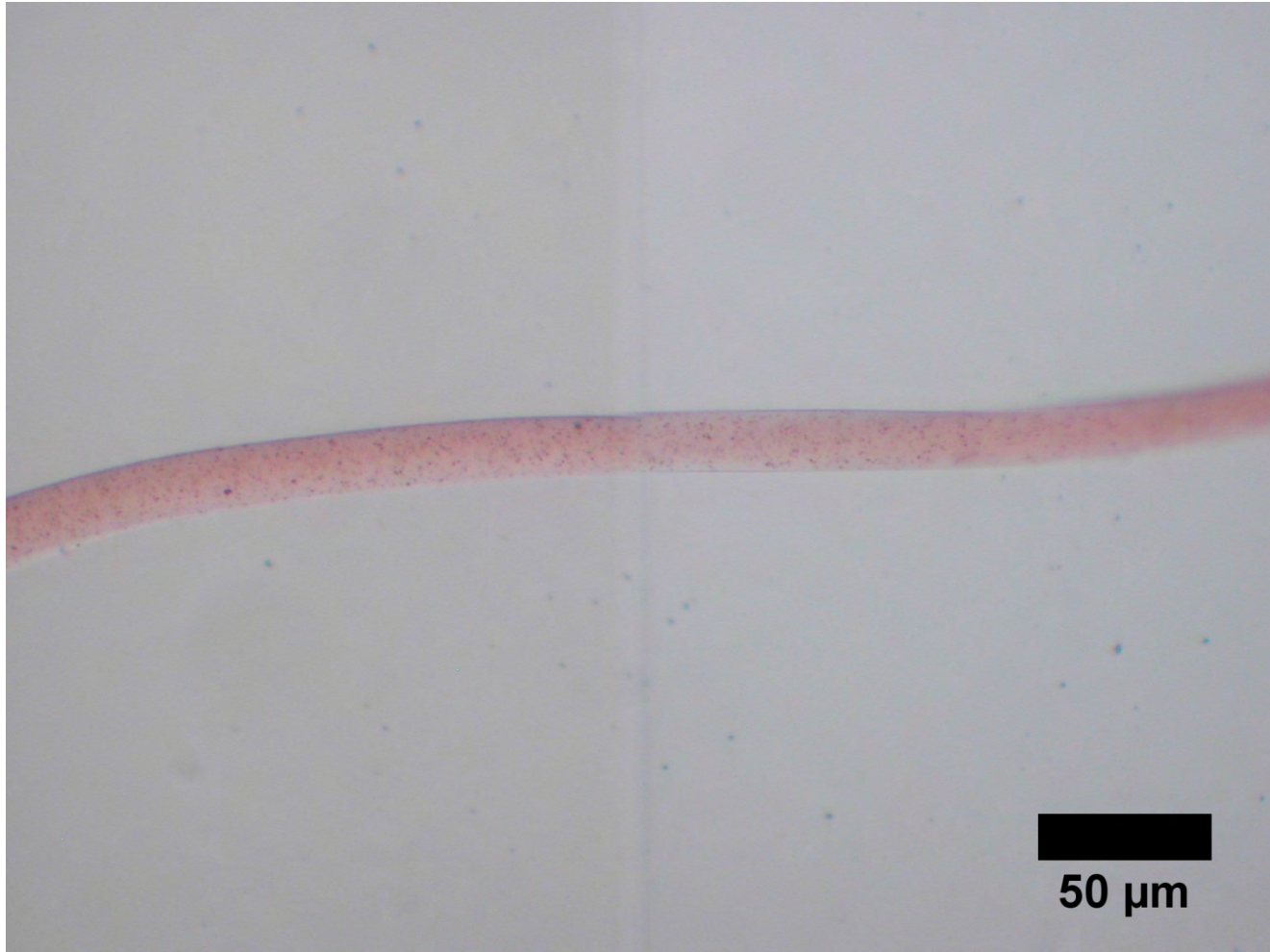


Figure 260. Comparison microscopy image of fibers dyed with Intralan Red 2G (1%) (left) and Intralan Fast Red RB (2%) (right).

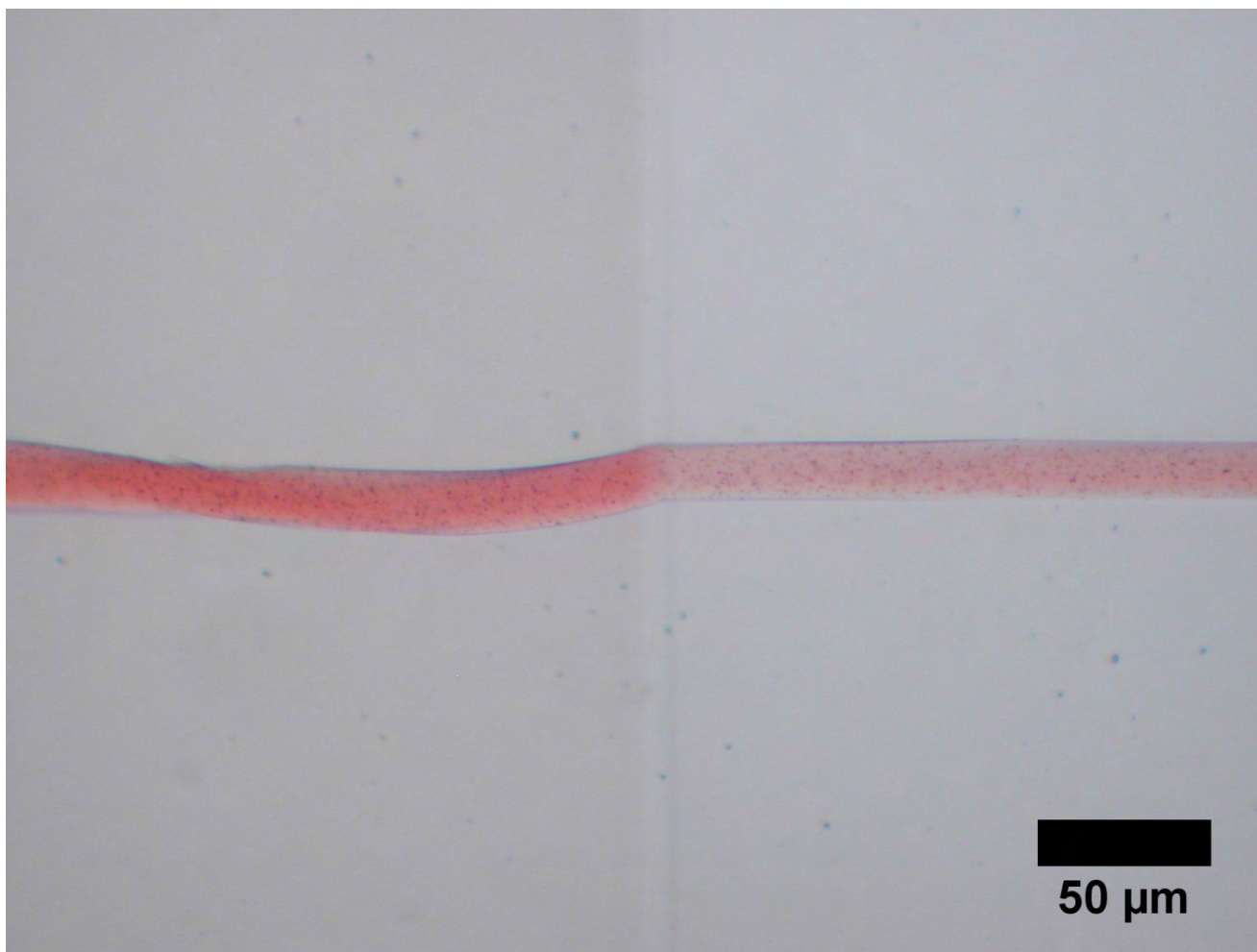


Figure 261. Comparison microscopy image of fibers dyed with Intralan Red SG (2%) (left) and Intralan Red 2G (1%) (right).

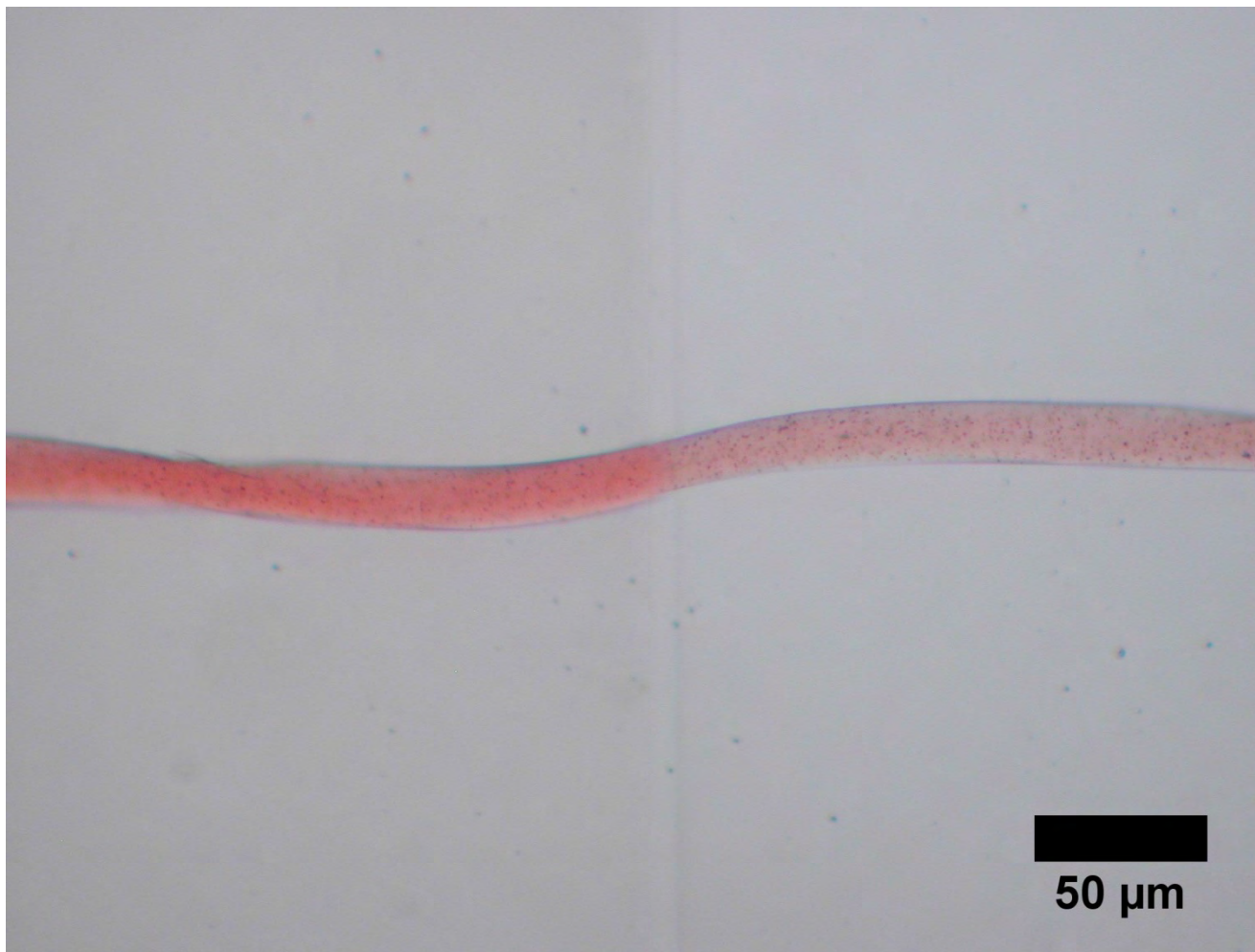


Figure 262. Comparison microscopy image of fibers dyed with Intralan Red SG (2%) (left) and Intralan Fast Red RB (2%) (right).

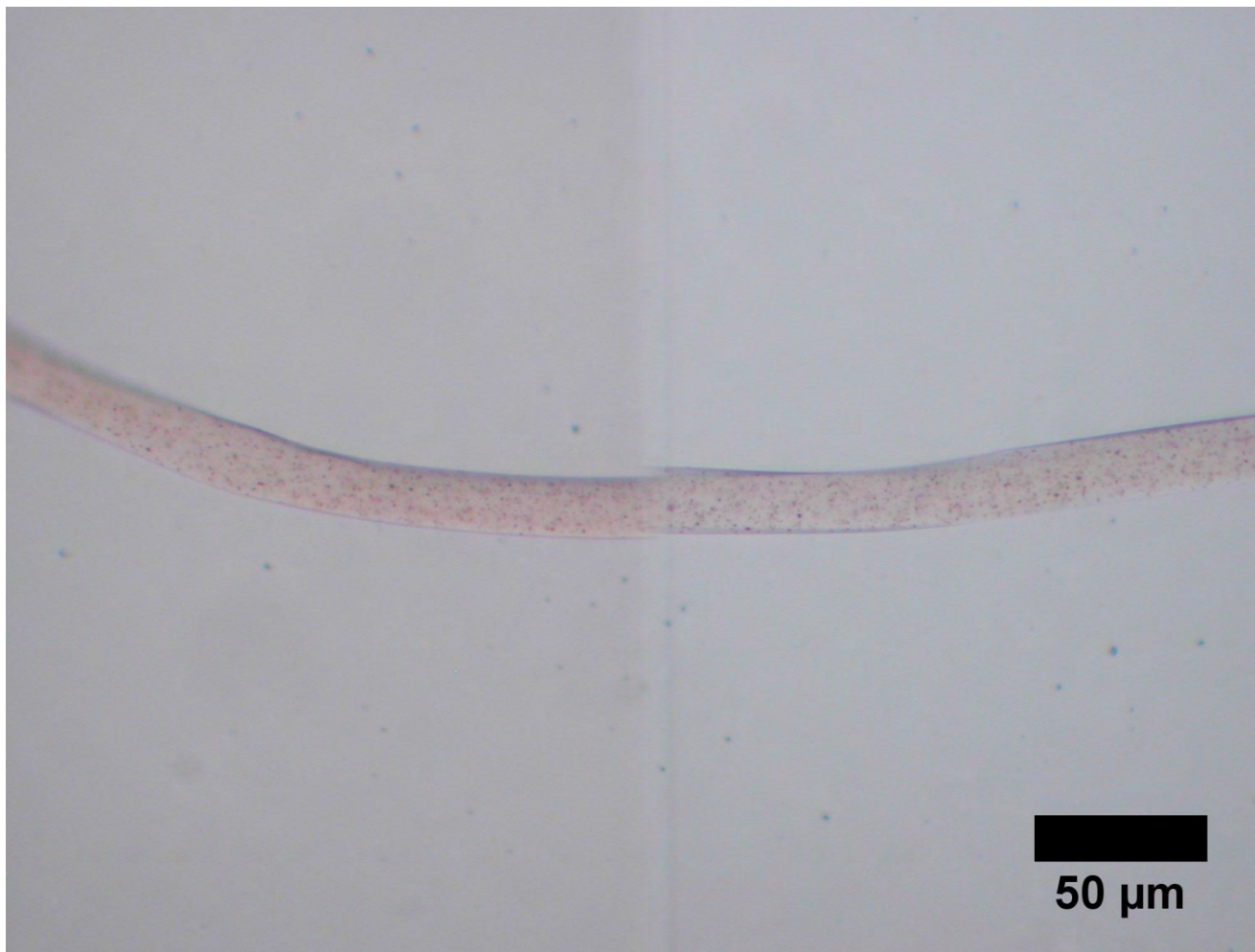


Figure 263. Comparison microscopy image of fibers dyed with Intralan Red SG (0.5%) (left) and Intralan Red 2G (0.25%) (right).

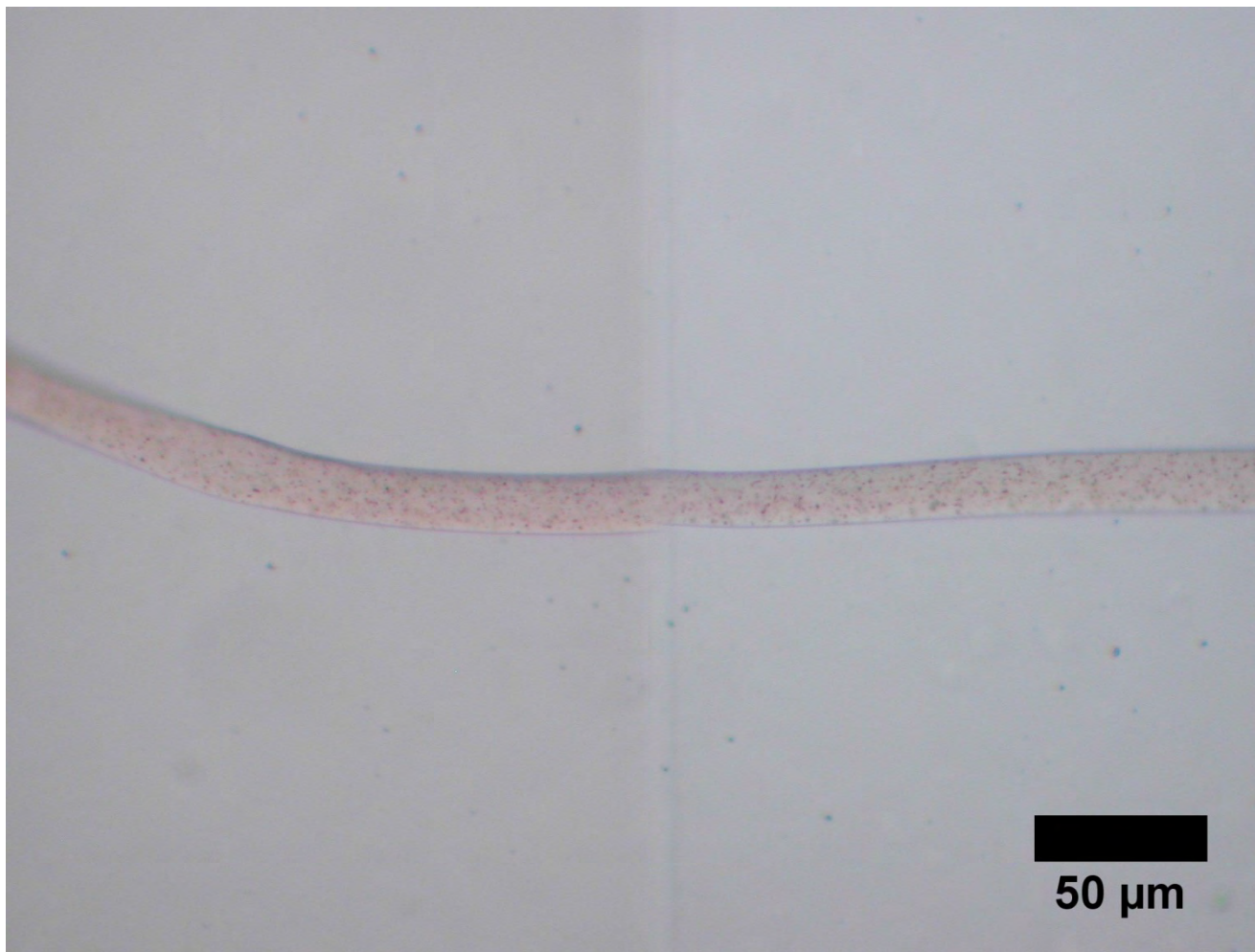


Figure 264. Comparison microscopy image of fibers dyed with Intralan Red SG (0.5%) (left) and Intralan Fast Red RB (0.5%) (right).

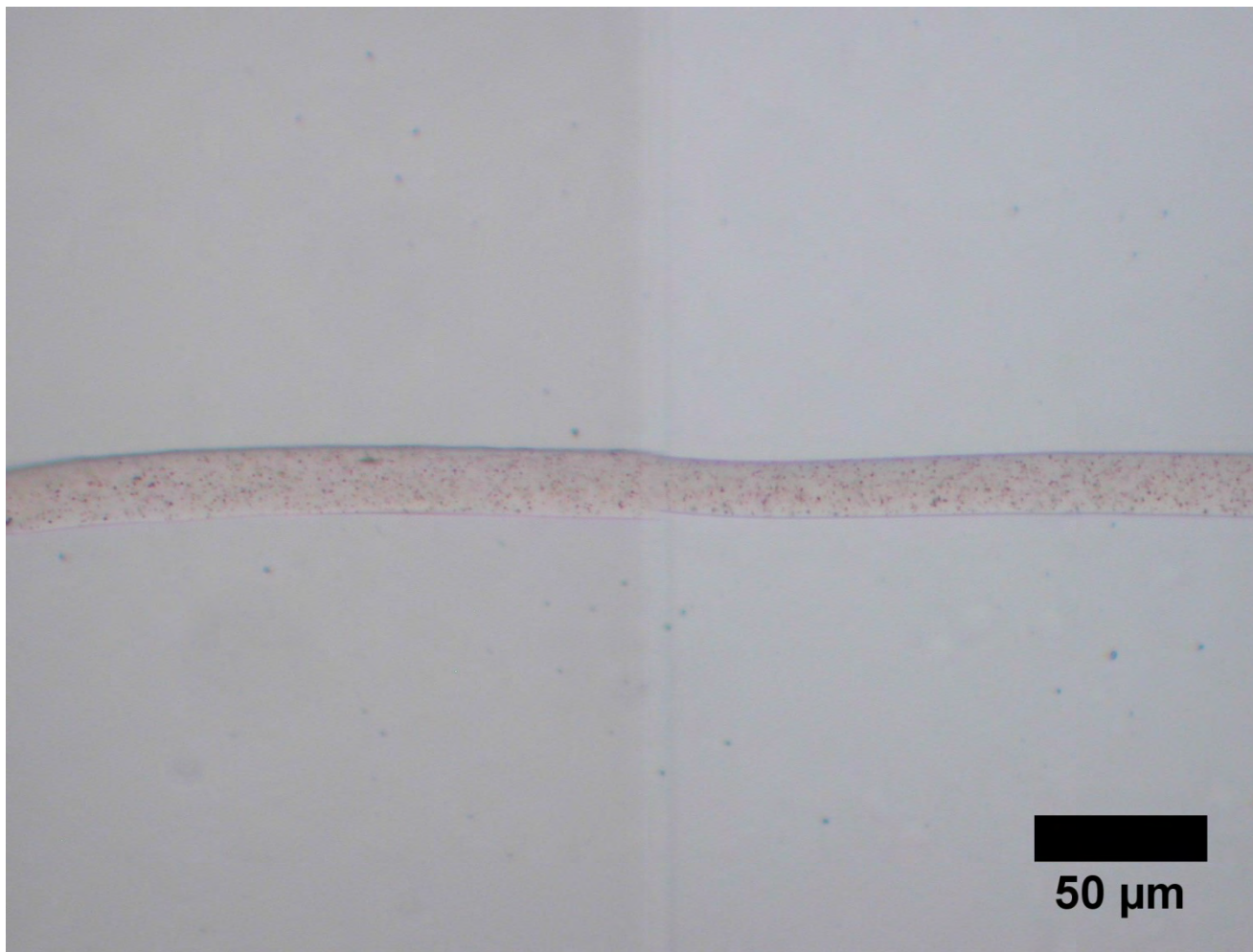


Figure 265. Comparison microscopy image of fibers dyed with Intralan Red 2G (0.25%) (left) and Intralan Fast Red RB (0.5%) (right).

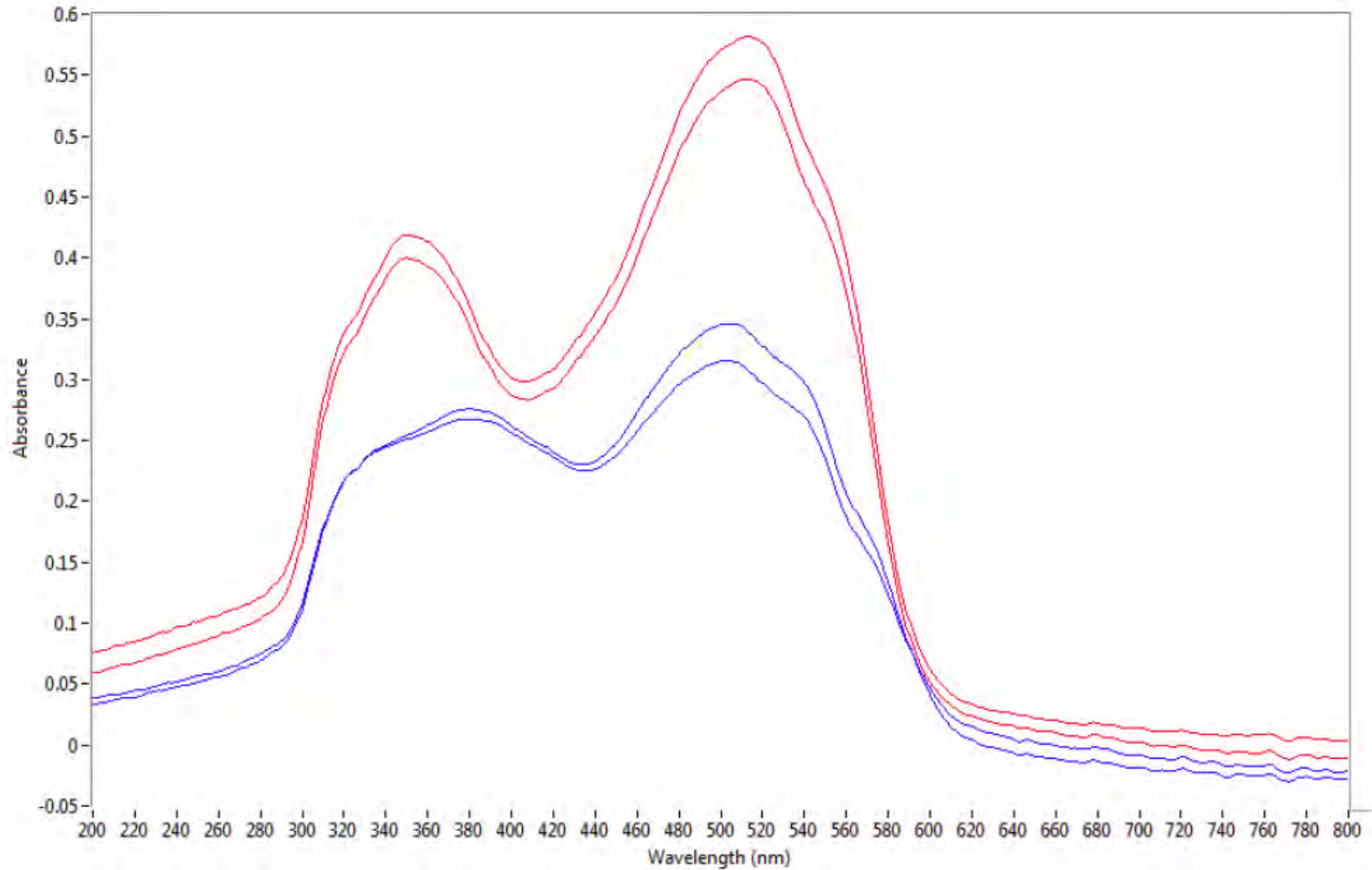


Figure 266. MSP spectra of fibers dyed with Intralan Fast Red RB 2% (blue) and Intralan Red SG 2% (red).

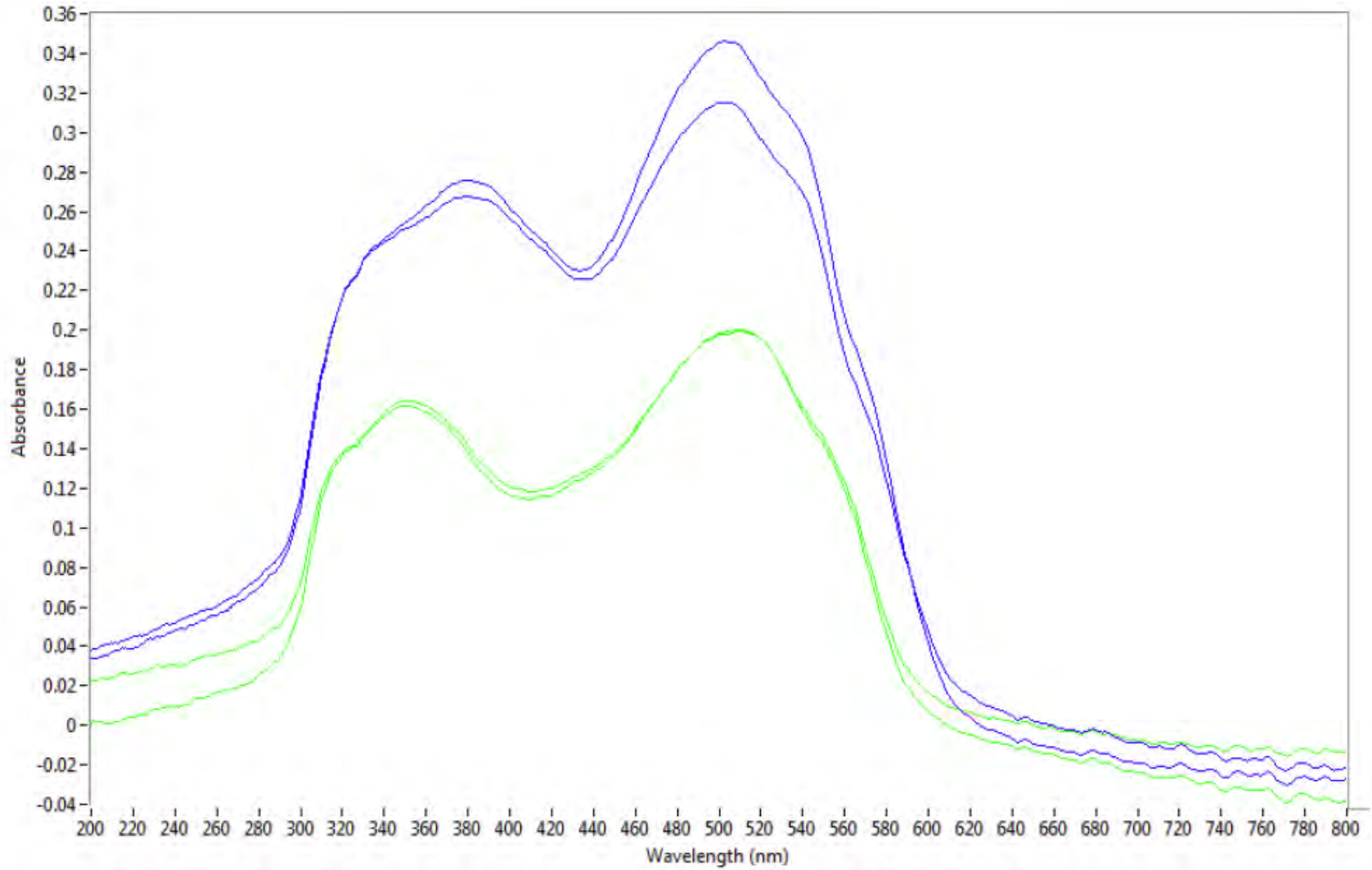


Figure 267. MSP spectra of fibers dyed with Intralan Fast Red RB 2% (blue) and Intralan Red 2G 1% (green).

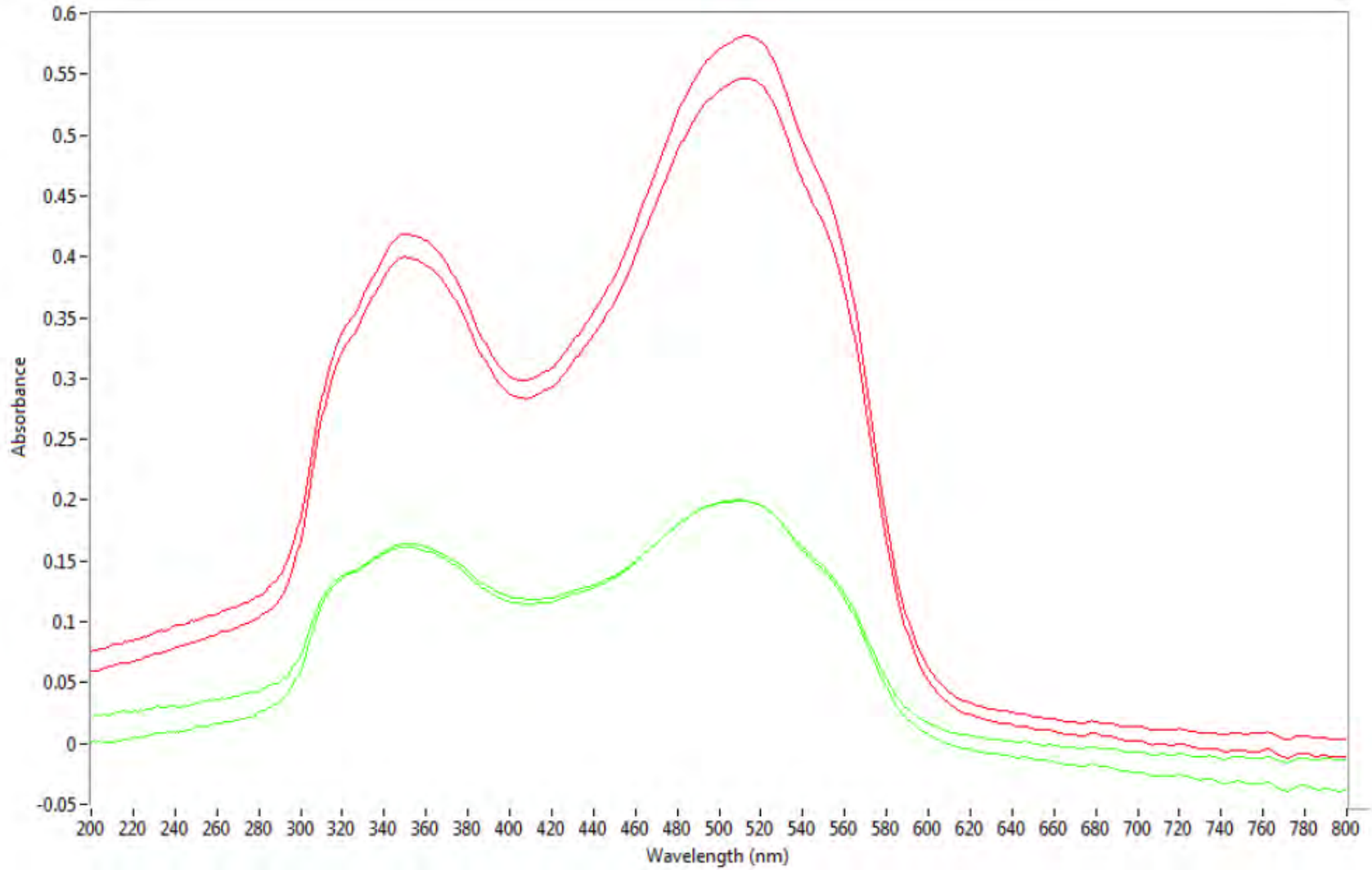


Figure 268. MSP spectra of fibers dyed with Intralan Red SG 2% (red) and Intralan Red 2G 1% (green).

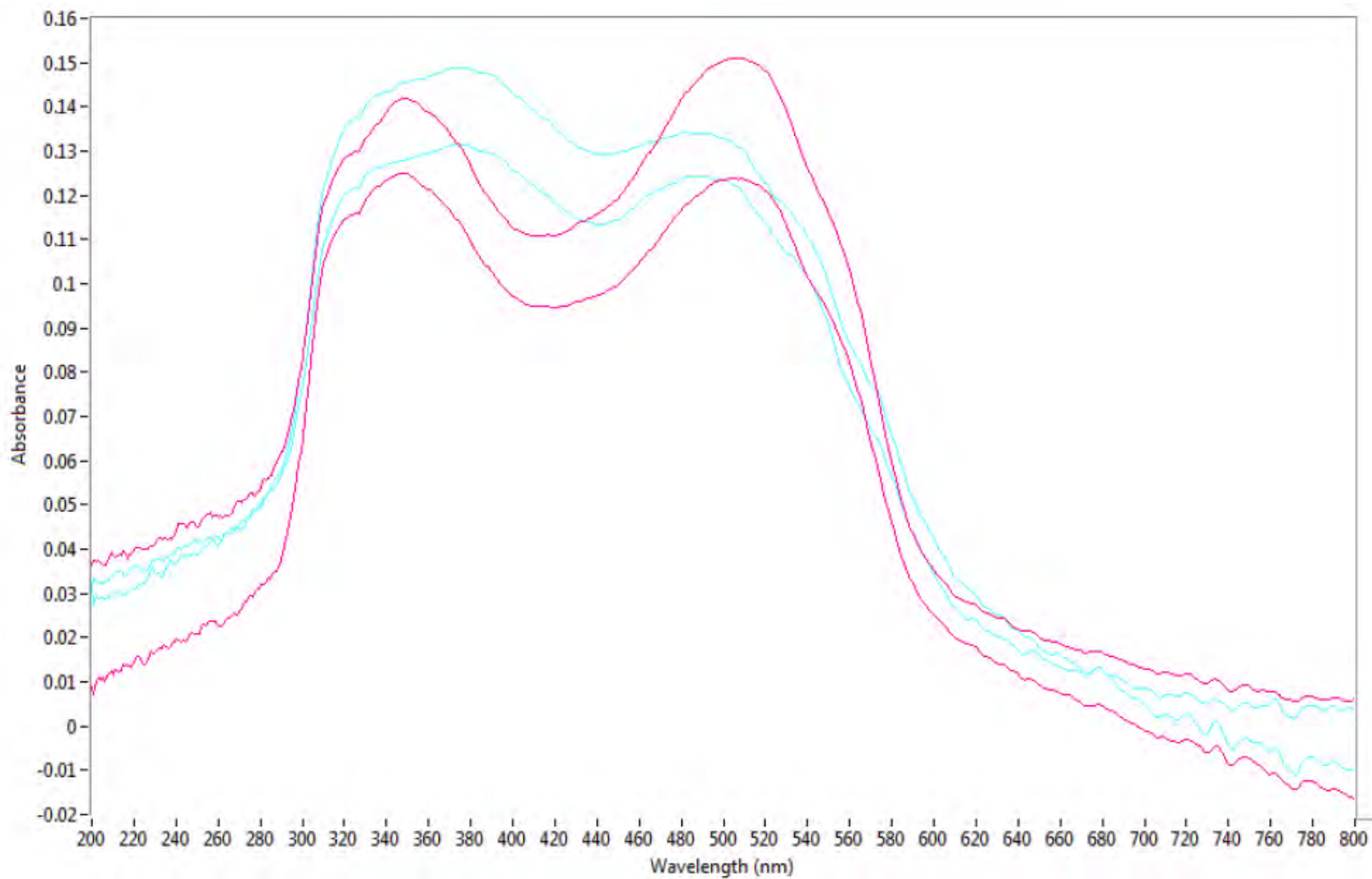


Figure 269. MSP spectra of fibers dyed with Intralan Fast Red RB 0.5% (light blue) and Intralan Red SG 0.5% (pink).

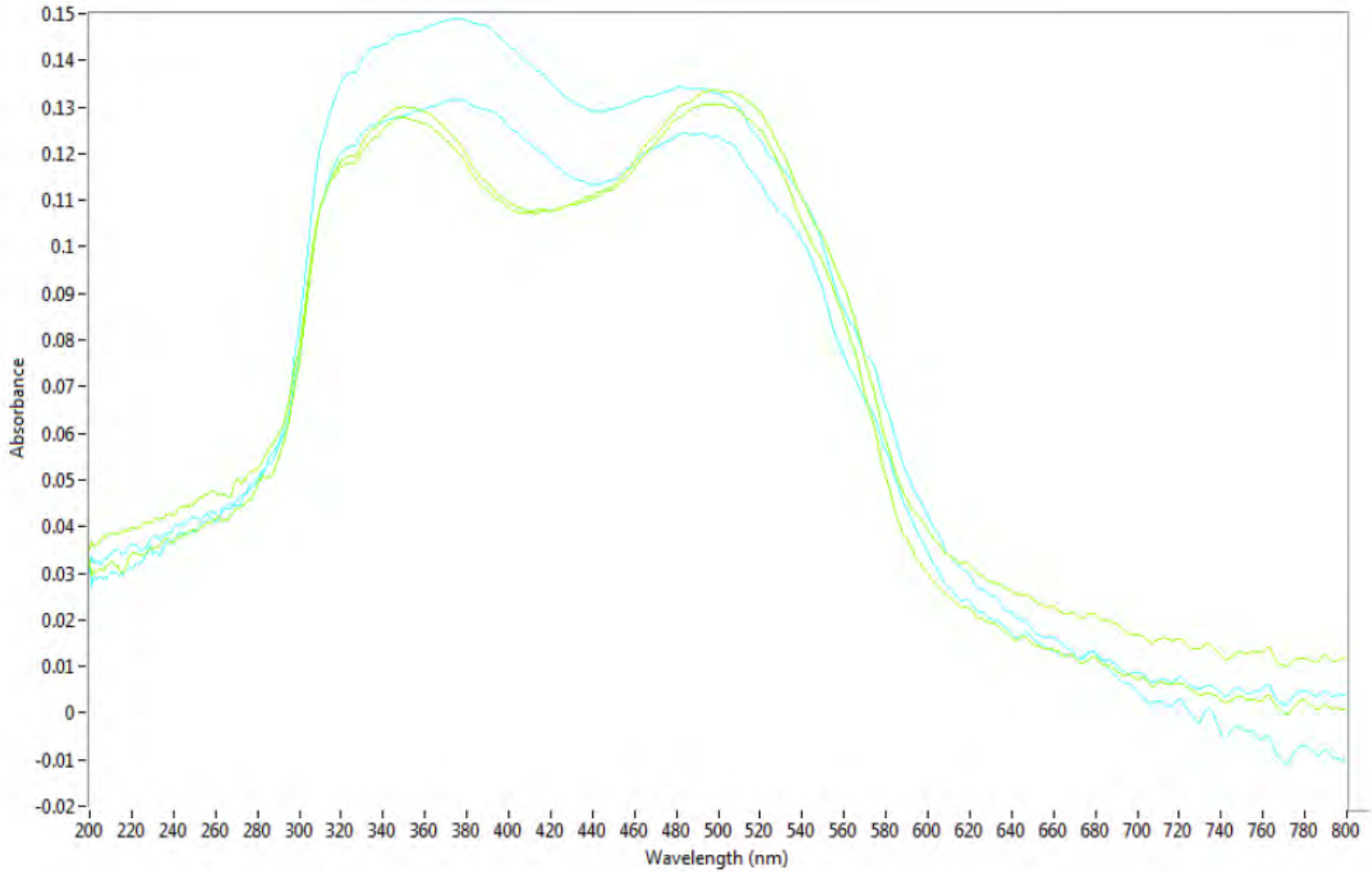


Figure 270. MSP spectra of fibers dyed with Intralan Fast Red RB 0.5% (light blue) and Intralan Red 2G 0.25% (lime green).

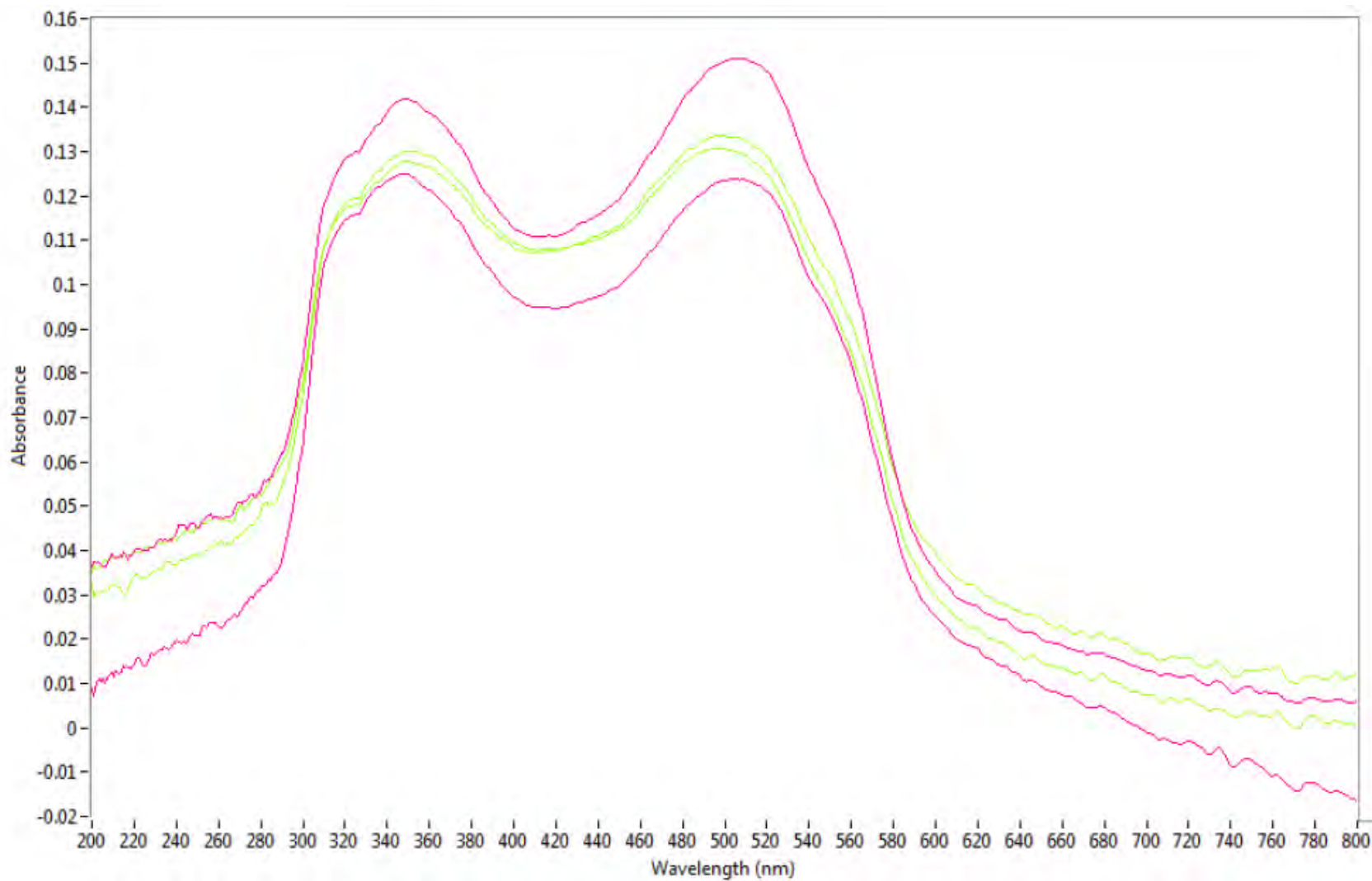


Figure 271. MSP spectra of fibers dyed with Intralan Red SG 0.5% (pink) and Intralan Red 2G 0.25% (lime green).

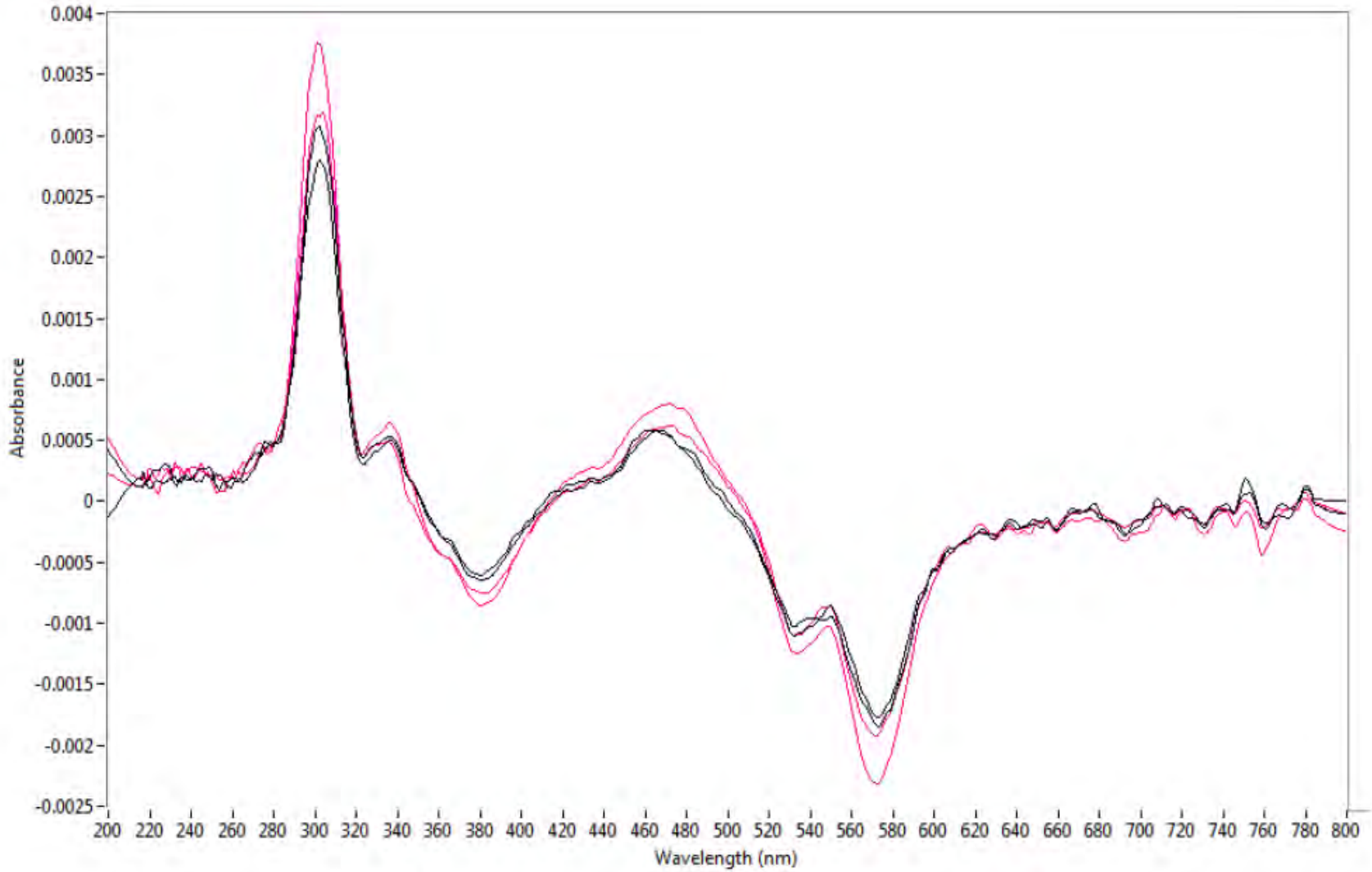


Figure 272. First derivative MSP spectra of fibers dyed with Intralan Red SG 0.5% (pink) and Intralan Red 2G 0.25% (black).

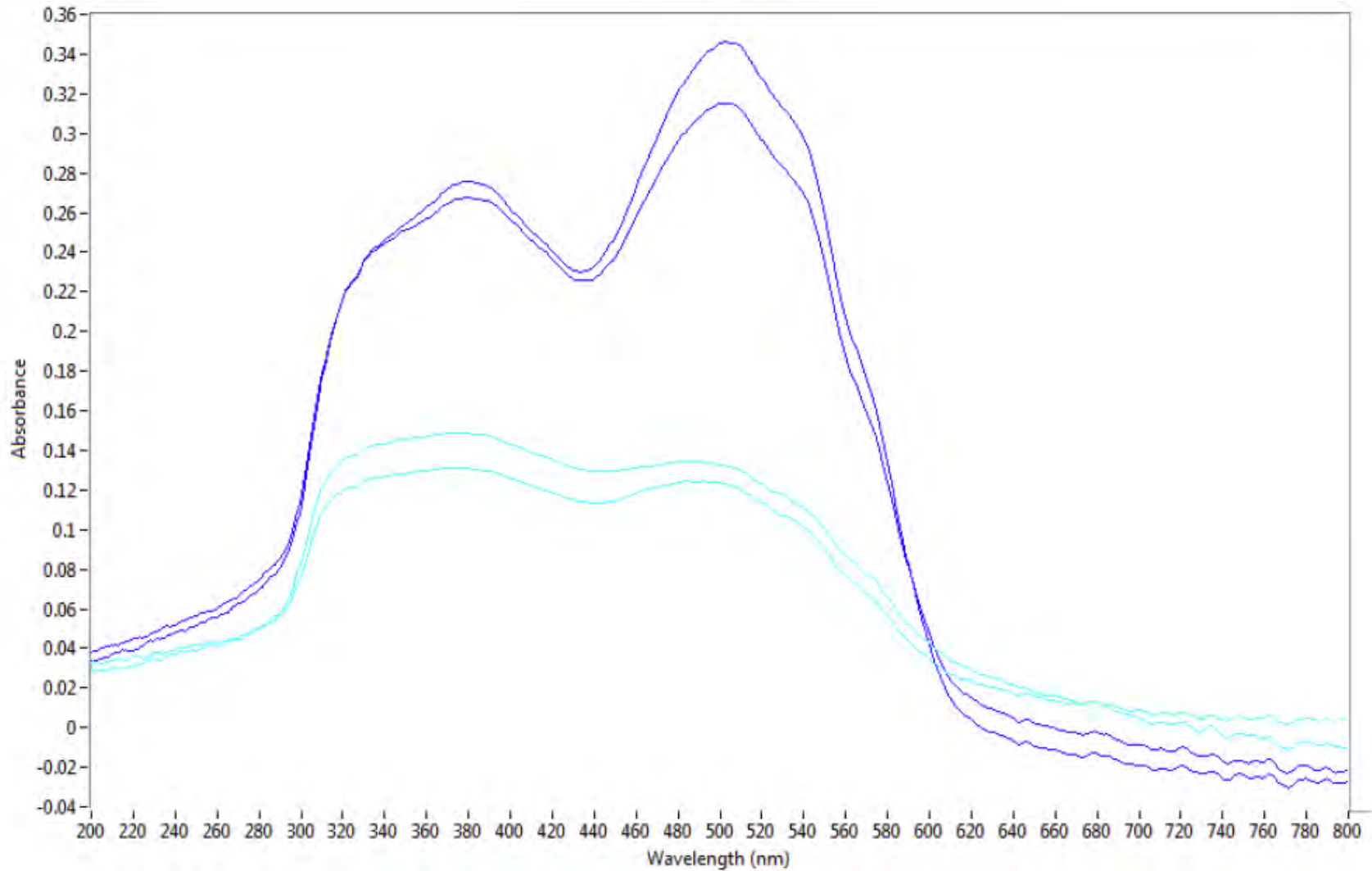


Figure 273. MSP spectra of fibers dyed with Intralan Fast Red RB 2% (blue) and 0.5% (light blue).

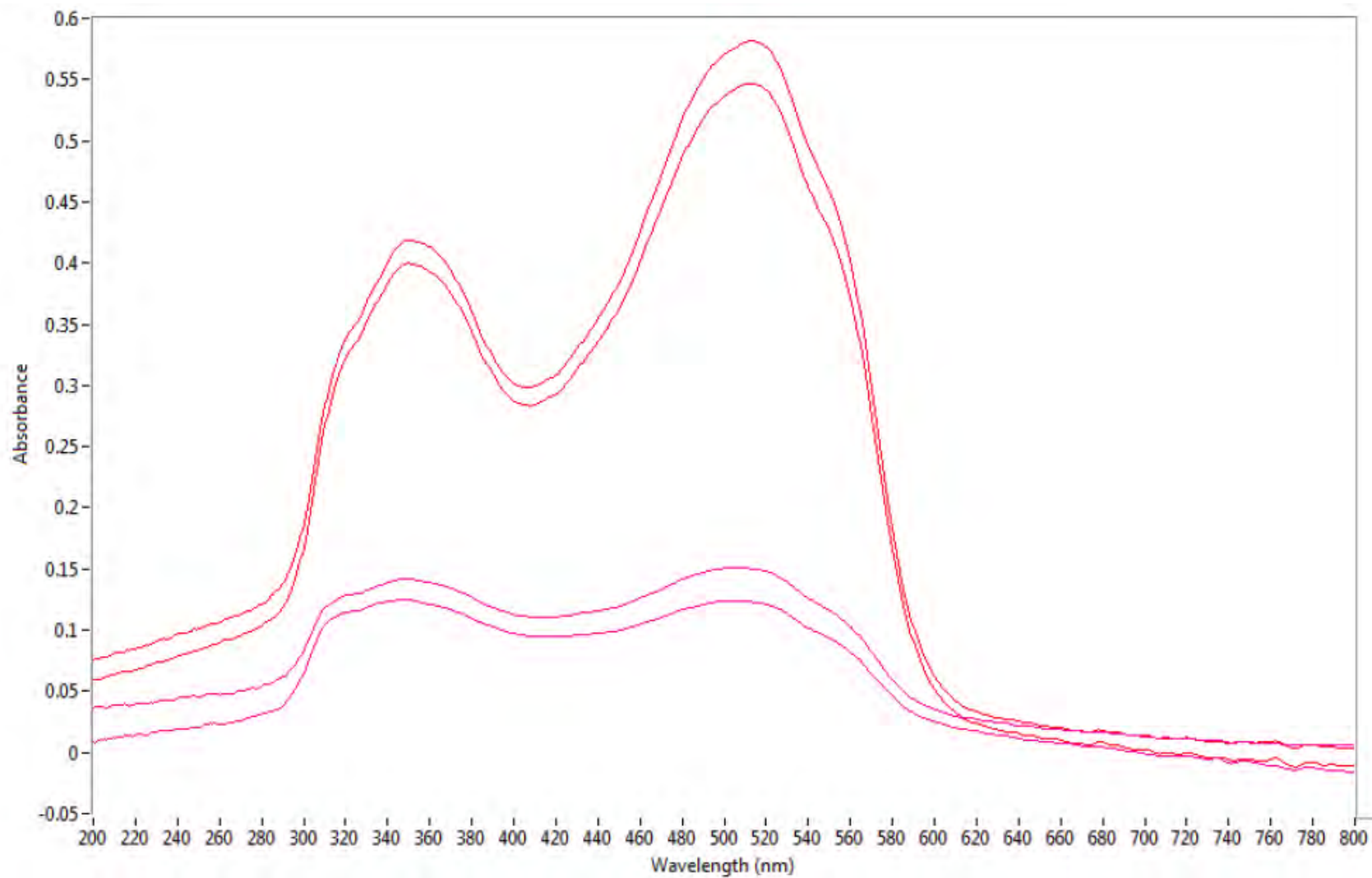


Figure 274. MSP spectra of fibers dyed with Intralan Red SG 2% (red) and 0.5% (pink).

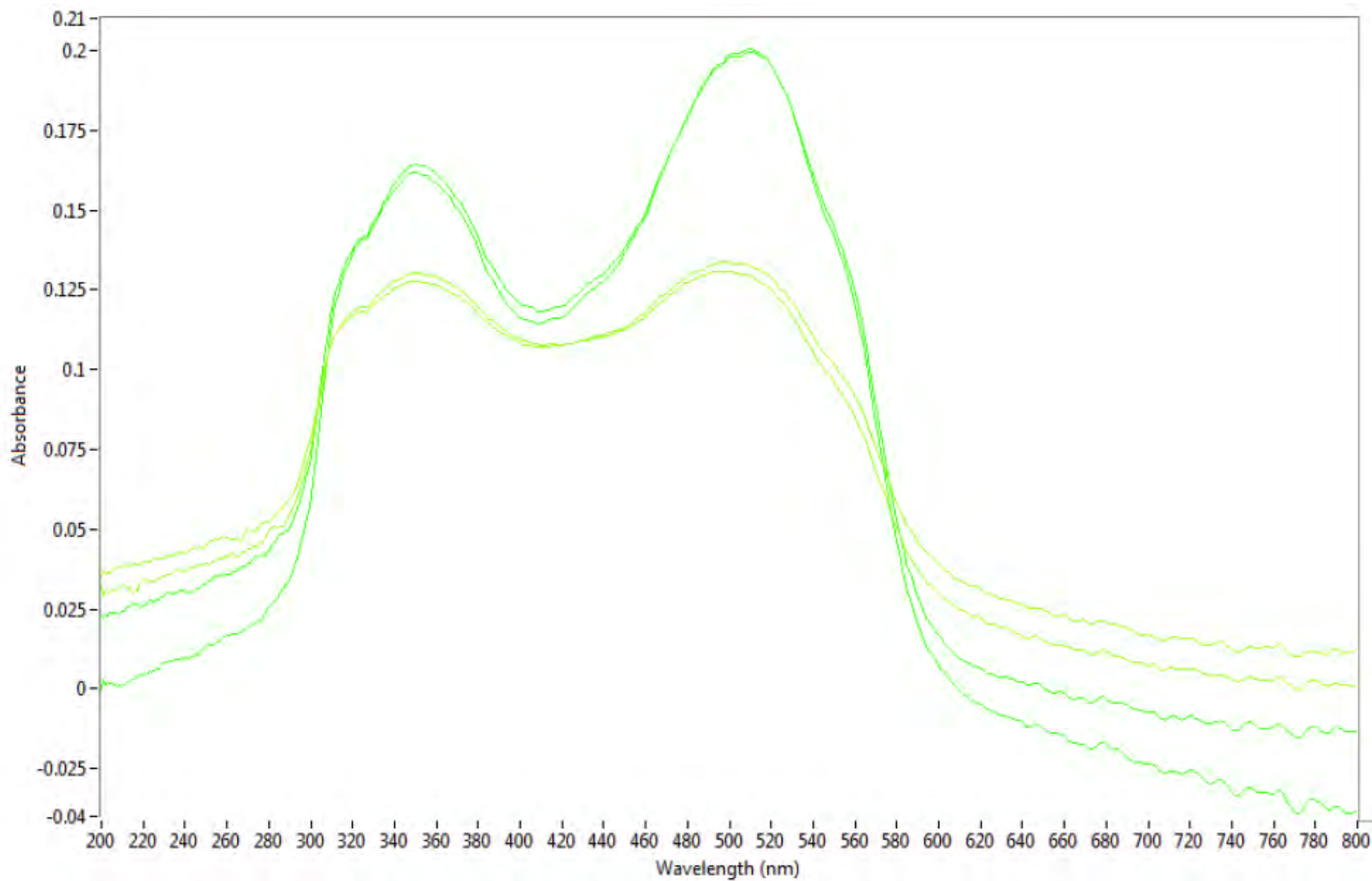


Figure 275. MSP spectra of fibers dyed with Intralan Red 2G 1% (green) and 0.25% (lime green).

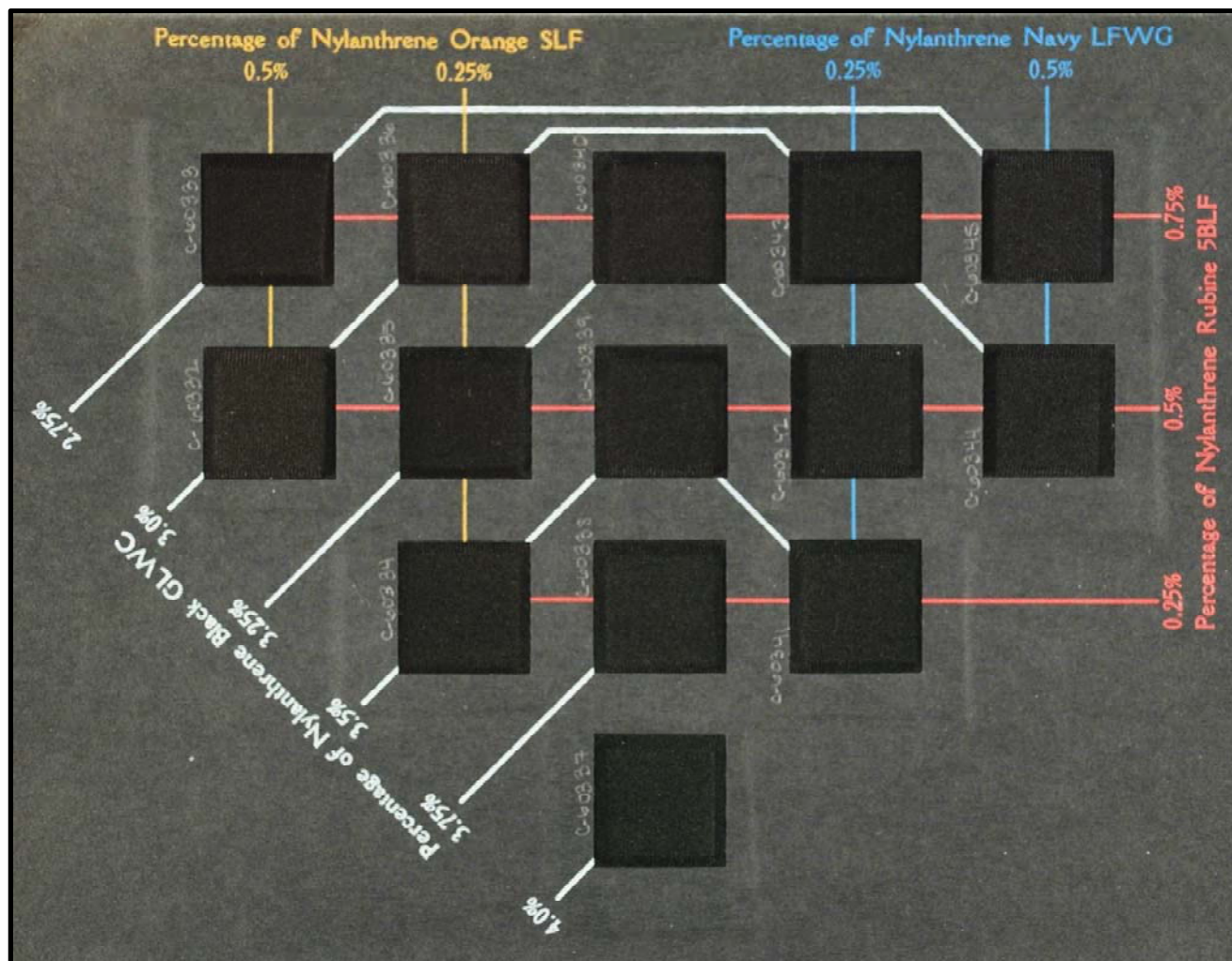
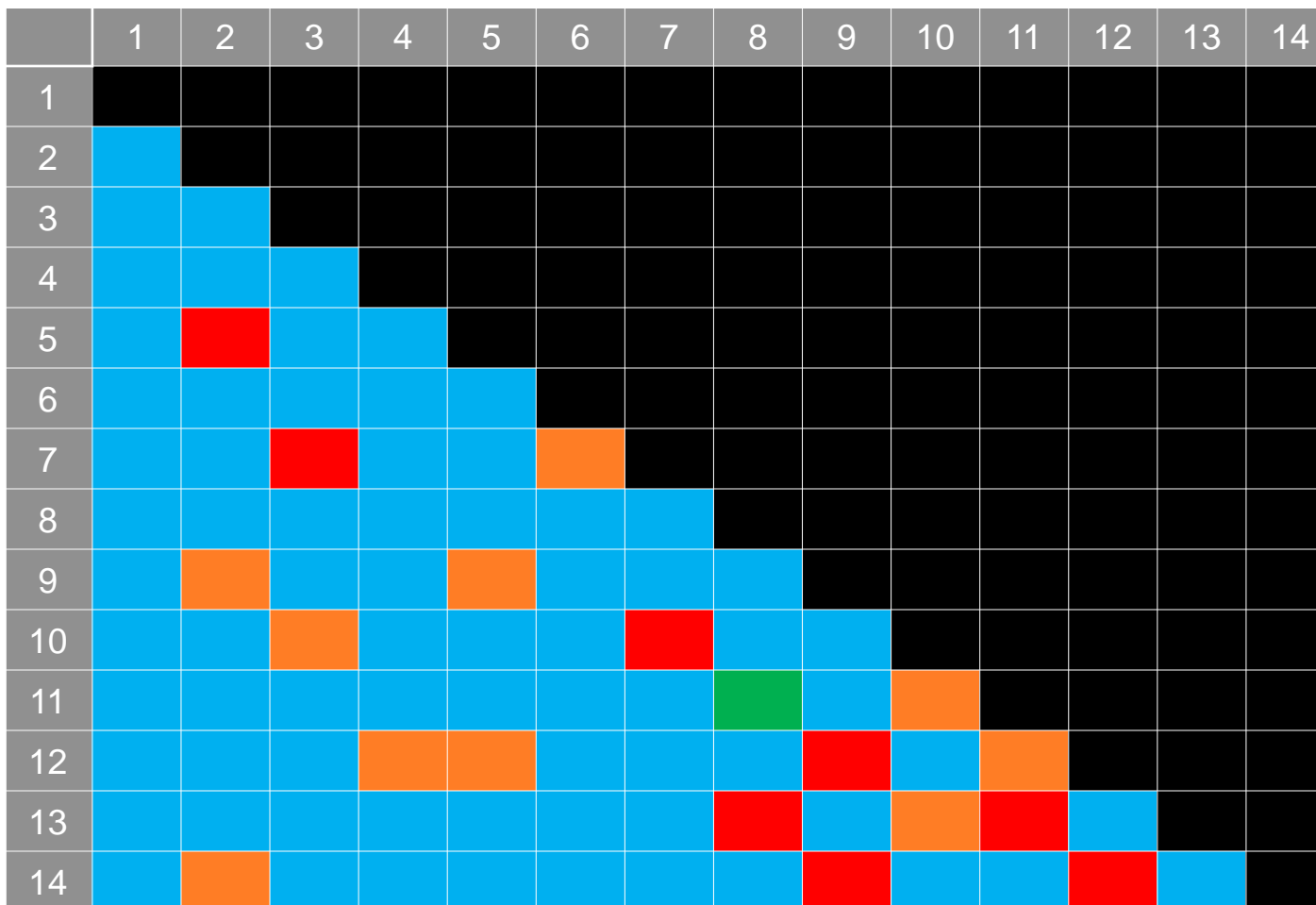


Figure 276. Fourteen black fabric swatches dyed with known concentrations of nylanthrene dyes.



- 72 Different by MSP and comparison microscopy
- 1 Similar MSP, different comparison microscopy
- 10 Different MSP, similar comparison microscopy
- 8 Similar MSP and comparison microscopy

Figure 277. Summary table of the 91 possible pairwise comparisons.

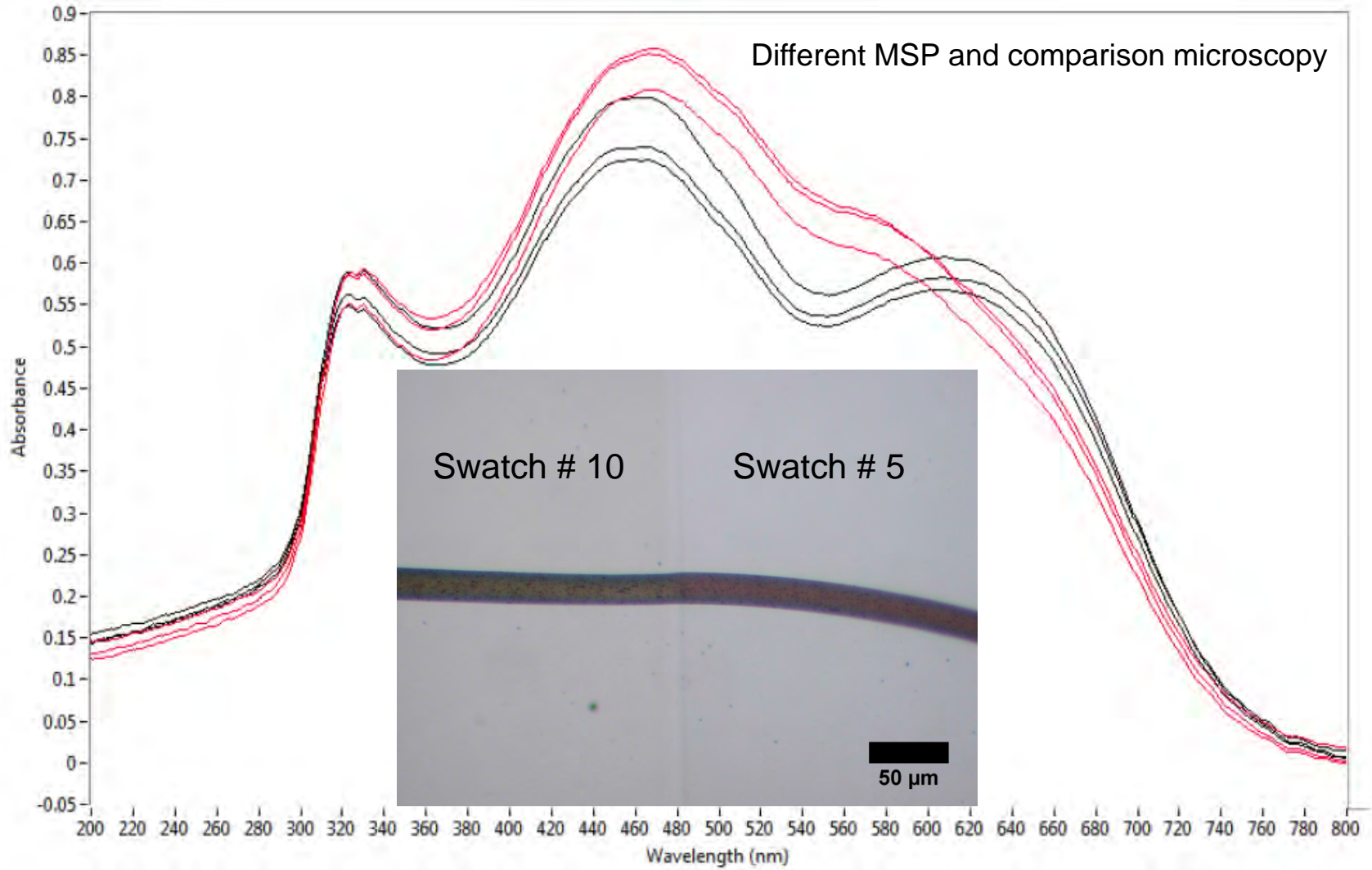


Figure 278. Comparison of MSP spectra collected from swatch #5 (red) and # 10 (black) with a comparison microscope image of fibers from the two samples.

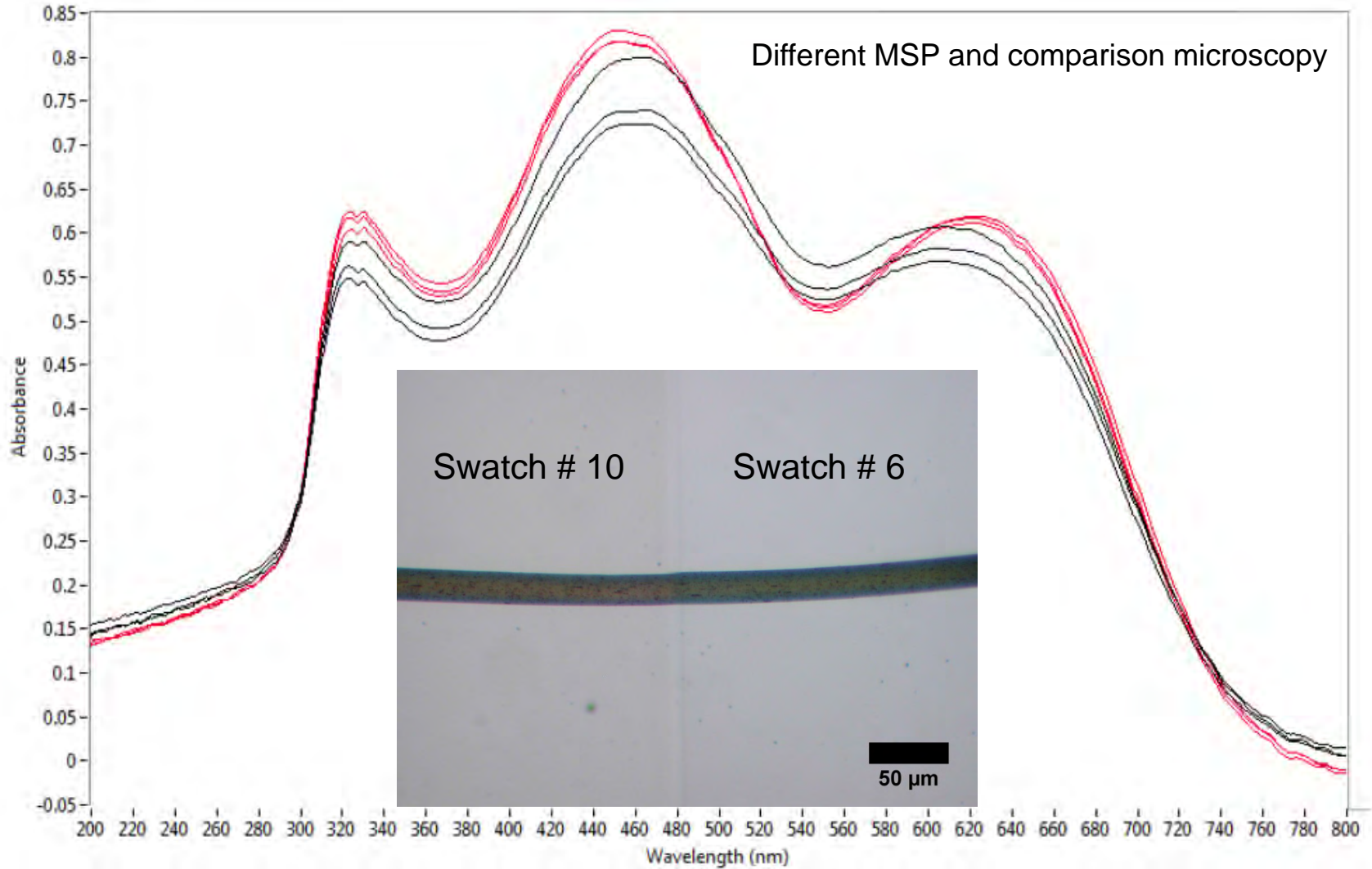


Figure 279. Comparison of MSP spectra collected from swatch #6 (red) and # 10 (black) with a comparison microscope image of fibers from the two samples.

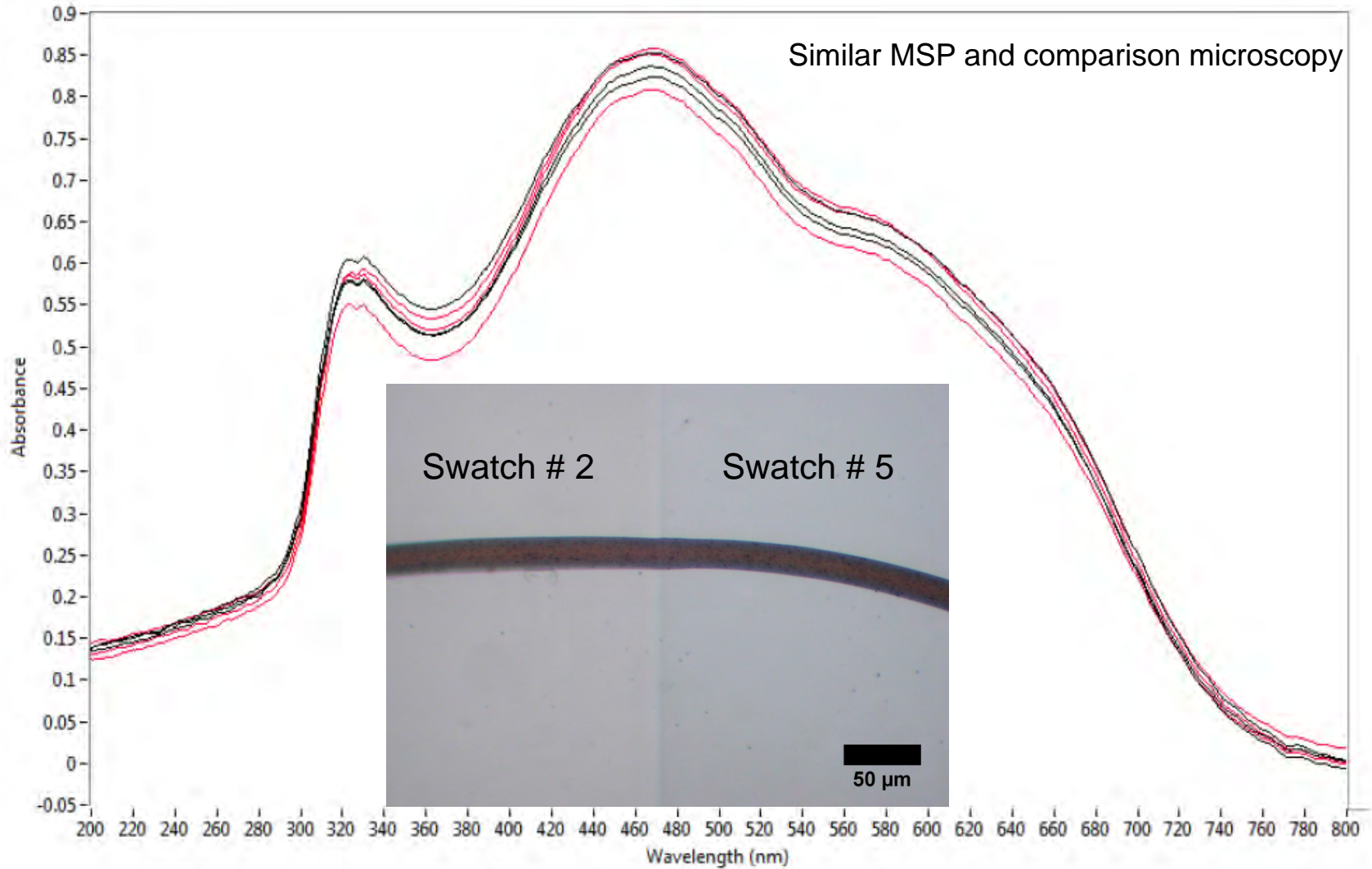


Figure 280. Comparison of MSP spectra collected from swatch #5 (red) and # 2 (black) with a comparison microscope image of fibers from the two samples.

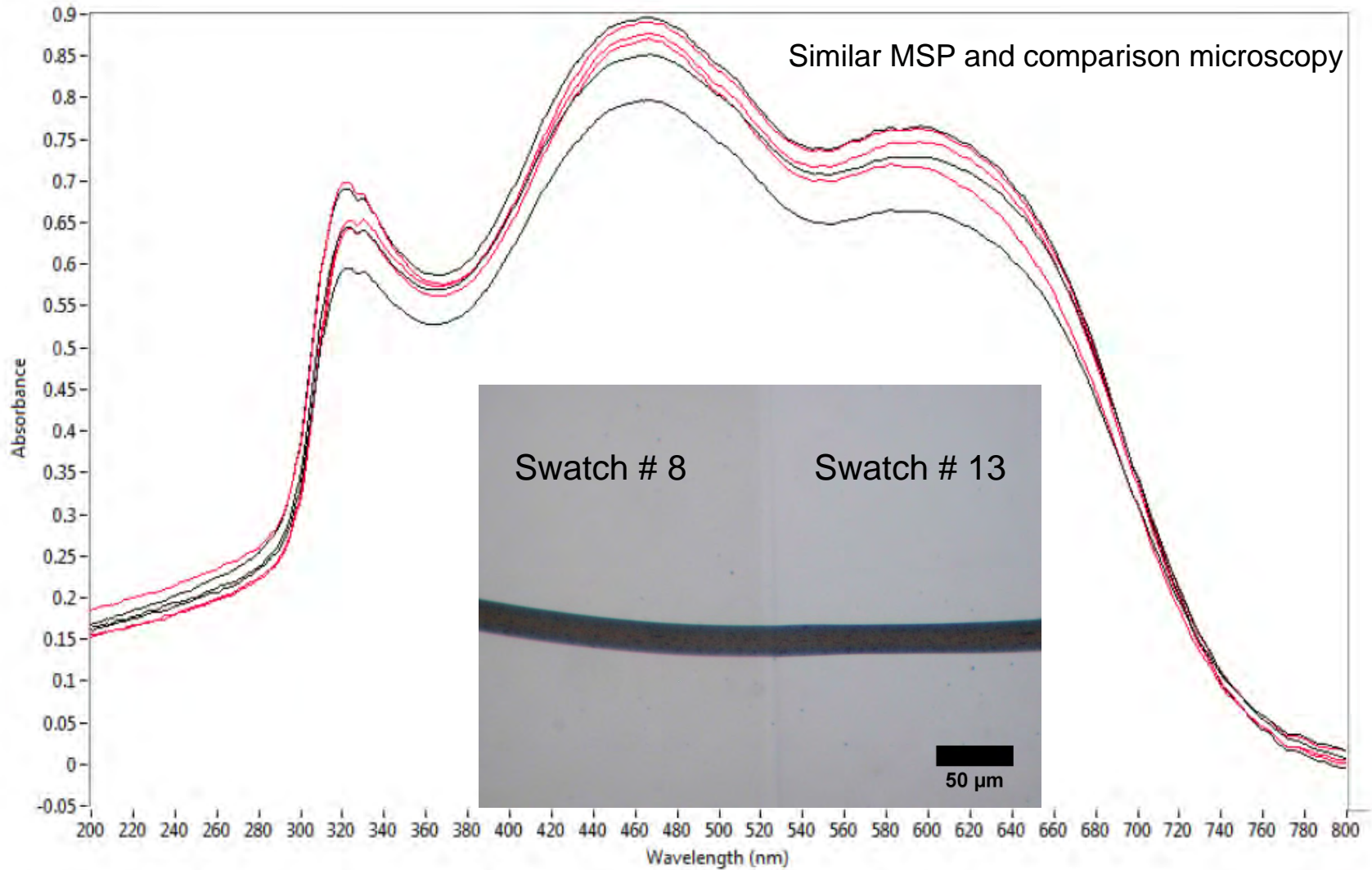


Figure 281. Comparison of MSP spectra collected from swatch #13 (red) and # 8 (black) with a comparison microscope image of fibers from the two samples.

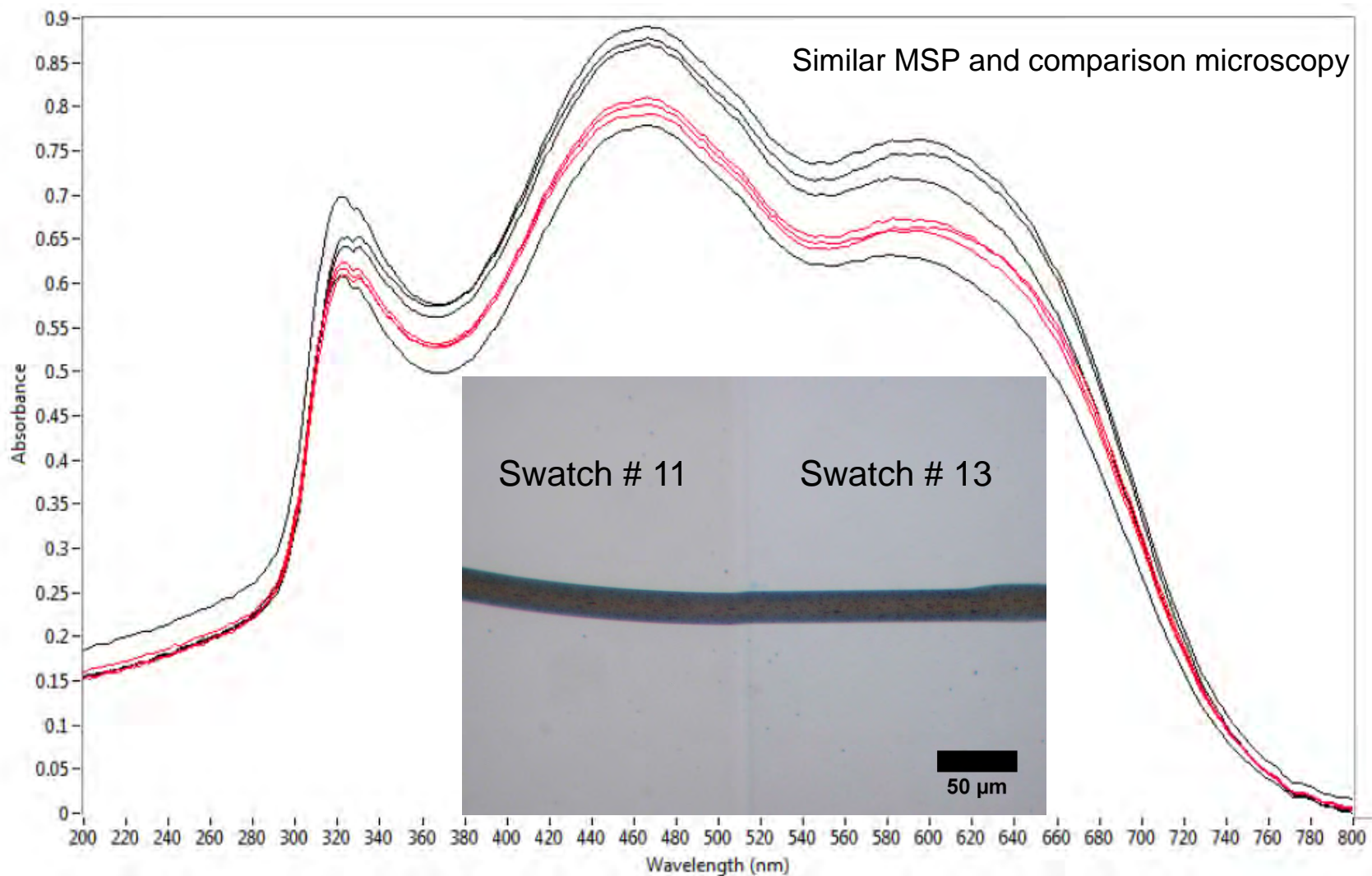


Figure 282. Comparison of MSP spectra collected from swatch #11 (red) and # 13 (black) with a comparison microscope image of fibers from the two samples.

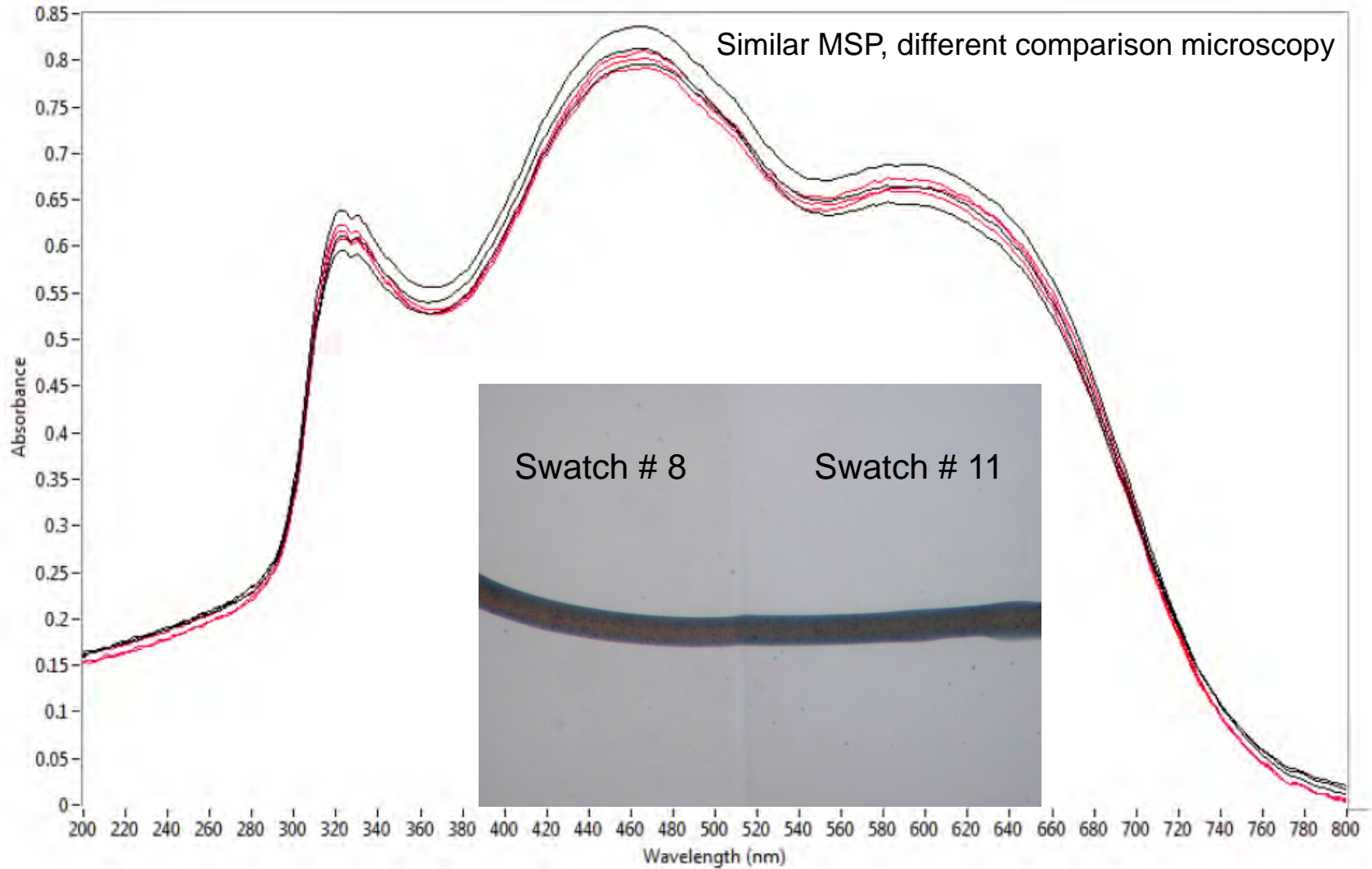


Figure 283. Comparison of MSP spectra collected from swatch #11 (red) and # 8 (black) with a comparison microscope image of fibers from the two samples.

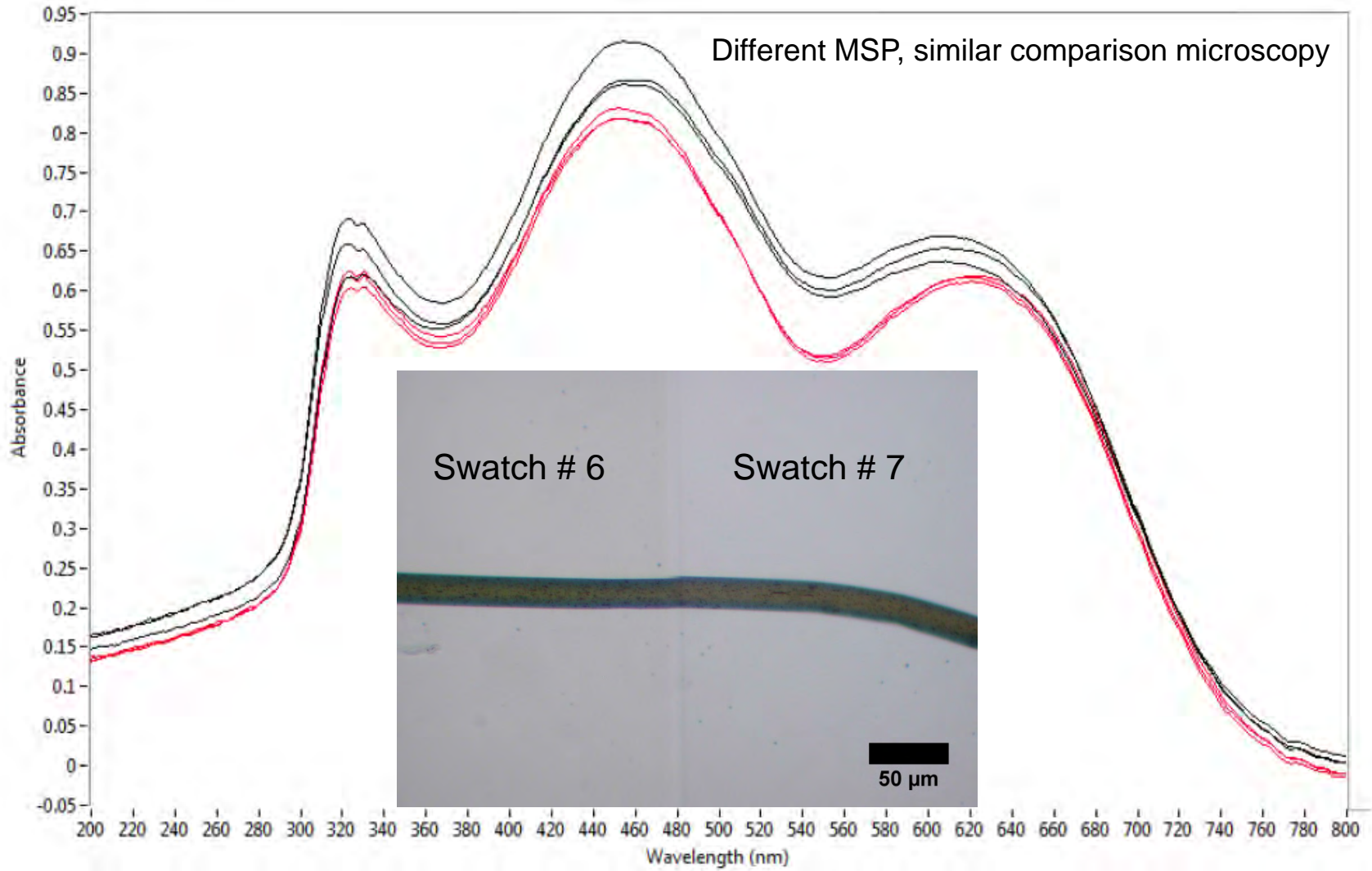


Figure 284. Comparison of MSP spectra collected from swatch #6 (red) and # 7 (black) with a comparison microscope image of fibers from the two samples.

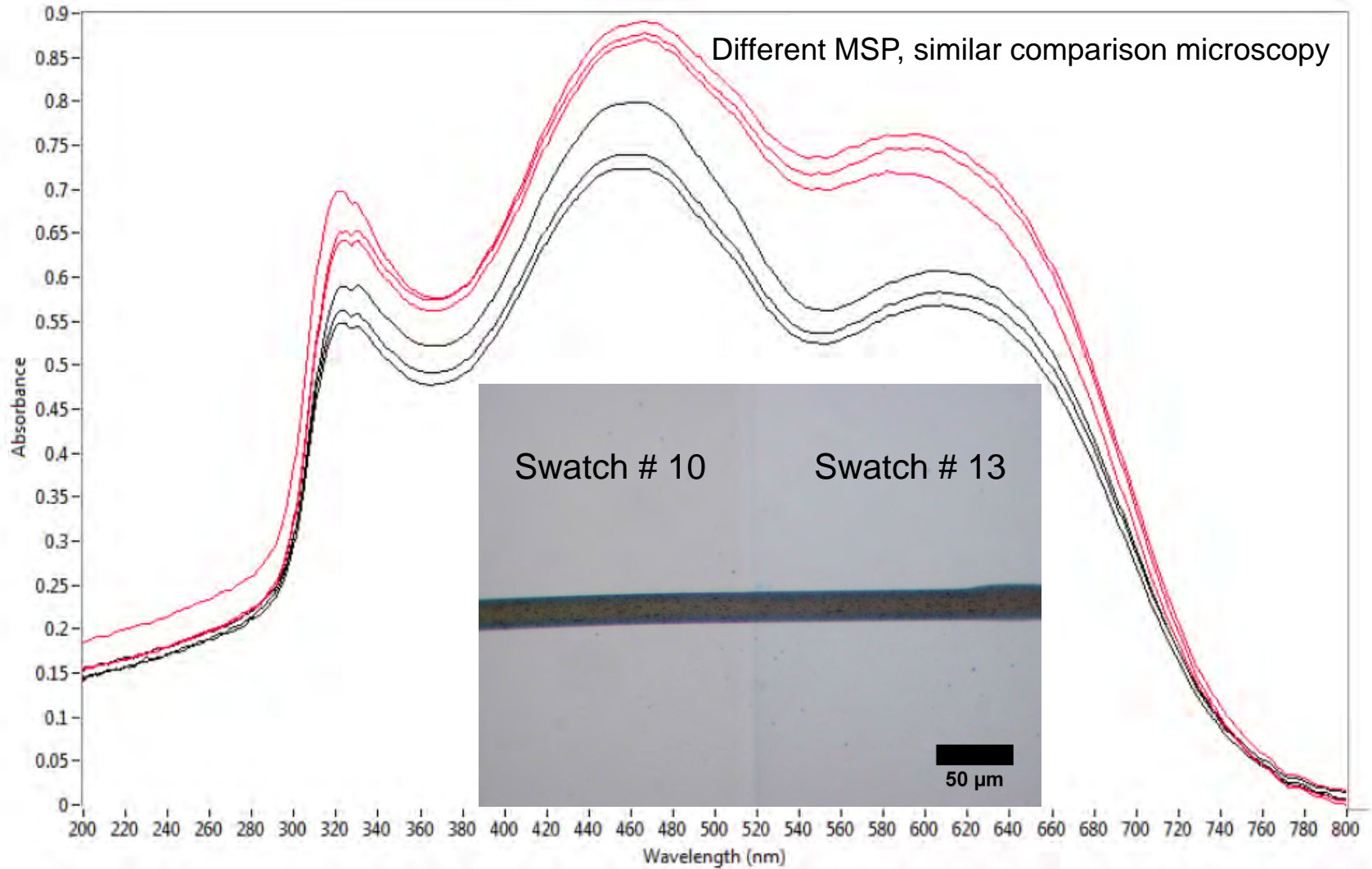


Figure 285. Comparison of MSP spectra collected from swatch #13 (red) and # 10 (black) with a comparison microscope image of fibers from the two samples.

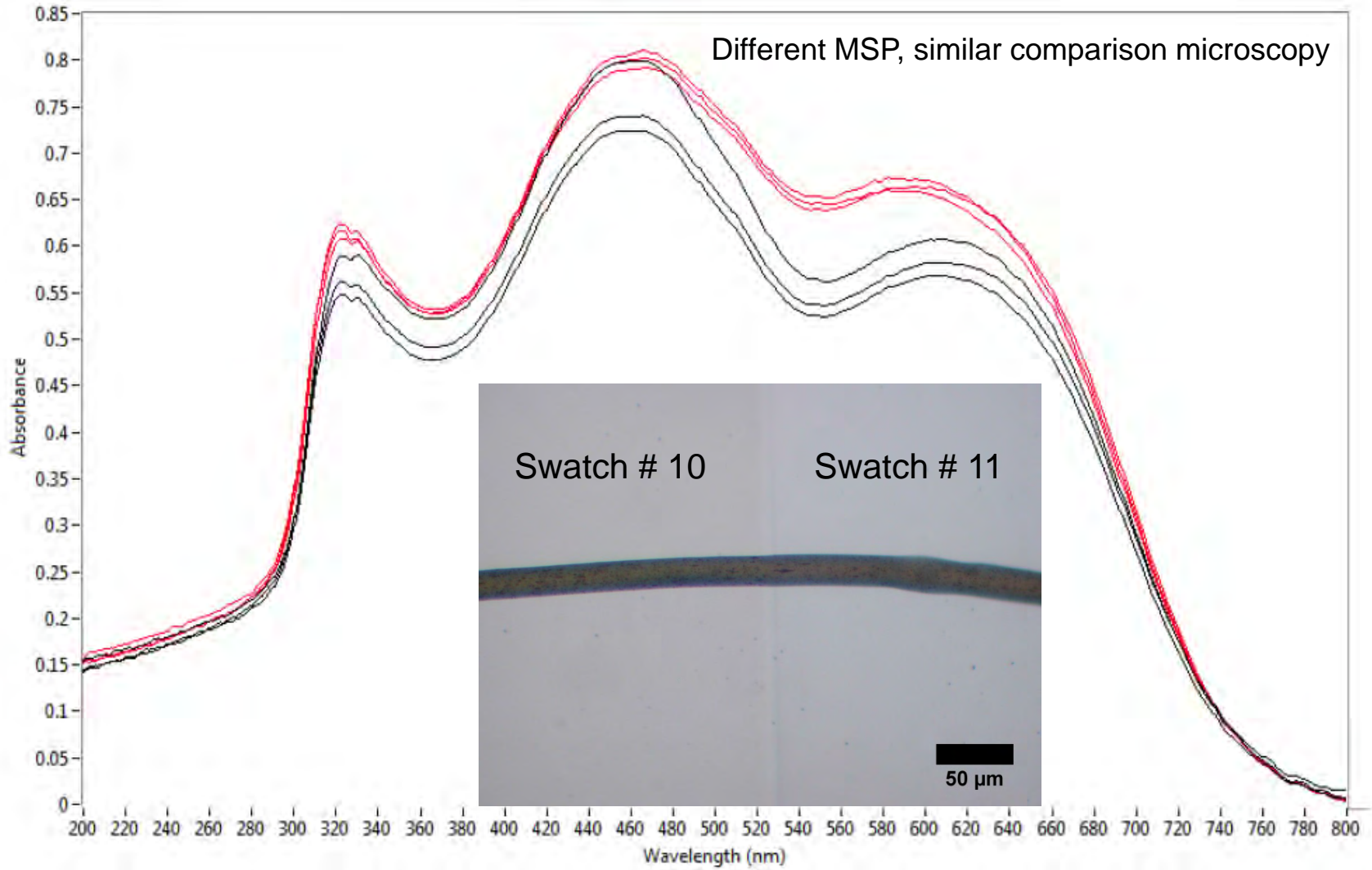


Figure 286. Comparison of MSP spectra collected from swatch #11 (red) and # 10 (black) with a comparison microscope image of fibers from the two samples.

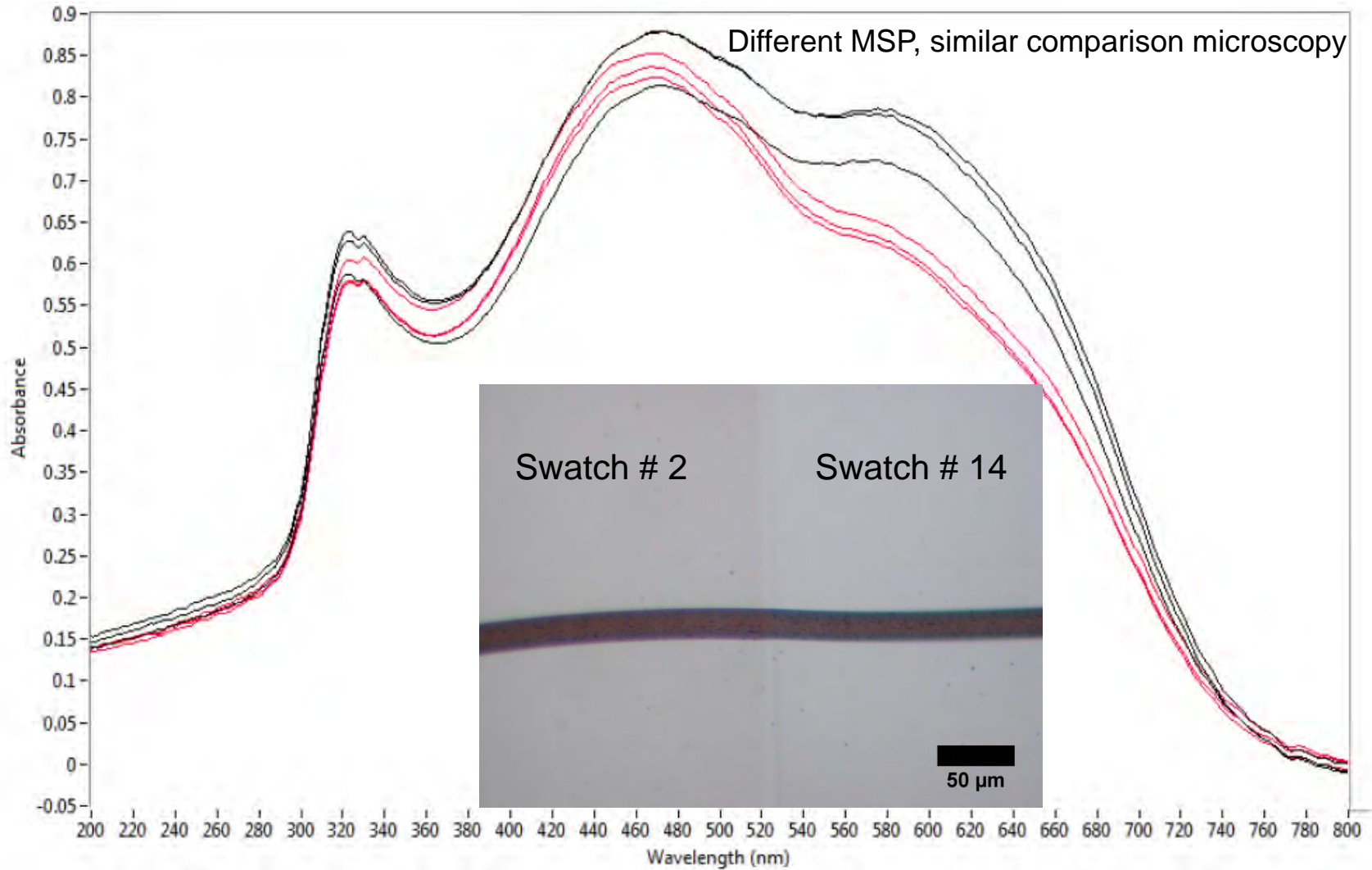


Figure 287. Comparison of MSP spectra collected from swatch #2 (red) and # 14 (black) with a comparison microscope image of fibers from the two samples.

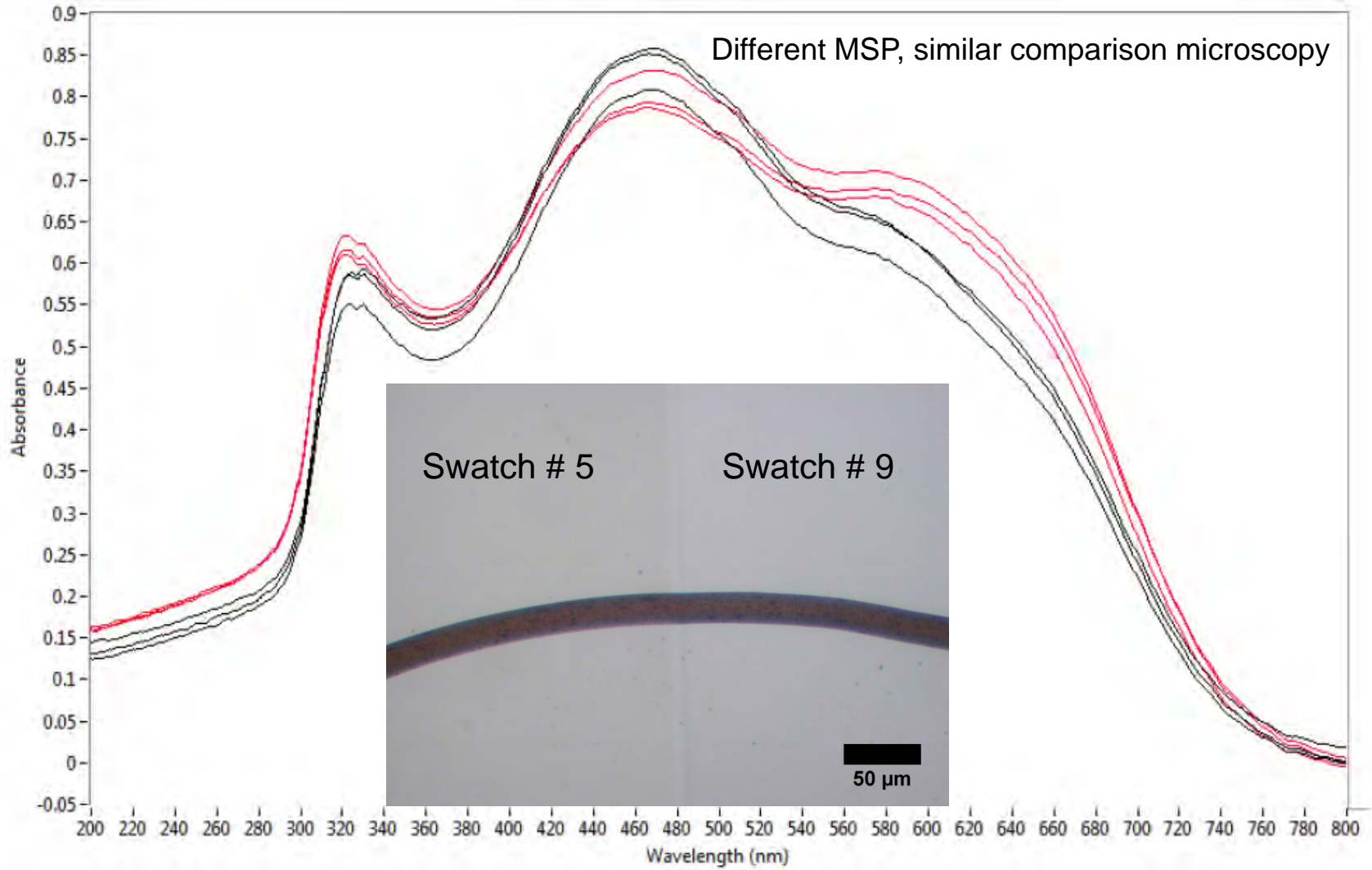


Figure 288. Comparison of MSP spectra collected from swatch #9 (red) and # 5 (black) with a comparison microscope image of fibers from the two samples.

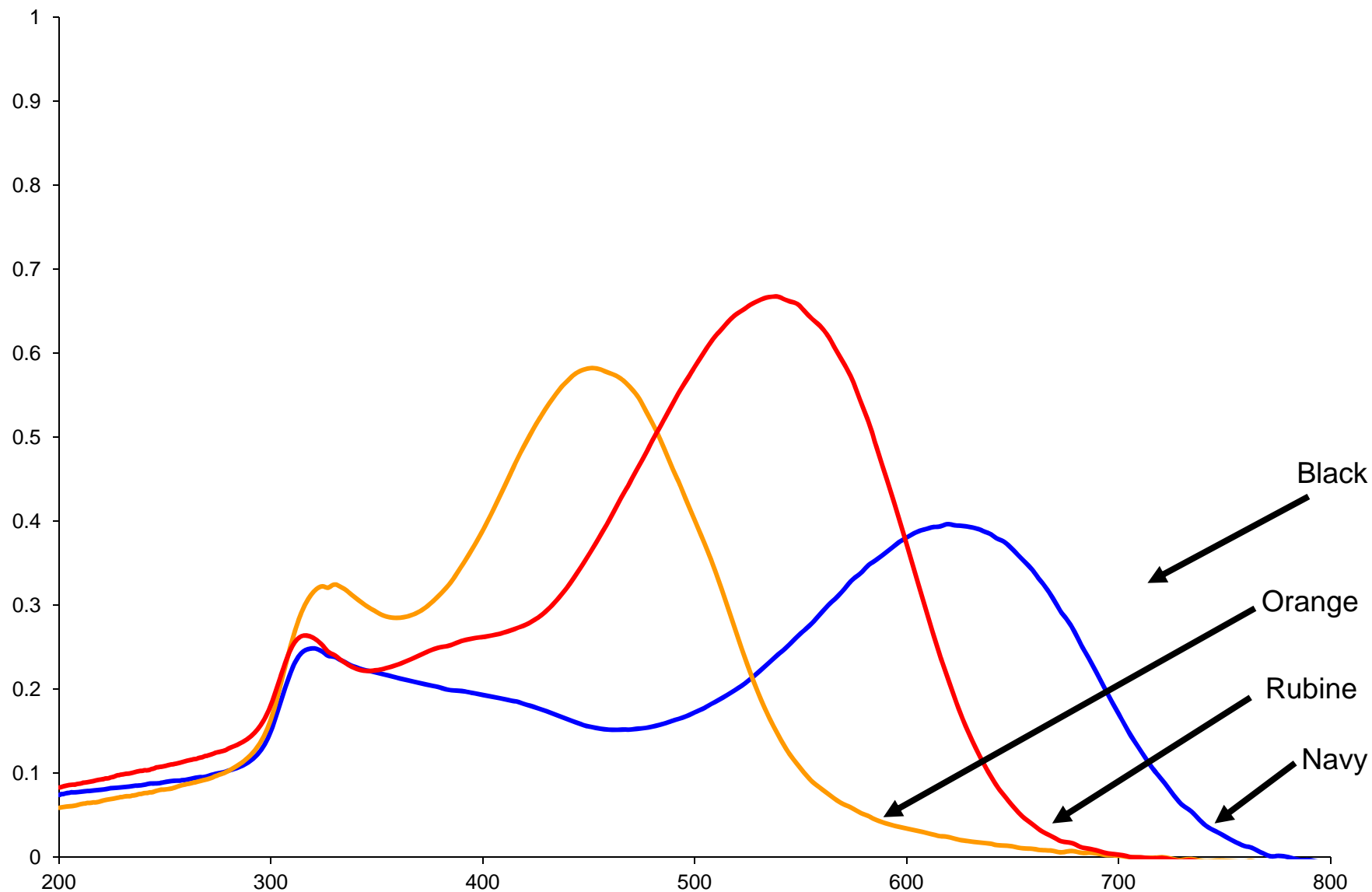


Figure 289. Comparison of MSP spectra collected from fibers colored with black, navy, orange, and rubine nylanthrene dyes (averages of fifteen spectra).

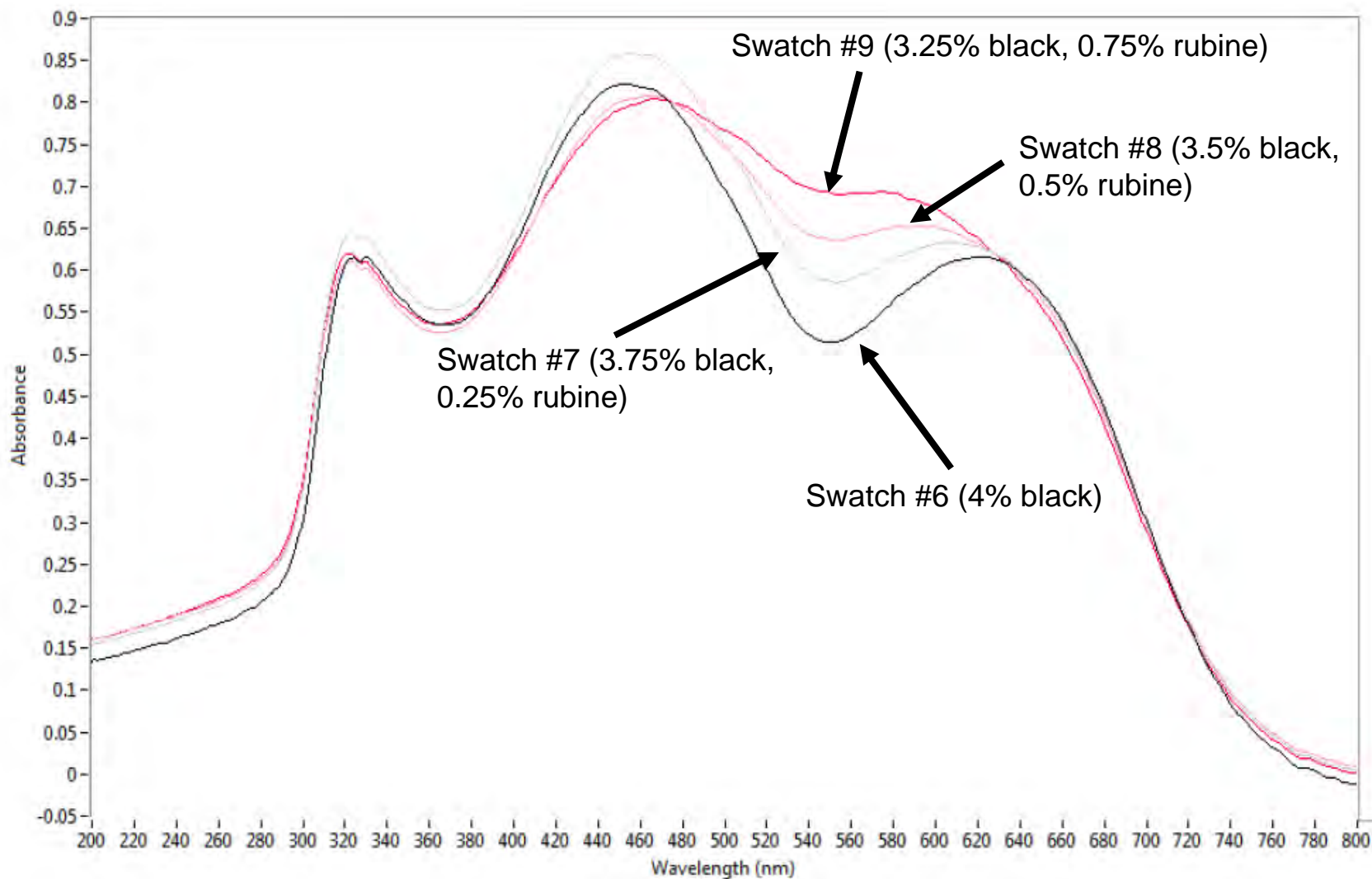


Figure 290. Comparison of MSP spectra collected from fibers from swatches 6 (black), 7 (gray), 8 (pink) and 9 (red) (averages of a minimum of nine spectra from each swatch).

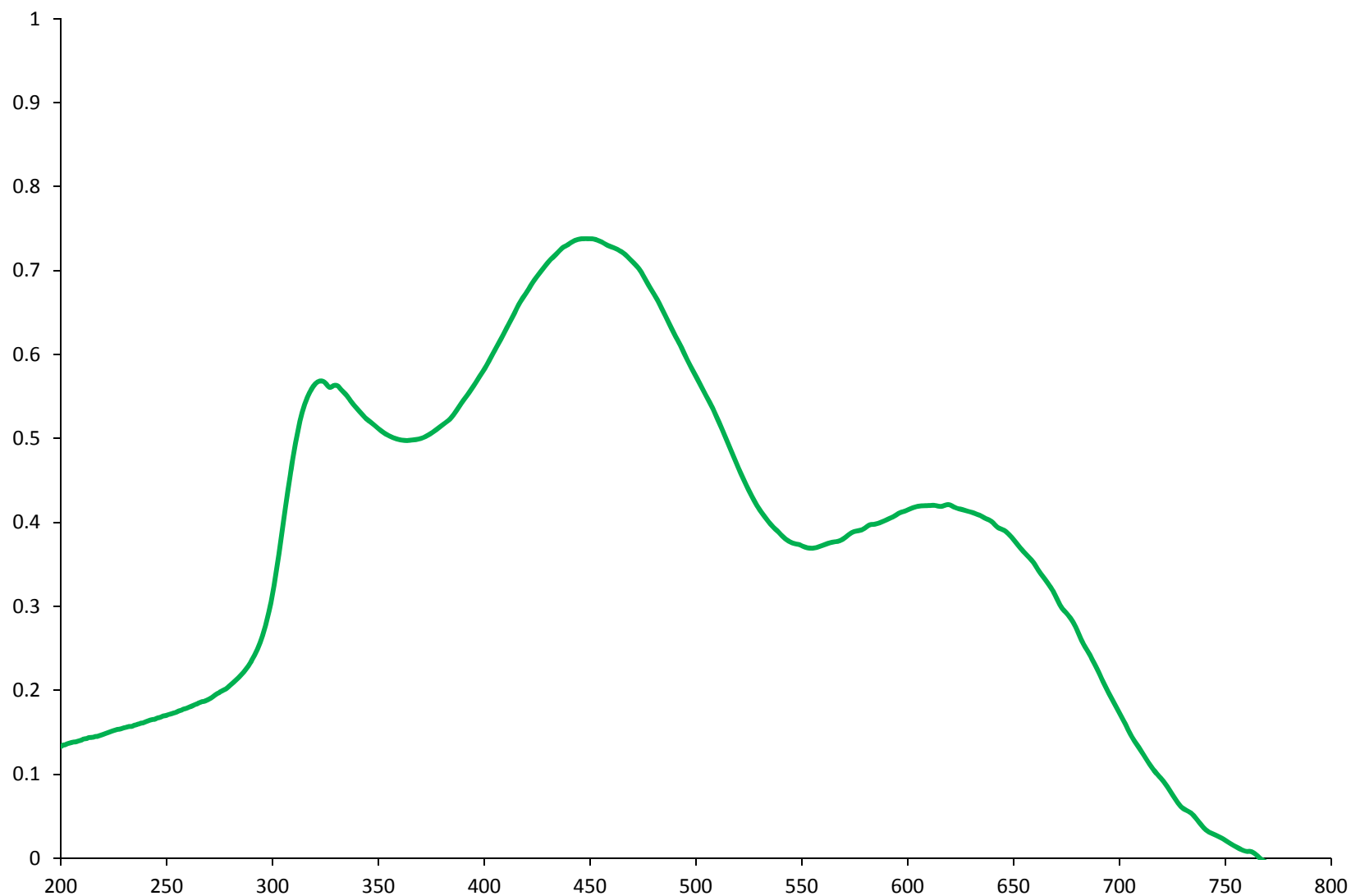


Figure 291. Comparison of MSP spectra collected from the fibers colored with only black dye (*i.e.*, swatch 6 – black) compared to the synthetic spectrum resulting from the addition of the spectra from the fibers dyed with the navy and orange dyes (green).

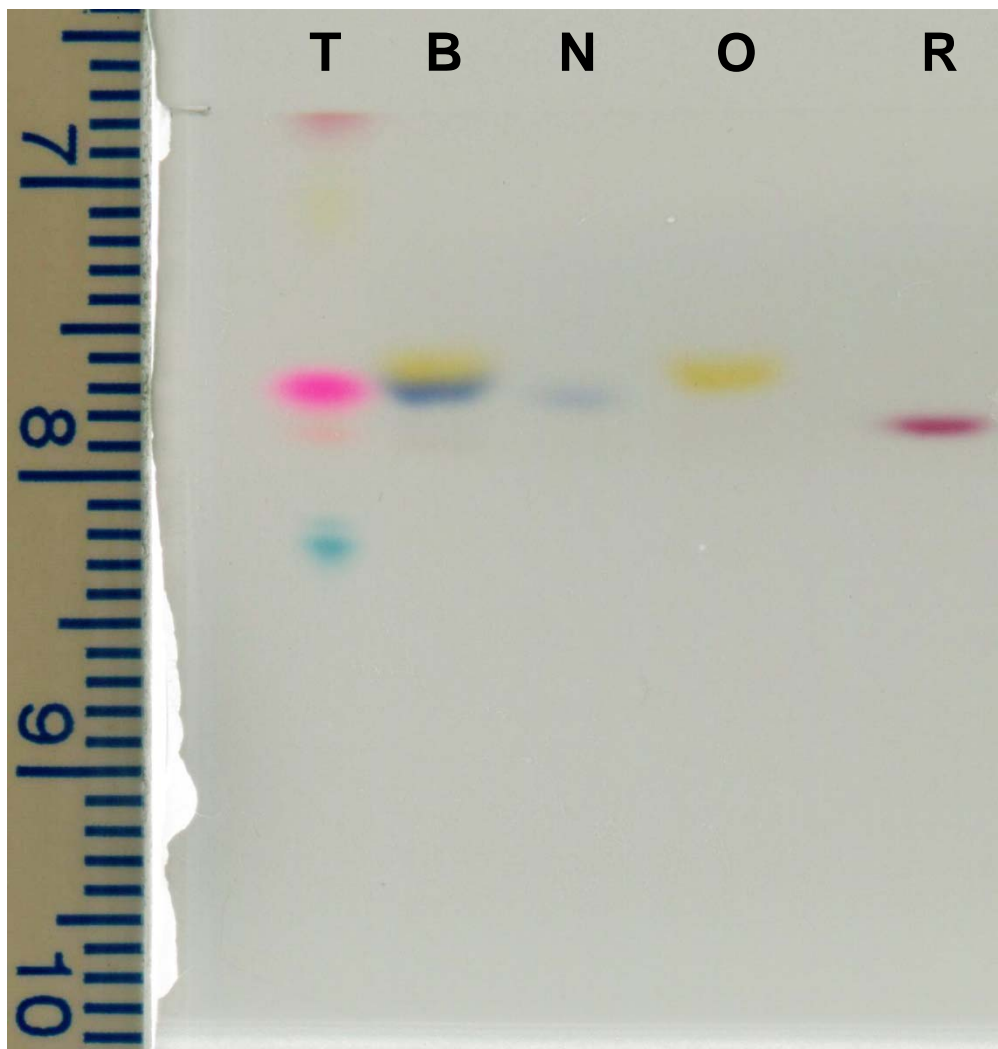


Figure 292. HPTLC plate showing the bands resulting from the extractions of the black (B), navy (N), orange (O), and rubine (R) fibers. The band on the left is a test dye mixture (T) used as an internal control.

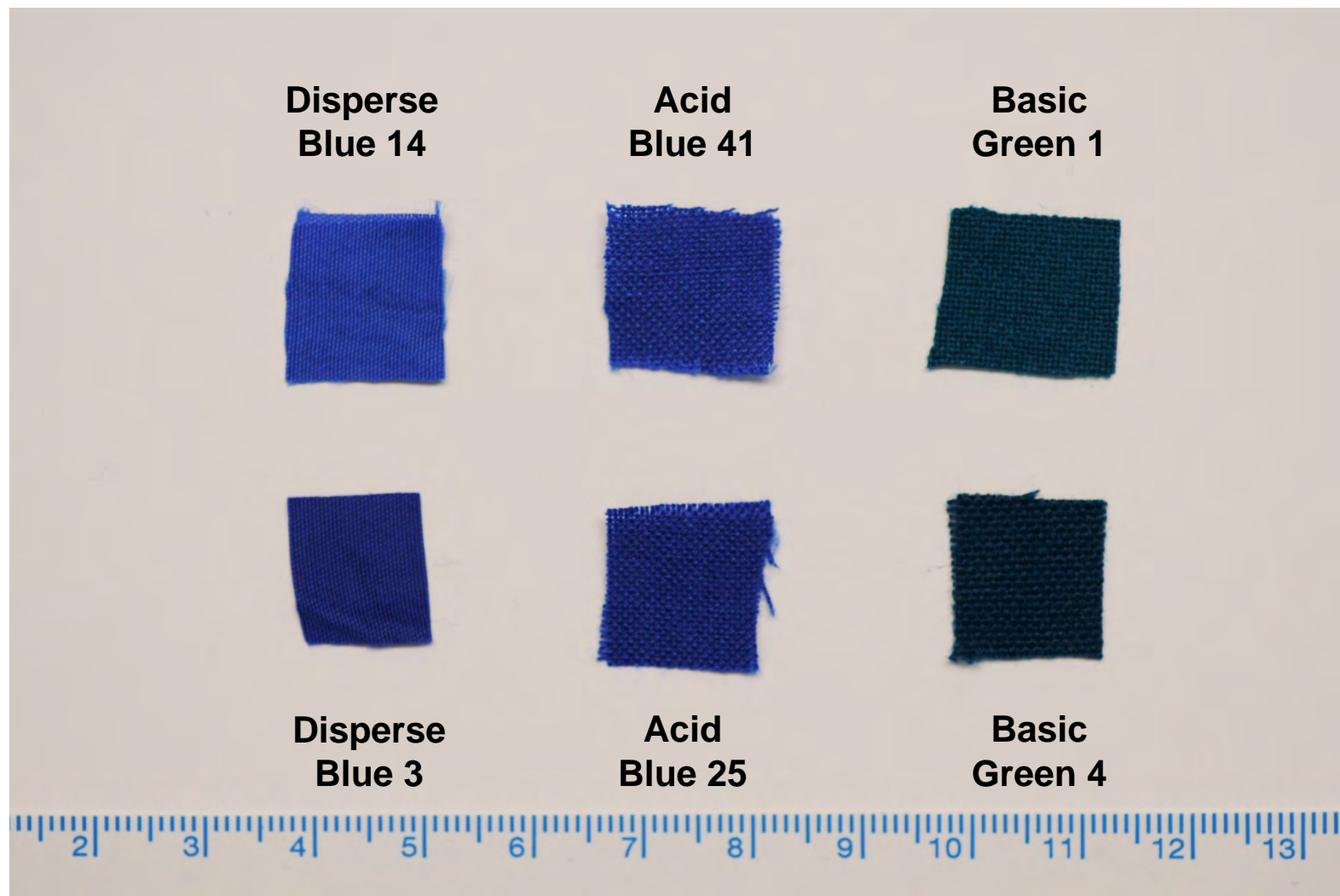


Figure 293. Six fabric swatches.

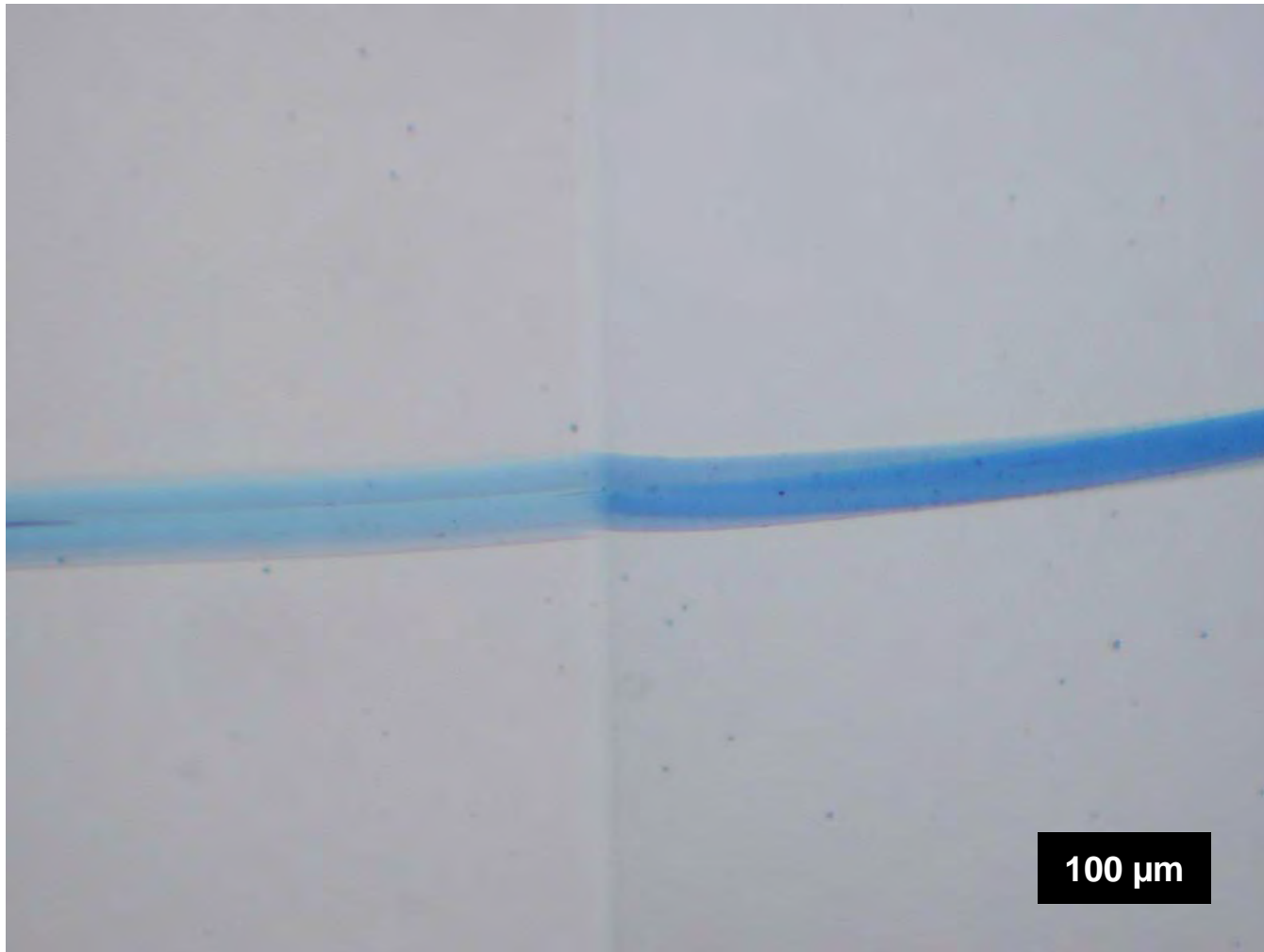


Figure 294. Comparison microscope image of fabric fibers dyed with Disperse Blue 14 (left) and Disperse Blue 3 (right).

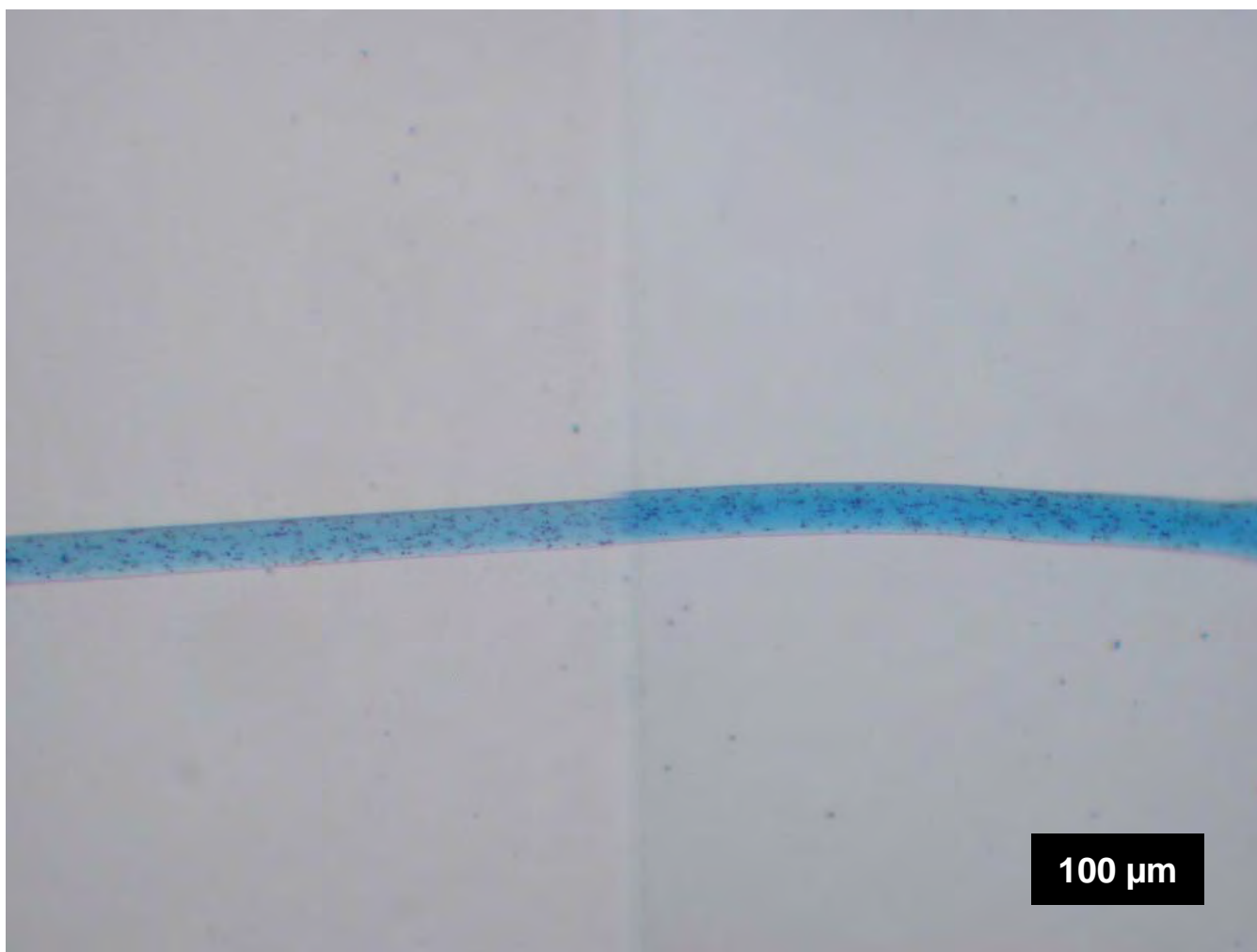


Figure 295. Comparison microscope image of fabric fibers dyed with Acid Blue 41 (left) and Acid Blue 25 (right).

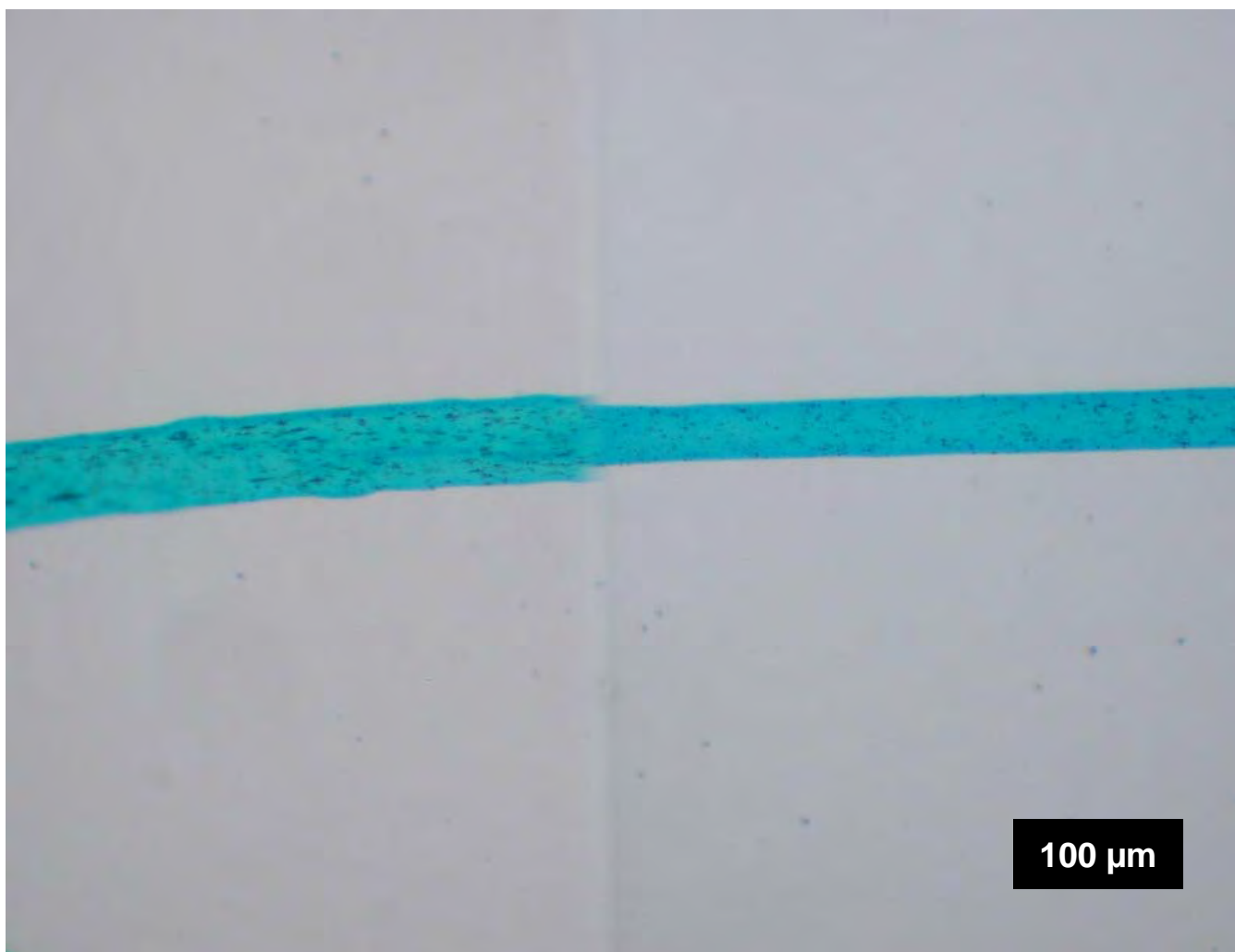


Figure 296. Comparison microscope image of fabric fibers dyed with Basic Green 1 (left) and Basic Green 4 (right).

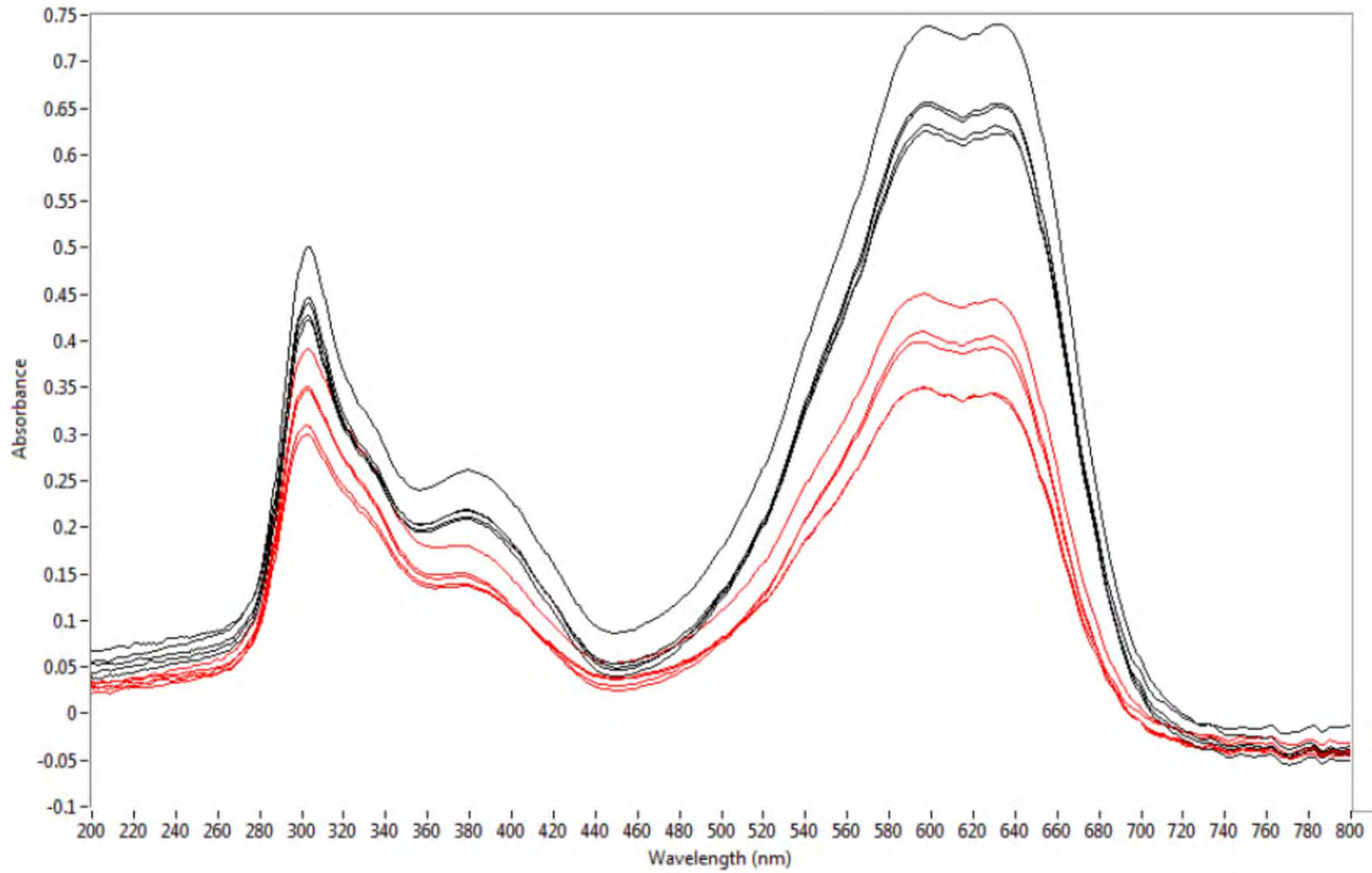


Figure 297. MSP spectral comparison of Acid Blue 25 (black) and Acid Blue 41 (red).

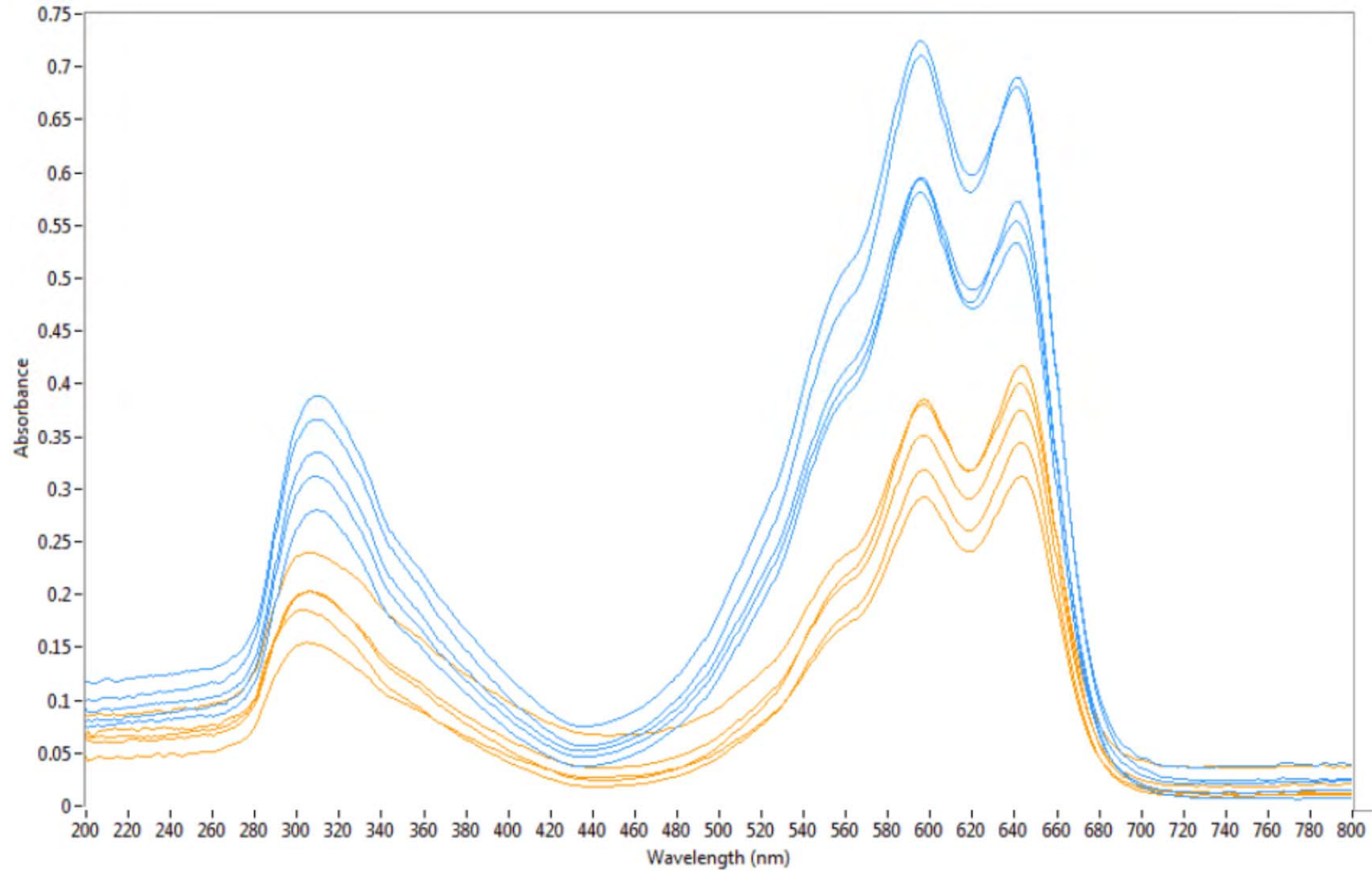


Figure 298. MSP spectral comparison of Disperse Blue 3 (blue) and Disperse Blue 14 (orange).

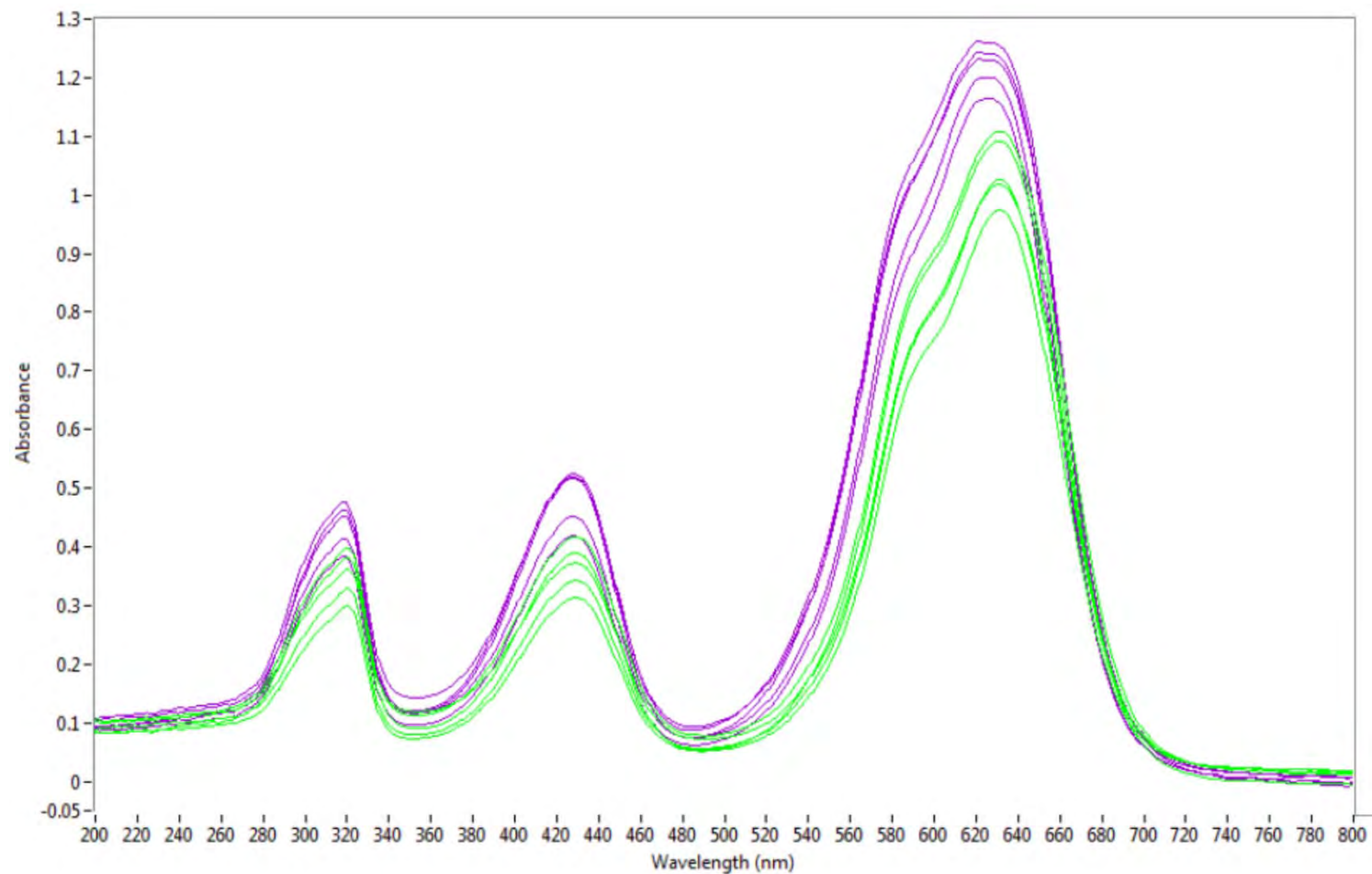


Figure 299. MSP spectral comparison of Basic Green 1 (green) and Basic Green 4 (purple).

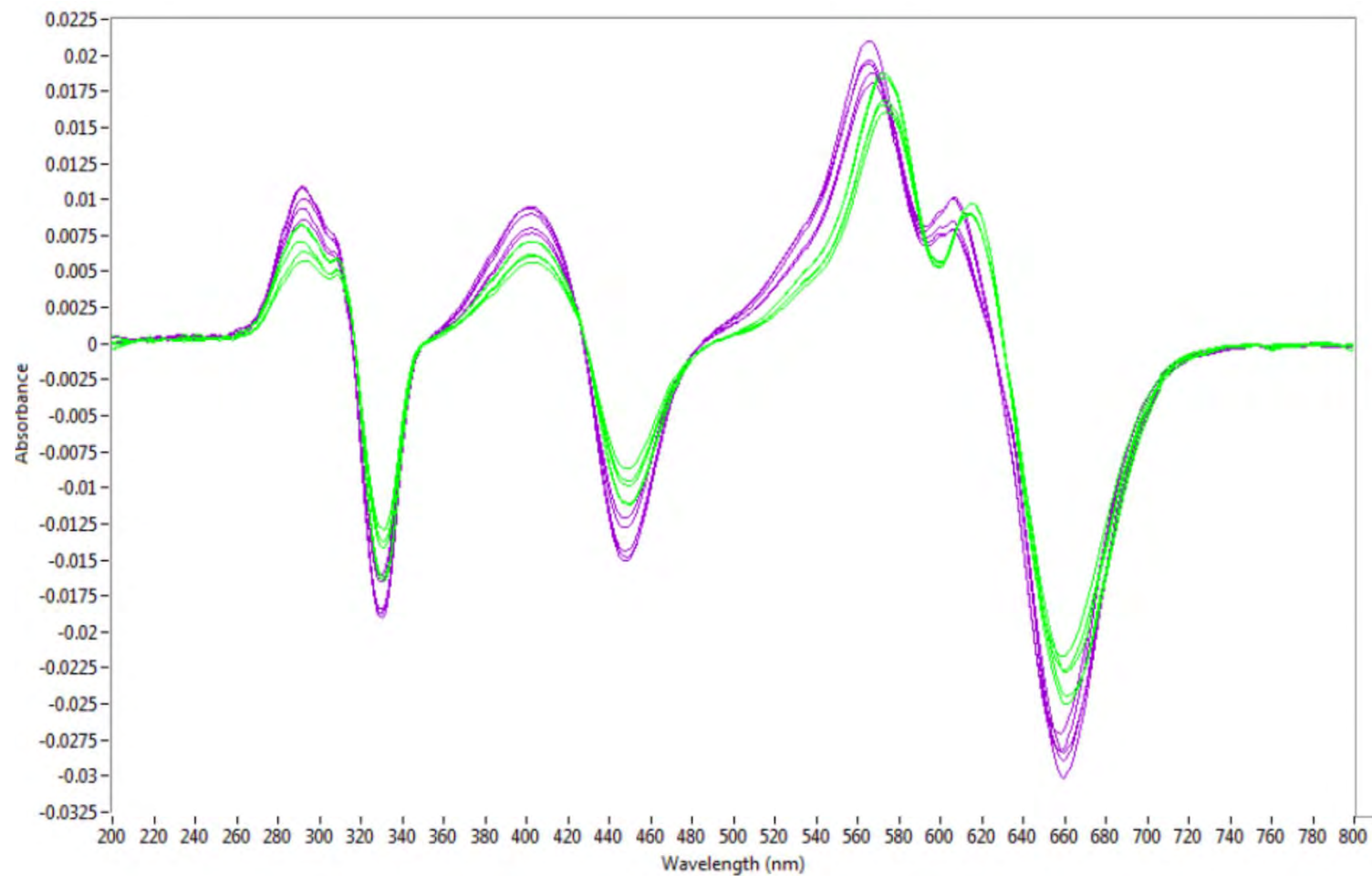


Figure 300. MSP first derivative spectral comparison of Basic Green 1 (green) and Basic Green 4 (purple).

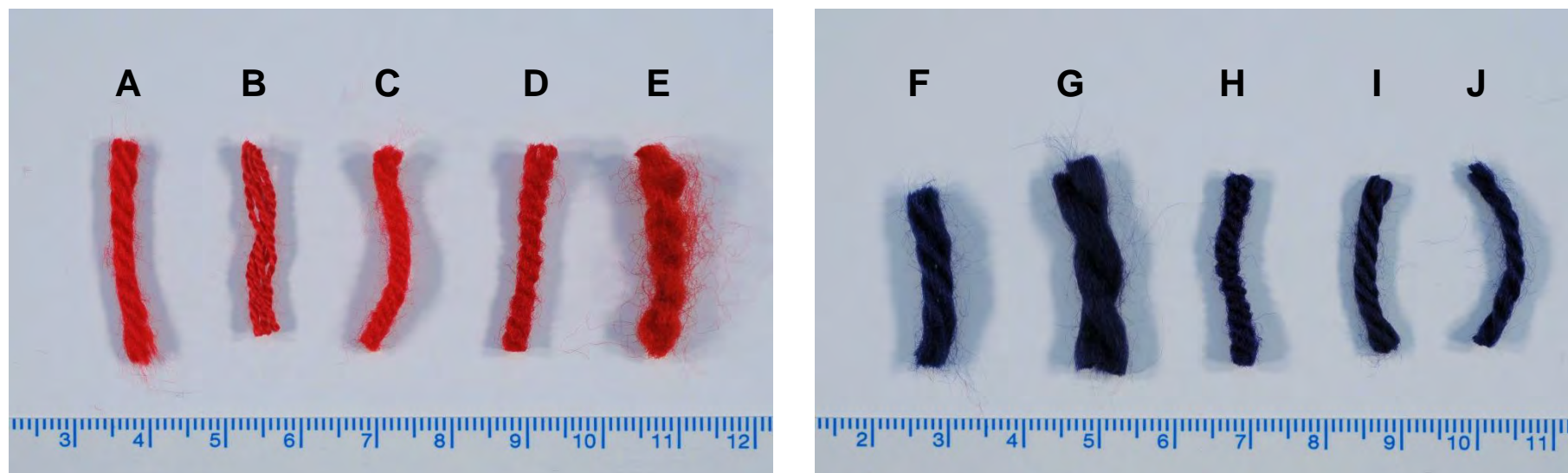


Figure 301. Five red (left) and blue (right) yarns.

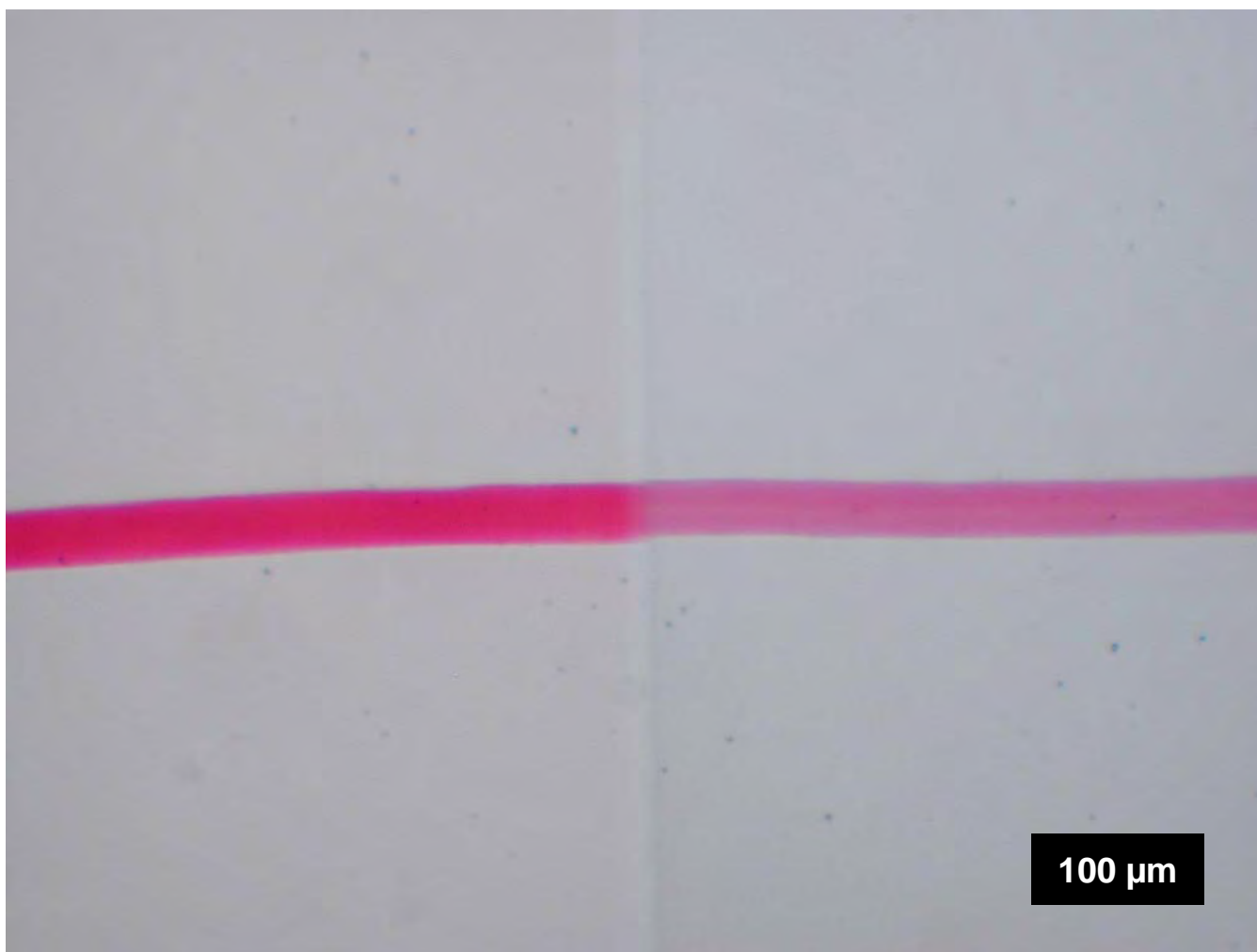


Figure 302. Comparison microscope image of Yarn A (left) and Yarn B (right).

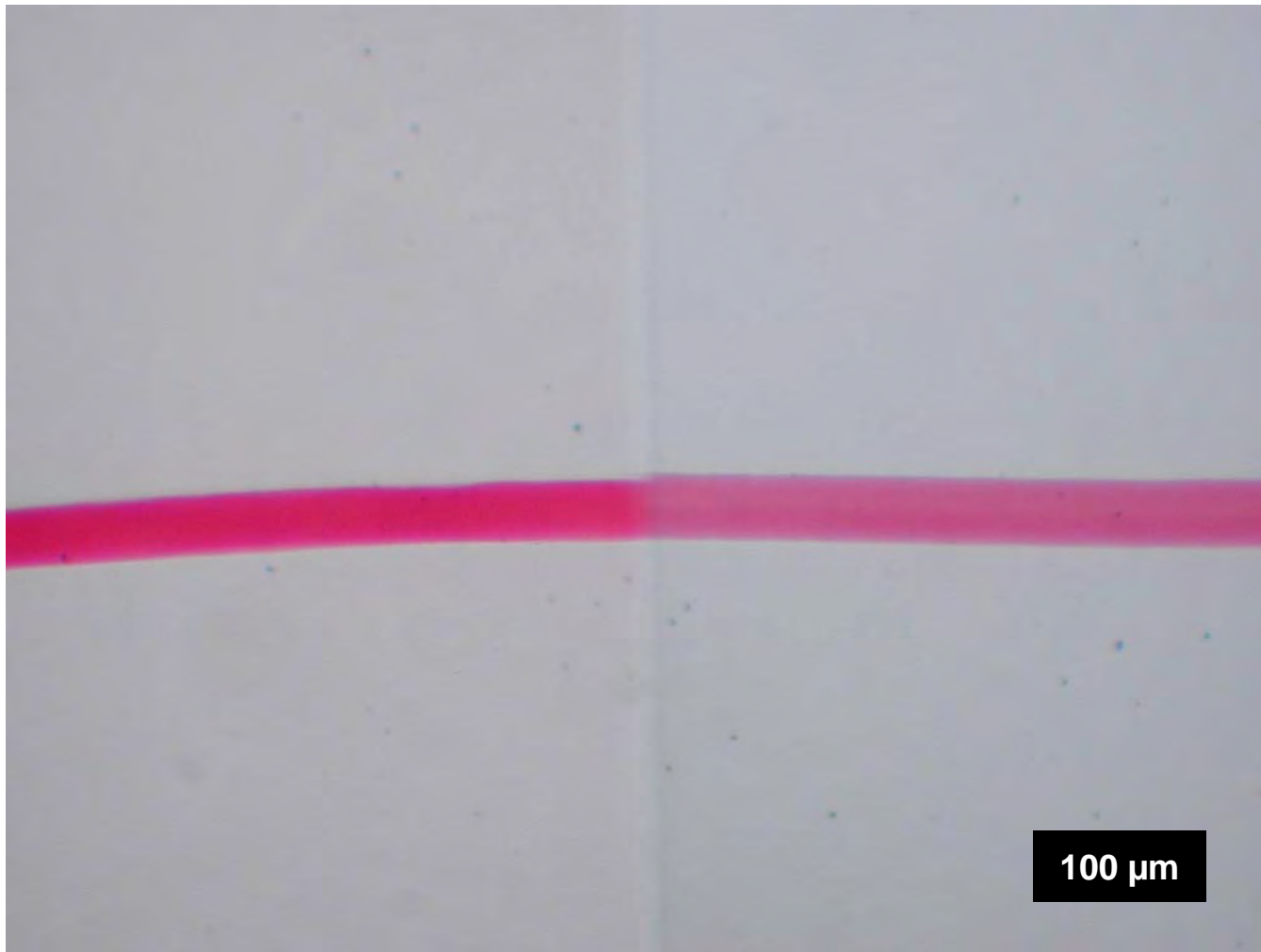


Figure 303. Comparison microscope image of Yarn A (left) and Yarn C (right).

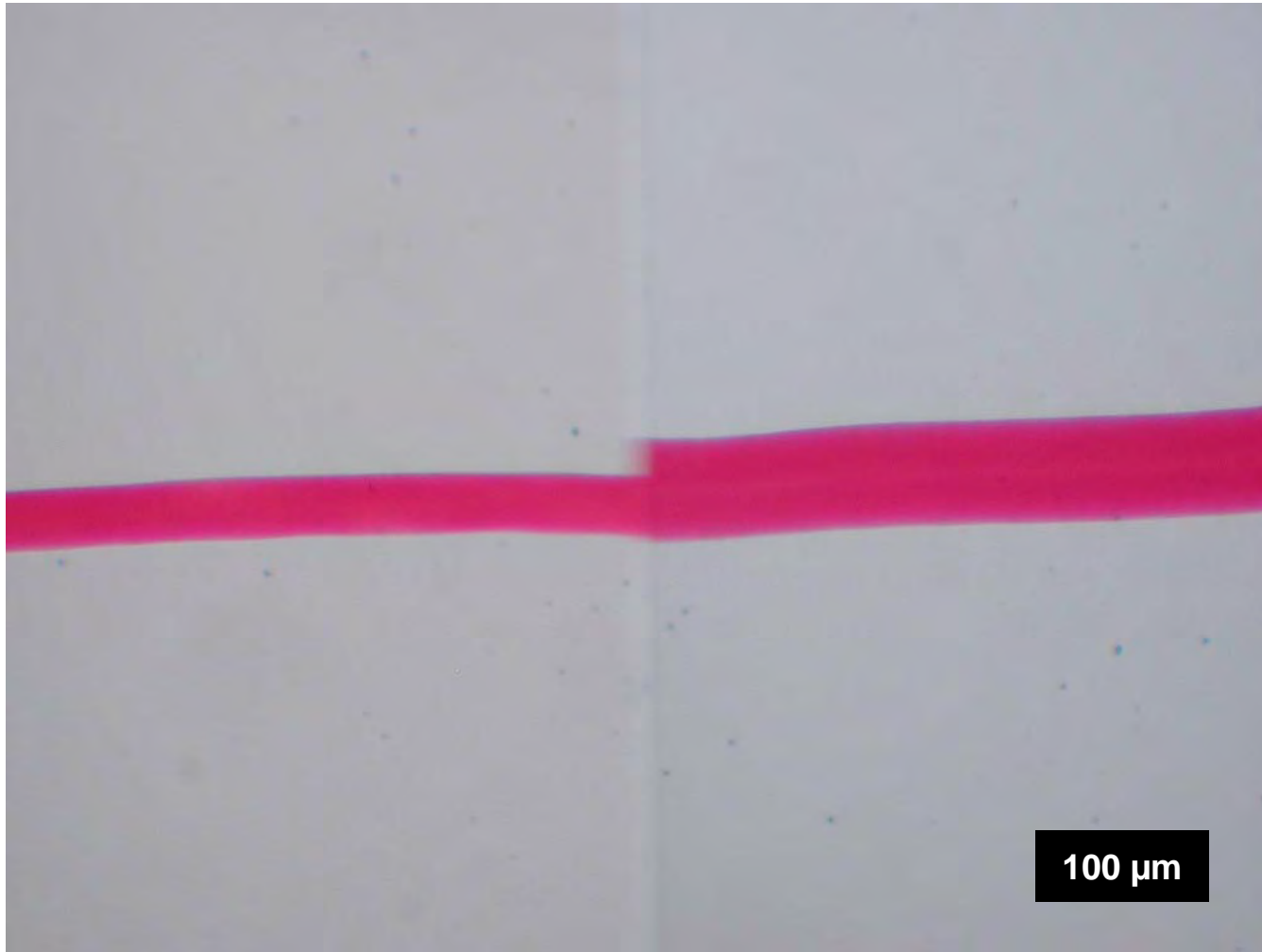


Figure 304. Comparison microscope image of Yarn A (left) and Yarn D (right).

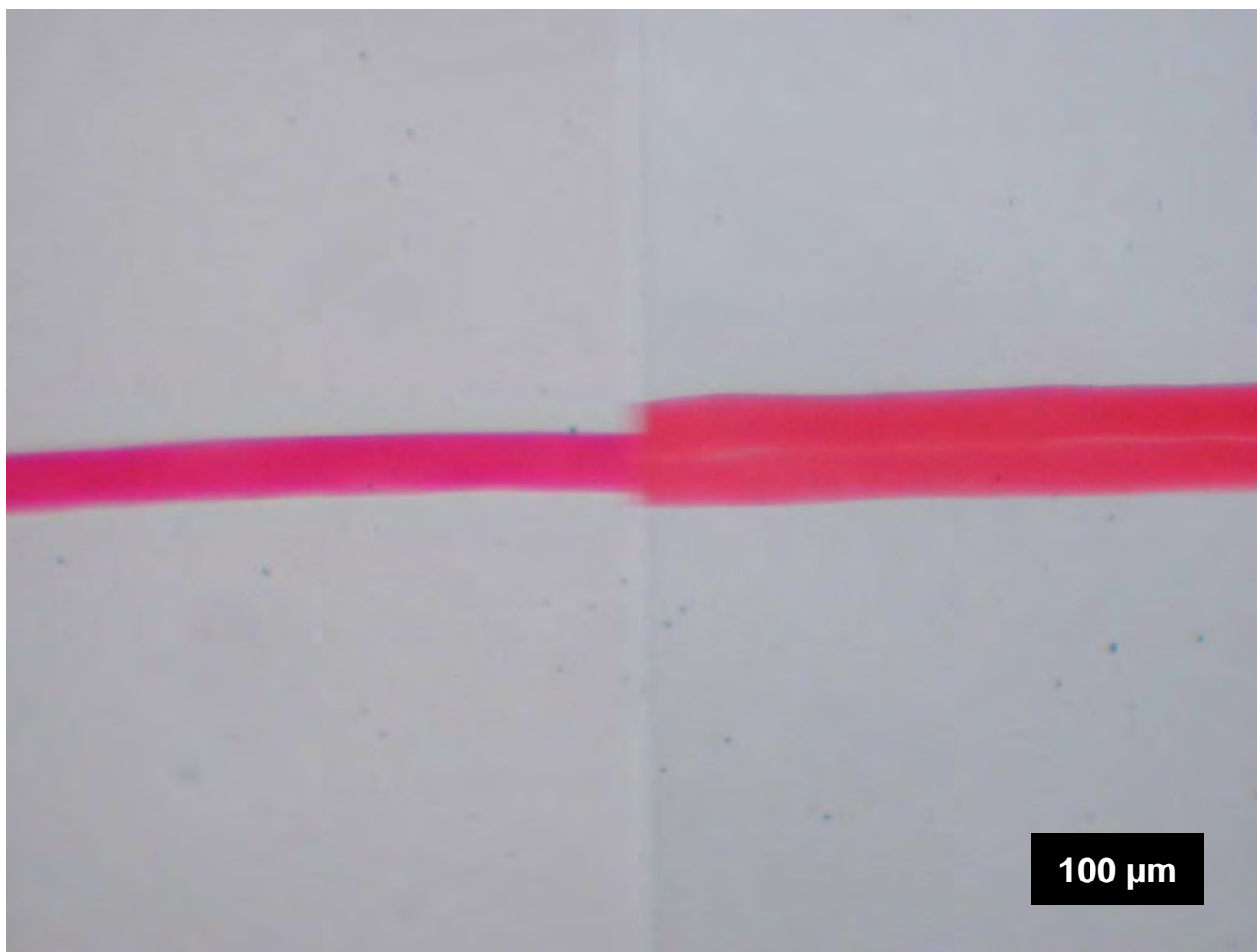


Figure 305. Comparison microscope image of Yarn A (left) and Yarn E (right).

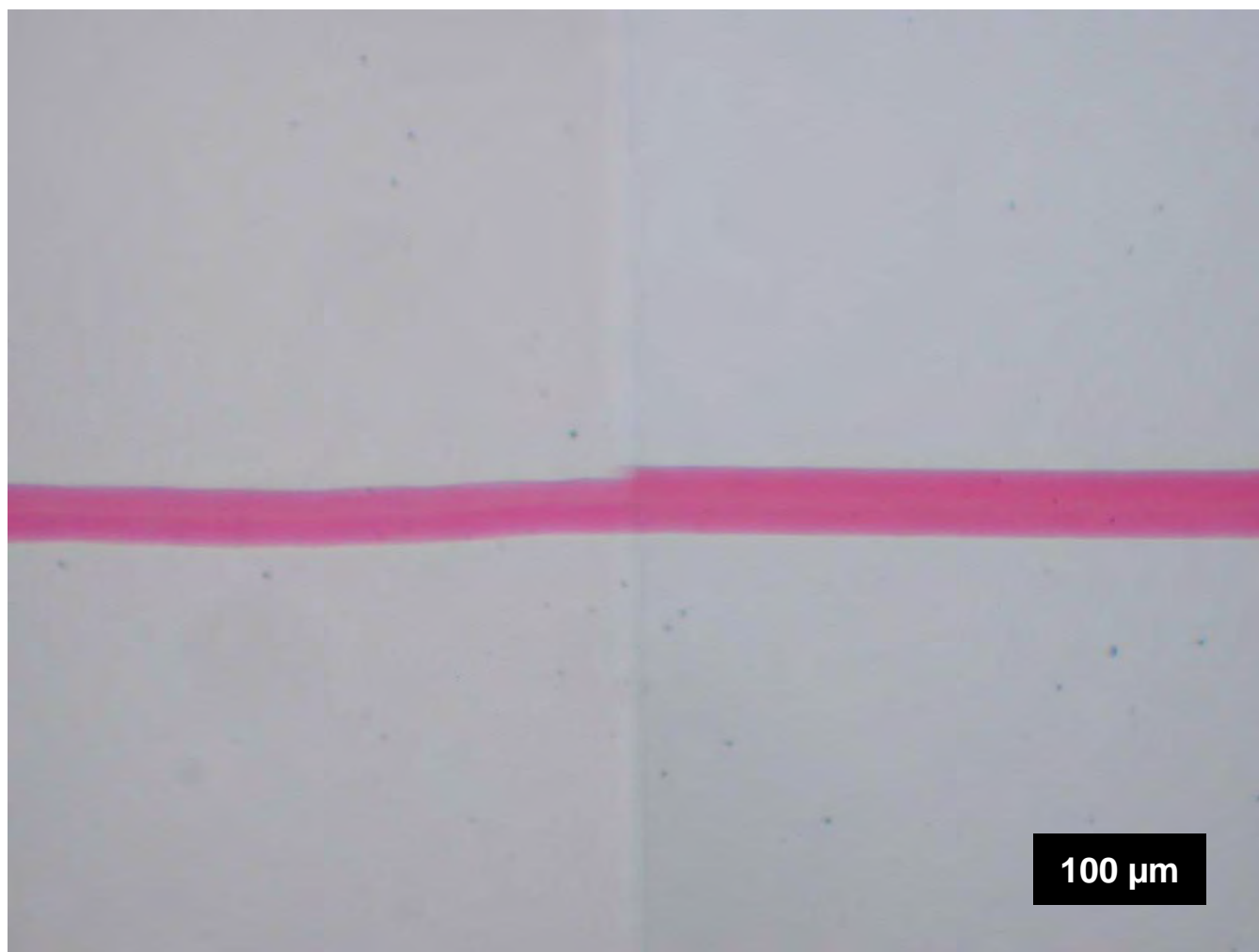


Figure 306. Comparison microscope image of Yarn B (left) and Yarn C (right).

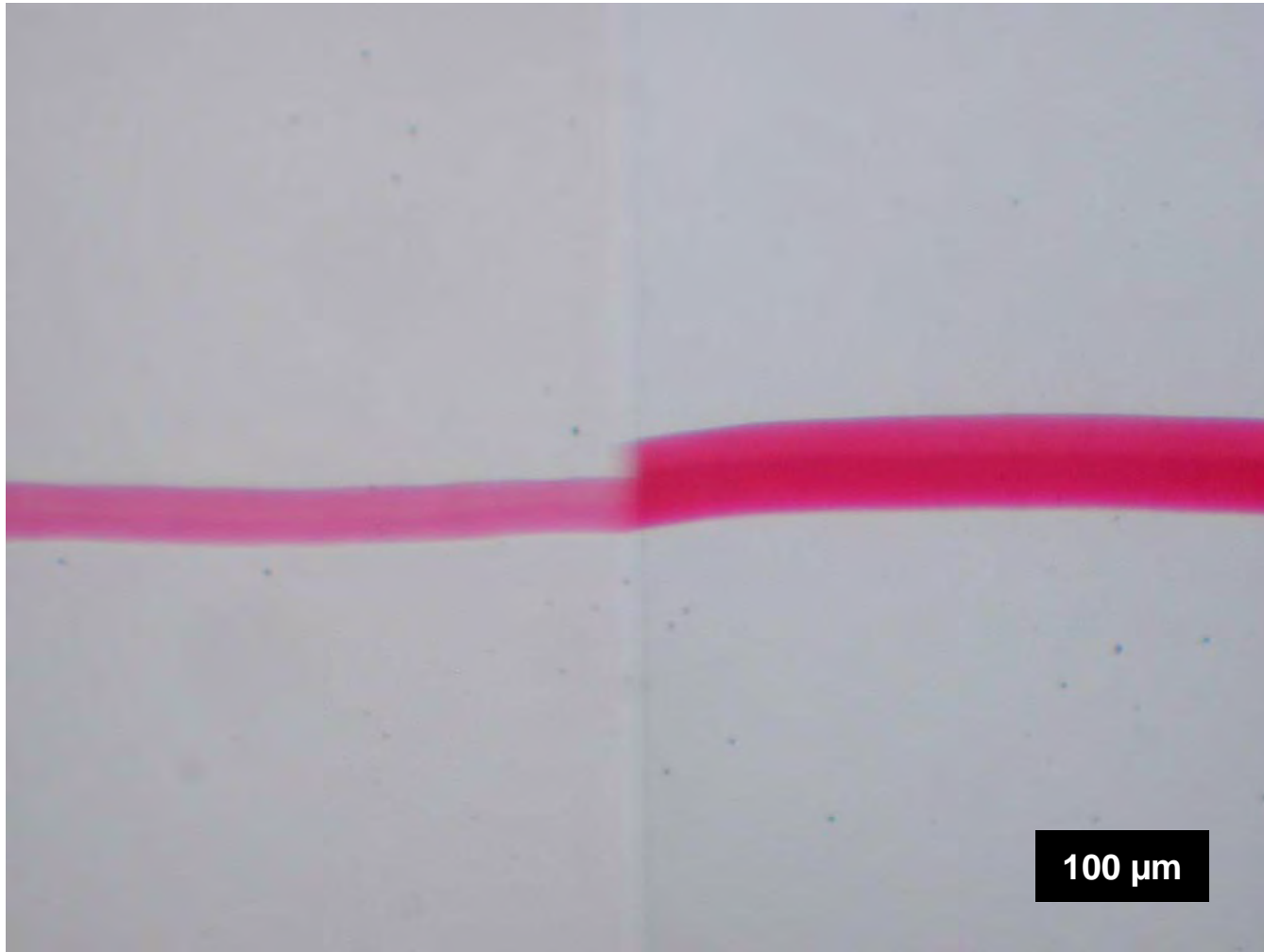


Figure 307. Comparison microscope image of Yarn B (left) and Yarn D (right).

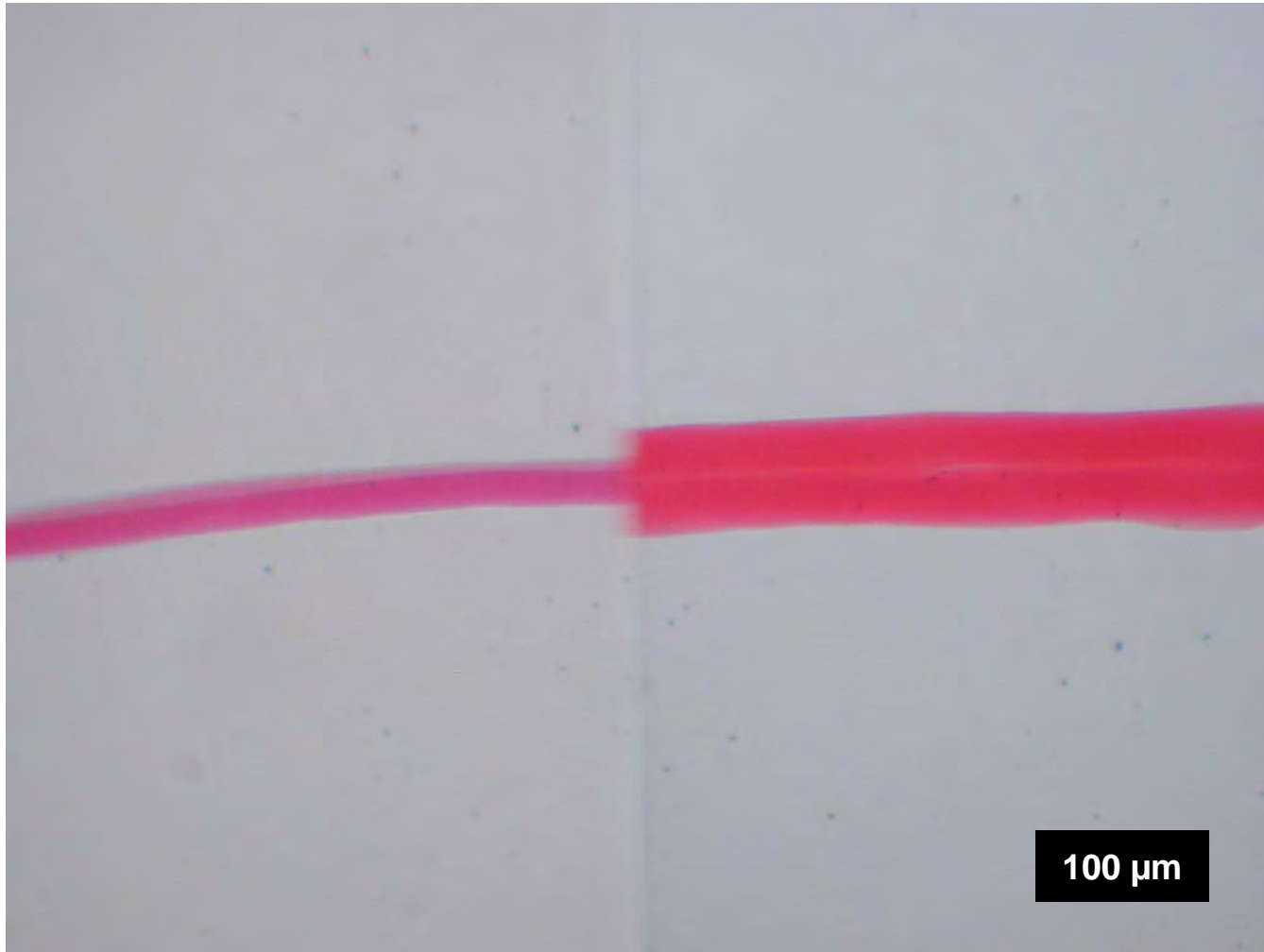


Figure 308. Comparison microscope image of Yarn B (left) and Yarn E (right).

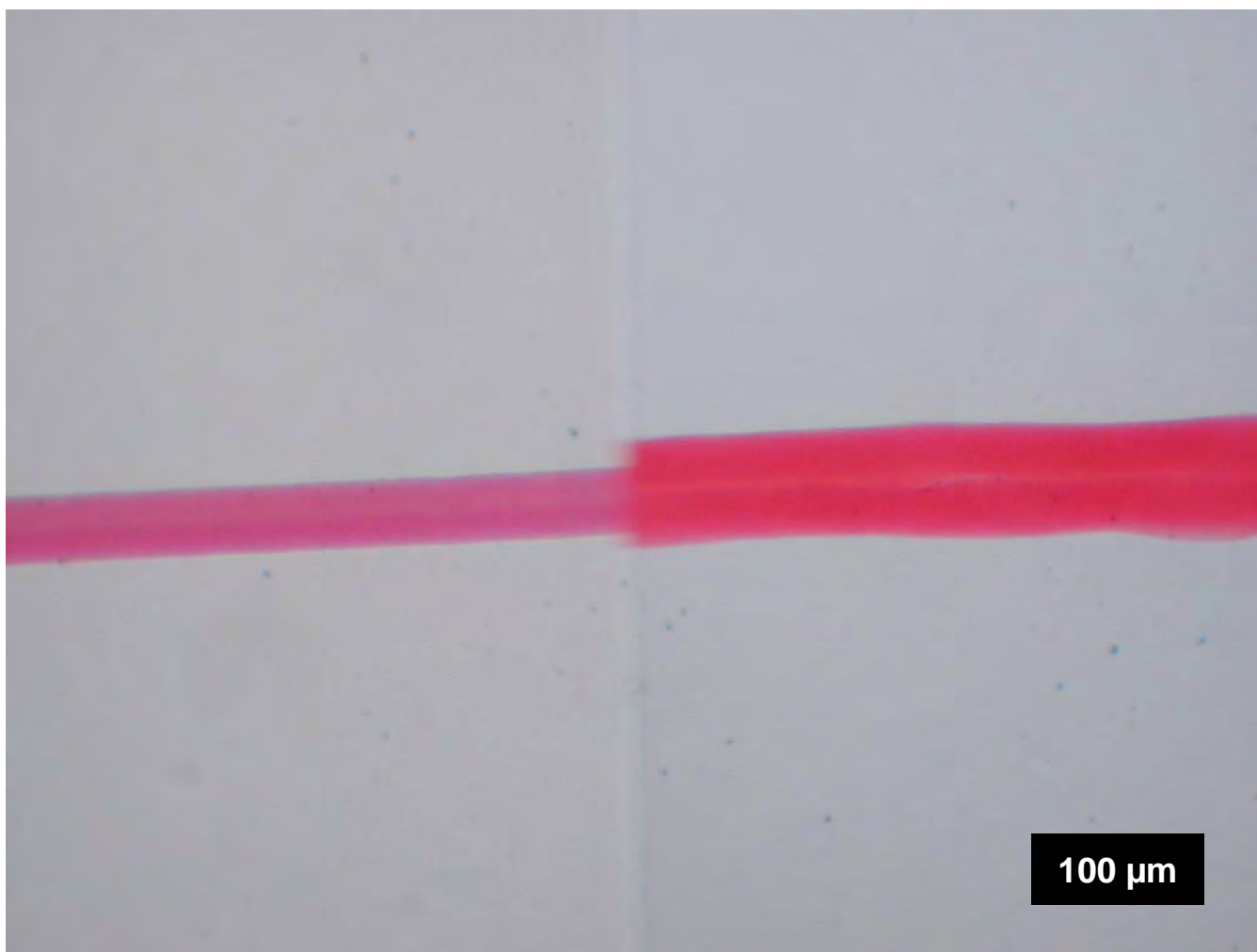


Figure 309. Comparison microscope image of Yarn C (left) and Yarn E (right).

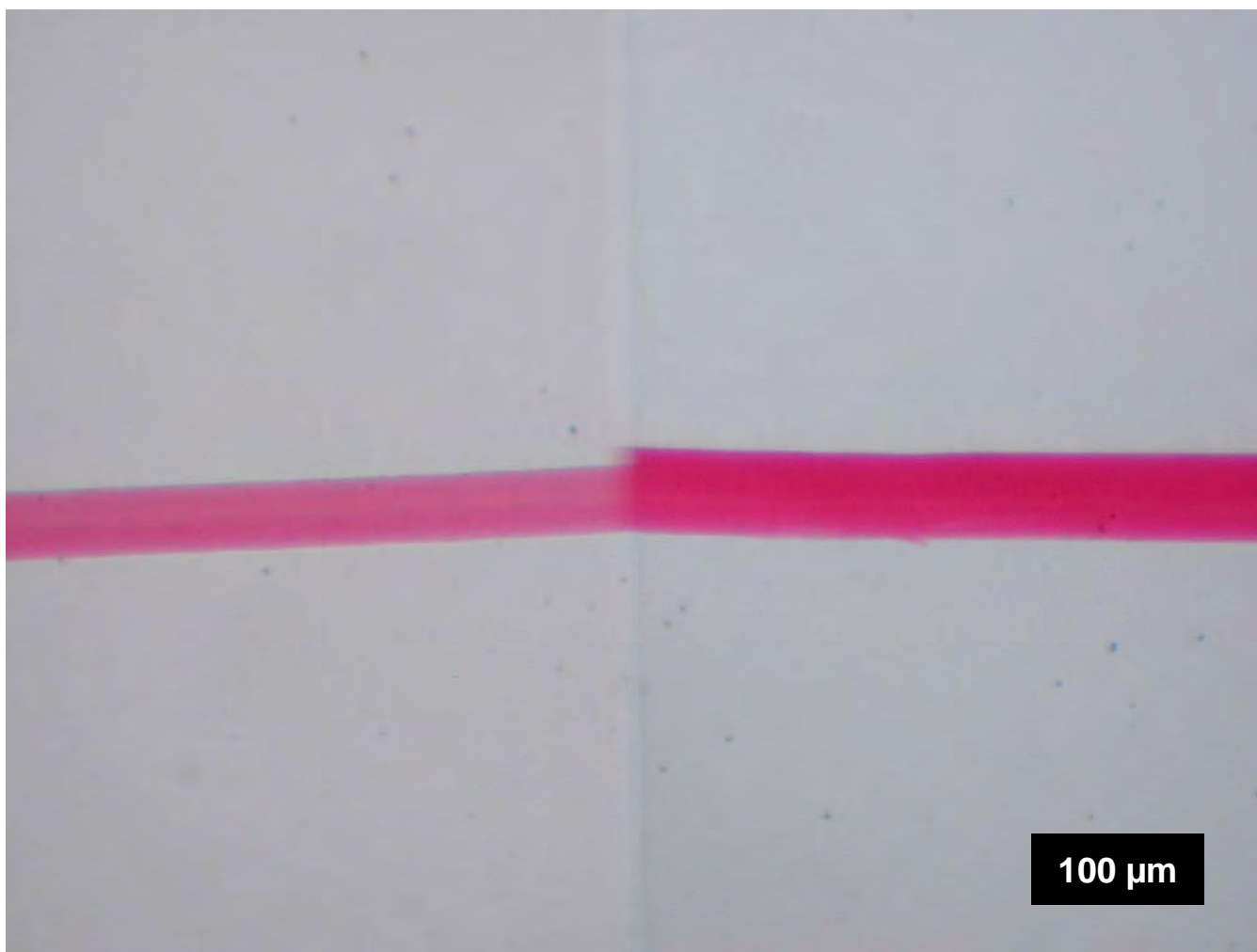


Figure 310. Comparison microscope image of Yarn C (left) and Yarn D (right).

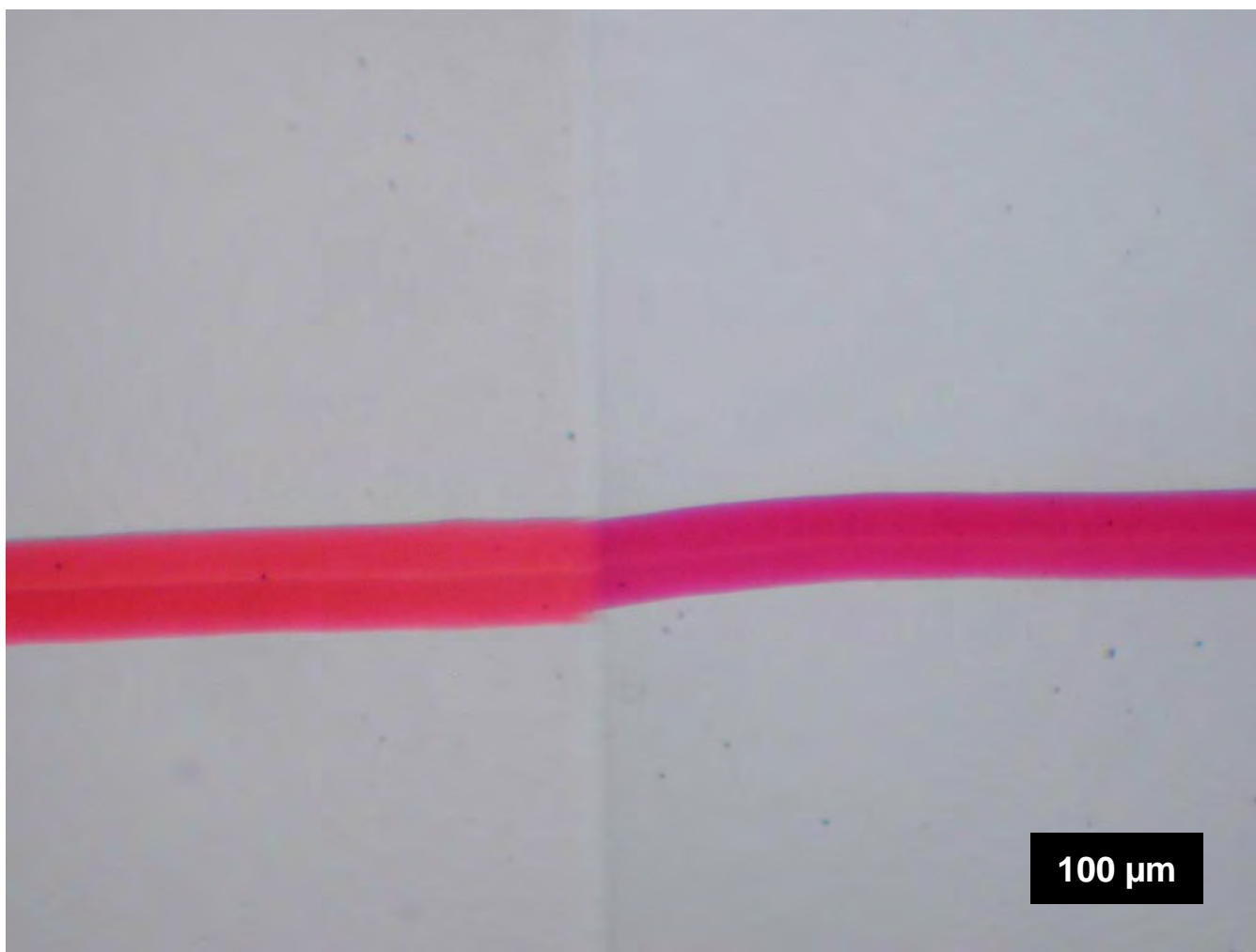


Figure 311. Comparison microscope image of Yarn E (left) and Yarn D (right).

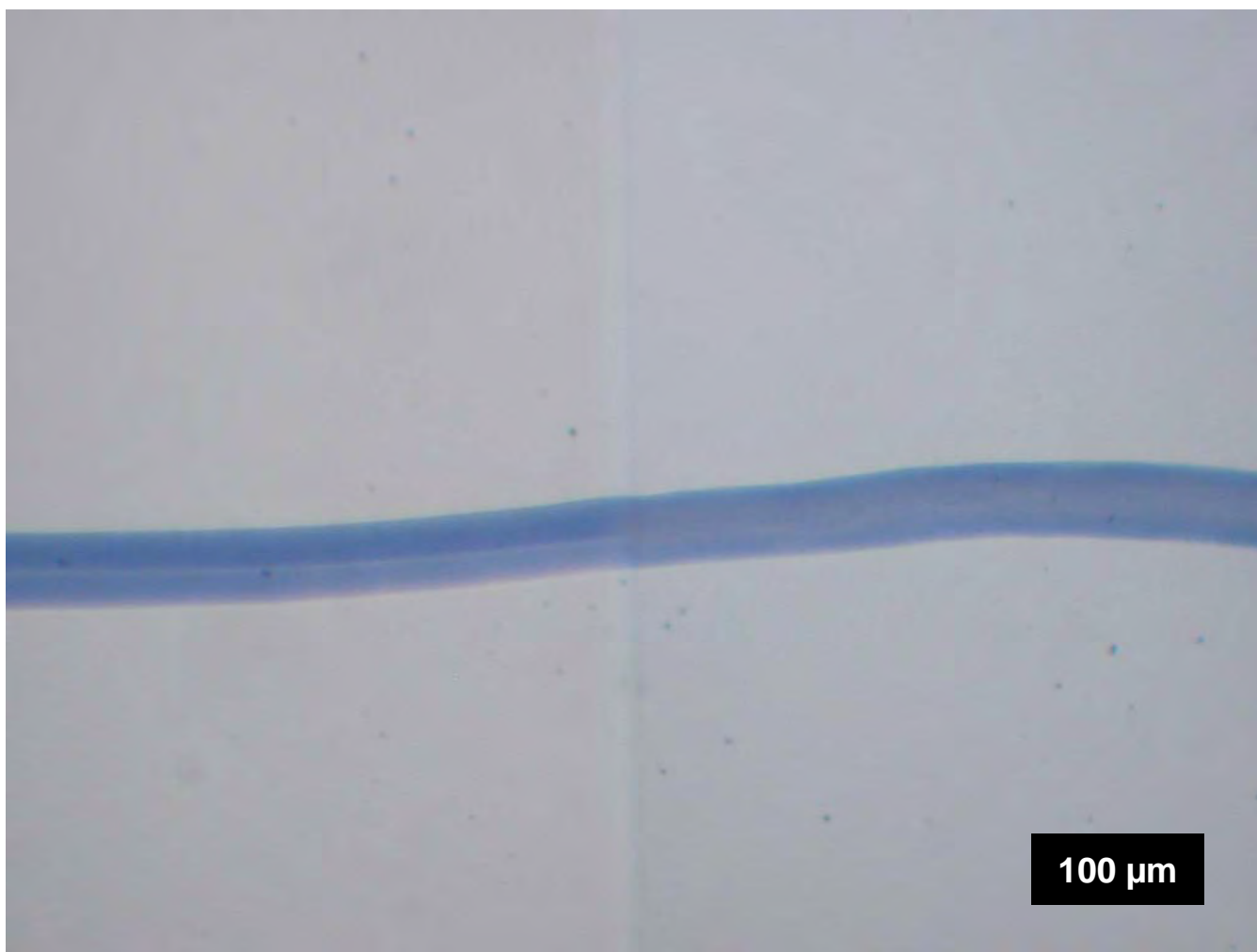


Figure 312. Comparison microscope image of Yarn F (left) and Yarn G (right).

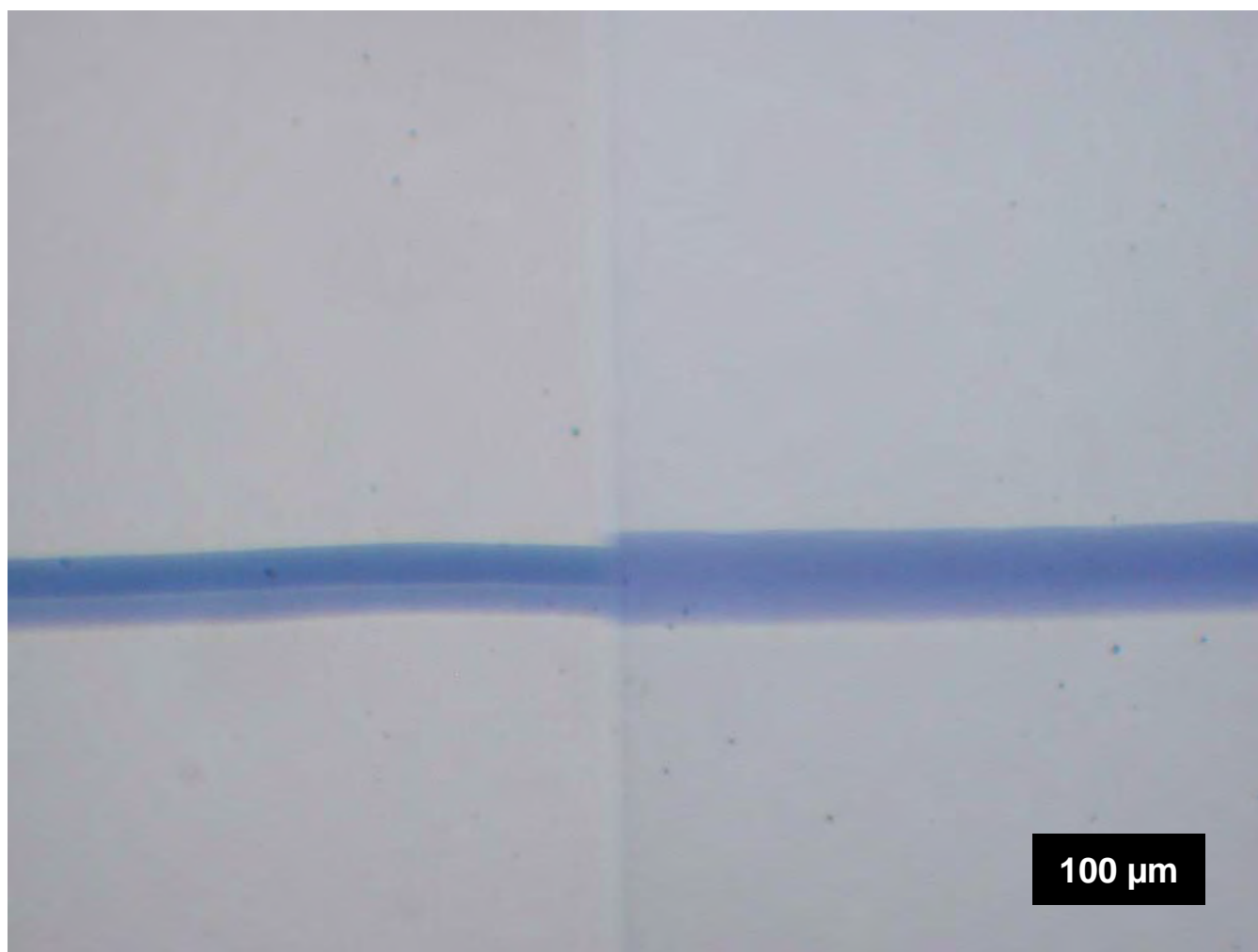


Figure 313. Comparison microscope image of Yarn F (left) and Yarn H (right).

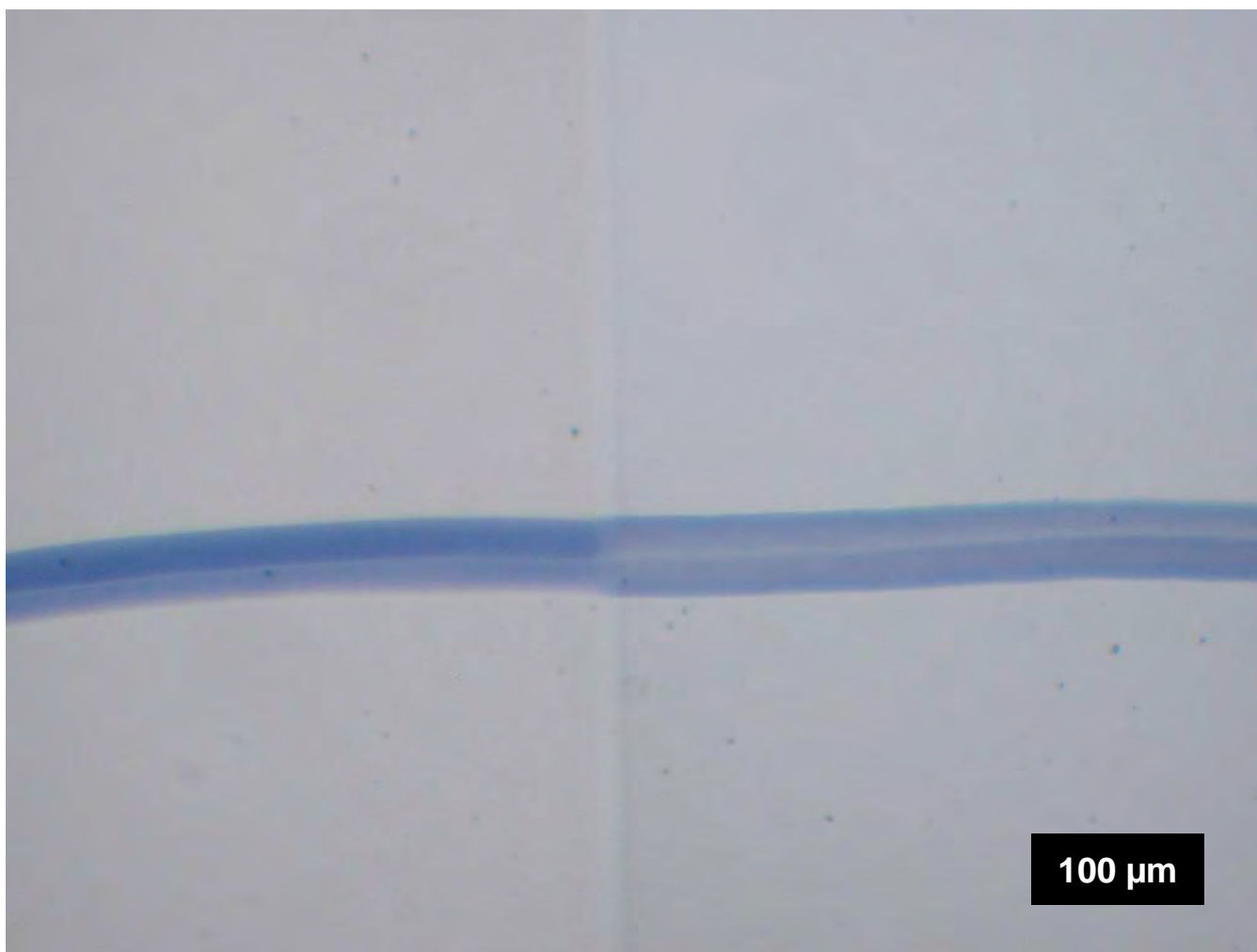


Figure 314. Comparison microscope image of Yarn F (left) and Yarn I (right).

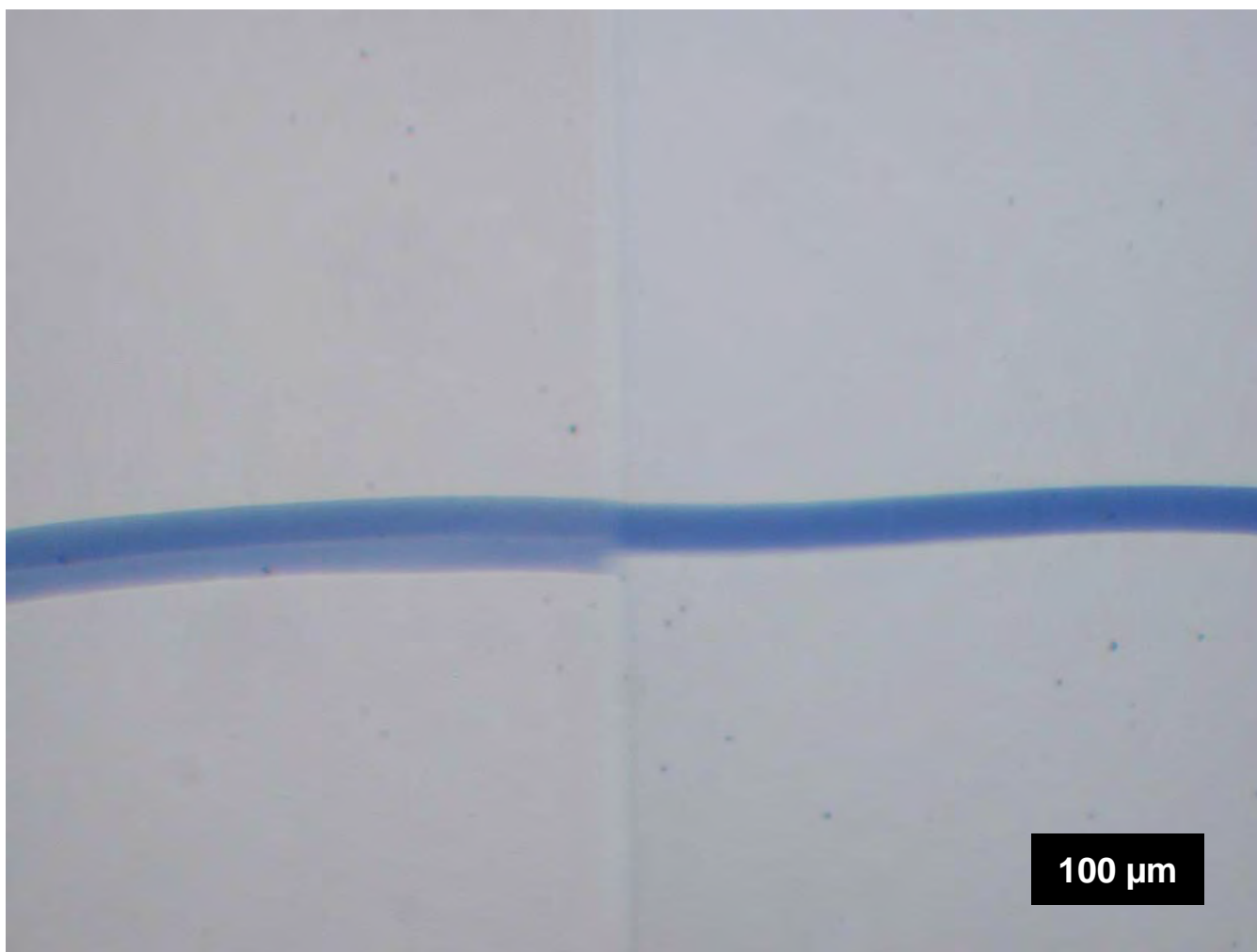


Figure 315. Comparison microscope image of Yarn F (left) and Yarn J (right).

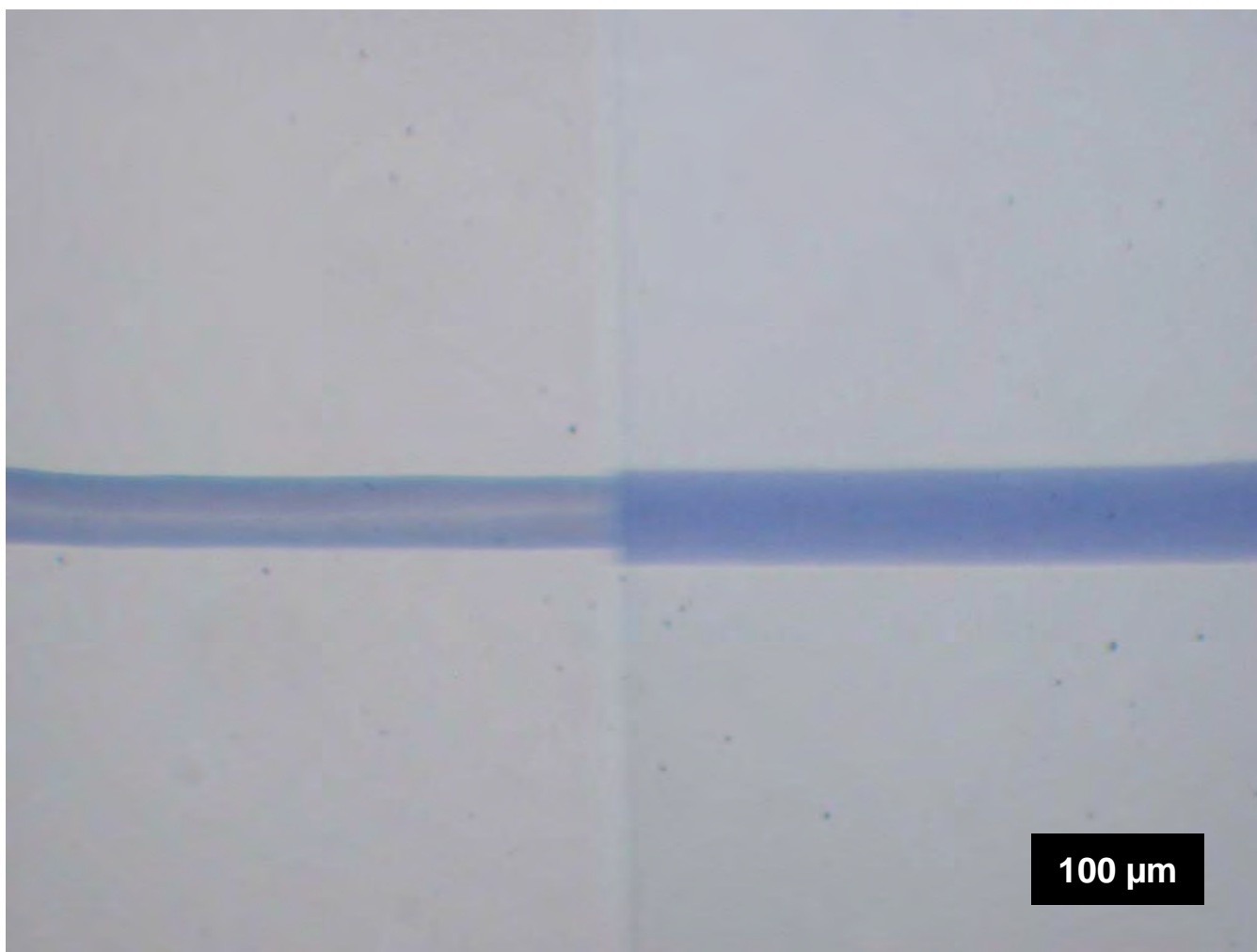


Figure 316. Comparison microscope image of Yarn G (left) and Yarn H (right).

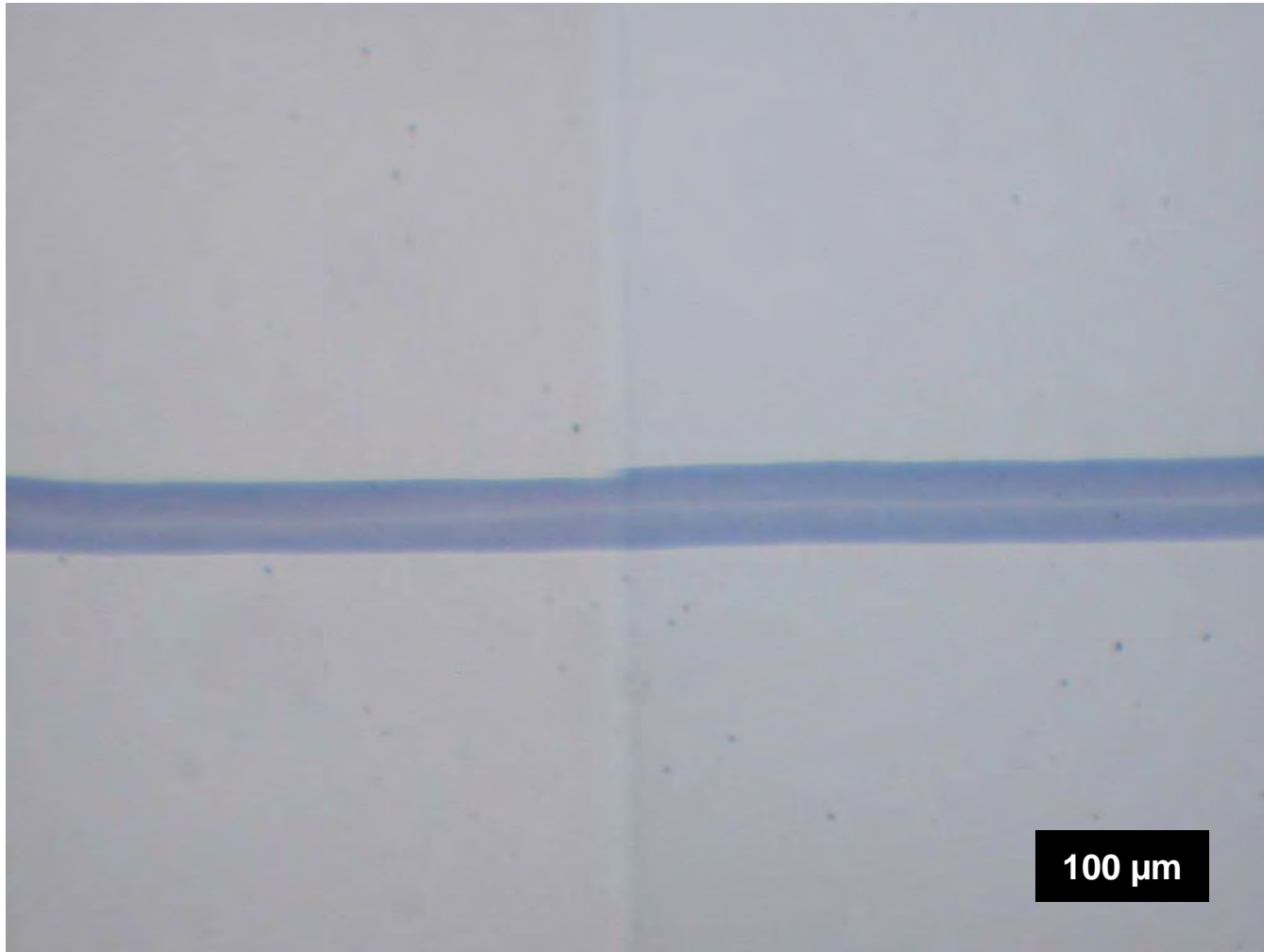


Figure 317. Comparison microscope image of Yarn G (left) and Yarn I (right).

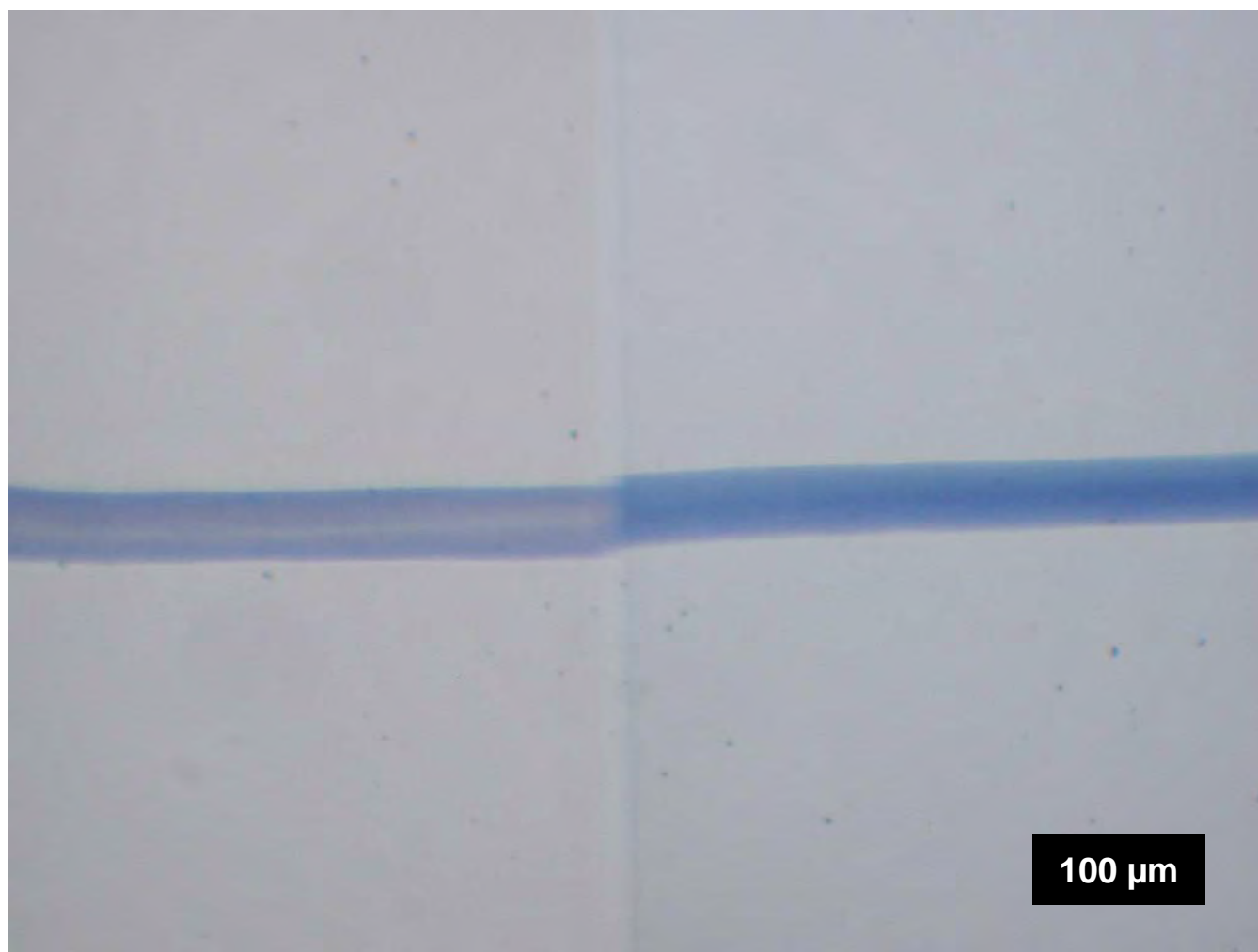


Figure 318. Comparison microscope image of Yarn G (left) and Yarn J (right).

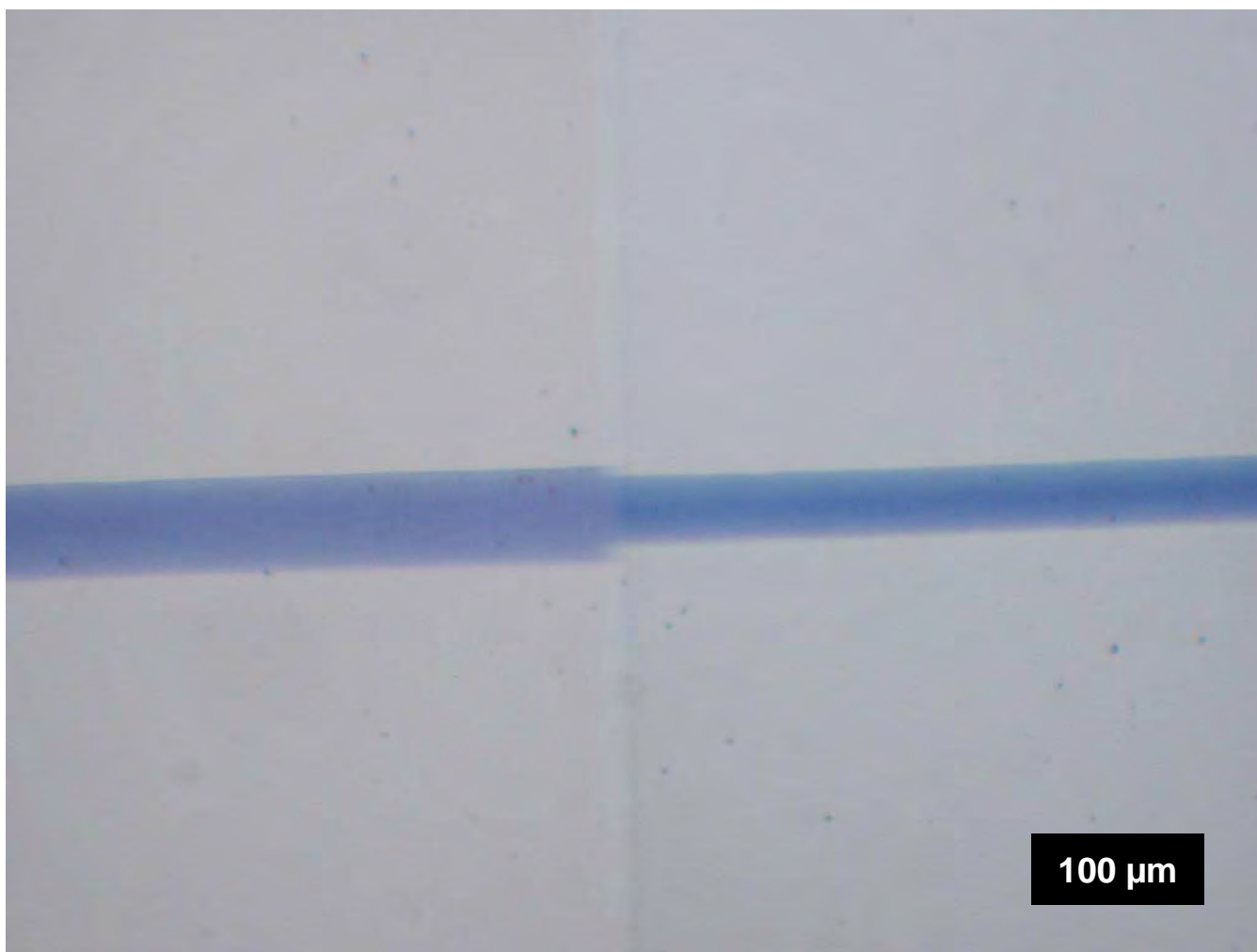


Figure 319. Comparison microscope image of Yarn H (left) and Yarn J (right).

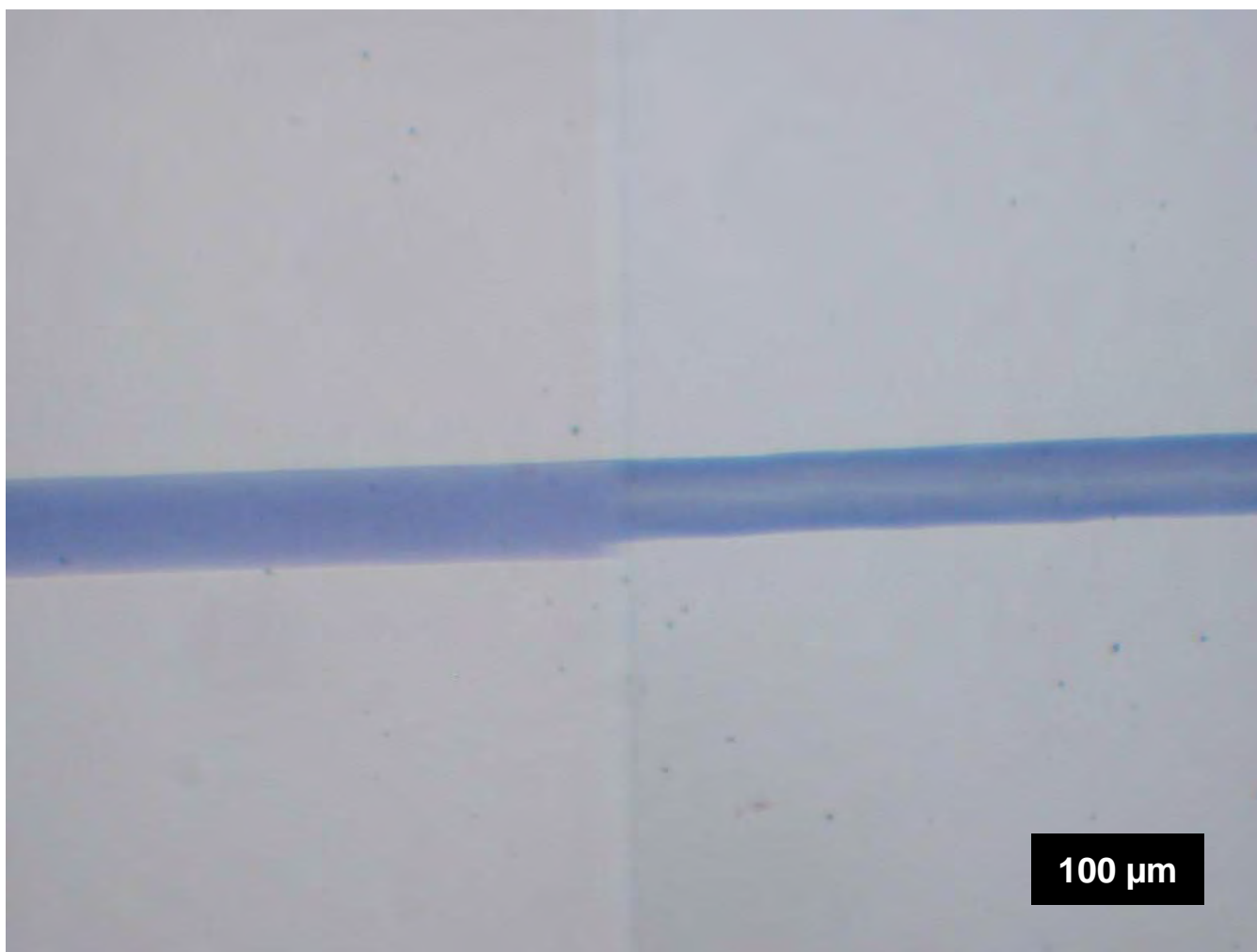


Figure 320. Comparison microscope image of Yarn H (left) and Yarn I (right).

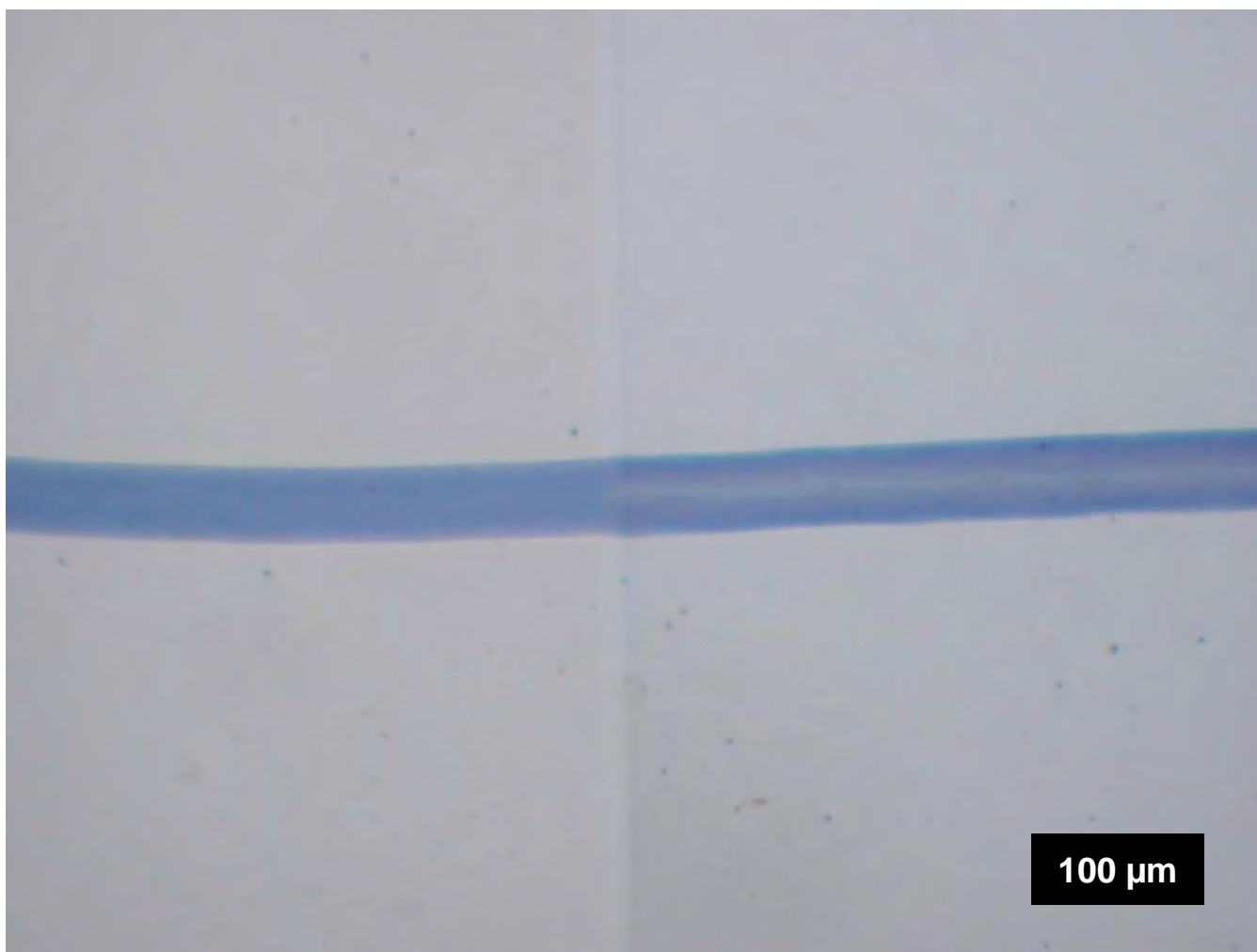


Figure 321. Comparison microscope image of Yarn J (left) and Yarn I (right).

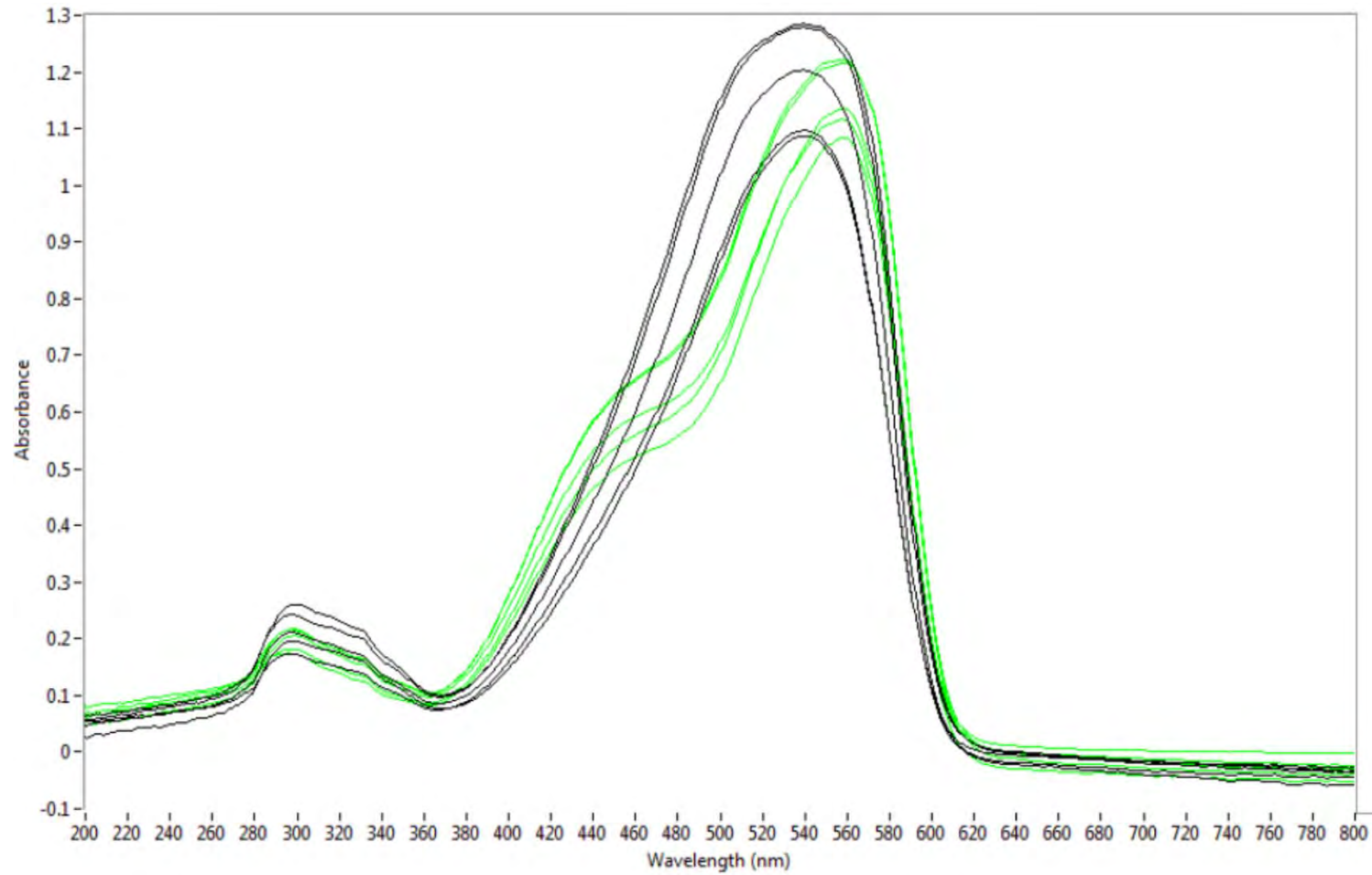


Figure 322. MSP spectral comparison of Yarn A (black) and Yarn D (green).

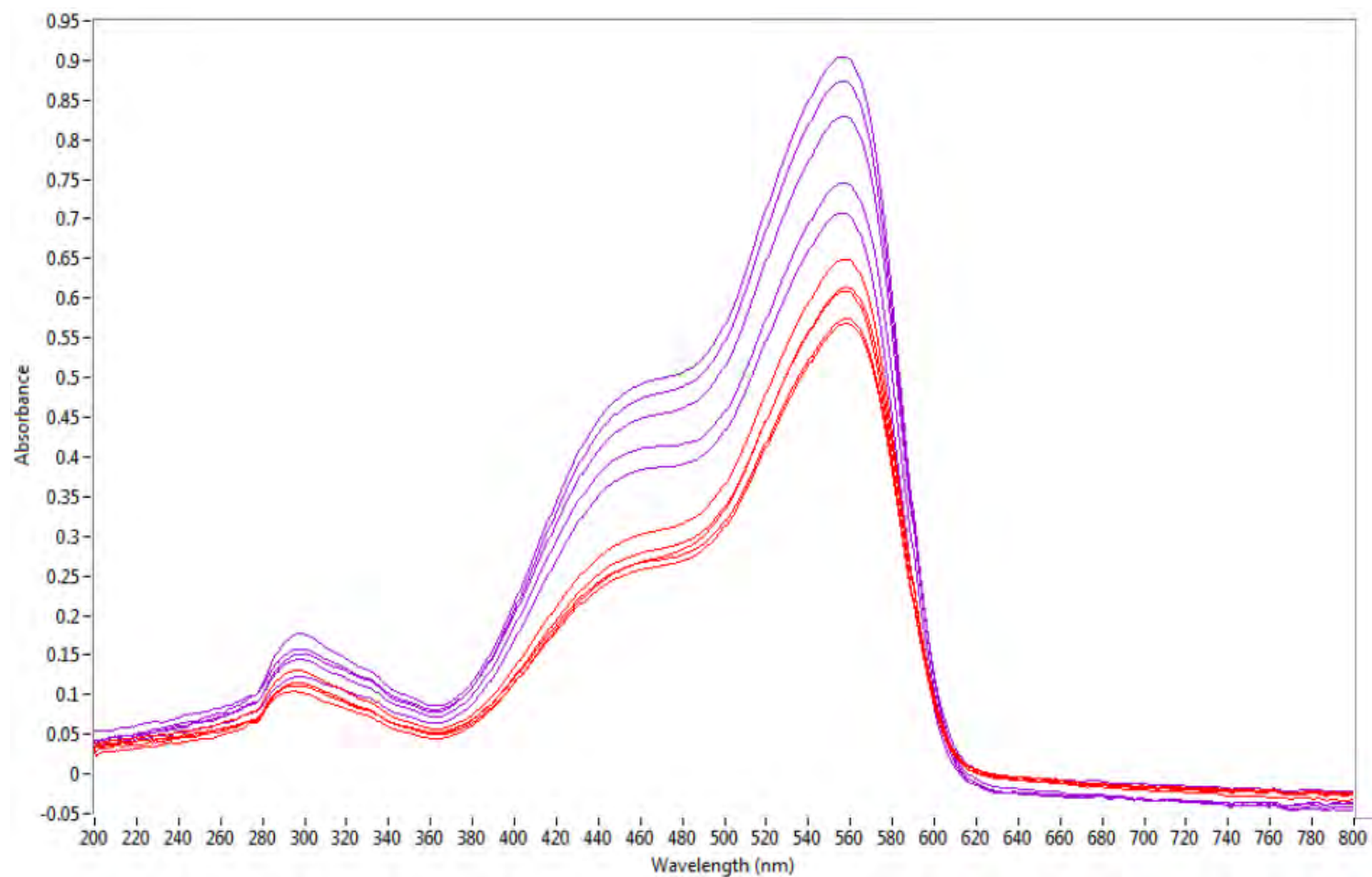


Figure 323. MSP spectral comparison of Yarn B (red) and Yarn C (purple).

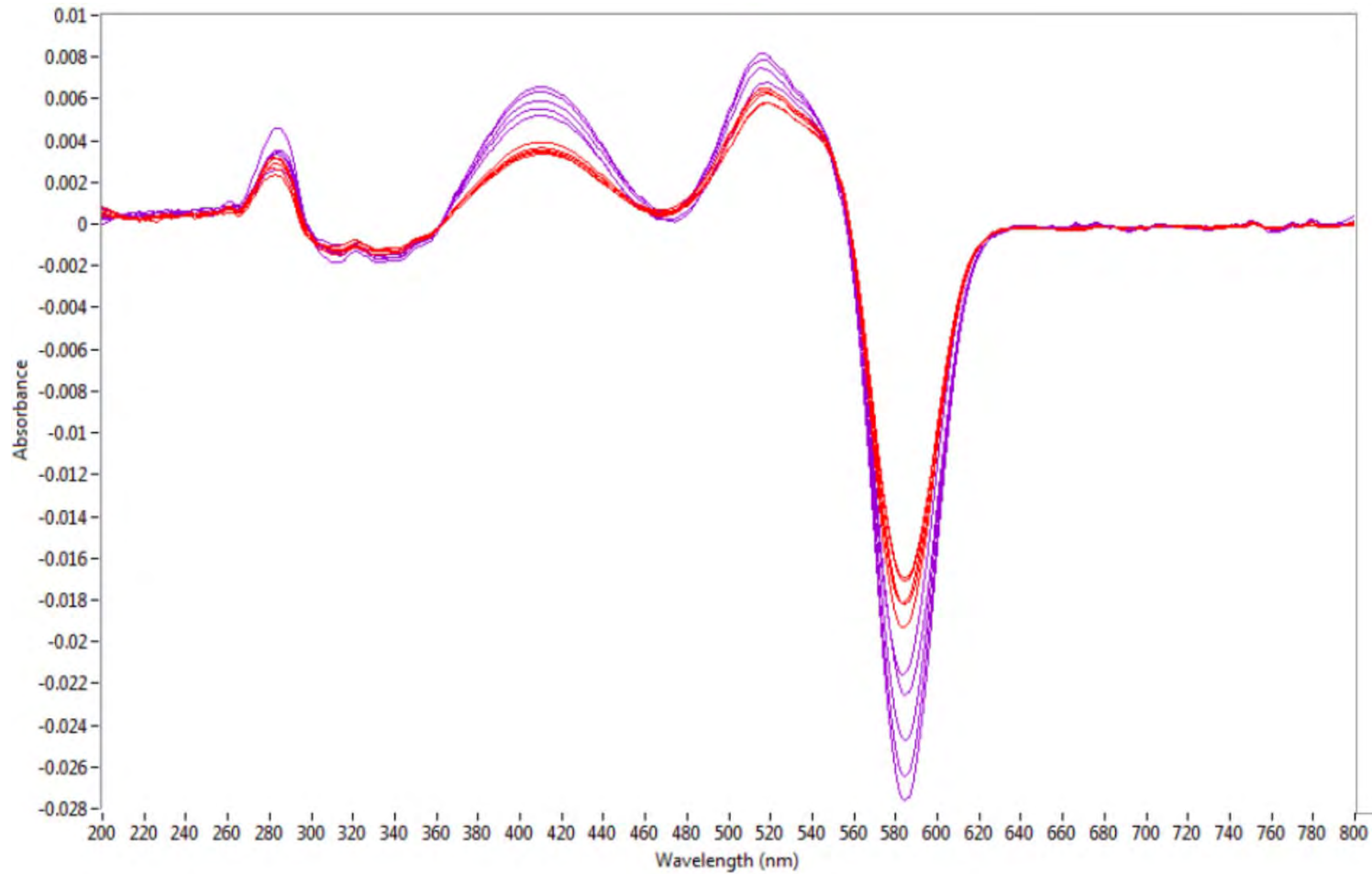


Figure 324. MSP first derivative spectral comparison of Yarn B (red) and Yarn C (purple).

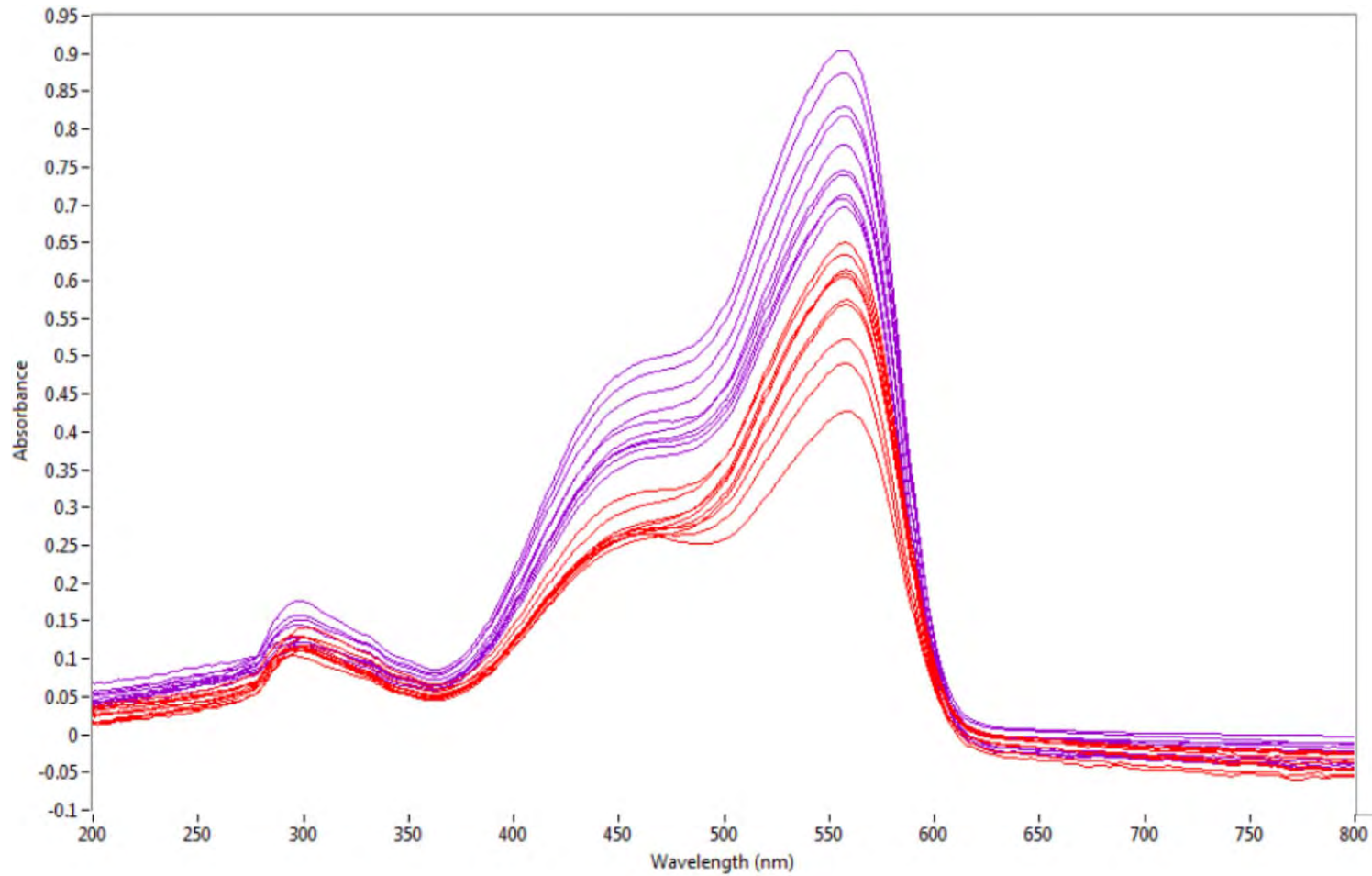


Figure 325. Additional MSP spectral comparison of Yarn B (red) and Yarn C (purple) to represent most of the variation in the fibers.

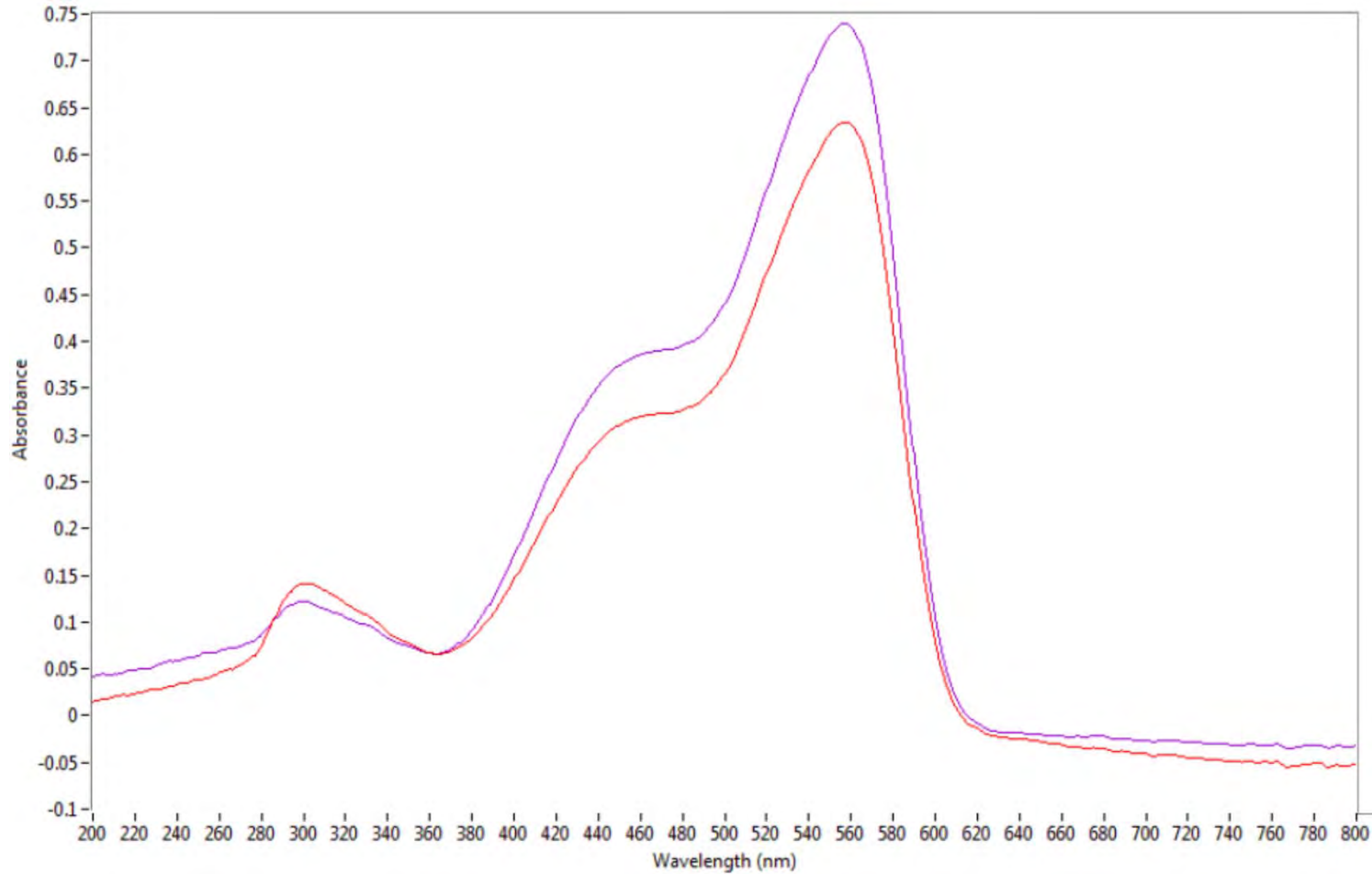


Figure 326. MSP best match spectral comparison of Yarn B (red) and Yarn C (purple).

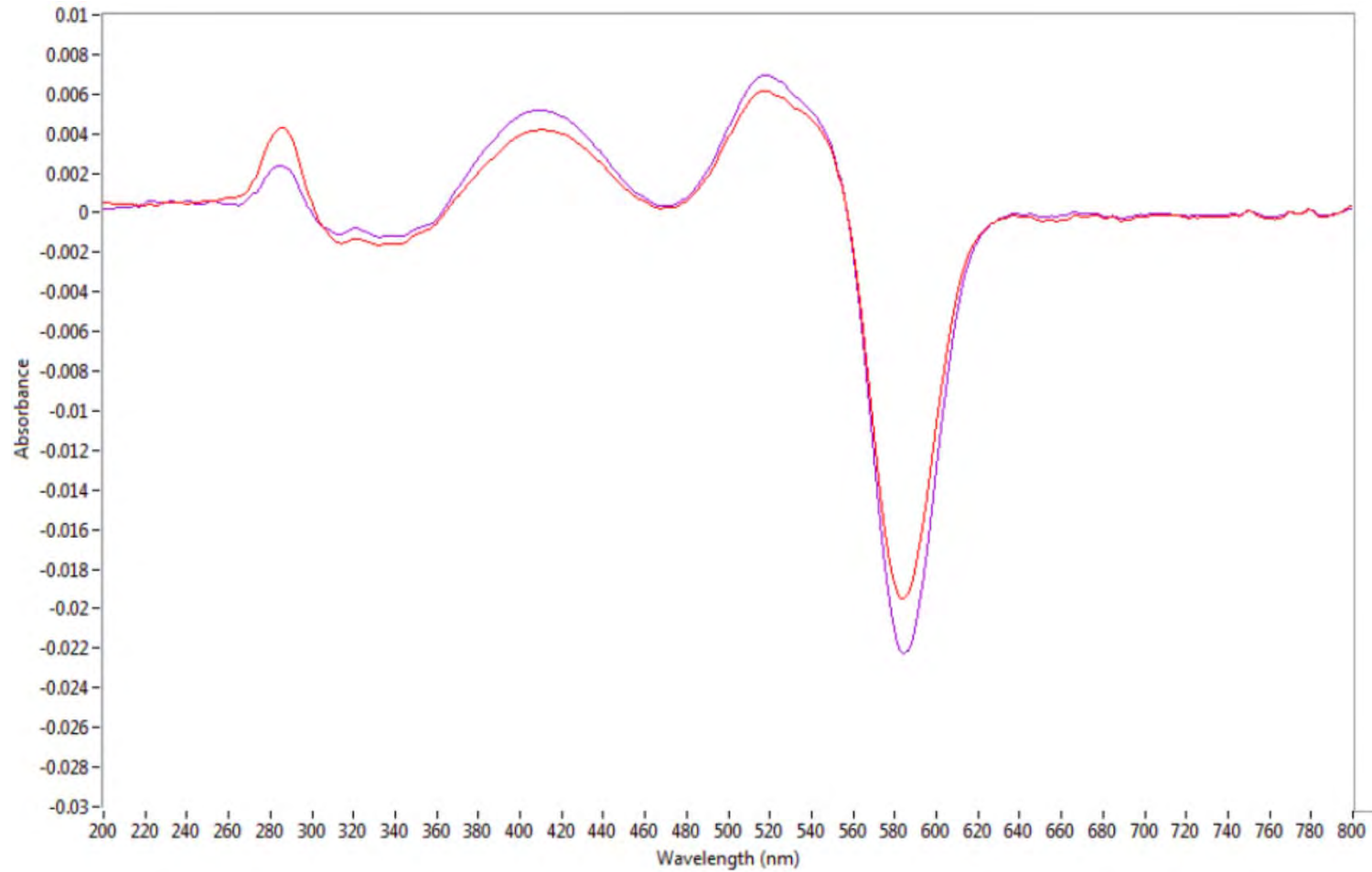


Figure 327. MSP best match first derivative spectral comparison of Yarn B (red) and Yarn C (purple).

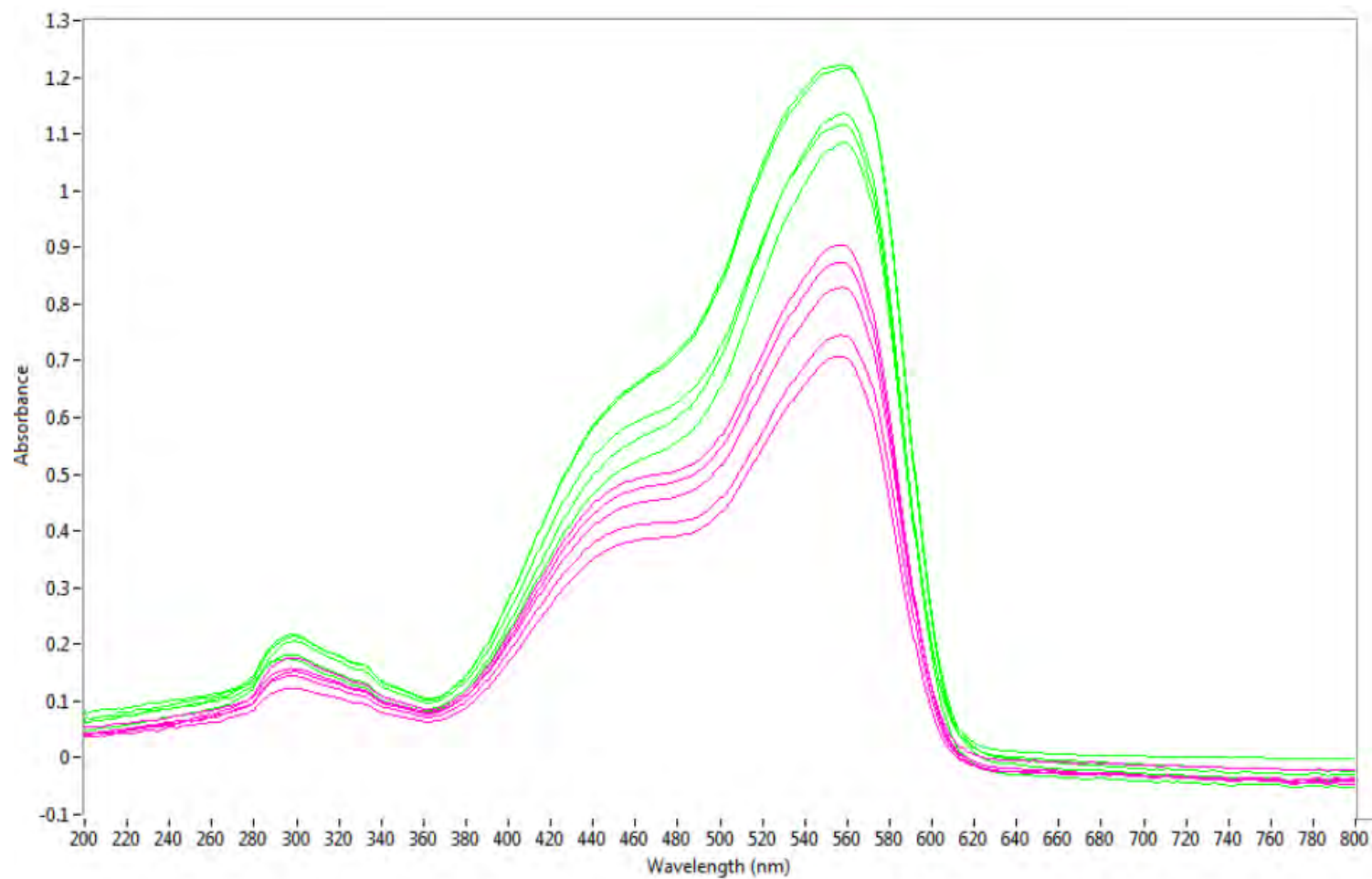


Figure 328. MSP spectral comparison of Yarn C (pink) and Yarn D (green).

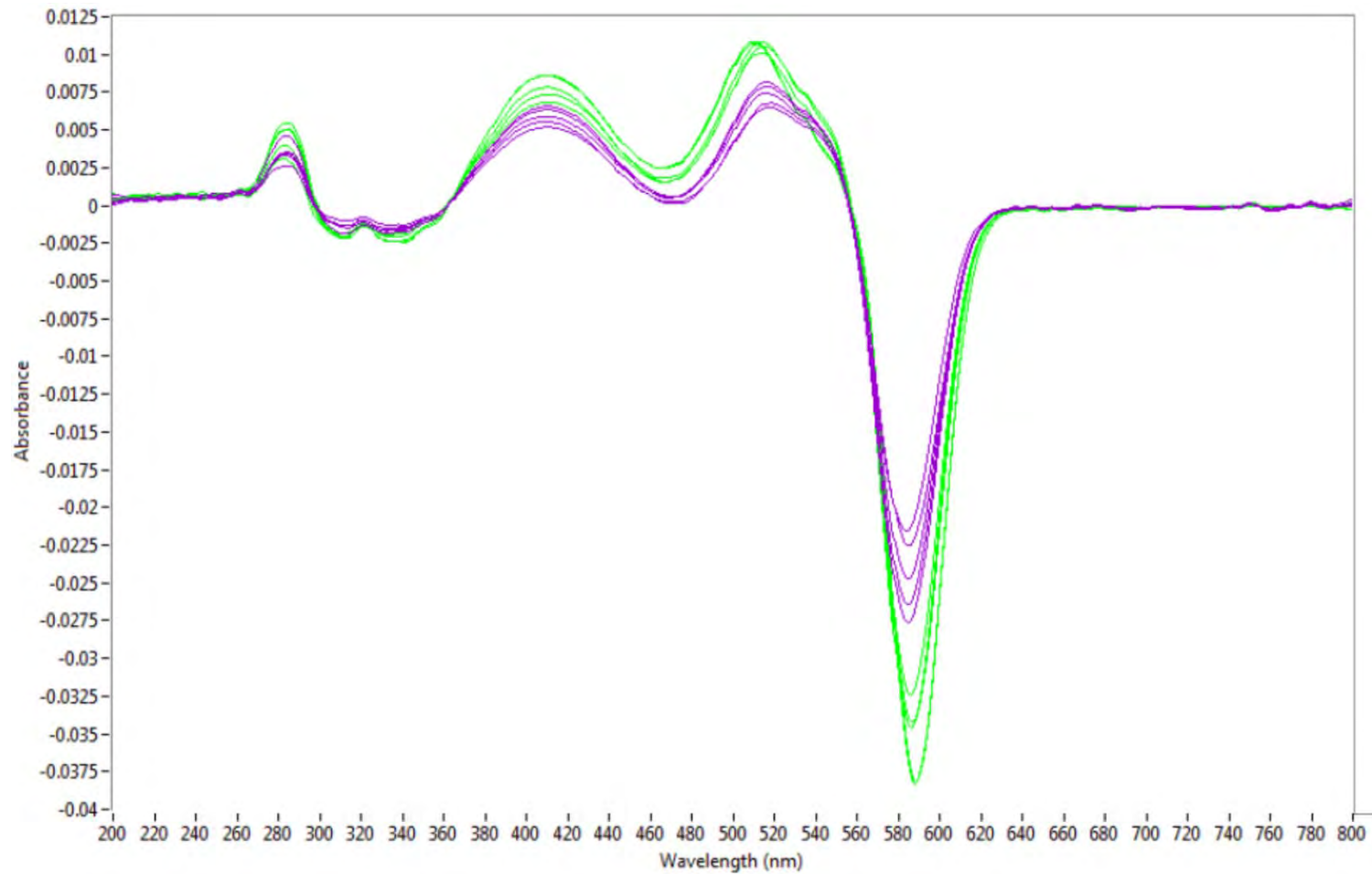


Figure 329. MSP first derivative spectral comparison of Yarn C (purple) and Yarn D (green).

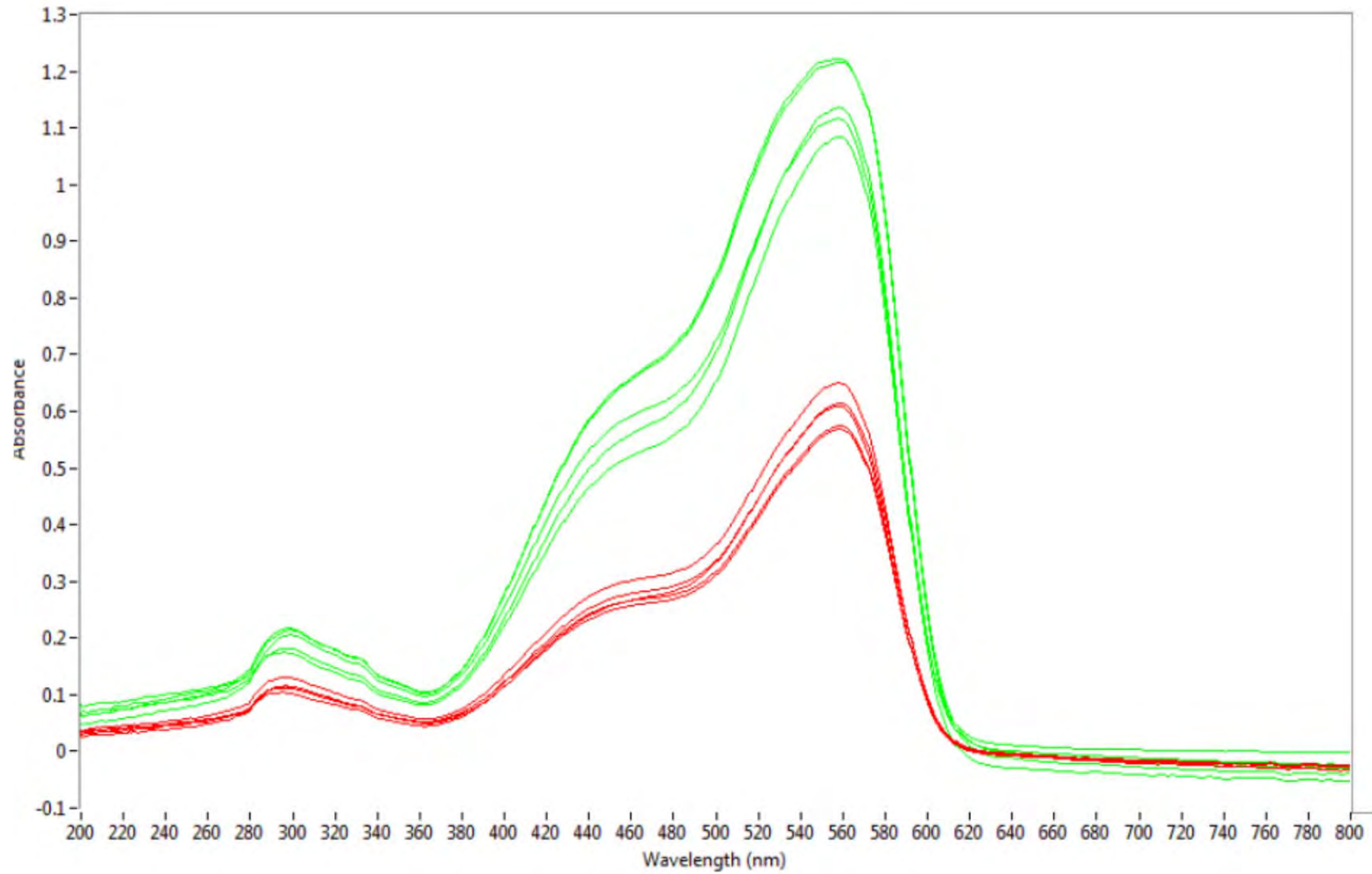


Figure 330. MSP spectral comparison of Yarn B (red) and Yarn D (green).

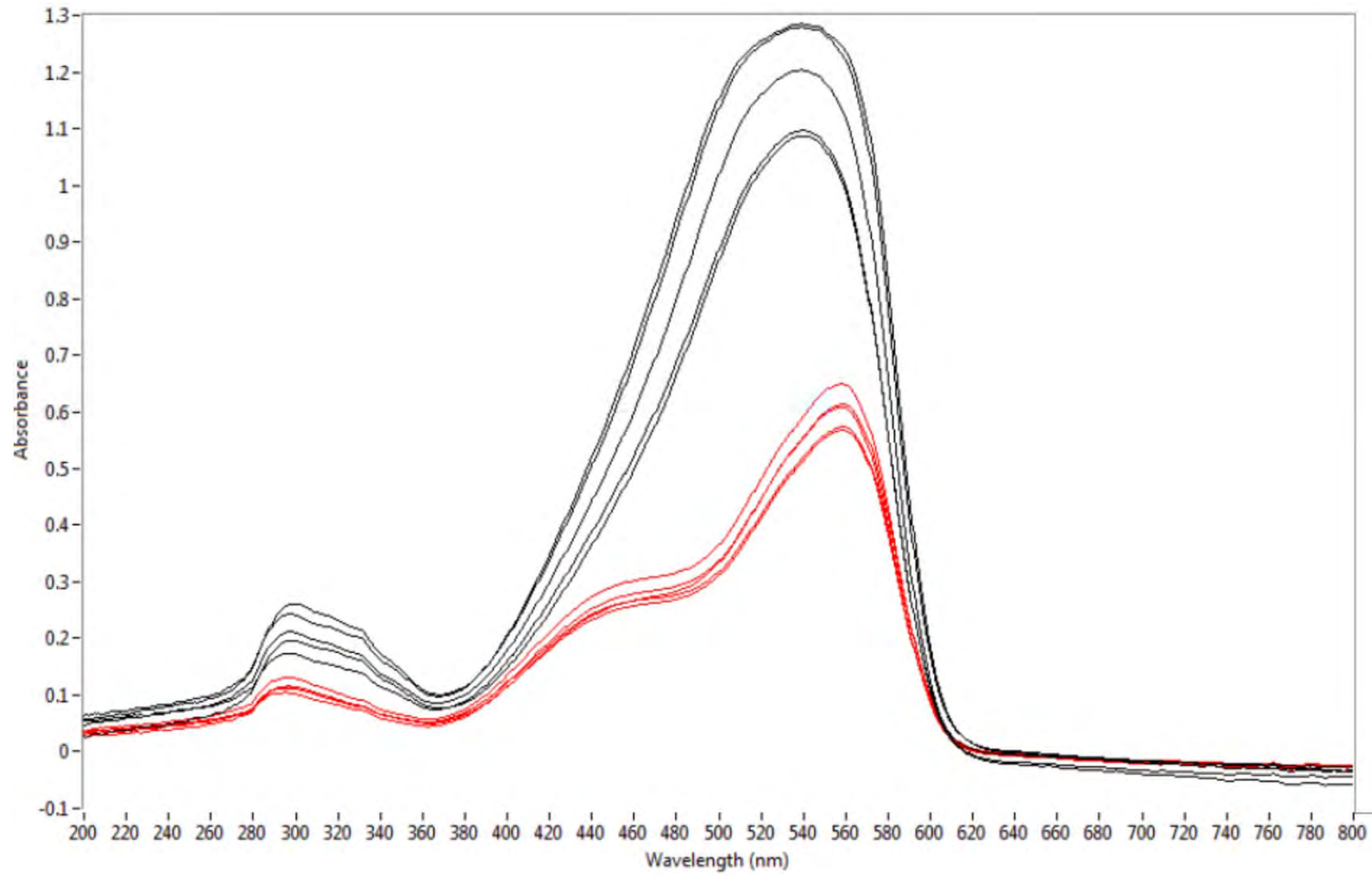


Figure 331. MSP spectral comparison of Yarn A (black) and Yarn B (red).

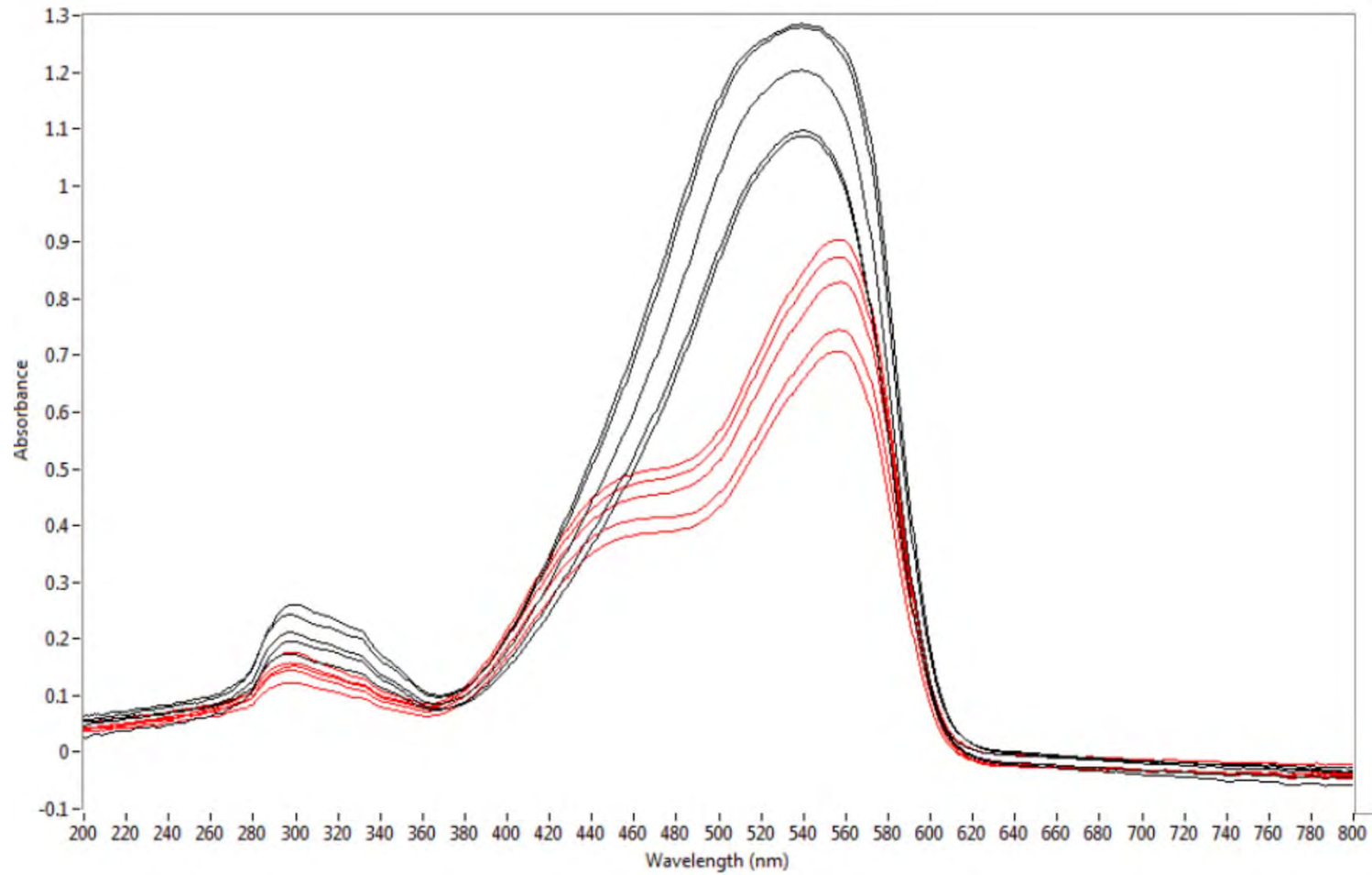


Figure 332. MSP spectral comparison of Yarn A (black) and Yarn C (red).

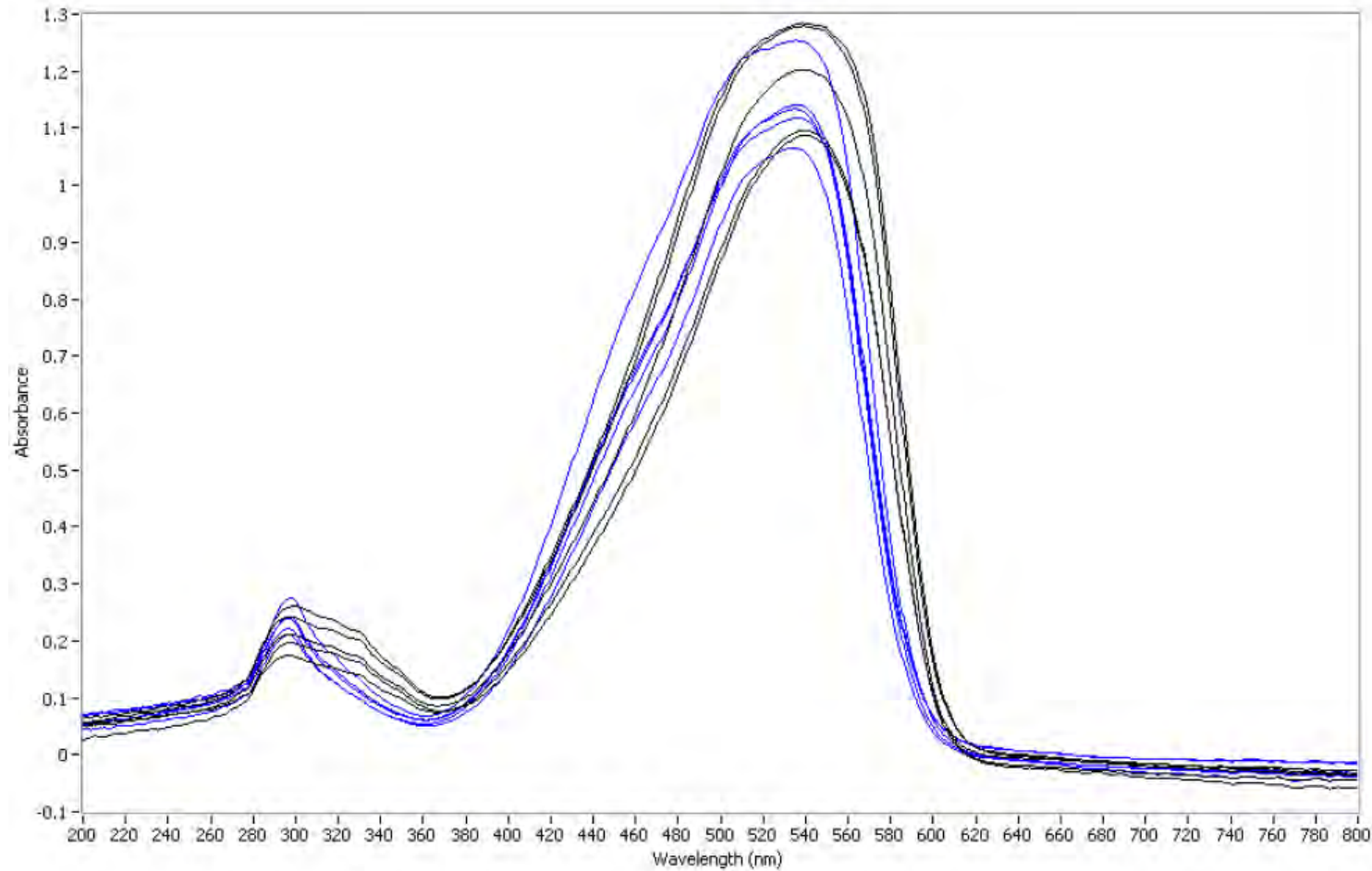


Figure 333. MSP spectral comparison of Yarn A (black) and Yarn E (blue).

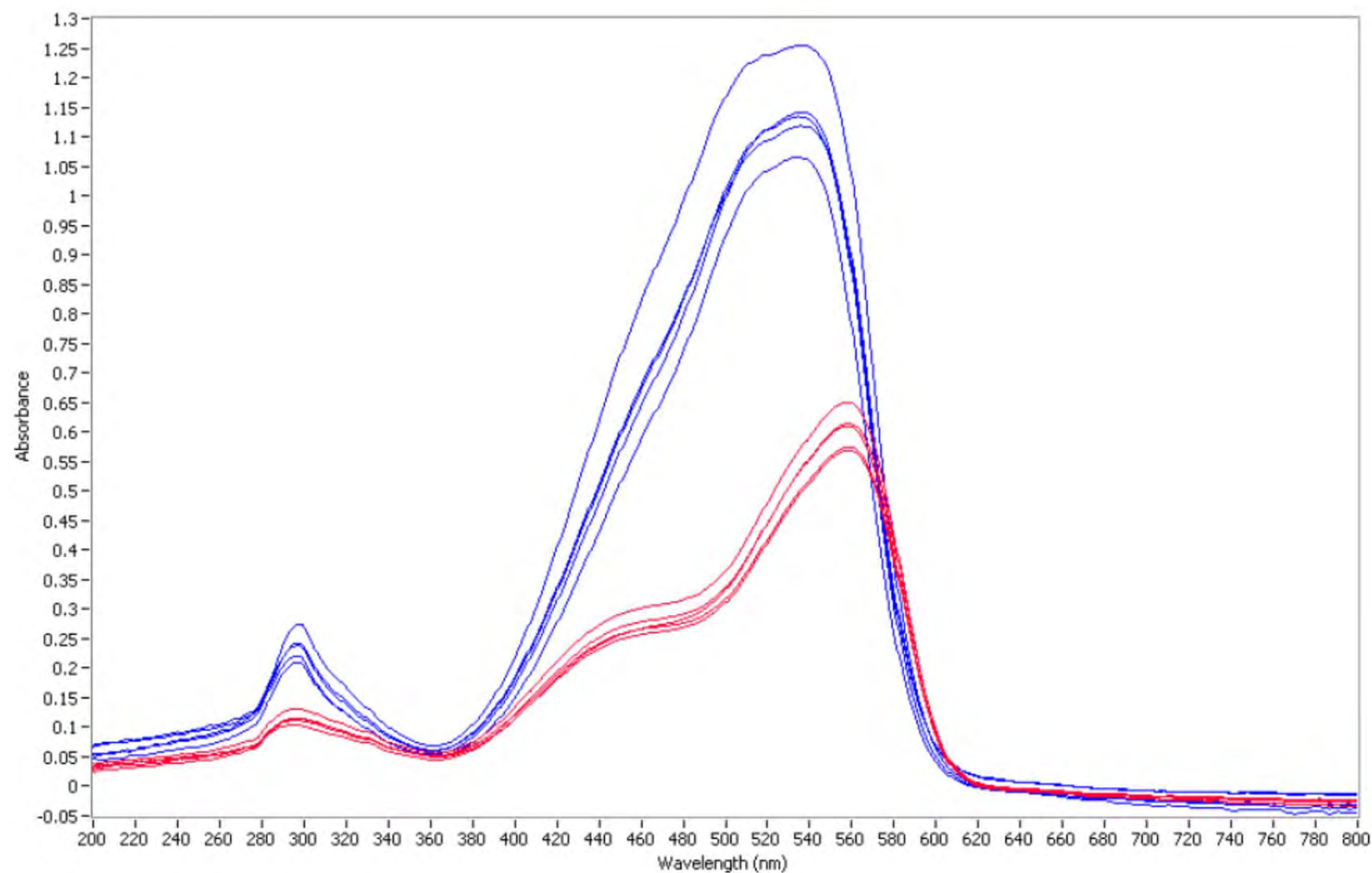


Figure 334. MSP spectral comparison of Yarn B (red) and Yarn E (blue).

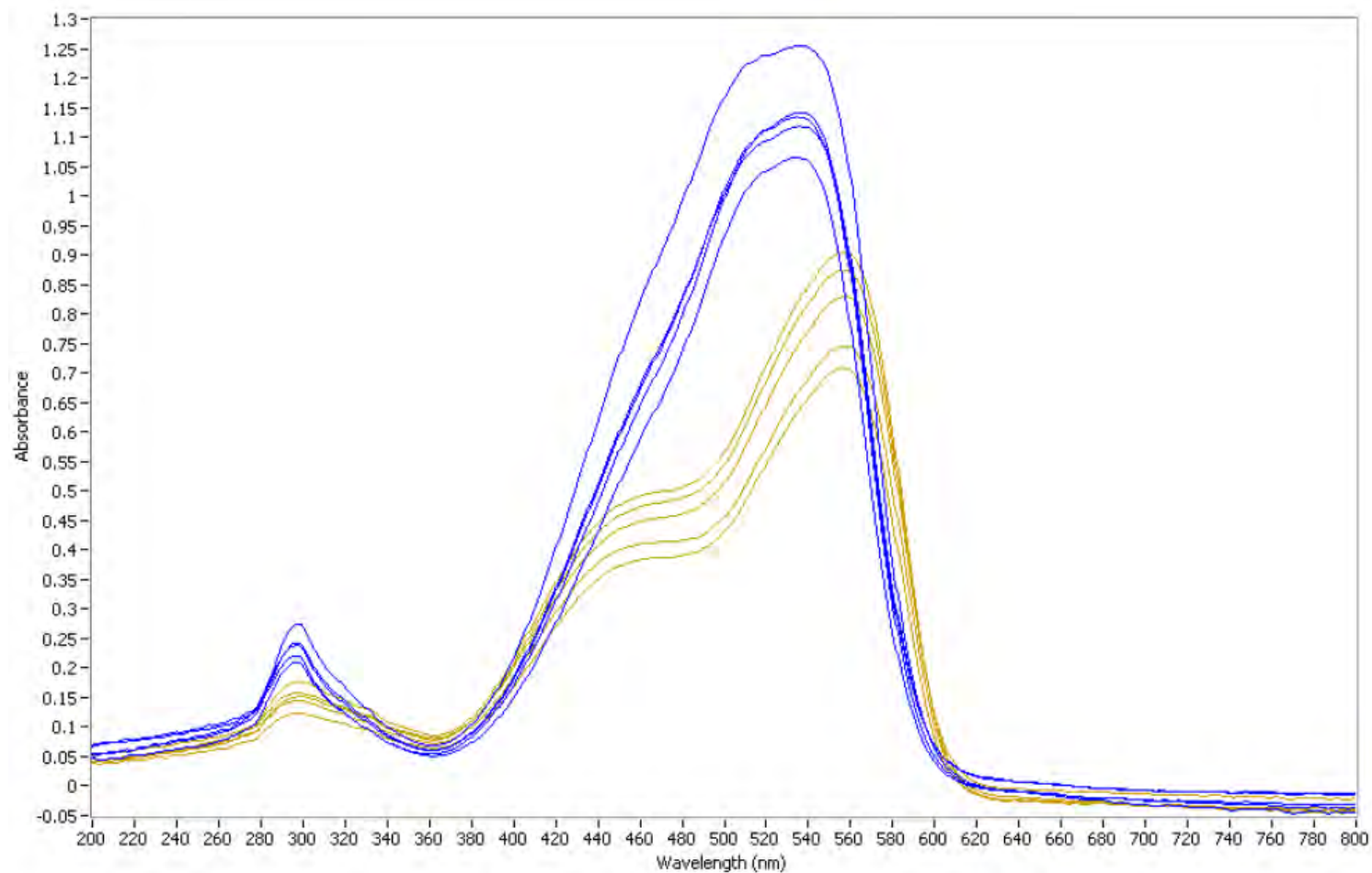


Figure 335. MSP spectral comparison of Yarn C (orange) and Yarn E (blue).

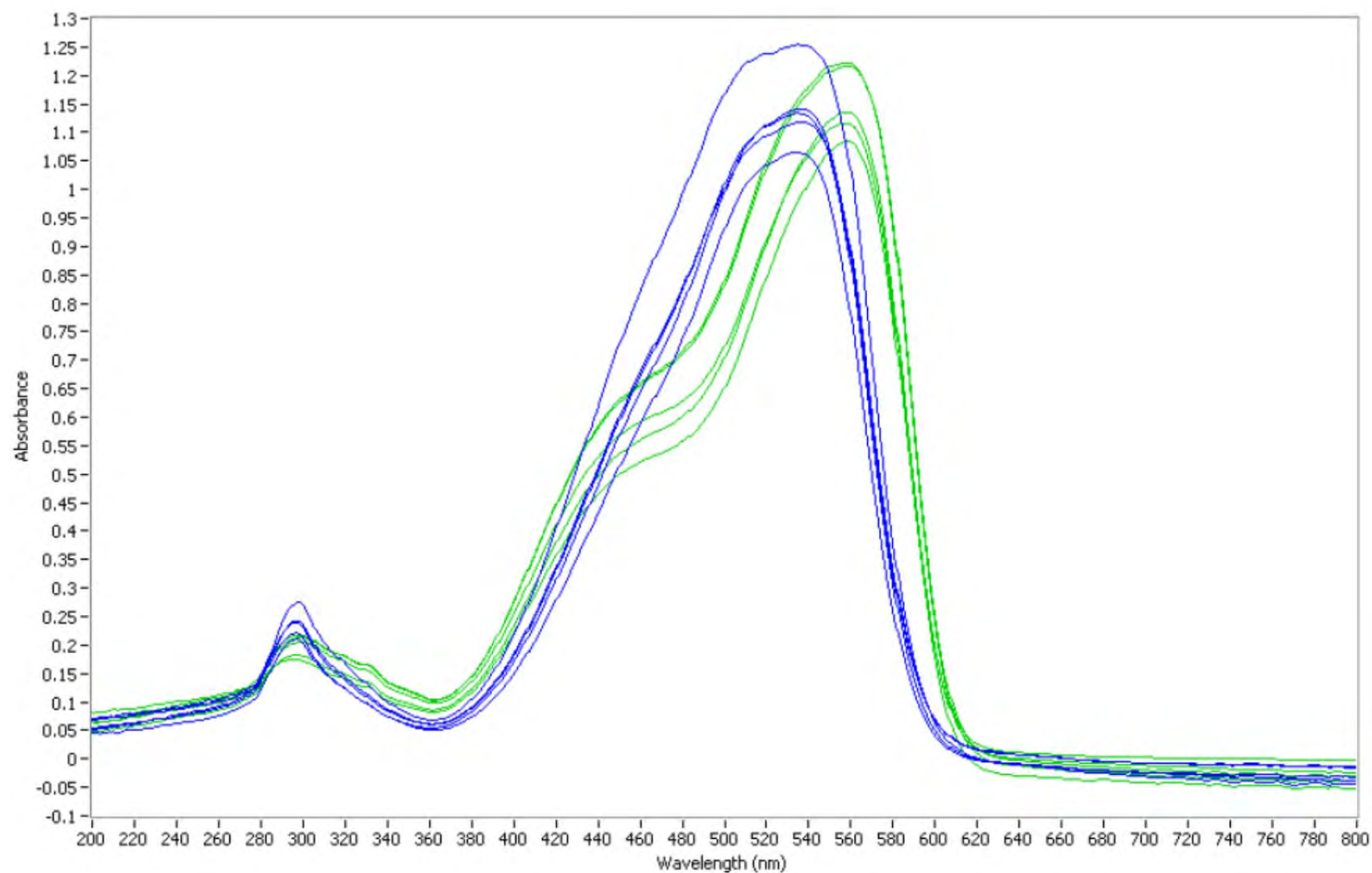


Figure 336. MSP spectral comparison of Yarn D (green) vs. Yarn E (blue)

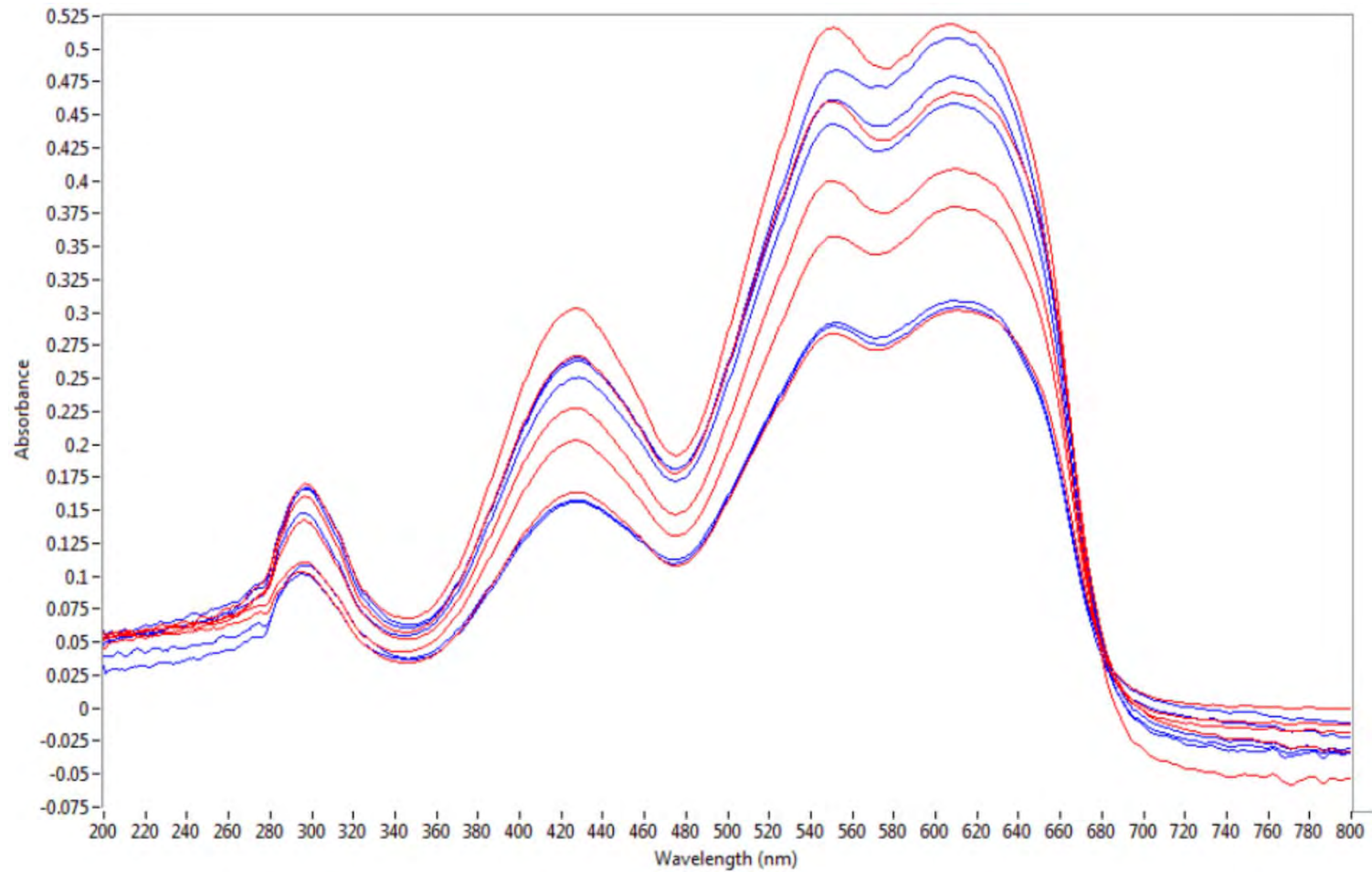


Figure 337. MSP spectral comparison of Yarn G (red) and Yarn I (blue).

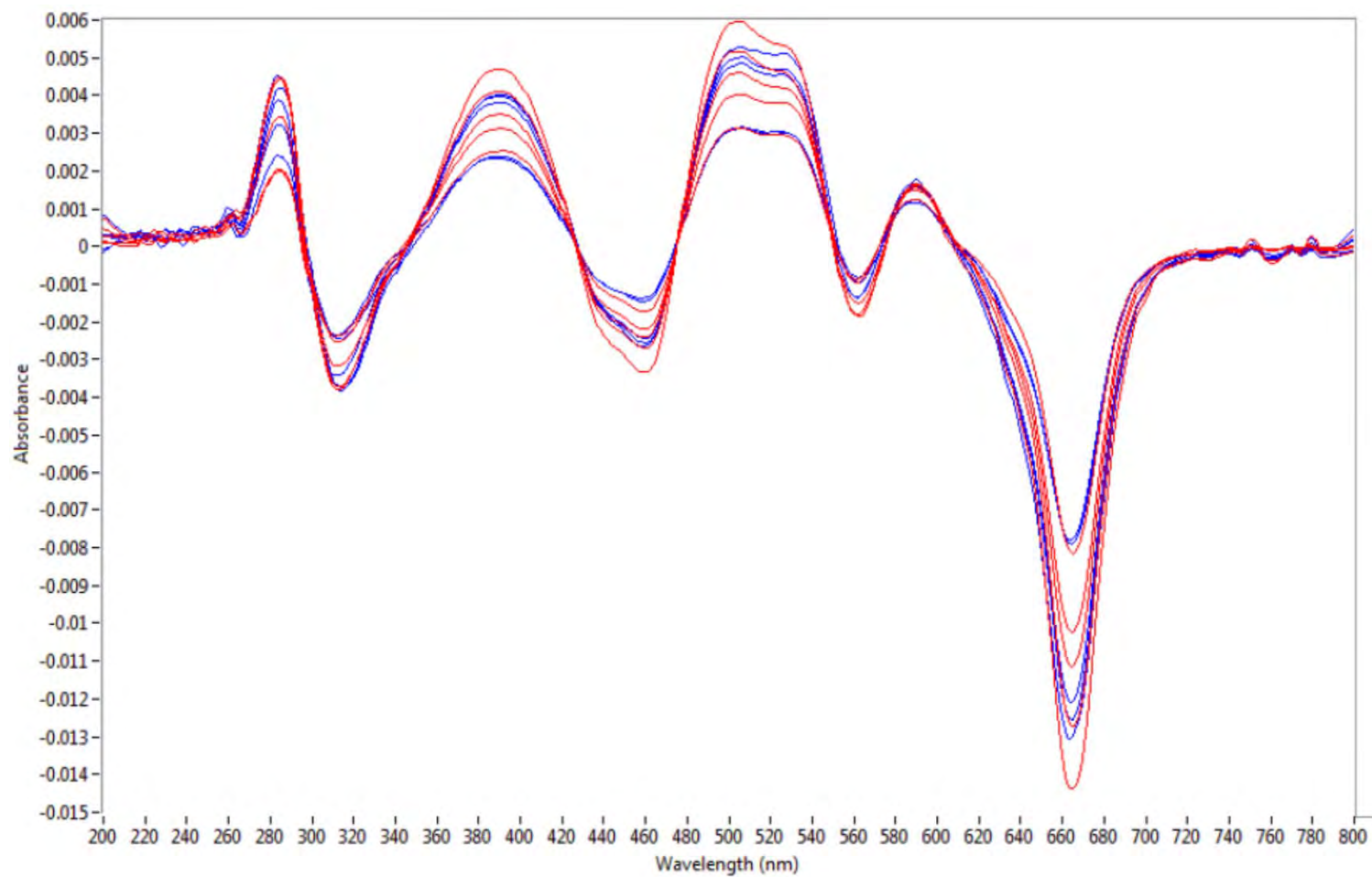


Figure 338. MSP first derivative spectral comparison of Yarn G (red) and Yarn I (blue).

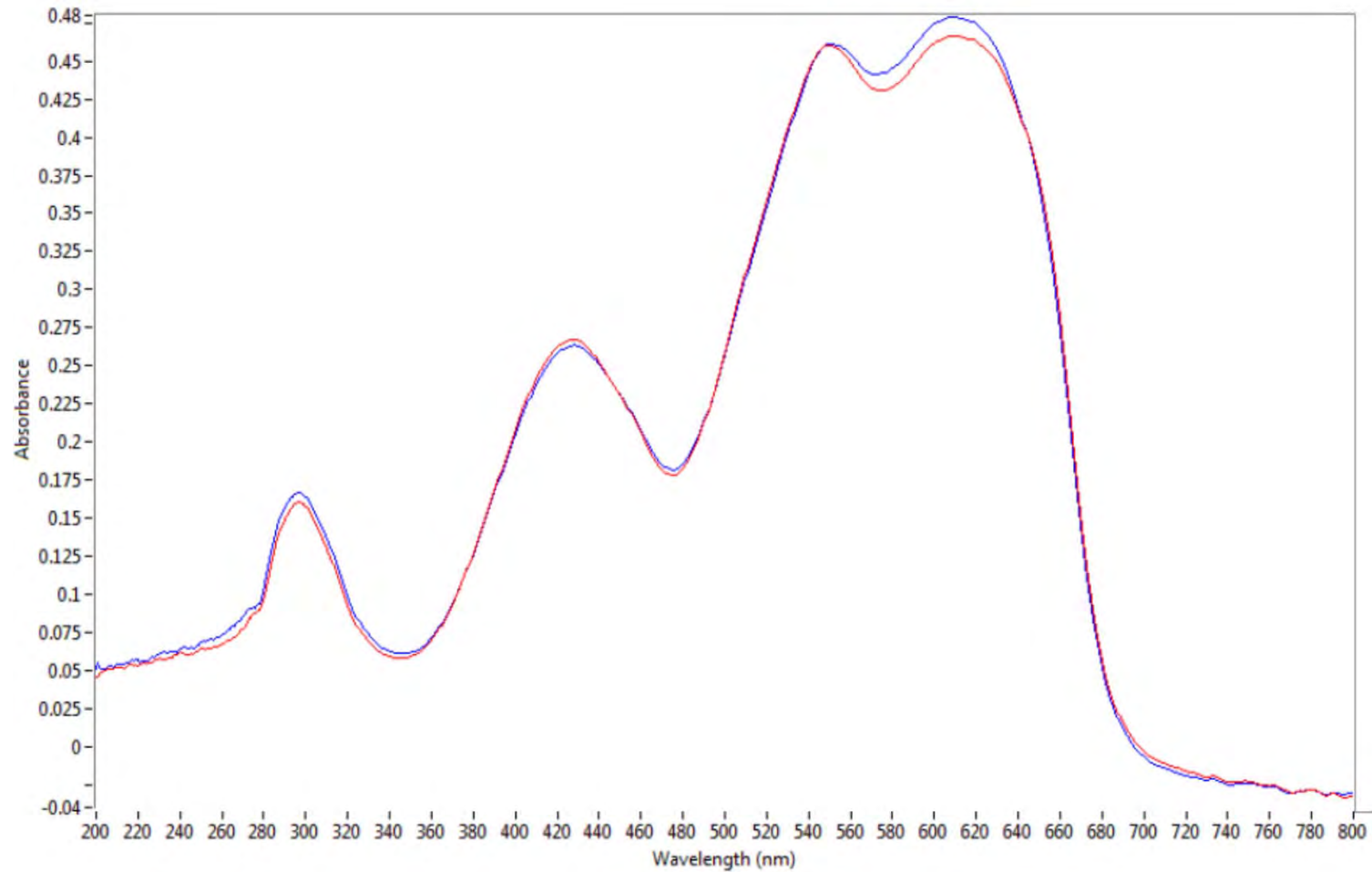


Figure 339. MSP best match spectral comparison of Yarn G (red) and Yarn I (blue).

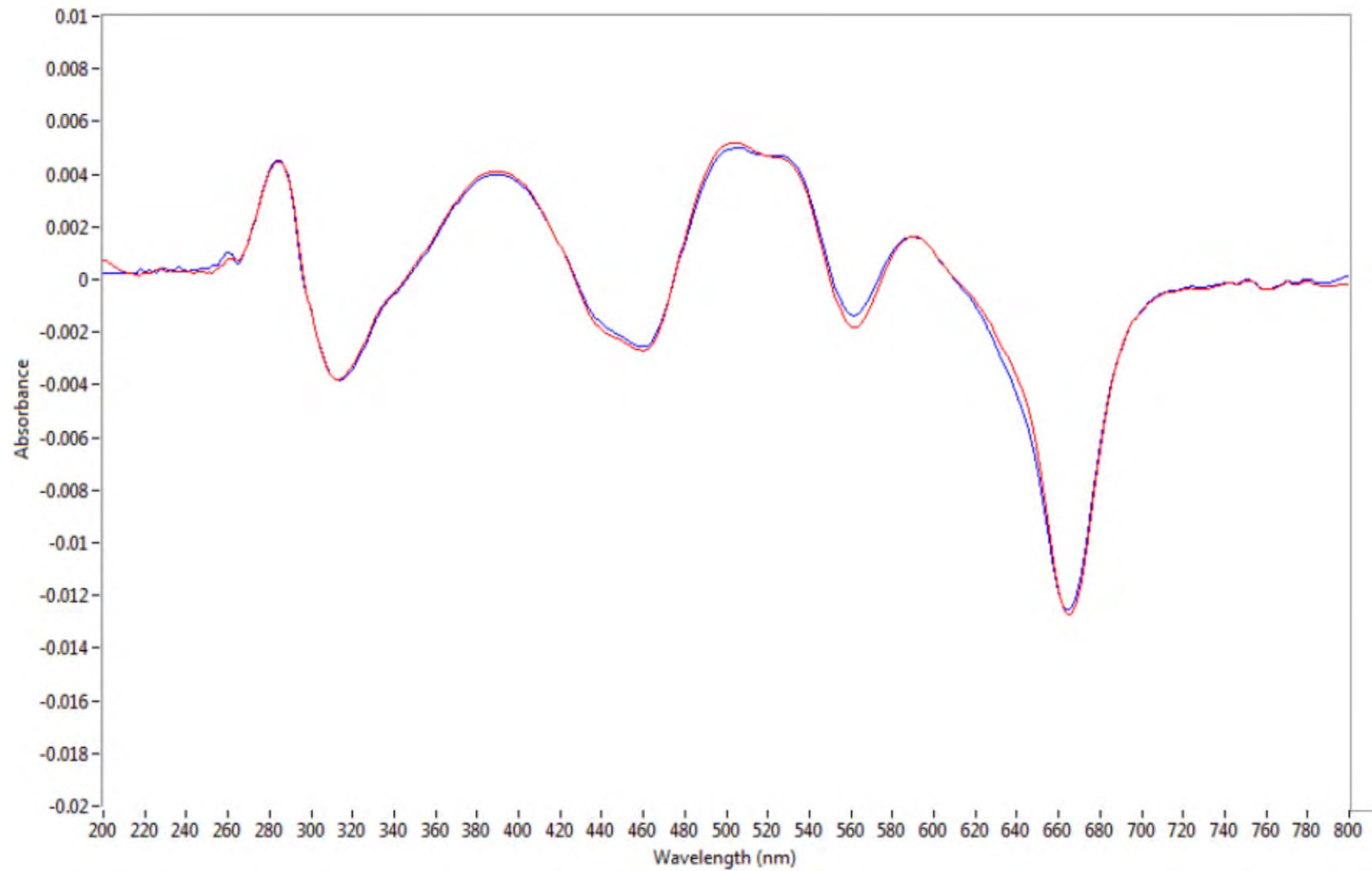


Figure 340. MSP best match first derivative spectral comparison of Yarn G (red) and Yarn I (blue).

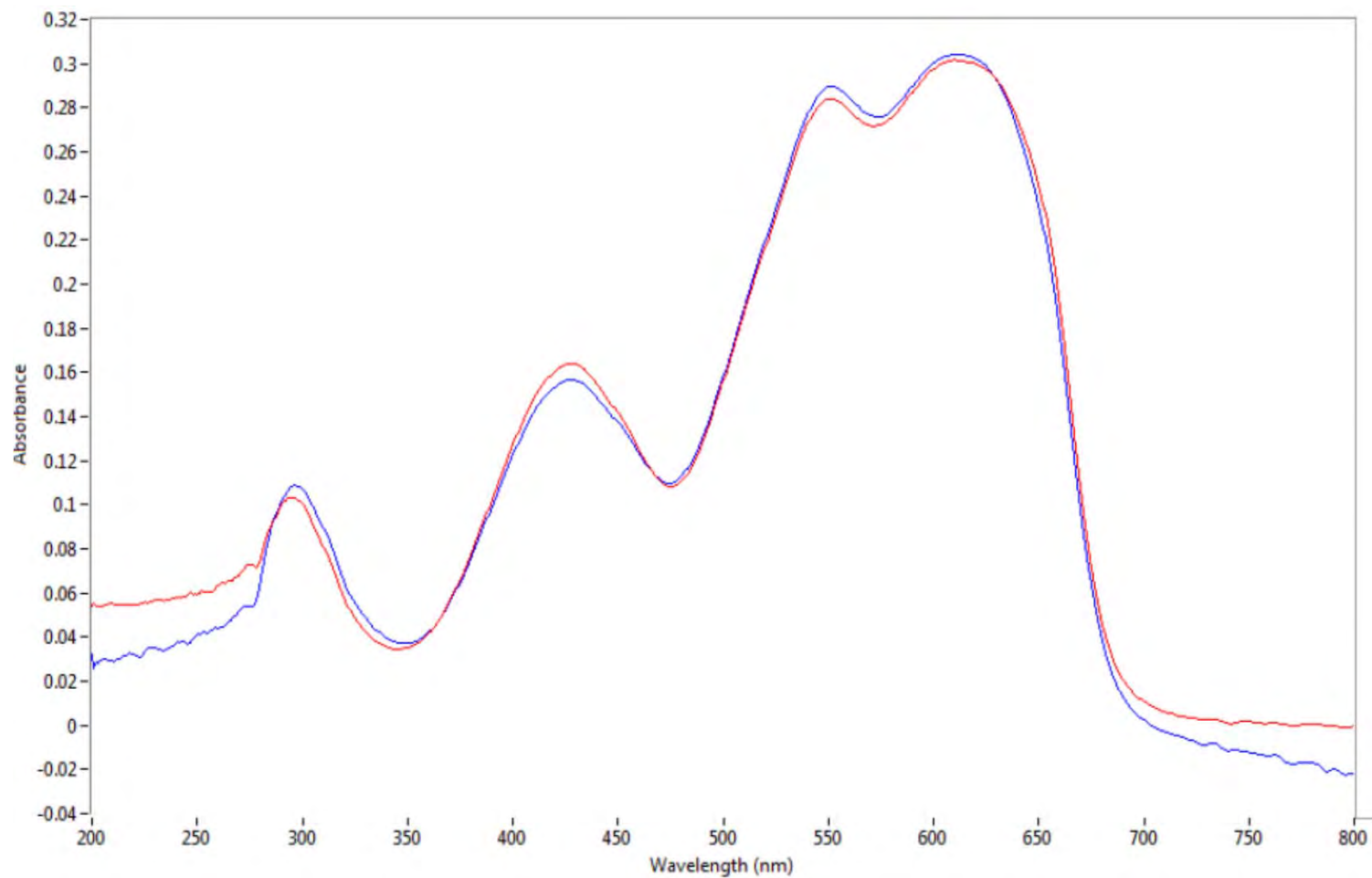


Figure 341. MSP best match spectral comparison from the lower grouping of Yarn G (red) and Yarn I (blue).

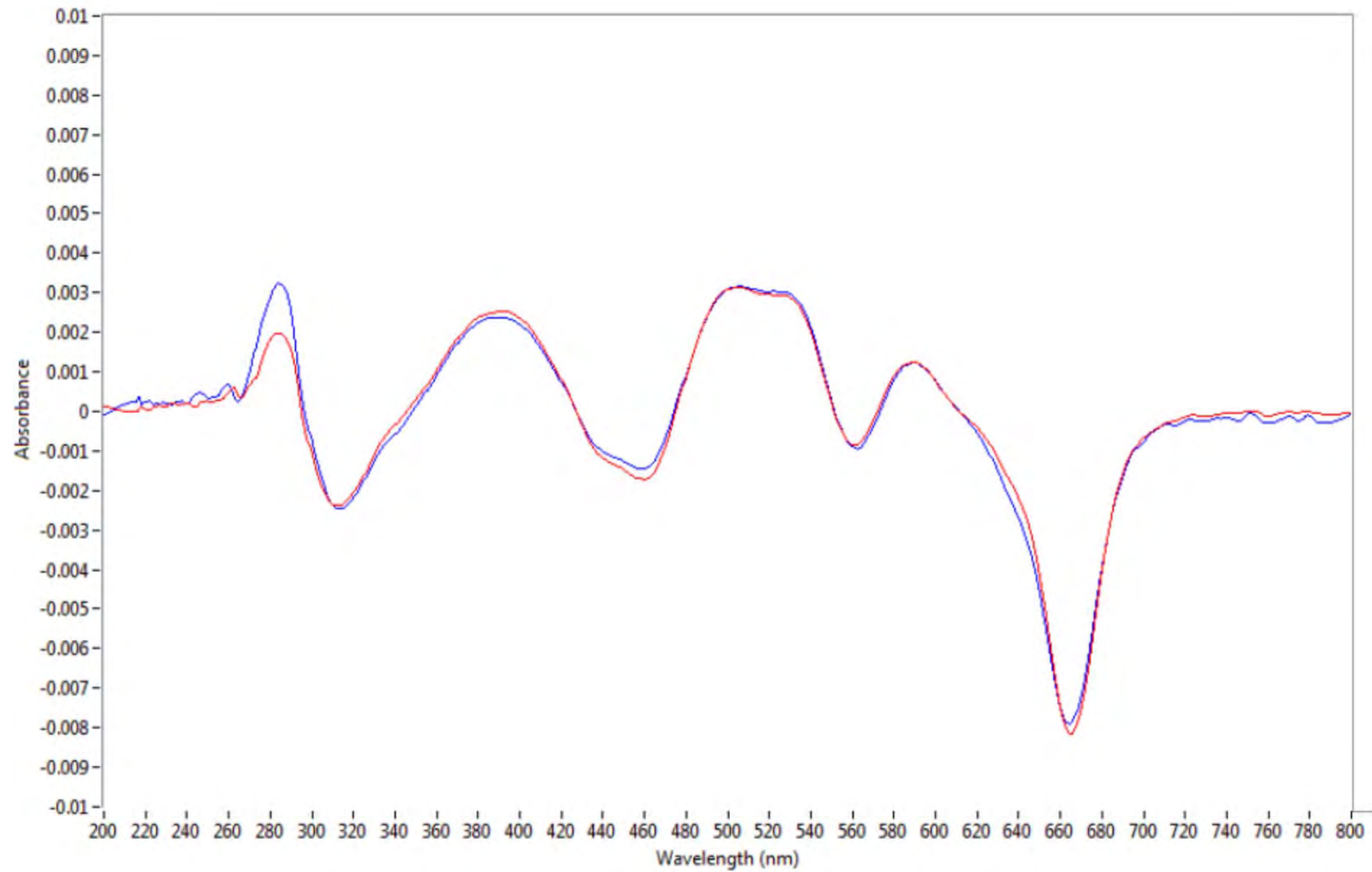


Figure 342. MSP best match first derivative spectral comparison from the lower grouping of Yarn G (red) and Yarn I (blue).

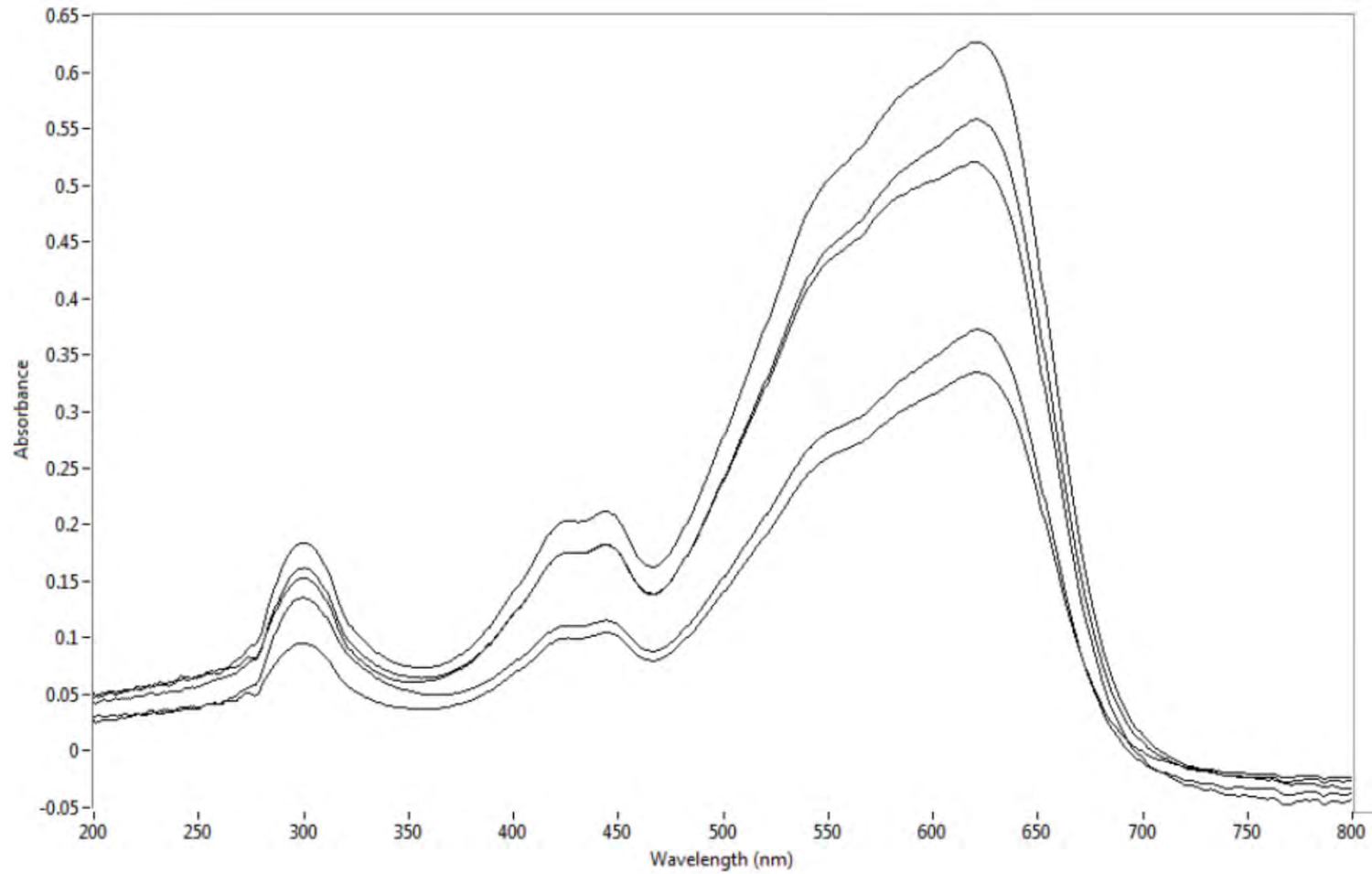


Figure 343. MSP spectra of the five fibers from Yarn J.

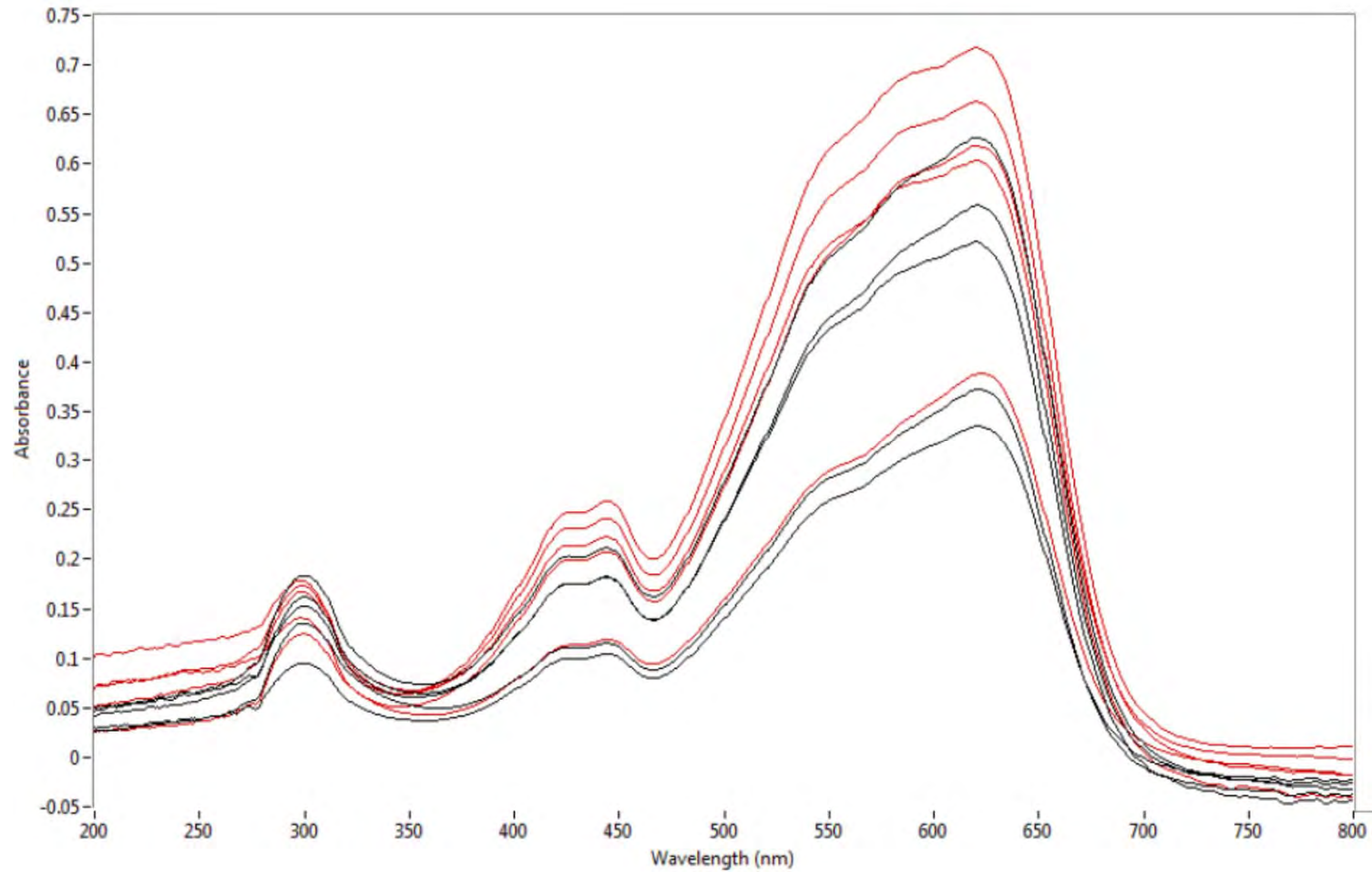


Figure 344. MSP spectra of the initial five fibers from Yarn J (black) compared to spectra from the additional fibers where fiber orientation was controlled (red).

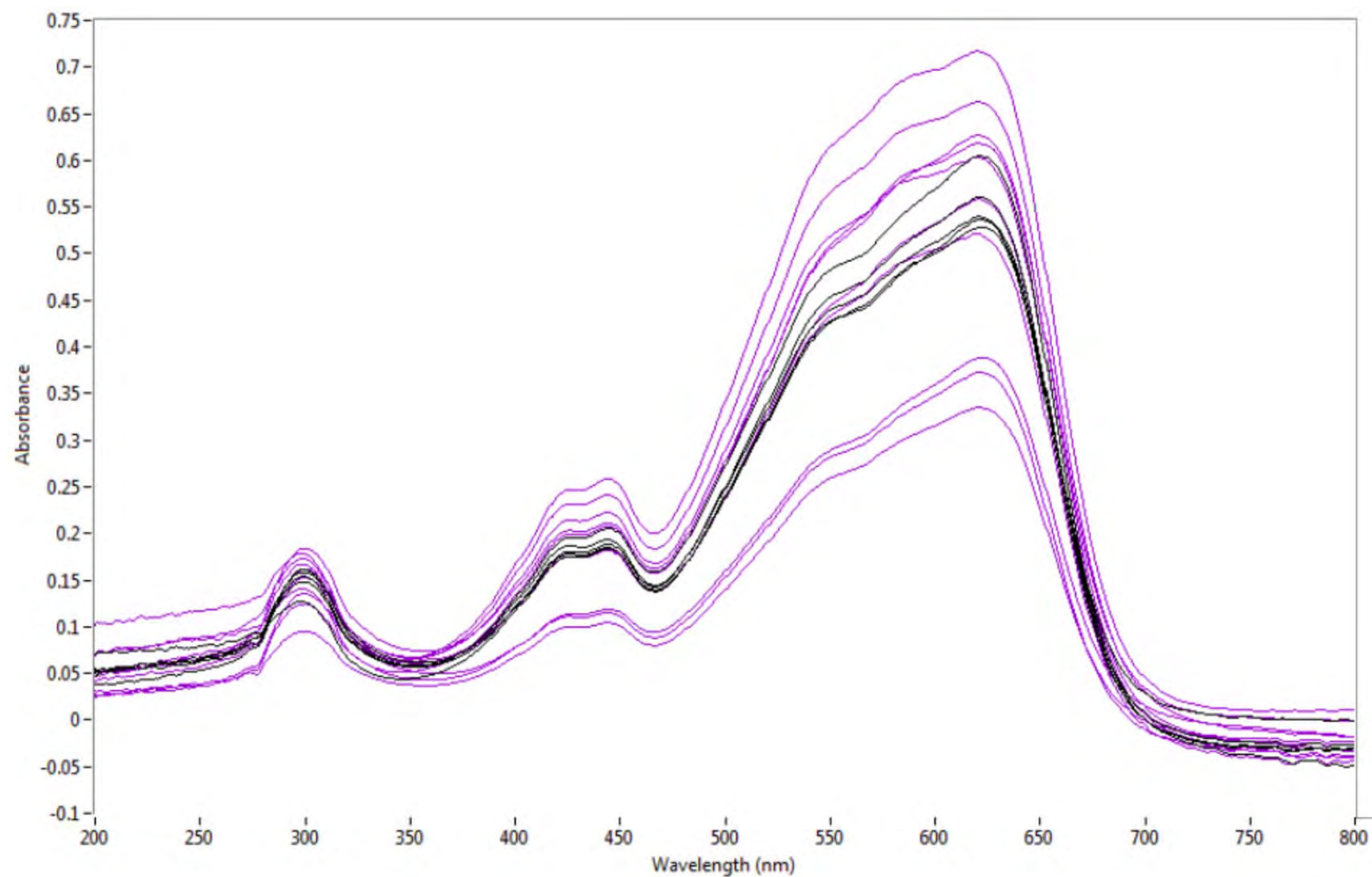


Figure 345. MSP spectral comparison of Yarn F (black) and Yarn J spectra (pink).

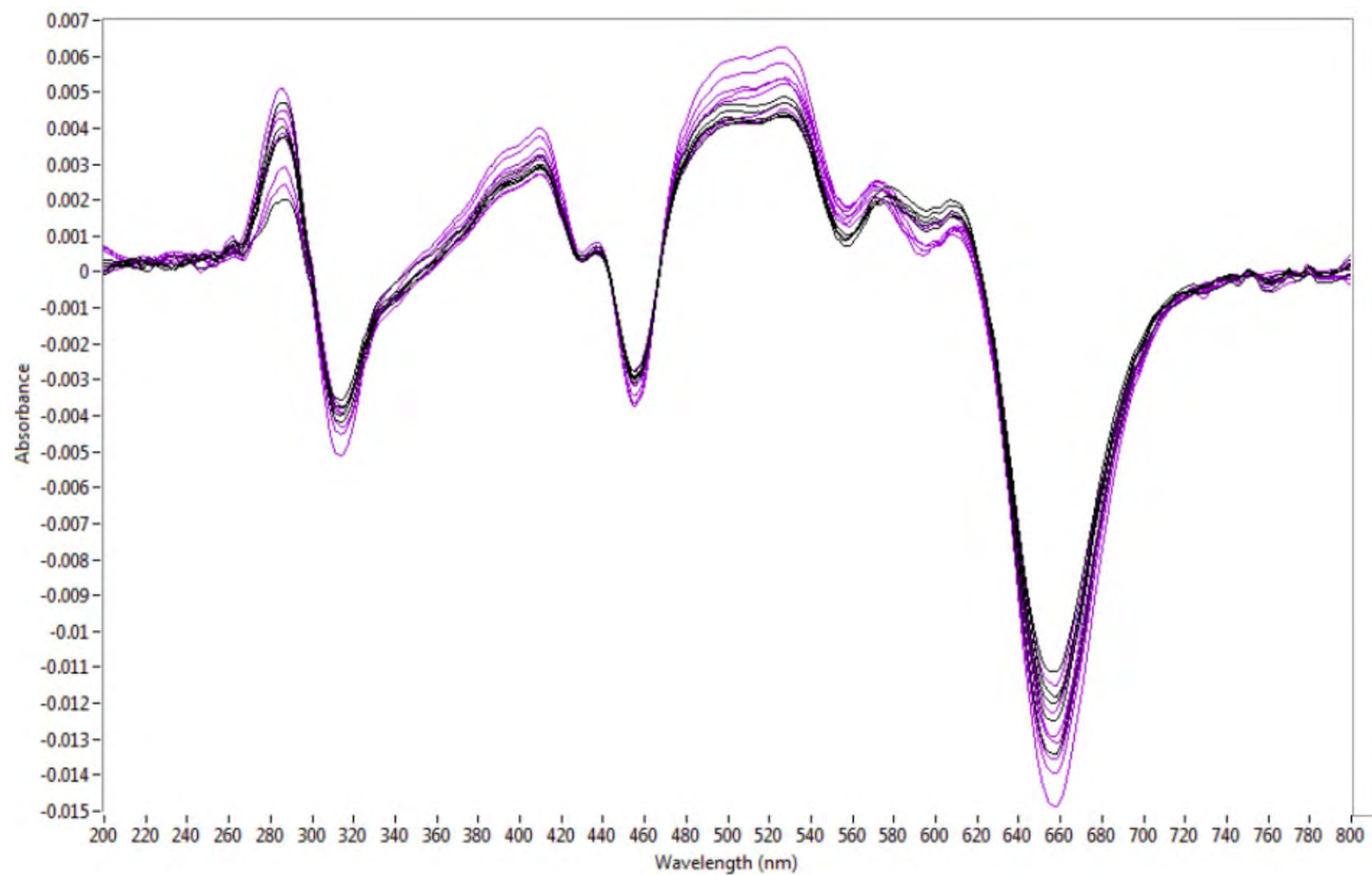


Figure 346. MSP first derivative spectral comparison of Yarn F (black) and Yarn J (pink).

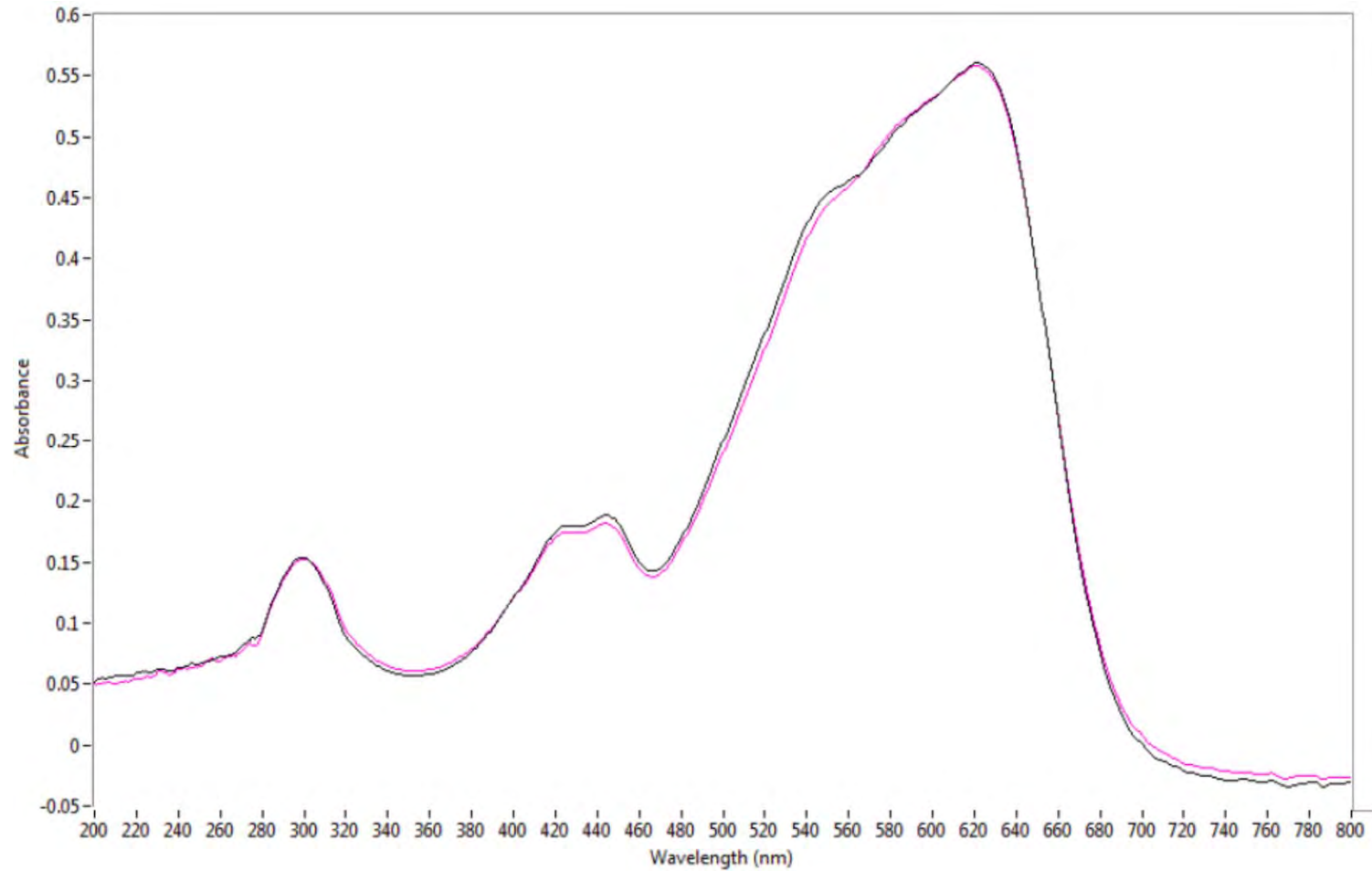


Figure 347. MSP best match spectral comparison of Yarn F (black) and Yarn J (pink).

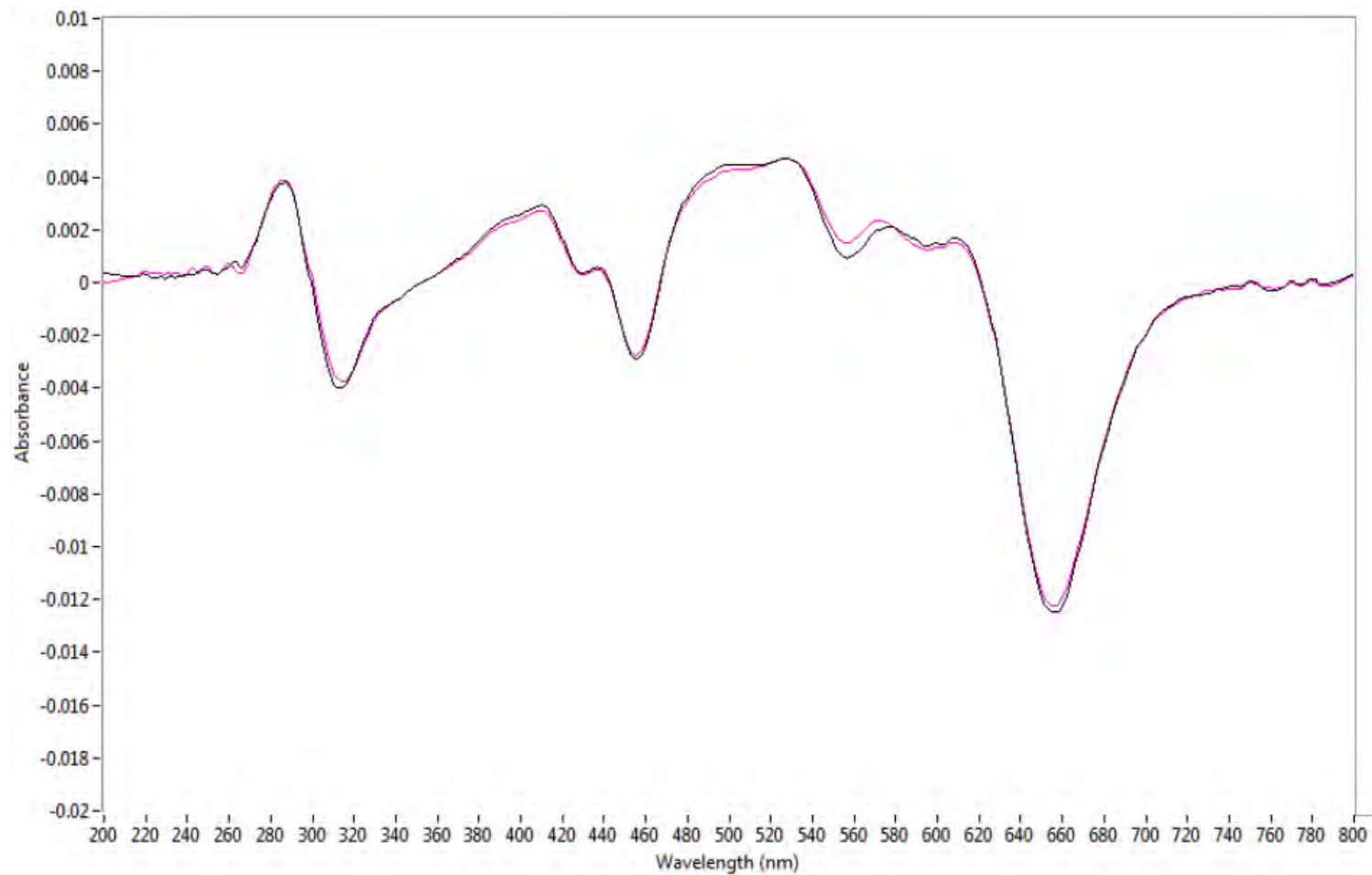


Figure 348. MSP best match first derivative spectral comparison of Yarn F (black) and Yarn J (pink).

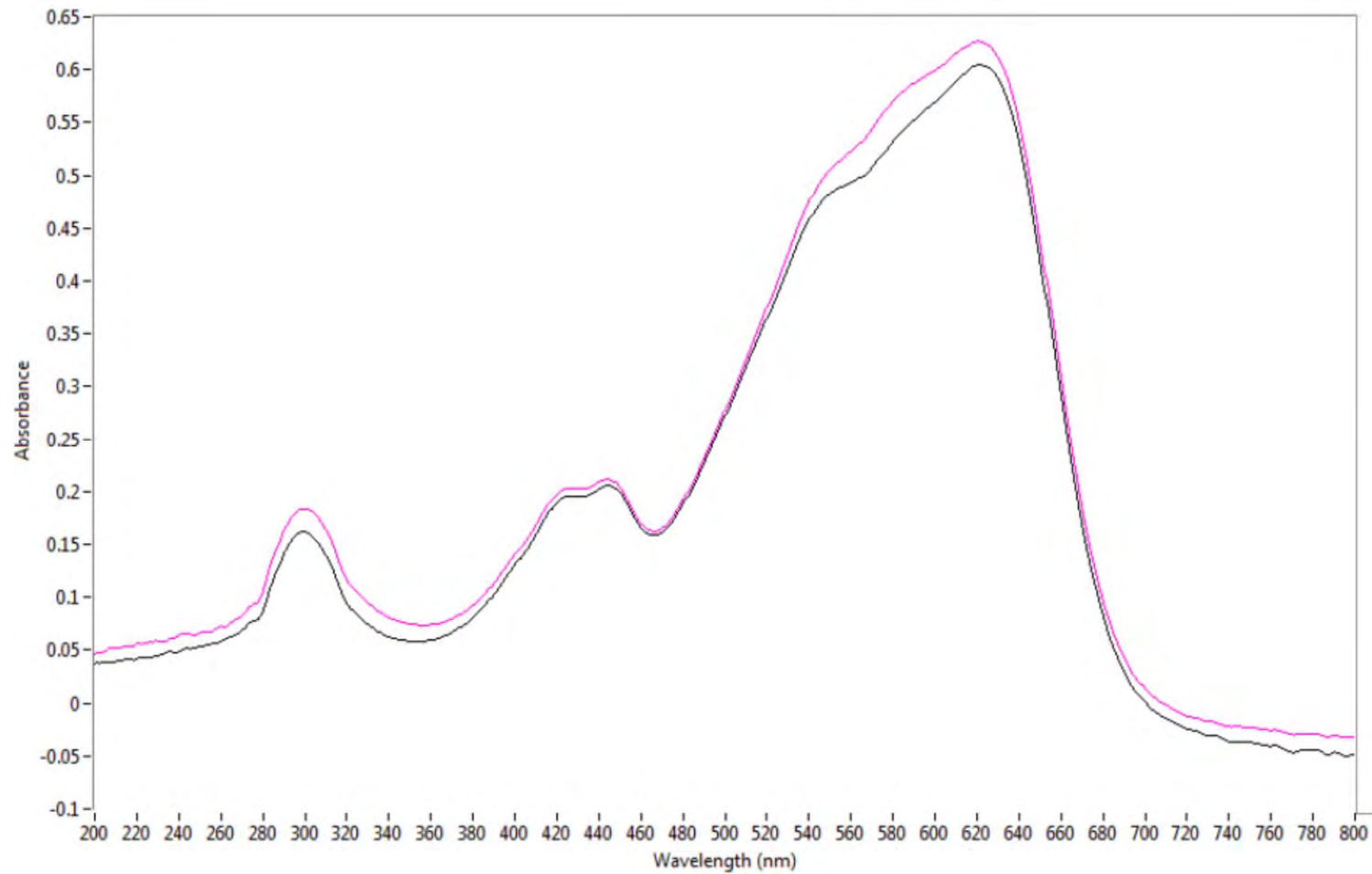


Figure 349. MSP best match spectral comparison of Yarn F (black) and Yarn J (pink), where the F and J spectra do not overlap.

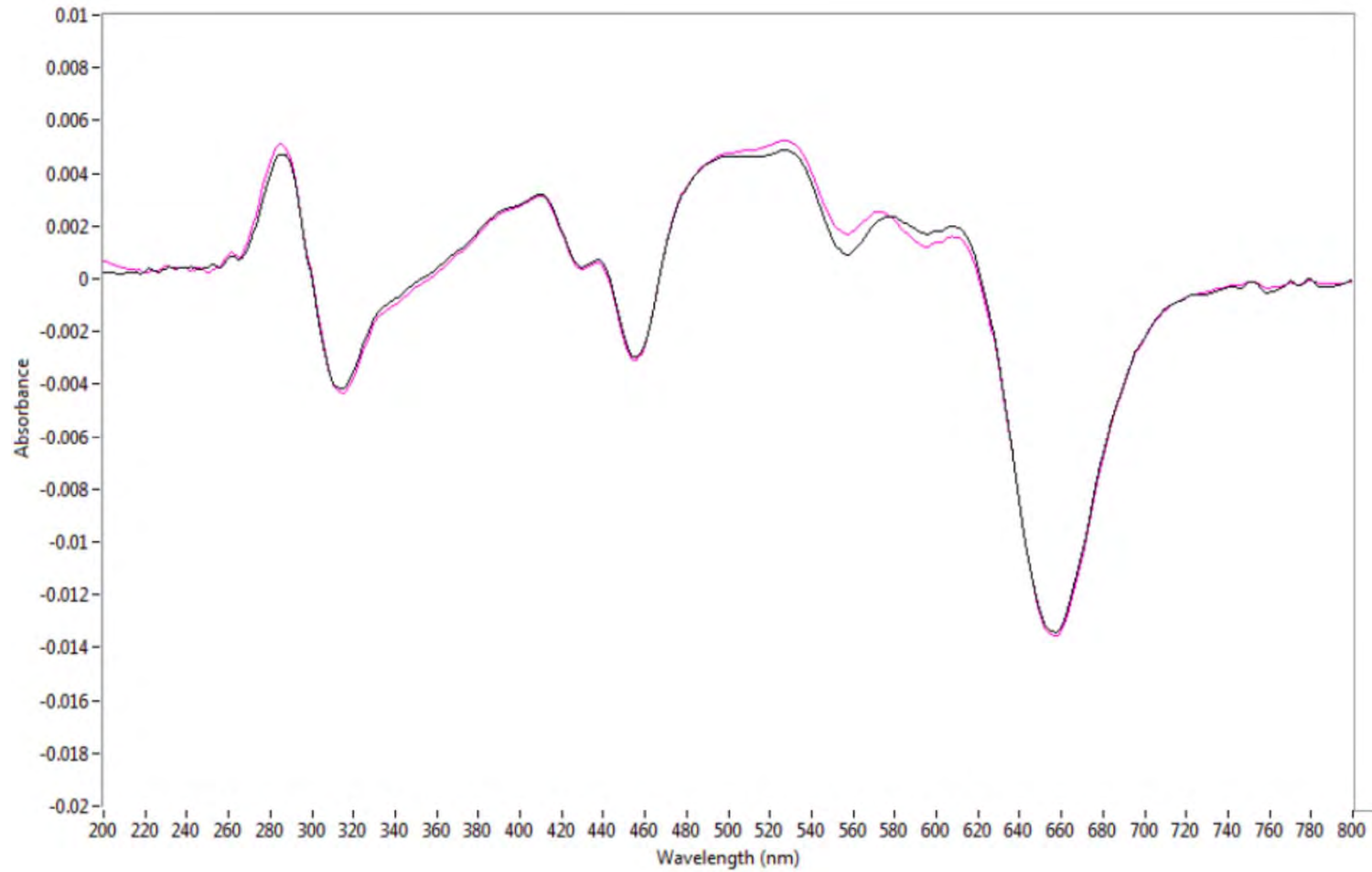


Figure 350. MSP best match first derivative spectral comparison of Yarn F (black) and Yarn J (pink) where the F and J spectra do not overlap.

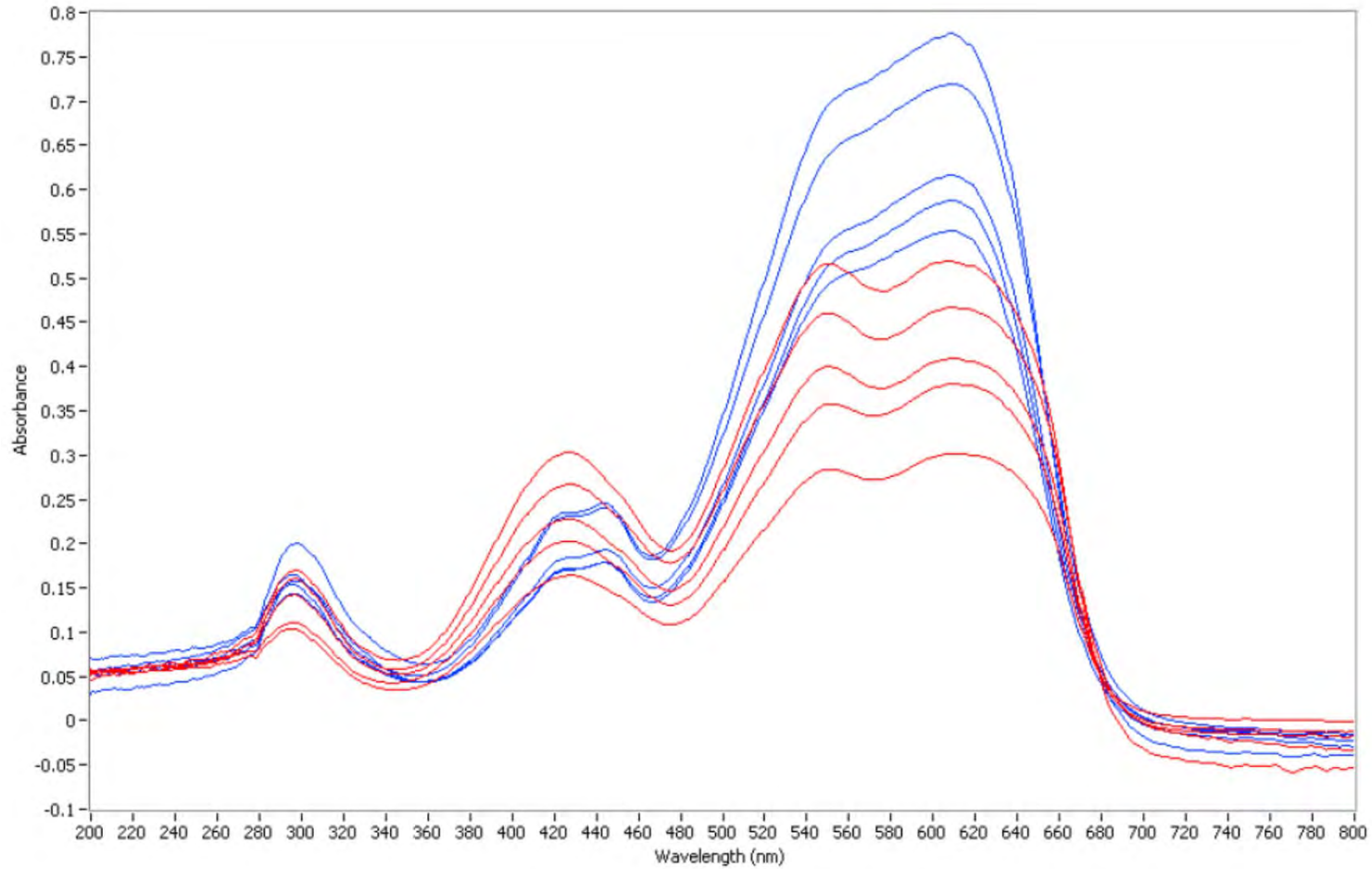


Figure 351. MSP spectral comparison of Yarn G (red) and Yarn H (blue).

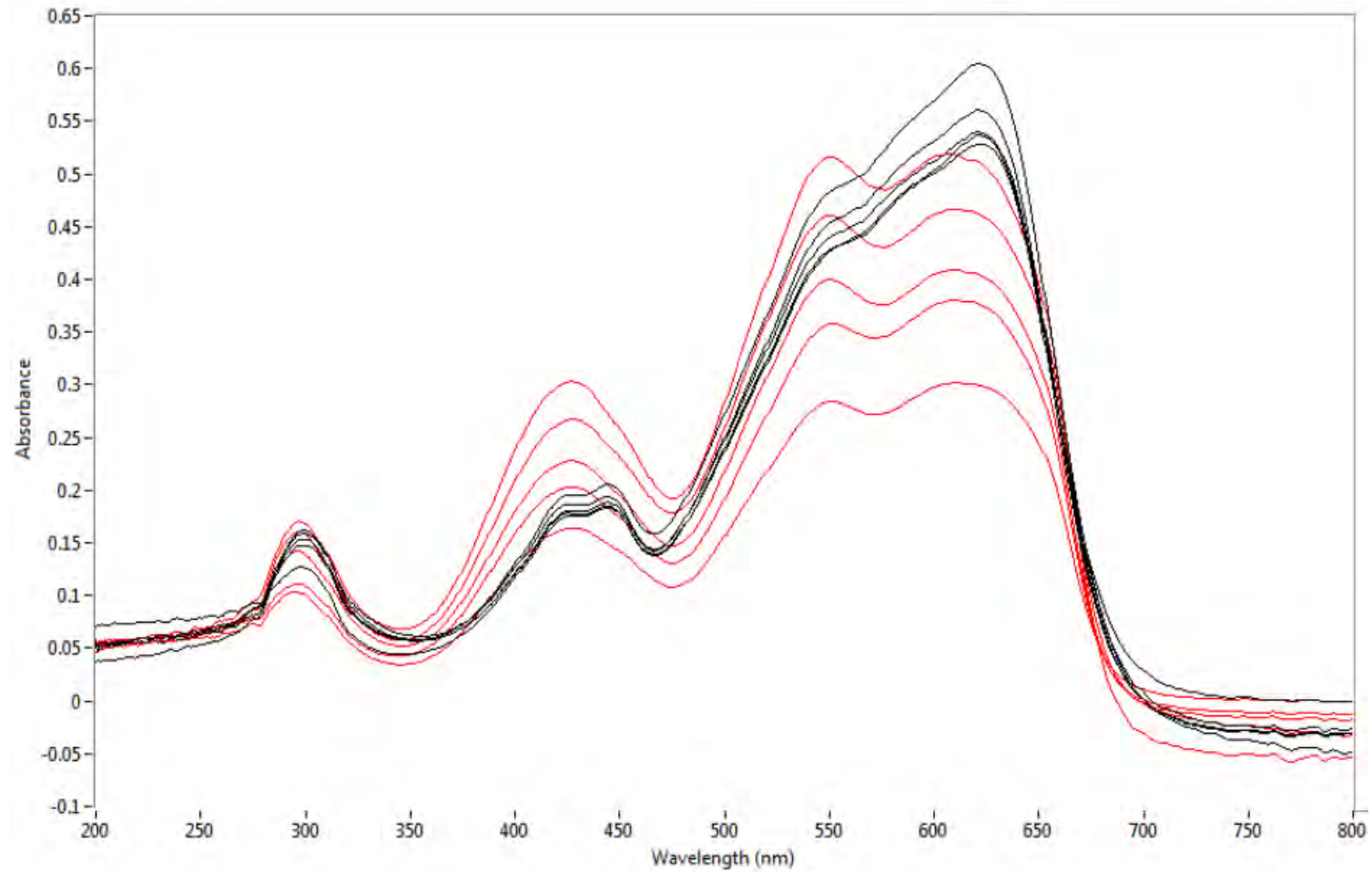


Figure 352. MSP spectral comparison of Yarn F (black) and Yarn G (red).

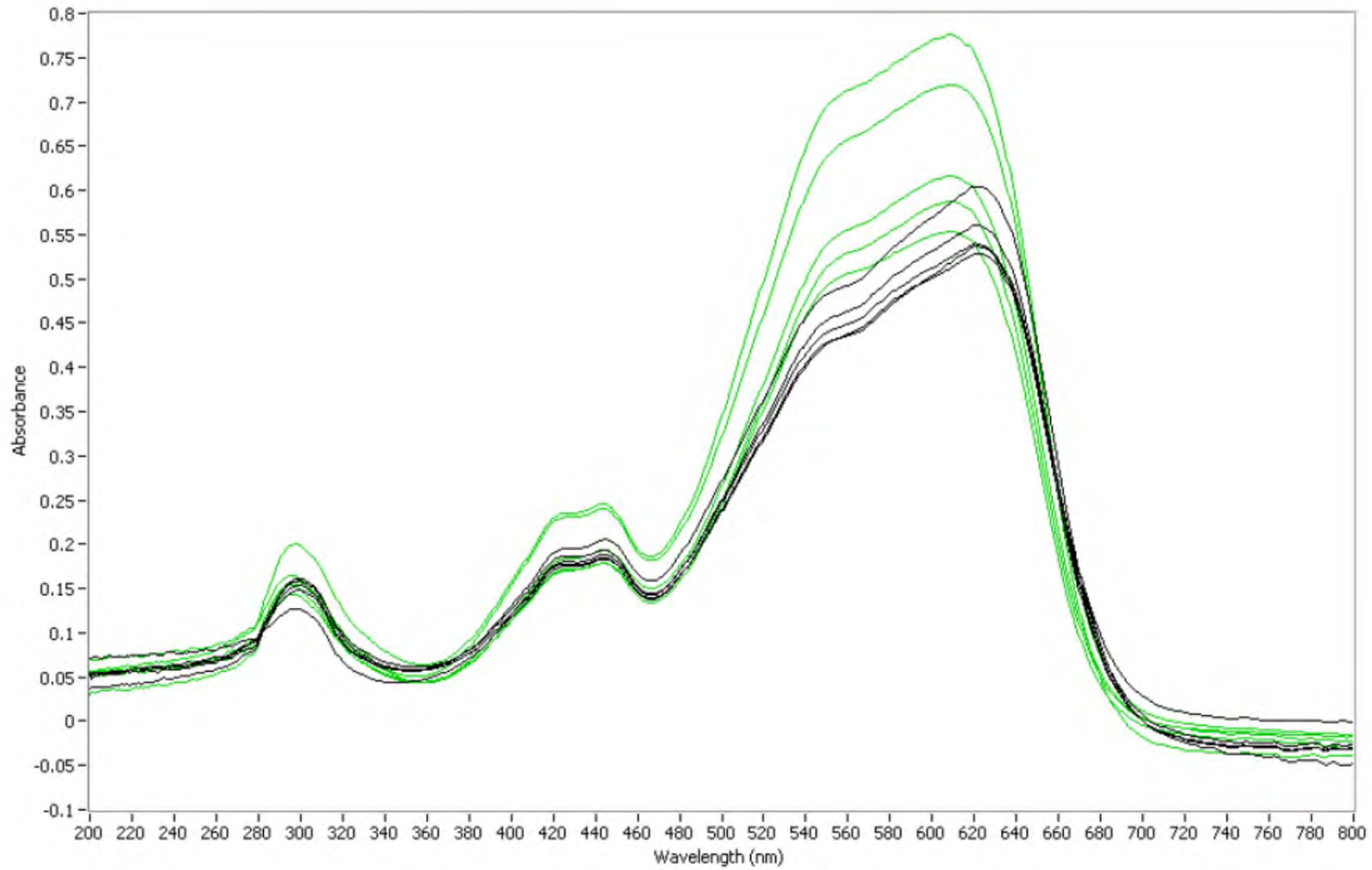


Figure 353. MSP spectral comparison of Yarn F (black) and Yarn H (green).

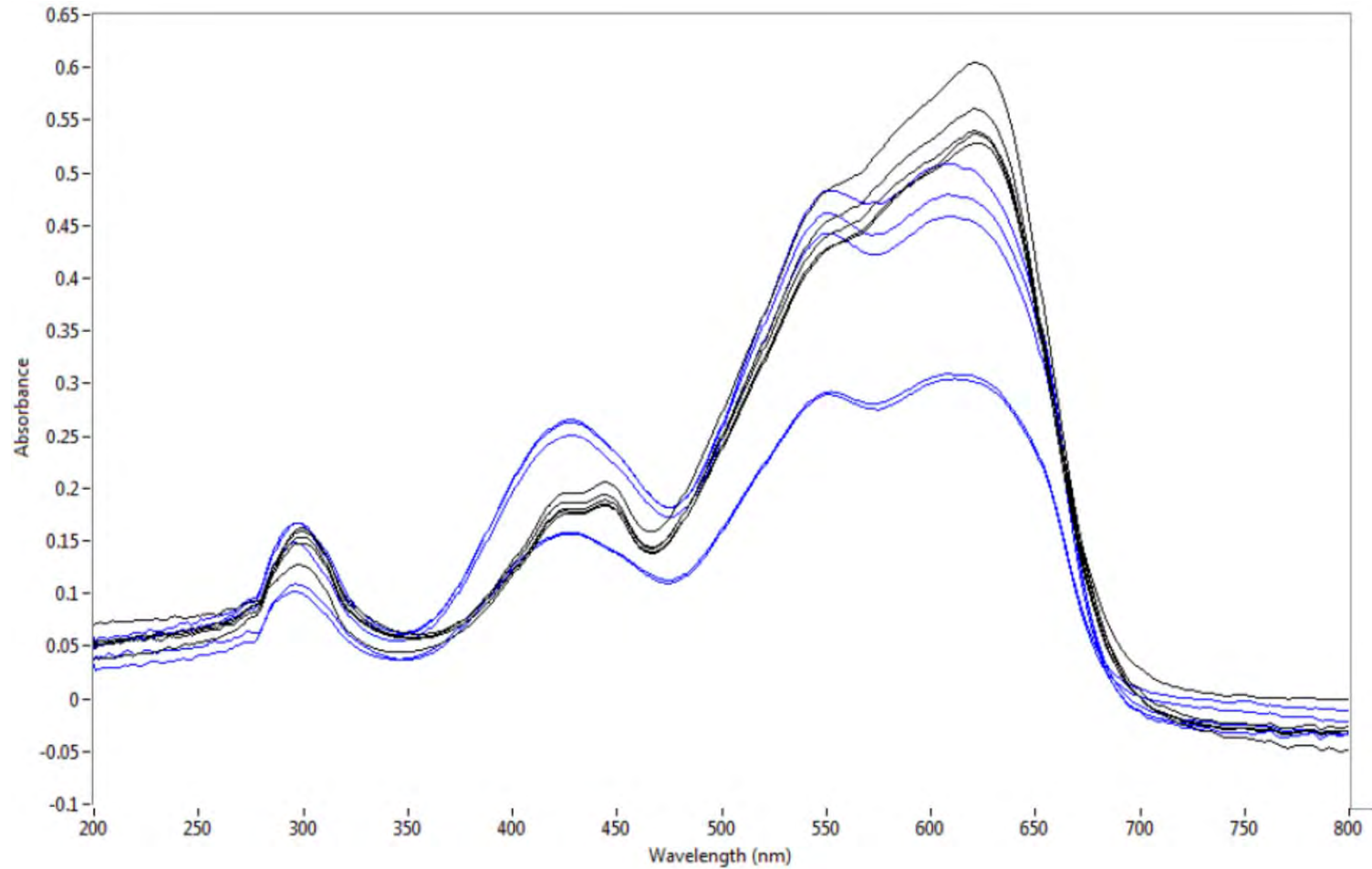


Figure 354. MSP spectral comparison of Yarn F (black) and Yarn I (blue).

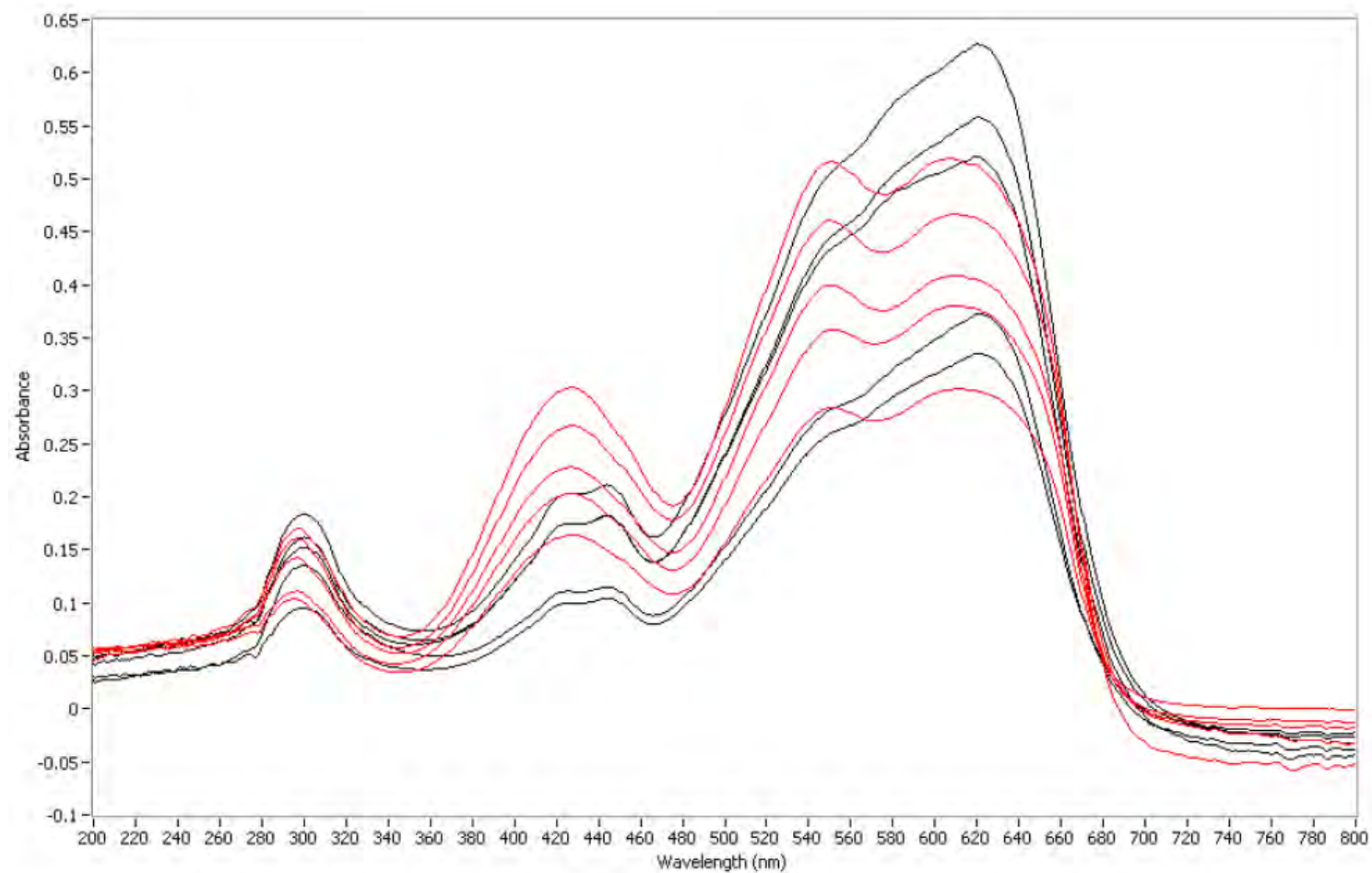


Figure 355. MSP spectral comparison of Yarn G (red) and Yarn J (black).

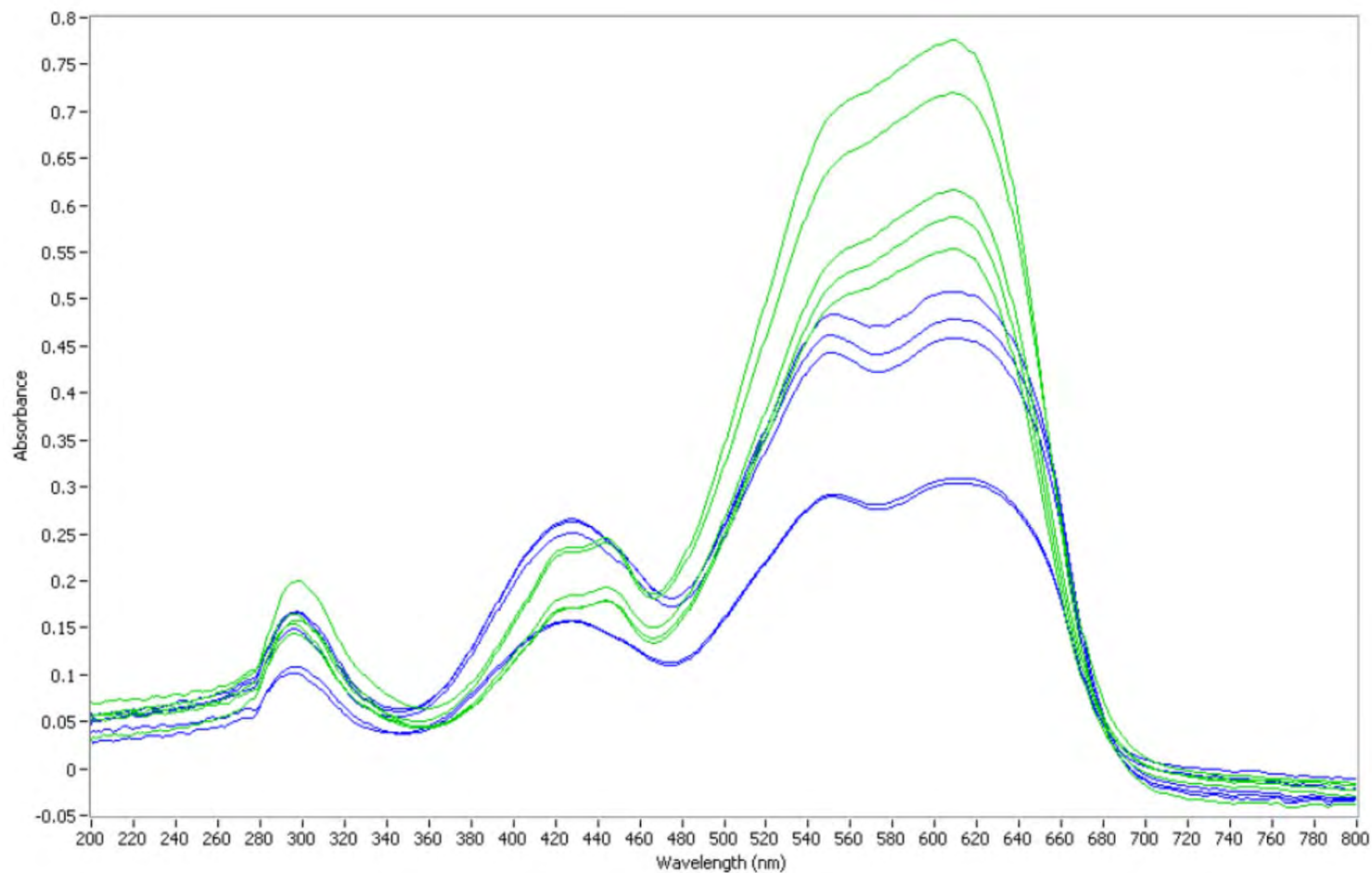


Figure 356. MSP spectral comparison of Yarn H (green) and Yarn I (blue).

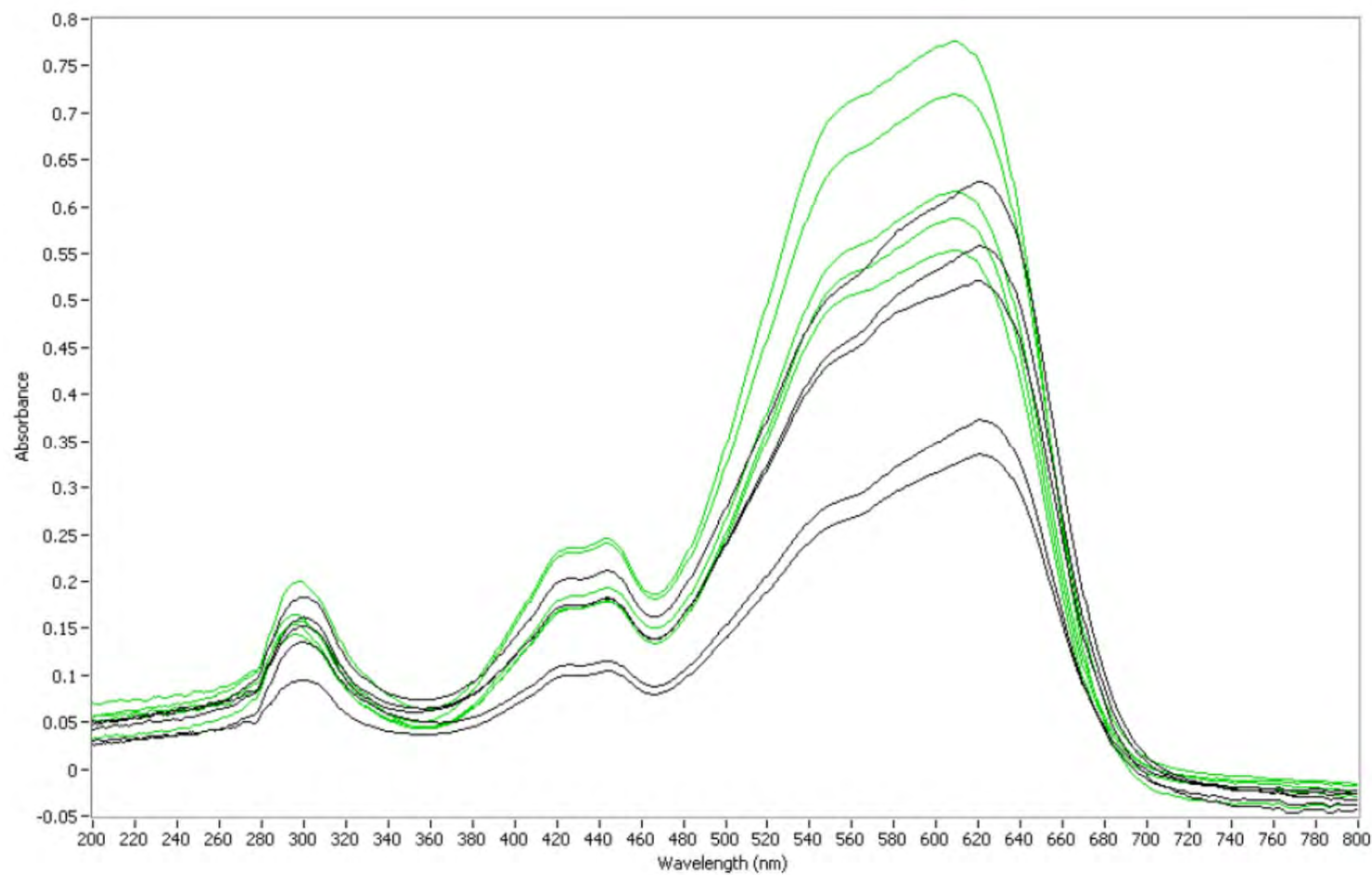


Figure 357. MSP spectral comparison of Yarn H (green) and Yarn J (blue).

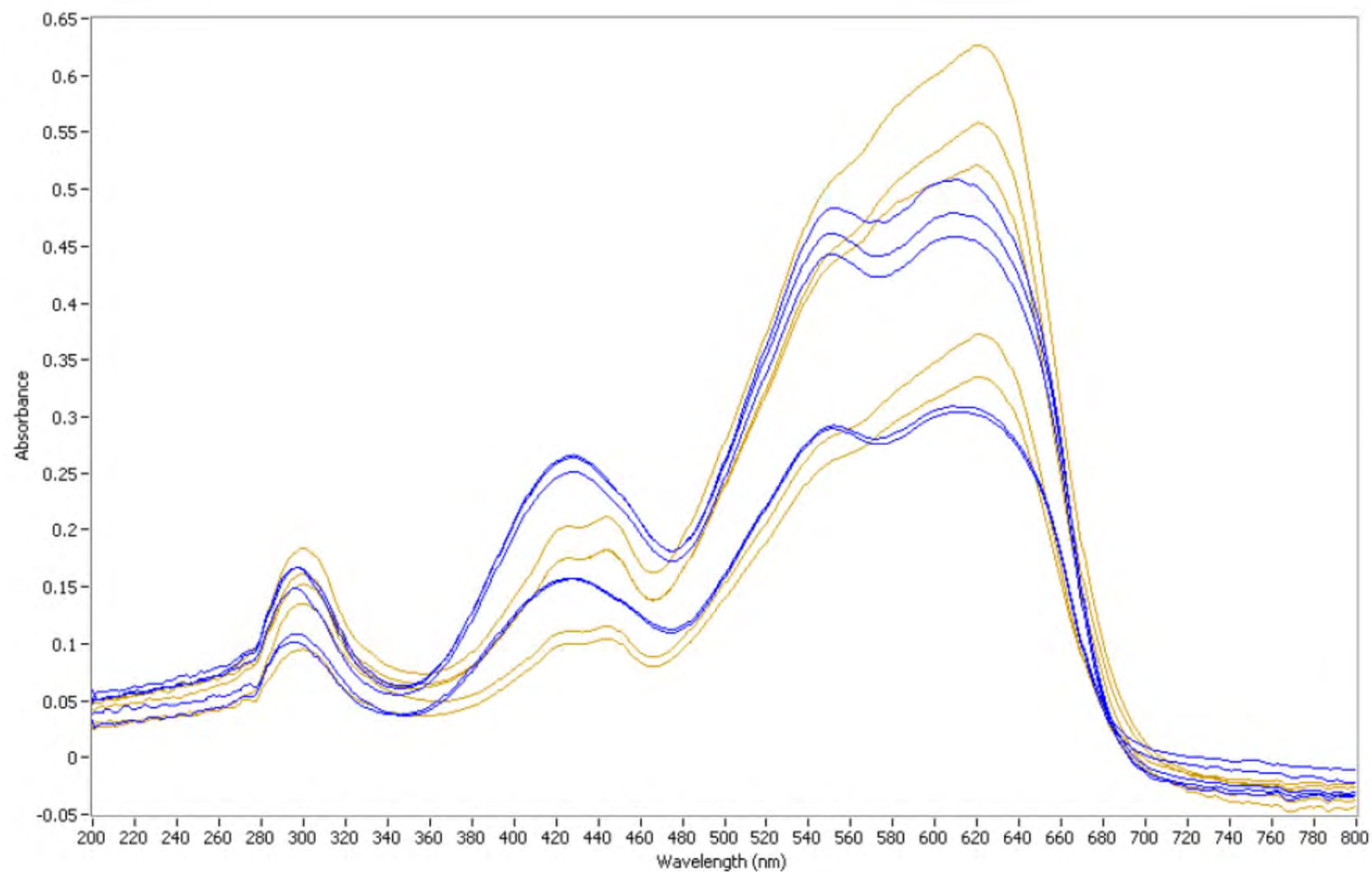


Figure 358. MSP spectral comparison of Yarn I (blue) and Yarn J (orange).